LATEST ADVANCES ON EXCITATORY SYNAPSE BIOLOGY

EDITED BY: Kimberly M. Huber, Pierre Paoletti and P. Jesper Sjöström
PUBLISHED IN: Frontiers in Synaptic Neuroscience,
Frontiers in Cellular Neuroscience and
Frontiers in Molecular Neuroscience

frontiers Research Topics

frontiers

ISSN 1664-8714
ISBN 978-2-88971-681-4
DOI 10.3389/978-2-88971-681-4

About Frontiers

Frontiers is more than just an open-access publisher of scholarly articles: it is a pioneering approach to the world of academia, radically improving the way scholarly research is managed. The grand vision of Frontiers is a world where all people have an equal opportunity to seek, share and generate knowledge. Frontiers provides immediate and permanent online open access to all its publications, but this alone is not enough to realize our grand goals.

Frontiers Journal Series

The Frontiers Journal Series is a multi-tier and interdisciplinary set of open-access, online journals, promising a paradigm shift from the current review, selection and dissemination processes in academic publishing. All Frontiers journals are driven by researchers for researchers; therefore, they constitute a service to the scholarly community. At the same time, the Frontiers Journal Series operates on a revolutionary invention, the tiered publishing system, initially addressing specific communities of scholars, and gradually climbing up to broader public understanding, thus serving the interests of the lay society, too.

Dedication to Quality

Each Frontiers article is a landmark of the highest quality, thanks to genuinely collaborative interactions between authors and review editors, who include some of the world's best academicians. Research must be certified by peers before entering a stream of knowledge that may eventually reach the public - and shape society; therefore, Frontiers only applies the most rigorous and unbiased reviews.
Frontiers revolutionizes research publishing by freely delivering the most outstanding research, evaluated with no bias from both the academic and social point of view. By applying the most advanced information technologies, Frontiers is catapulting scholarly publishing into a new generation.

What are Frontiers Research Topics?

Frontiers Research Topics are very popular trademarks of the Frontiers Journals Series: they are collections of at least ten articles, all centered on a particular subject. With their unique mix of varied contributions from Original Research to Review Articles, Frontiers Research Topics unify the most influential researchers, the latest key findings and historical advances in a hot research area! Find out more on how to host your own Frontiers Research Topic or contribute to one as an author by contacting the Frontiers Editorial Office: frontiersin.org/about/contact

LATEST ADVANCES ON EXCITATORY SYNAPSE BIOLOGY

Topic Editors:
Kimberly M. Huber, University of Texas Southwestern Medical Center, United States
Pierre Paoletti, Institut National de la Santé et de la Recherche Médicale (INSERM), France
P. Jesper Sjöström, McGill University, Canada

Citation: Huber, K. M., Paoletti, P., Sjöström, P. J., eds. (2021). Latest Advances on Excitatory Synapse Biology. Lausanne: Frontiers Media SA.
doi: 10.3389/978-2-88971-681-4

Table of Contents

frontiers in Synaptic Neuroscience

EDITORIAL
published: 28 September 2021
doi: 10.3389/fnsyn.2021.768651

Editorial: Latest Advances on Excitatory Synapse Biology

Kimberly M. Huber[1], *Pierre Paoletti*[2] *and P. Jesper Sjöström*[3]*

[1] Department of Neuroscience, O'Donnell Brain Institute, University of Texas Southwestern Medical Center, Dallas, TX, United States, [2] Institut de Biologie de l'Ecole Normale Supérieure (IBENS), Ecole Normale Supérieure, Université PSL, CNRS, INSERM, Paris, France, [3] Centre for Research in Neuroscience, Brain Repair and Integrative Neuroscience Program, Department of Medicine, Department of Neurology and Neurosurgery, The Research Institute of the McGill University Health Centre, Montreal General Hospital, Montreal, QC, Canada

Keywords: synapse, excitation, plasticity, electrophysiology, microscopy, optogenetics

Editorial on the Research Topic

Latest Advances on Excitatory Synapse Biology

INTRODUCTION

The development and function of the human brain as well as its remarkable capacity for experience dependent change hinge on the organization and dynamics of synapses. In the central nervous system, excitatory synapses represent the primary means of information processing by local circuits and communication between brain regions. The molecular composition, structural organization, signaling function, and plasticity of excitatory synapses underlie experience-dependent changes in brain function associated with learning and memory. Not surprisingly, disruption of excitatory synapse signaling, function, and plasticity has been implicated in a broad range of neurological and psychiatric diseases, including schizophrenia, autism, depression, substance abuse and addiction, Parkinson's disease, Alzheimer's disease, traumatic brain injury, stroke, and epilepsy. Therefore, synaptic studies not only provide fundamental insight into a linchpin of the nervous system but also is essential to develop novel therapeutics and progress in lessening the burden of human neurological diseases and improving mental health.

In the past decade, major progress has been made in understanding the architecture and functionalities of excitatory synapses. These advances, largely triggered by the advent of novel technologies—such as cryo-electron and super-resolution microscopy, optogenetics and opto-pharmacology, deep sequencing, single-cell genetics, etc. —have had profound implications for our understanding of the normal and diseased brain. In this Research Topic, we have collected articles to highlight recent progress and excitement across the breadth of synapse biology, with a focus on glutamatergic synapses of the mammalian brain and an emphasis on molecular, cellular, physiological, and physiopathological mechanisms.

PAPERS IN THIS COLLECTION

Synapse Development and Neurodevelopmental Disorders

Understanding how brain circuits form and how proper synaptic connectivity is established during brain development is an active area of neuroscience research that is essential for clarifying the mechanisms of neurodevelopmental disorders such as autism and intellectual disability. To study synapse development, culture methods are invaluable, as these provide direct access to these processes. In this collection, Moutin et al. detail a method for making postnatal cultures of mouse hippocampal neurons and for efficient genetic manipulation using lentiviruses. Because

OPEN ACCESS

Edited and reviewed by:
Alfredo Kirkwood,
Johns Hopkins University,
United States

***Correspondence:**
P. Jesper Sjöström
jesper.sjostrom@mcgill.ca

Received: *01 September 2021*
Accepted: *08 September 2021*
Published: *28 September 2021*

Citation:
Huber KM, Paoletti P and Sjöström PJ (2021) Editorial: Latest Advances on Excitatory Synapse Biology. Front. Synaptic Neurosci. 13:768651. doi: 10.3389/fnsyn.2021.768651

most excitatory synapse development in hippocampus occurs after birth, this method provides incredible access for imaging, functional studies, as well as for genetic and chronic pharmacological treatments to study synapse development. Lentiviral transfection also allows manipulation of neurodevelopment-related genes, to determine acute and direct effects of these genes on synapses.

The interaction between GABAergic and glutamatergic synapses during brain development and how they impact each other's maturation has been unclear. Using organotypic hippocampal slice cultures, Salmon et al. discovered a role for depolarizing GABA in limiting excitatory synapse development. Over the course of neuron development, GABA receptor (GABAR) mediated synaptic currents switch from depolarizing to hyperpolarizing after the first postnatal week, due to a developmental expression of the KCC2 chloride transporter. Salmon et al. demonstrated a developmental switch in GABAR current polarity in slice cultures and find that pharmacological blockade of GABARs during the first postnatal week, even transiently, induces a persistent increase excitatory synapse number. They also demonstrate that this effect requires action potential firing of neurons, suggesting that it is the depolarizing action of GABARs that restrains excitatory synapse development. This activity-dependent inhibition of synapse development may utilize similar mechanisms to the activity-induced synaptic depression or elimination mechanisms that occur in the brain.

Loss of the fragile X mental retardation protein FMRP is a leading monogenic cause of autism, called Fragile X Syndrome (FXS). FXS is also characterized by repetitive, stereotyped behaviors and hyperactivity—all of which are associated with striatal function. FMRP regulates structural and functional synapse development and plasticity in the neocortex and hippocampus, but little is known of FMRP function in the striatum. Using cortical-striatal co-culture Huebschman et al. find that medium-spiny neurons (MSNs) without FMRP, have deficits in of excitatory synapse development, as measured by colocalized PSD-95 puncta at synapses and dendritic spines. Surprisingly, re- or overexpression of FMRP also suppressed synapse development, suggesting a *U*-shaped effect of FMRP on synapse development. Using different mutants of FMRP, some implicated in FXS, Huebschman et al. reveal roles for specific RNA binding domains of FMRP in development of cortical striatal synapses.

A fascinating review article by Nguyen et al. discusses recent literature on the mutations in the Neuroligin (*Nlgn1-4*) gene family of postsynaptic cell adhesion molecules and the interactions of distinct family members on synapse development and implications for diseases such as autism. NLGNs, generally, promote synapse development and stabilization and NLGN3 and NLGN4 mutations are linked to autism. Nguyen et al. review recent work that revealed distinct protein sequences, trafficking and functions for NLGN4 on synapses when expressed on the X (NLGN4X) or Y (NLGN4Y) chromosomes that may help to explain the male bias of autism diagnoses with NLGN mutations.

Plasticity of Excitatory Synapses, AMPA Receptors, and Disease

A major mechanism of plasticity of excitatory synapses, both during development and in the mature brain, is trafficking of the AMPA receptor (AMPAR) subtype of ionotropic glutamate receptors. Synaptic strength changes during long-term potentiation (LTP) and long-term depression (LTD) can occur by insertion or removal of GluA2 lacking AMPARs at synapses, in part because they have a higher conductance. GluA2-lacking AMPARs are typically GluA1 homomers and are Ca^{2+} permeable. Little has been known of the molecular mechanisms that control trafficking of GluA2- lacking, Ca^{2+} permeable AMPARs. Purkey and Dell'Acqua provide a comprehensive review of how phosphorylation and dephosphorylation of GluA1 regulates trafficking of Ca^{2+} permeable AMPARs at synapses during plasticity. The authors also provide important knowledge of the molecular mechanisms of synaptic plasticity that contribute to learning and memory.

Long-term synaptic plasticity and memory storage in the brain are well-known for depending on neuromodulation. Precisely how remains poorly understood, however. In a modeling study, Mihalas et al. explore how the expression of LTP and LTD is limited by the occupancy of AMPARs at small perisynaptic compartments, and how this is modulated by push-pull regulation by the G-proteins Gs and Gq. In addition to showing how their model captures the key features of the pull-push neuromodulation of synaptic plasticity, Mihalas et al. also demonstrate that it is consistent with other actions of neuromodulators observed in slice, for a view that is compatible with our current understanding of AMPAR trafficking in synaptic plasticity.

Caffeine modulates synaptic function through its antagonistic action at adenosine receptors, but little has been known of the age- and brain-region-specific functions of adenosine at synapses. New work from Caruana and Dudek reveals that activation of adenosine receptors induces a long-lasting depression of synaptic transmission at hippocampal CA1 and CA2 neurons in young rats, but selectively induces depression in CA2 in adults. They also find distinct sensitivity of CA1 and CA2 synaptic transmission to regulators of cAMP levels, a downstream effector of adenosine, which provides mechanistic insight into the CA2-specific actions of adenosine.

A wide range of neuropathologies, including psychiatric and neurodegenerative disorders, have aberrations in synaptic transmission and plasticity that are specific to brain region and to AMPAR subunits. In an interesting mini review, Zhang and Bramham provide a summary of AMPAR dysregulation in animal models of neuropathology. They also discuss preclinical findings regarding the targeting of AMPARs therapeutically.

Epileptogenesis is the process by which the healthy brain becomes epileptic. This process is not well-understood, to a large extent because of a limited availability of relevant probes to monitor the key players in epileptogenesis, for example the gelatinases Matrix Metalloproteinase 2 and 9 (MMP-2 and MMP-9, respectively). To address this, Bouquier et al. created a peptide-based biosensor for reporting gelatinase activity. As a proof of

principle, they applied their new biosensor to the kainate model of epilepsy. Bouquier et al. propose that this biosensor is useful for localizing cellular reactive changes in epileptogenesis and that it could enable selective, local therapy by pharmacologically targeting gelatinase activity.

Neuronal and Synaptic Heterogeneity in Humans and Rodents

There is much heterogeneity of neuronal and synaptic morphology and function in the brain, but little is known of this heterogeneity in human brain and how it relates to the evolution of cortical areas. In a hypothesis-and-theory article, Rasia-Filho et al. present new data and discuss previous work from 3D reconstruction of pyramidal neurons that demonstrate a morphological heterogeneity across the subcortical, allocortical, and neocortical regions of the human brain, focusing on the amygdala, hippocampus, and neocortex. They also demonstrate and discuss the large variability in dendritic spine morphologies within an individual pyramidal neuron in each region and discuss the functional implications of such diversity.

The cingulate cortex of humans has been implicated in emotion, attention, cognition, and social behavior. Interestingly, in layer 5 of the human cingulate cortex, one does not only find the classical pyramidal neurons, but also a specialized neuronal type with an elongated spindle-shaped cell body, known as the von Economo neuron, or VEN. Using advanced histological techniques, Correa-Júnior et al. studied these intriguing VENs in tissue from four neurologically normal adult subjects, which revealed a continuum of morphological properties. Morphometry suggested to Correa-Júnior et al. that this spectrum could be subdivided into three classes, VENs 1 through 3, with progressively increased dendritic ramifications and higher spine densities. The authors suggest that this interesting heterogeneity may underlie diverse functionality and forms of information processing.

Synapses in the brain are strikingly diverse. Even within a relatively restricted portion of the brain, such as the CA1 region of the hippocampus, there is a high degree of synaptic variability due to molecular and morphological differences present among individual synapses of the same type. However, most of today's electrophysiological methods record from synapse populations, thus averaging across individual synapses while discarding the individual variability. In a thought-provoking hypothesis-and-theory article, Grant and Fransén discuss the implications of synapse diversity for studies of synaptic physiology, plasticity, development, and behavior, as well as for phenotypes arising from pharmacological and genetic perturbations. Grant and Fransén propose that present models that are based on measurements averaged across diverse populations may need to be re-examined, since single-synapse resolution methods are required to test and validate current synaptic models of behavior. This fresh view suggests that novel, more detailed models of physiology and behavior could be created based on this traditionally ignored functional and molecular diversity of different synapses.

CONCLUDING REMARKS

This collection highlights the varied and latest research concerning excitatory synapses. These works describe methods used to study synapses, as well as current efforts to understand the development, plasticity and function of excitatory synapses in both humans and animals. Importantly, several articles illustrate how research in excitatory synapses contributes to the understanding and treatment of brain disease. We hope this collection will inform and inspire future studies in many areas of neuroscience.

AUTHOR CONTRIBUTIONS

KH, PP, and PJS wrote the manuscript. All authors contributed to the article and approved the submitted version.

ACKNOWLEDGMENTS

We thank Alanna Watt for help and useful discussions. KH was supported by NIH grants HD052731 and HD082008. PP was supported by grants from the ANR (GluBrain3A, EXCIGLY) and by the ERC (#693021). PJS was supported by FRQS *Chercheurs-Boursiers* Senior 9 Award #254033.

Conflict of Interest: The authors declare that the research was conducted in the absence of any commercial or financial relationships that could be construed as a potential conflict of interest.

Publisher's Note: All claims expressed in this article are solely those of the authors and do not necessarily represent those of their affiliated organizations, or those of the publisher, the editors and the reviewers. Any product that may be evaluated in this article, or claim that may be made by its manufacturer, is not guaranteed or endorsed by the publisher.

frontiers in Cellular Neuroscience

ORIGINAL RESEARCH
published: 25 February 2020
doi: 10.3389/fncel.2020.00036

Depolarizing GABA Transmission Restrains Activity-Dependent Glutamatergic Synapse Formation in the Developing Hippocampal Circuit

Christopher K. Salmon[1], Horia Pribiag[1], Claire Gizowski[1], W. Todd Farmer[1], Scott Cameron[1], Emma V. Jones[1], Vivek Mahadevan[2], Charles W. Bourque[1], David Stellwagen[1], Melanie A. Woodin[2] and Keith K. Murai[1]**

[1]Centre for Research in Neuroscience, Department of Neurology and Neurosurgery, Brain Repair and Integrative Neuroscience Program, The Research Institute of the McGill University Health Centre, Montreal General Hospital, Montreal, QC, Canada, [2]Department of Cell & Systems Biology, University of Toronto, Toronto, ON, Canada

γ-Aminobutyric acid (GABA) is the main inhibitory neurotransmitter in the mature brain but has the paradoxical property of depolarizing neurons during early development. Depolarization provided by $GABA_A$ transmission during this early phase regulates neural stem cell proliferation, neural migration, neurite outgrowth, synapse formation, and circuit refinement, making GABA a key factor in neural circuit development. Importantly, depending on the context, depolarizing $GABA_A$ transmission can either drive neural activity or inhibit it through shunting inhibition. The varying roles of depolarizing $GABA_A$ transmission during development, and its ability to both drive and inhibit neural activity, makes it a difficult developmental cue to study. This is particularly true in the later stages of development when the majority of synapses form and $GABA_A$ transmission switches from depolarizing to hyperpolarizing. Here, we addressed the importance of depolarizing but inhibitory (or shunting) $GABA_A$ transmission in glutamatergic synapse formation in hippocampal CA1 pyramidal neurons. We first showed that the developmental depolarizing-to-hyperpolarizing switch in $GABA_A$ transmission is recapitulated in organotypic hippocampal slice cultures. Based on the expression profile of K^+-Cl^- co-transporter 2 (KCC2) and changes in the GABA reversal potential, we pinpointed the timing of the switch from depolarizing to hyperpolarizing $GABA_A$ transmission in CA1 neurons. We found that blocking depolarizing but shunting $GABA_A$ transmission increased excitatory synapse number and strength, indicating that depolarizing $GABA_A$ transmission can restrain glutamatergic synapse formation. The increase in glutamatergic synapses was activity-dependent but independent of BDNF signaling. Importantly, the elevated number of synapses was stable for more than a week after $GABA_A$ inhibitors were washed out. Together these findings point to the ability of immature GABAergic transmission to restrain glutamatergic synapse formation and suggest an unexpected role for depolarizing $GABA_A$ transmission in shaping excitatory connectivity during neural circuit development.

Keywords: synapse formation, hippocampus, GABA transmission, dendritic spines, chloride homeostasis, KCC2, circuit development, autism

OPEN ACCESS

Edited by:
Kimberly M. Huber, UT Southwestern Medical Center, United States

Reviewed by:
Shiva K. Tyagarajan, University of Zurich, Switzerland
Knut Holthoff, Friedrich Schiller University Jena, Germany

****Correspondence:***
Christopher K. Salmon
chris.salmon@mail.mcgill.ca
Keith K. Murai
keith.murai@mcgill.ca

Received: *29 September 2019*
Accepted: *05 February 2020*
Published: *25 February 2020*

Citation:
Salmon CK, Pribiag H, Gizowski C, Farmer WT, Cameron S, Jones EV, Mahadevan V, Bourque CW, Stellwagen D, Woodin MA and Murai KK (2020) Depolarizing GABA Transmission Restrains Activity-Dependent Glutamatergic Synapse Formation in the Developing Hippocampal Circuit. Front. Cell. Neurosci. 14:36. doi: 10.3389/fncel.2020.00036

INTRODUCTION

γ-Aminobutyric acid (GABA) is the main inhibitory neurotransmitter in the mature brain. However, GABA is paradoxically depolarizing during nervous system development. Many *in vitro* studies in rodents have shown that depolarizing $GABA_A$ transmission provides excitatory drive during gestation and early postnatal CNS development, driving early network oscillations (ENOs) thought to promote activity-dependent maturation of neural circuits (Ben-Ari et al., 2012). However, recent work suggests that despite providing local depolarization, immature $GABA_A$ transmission has inhibitory effects *in vivo* (Kirmse et al., 2015; Oh et al., 2016; Valeeva et al., 2016). This ability of GABA to be simultaneously depolarizing and inhibitory relies on shunting inhibition, which results from a decrease in input resistance and membrane time constant when $GABA_A$ receptors open, regardless of the direction of Cl^- flux (Staley and Mody, 1992).

Depolarizing $GABA_A$ transmission is implicated in numerous neurodevelopmental processes in vertebrates, including neural stem cell proliferation (Liu et al., 2005), cell migration (Behar et al., 2000), neurite outgrowth (Cancedda et al., 2007), synapse formation, and circuit refinement (Akerman and Cline, 2006; Cancedda et al., 2007; Wang and Kriegstein, 2008). Critically, circuit activity supported by depolarizing $GABA_A$ transmission *in vitro* drives calcium influx thought to be important for glutamatergic synapse development (Leinekugel et al., 1995; Ben-Ari et al., 1997; Griguoli and Cherubini, 2017). Indeed, disrupting the depolarizing nature of $GABA_A$ transmission by interfering with chloride homeostasis alters glutamatergic synapse formation and maturation (Akerman and Cline, 2006; Wang and Kriegstein, 2008). However, the effects of $GABA_A$ transmission itself on glutamatergic synapse development and the timing of these effects remain poorly defined. This is partly due to the difficulty in manipulating depolarizing $GABA_A$ transmission in defined cell types and circuits with sufficient temporal resolution to specifically target the period when glutamatergic synapses are forming while sparing the preceding developmental roles of GABA. Several studies have prematurely hyperpolarized the reversal potential for chloride (E_{Cl}) by disrupting chloride homeostasis for more than a week during perinatal development, across a time span in which the targeted neurons terminally divide, migrate, extend neurites and are incorporated into the surrounding circuitry (Ge et al., 2006; Cancedda et al., 2007; Wang and Kriegstein, 2008). This work suggests that disrupting E_{Cl} alters neurite and synapse maturation, however, it has been noted that additional studies with the higher temporal resolution are needed (Akerman and Cline, 2007; Kirmse et al., 2018). Closing this gap in our understanding of how $GABA_A$ transmission and its transition from a depolarizing to a hyperpolarizing state impacts glutamatergic synapse development will help solve a now-classic problem in developmental neurobiology, and will likely be of clinical significance as disruptions of $GABA_A$ transmission during brain development are associated with neurodevelopmental disorders (El Marroun et al., 2014; He et al., 2014; Tyzio et al., 2014).

Here, we investigated the role of depolarizing $GABA_A$ transmission in glutamatergic synapse formation on hippocampal CA1 pyramidal cells. To perform temporally precise pharmacological manipulations of $GABA_A$ transmission during neural circuit development, we took advantage of the properties of the organotypic hippocampal slice culture. This preparation preserves the anatomy and the developmental progression of the hippocampus, including the time course of excitatory synapse formation (Buchs et al., 1993; Muller et al., 1993; De Simoni et al., 2003). This system enabled us to define a narrow time window during the first week of slice development in which $GABA_A$ transmission shifts from immature, depolarizing transmission, to hyperpolarizing transmission in CA1 pyramidal cells. Previous work suggests that blocking depolarizing $GABA_A$ transmission during development will remove the excitatory drive and decrease excitatory synapse formation and maturation (Ben-Ari et al., 2007; Wang and Kriegstein, 2008). Contrary to these predictions, we found that transient blockade of immature, depolarizing $GABA_A$ transmission increased glutamatergic synapse number and function on CA1 pyramidal cells. This unexpected effect was explained by the finding that, at this stage of development, depolarizing $GABA_A$ transmission provides shunting inhibition, which when blocked alleviated a restraint on activity-dependent synapse formation. Interestingly, the activity-dependent increase in glutamatergic synapses was stable for at least a week. Furthermore, the effect could not be reproduced by prematurely hyperpolarizing E_{GABA}, and was independent of BDNF signaling. Our results, therefore, point to an important time window during hippocampal development when immature $GABA_A$ transmission can restrain excitatory synapse development, and demonstrate that interfering with $GABA_A$ transmission at this stage can have lasting effects on neural circuitry.

MATERIALS AND METHODS

Animals

Experiments were approved by the Montreal General Hospital Facility Animal Care Committee and followed guidelines of the Canadian Council on Animal Care. Male and female C57BL6 mice kept on a 12:12 light-dark cycle were used to prepare organotypic cultures.

Slice Preparation

Organotypic hippocampal slices were prepared as described previously (Haber et al., 2006). Briefly, hippocampi were extracted from postnatal day five mice and cut into 300 μm slices with a McIllwain tissue chopper (Stoelting). Slices were cultured on semi-porous tissue culture inserts (Millipore, Cat. No. PICMORG50) that sat in culture medium composed of minimal essential medium (MEM) supplemented with Glutamax (Invitrogen, Cat. No. 42360032), 25% horse serum (Invitrogen, Cat. No. 26050088), 25% HBSS (Invitrogen, Cat. No. 14025092), 6.5 mg/ml D-glucose and 0.5% penicillin/streptomycin. Slices were cultured for 5–14 days with full medium changes every 2 days.

Labeling of CA1 Cells

Dendrites and spines of CA1 pyramidal cells were labeled using a Semliki Forest Virus (SFV)-mediated approach described in detail elsewhere (Haber et al., 2006). Briefly, SFV driving expression of enhanced green fluorescent protein, targeted to the cell membrane through a farnesylation sequence (EGFPf), was injected into the stratum oriens *via* a pulled glass pipette, broken to a diameter of approximately 50–100 μm. Glass pipettes were attached to a Picospritzer III (Parker Hannifin) and SFV was delivered with 10 ms pulses at 14–18 psi 18–20 h before fixation in 4% formaldehyde/0.1 M PO_4^{2-} for 30 min.

Confocal Imaging and Spine Analysis

Imaging was performed using an Ultraview Spinning Disc confocal system (Perkin Elmer) attached to a Nikon TE-2000 microscope and an FV1000 laser scanning confocal microscope (Olympus). Z-stacks were acquired from approximately 100 μm of CA1 primary apical dendrites, just above the primary dendrite bifurcation. This dendritic subfield is consistently identifiable, fully formed by the period of interest, harbors the highest density of asymmetric synapses, and retains its native connectivity in organotypic slices (Megías et al., 2001; Amaral and Lavenex, 2007). Ten to forty z-stacks were acquired per animal. Experiments were comprised of cultures from animals originating from at least two litters. Two-dimensional spine counts and geometric measurements of spines were quantified using Reconstruct (Fiala, 2005) and a custom ImageJ macro. Three-dimensional spine classification was performed with NeuronStudio (Rodriguez et al., 2008). All spine analysis was performed by an investigator blinded to the experimental condition.

Western Blot Analysis

For Western blots, 4–6 organotypic slices were lifted from nylon culture inserts with a No. 10 scalpel blade, rinsed in cold PBS and incubated on ice in 100 μl of Triton lysis buffer (20 mM Tris pH 7.4, 137 mM NaCl, 2 mM EDTA, 1% Triton X-100 (TX-100), 0.1% SDS, 10% glycerol, with protease inhibitors and sodium orthovanadate) for 30 min. Lysates were centrifuged at high speed for 10 min and stored at −80°C in sample buffer. Supernatants were warmed to room temperature and run under standard SDS-PAGE conditions. Membranes were immunoblotted with anti-K^+-Cl^- co-transporter 2 (KCC2) 1:1,000 (N1/12, NeuroMab) and GAPDH 1:300,000 (MAB374, Millipore). KCC2 blots were run immediately after developmental time courses ended to reduce experimentally-induced aggregation of KCC2 oligomers, which we observe to increase with time at -80°C.

Electrophysiology

Gramicidin perforated patch whole-cell recordings were performed similarly to previously described (Acton et al., 2012). Briefly, current-voltage (IV) curves were generated by step depolarizing the membrane potential in 10 mV increments from ∼−95 to −35 mV (**Figure 1C**) and during each increment GABAergic transmission was elicited *via* extracellular stimulation in the stratum radiatum. Pipettes had a resistance of 7–12 MΩ and were filled with an internal solution containing 150 mM KCl, 10 mM HEPES, and 50 mM μg/ml gramicidin (pH 7.4, 300 mOsm). We recorded E_{GABA} in the current-clamp mode. The glutamatergic transmission was inhibited with CNQX.

Miniature EPSCs (mEPSCs) were recorded using the whole-cell patch clamp configuration (V_h = −70 mV), at 30°C, in ACSF containing (in mM): 119 NaCl, 26.2 $NaHCO_3$, 11 D-glucose, 2.5 KCl, 1 NaH_2PO_4, 2.5 $CaCl_2$, 1.3 $MgCl_2$, 0.0002 TTX, 0.025 D-APV, 0.05 picrotoxin. Recording pipettes (2–5 MΩ) were filled with (in mM): 122 $CsMeSO_4$, 8 NaCl, 10 D-glucose, 1 $CaCl_2$, 10 EGTA, 10 HEPES, 0.3 Na_3GTP, 2 MgATP, pH 7.2. Signals were low-pass filtered at 2 kHz, acquired at 10 kHz, and analyzed using Clampfit 10.3 (Molecular Devices).

For cell-attached recordings, ACSF and pipette solutions were as described above for mEPSC recordings, but ACSF lacked TTX, D-APV and picrotoxin. Low resistance recording pipettes (1–2 MΩ) were used to form loose patch seals (approximately 100–350 MΩ). Recordings were performed in I = 0 mode. GABA was diluted in ACSF to 100 μM and puffed in close proximity to the recorded cell using a glass pipette connected to a Picospritzer III (Parker Hannifin) delivering 10 ms duration air puffs at 14 psi. Electrically-evoked stimulations (1.3 V, 0.5 ms) were delivered by the recording amplifier *via* the recording pipette. Recorded signals were analyzed using threshold-based detection of spikes in Clampfit 10.3 (Molecular Devices).

Experiments comprised slices from at least three separate animals taken from at least two litters.

Pharmacology

Pharmacological agents (Tocris unless otherwise noted) were applied to the culture medium during a regular medium change. Gabazine (GBZ; 20 μM), bicuculline-methiodide (20 μM) and diazepam (5 μM) were used to manipulate $GABA_A$ transmission. GBZ was washed out by incubating slices in fresh medium for 30 min, then washing the top of the slices with equilibrated medium for 1–2 min before changing to fresh dishes and medium. Bumetanide (Bume, 10 μM), TrkB-Fc bodies (5 mg/mL, R&D Systems) and K252a (200 nM) were added to cultures 30 min before adding GBZ.

Quantitative Reverse Transcriptase PCR (qRT-PCR)

Six to eight organotypic slices per sample were lifted from nylon culture inserts with a No. 10 scalpel blade, washed briefly in ice-cold PBS and flash-frozen in microcentrifuge tubes in a 100% EtOH/dry ice slurry. Total RNA was extracted using the RNeasy Lipid Tissue Kit (Qiagen). cDNA libraries were created using the QuantiTect Reverse Transcription Kit (Qiagen). Quantitative PCR was performed using Sybr Green Master Mix (Applied Biosystems Systems) on a StepOne Plus thermocycler (Applied Biosystems). Relative levels of mRNA were calculated using the ΔΔCT method with GAPDH as the internal control. Primer sequences were as follows: GAPDH forward TTG AAG TCG CAG GAG ACA ACC; GAPDH reverse ATG TGT CCG TCG TGG ATC; BDNF forward GTG ACA GTA TTA GCG AGT GGG; BDNF reverse GGG ATT ACA CTT GGT CTC GTA G;

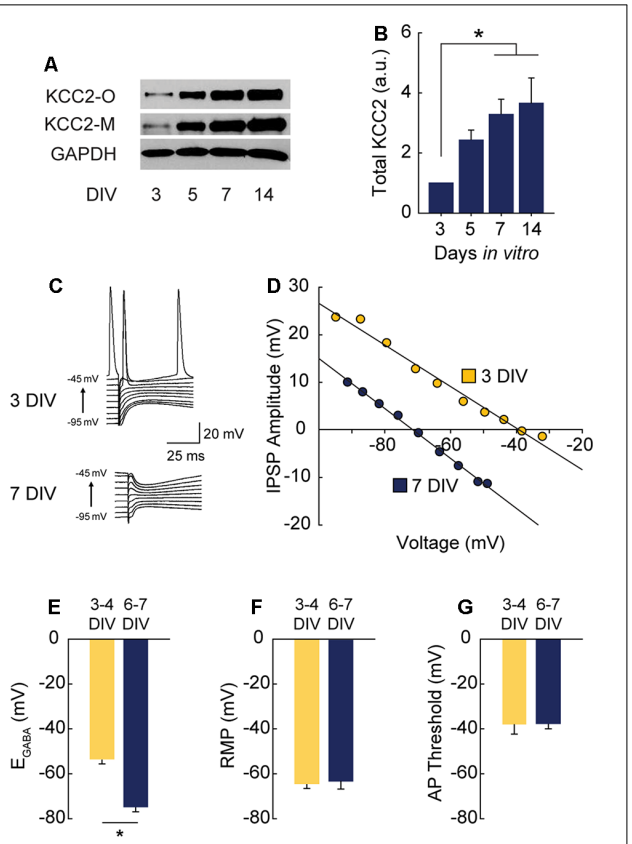

FIGURE 1 | γ-Aminobutyric acid (GABA) reversal potential (E_{GABA}) shifts from depolarizing to hyperpolarizing between 3 and 7 DIV. **(A,B)** Western blot of K^+-CL^- co-transporter 2 (KCC2) expression time course **(A)** and summary data, normalized to expression level at 3 DIV (**B**: 5 DIV 1.43 ± 0.34, 7 DIV 3.28 ± 0.51, 14 DIV 3.66 ± 0.84; $n = 5$; ANOVA $p = 0.011$; 3 vs. 5 DIV $p = 0.25$, 3 vs. 7 DIV $p = 0.03$, 3 vs. 14 DIV $p = 0.01$, Tukey post test). **(C,D)** Representative gramicidin perforated patch traces and representative IV curves from GABAergic responses at 3 DIV and 7 DIV. **(E)** E_{GABA} summary plots (3/4 DIV: −53.3 ± 6.1 mV, $n = 5$; 6/7 DIV: −74.7 ± 6.4 mV, $n = 5$, $p = 0.04$). **(F)** Resting membrane potential (RMP) summary plots (3/4 DIV: −64.5 ± 2.3 mV, $n = 5$; 6/7 DIV: −63.4 ± 3.8 mV, $n = 5$). **(G)** Action potential (AP) threshold summary plot (3/4 DIV: −38.2 ± 4.2 mV, $n = 5$; 6/7 DIV-37.7 ± 2.3 mV, $n = 5$). $^*p < 0.05$.

Fos forward TCC CCA AAC TTC GAC CAT G; Fos reverse CAT GCT GGA GAA GGA GTC G.

Immunofluorescence

Slice cultures were fixed as described above, permeabilized for 30 min in 1% TritonX 100/PBS, blocked in 10% normal donkey serum (NDS, Jackson Immuno Research)/0.2% TX-100/PBS, and incubated with anti-c-Fos antibody (1:5,000, Cat. No. 226 003, Synaptic Systems) in 1% NDS/0.2% TX-100/PBS rocking at 4°C for 5–8 days. The primary antibody solution was washed with three rinses in 1% NDS/0.2% TX-100/PBS, followed by secondary antibodies at 1:1,000 for 2 h at room temp. TOPRO-3-iodide (Jackson Immuno Research) was applied at 1:10,000 for 10 min in the second of three washes following incubation with secondary antibodies. Quantification of Fos immunofluorescence intensity with background correction was performed with ImageJ. Full-field immunofluorescence within the CA1 *stratum pyramidale* was quantified and normalized within timepoint to the mean of the control.

Statistics

Data are presented as mean ± SEM, n sample size, N animals. Student t-tests were used except where noted that Mann–Whitney tests were used with datasets with non-normal distribution. *Post hoc* pairwise comparisons following ANOVA were performed with Tukey's honestly significant difference (HSD) test. For mean comparisons: $^*p < 0.05$, $^{**}p < 0.01$, $^{***}p < 0.001$. For Kolmogorov–Smirnov tests: $^{***}p < 0.0001$.

RESULTS

$GABA_A$ Transmission Switches From Depolarizing to Hyperpolarizing in CA1 Cells During the First Week in Hippocampal Slice Culture

Depolarizing $GABA_A$ transmission relies on relatively high intracellular chloride ($[Cl^-]_i$) during development. As neurons mature during the first weeks of postnatal CNS development, Na^+-K^+-Cl^- cotransporter (NKCC1) expression is downregulated and KCC2 is upregulated, lowering $[Cl^-]_i$ (Rivera et al., 1999; Yamada et al., 2004). $GABA_A$ receptors are largely permeable to Cl^-, and to a lesser extent bicarbonate (HCO_3^-; Kaila, 1994; Staley and Proctor, 1999). When $[Cl^-]_i$ lowers to the point at which the reversal potential for GABA (E_{GABA}) hyperpolarizes below the resting membrane potential (RMP), $GABA_A$ transmission switches from depolarizing to hyperpolarizing. To pinpoint when this switch from depolarization to hyperpolarization occurs in CA1 pyramidal cells in hippocampal organotypic slices, we first assessed the timing of KCC2 upregulation across the first 2 weeks *in vitro* and found expression of KCC2 underwent a large and graded increase between 3 and 14 days *in vitro* (DIV), reaching near-maximal levels by 7 DIV (**Figures 1A,B**). Using this timeframe as a guide, we performed gramicidin perforated patch recordings to determine the $GABA_A$ reversal potential (E_{GABA}) in CA1 pyramidal cells (exemplary traces and IV curves shown in **Figures 1C,D**). At 3–4 DIV, E_{GABA} was depolarized with respect to RMP (**Figures 1E–G**). However, by 6–7 DIV E_{GABA} was hyperpolarized with respect to RMP, indicating a switch to hyperpolarizing $GABA_A$ transmission by 6–7 DIV (**Figures 1C–G**), a timeframe similar to that reported previously for CA1 pyramidal cells (Swann et al., 1989). E_{GABA} was more negative than action potential (AP) threshold at 3–4 DIV (**Figures 1E,G**), suggesting GABA is depolarizing but not capable of directly depolarizing neurons past AP threshold from rest at this stage.

Blocking Depolarizing $GABA_A$ Transmission Increases Glutamatergic Synapse Number and Function

Overexciting mature neurons by blocking hyperpolarizing $GABA_A$ transmission is known to cause a collapse of dendritic spines both *in vivo* (Zeng et al., 2007) and *in vitro*

(Muller et al., 1993; Drakew et al., 1996; Jourdain et al., 2002; Zha et al., 2005). In particular, applying $GABA_A$ antagonists to organotypic hippocampal cultures at 5 or 23 DIV over a period of 2–3 days has been shown to cause a marked loss of spines (Drakew et al., 1996; Zha et al., 2005). Consistent with this, when we blocked $GABA_A$ transmission with the $GABA_AR$ antagonist, bicuculline (BIC) from 5 to 7 DIV [when $GABA_A$ transmission is hyperpolarizing (**Figures 1C–G**)], spine density decreased by 34% (**Figures 2A–C**). This suggests that by this stage, excitatory transmission causes overexcitation and spine loss in the absence of hyperpolarizing $GABA_A$ transmission.

To assess the role of immature, depolarizing $GABA_A$ transmission on dendritic spine development, we inhibited $GABA_A$ transmission earlier, from 3 to 5 DIV (**Figure 2D**). Previous work suggests that inhibiting depolarizing $GABA_A$ transmission during development would decrease glutamatergic synapse formation and maturation (Ben-Ari et al., 1997; Hanse et al., 1997; Cancedda et al., 2007; Wang and Kriegstein, 2008). However, in contrast to these findings, BIC applied for 48 h from 3 to 5 DIV significantly increased dendritic spine density (25% increase; **Figures 2E,F**). This effect was fully reproducible with the $GABA_AR$ antagonist gabazine (GBZ; 31% increase; **Figures 2E,G**), which is a more specific antagonist of $GABA_ARs$ (Heaulme et al., 1986) and blocks inhibition more consistently in hippocampal neurons (Sokal et al., 2000).

To assess whether the supernumerary spines induced by blocking depolarizing $GABA_A$ transmission showed structural differences, we analyzed spine morphology. GBZ treatment did not affect the proportions of mushroom, thin, and stubby spines (**Figure 2H**), 2-dimensional head area (Control: $0.32 \pm 0.02\ \mu m^2$; GBZ: $0.37 \pm 0.04\ \mu m^2$, $p < 0.10$), head diameter (Control: $0.58 \pm 0.02\ \mu m^2$; GBZ: $0.62 \pm 0.03\ \mu m^2$, $p < 0.1$), spine length (Control $1.66 \pm 0.09\ \mu m^2$; GBZ: $1.83 \pm 0.08\ \mu m^2$, $p < 0.1$) or dendrite diameter (**Figure 2I**).

We next asked whether the increased number of spines constituted an increase in *bona fide* glutamatergic synapses on CA1 cells by recording miniature EPSCs (mEPSCs). Consistent with the increase in dendritic spine density, GBZ treatment (3–5 DIV) increased mESPC frequency 3-fold (**Figures 2J,K**). Miniature EPSC amplitude also increased, indicating enhanced synaptic strength (**Figures 2L,M**). Together, these results suggest that immature $GABA_A$ transmission restrains glutamatergic synapse formation and maturation.

The narrow time window we examined raised the possibility that the spine-enhancing effect of $GABA_A$ blockade is limited to a short period directly prior to the depolarizing to hyperpolarizing shift in $GABA_A$ transmission. This would suggest that $GABA_A$ transmission restrains glutamatergic synapse formation only during a very short transition state. To test whether this was the case, we prepared slices 3 days earlier (P2) and applied GBZ at 3 DIV for 48 h (**Figures 2N–P**). We found that $GABA_AR$ blockade in these younger slices also caused a significant increase in spines (**Figures 2O,P**), suggesting that depolarizing $GABA_A$ transmission is capable of restraining synapse formation for an appreciable period during postnatal development.

We also verified that the presence of penicillin-streptomycin in the culture medium was not associated with the spine-enhancing effect of blocking depolarizing $GABA_A$ transmission by applying GBZ from 3 to 5 DIV in the absence of antibiotics, and found the same increase in dendritic spines (**Figures 2Q–S**).

Bumetanide Treatment Has No Effect on Spine Numbers

Previous work suggests that abrogating GABAergic depolarization by prematurely rendering GABA hyperpolarizing decreases glutamatergic synapse formation (Ge et al., 2006; Wang and Kriegstein, 2008). However, our data show that blocking depolarizing $GABA_A$ transmission increased glutamatergic synapse formation. These contrasting results raise the question of whether the depolarizing nature of $GABA_A$ transmission is important for the normal development of glutamatergic synapse number in our period of interest (3–5 DIV). To address this, we asked whether prematurely rendering E_{GABA} hyperpolarizing could mimic the effect of $GABA_A$ blockade by treating slices with the NKCC1 blocker bumetanide (BUME) from 3 to 5 DIV. BUME is well established to lower E_{GABA} in immature neurons (Dzhala et al., 2005) and prematurely render GABA hyperpolarizing (Wang and Kriegstein, 2011), and we verified that this was the case in the organotypic slice preparation (**Figures 3A–C**). We then applied BUME to organotypic slices from 3 to 5 DIV in the presence and absence of GBZ. BUME did not alter spine density on its own (**Figures 3D,E**), indicating that the depolarized nature of E_{GABA} is not important for regulating spine numbers at this stage of development. Furthermore, BUME did not alter the effect of GBZ on spine density, indicating that if E_{GABA} is prematurely decreased this does not change the role of $GABA_A$ transmission in regulating synapse formation at this stage.

Since KCC2 overexpression can cause an increase in spines through its non-transport, scaffolding function (Li et al., 2007; Fiumelli et al., 2012), we also assessed KCC2 expression following GBZ treatment. GBZ did not significantly elevate the expression of KCC2 oligomers or monomers (**Figures 3F,G**).

Driving Depolarizing $GABA_A$ Transmission Does Not Alter Glutamatergic Synapse Number

Next, we investigated if increasing $GABA_A$ transmission over the 3–5 DIV period would have the opposite effect of GABA-blockade and reduce excitatory synapse number. Previous work has demonstrated that propofol, a positive allosteric modulator of $GABA_ARs$, decreases spine density in developing layer 2/3 principal cells of the somatosensory cortex when administered to rat pups over a 6 h period at postnatal day 10 when $GABA_A$ transmission is still depolarizing (Puskarjov et al., 2017). To test this in CA1 pyramidal cells, we pharmacologically enhanced depolarizing $GABA_A$ transmission from 3 to 5 DIV with diazepam (DZP). We first confirmed that bath applied-DZP caused the expected slower decay kinetics of mIPSCs (**Figures 4A,B**) and also that this led to enhanced charge transfer (**Figure 4C**). Miniature IPSC frequency and amplitude were unaffected by DZP, as expected (Not shown graphically; Frequency: Ctrl 0.27 ± 0.08 Hz, DZP

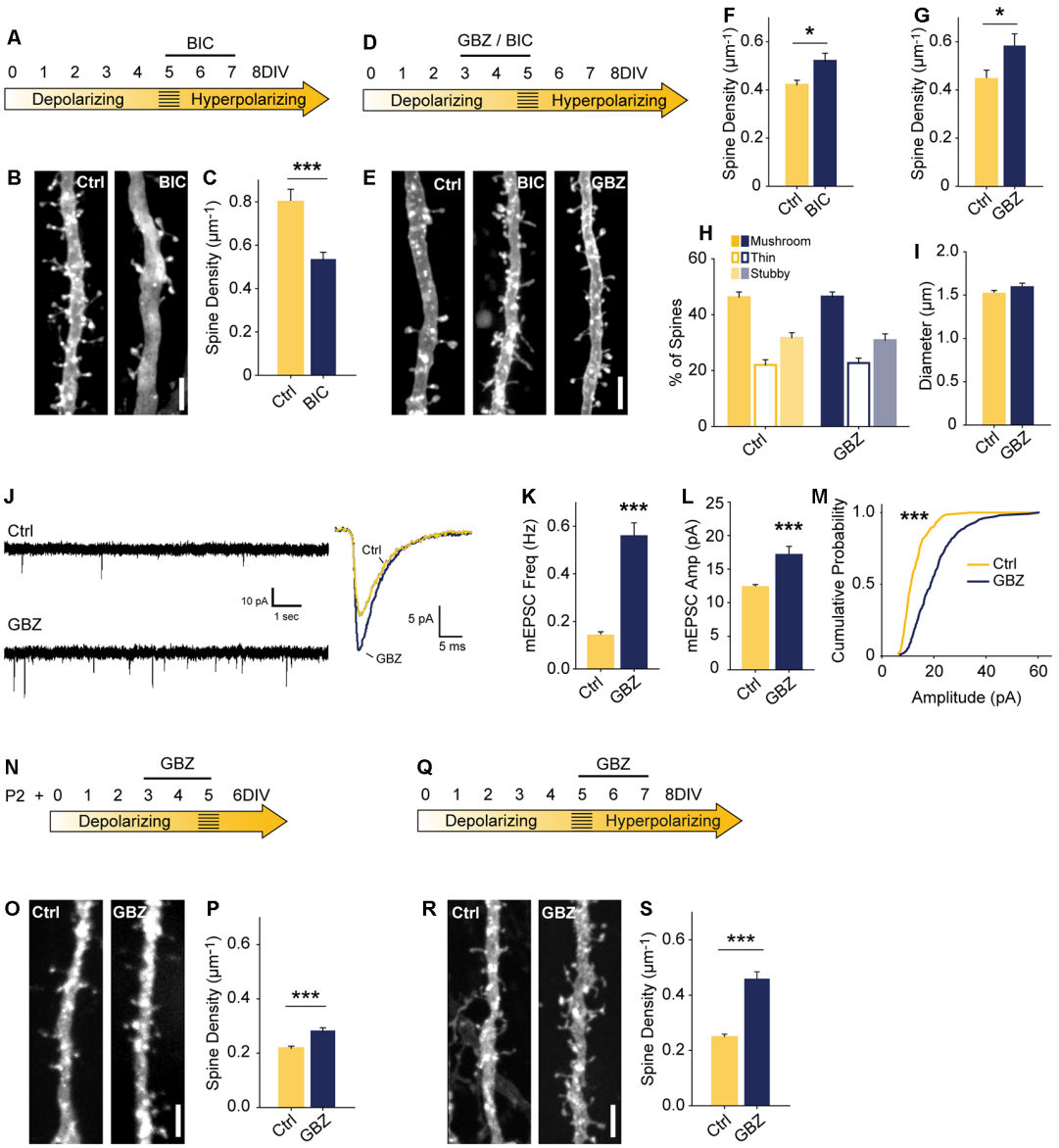

FIGURE 2 | Blocking depolarizing $GABA_A$ transmission increases excitatory synapse number. **(A)** Time course of bicuculline (BIC) treatment for **(B,C)**. **(B,C)** Spine density after 5–7 DIV BIC treatment (Control 0.80 ± 0.06 spines/µm, n = 36, BIC 0.53 ± 0.03, n = 50; N = 3; $p < 0.001$, Mann–Whitney). **(D)** Time course of pharmacological treatments for **(E–M)**. **(E–G)** Spine density after 3–5 DIV GBZ (**G**: Control 0.44 ± 0.12 spines/µm, n = 145, GBZ 0.58 ± 0.17, n = 77; N = 11; p = 0.04) and BIC treatment (**F**: Control 0.42 ± 0.02 spines/µm, n = 55, BIC 0.52 ± 0.03 spines/µm, n = 41; N = 9; P = 0.027, Mann–Whitney). **(H,I)** Three dimensional spine morphology and dendrite diameter after GBZ. **(J)** Representative and mean traces of miniature EPSCs (mEPSCs). **(K)** mEPSC frequency summary plot (Control 0.14 ± 0.02 Hz, GBZ 0.56 ± 0.06 Hz, $p < 0.001$, Mann–Whitney). **(L)** mEPSC amplitude summary plot (Control 12.32 ± 0.37 pA, n = 8, GBZ 17.12 ± 1.27 pA, n = 10, $p < 0.001$, Mann–Whitney). **(M)** Cumulative distributions of amplitudes ($p < 0.0001$, Kolmogorov–Smirnov test). Scale bars 3 µm. **(N)** Time course of treatment of slices prepared from P2 pups. **(O,P)** Exemplary images and quantification of spine enhancing effect of GBZ when applied to slices from P2 pups (Ctrl 0.22 ± 0.008 μm^{-1}, n = 217, GBZ 0.28 ± 0.01 spines/μm^{-1}, n = 156; N = 3; $p < 0.001$, Mann Whitney). **(Q)** Time course of antibiotic-free GBZ treatment. **(R,S)** Exemplary images and quantification of the spine enhancing effect of GBZ on slices cultured in antibiotic-free culture medium (Ctrl 0.248 ± 0.0109 μm^{-1}, n = 198, GBZ 0.458 ± 0.0264 μm^{-1}, n = 70; N = 4; $p < 0.001$, Mann–Whitney). *$p < 0.05$, ***$p < 0.001$.

0.39 ± 0.2 Hz, p = 0.43; Amplitude: Ctrl 5.05 ± 1.11 pA, DZP 5.2 ± 1.21 pA, p = 0.55). However, contrary to the *in vivo* propofol administration (Puskarjov et al., 2017), DZP (5 µM) applied to organotypic slices from 3 to 5 DIV had no effect on spine density or mEPSCs (**Figures 4D–I**). Based on these results, increasing $GABA_A$ transmission was not sufficient to decrease glutamatergic synapse number or function, suggesting depolarizing $GABA_A$ transmission can only limit synapse formation up to a certain point at this stage of circuit development in our preparation. However, these results do not rule out the possibility that enhancing immature $GABA_A$ transmission on different timescales or

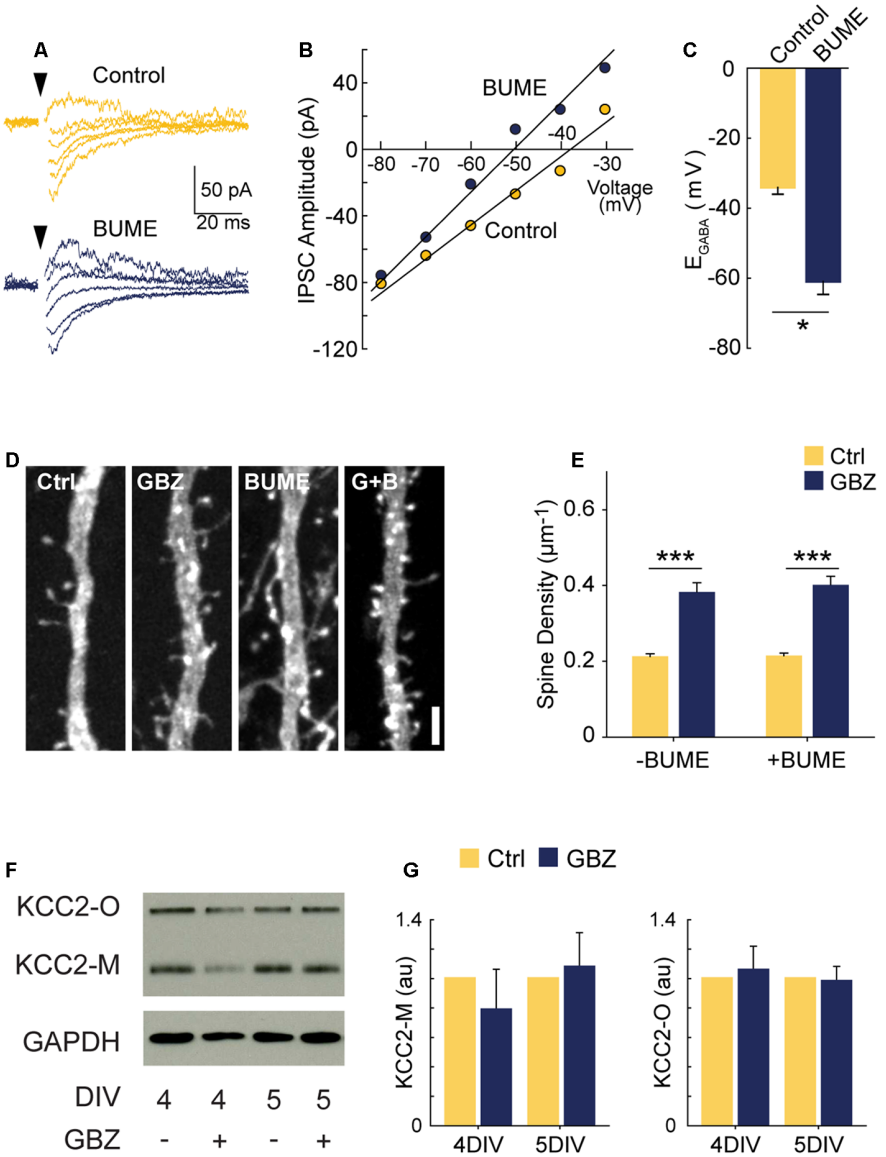

FIGURE 3 | GBZ-induced increase in spines is not reproduced by bumetanide and is not associated with changes in KCC2 expression. **(A–C)** Sample traces from which IV curves were generated **(A)** and resulting sample IV curve **(B)**, and summary plots showing BUME hyperpolarizes E_{GABA} in organotypic slices (**C**, Ctrl −34.0 ± 2.0 mV, n = 3, GBZ −60.8 ± 3.8 mV, n = 3, p = 0.02). **(D,E)** Bumetanide does not increase spine density above control levels or change the effect of GBZ on spine density, (**E**, Control 0.21 ± 0.01 µm^{-1}, n = 102; GBZ 0.38 ± 0.02 µm^{-1}, n = 47; BUME 0.21 ± 0.02 µm^{-1}, n = 88; BUME+ GBZ 0.40 ± 0.02 µm^{-1}, n = 53; N = 3; two-way ANOVA indicated no significant interaction between GBZ and BUME treatment (p = 0.633). Tukey honestly significant difference (HSD) post-test indicates significant differences between Ctrl and GBZ in the absence of BUME ($p < 0.001$) and in the presence of BUME ($p < 0.001$). **(F,G)** Western blot **(F)** showing no changes in monomeric (KCC2-M) or oligomeric (KCC2-O) KCC2 expression following GBZ from 3 to 4 DIV (p = 0.52 and 0.77, respectively, one-sample t-test, n = 3) and 3–5 DIV (p = 0.76 and 0.87, respectively, one-sample t-test, n = 3) **(G)**. Scale bar 3 µm. *$p < 0.05$, ***$p < 0.001$.

in other systems decreases glutamatergic synapse formation (Puskarjov et al., 2017).

An Increase in Glutamatergic Synapses Following Blockade of Depolarizing $GABA_A$ Transmission is Activity-Dependent

Based on our recordings showing that at 3–4 DIV E_{GABA} is depolarized relative to RMP, but lower than AP threshold (**Figures 1E–G**), we hypothesized that GABA is likely to mediate shunting inhibition despite being depolarizing at this stage (schematized in **Figure 5A**). To test this, we puffed GABA locally while recording spontaneous or electrically evoked firing. GABA inhibited both spontaneous (**Figures 5B,C**) and evoked spiking (**Figures 5D,E**), suggesting that although E_{GABA} is depolarizing relative to RMP, $GABA_A$ transmission is inhibitory through shunting inhibition during the 3–5 DIV timeframe.

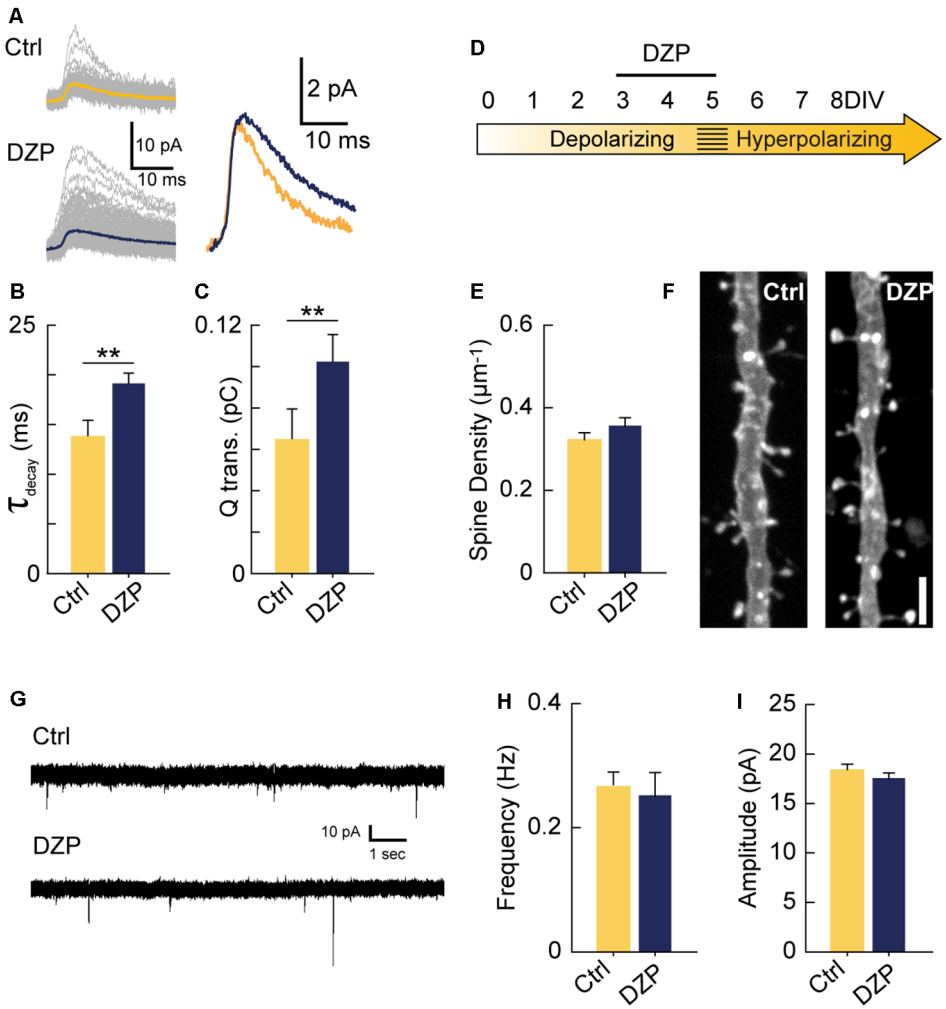

FIGURE 4 | Driving depolarizing $GABA_A$ transmission does not decrease glutamatergic synapse numbers. **(A)** Sample mIPSC traces with superimposed mean traces in color for Ctrl (n = 104) and DZP (n = 197) conditions (left), and enlarged overlay of mean Ctrl and DZP mIPSCs (right). DZP was applied at 5 µM. **(B,C)** Summary data for mIPSC decay constant (Ctrl 13.7 ± 1.73 ms, DZP 19.1 ± 1.15 ms, p = 0.007, n = 3 cells) and charge transfer (Ctrl 0.063 ± 0.015 pC; DZP 0.101 ± 0.013 pC, p = 0.006, n = 3 cells). **(D)** Time course of DZP treatment in organotypic slices. **(E,F)** Spine density after 3–5 DIV DZP treatment (Ctrl 0.321 ± 0.02, n = 116; DZP 0.36 ± 0.02, n = 88; N = 6; p = 0.11, Mann–Whitney). **(G)** Representative traces of mEPSCs following 3–5 DIV treatment with DZP. **(H)** mEPSC frequency summary plot (Ctrl 0.27 ± 0.02 Hz, n = 9; DZP 0.25 ± 0.04 Hz, n = 8; p = 0.41 Mann–Whitney). **(I)** mEPSC amplitude summary plot (Ctrl 18.3 ± 0.7 pA, n = 9; DZP 17.5 ± 0.6 pA, n = 8; p = 0.39). $^{**}p < 0.01$.

Blocking this depolarizing but shunting $GABA_A$ transmission likely increased activity in our preparation, suggesting that the increase in glutamatergic synapses following $GABA_A$-blockade at 3 DIV was driven by activity-dependent mechanisms (Balkowiec and Katz, 2002; Pérez-Gómez and Tasker, 2013). To begin to address this possibility, we measured levels of *Bdnf* and *Fos* mRNA, two activity-regulated genes associated with glutamatergic synapse formation (Vicario-Abejón et al., 1998, 2002; Tyler and Pozzo-Miller, 2003; Chapleau et al., 2009). Both transcripts were significantly upregulated following a 48-h blockade of depolarizing $GABA_A$ transmission from 3 to 5 DIV (*Bdnf*: 5-fold increase, *Fos*: 2.5-fold increase; **Figure 5F**). $GABA_A$-blockade also significantly increased Fos protein expression by 2 h after commencing GBZ treatment at 3 DIV (**Figure 5G**). Furthermore, GBZ treatment elevated Fos expression relative to control across the 48 h treatment window, with a slow decay in the elevation later on (**Figures 5H,I**). Both the increased Fos expression and the partial decay of this expression over time are consistent with a sustained increase in neural activity as examined in previous studies (Tyssowski et al., 2018). Thus, the above data indicate that blocking immature depolarizing $GABA_A$ transmission at this point increased activity in CA1 pyramidal cells across the 3–5 DIV window. To test whether the increased synapse formation we observed following 3–5 DIV $GABA_A$-blockade was activity-dependent, we treated slice cultures with GBZ and/or TTX, and found that while TTX alone had no effect on spine density, TTX blocked the GBZ-induced increase in spines (**Figure 5J**).

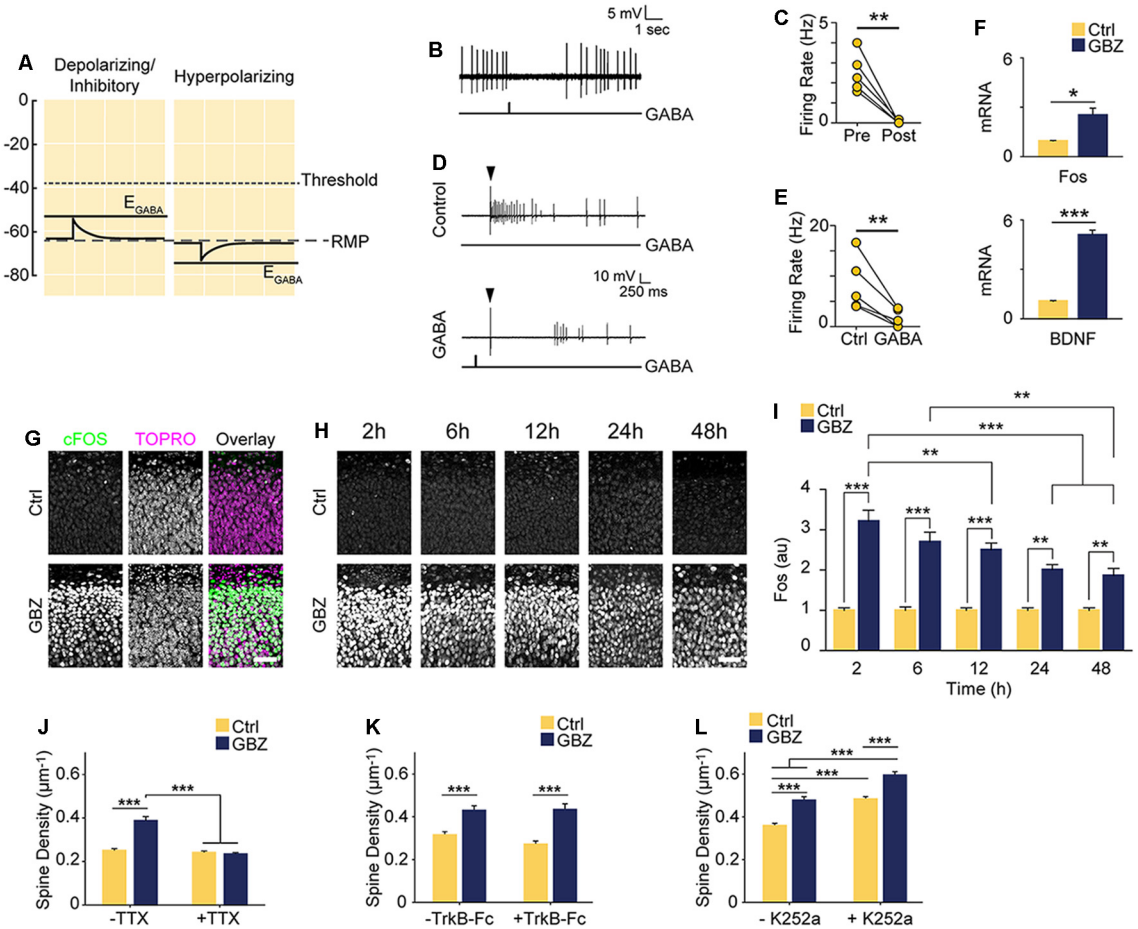

FIGURE 5 | Increased spine density following blockade of depolarizing $GABA_A$ transmission is activity-dependent but does not rely on BDNF signaling. **(A)** Schematic demonstrating the likely shunting and hence inhibitory nature of depolarizing $GABA_A$ transmission at 3–4 DIV due to the relative values of AP Threshold < E_{GABA} < RMP. The scale in **(A)** aligns with that of **Figures 1E–G** such that the threshold, RMP and E_{GABA} values are represented accurately relative to each other. **(B)** Sample trace of spontaneous activity inhibited by puffing on GABA. The line trace below indicates the time of GABA puff. **(C)** Summary plots of spontaneous activity pre- and post-GABA puff. **(D)** Sample traces from the same cell demonstrating that activity could be evoked electrically (Control) and that puffed GABA inhibited electrically evoked activity (GABA). The arrow above the traces denotes the timing of electrical stimulation, while the line trace below denotes the timing of the GABA puff. **(E)** Summary plots of electrically evoked activity in the absence and presence of puffed GABA. **(F)** Fos and BDNF transcript levels following GBZ from 3 to 5 DIV (BDNF: Ctrl 1.07 ± 0.04, GBZ 5.08 ± 0.3, $N = 3$, $p < 0.001$; Fos: Ctrl 0.94 ± 0.04, GBZ 2.52 ± 0.4, $N = 3$, $p = 0.02$). **(G)** Fos immunofluorescence 2 h after GBZ treatment beginning at 3 DIV. Images depict the top of the *stratum pyramidale*, including the lower extremity of the *stratum oriens*, in area CA1. TOPRO-3-Iodide was used to visualize nuclei. **(H,I)** GBZ significantly increased Fos immunofluorescence after 2 h (Ctrl 1 ± 0.06 au, $n = 13$, GBZ 3.21 ± 0.26 au, $n = 13$), 6 h (Ctrl 1 ± 0.08 au, $n = 14$, GBZ 2.70 ± 0.23 au, $n = 14$), 12 h (Ctrl 1 ± 0.07 au, $n = 15$, GBZ 2.51 ± 0.16 au, $n = 14$), 24 h (Ctrl 1 ± 0.06 au, $n = 10$, GBZ 2.00 ± 0.12 au, $n = 11$) and 48 h (Ctrl 1 ± 0.06 au, $n = 10$, GBZ 1.86 ± 0.18 au, $n = 10$; two-way ANOVA, Tukey post test, $p < 0.001$ for population comparisons and interaction). **(J)** Quantification of spine density following GBZ and/or TTX treatment beginning at 3 DIV (Ctrl 0.25 ± 0.01 μm^{-1}, $n = 196$, GBZ 0.39 ± 0.01 μm^{-1}, $n = 110$, TTX 0.24 ± 0.01 μm^{-1}, $n = 166$, GBZ + TTX 0.23 ± 0.01 μm^{-1}, $n = 154$; $N = 5$). Two-way ANOVA indicates a significant interaction between GBZ and TTX conditions, $p < 0.001$. Significant differences between GBZ and all other conditions, $p < 0.001$, Tukey post-test. **(K)** Quantification of spine density following GBZ and/or TrkB-Fc treatment (Ctrl 0.31 ± 0.02, $n = 86$, GBZ 0.42 ± 0.02, $n = 68$, TrkB-Fc 0.27 ± 0.02, $n = 96$, TrkB-Fc + GBZ 0.43 ± 0.02, $n = 61$; $N = 3$; two-way ANOVA, no interaction, Tukey post-test). **(L)** Quantification of spine density following GBZ and/or K252a treatment (Ctrl 0.35 ± 0.01, $n = 198$, GBZ 0.49 ± 0.03, $n = 144$, K252a 0.47 ± 0.02, $n = 216$, K252a+GBZ 0.58 ± 0.04, $n = 185$; all significant differences <0.001, two-way ANOVA, no interaction, Tukey post-test). Scale bar 60 µm. $^*p < 0.05$, $^{**}p < 0.01$, $^{***}p < 0.001$.

From this, we conclude that depolarizing $GABA_A$ transmission limits activity-dependent glutamatergic synapse formation at this point in the development of hippocampal circuitry in slice culture.

BDNF is known to regulate activity-dependent synapse formation (Park and Poo, 2013). We therefore asked whether BDNF signaling was responsible for the increase in spines following blockade of depolarizing $GABA_A$ transmission. We inhibited BDNF signaling during the 3–5 DIV GBZ treatment using TrkB-Fc bodies or K252a (Ji et al., 2010; Puskarjov et al., 2015), however, neither manipulation blocked the increase in spine density (**Figures 5K,L**), suggesting that BDNF signaling is not necessary for the observed increase in spines.

Blocking Depolarizing $GABA_A$ Transmission Leads to a Sustained Increase in Glutamatergic Synapse Number

The observed increase in spine density induced by blocking depolarizing $GABA_A$ transmission may only lead to a transient alteration without a longer-lasting effect on glutamatergic synapses. To determine whether blockade of $GABA_A$ transmission caused a temporary or sustained increase in glutamatergic synapses, we treated slices with GBZ from 3 to 5 DIV and allowed them to recover for an additional 5–9 days in the absence of GBZ (**Figure 6A**). This temporary $GABA_A$ blockade resulted in a 37% increase in spine density after a 5-day recovery period (**Figures 6B,C**). Furthermore, after this recovery period, CA1 cells had more thin spines than mushroom spines, a difference not present in the control condition (**Figure 6D**). No changes in dendrite diameter were observed (**Figure 6E**). To determine if transient GBZ treatment led to long-term functional changes in glutamatergic synapses, we recorded mEPSC frequency and amplitude after 8–9 days of recovery. We found that mEPSC frequency was enhanced by 79%, while mEPSC amplitude was unchanged at this stage (**Figures 6F–I**). Together these data suggest that inhibiting depolarizing $GABA_A$ transmission during a narrow time window can lead to persistent changes in glutamatergic synapse number in the hippocampus.

DISCUSSION

Immature, depolarizing $GABA_A$ transmission is believed to promote glutamatergic synapse formation and maturation (Ben-Ari et al., 1997; Hanse et al., 1997; Wang and Kriegstein, 2009; Chancey et al., 2013). However, when and how GABA affects glutamatergic synapse formation remains to be fully understood. Indeed, several groups have noted that tools and approaches for manipulating depolarizing $GABA_A$ transmission with higher temporal and spatial precision are needed to resolve this question (Akerman and Cline, 2007; Chancey et al., 2013; Kirmse et al., 2018). We, therefore, sought to address the role of $GABA_A$ transmission in glutamatergic synapse formation by performing precisely timed pharmacological manipulations in hippocampal slice cultures. We first mapped the depolarizing-to-hyperpolarizing shift of $GABA_A$ transmission in CA1 cells. This was followed by a structural and electrophysiological analysis which showed that blocking immature, depolarizing $GABA_A$ transmission enhanced glutamatergic synapse function and number. Interestingly, the enhanced synapse number was stable following a recovery period. These results suggest that immature $GABA_A$ transmission restrains glutamatergic synapse formation during an early phase of hippocampal circuit development. Using slice cultures allowed for more temporally precise manipulations that revealed this effect, though limitations of this model system must be considered when interpreting our results. In particular, exuberant glutamatergic synapse formation has been observed in slice cultures and has been attributed to increases in distal dendritic branching (De Simoni et al., 2003). However, we minimized this confound by focusing on primary apical

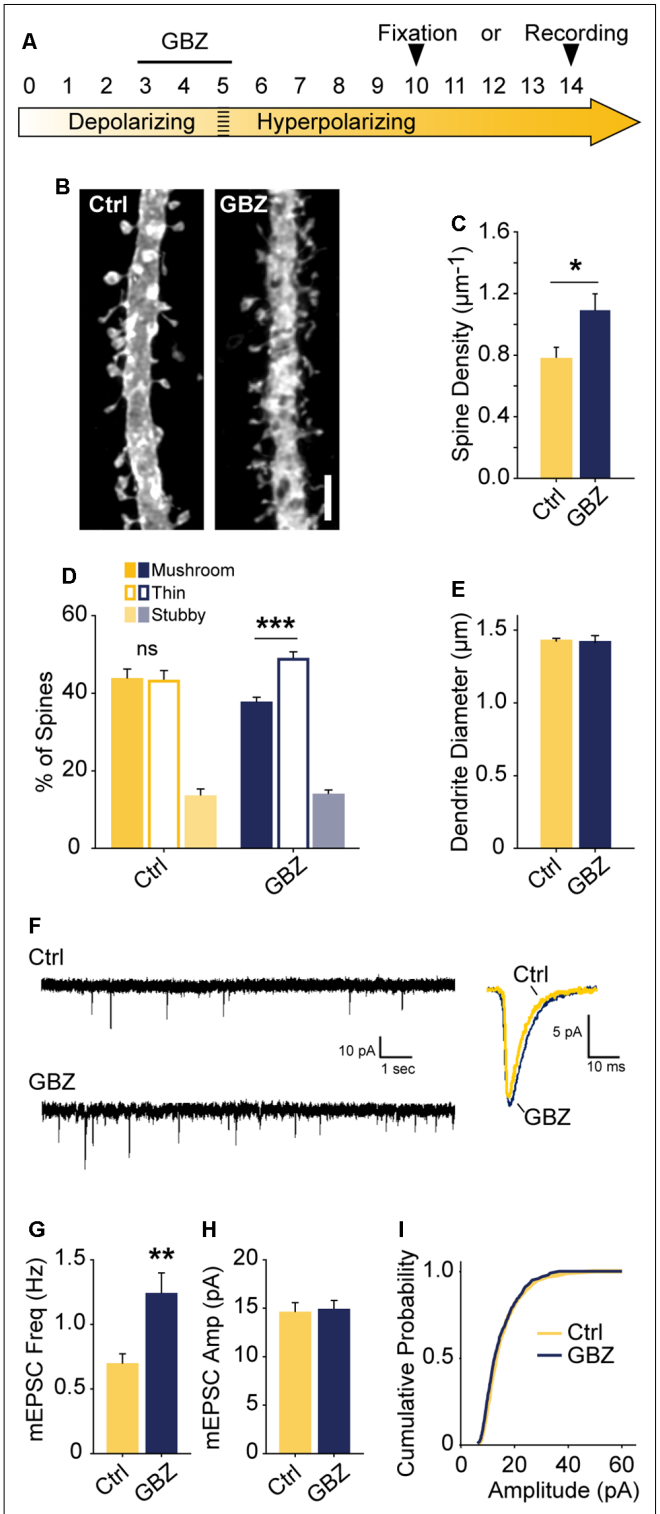

FIGURE 6 | Transient blockade of depolarizing $GABA_A$ transmission causes a lasting increase in excitatory synapse number and alters spine morphology. **(A)** Schematic time course of GBZ treatment and experimental endpoints. **(B,C)** Spine density after 3–5 DIV GBZ treatment and 5 days of recovery (Control 0.78 ± 0.08 spines/µm, n = 127; GBZ washout 1.07 ± 0.07 spines/µm, n = 112; N = 6; p = 0.024). **(D)** 3D spine

(*Continued*)

FIGURE 6 | Continued
morphology after 5 days of recovery (***$p < 0.001$, critical level 0.05, two-way ANOVA with Holm Sidak Post Test). **(E)** Dendrite diameter after recovery ($p = 0.86$). **(F)** Representative mEPSC traces from slices after 8–9 days of recovery. **(G)** mEPSC frequency summary plot (Control: 0.70 ± 0.08 Hz, $n = 10$ GBZ: 1.23 ± 0.17 Hz, $n = 10$, $p = 0.009$). **(H)** mEPSC amplitude summary plot (Control: 14.50 ± 1.07 pA, $n = 10$, GBZ: 14.80 ± 1.00 pA, $n = 10$, $p = 0.84$). **(I)** Cumulative mEPSC distributions ($p = 0.58$, Kolmogorov–Smirnov test). Scale bar 3 μm. *$p < 0.05$, **$p < 0.01$, ***$p < 0.001$.

dendrites, which are fully formed by the time of pharmacological treatment. Thus, while further work will be required to extend our findings to other systems, the results of this study show that immature, depolarizing $GABA_A$ transmission is capable of restraining glutamatergic synapse formation in certain contexts, and that the removal of this restraint by interfering with $GABA_A$ transmission during development may cause a long-term increase in glutamatergic synapses.

An Unpredicted Role for Immature $GABA_A$ Transmission in Restraining Glutamatergic Synapse Formation

In the time window we examined, $GABA_A$ transmission provides subthreshold depolarization and shunting inhibition, which when blocked alleviates a brake on glutamatergic synapse development. Taken in the context of previous work, our results suggest a couple of models for how immature $GABA_A$ transmission affects hippocampal excitatory connectivity (**Figure 7**). Firstly, the GABA-mediated restraint on glutamatergic synapse formation may be a short-lived feature of a "depolarizing but inhibitory" transition state that GABA passes through as E_{Cl} matures from depolarizing and excitatory to hyperpolarizing (Model 1, **Figures 7A–C**). However, recent work suggests GABA may be inhibitory throughout most or all of postnatal development. Therefore, in a second model, depolarizing but inhibitory $GABA_A$ transmission may inhibit circuit activity from birth onward (Model 2, **Figures 7B,C**), thus restraining glutamatergic synapse formation across development. In both of these cases we specify "depolarizing but inhibitory" rather than simply shunting, since shunting inhibition occurs in conjunction with both depolarizing and hyperpolarizing GABA transmission.

The first model is based on evidence from acute slices suggesting that immature $GABA_A$ transmission is capable of driving excitation (Gulledge and Stuart, 2003) and that depolarizing $GABA_A$ transmission drives ENOs, which in turn promote glutamatergic synapse formation and unsilencing, and circuit refinement (Hanse et al., 1997; Ben-Ari, 2002; Wang and Kriegstein, 2009; Griguoli and Cherubini, 2017). Disrupting E_{Cl} or $GABA_A$ transmission in this phase of development is hypothesized to interfere with synapse formation (**Figure 7A**), and this has been borne out by experimentally lowering E_{Cl} across the postmitotic period in immature neurons (Ge et al., 2006; Cancedda et al., 2007; Wang and Kriegstein, 2008). Assuming this model is correct, incorporating our results refines the model and accounts for the role of $GABA_A$ transmission in circuit development as it transitions from a depolarizing and excitatory to a hyperpolarizing state. Our work suggests that following an initial depolarizing phase in which GABA promotes excitation, as E_{Cl} progressively matures, $GABA_A$ transmission passes through a transient but developmentally relevant depolarizing but inhibitory phase (**Figure 7B**). Such a transition phase is hinted at in the literature, as certain studies have shown that blocking depolarizing $GABA_A$ transmission can silence ENOs (Ben-Ari et al., 1989; Garaschuk et al., 1998; Mohajerani and Cherubini, 2005), while others show that blocking depolarizing $GABA_A$ transmission increases circuit activity, eliciting interictal discharges or paroxysmal activity (Khazipov et al., 1997; Khalilov et al., 1999; Lamsa et al., 2000; Wells et al., 2000; Le Magueresse et al., 2006; Ben-Ari et al., 2007). This latter group of studies indicates a role for depolarizing GABA in inhibiting circuit activity, as GABA transitions from depolarizing and excitatory to hyperpolarizing. Our results suggest that during the transition phase, depolarizing but inhibitory $GABA_A$ transmission restrains glutamatergic synapse formation. Blocking $GABA_A$ transmission at this time alleviates the restraint, allowing for activity-dependent synapse formation (**Figure 7B**). Following this transition phase, $GABA_A$ transmission becomes fully hyperpolarizing, and the glutamatergic system becomes capable of overexcitation. The result of $GABA_A$ blockade at this stage is the loss of spines (**Figures 2**, **7C**; Swann et al., 1989; Drakew et al., 1996; Zeng et al., 2007). Crucially, in the present study, a similar spine loss following blockade of depolarizing but inhibitory $GABA_A$ transmission at 3 DIV does not occur, despite the fact that GABA is inhibitory at this stage. This may be explained by a glutamatergic system that is not yet mature enough to drive overexcitation capable of causing pathological collapse of synapse numbers similar to that seen in models of epilepsy (Zha et al., 2005; Zeng et al., 2007).

Alternatively, in the second model, it is possible that depolarizing $GABA_A$ transmission provides shunting inhibition throughout the postnatal period, thereby restraining synapse formation and circuit activity during development (Model 2, **Figures 7B,C**). Indeed, emerging evidence suggests that depolarizing $GABA_A$ transmission exerts inhibitory effects on ENOs *in vivo*, from at least P3 onward (Kirmse et al., 2015; Valeeva et al., 2016; Che et al., 2018). Consistent with this, our results in slices cultured from younger mice (**Figures 2N–P**) show that $GABA_A$ transmission restrains synapse formation over a period of at least 5 days of hippocampal circuit development. While previous work has admittedly demonstrated that prematurely rendering $GABA_A$ transmission hyperpolarizing *in vivo* decreases glutamatergic synapse formation (Ge et al., 2006; Cancedda et al., 2007; Wang and Kriegstein, 2008, 2011), it is noteworthy that these earlier studies manipulated E_{Cl} over extended periods that spanned multiple phases of postmitotic neuronal development, including cell migration, axonal/dendritic growth, synapse formation, and circuit refinement. Depolarizing $GABA_A$ transmission is thought to play important roles in all of these processes (Owens and Kriegstein, 2002), and hence the observed effects of prematurely reducing E_{Cl} on synapses may be secondary to

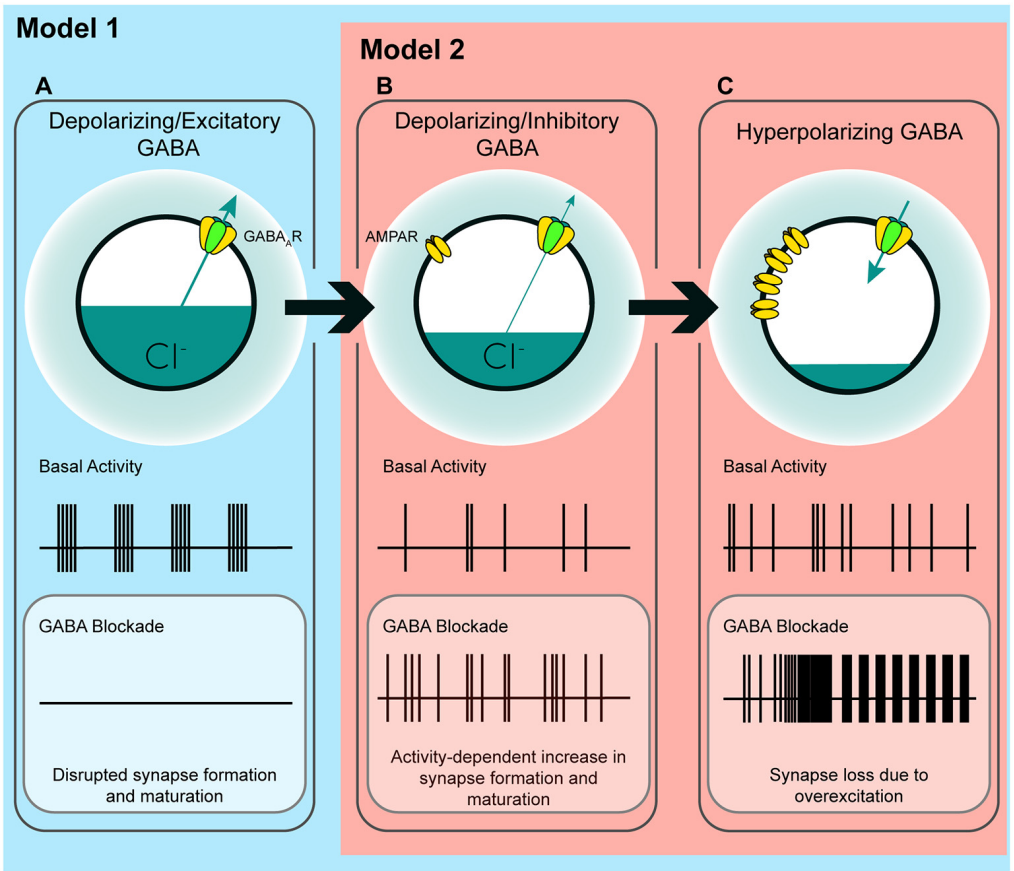

FIGURE 7 | A model of the possible roles of $GABA_A$ transmission in glutamatergic synapse formation as chloride homeostasis matures. **(A)** Work performed in acute slices suggests that depolarizing $GABA_A$ transmission provides the initial excitatory drive required for activity- and calcium-dependent formation and maturation of glutamatergic synapses. The *in vitro* work supporting a phase in which GABA drives network activity suggests that blocking $GABA_A$ transmission at this stage eliminates early network oscillations (ENOs). **(B)** Our work suggests a possible transition state wherein blocking depolarizing but inhibitory transmission alleviates an inhibitory restraint on circuit activity, allowing for activity-dependent formation of glutamatergic synapses. Such a transition state would likely rely on a still underdeveloped glutamatergic system that is not yet capable of pathological levels of overexcitation. Conversely, recent *in vivo* work suggests that GABA may inhibit circuit activity throughout postnatal development, indicating that blocking $GABA_A$ transmission might enhance circuit activity and glutamatergic synapse formation from birth until GABA becomes fully hyperpolarizing (Model 2; although the basal activity here is depicted as uncoordinated to clearly differentiate **(B)** from **(A)**, the activity pattern in this transition state, as well as in **(C)**, may very well be oscillatory depending on the state of the system being studied). **(C)** When E_{Cl} and the glutamatergic system are mature, blocking hyperpolarizing $GABA_A$ transmission causes overexcitation and loss of glutamatergic synapses.

other alterations in neuronal and circuit development. Indeed, soma size and dendritic branching are altered when GABA is prematurely rendered hyperpolarizing over an extended time period (Cancedda et al., 2007; Wang and Kriegstein, 2008). More temporally precise manipulations of $GABA_A$ transmission and E_{Cl} are therefore essential for clarifying the roles of GABA during critical phases of synapse formation *in vivo*. Interestingly, the finding that propofol administered to postnatal day 10 rats decreased spine number supports the notion that there is a developmental period *in vivo* during which immature $GABA_A$ transmission restrains glutamatergic synapse formation (Puskarjov et al., 2017).

When considering these two models, it is important to note that an inhibitory effect of depolarizing $GABA_A$ transmission does not preclude a role for GABA in driving ENOs, as it has been demonstrated that depolarizing chloride currents are only involved in the initial generation of ENOs in acute slices, after which they inhibit the continuation of the same ENOs (Khalilov et al., 2015). Thus, depolarizing $GABA_A$ transmission may simultaneously aid in generating ENOs, while also maintaining control of wider circuit activity, thereby limiting runaway glutamatergic synapse formation. These dichotomous effects of GABA may rely on where GABAergic inputs impinge on the postsynaptic neuron. Gulledge and Stuart (2003) showed that in young rats, puffing GABA on distal dendrites of Layer 5 pyramidal cells facilitated firing while puffing GABA on the cell body inhibited firing. Thus, different GABAergic interneuron subtypes may be responsible for driving ENOs vs. restraining glutamatergic synapse formation. Furthermore, despite the evidence suggesting GABA is inhibitory throughout most of the postnatal development *in vivo*, it has been shown that high frequency uncaging or stimulated release of GABA

onto dendrites of layer 2/3 pyramidal cells in the neocortex can elicit formation of glutamatergic and GABAergic synapses during development *in vivo* (Oh et al., 2016). Although it remains to be seen whether endogenous patterns of GABA release can have similar effects, it appears there may be a local trophic role for depolarizing $GABA_A$ transmission, which may promote synapse formation even as its circuit-wide inhibitory effects restrain the same process as we have demonstrated. More work is needed to dissect the possible roles of GABA in local synapse formation and more global circuit development, and to understand how the role of $GABA_A$ transmission changes across development.

Depolarizing $GABA_A$ Transmission and Sustained Changes in Glutamatergic Synapses

Remarkably, we found that a transient blockade of depolarizing $GABA_A$ transmission led to a sustained increase in both the number of glutamatergic synapses and the proportion of thin spines, indicating that transient manipulations of immature $GABA_A$ transmission can profoundly alter hippocampal connectivity (**Figure 6**). Importantly, the observed changes in synapse number may elicit compensatory homeostatic responses. For instance, increased synapse number can be compensated for by decreasing overall dendritic length (Tripodi et al., 2008), however, the increased mEPSC frequency we observed after GBZ washout suggests that overall synapse number was indeed elevated at the time point examined. Using slice cultures allowed for more temporally precise manipulations that revealed this effect, though it remains to be seen if the phenomenon persists *in vivo*. These questions are clinically relevant, as a role for GABA in restraining synapse formation may change how we understand and mitigate the effects of anticonvulsants, anesthetics and drugs of abuse on neonatal, as well as fetal development, as GABA is believed to be depolarizing mainly in late gestation in humans (Vanhatalo et al., 2005; Sedmak et al., 2016). Furthermore, both the persistent increase in synapses and spines and the shift in spine morphologies we observed after recovery from transient GBZ treatment are reminiscent of "spinopathies" seen in intellectual disabilities including Fragile X syndrome and autism spectrum disorders (Lacey and Terplan, 1987; Irwin et al., 2000, 2001; Kaufmann and Moser, 2000; Fiala et al., 2002; Hutsler and Zhang, 2010). Importantly, such neurodevelopmental disorders are often associated with altered excitatory/inhibitory (E/I) balance, thus when testing the findings of the current study *in vivo*, it will be important to examine excitatory and inhibitory synapse development in parallel. Interestingly, there are a number of potential molecular targets that are thought to both limit glutamatergic synapse formation and regulate E/I balance, such as the SRGAP2s (Fossati et al., 2016; Schmidt et al., 2019) and the activity-regulated MEF2C (Harrington et al., 2016). These potential mechanisms should be investigated as the role of depolarizing $GABA_A$ transmission in synapse formation continues to be more finely dissected.

Numerous models of ASDs are associated with a delay in the depolarizing to hyperpolarizing shift in E_{GABA} (He et al., 2014; Tyzio et al., 2014; Leonzino et al., 2016). Such a delayed transition to hyperpolarized E_{GABA} is likely associated with a delay in the onset of adequate shunting inhibition when GABA is still depolarizing, which may increase glutamatergic synapse formation in a manner similar to that which we observed when blocking depolarizing $GABA_A$ transmission. Furthermore, mutation of the β3 $GABA_A$ receptor subunit, the expression of which peaks during development when GABA is depolarizing, has been observed in ASD (Menold et al., 2001; Buxbaum et al., 2002; Chen et al., 2014). The findings presented in the current study may provide a causal link between these mutations and the hyperconnectivity observed in ASDs. Thus, further investigation is required to understand if impairments of depolarizing $GABA_A$ transmission contribute to the lasting alterations of spines and synapses in these conditions. Finally, the possibility that GABA bidirectionally controls synapse formation may yield novel clinical approaches for correcting synaptic deficits in neurodevelopmental disorders.

DATA AVAILABILITY STATEMENT

The datasets generated for this study are available on request to the corresponding author.

ETHICS STATEMENT

All procedures were performed in accordance to guidelines established by the Canadian Council on Animal Care and by the Montreal General Hospital Facility Animal Care Committee.

AUTHOR CONTRIBUTIONS

CS and KM conceived of the project. CS, HP, SC, DS, CB, MW, and KM designed experiments. CS, HP, CG, SC, EJ, VM, MW, and WF performed and analyzed experiments. CS and KM wrote the manuscript.

FUNDING

This work was supported by the Canadian Institutes of Health Research (OGB 111152, PJT148569, 156247 to KM) and Natural Sciences and Engineering Research Council of Canada (482622 to MW and 408044-2011 and 69404 to KM). CS was supported through a CGS-M from the CIHR (201002GSM-222639-198785) and a Doctoral Award from the Fonds de Recherche du Québec-Santé (FF6-15D).

ACKNOWLEDGMENTS

We would like to thank Dr. Edward Ruthazer for valuable input throughout the course of this study, as well as Dr. Andrew Greenhalgh and Andy YL Gao for a critical review of the manuscript. A version of this article has been released as a bioRxiv preprint at: https://doi.org/10.1101/742148 (Salmon et al., 2019).

REFERENCES

Acton, B. A., Mahadevan, V., Mercado, A., Uvarov, P., Ding, Y., Pressey, J., et al. (2012). Hyperpolarizing GABAergic transmission requires the KCC2 C-terminal ISO domain. *J. Neurosci.* 32, 8746–8751. doi: 10.1523/JNEUROSCI.6089-11.2012

Akerman, C. J., and Cline, H. T. (2006). Depolarizing GABAergic conductances regulate the balance of excitation to inhibition in the developing retinotectal circuit *in vivo*. *J. Neurosci.* 26, 5117–5130. doi: 10.1523/JNEUROSCI.0319-06.2006

Akerman, C. J., and Cline, H. T. (2007). Refining the roles of GABAergic signaling during neural circuit formation. *Trends Neurosci.* 30, 382–389. doi: 10.1016/j.tins.2007.06.002

Amaral, D., and Lavenex, P. (2007). *Hippocampal Neuroanatomy*," in *The Hippocampus Book*, eds P. Andersen, R. Morris, D. Amaral, T. Bliss and J. O'Keefe (Oxford: Oxford University Press), 37–115.

Balkowiec, A., and Katz, D. M. (2002). Cellular mechanisms regulating activity-dependent release of native brain-derived neurotrophic factor from hippocampal neurons. *J. Neurosci.* 22, 10399–10407. doi: 10.1523/JNEUROSCI.22-23-10399.2002

Behar, T. N., Schaffner, A. E., Scott, C. A., Greene, C. L., and Barker, J. L. (2000). GABA receptor antagonists modulate postmitotic cell migration in slice cultures of embryonic rat cortex. *Cereb. Cortex* 10, 899–909. doi: 10.1093/cercor/10.9.899

Ben-Ari, Y. (2002). Excitatory actions of GABA during development: the nature of the nurture. *Nat. Rev. Neurosci.* 3, 728–739. doi: 10.1038/nrn920

Ben-Ari, Y., Cherubini, E., Corradetti, R., and Gaiarsa, J. (1989). Giant synaptic potentials in immature rat CA3 hippocampal neurones. *J. Physiol.* 416, 303–325. doi: 10.1113/jphysiol.1989.sp017762

Ben-Ari, Y., Gaiarsa, J.-L., Tyzio, R., and Khazipov, R. (2007). GABA: a pioneer transmitter that excites immature neurons and generates primitive oscillations. *Physiol. Rev.* 87, 1215–1284. doi: 10.1152/physrev.00017.2006

Ben-Ari, Y., Khazipov, R., Leinekugel, X., Caillard, O., and Gaiarsa, J. (1997). GABAA, NMDA and AMPA receptors: a developmentally regulated 'ménage à trois.'. *Trends Neurosci.* 20, 523–529. doi: 10.1016/s0166-2236(97)01147-8

Ben-Ari, Y., Woodin, M. A., Sernagor, E., Cancedda, L., Vinay, L., Rivera, C., et al. (2012). Refuting the challenges of the developmental shift of polarity of GABA actions: GABA more exciting than ever!. *Front. Cell. Neurosci.* 6:35. doi: 10.3389/fncel.2012.00035

Buchs, P.-A., Stoppini, L., and Muller, D. (1993). Structural modifications associated with synaptic development in area CA1 of rat hippocampal organotypic cultures. *Dev. Brain Res.* 71, 81–91. doi: 10.1016/0165-3806(93)90108-m

Buxbaum, J. D., Silverman, J. M., Smith, C. J., Greenberg, D. A., Kilifarski, M., Reichert, J., et al. (2002). Association between a GABRB3 polymorphism and autism. *Mol. Psychiatry* 7, 311–316. doi: 10.1038/sj.mp.4001011

Cancedda, L., Fiumelli, H., Chen, K., and Poo, M. (2007). Excitatory GABA action is essential for morphological maturation of cortical neurons *in vivo*. *J. Neurosci.* 27, 5224–5235. doi: 10.1523/JNEUROSCI.5169-06.2007

Chancey, J. H., Adlaf, E. W., Sapp, M. C., Pugh, P. C., Wadiche, J. I., and Overstreet-Wadiche, L. S. (2013). GABA depolarization is required for experience-dependent synapse unsilencing in adult-born neurons. *J. Neurosci.* 33, 6614–6622. doi: 10.1523/JNEUROSCI.0781-13.2013

Chapleau, C. A., Larimore, J. L., Theibert, A., and Pozzo-Miller, L. (2009). Modulation of dendritic spine development and plasticity by BDNF and vesicular trafficking: fundamental roles in neurodevelopmental disorders associated with mental retardation and autism. *J. Neurodev. Disord.* 1, 185–196. doi: 10.1007/s11689-009-9027-6

Che, A., Babij, R., Iannone, A. F., Fetcho, R. N., Ferrer, M., Liston, C., et al. (2018). Layer I interneurons sharpen sensory maps during neonatal development. *Neuron* 99, 98.e7–116.e7. doi: 10.1016/j.neuron.2018.06.002

Chen, C.-H., Huang, C.-C., Cheng, M.-C., Chiu, Y.-N., Tsai, W.-C., Wu, Y.-Y., et al. (2014). Genetic analysis of GABRB3 as a candidate gene of autism spectrum disorders. *Mol. Autism* 5:36. doi: 10.1186/2040-2392-5-36

De Simoni, A., Griesinger, C. B., and Edwards, F. A. (2003). Development of rat CA1 neurones in acute versus organotypic slices: role of experience in synaptic morphology and activity. *J. Physiol.* 550, 135–147. doi: 10.1113/jphysiol.2003.039099

Drakew, A., Müller, M., Gahwiler, B., Thompson, S., and Frotscher, M. (1996). Spine loss in experimental epilepsy: quantitative light and electron miscroscopic analysis of intracellularly stained CA3 pyramidal cells in hippocampal slice cultures. *Neuroscience* 70, 31–45. doi: 10.1016/0306-4522(95)00379-w

Dzhala, V. I., Talos, D. M., Sdrulla, D. A., Brumback, A. C., Mathews, G. C., Benke, T. A., et al. (2005). NKCC1 transporter facilitates seizures in the developing brain. *Nat. Med.* 11, 1205–1213. doi: 10.1038/nm1301

El Marroun, H., White, T., Verhulst, F. C., and Tiemeier, H. (2014). Maternal use of antidepressant or anxiolytic medication during pregnancy and childhood neurodevelopmental outcomes: a systematic review. *Eur. Child Adolesc. Psychiatry* 23, 973–992. doi: 10.1007/s00787-014-0558-3

Fiala, J. C. (2005). Reconstruct: a free editor for serial section microscopy. *J. Microsc.* 218, 52–61. doi: 10.1111/j.1365-2818.2005.01466.x

Fiala, J. C., Spacek, J., and Harris, K. M. (2002). Dendritic spine pathology: cause or consequence of neurological disorders? *Brain Res. Rev.* 39, 29–54. doi: 10.1016/s0165-0173(02)00158-3

Fiumelli, H., Briner, A., Puskarjov, M., Blaesse, P., Belem, B. J., Dayer, A. G., et al. (2012). An ion transport-independent role for the cation-chloride cotransporter KCC2 in dendritic spinogenesis *in vivo*. *Cereb. Cortex* 23, 378–388. doi: 10.1093/cercor/bhs027

Fossati, M., Pizzarelli, R., Schmidt, E. R., Kupferman, J. V., Stroebel, D., Polleux, F., et al. (2016). SRGAP2 and its human-specific paralog co-regulate the development of excitatory and inhibitory synapses. *Neuron* 91, 356–369. doi: 10.1016/j.neuron.2016.06.013

Garaschuk, O., Hanse, E., and Konnerth, A. (1998). Developmental profile and synaptic origin of early network oscillations in the CA1 region of rat neonatal hippocampus. *J. Physiol.* 507, 219–236. doi: 10.1111/j.1469-7793.1998.219bu.x

Ge, S., Goh, E. L. K., Sailor, K. A., Kitabatake, Y., Ming, G., and Song, H. (2006). GABA regulates synaptic integration of newly generated neurons in the adult brain. *Nature* 439, 589–593. doi: 10.1038/nature04404

Griguoli, M., and Cherubini, E. (2017). Early correlated network activity in the hippocampus: its putative role in shaping neuronal circuits. *Front. Cell. Neurosci.* 11:255. doi: 10.3389/fncel.2017.00255

Gulledge, A. T., and Stuart, G. J. (2003). Excitatory actions of GABA in the cortex. *Neuron* 37, 299–309. doi: 10.1016/s0896-6273(02)01146-7

Haber, M., Zhou, L., and Murai, K. K. (2006). Cooperative astrocyte and dendritic spine dynamics at hippocampal excitatory synapses. *J. Neurosci.* 26, 8881–8891. doi: 10.1523/JNEUROSCI.1302-06.2006

Hanse, E., Durand, G. M., Garaschuk, O., and Konnerth, A. (1997). Activity-dependent wiring of the developing hippocampal neuronal circuit. *Semin. Cell Dev. Biol.* 8, 35–42. doi: 10.1006/scdb.1996.0119

Harrington, A. J., Raissi, A., Rajkovich, K., Berto, S., Kumar, J., Molinaro, G., et al. (2016). MEF2C regulates cortical inhibitory and excitatory synapses and behaviors relevant to neurodevelopmental disorders. *Elife* 5:e20059. doi: 10.7554/eLife.20059

He, Q., Nomura, T., Xu, J., and Contractor, A. (2014). The developmental switch in GABA polarity is delayed in fragile X mice. *J. Neurosci.* 34, 446–450. doi: 10.1523/JNEUROSCI.4447-13.2014

Heaulme, M., Chambon, J. P., Leyris, R., Molimard, J. C., Wermuth, C. G., and Biziere, K. (1986). Biochemical characterization of the interaction of three pyridazinyl-GABA derivatives with the $GABA_A$ receptor site. *Brain Res.* 384, 224–231. doi: 10.1016/0006-8993(86)91158-3

Hutsler, J. J., and Zhang, H. (2010). Increased dendritic spine densities on cortical projection neurons in autism spectrum disorders. *Brain Res.* 1309, 83–94. doi: 10.1016/j.brainres.2009.09.120

Irwin, S. A., Galvez, R., and William, T. (2000). Dendritic spine structural anomalies in fragile-X mental retardation syndrome. *Cereb. Cortex* 10, 1038–1044. doi: 10.1093/cercor/10.10.1038

Irwin, S. A., Patel, B., Idupulapati, M., Harris, J. B., Crisostomo, R. A., Larsen, B. P., et al. (2001). Abnormal dendritic spine characteristics in the temporal and visual cortices of patients with fragile-X syndrome: a quantitative examination. *Am. J. Med. Genet.* 98, 161–167. doi: 10.1002/1096-8628(20010115)98:2<161::aid-ajmg1025>3.0.co;2-b

Ji, Y., Lu, Y., Yang, F., Shen, W., Tang, T. T. T., Feng, L., et al. (2010). Acute and gradual increases in BDNF concentration elicit distinct signaling and functions in neurons. *Nat. Neurosci.* 13, 302–309. doi: 10.1038/nn.2505

Jourdain, P., Nikonenko, I., Alberi, S., and Muller, D. (2002). Remodeling of hippocampal synaptic networks by a brief anoxia—hypoglycemia. *J. Neurosci.* 22, 3108–3116. doi: 10.1523/JNEUROSCI.22-08-03108.2002

Kaila, K. (1994). Ionic basis of $GABA_A$ receptor channel function in the nervous system. *Prog. Neurobiol.* 42, 489–537. doi: 10.1016/0301-0082(94)90049-3

Kaufmann, W. E., and Moser, H. W. (2000). Dendritic anomalies in disorders associated with mental retardation. *Cereb. Cortex* 10, 981–991. doi: 10.1093/cercor/10.10.981

Khalilov, I., Dzhala, V., Ben-Ari, Y., and Khazipov, R. (1999). Dual role of GABA in the neonatal rat hippocampus. *Dev. Neurosci.* 21, 310–319. doi: 10.1159/000017380

Khalilov, I., Minlebaev, M., Mukhtarov, M., and Khazipov, R. (2015). Dynamic changes from depolarizing to hyperpolarizing GABAergic actions during giant depolarizing potentials in the neonatal rat hippocampus. *J. Neurosci.* 35, 12635–12642. doi: 10.1523/JNEUROSCI.1922-15.2015

Khazipov, R., Leinekugel, X., Khalilov, I., Gaiarsa, J., and Ben-Ari, Y. (1997). Synchronization of GABAergic interneuronal network in CA3 subfield of neonatal rat hippocampal slices. *J. Physiol.* 483, 763–772. doi: 10.1113/jphysiol.1997.sp021900

Kirmse, K., Hübner, C. A., Isbrandt, D., and Witte, O. W. (2018). GABAergic transmission during brain development: multiple effects at multiple stages. *Neuroscientist* 24, 36–53. doi: 10.1177/1073858417701382

Kirmse, K., Kummer, M., Kovalchuk, Y., Witte, O. W., Garaschuk, O., and Holthoff, K. (2015). GABA depolarizes immature neurons and inhibits network activity in the neonatal neocortex *in vivo*. *Nat. Commun.* 6:7750. doi: 10.1038/ncomms8750

Lacey, D. J., and Terplan, K. (1987). Abnormal cerebral cortical neurons in a child with maternal PKU syndrome. *J. Child Neurol.* 2, 201–204. doi: 10.1177/088307388700200306

Lamsa, K. P., Palva, J. M., Ruusuvuori, E., Kaila, K., and Taira, T. (2000). Synaptic $GABA_A$ activation inhibits AMPA-kainate receptor—mediated bursting in the newborn (*P0—P2*) rat hippocampus. *J. Neurophysiol.* 83, 359–366. doi: 10.1152/jn.2000.83.1.359

Le Magueresse, C., Safiulina, V., Changeux, J.-P., and Cherubini, E. (2006). Nicotinic modulation of network and synaptic transmission in the immature hippocampus investigated with genetically modified mice. *J. Physiol.* 576, 533–546. doi: 10.1113/jphysiol.2006.117572

Leinekugel, X., Tseeb, V., Ben-Ari, Y., and Bregestovski, P. (1995). Synaptic $GABA_A$ activation induces Ca^{2+} rise in pyramidal cells and interneurons from rat neonatal hippocampal slices. *J. Physiol.* 487, 319–329. doi: 10.1113/jphysiol.1995.sp020882

Leonzino, M., Busnelli, M., Antonucci, F., Verderio, C., Mazzanti, M., Chini, B., et al. (2016). The timing of the excitatory-to-inhibitory GABA switch is regulated by the oxytocin receptor report the timing of the excitatory-to-inhibitory GABA switch is regulated by the oxytocin receptor *via* KCC2. *Cell Rep.* 15, 96–103. doi: 10.1016/j.celrep.2016.03.013

Li, H., Khirug, S., Cai, C., Ludwig, A., Blaesse, P., Kolikova, J., et al. (2007). KCC2 interacts with the dendritic cytoskeleton to promote spine development. *Neuron* 56, 1019–1033. doi: 10.1016/j.neuron.2007.10.039

Liu, X., Wang, Q., Haydar, T. F., and Bordey, A. (2005). Nonsynaptic GABA signaling in postnatal subventricular zone controls proliferation of GFAP-expressing progenitors. *Nat. Neurosci.* 8, 1179–1187. doi: 10.1038/nn1522

Megías, M., Emri, Z., Freund, T. F., and Gulyás, A. I. (2001). Total number and distribution of inhibitory and excitatory synapses on hippocampal CA1 pyramidal cells. *Neuroscience* 102, 527–540. doi: 10.1016/s0306-4522(00)00496-6

Menold, M. M., Shao, Y., Wolpert, C. M., Donnelly, S. L., Raiford, K. L., Martin, E. R., et al. (2001). Association analysis of chromosome 15 gabaa receptor subunit genes in autistic disorder. *J. Neurogenet.* 15, 245–259. doi: 10.3109/01677060109167380

Mohajerani, M. H., and Cherubini, E. (2005). Spontaneous recurrent network activity in organotypic rat hippocampal slices. *Eur. J. Neurosci.* 22, 107–118. doi: 10.1111/j.1460-9568.2005.04198.x

Muller, D., Buchs, P.-A., and Stoppini, L. (1993). Time course of synaptic development in hippocampal organotypic cultures. *Dev. Brain Res.* 71, 93–100. doi: 10.1016/0165-3806(93)90109-n

Oh, W. C., Lutzu, S., Castillo, P. E., and Kwon, H. B. (2016). *De novo* synaptogenesis induced by GABA in the developing mouse cortex. *Science* 353, 1037–1040. doi: 10.1126/science.aaf5206

Owens, D. F., and Kriegstein, A. R. (2002). Is there more to GABA than synaptic inhibition? *Nat. Rev. Neurosci.* 3, 715–727. doi: 10.1038/nrn919

Park, H., and Poo, M. M. (2013). Neurotrophin regulation of neural circuit development and function. *Nat. Rev. Neurosci.* 14, 7–23. doi: 10.1038/nrn3379

Pérez-Gómez, A., and Tasker, R. A. (2013). Transient domoic acid excitotoxicity increases BDNF expression and activates both MEK- and PKA-dependent neurogenesis in organotypic hippocampal slices. *BMC Neurosci.* 14:72. doi: 10.1186/1471-2202-14-72

Puskarjov, M., Ahmad, F., Khirug, S., Sivakumaran, S., Kaila, K., and Blaesse, P. (2015). BDNF is required for seizure-induced but not developmental up-regulation of KCC2 in the neonatal hippocampus. *Neuropharmacology* 88, 103–109. doi: 10.1016/j.neuropharm.2014.09.005

Puskarjov, M., Fiumelli, H., Briner, A., Bodogan, T., Demeter, K., Lacoh, C., et al. (2017). K-Cl Cotransporter 2-mediated Cl− extrusion determine developmental stage-dependent impact of propofol mediated anesthesia on dendritic spines. *Anesthesiology* 126, 855–867. doi: 10.1097/aln.0000000000001587

Rivera, C., Voipio, J., Payne, J. A., Ruusuvuori, E., Lahtinen, H., Lamsa, K., et al. (1999). The K^+/Cl^- co-transporter KCC2 renders GABA hyperpolarizing during neuronal maturation. *Nature* 397, 251–255. doi: 10.1038/16697

Rodriguez, A., Ehlenberger, D. B., Dickstein, D. L., Hof, P. R., and Wearne, S. L. (2008). Automated three-dimensional detection and shape classification of dendritic spines from fluorescence microscopy images. *PLoS One* 3:e1997. doi: 10.1371/journal.pone.0001997

Salmon, C. K., Pribiag, H., Farmer, W. T., Cameron, S., Jones, E. V., Mahadevan, V., et al. (2019). Depolarizing GABA transmission restrains activity-dependent glutamatergic synapse formation in the developing hippocampal circuit. *bioRxiv* [Preprint]. doi: 10.1101/596940

Schmidt, E. R., Kupferman, J. V., Stackmann, M., and Polleux, F. (2019). The human-specific paralogs SRGAP2B and SRGAP2C differentially modulate SRGAP2A-dependent synaptic development. *bioRxiv* [Preprint]. doi: 10.1101/74214810.1101/596940

Sedmak, G., Jovanov-Milošević , N., Puskarjov, M., Ulamec, M., Krušlin, B., Kaila, K., et al. (2016). Developmental expression patterns of KCC2 and functionally associated molecules in the human brain. *Cereb. Cortex* 26, 4574–4589. doi: 10.1093/cercor/bhv218

Sokal, D. M., Mason, R., and Parker, T. L. (2000). Multi-neuronal recordings reveal a differential effect of thapsigargin on bicuculline- or gabazine-induced epileptiform excitability in rat hippocampal neuronal networks. *Neuropharmacology* 39, 2408–2417. doi: 10.1016/s0028-3908(00)00095-2

Staley, K. J., and Mody, I. (1992). Shunting of excitatory input to dentate gyrus granule cells by a depolarizing GABAA receptor-mediated postsynaptic conductance. *J. Neurophysiol.* 68, 197–212. doi: 10.1152/jn.1992.68.1.197

Staley, K. J., and Proctor, W. R. (1999). Modulation of mammalian dendritic GABAA receptor function by the kinetics of Cl^- and HCO_3^- transport. *J. Physiol.* 519, 693–712. doi: 10.1111/j.1469-7793.1999.0693n.x

Swann, J. W., Brady, R. J., and Martin, D. L. (1989). Postnatal development of GABA-mediated synaptic inhibition in rat hippocampus. *Neuroscience* 28, 551–561. doi: 10.1016/0306-4522(89)90004-3

Tripodi, M., Evers, J. F., Mauss, A., Bate, M., and Landgraf, M. (2008). Structural homeostasis: compensatory adjustments of dendritic arbor geometry in response to variations of synaptic input. *PLoS Biol.* 6:e260. doi: 10.1371/journal.pbio.0060260

Tyler, W. J., and Pozzo-Miller, L. (2003). Miniature synaptic transmission and BDNF modulate dendritic spine growth and form in rat CA1 neurones. *J. Physiol.* 553, 497–509. doi: 10.1113/jphysiol.2003.052639

Tyssowski, K. M., DeStefino, N. R., Cho, J.-H., Dunn, C. J., Poston, R. G., Carty, C. E., et al. (2018). Different neuronal activity patterns induce different article different neuronal activity patterns induce different gene expression programs. *Neuron* 98, 530.e11–546.e11. doi: 10.1016/j.neuron.2018.04.001

Tyzio, R., Nardou, R., Ferrari, D. C., Tsintsadze, T., Shahrokhi, A., Eftekhari, S., et al. (2014). Oxytocin-mediated GABA inhibition during delivery

attenuates autism pathogenesis in rodent offspring. *Science* 343, 675–679. doi: 10.1126/science.1247190

Valeeva, G., Tressard, T., Mukhtarov, M., Baude, A., and Khazipov, R. (2016). An optogenetic approach for investigation of excitatory and inhibitory network GABA actions in mice expressing channelrhodopsin-2 in GABAergic neurons. *J. Neurosci.* 36, 5961–5973. doi: 10.1523/jneurosci.3482-15.2016

Vanhatalo, S., Palva, J. M., Andersson, S., Rivera, C., Voipio, J., and Kaila, K. (2005). Slow endogenous activity transients and developmental expression of K^+-Cl^- cotransporter 2 in the immature human cortex. *Eur. J. Neurosci.* 22, 2799–2804. doi: 10.1111/j.1460-9568.2005.04459.x

Vicario-Abejón, C., Collin, C., McKay, R. D., and Segal, M. (1998). Neurotrophins induce formation of functional excitatory and inhibitory synapses between cultured hippocampal neurons. *J. Neurosci.* 18, 7256–7271. doi: 10.1523/jneurosci.18-18-07256.1998

Vicario-Abejón, C., Owens, D., McKay, R., and Segal, M. (2002). Role of neurotrophins in central synapse formation and stabilization. *Nat. Rev. Neurosci.* 3, 965–974. doi: 10.1038/nrn988

Wang, D. D., and Kriegstein, A. R. (2008). GABA regulates excitatory synapse formation in the neocortex *via* NMDA receptor activation. *J. Neurosci.* 28, 5547–5558. doi: 10.1523/jneurosci.5599-07.2008

Wang, D. D., and Kriegstein, A. R. (2009). Defining the role of GABA in cortical development. *J. Physiol.* 587, 1873–1879. doi: 10.1113/jphysiol.2008.167635

Wang, D. D., and Kriegstein, A. R. (2011). Blocking early GABA depolarization with bumetanide results in permanent alterations in cortical circuits and sensorimotor gating deficits. *Cereb. Cortex* 21, 574–587. doi: 10.1093/cercor/bhq124

Wells, J. E., Porter, J. T., Agmon, A., and Virginia, W. (2000). GABAergic inhibition suppresses paroxysmal network activity in the neonatal rodent hippocampus and neocortex. *J. Neurosci.* 20, 8822–8830. doi: 10.1523/jneurosci.20-23-08822.2000

Yamada, J., Okabe, A., Toyoda, H., Kilb, W., Luhmann, H. J., and Fukuda, A. (2004). Cl- uptake promoting depolarizing GABA actions in immature rat neocortical neurones is mediated by NKCC1. *J. Physiol.* 557, 829–841. doi: 10.1113/jphysiol.2004.062471

Zeng, L., Xu, L., Rensing, N. R., Sinatra, P. M., Rothman, S. M., and Wong, M. (2007). Kainate seizures cause acute dendritic injury and actin depolymerization *in vivo*. *J. Neurosci.* 27, 11604–11613. doi: 10.1523/jneurosci.0983-07.2007

Zha, X.-M., Green, S. H., and Dailey, M. E. (2005). Regulation of hippocampal synapse remodeling by epileptiform activity. *Mol. Cell. Neurosci.* 29, 494–506. doi: 10.1016/j.mcn.2005.04.007

Conflict of Interest: The authors declare that the research was conducted in the absence of any commercial or financial relationships that could be construed as a potential conflict of interest.

frontiers in Synaptic Neuroscience

REVIEW
published: 27 March 2020
doi: 10.3389/fnsyn.2020.00008

Phosphorylation-Dependent Regulation of Ca^{2+}-Permeable AMPA Receptors During Hippocampal Synaptic Plasticity

Alicia M. Purkey† *and Mark L. Dell'Acqua**

Department of Pharmacology, University of Colorado School of Medicine, Anschutz Medical Campus, Aurora, CO, United States

Experience-dependent learning and memory require multiple forms of plasticity at hippocampal and cortical synapses that are regulated by N-methyl-D-aspartate receptors (NMDA) and α-amino-3-hydroxy-5-methyl-4-isoxazolepropionic acid (AMPA)-type ionotropic glutamate receptors (NMDAR, AMPAR). These plasticity mechanisms include long-term potentiation (LTP) and depression (LTD), which are Hebbian input-specific mechanisms that rapidly increase or decrease AMPAR synaptic strength at specific inputs, and homeostatic plasticity that globally scales-up or -down AMPAR synaptic strength across many or even all inputs. Frequently, these changes in synaptic strength are also accompanied by a change in the subunit composition of AMPARs at the synapse due to the trafficking to and from the synapse of receptors lacking GluA2 subunits. These GluA2-lacking receptors are most often GluA1 homomeric receptors that exhibit higher single-channel conductance and are Ca^{2+}-permeable (CP-AMPAR). This review article will focus on the role of protein phosphorylation in regulation of GluA1 CP-AMPAR recruitment and removal from hippocampal synapses during synaptic plasticity with an emphasis on the crucial role of local signaling by the cAMP-dependent protein kinase (PKA) and the Ca^{2+}calmodulin-dependent protein phosphatase 2B/calcineurin (CaN) that is coordinated by the postsynaptic scaffold protein A-kinase anchoring protein 79/150 (AKAP79/150).

Keywords: synaptic plasticity, LTP, LTD, Ca^{2+}-permeable AMPA receptor, phosphorylation, PKA, calcineurin, AKAP

OPEN ACCESS

Edited by:
Kimberly M. Huber, University of Texas Southwestern Medical Center, United States

Reviewed by:
Johannes W. Hell, University of California, Davis, United States
Edward B. Ziff, New York University, United States

****Correspondence:***
Mark L. Dell'Acqua
mark.dellacqua@cuanschutz.edu

†Present address:
Alicia M. Purkey, Department of Cell Biology, Duke University Medical School, Durham, NC, United States

Received: *20 December 2019*
Accepted: *18 February 2020*
Published: *27 March 2020*

Citation:
Purkey AM and Dell'Acqua ML (2020) Phosphorylation-Dependent Regulation of Ca^{2+}-Permeable AMPA Receptors During Hippocampal Synaptic Plasticity. Front. Synaptic Neurosci. 12:8. doi: 10.3389/fnsyn.2020.00008

INTRODUCTION

Long-term potentiation (LTP) and depression (LTD) can be induced by brief, strong vs. prolonged, weak activation of N-methyl-D-aspartate receptor (NMDAR) Ca^{2+} influx and are expressed by long-lasting increases or decreases, respectively, in α-amino-3-hydroxy-5-methyl-4-isoxazolepropionic acid receptor (AMPAR) activity. LTP/LTD at excitatory synapses can be induced rapidly (seconds-minutes) but expressed persistently (hours-days; Collingridge et al., 2010; Huganir and Nicoll, 2013). Hippocampal and cortical pyramidal neurons can also homeostatically scale-up or -down excitatory synaptic strength across all inputs in response to chronic (hours-days) decreases or increases, respectively, in overall input and firing (Turrigiano, 2012; Chen et al., 2013; Lee et al., 2013). Homeostatic synaptic plasticity, like Hebbian, is

expressed through changes in AMPAR synaptic localization (O'Brien et al., 1998; Turrigiano et al., 1998; Thiagarajan et al., 2005; Sutton et al., 2006; Aoto et al., 2008; Ibata et al., 2008; Lee and Chung, 2014). However, it was originally thought that the mechanisms mediating Hebbian and homeostatic AMPAR regulation would not be identical due to several opposing features. For instance, LTP and homeostatic scaling-up are triggered by brief, elevated vs. prolonged, decreased Ca^{2+} signaling. Nonetheless, accumulating evidence indicates that the mechanistic lines separating Hebbian and homeostatic plasticity are becoming blurred with common signaling machinery controlling both processes. Importantly, Hebbian and homeostatic synaptic plasticity alterations are implicated in many nervous system disorders, including Alzheimer's disease, Fragile X, Rett syndrome, and autism, thus, we need to understand the underlying signaling mechanisms (Thiagarajan et al., 2007; Keck et al., 2017). This review article will briefly review the respective roles of NMDARs and AMPARs in synaptic transmission but will primarily focus on mechanisms regulating the activity, trafficking, and subunit composition of synaptic AMPARs during synaptic plasticity, with emphasis on CP-AMPAR regulation in CA1 hippocampal pyramidal neurons.

IONOTROPIC GLUTAMATE RECEPTORS AND THE POSTSYNAPTIC DENSITY (PSD)

Glutamatergic synapses on principal cells in the CNS, such as hippocampal and cortical pyramidal neurons, are predominately located on dendritic spines and contain a structure known as the postsynaptic density (PSD), so named based on its appearance in electron micrographs due to the densely-packed protein network it contains (Sheng and Hoogenraad, 2007). In the 1970s, the first PSD purification experiments were carried out and in the 1990s the first molecular constituents of the PSD components were identified. Owing largely to the development of mass spectrometry-based proteomics, many PSD proteins have been identified in the past few decades. The average PSD has a molecular mass of ∼1 gigadalton (Chen et al., 2005) and contains 100–1,000 different proteins, including most prominently NMDARs and AMPARs, scaffolding proteins, voltage-gated ion channels, cell adhesion molecules, cytoskeletal elements and intracellular signaling enzymes. One of the most abundant and first identified components of the PSD is postsynaptic density protein 95 (PSD-95; Cho et al., 1992), which is the most prominent member of a family of PDZ-domain-containing membrane-associated guanylate kinase (MAGUK) scaffold proteins that serve as primary organizers of PSD structure and master regulators of excitatory synapse function (Won et al., 2017). Despite its complex composition, the PSD is a dynamic structure with changes in protein composition taking place in hours-days over the course of synaptic development and homeostatic plasticity and in seconds-minutes following the induction LTP or LTD. While we now appreciate a whole host of molecular players within the PSD, we still do not have a thorough understanding of the molecular organization of the PSD or how its protein composition and those of the associated synaptic membrane plus neighboring perisynaptic (within 100 nm of the PSD) and extrasynaptic regions of the dendritic spine plasma membrane are regulated during plasticity (Sheng and Hoogenraad, 2007).

Ionotropic glutamate receptors are the major functional component of the PSD that mediate excitatory synaptic transmission. These receptors are integral membrane proteins that form ion channels from four individual subunits coming together to form tetrameric receptors with cation-selective pores (Traynelis et al., 2010). Each subunit is composed of four domains: an amino (N)-terminal domain (NTD) that drives multimerization, a highly conserved extracellular clamshell-like ligand-binding domain (LBD), which together comprise ∼85% of receptor mass and protrude ∼130 Angstroms into the synaptic cleft (Sobolevsky et al., 2009; Meyerson et al., 2014; García-Nafría et al., 2016), the transmembrane domain (TMD) containing the ion-conducting pore, and a variable intracellular carboxy (C)-terminal domain (CTD; **Figure 1A**). There are three major classes of ionotropic glutamate receptors that mediate synaptic transmission at cortical and hippocampal synapses: AMPA receptors, kainate receptors (KARs), and NMDA receptors. AMPARs, KARs, and NMDARs are all activated by glutamate binding to their LBDs but with NMDARs also requiring binding of glycine or D-serine as a co-agonist. Upon agonist binding the LBDs change conformation causing the ion channel pore in the TMD to open and allow Na^+, K^+, and in some cases Ca^{2+} and Zn^{2+} cation flux (Traynelis et al., 2010). The forms of hippocampal synaptic plasticity covered in this review are only regulated by AMPARs and NMDARs, thus KARs will not be further discussed.

NMDA RECEPTORS

NMDARs form the functional core of the synapse with ∼20 NMDARs per PSD (Sheng and Hoogenraad, 2007). Unlike AMPARs that are highly variable in number from spine to spine, the number of NMDARs is fairly consistent across synapses and in general is more stable over time (Sheng and Hoogenraad, 2007). NMDARs are heterotetramers formed by two GluN1 subunits (*Grin1* gene) that bind the co-agonists glycine and D-serine and two-variable GluN2 or GluN3 subunits that bind glutamate or glycine, respectively (Traynelis et al., 2010; Gray et al., 2011). NMDAR subunit expression is variable throughout the brain across different cell types and during development and can contribute to differences in NMDAR channel properties, including desensitization and Ca^{2+}-conductance. The majority of NMDARs in hippocampal CA1 neurons contain GluN1 in various combinations with GluN2A (*Grin2A* gene) and GluN2B (*Grin2b* gene) subunits (Traynelis et al., 2010). While AMPARs are purely ligand-gated, NMDARs are not only directly ligand-gated but are also indirectly voltage-gated by virtue of the requirement for membrane depolarization to relieve pore block by Mg^{2+} ions. As a result of this voltage-dependent Mg^{2+} pore block, NMDARs are not responsible for much of the current at the resting membrane potential of −70 mV during basal transmission, but when activated in response to repetitive stimuli that induce synaptic plasticity, glutamate binding coincident with

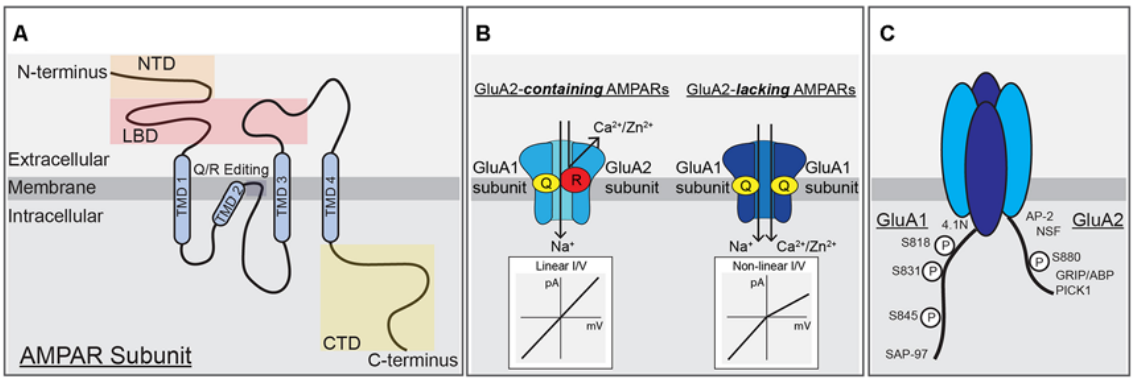

FIGURE 1 | α-amino-3-hydroxy-5-methyl-4-isoxazolepropionic acid (AMPA) receptor subunit structure, function and modifications. **(A)** A single AMPAR subunit with (N)-terminal domain (NTD), ligand-binding domain (LBD), transmembrane domain (TMD), and (C)-terminal domain (CTD) structural domains indicated. **(B)** AMPARs containing the GluA2-subunit are unable to pass calcium due to the positive charge of arginine residues within the pore, *left*. AMPARs lacking the GluA2-subunit can pass calcium and have a non-linear, inwardly rectifying current-voltage relationship due to block of outward current by intracellular polyamines, *right*. **(C)** Schematic of the CTDs of GluA1 and GluA2 highlighting phosphorylation sites and protein-protein interaction domains.

postsynaptic depolarization mediated by AMPAR activation allows the NMDAR to open and conduct Na^+ and Ca^{2+} inward and K^+ outward. While NMDAR Ca^{2+}-current makes up only a small percentage of the total current passed through the channel, it is essential for neuronal signaling that regulates AMPAR activity in synaptic plasticity.

AMPA RECEPTORS

AMPARs are the primary mediators of fast excitatory glutamatergic neurotransmission in the CNS under basal conditions. Due to their rapid kinetics, opening and closing on the timescale of milliseconds, AMPARs allow for fast depolarization of the postsynaptic membrane *via* Na^+ influx and thus high-fidelity propagation of signaling between pre- and postsynaptic neurons. AMPARs form tetramers of homo- and heterodimers composed of GluA1–4 subunits (genes *Gria1–4*), and are, like NMDARs, dimers of dimers (Lu et al., 2009; Traynelis et al., 2010). Channel opening depends on glutamate binding to all subunits of the tetramer (Lisman et al., 2007). GluA1–4 subunits can contribute differently to receptor properties like channel kinetics, ion selectivity, and intracellular trafficking. In addition to innate subunit-specific properties, mRNA processing, auxiliary proteins and phosphorylation add additional complexity to subunit control of receptor properties. AMPAR GluA1–4 subunits differ the most from each other in their divergent CTDs that vary in length and serve as a major site for regulatory intracellular protein-protein interactions and post-translational modifications (**Figures 1A,C**; Shepherd and Huganir, 2007; Traynelis et al., 2010; Benke and Traynelis, 2019).

AMPAR synaptic number varies widely from synapse to synapse reflecting differences in synaptic strength (Sheng and Hoogenraad, 2007). Using super-resolution imaging techniques, individual hippocampal synapses are thought to contain 20–100 AMPARs organized into distinct nanoclusters containing on the order of 20–40 receptors (Biederer et al., 2017; Chen et al., 2018; Choquet, 2018). AMPARs are highly mobile and their synaptic abundance is highly regulated developmentally and during synaptic plasticity. Much work has gone into understanding AMPAR trafficking to and from synapses to control synaptic strength and how receptor subunit composition can influence AMPAR properties.

Ca^{2+}-Permeable AMPA Receptors

AMPAR channel function is prominently controlled by the presence or absence of the GluA2 subunit. Interestingly, the impacts of GluA2 on AMPAR function are a product of adenosine deaminase mediated post-transcriptional editing of the *Gria2* mRNA that precedes mRNA splicing and translation. This mRNA-editing occurs at codon 607 and the resulting residue of the GluA2 protein is located in the membrane re-entrant pore loop (**Figures 1A,B**). Editing at this position results in a Glutamine to Arginine (Q/R) substitution that reduces overall channel conductance, limits permeability to Ca^{2+} (and Zn^{2+}), and prevents pore block by positively charged polyamines, all due to the introduction of two large positively charged R residues in the pore. The introduction of R residues into the pore of GluA2-containing AMPARs also influences receptor assembly in endoplasmic reticulum (ER) to favor heterodimerization with other subunits and ER exit over homodimerization to form GluA2-homomers that are retained in ER and if they reached the surface would have very little activity (Greger et al., 2003; Traynelis et al., 2010). However, the process of AMPAR dimer assembly itself is driven by interactions between the NTDs, and recently GluA1 NTD interactions have been shown to be key for regulating synaptic incorporation (Díaz-Alonso et al., 2017; Watson et al., 2017). As the mRNA editing process is normally very efficient, most GluA2 subunits are Q/R edited, resulting in low Ca^{2+}-permeability and insensitivity to polyamine blockade (Ca^{2+}-impermeable AMPARs, CI-AMPARs). Alternatively, AMPAR assemblies lacking GluA2 subunits, such as GluA1 homomers, are Ca^{2+}-permeable (i.e., CP-AMPARs), though still less so

than NMDARs (Isaac et al., 2007; Traynelis et al., 2010). CP-AMPARs are sensitive to channel block by endogenous intracellular polyamines, such as spermine, and exogenously applied extracellular polyamine toxins and compounds, such as philanthotoxin (PhTx), joro spider toxin, argiotoxin, IEM-1460, and 1-naphthylacetyl-spermine (NASPM; Blaschke et al., 1993; Herlitze et al., 1993; Bowie and Mayer, 1995; Koike et al., 1997; Magazanik et al., 1997; Washburn et al., 1997; Toth and McBain, 1998). These exogenous polyamine-derivatives can be extracellularly applied to produce open-channel block of CP-AMPARs, and are thus frequently used to probe receptor subunit composition in neurons (Toth and McBain, 1998; Liu and Cull-Candy, 2000; Kumar et al., 2002; Terashima et al., 2004; Plant et al., 2006).

In addition, CI-AMPARs and CP-AMPARs display different current-voltage (I–V) relationships due to block of CP-AMPARs by intracellular polyamines at positive potentials. All AMPARs, like NMDARs, have a reversal potential near 0 mV due to lack of selectivity for Na^+ vs. K^+, but while GluA2-containing CI-AMPARs exhibit a linear I-V relationship at potentials both negative and positive to 0 mV, GluA2-lacking CP-AMPARs exhibit very little current at membrane potentials greater than 0 mV due to endogenous polyamines being driven into the pore in a voltage-dependent manner and preventing outward flux of K^+ ions. This phenomenon of passing less outward current than inward current is called inward rectification (**Figure 1B**). As mentioned above, the presence of GluA2 also regulates AMPAR single-channel conductance, with GluA1 homomers conducting an average of ∼12 pS and GluA1/2 heteromers passing much less current at ∼3 pS (Benke and Traynelis, 2019). From numerous studies it appears the majority of AMPARs under basal conditions at most synapses on most principal cells in the brain, including in CA1 hippocampal pyramidal cells (Lu et al., 2009), are heteromeric GluA2-containing CI-AMPARs with low single-channel conductance. However, under certain conditions, both physiological and pathophysiological, a small number of GluA2-lacking CP-AMPARs with high single-channel conductance can be recruited to synapses to play a critical role in modifying synaptic signaling during plasticity and disease (Cull-Candy et al., 2006; Liu and Zukin, 2007; Man, 2011). In cortical and CA1 pyramidal cells, these CP-AMPARs are mainly thought to be GluA1 homomers, except very early in development when GluA4 is more abundantly expressed (Zhu et al., 2000).

AMPAR Variable CTD Contributions to Subunit Regulation

Because AMPAR subunits are otherwise highly homologous, the variable CTD is thought to be a site of conferring distinct modes of regulation between the subunits, including membrane trafficking, stabilization, and degradation. GluA1 and GluA4 have long CTDs and GluA2 and GluA3 have short CTDs that contain a number of sites for subunit-specific post-translational modification, including phosphorylation, and protein-protein interactions, such as with different scaffold proteins and cytoskeletal elements (Henley et al., 2011; **Figure 1C**). Initially, the NMDAR GluN2A and GluN2B CTDs were identified as directly binding to the PDZ domain-containing MAGUK scaffold protein PSD-95 (Sheng and Kim, 2011) and the AMPAR GluA1 CTD as directly binding to the related MAGUK Synapse-associated protein 97 (SAP97; Leonard et al., 1998). This MAGUK family of PDZ scaffolds also includes PSD-93 and SAP102, with functions of these four MAGUKs having some overlap (Xu, 2011; Zheng et al., 2011). Overall, the expression of MAGUKs, PSD-95 in particular, is important for maintaining both AMPAR and NMDAR targeting to the synapse (Chen et al., 2015). Accordingly, PSD-95 indirectly interacts with AMPARs independent of subunit composition through PDZ binding to the C-terminal tail of the auxiliary transmembrane AMPA receptor regulatory proteins (TARPs), which both modify channel biophysical properties and promote AMPAR retention at synapses (Straub and Tomita, 2012).

CTD phosphorylation of different AMPAR subunits can regulate channel properties and localization. GluA1–4 subunits are phosphorylated at over 20 serine, threonine, and tyrosine residues by many kinases, such as Calcium/calmodulin-dependent protein kinase II (CaMKII), PKA, Protein Kinase C (PKC), Protein Kinase G (PKG), proto-oncogene tyrosine-protein kinases Src and Fyn, and c-Jun N-terminal kinase (JNK; Shepherd and Huganir, 2007; Lu and Roche, 2012). In particular, GluA1 CTD phosphorylation has been extensively studied with three sites prominently featured in control of receptor activity and trafficking: Serine 818 (S818), Serine 831 (S831), and Serine 845 (S845; **Figures 1C**, **2A**). Phosphorylation of S818 by PKC both increases single-channel conductance and promotes GluA1 surface delivery and synaptic incorporation (**Figure 2A**; Diering and Huganir, 2018). CaMKII and PKC phosphorylate S831, which can increase single-channel conductance and control receptor trafficking and synaptic incorporation (**Figure 2A**; Diering and Huganir, 2018; Summers et al., 2019). GluA1 S845 is phosphorylated by PKA and PKG and is involved in both regulation of open probability (Banke et al., 2000) and receptor recycling between intracellular endosomes and the extrasynaptic plasma membrane (**Figures 2A,B**; Traynelis et al., 2010). In particular, S845 phosphorylation appears to promote endosomal recycling of GluA1 containing receptors, including GluA1 homomeric CP-AMPARs, to prevent their sorting to late endosomes and the lysosome for degradation (He et al., 2009; Fernández-Monreal et al., 2012), and to promote GluA1 delivery to the extrasynaptic membrane (Sun et al., 2005; Oh et al., 2006; Man et al., 2007; Yang et al., 2008, 2010; He et al., 2009). It has been determined that ∼15% of receptors are phosphorylated at S831 and S845 at rest (Diering et al., 2016; but see also Hosokawa et al., 2015). As detailed more below, these phosphorylation events appear to play a critical role in controlling receptor trafficking and function during LTP, LTD and homeostatic synaptic plasticity.

GluA2 trafficking and synaptic localization are also regulated by phosphorylation and protein-protein interactions with its CTD. In the 1990s, yeast two-hybrid screens identified a number of proteins that interact with the GluA2 CTD, including the PDZ interactions between GluA2 (and GluA3) and GRIP 1 and 2 [Glutamate Receptor Interacting Protein (GRIP1)/AMPAR Binding Protein (ABP)] and Protein Interacting with C Kinase (PICK1; **Figure 1C**; Dong et al., 1997, 1999; Lüscher et al.,

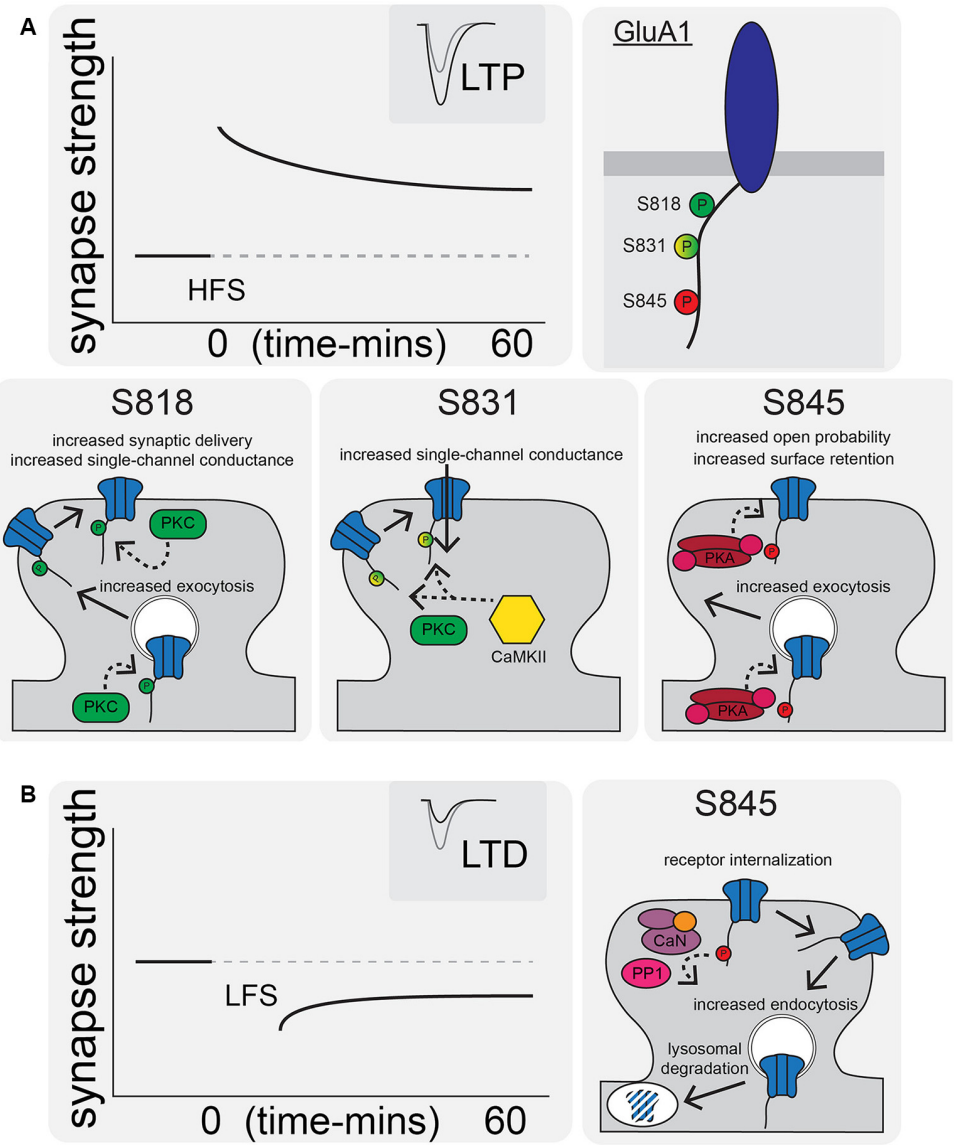

FIGURE 2 | AMPAR synaptic trafficking regulation by CTD phosphorylation during long-term potentiation (LTP) and depression (LTD). **(A)** LTP stimuli induce phosphorylation at S818, S831, and S845 on the GluA1 CTD. Phosphorylation of these sites by CaMKII, PKC, and/or PKA increases synaptic AMPAR content and increases receptor transmission by a variety of indicated mechanisms. **(B)** LTD is characterized by AMPAR internalization and increased lysosomal degradation *via* CaN- and protein phosphatase 1 (PP1)-mediated dephosphorylation of GluA1 S845.

1999; Srivastava and Ziff, 1999; Dev et al., 2000; Xia et al., 2000). In addition, both N-ethylamine-Sensitive Factor (NSF), a protein required for membrane fusion and exocytosis, and AP2, a protein required for clathrin-dependent endocytosis, interact with the juxtamembrane region of GluA2 CTD. Accordingly, the GluA2-NSF interaction is important in maintaining AMPAR content at the synapse, while the AP2 motif mediates endocytic removal (Nishimune et al., 1998; Osten et al., 1998; Song et al., 1998; Lüscher et al., 1999; Lüthi et al., 1999; Noel et al., 1999; Lee et al., 2002). The GluA2 subunit CTD can also be modulated by phosphorylation of Y875 by Src, which is then dephosphorylated to favor endocytosis during LTD. Phosphorylation of Serine 880 within the PDZ ligand domain by PKC (**Figure 1C**) disrupts GluA2 binding to GRIP1/2 but increases binding to PICK1 to promote trafficking in both directions between the plasma membrane and endosomes (Matsuda et al., 1999; Chung et al., 2000; Gladding et al., 2009; Collingridge et al., 2010).

AMPAR REGULATION DURING LTP AND LTD

During LTP induction, AMPARs are activated and relieve NMDAR pore blockade by Mg^{2+} to permit Ca^{2+} entry into the postsynaptic cell and initiate signaling cascades

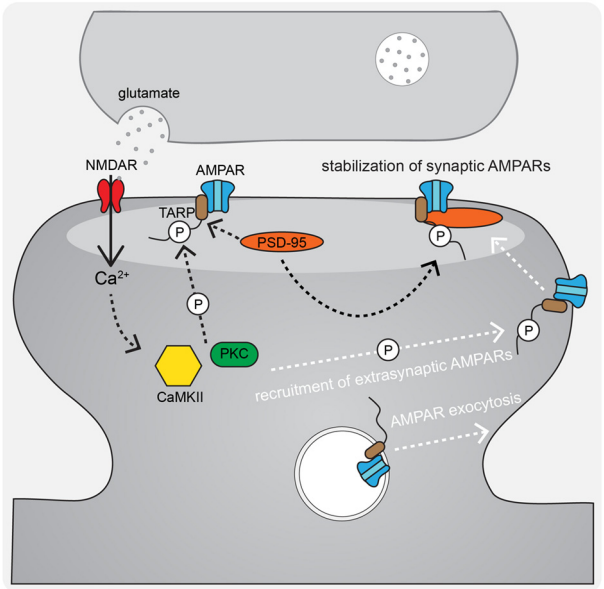

FIGURE 3 | AMPAR-TARP interaction and TARP phosphorylation regulate AMPAR diffusional trapping in the postsynaptic density (PSD) during LTP. During LTP stimuli, N-methyl-D-aspartate receptors (NMDAR)-Ca^{2+} activated CaMKII and PKC phosphorylate AMPAR-associated TARPs both to trap newly exocytosed extrasynaptic receptors in the synapse after lateral diffusion and to stabilize existing synaptic receptors by binding to the synaptic scaffold PSD-95.

that result in changes in synaptic strength (Kessels and Malinow, 2009; Huganir and Nicoll, 2013). The postsynaptic mechanisms required for LTP downstream of NMDAR-Ca^{2+} include, most prominently, signaling by the protein kinases CaMKII (*via* Ca^{2+}-calmodulin), PKA (*via* Ca^{2+}-sensitive adenylyl cyclase-mediated cAMP production), and PKC (*via* Ca^{2+} and phospholipase C lipid signaling). In particular, CaMKII activity is necessary and can even be sufficient for mediating LTP induction and expression (Nicoll, 2017). AMPAR regulation downstream of these kinase signaling cascades involves changes in phosphorylation state of the AMPARs themselves (**Figure 2A**) as well as the auxiliary TARP proteins (**Figure 3**) to control both channel biophysical properties and synaptic receptor number *via* endo- and exocytosis and lateral diffusion and synaptic insertion (Shepherd and Huganir, 2007; Newpher and Ehlers, 2008; Opazo and Choquet, 2011; Huganir and Nicoll, 2013; Buonarati et al., 2019).

CP-AMPARs in LTP and LTD

Although early studies found mainly a role for AMPARs in LTP expression and no requirement in LTP induction, beyond facilitating relief of NMDAR Mg^{2+} block (Kauer et al., 1988; Muller et al., 1988), considerable research has since indicated that AMPARs can play more active roles in controlling both plasticity induction and expression in the hippocampus and other brain regions. While it has long been appreciated that NMDARs are required for induction of LTP at CA1 synapses and that the Ca^{2+} they provide is an important signal for LTP (the NMDAR competitive antagonist AP5 and open channel blocker MK801 both prevent induction of LTP), more recent studies (Plant et al., 2006; Lu et al., 2007; Guire et al., 2008; Yang et al., 2010; Sanderson et al., 2016) have implicated another Ca^{2+} source, the CP-AMPAR, as an additional key regulator of LTP, as well as LTD (but see also Adesnik and Nicoll, 2007; Gray et al., 2007). While GluA2-lacking, GluA1 homomeric CP-AMPARs are largely excluded from hippocampal synapses basally (Lu et al., 2009; Rozov et al., 2012), both Hebbian and homeostatic plasticity can modify synaptic strength *via* recruiting CP-AMPARs to synapses (Thiagarajan et al., 2005; Plant et al., 2006; Sutton et al., 2006; Lu et al., 2007; Aoto et al., 2008; Yang et al., 2010; Soares et al., 2013; Park et al., 2016; Sanderson et al., 2016; but see Adesnik and Nicoll, 2007; Ancona Esselmann et al., 2017). These recruited CP-AMPARs, due to both greater single-channel conductance and Ca^{2+} permeability described above, can in turn not only influence the level of plasticity expression but also confer changes in synaptic signaling resulting in the plasticity of plasticity i.e., metaplasticity. Importantly, CP-AMPAR metaplasticity in the VTA, nucleus accumbens and amygdala has been linked to drug addiction and fear extinction (Clem and Huganir, 2010; Wolf and Tseng, 2012). However, the roles of CP-AMPARs in plasticity and metaplasticity in the cortex and at CA1 synapses in the hippocampus remain controversial, in large part because we do not have an adequate understanding of the mechanisms that determine whether CP-AMPARs are recruited to or removed from synapses.

CP-AMPARs, as identified both by their inward rectification and sensitivity to polyamine-derived drugs [such as NASPM, IEM, and PhTx (Traynelis et al., 2010)], have been found to be transiently recruited to synapses in CA1 pyramidal neurons in response to induction of both LTP and LTD (Plant et al., 2006; Lu et al., 2007; Guire et al., 2008; Yang et al., 2010; Jaafari et al., 2012; Park et al., 2016; Sanderson et al., 2016). These recruited CP-AMPARs are then subsequently removed within ∼15–30 min of the LTP induction stimulus (Plant et al., 2006) or during the prolonged (6–15 min) LTD induction stimulus (Sanderson et al., 2016). Accordingly, blocking CP-AMPARs with antagonists at early time points after LTP induction will prevent LTP, but not at later time points ∼30 min after induction, when LTP expression is fully established (Washburn and Dingledine, 1996; Plant et al., 2006; Yang et al., 2010; Jaafari et al., 2012). These observations indicate that CP-AMPARs are important in a short window following induction and that early Ca^{2+} entry through these receptors can be important for establishing the stable expression of LTP but not in maintaining LTP expression once fully established. Likewise, CP-AMPAR antagonists reduce the amount of resulting LTD expression only when applied during LTD induction, when they are present, but not later after induction of LTD, when expression is established and the previously recruited CP-AMPARs have already been removed (Sanderson et al., 2016). Because there are few or no synaptic CP-AMPARs basally, transient introduction of a very small number of these high conductance receptors can have a large impact on CA1 synaptic strength; only a ∼5% increase in synaptic CP-AMPAR content is needed to account for the increased conductance seen during a typical

LTP experiment (Guire et al., 2008; Stubblefield and Benke, 2010; Benke and Traynelis, 2019). Hence, an attractive and experimentally supported model is that CP-AMPARs help to increase postsynaptic currents for a short yet critical period after LTP induction or during LTD induction to promote additional Ca^{2+} signaling that is required for promoting stable expression in the case of LTP or maximal induction in the case of LTD. However, it not yet known what specific downstream signaling pathways this additional CP-AMPAR synaptic Ca^{2+} influx is engaging to promote LTP vs. LTD.

Controversy Surrounding CP-AMPAR Involvement in LTP

Although multiple lines of investigation suggest that CP-AMPARs can be recruited during LTP, significant controversy still exists due to other studies showing there is no GluA1 homomer involvement (Adesnik and Nicoll, 2007; Gray et al., 2007; Granger et al., 2013). It has become clear over time and with more experimental evidence that a number of variables could be contributing to these inconsistencies regarding CP-AMPAR involvement in LTP, including most prominently developmental age of the animals (which also makes it difficult to directly compare between rats and mice), the recording methods (extracellular vs. whole-cell), and the induction protocols used (**Table 1**). Our laboratory and others found that in mice at ∼P14 (2 weeks of age), robust recruitment of CP-AMPARs can be observed following 1 × 100 Hz induction of LTP using extracellular field recording, but this CP-AMPAR recruitment by 1 × 100 Hz LTP disappears by between ∼P17–21 and then reappears at ages >P42 (Lu et al., 2007; Sanderson et al., 2016). However, another variable impacting CP-AMPAR involvement in LTP is the specific type of plasticity being induced. Not only has it emerged that there exist many types of plasticity *in vivo* (Lisman, 2017), but also within the literature there exist many diverse protocols for inducing LTP *ex vivo* in brain slices, whether using an extracellular or whole-cell recording. The choice of induction protocol likely plays a pivotal role in the signaling pathways initiated and how they interact with the mechanisms that recruit CP-AMPARs. In general, it appears that CP-AMPAR recruitment after LTP is more likely to be observed when induced using relatively brief, weak stimuli (1–2× HFS tetani, single or spaced theta-burst stimulation (sTBS), briefer 0 mV pairing) compared to stronger stimuli (multiple HFS tetani, massed/continuous theta burst (cTBS), prolonged 0 mV pairing), such that at even a single developmental age one can observe both CP-AMPAR dependent and independent forms of LTP depending on the induction protocol. For example, we found using whole-cell recording in ∼2–3 week-old mice that a relatively weaker, brief 2 × 100 Hz, 1 s HFS, 0 mV pairing induction protocol resulted in moderate LTP expression that was sensitive to the CP-AMPAR blocker NASPM, while a stronger, prolonged 3 Hz, 90 s 0 mV pairing induction protocol resulted in more robust LTP expression that was insensitive to NASPM (Purkey et al., 2018). In addition, work from Guire et al. (2008) found using extracellular field recording from 4 to 6 week-old rats that a weaker, brief TBS induction stimulus-induced LTP was CP-AMPAR dependent, while a stronger 3 × 100 Hz HFS induction stimulus-induced LTP was CP-AMPAR independent.

However, what constitutes a weak vs. strong LTP induction protocol may be different between whole-cell and extracellular recording approaches; for instance, in mice at ∼2 weeks of age, we found that 2 × 100 Hz HFS with 0 mV pairing induces CP-AMPAR dependent LTP while others using 2 × 100 Hz induction in extracellular field recording found LTP at this same age that was insensitive to CP-AMPAR blockers (Gray et al., 2007; Purkey et al., 2018). Accordingly, in mice at ∼8 weeks of age 1 × 100 Hz, HFS induces CP-AMPAR-dependent LTP in field recordings but 2 × 100 Hz induces LTP that is insensitive to CP-AMPAR antagonists (Gray et al., 2007; Lu et al., 2007). Thus, one must consider developmental age, recording method, and induction protocols. The early controversy between Plant et al. (2006) which observed CP-AMPAR recruitment following LTP induction, and Adesnik and Nicoll (2007), which did not, might be explained by the relatively small differences in induction protocol; while both studies used mice ∼2–3 weeks of age and whole-cell recording pairing protocols to induce LTP, Plant et al. (2006) used slightly weaker, briefer pairing protocols on average than Adesnik and Nicoll (2007; **Table 1**).

However, the question still remains why might relatively weaker induction of LTP recruit CP-AMPARs while stronger induction does not? Even when CP-AMPARs are recruited to CA1 synapses after LTP (or LTD) induction, the presence of these receptors in the synapse is transient, with their own activity triggering subsequent removal (Plant et al., 2006; Sanderson et al., 2016). Thus, it is possible that when LTP is induced by stronger and/or more prolonged induction protocols, the greater resulting NMDAR Ca^{2+} influx (with no need for any Ca^{2+} contributed by CP-AMPARs) rapidly triggers these CP-AMPAR removal mechanisms to prevent even transient recruitment to the synapse. As discussed in more detail below, the CP-AMPARs transiently recruited to CA1 synapses during LTD are rapidly removed by AKAP79/150-anchored CaN signaling that promotes GluA1 S845 dephosphorylation (Sanderson et al., 2012, 2016); however, it remains to be seen whether activation of this AKAP-CaN pathway also prevents CP-AMPAR recruitment in response to strong, prolonged LTP induction stimuli.

A further complication exists whereby many studies have tried to understand AMPAR regulatory mechanisms in plasticity by manipulating the receptor itself with subunit-specific knock-outs (KO) and mutations. But there are clear problems with the "receptor-centric" approach to understanding AMPAR subunit-specific regulatory mechanism because AMPAR activity is the measurement that is used to determine synaptic strength, thus when manipulations are made to the receptor itself (*via* knockout, point mutation, deletions, etc.) it can complicate interpretations, as the manipulations can fundamentally impact receptor function even basally. Whole receptor subunit knockouts are further complicated due to compensation by other receptor subunits, and even when combined with rescue approaches can potentially produce non-physiological receptors and signaling conditions. Therefore, while there is strong evidence to

TABLE 1 | Ca^{2+}-permeable α-amino-3-hydroxy-5-methyl-4-isoxazolepropionic acid receptors (CP-AMPAR) plasticity studies.

References	Age/Species	LTP induction protocol	CP-AMPAR? (*no*; *yes*)
Gray et al. (2007)	2 (P15–17)-3 (P21–23) weeks, 8–12 weeks, Mouse	Fields: 2 × 100 Hz, 10 s interval; Whole-cell: 2 Hz, 100 pulses paired −10 mV holding; current-clamp recordings	All were insensitive to 100–200 μM IEM1460.
Adesnik and Nicoll (2007)	2–3 weeks, Mouse and Rat	Fields: 4 × 100 Hz, 20 s interval; Whole-cell: 2 Hz, 120 pulses paired between −10 to 0 mV	All insensitive to 10 μM PhTx-433. No rectification changes observed any time after LTP induction.
Granger et al. (2013)	P17–20, Mouse	Whole-cell: 2 Hz, 90 s at 0 mV	*Gria1–3*$^{fl/fl}$; rescued with mutant receptors (all were Ca^{2+} permeable). No single AMPAR subunit found to be important for LTP.
Plant et al. (2006)	2–3 weeks, Mouse	Whole-cell: 0.5–2 Hz, 50–100 pulses paired to 0 or −10 mV	Rectification changes observed for ∼15–30 min post-induction; sensitive to 10 μM PhTx-433.
Guire et al. (2008)	4–6 weeks, Rat	Fields: TBS (five trains at 5 Hz, four pulses at 100 Hz per train) or HFS (3 × 100 Hz, 1 s, 20 s interval)	TBS stim (not HFS) sensitive to 30 μM IEM1460 immediately after induction (not 20 min later).
Lu et al. (2007)	2 (P12–14), 3 (P20–22), 4, 8 weeks, Mouse	Fields: 1 × 100 Hz, 1 s	1 × 100 Hz: 2 and 8 week-old sensitive to 2.5 μM PhTx and 20 μM NASPM; 3 and 4 week-old insensitive.
		2 × 100 Hz, 1 s spaced 20 s	2 × 100 Hz: insensitive.
Yang et al. (2010)	P13–18, Rat	Fields: TBS (three trains at 5 Hz, five pulses at 100 Hz per train, 2 ×, 20 s interval)	Incomplete expression of LTP with 10 μM PhTx-433, Ca^{2+} entry from CP-AMPARs required for LTP.
Sanderson et al. (2016)	2 (P11–14), 3 (P17–21) weeks, Mouse	Fields: LTP 1 × 100 Hz, 1 s; LTD 1 Hz, 15 min; Whole-cell: LTD 1 Hz, 6 min paired at −30 mV.	2 week-old LTP 70 μM IEM1460 sensitive when added immediately post-induction, 3 week-old LTP insensitive. 2 week-old LTD sensitive to 30 μM NASPM added during induction. Rectification changes observed transiently during LTD induction but not after.
Park et al. (2016)	3–12 weeks, Rat	Fields: cTBS 3 TBS episodes, 10 s interval; sTBS 3 TBS episodes, 2 min-1 h interval; wTBS 1 TBS episode	wTBS, cTBS insensitive to 30 μM IEM1460; sTBS sensitive to 30 μM IEM1460.
Zhou et al. (2018)	3–4 weeks, Mouse	Whole-cell: LTP 1 × 100 Hz, 4 × 100 Hz; Fields: 100 Hz, 1 s 1 or 4 times with inter-train interval of 10 s or 5 min	LTP depends on GluA1 C- tail; did not address CP-AMPARs but may be involved - GluA1 requirement and conductance change.
Purkey et al. (2018)	2–3 weeks (P14-P21), Mouse	Whole-cell: LTP 2 × 100 Hz at 0 mV, 3 Hz, 90 s at 0 mV	Weaker 2 × 100 Hz LTP sensitive to NASPM but stronger 3 Hz, 90 s LTP insensitive to NASPM.

suggest the involvement of CP-AMPARs in LTP, there still remains controversy and questions about the precise forms of plasticity involved and signaling mechanisms implicated. As discussed more below, a strong picture is now emerging that CP-AMPAR recruitment to synapses is heavily controlled by postsynaptic PKA signaling through GluA1 S845 phosphorylation.

AMPAR LTP Models: Exocytosis and Lateral Diffusion

Despite the controversy of the involvement of CP-AMPARs in LTP, it is widely accepted that AMPARs are recruited to the synapse in order to increase synaptic strength. A number of non-mutually exclusive mechanisms have been proposed to explain how AMPARs get retained/recruited to the PSD in an activity-dependent manner. The overall AMPAR insertion model of LTP includes both AMPAR trafficking to the extrasynaptic plasma membrane from intracellular stores and lateral diffusion and trapping in the synapse as key mechanisms (Passafaro et al., 2001; Kennedy and Ehlers, 2006; Ehlers, 2007; Petrini et al., 2009; Opazo and Choquet, 2011; Penn et al., 2017). The primary proposed mechanism for regulated AMPAR delivery to the extrasynaptic plasma membrane is through activity-triggered exocytosis from internal stores. A seminal contribution to elucidating this plasticity mechanism was the discovery that dynamic postsynaptic membrane trafficking is required for the expression of LTP (Lledo et al., 1998; Lüscher et al., 1999; Lu et al., 2001). In addition, LTP induction acutely increases exocytosis of GluA1 AMPARs at the extrasynaptic plasma membrane (Kopec et al., 2006; Yudowski et al., 2007; Lin et al., 2009; Kennedy et al., 2010; Patterson et al., 2010; Hiester et al., 2017) that can then laterally diffuse into the PSD and be captured (Borgdorff and Choquet, 2002; Opazo and Choquet, 2011; Opazo et al., 2012; Penn et al., 2017). This AMPAR trapping is thought to involve the retention of AMPARs in "slots" in the PSD where they are optimally positioned to respond to release of glutamate from the presynaptic terminal (MacGillavry et al., 2013; Nair et al., 2013; Tang et al., 2016; Sinnen et al., 2017). In this PSD slot model, CaMKII acts on structural regulatory proteins in the PSD to create additional AMPAR slots during LTP (Araki et al., 2015; Herring and Nicoll, 2016; Walkup et al., 2016; Zeng et al., 2016, 2019), possibly by reorganizing the PSD *via* liquid-liquid phase transition, which then can effectively trap the highly mobile AMPARs through additional CaMKII phosphorylation of TARPs that increases the affinity of AMPAR-TARP complexes for the underlying synaptic architecture (**Figure 3**; Tomita et al., 2005; Opazo et al., 2010, 2012; Park et al., 2016). Thus, AMPAR mobilization from internal stores followed by lateral diffusion and synaptic trapping likely cooperate to increase synaptic strength during LTP.

Accordingly, most models of LTP now include the requirement for an extrasynaptic plasma membrane reserve pool of surface receptors that move laterally into the PSD to support LTP expression, with receptors residing in internal stores then being recruited to the plasma membrane to replenish this extrasynaptic reserve pool (Opazo and Choquet, 2011; Granger et al., 2013; Nicoll and Roche, 2013). Indeed, a recent article from the Choquet laboratory showed that preventing lateral mobility of AMPARs blocks the initial potentiation observed after LTP induction while blocking exocytosis from internal stores decreases potentiation only at later time points (Penn et al., 2017). One prominent pool of internal AMPARs resides in the recycling endosome (RE). REs have been observed in dendritic spines (Kennedy et al., 2010; Hiester et al., 2017) and in the dendrite shaft near the bases of spines (Park et al., 2006; Kelly et al., 2011), and it has been demonstrated that LTP relies on AMPARs that are supplied by recycling through REs (Petrini et al., 2009). Additional evidence for a requirement for receptor delivery from REs during LTP includes findings that RE trafficking proteins, including Rab11, and the vesicular fusion machinery, including multiple SNARE proteins that regulate exocytosis, are all required for LTP expression (Lledo et al., 1998; Park et al., 2004, 2006; Kennedy et al., 2010; Ahmad et al., 2012; Jurado et al., 2013; Wu et al., 2017). In addition, NMDAR activity during LTP can influence postsynaptic RE dynamics to increase recycling exocytosis (Kennedy et al., 2010; Keith et al., 2012; Woolfrey et al., 2015; Hiester et al., 2017), promote RE translocation into spines (Park et al., 2006), and increase GluA1 exocytosis (Kopec et al., 2006; Yudowski et al., 2007; Lin et al., 2009; Kennedy et al., 2010; Patterson et al., 2010; Hiester et al., 2017). As mentioned above, multiple lines of evidence suggest that when GluA2-lacking CP-AMPARs are recruited to synapses following LTP, this recruitment is transient and they are quickly replaced with GluA2-containing CI-AMPARs (McCormack et al., 2006; Plant et al., 2006; Shepherd and Huganir, 2007; Kessels and Malinow, 2009). Accordingly, PICK1 associated with GluA2 and seems to be involved in the regulated recycling/endocytosis of GluA2-containing receptors during LTP and promoting GluA1 CP-AMPAR insertion (Jaafari et al., 2012). Importantly, both PICK1 and GRIP1 are known to localize to REs (Jaafari et al., 2012; Thomas et al., 2012).

AMPAR Regulation by Phosphorylation During LTP

Regardless of the extent to which AMPARs are recruited to the synapse from internal vs. extrasynaptic pools, there still exists the fundamental question of what signals mobilize AMPARs from these pools to the synapse? One mechanism regulating AMPAR plasma membrane insertion and synaptic recruitment is phosphorylation. In the late 1980s, it was demonstrated that kinase activity was required for the induction of LTP (Malenka et al., 1989; Malinow et al., 1989; Wyllie and Nicoll, 1994). This quickly led to a hypothesis that AMPAR subunits were phosphorylated during LTP to increase synaptic currents (Swope et al., 1992; Soderling, 1993). Since then, studies of activity-dependent AMPAR phosphorylation have focused on modification of GluA1 and GluA2 subunits, as the phosphorylation sites on these subunits were shown to be regulated by neuronal activity (Shepherd and Huganir, 2007; Lu and Roche, 2012). Strong evidence supporting the importance of phosphorylation control of AMPARs in plasticity was shown in the late 1990s, with increased GluA1 phosphorylation correlated with LTP and decreased GluA1 phosphorylation with LTD (**Figures 2A,B**; Barria et al., 1997; Kameyama et al., 1998;

Lee et al., 1998, 2000). GluA1 phosphorylation at S831 by CaMKII and/or PKC has been shown to increase channel conductance (Derkach et al., 2007; Kristensen et al., 2011). PKA-dependent phosphorylation of S845 increases mean open time (Banke et al., 2000) and also promotes plasma membrane insertion of the receptor, especially extrasynaptically, to make GluA1 AMPARs available for subsequent synaptic recruitment during LTP (Sun et al., 2005; Oh et al., 2006; Man et al., 2007; Yang et al., 2008; He et al., 2009; Yang et al., 2010). In addition, PKC phosphorylation of GluA1 S818 increases single-channel conductance and also promotes AMPAR plasma membrane insertion, working in concert with S845 and S831 (Boehm et al., 2006; Lin et al., 2009; Jenkins et al., 2014). Recently, it was discovered that cAMP-PKA signaling can also recruit GluA3-containing receptors to synapses to increase synaptic strength, although the specific phosphorylation targets of PKA involved in this mechanism remain to be determined (Renner et al., 2017).

To study the subunit-specific requirements of LTP, many labs have used knockout, knock-in or molecular replacement approaches (**Table 2**). Through a combination of *in vitro* studies in organotypic slices and *ex vivo* studies in acute slices from mutant mice the three GluA1 phosphorylation sites (S818, S831, and S845) have each been shown to contribute to CA1 LTP either in combination or separately depending on the experimental conditions (Esteban et al., 2003; Lee et al., 2003, 2010; Boehm et al., 2006; Qian et al., 2012). However, it is not surprising that, as in the CP-AMPAR literature, the role of GluA1 and subunit specificity in plasticity is contentious. In particular, no manipulation that blocks phosphorylation of the AMPAR CTD residues completely blocks LTP under all conditions. For example, TBS induced LTP is normal in juvenile GluA1 S831/845A double mutant mice but is strongly impaired in adults (Lee et al., 2003). Similarly, LTP is only impaired in adult but not juvenile GluA1 knockout mice (Zamanillo et al., 1999; Jensen et al., 2003; Kolleker et al., 2003). Yet, the S845A and S831A single mutant mice show normal hippocampal LTP at all ages (Lee et al., 2010). However, young adult S845A mice are deficient in prolonged theta-train (PTT) induction of LTP that depends on CP-AMPARs, activation of postsynaptic PKA signaling by β_2-adrenergic receptors, and PKA phosphorylation-mediated enhancement of L-type voltage-gated Ca^{2+} channels (Qian et al., 2012, 2017). Importantly, for most conditions where GluA1 KO and GluA1 phosphorylation-deficient mutant mice exhibited LTP deficits, there is evidence from other studies using the same or similar conditions (discussed in more detail below) that PKA signaling and CP-AMPARs are also required (Lu et al., 2007; Qian et al., 2012; Zhang et al., 2013; Sanderson et al., 2016).

Interestingly, a recent study examining the requirement of the CTDs of GluA1 and GluA2 using chimeric knock-in mice, showed that replacing the GluA1 CTD with that of GluA2 blocks LTP, but this deficit can be rescued by reintroducing the GluA1 CTD fused to GluA2 (Zhou et al., 2018). Thus, this study reinforces that the GluA1 CTD is somehow essential for AMPAR trafficking and LTP expression, although the involvement of GluA1 CP-AMPARs was not specifically addressed. In contrast, an earlier study using KO and molecular replacement approaches reached very different conclusions; normal LTP was observed with a GluA1 construct lacking the entire C-terminal tail or by an unedited GluA2-Q construct when expressed on a conditional AMPAR GluA1–3 triple knockout background (Granger et al., 2013). However, these studies in many cases used varying protocols for inducing LTP and in some cases also used different developmental ages, which as discussed both above and below could contribute to differences in results and conclusions (**Table 2**). Nevertheless, a consistent result of many studies is that knocking out GluA1 results in strongly reduced extrasynaptic AMPAR surface expression and impaired LTP (Zamanillo et al., 1999; Granger et al., 2013), but knocking out GluA2 and GluA3 results in normal extrasynaptic AMPAR surface expression and LTP (Meng et al., 2003). Taken together, these findings indicate that under most circumstances GluA1 subunit trafficking maintains the reserve pool of AMPARs necessary to support LTP, and GluA1 CTD phosphorylation appears to play a crucial but complicated role in regulating this process, in part through controlling whether GluA1 homomeric CP-AMPARs contribute to this pool and can be recruited to the plasma membrane and synapse during LTP.

AMPAR Regulation by Phosphorylation During LTD

There are multiple protocols for experimentally inducing NMDAR-dependent LTD of AMPAR synaptic strength, such as low-frequency stimulation (LFS), spike-timing-dependent plasticity (STDP) and chemical LTD with bath NMDA application (cLTD; Kameyama et al., 1998). Apart from NMDAR-dependent LTD, another mechanism for LTD induction is through a mGluR-dependent pathway. This mGluR-LTD can be induced with similar activation patterns as NMDAR-LTD, such as paired-pulse LFS (Massey and Bashir, 2007), or the group I mGluR agonist dihydroxyphenylglycine (DHPG; Palmer et al., 1997). This mGluR-dependent form of LTD will not be further discussed, and any use of LTD hereafter will be referring to NMDAR-dependent LTD. NMDAR-dependent LTD requires postsynaptic Ca^{2+} and phosphatase activity as supported by evidence that LTD expression is blocked by AP5, intracellular BAPTA (Ca^{2+} chelator; Mulkey and Malenka, 1992) and CaN or protein phosphatase 1 (PP1) inhibitors (Mulkey et al., 1994). Low-level Ca^{2+} influx from NMDARs or even basal postsynaptic Ca^{2+} levels of ∼100 nM have been shown to be sufficient to support CaN and PP1 phosphatase signaling that are required for LTD (Lisman, 1989; Mulkey et al., 1993; Malenka and Bear, 2004), along with a more recently identified NMDAR conformational signaling to the kinase p38 Mitogen-Activated Kinase (MAPK; Nabavi et al., 2013; Stein et al., 2015).

Among the targets of CaN and PP1 phosphatase activity implicated in LTD is GluA1 S845; AMPARs are dephosphorylated at S845 during LTD to promote receptor endocytosis and degradation (**Figure 2B**; Lee et al., 1998, 2003, 2010; Fernández-Monreal et al., 2012; Sanderson et al., 2016). Endocytic zones have been discovered at the periphery of excitatory synapses (Blanpied et al., 2002) and these zones are

TABLE 2 | AMPAR studies in transgenic mice.

Reference(s)	Mutation	Age	Result
Kim et al. (2005; PDZ ligand)	KI mutant mice lacking the last 7 a.a. GluA1; male	3 weeks–7 months	Unaffected: Basal localization and transmission, LTP (Fields: 1 TBS, whole-cell pairing: 2 Hz, 200 pulses at 0 mV) and LTD (Fields: 1 Hz, 900 pulses, whole-cell pairing: 0.5–1 Hz, 200–300 pulses at −40 mV).
Granger et al. (2013) and Granger and Nicoll (2014a)	*Gria1–3*$^{fl/fl}$; replaced with different mutant receptors	P17–20	No single portion of the GluA1 C-terminal tail is required for LTP (2 Hz, 90 s at 0 mV), GluA2, GluA2(Q) or GluK1 replacement sufficient to rescue LTP. GluA1 and GluA2 conditional knockouts have normal LTD (1 Hz, 15 min), GluK1 replacement in GluA1–3 conditional knockout sufficient to rescue LTD.
Zamanillo et al. (1999), Hoffman et al. (2002), Reisel et al. (2002) and Jensen et al. (2003)	GluA1 knockout	3 months, P14–42, P41–56, Adult	LTP (Fields: 1 × 100 Hz, 1 s): impaired; normal spatial learning in Morris Water Maze; LTP (Fields: 1 × 100 Hz, 1 s/Whole-cell 0.67 Hz, 3 min at 0 mV): modest/normal amount of LTP at P14 disappears by P42; LTP (TBS): decreased initially but normalizes to WT after 25 min; Normal spatial memory; spatial working memory deficits.
Meng et al. (2003)	GluA3 knockout	2–3 weeks, 2–3 months	Normal basal transmission and pre-synaptic function; LTD (1 Hz, 15 min) 12–16 days: normal; Depotentiation 2–3 weeks: normal; Enhanced LTP (100 Hz, 1 s) in adults and enhanced level of LTP saturation (6 trains of 100 Hz, 1 s with 5 min interval) in adults.
Jia et al. (1996), Gerlai et al. (1998) and Meng et al. (2003)	GluA2 knockout	P16–30, 5–8 weeks, 2–3 weeks, 2–3 months	LTP (Fields: 5 × 100 Hz, 200 ms pulses): enhanced; growth retardation and motor deficits, normal brain anatomy, increased excitability, alterations in a number of behaviors across multiple brain areas; LTD (Fields: 1 Hz, 15 min): normal; Depotentiation (HFS 100 Hz 1 s followed by LFS 1 Hz, 15 min): impaired depotentiation but enhanced LTP (100 Hz, 1 s) in adults.
Meng et al. (2003)	GluA2/3 double knockout	2-3 weeks, 2-3 months	Reduced basal transmission in adults; Normal PPR in adults; Enhanced LTD and de-depression (12–16 days); Enhanced LTP and de-potentiation (2–3 weeks old); Enhanced LTP in adult mice.
Lee et al. (2003)	GluA1 S831/845A knock-in	Young (P21–P28) and old (3 months or older)	Normal basal transmission; LTP (Fields TBS) old mostly blocked, young normal; LTD (Fields: old PP 1 Hz, 15 min and young 1 Hz, 15 min): blocked likely due to lack of receptor internalization; MWM: learning normal, impaired retention of spatial memory (delayed sessions).
Lee et al. (2010)	GluA1 S831A knock-in	Young (3 weeks) and old (3 months+)	Young-Normal basal transmission; LTP (Fields: 4 × TBS) normal; LTD: (Fields: 1 Hz) slight decrease but not statistically significant. Old-Normal basal transmission; LTP: (Fields: 4 × TBS and 1 × TBS) normal; LTD: (Fields: PP-1 Hz) normal. Normal de-potentiation and de-depression.
Lee et al. (2010) and Qian et al. (2012)	GluA1 S845A knock-in	Young (3 weeks) and old (3 months+), 6–8 weeks	Young mice have normal basal transmission and normal LTP (Fields: 4 × TBS) but virtually absent LTD (Fields: 1 Hz). Old mice have normal basal transmission and normal LTP (Fields: 4× TBS and 1 × TBS) but mostly blocked LTD (Fields: PP 1 Hz) and normal de-potentiation. At 6–8 weeks, PTT-LTP (5 Hz, 3 min in presence of β-adrenergic receptor agonist) is impaired.
Zhou et al. (2018)	GluA1 and GluA2 C-terminal tail swap knock-ins	3–4 weeks for LTP; 13–15 days for LTD	Both show normal basal transmission GluA1-C2KI has normal NMDAR LTD, impaired LTP (1 × 100 Hz, 4 × 100 Hz); GluA2-C1KI has normal mGluR LTD (100 μM (RS)-3,5-DHPG for 10 min), no NMDAR LTD (900 pulses at 1 Hz), enhanced LTP (4 × 100 Hz). With the double replacement, LTP and LTD are normal. Behavior: GluA1-C2KI impaired spatial learning and memory, GluA2-C1KI impaired contextual fear memory.

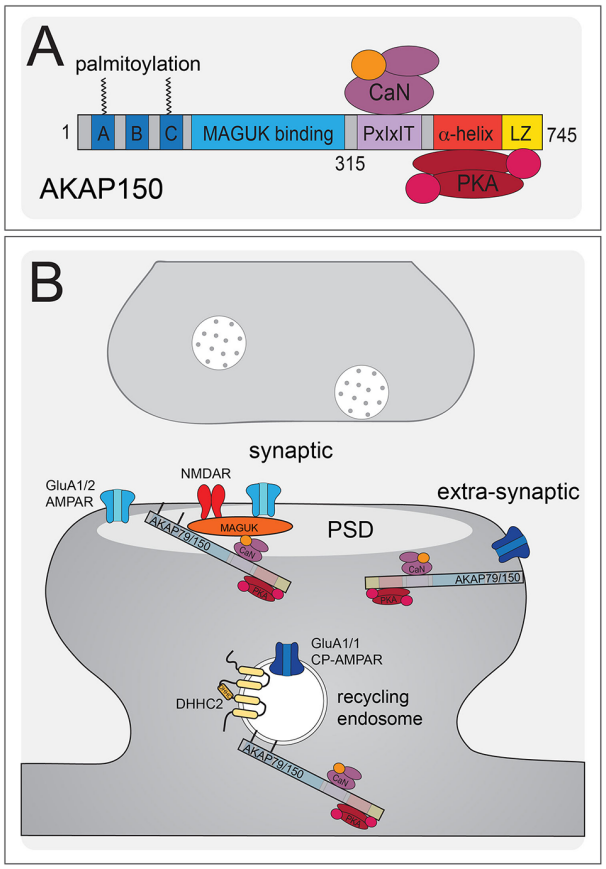

FIGURE 4 | AKAP79/150 localizes bidirectional PKA-CaN signaling to key postsynaptic signaling nodes. **(A)** Schematic of AKAP79/150 highlighting the C-terminal PKA and CaN signaling protein binding partners and anchoring domains, the internal MAGUK binding domain, and the N-terminal polybasic membrane targeting domains (A–C) containing two sites of S-palmitoylation. **(B)** AKAP79/150 is targeted to the PSD, extrasynaptic membrane, and recycling endosome (RE) through protein-protein and membrane lipid interactions that are modulated by S-palmitoylation within the N-terminal polybasic domains. AKAP79/150 anchors the phosphatase CaN and kinase PKA to provide bidirectional signaling in control of AMPARs.

the sites of clathrin-coated pit formation (Spacek and Harris, 1997) and AMPAR internalization (Rácz et al., 2004). Using a cLTD treatment, it was discovered that there is rapid AMPAR endocytosis (Carroll et al., 1999a,b; Beattie et al., 2000; Ehlers, 2000). It was also observed that there is decreased synaptic AMPAR content with *in vivo* LTD induction (Heynen et al., 2000). For NMDAR-dependent AMPAR internalization (like LTD) Ca^{2+} influx and activation of CaN are needed (Beattie et al., 2000; Ehlers, 2000; Zhou et al., 2001). Interestingly, as mentioned above it was recently identified that transient incorporation of CP-AMPARs also occurs during LTD induction downstream of PKA signaling, but these receptors are rapidly removed before the end of the induction stimulus by CaN signaling (Sanderson et al., 2016). This transient CP-AMPAR recruitment is reminiscent of some forms of LTP discussed above; however, the time-scale of removal of the recently recruited CP-AMPAR is different (removal within ∼15–30 min post-LTP induction vs. within 6–15 min during LTD induction).

Though it is widely accepted that AMPARs are removed during LTD, there is no coherent mechanistic model. The activities of PKA, CaMKII, Cyclic Dependent Kinase 5 (CDK5), p38MAPK, and Glycogen Synthase Kinase (GSK3) have all been implicated in LTD (Collingridge et al., 2010; Coultrap et al., 2014). The CTD of GluA2 is phosphorylated at S880 in the PDZ ligand to inhibit GRIP/ABP binding and promote PICK1 binding and disrupting scaffolding interactions with this PDZ ligand can block LTD (Daw et al., 2000; Kim et al., 2001; Seidenman et al., 2003). Accordingly, experiments using GluA1 and GluA2 CTD chimera mice found a requirement for GluA2 CTD but not the GluA1 CTD in LTD (Park et al., 2016). Nonetheless, both GluA2 and GluA2/3 double knockout retain LTD (Meng et al., 2003). In addition, similar to LTP above, single-subunit replacement approaches in a GluA1–3 triple conditional knockout background found that either GluA1 or unedited GluA2-Q alone can support LTD (Granger and Nicoll, 2014b). However, while LTD is normal in complete GluA1 knock-out (Selcher et al., 2012), it is impaired in the GluA1 S845A mutant (Lee et al., 2010). Thus, like AMPAR recruitment in LTP, these studies together indicate that the mechanisms controlling AMPAR removal during LTD can act through multiple subunits. However, none of the above studies specifically examined a role for CP-AMPARs, although the finding that the GluA1 S845A mutant, which lacks extrasynaptic GluA1 homomers in the hippocampus, exhibits impaired LTD suggested their possible involvement (He et al., 2009). This possible involvement of CP-AMPARs in LTD was later confirmed in studies discussed more below characterizing how PKA and CaN signaling organized by the postsynaptic scaffold protein AKAP79/150 regulates CP-AMPARs in LTD as well as LTP (**Figures 4**, **5**).

REGULATION OF CP-AMPAR-MEDIATED PLASTICITY BY AKAP79/150-ANCHORED PKA AND CaN

Regardless of these remaining mechanistic questions regarding GluA1 vs. GluA2 involvement in LTP and LTD, emerging evidence indicates that many of the kinases and phosphatases that regulate GluA1 phosphorylation and AMPAR trafficking, including CaMKII (Thiagarajan et al., 2002, 2005; Groth et al., 2011), PKA (Goel et al., 2011; Diering et al., 2014), and CaN (Kim and Ziff, 2014), play key roles regulating CP-AMPARs to impact LTP, LTD, and homeostatic plasticity (Thiagarajan et al., 2005; Plant et al., 2006; Lu et al., 2007; Yang et al., 2010; Goel et al., 2011; Soares et al., 2013; Kim and Ziff, 2014; Kim et al., 2015; Megill et al., 2015; Woolfrey and Dell'Acqua, 2015; Sanderson et al., 2016). By creating knock-in mice to disrupt PKA (D36, ΔPKA) and CaN (ΔPIX) anchoring to the postsynaptic scaffold protein AKAP79/150 (79 human/150 rodent; *Akap5* gene; **Figure 4A**; **Table 3**), we and others found that AKAP-PKA/CaN signaling bi-directionally regulates GluA1-S845 phosphorylation to control the balance

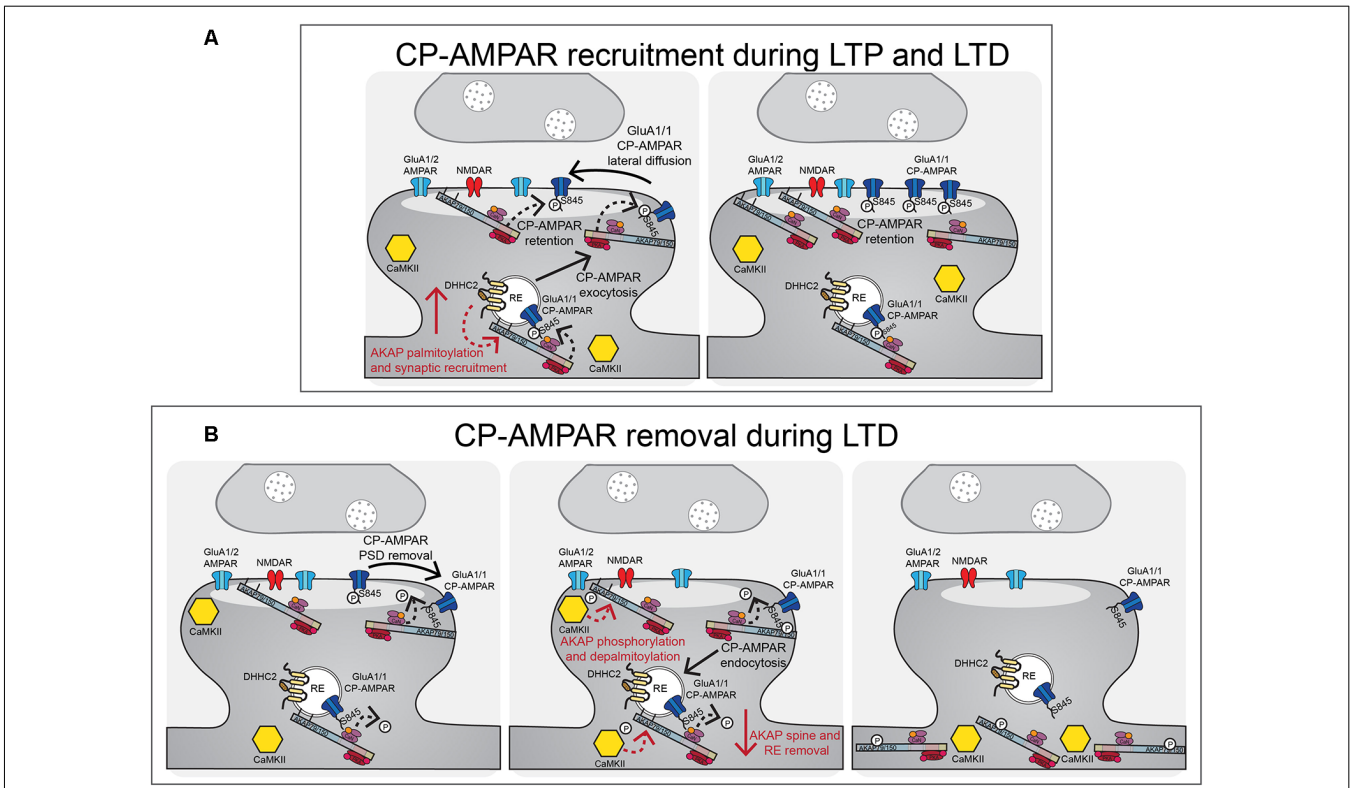

FIGURE 5 | AKAP79/150-anchored PKA and CaN control CP-AMPAR trafficking during LTP and LTD. **(A)** During LTP and LTD, AKAP79/150 is recruited to dendritic spines and recycling endosomes through palmitoylation by DHHC2. AKAP-anchored PKA phosphorylates GluA1 at S845 to promote CP-AMPAR synaptic recruitment during both LTP and LTD. **(B)** During LTD, AKAP-anchored CaN then dephosphorylates GluA1 at S845 resulting in CP-AMPAR removal from the synapse and endocytosis. AKAP79/150 itself is then subsequently removed from spines and recycling endosomes to prevent rephosphorylation of GluA1 by PKA. This AKAP79/150 translocation from the synapse is downstream of CaN-dependent F-actin reorganization and AKAP depalmitoylation that is promoted by CaMKII mediated in part by through phosphorylation of the N-terminal targeting domain.

of CP-AMPAR recruitment/removal at CA1 synapses basally and during LTP/LTD (**Figure 5**; Lu et al., 2007; Sanderson et al., 2012, 2016; Zhang et al., 2013). Because of four S845 phosphorylation sites in a GluA1 homomer (compared to two in a GluA1/2 heteromer), this PKA/CaN metaplasticity appears to be especially key for CP-AMPAR regulation.

PKA phosphorylation of S845 has also been linked to CP-AMPAR synaptic incorporation during homeostatic scaling-up in cultured cortical neurons (Kim and Ziff, 2014; Diering et al., 2014) and in visual cortex in response to light deprivation (Goel et al., 2011), with phospho-deficient S845A knock-in mice exhibiting impaired scaling-up in both systems. Yet inhibition of CaN, which also occurs during neuronal silencing due to decreased Ca^{2+}, is sufficient to increase S845 phosphorylation and induce scaling-up through CP-AMPARs in cortical neurons (Kim and Ziff, 2014). Thus, it may not be the absolute levels but the *balance* of PKA vs. CaN signaling that exerts metaplastic control over not only LTP/LTD but also homeostatic plasticity. Consistent with this idea, using hippocampal neurons cultured from AKAP150 ΔPKA and ΔPIX knock-in mice, we recently demonstrated that AKAP-anchored PKA and CaN also oppose each other to control S845 phosphorylation and CP-AMPAR incorporation during homeostatic scaling-up *in vitro* in hippocampal neuron cultures (Sanderson et al., 2018).

AKAP79/150 is highly enriched in the hippocampus at the PSD with AMPARs (Carr et al., 1992b; Gomez et al., 2002; Lu et al., 2007; Li et al., 2012), in REs (Keith et al., 2012; Woolfrey et al., 2015; Purkey et al., 2018), and in the extrasynaptic plasma membrane (Dell'Acqua et al., 1998). AKAP79/150 is known to bind the kinase PKA (Carr et al., 1992a,b) at the distal C-terminus of the scaffold using a canonical amphipathic α-helix that is also found in other AKAP family members (**Figure 4A**). However, unlike most other AKAPs, AKAP79/150 can also bind the CaN phosphatase catalytic A subunit through a PxIxIT-type docking motif located just N-terminal to the PKA binding site (Coghlan et al., 1995; Dell'Acqua et al., 2002; Oliveria et al., 2007, 2012; Li et al., 2012). Finally, AKAP79/150 interacts with PKC (Klauck et al., 1996; Faux et al., 1999), which is activated by Ca^{2+} and diacylglycerol (DAG), near the N-terminus through an inhibitory pseudo-substrate-like motif that is regulated by Ca^{2+}-calmodulin binding (Faux and Scott, 1997). This multivalent scaffolding is particularly important when considering the synaptic signaling that requires bidirectional kinase and phosphatase signaling to control the phosphorylation state of AMPARs and other synaptic proteins during plasticity.

The N-terminus of the AKAP79/150 protein participates in many different cellular activities in addition to PKC anchoring (Klauck et al., 1996; Dell'Acqua et al., 1998; Gomez et al., 2002; Gorski et al., 2005; Tavalin, 2008), including most importantly targeting to the plasma membrane. Immunocytochemistry for AKAP150 in hippocampal neurons shows a clear association with the somatodendritic plasma membrane with notable enrichment in dendritic spines. Which begs the question: how is AKAP79/150 itself targeted to the synapses? Previous studies showed that within the N-terminus exist three membrane targeting polybasic domains (A, B, and C; Dell'Acqua et al., 1998), two of which also contain conserved palmitoylation sites that will be discussed further below (Delint-Ramirez et al., 2011; Keith et al., 2012; Woolfrey and Dell'Acqua, 2015; Woolfrey et al., 2018). AKAP79/150 interacts with the plasma membrane directly through electrostatic interactions of the three polybasic domains with the acidic phospholipid phosphatidylinositol 4,5-bisphosphate (PIP_2; Dell'Acqua et al., 1998). AKAP79/150 can also bind N-cadherin (a transsynaptic cell adhesion molecule) and the actin cytoskeleton (F-actin) *via* these domains (Dell'Acqua et al., 2002; Gomez et al., 2002; Gorski et al., 2005). AKAP79/150 is further targeted to postsynaptic glutamate receptor signaling complexes in the PSD through its internal MAGUK binding domain (Colledge et al., 2000; Bhattacharyya et al., 2009; Nikandrova et al., 2010). The MAGUK family of proteins, specifically PSD-95 and SAP97 (Colledge et al., 2000; Robertson et al., 2009), interact with AKAP79/150 by way of their C-terminal SH3 and GK domains (Colledge et al., 2000) and these interactions allow assembly of large signaling complexes by bringing the AKAP near AMPARs and NMDARs in the PSD as well as other subcellular compartments (discussed more below). Accordingly, AKAP79/150 can control synaptic AMPAR content both through acting as structural protein and through anchored PKA and CaN signaling (Robertson et al., 2009; Sanderson et al., 2012, 2016).

The first evidence of AKAP-anchored PKA influencing AMPAR-mediated transmission came from pharmacological studies utilizing a peptide Ht31 that interferes with AKAP-PKA binding (Carr et al., 1992a), revealing that blocking this interaction resulted in decreased synaptic and extrasynaptic AMPAR currents (Rosenmund et al., 1994). Later studies found that AKAP79/150 is the primary AKAP targeting PKA to postsynaptic spines and the PSD and that AKAP-anchored CaN signaling was responsible for the decreased AMPAR activity observed when PKA anchoring was disrupted (Dell'Acqua et al., 2002; Tavalin et al., 2002; Hoshi et al., 2005). AKAP79/150 can interact indirectly with GluA1-AMPARs *via* SAP97 and also *via* PSD-95 and TARPs (Colledge et al., 2000; Tavalin et al., 2002; Bhattacharyya et al., 2009). Importantly, several studies have also shown that AKAP79/150-anchoring of PKA promotes phosphorylation of S845 on GluA1 to impact the regulation of LTP, LTD, and homeostatic plasticity by CP-AMPARs (Lu et al., 2007, 2008; Tunquist et al., 2008; Weisenhaus et al., 2010; Zhang et al., 2013; Diering et al., 2014; Sanderson et al., 2016, 2018). Additional studies in heterologous systems found that assembly and trafficking of CP-AMPARs can be further regulated by AKAP-anchored PKC through phosphorylation of GluA1 S831; however, it remains to be determined whether these PKC mechanisms also operate *in vivo* to control plasticity at CA1 synapses (Tavalin, 2008; Summers et al., 2019). Interestingly, as discussed in more detail below, during both LTP and LTD, AKAP79/150 facilitates CP-AMPAR recruitment to and removal from CA1 synapses *via* its anchoring of PKA and CaN, respectively (Bhattacharyya et al., 2009; Jurado et al., 2010; Sanderson et al., 2012, 2016, 2018). In line with their clear importance in controlling neuronal functions, AKAP79/150 and other AKAPs have been implicated in diseases such as seizures, addiction, pain, and neurodegeneration like AD and Parkinson's disease (Wild and Dell'Acqua, 2018).

A number of mutant mouse models have been used to understand the functional implications of manipulating AKAP79/150 anchoring at the synapse (**Table 3**). As explained below, the AKAP150 total knockout in general exhibits surprisingly mild phenotypes, especially with respect to synaptic function given the deletion of such an important signaling hub. It is a notable caveat that compensation can occur especially when knocking out a protein from birth. For example, other AKAPs, such as AKAP250/Gravin (Havekes et al., 2012), that also anchor a similar set of signaling molecules could compensate for a total AKAP150 knockout. Further, it can be complicated figuring out what particular component of the scaffold is responsible for what phenotypic expression due to the multivalent capacity of the protein, especially considering that some of these components functionally oppose each other (i.e., PKA and CaN). So, to circumvent these issues, our laboratory and others have studied the importance of AKAP79/150 PKA and CaN anchoring in hippocampal neurons using knockdown/replacement and knock-in mutations to specifically alter the different enzyme anchoring sites (**Table 3**).

AKAP150-PKA Binding Deficient Mutants ΔPKA and D36

To study AKAP150-PKA uncoupling, specific mutations that perturb AKAP-PKA binding through mutating the amphipathic α-helix that PKA-RII binds to on the AKAP were generated in two different knock-in mouse models, D36 and ΔPKA (**Table 3**). The D36 AKAP150 PKA-binding mutant was developed first by truncating the last 36 amino acids of the C-terminal domain of the AKAP. D36 mice were found to have normal basal excitatory transmission and S845 phosphorylation (in 2, 4–5 and 7–12 week old animals) but impaired activity-induced phosphorylation of GluA1 S845 (Lu et al., 2007, 2008). LTP was normal in ∼4 week-old D36 animals when LTP induced with 1 × 100 Hz stimulation was found to be insensitive to inhibitors of PKA and CP-AMPARs, but impaired at ∼8 weeks of age when this LTP was prevented by PKA and CP-AMPAR inhibitors (Lu et al., 2007). Furthermore, LTD was impaired in 2-week-old D36 animals but depotentiation of prior LTP was normal (Lu et al., 2008). These mice also exhibited impairment in the reversal-learning phase in an operant conditioning task (Weisenhaus et al., 2010). Interestingly, in parallel analyses, complete AKAP150 KO mice exhibited no alterations in LTD in juveniles, LTP in juveniles or adults, or operant

TABLE 3 | AKAP150 transgenic mouse model studies.

AKAP150 mutation	Phenotype	References
Knockout (two different lines)	**Basal**	Tunquist et al. (2008)
	2 weeks normal or slightly enhanced	
	8 weeks normal	
	LTP (100 Hz, 1 s)	
	8 weeks normal	
	LTD (1 Hz, 15 min)	
	2 weeks normal	
	8–16 weeks impaired (NMDAR vs. mGluR? Not determined)	Weisenhaus et al. (2010)
	Behavior	
	Modest deficits in spatial memory	
	Normal reversal learning	
	Impaired cerebellar behaviors	
	Reduced pilocarpine seizures	
	PTT-LTP (5 Hz, 3 min in presence of a β-adrenergic receptor agonist)	Zhang et al. (2013)
	CP-AMPAR dependent, 6–8 weeks impaired	
D36 (PKA anchoring-deficient)	**Basal**	Lu et al. (2007)
	Normal	
	LTP (100 Hz, 1 s)	
	CP-AMPAR and PKA independent, 4–5 weeks normal	Lu et al. (2008)
	CP-AMPAR and PKA dependent, 8 weeks impaired	
	LTD (1 Hz, 15 min)	Weisenhaus et al. (2010)
	2 weeks, impaired (retain ∼10%)	
	Depotentiation (100 Hz, 1 s and 5 min later 1 Hz, 15 min)	
	Normal	
	Behavior	
	Impaired reversal learning	
	Normal spatial learning, working memory, and open field behaviors	
	PTT-LTP (5 Hz, 3 min in presence of a β-adrenergic receptor agonist)	Zhang et al. (2013)
	6–8 weeks partially impaired	
ΔPKA (PKA anchoring-deficient)	**Basal**	Sanderson et al. (2016)
	Normal	
	LTP (100 Hz, 1 s)	
	2 weeks normal magnitude (but unlike WT is not CP-AMPAR dependent)	
	LTD (1 Hz, 15 min)	
	CP-AMPAR dependent, 2 weeks impaired (retain ∼10%)	
ΔPIX (CaN anchoring-deficient)	**Basal**	Sanderson et al. (2012)
	Normal but increased CP-AMPARs	
	LTP (100 Hz, 1 s)	
	2–3 weeks enhanced due to increased CP-AMPAR synaptic recruitment, but 50 Hz, 2 s normal	
	Depotentiation (100 Hz, 1 s and 30 min later 1 Hz, 15 min)	
	Impaired: de-potentiates to a similar amount but does not reach WT baseline levels	
	LTD (Fields 1 Hz, 15 min or Whole-cell 1 Hz, 6 min paired at −30 mV)	
	2 weeks impaired due to decreased CP-AMPAR synaptic removal (1 Hz PP 900 pulses, 50 ms interval LTD and 10 Hz transient depression also impaired)	
CS (palmitoylation-deficient)	**Basal**	Purkey et al. (2018)
	Normal but increased CP-AMPARs	
	LTP (Fields 100 Hz, 1 s)	
	2–3 weeks impaired	
	LTP (Whole-cell 2 × 100 Hz, 0 mV)	
	CP-AMPAR dependent, 2–3 weeks impaired	
	LTP (Whole-cell 3 Hz, 90 s, 0 mV)	
	CP-AMPAR independent, 2–3 weeks normal	
	LTD (Fields 1 Hz, 15 min)	
	2 weeks normal	
	De-depression (Fields 1 Hz LTD, 15 min and 15 min later 100 Hz, 1 s LTP)	
	CP-AMPAR dependent, 2 weeks enhanced	

learning (Weisenhaus et al., 2010). However, in another study, an independent AKAP150 KO line exhibited reduced basal GluA1 S845 phosphorylation, impaired LTD (but normal LTP) in adult animals, and mild spatial learning impairment in the Morris water maze (**Table 3,** Tunquist et al., 2008).

The D36 model is more specific than complete loss of all AKAP150 functions in KO animals but results in deletion of not only the PKA anchoring site but also of a modified leucine-zipper (LZ) motif that helps recruit the AKAP to L-type Ca^{2+} channel signaling complexes (Oliveria et al.,

2007; Murphy et al., 2019). To circumvent any issues with deleting this LZ motif, our laboratory independently developed the PKA anchoring-deficient mutant AKAP150ΔPKA that just removes 10 amino acids (709–718) from the N-terminal portion of the amphipathic α-helix PKA-RII binding site (**Table 3,** Murphy et al., 2014; Sanderson et al., 2016). Overall, phenotypes for the D36 and ΔPKA animals are very similar. ΔPKA animals have normal basal CA1 synaptic transmission (both excitatory and inhibitory) at 2–3 weeks of age but decreased GluA1 S845 phosphorylation basally. Similar to D36, 2 week-old ΔPKA animals retained only ∼10% of CA1 LTD expression, a deficit which was subsequently shown to be due to a failure, compared to WT, to transiently recruit CP-AMPARs to synapses during the 1 Hz induction stimulus, as assessed by both rectification measurements and use of the CP-AMPAR antagonists NASPM and IEM1460. Yet interestingly, 1 × 100 Hz LTP expression in 2 week-old ΔPKA animals was normal but insensitive to IEM1460, unlike WT LTP that was sensitive to IEM1460 at this age. Importantly, D36 and complete AKAP150 KO mice were also found to be deficient in PTT-LTP at CA1 synapses, which requires β-adrenergic-cAMP-PKA signaling and CP-AMPARs (Zhang et al., 2013). Overall, these AKAP150 KO, ΔPKA and D36 mouse studies indicate that AKAP-anchored PKA promotes GluA1 S845 phosphorylation and CP-AMPAR recruitment both during LTP and LTD (**Figure 5**).

AKAP150-CaN Binding Deficient Mutant ΔPIX

To study the disruption of AKAP150-CaN anchoring, our laboratory generated a mutant mouse model that deletes seven amino acids (655-PIAIIIT-661), which we call ΔPIX, containing the CaN docking PxIxIT motif (**Table 3**). AKAP150ΔPIX mice at 2–3 weeks of age exhibit overall normal basal synaptic strength at CA1 synapses but with enhanced basal GluA1 S845 phosphorylation (Sanderson et al., 2012). Mice with the ΔPIX mutation at 2–3 weeks of age also exhibited impaired NMDAR-dependent LTD and enhanced 1 × 100 Hz LTP. This LTD impairment in ΔPIX mice was associated with impaired dephosphorylation of GluA-S845 and a lack of removal of GluA1 and AKAP150 from the PSD following LTD. Furthermore, ΔPIX animals showed enhanced basal activity of CP-AMPARs at CA1 synapses that acted to both inhibit LTD, due to impaired removal, and facilitate enhanced LTP, due to additional recruitment. Thus, AKAP-anchored CaN appears to be important for restricting both basal and plasticity-induced synaptic incorporation of CP-AMPARs by opposing PKA-mediated phosphorylation of S845 and is essential for dephosphorylation and the removal of CP-AMPARs that are transiently recruited to CA1 synapses during LTD (**Figure 5**; Sanderson et al., 2012, 2016).

AKAP79/150 Palmitoylation and Postsynaptic Trafficking During LTP and LTD

AKAP79/150 is targeted to dendritic spines where it is present in both the PSD and extrasynaptic plasma membrane (Carr et al., 1992b; Colledge et al., 2000; Gomez et al., 2002; Tunquist et al., 2008; Weisenhaus et al., 2010), but we more recently discovered that it is also localized to dendritic REs (Keith et al., 2012; Woolfrey et al., 2015). Importantly, as discussed above, PKA/CaN regulation of AMPAR phosphorylation is thought to control recruitment/removal of synaptic AMPARs during LTP/LTD in part through coordinately regulating RE exocytosis and endocytosis at the extrasynaptic membrane to provide the reserve pool of extrasynaptic receptors available for lateral exchange in and out of the PSD (Beattie et al., 2000; Ehlers, 2000; Esteban et al., 2003; Park et al., 2004; Brown et al., 2005; Oh et al., 2006; Ehlers et al., 2007; Petrini et al., 2009; Opazo et al., 2010; Opazo and Choquet, 2011; Fernández-Monreal et al., 2012). While our previous work demonstrated AKAP79/150 targeting to the plasma membrane, in general, is mediated by binding of its three N-terminal polybasic domains (A, B, C) to acidic lipids (i.e., PI-4, 5-P_2) and cortical F-actin (Dell'Acqua et al., 1998; Gomez et al., 2002; Horne and Dell'Acqua, 2007), our recent work found that AKAP targeting to REs requires additional S-palmitoylation on two Cys residues (C36 and C129 human/123 mouse) in this N-terminal domain (**Figures 4A,B**; Keith et al., 2012; Woolfrey et al., 2015).

S-palmitoylation is catalyzed by a family of DHHC palmitoyl acyltransferases (PATs) that covalently attach the C-16 fatty acid palmitate to Cys residues *via* a thioester linkage (Fukata and Fukata, 2010; Greaves and Chamberlain, 2011). In contrast to other lipidations like myristoylation and prenylation, palmitoylation is reversible, with palmitate removal being catalyzed by thioesterases. Of note, the palmitoylation levels of AKAP150 and other synaptic proteins can be affected by seizures and anticonvulsants (Kang et al., 2008; Keith et al., 2012; Kay et al., 2015), and several DHHC PATs have been linked to nervous system disorders, including Huntington's, schizophrenia, and X-linked intellectual disability (Huang et al., 2004; Mukai et al., 2004, 2008; Mansouri et al., 2005; Fukata and Fukata, 2010). Palmitoylation frequently directs proteins to cholesterol-rich, detergent-resistant lipid-raft membrane domains (Fukata and Fukata, 2010; Greaves and Chamberlain, 2011). Notably, the PSD is biochemically defined by its detergent-insolubility and many PSD proteins are palmitoylated and show lipid-raft association (Fukata and Fukata, 2010), including the central PSD scaffold and AKAP binding partner PSD-95 (Topinka and Bredt, 1998; Craven et al., 1999; Colledge et al., 2000; Robertson et al., 2009). Accordingly, our recent work (Purkey et al., 2018) indicates that AKAP palmitoylation increases its association with the PSD and is required for CP-AMPAR synaptic incorporation during LTP (**Figure 5**), as discussed in more detail below.

Palmitoylation of AKAP79/150, unlike for PSD-95, is not a requirement for general plasma membrane targeting, because AKAP79/150 CS mutants that cannot be palmitoylated are still targeted to the plasma membrane. Further work by our group identified DHHC2 as the PAT responsible for AKAP79/150 palmitoylation (Woolfrey et al., 2015) and found that palmitoylation specifically targets AKAP79/150 to the RE

and lipid rafts in the core PSD (**Figure 4B**; Delint-Ramirez et al., 2011; Keith et al., 2012; Woolfrey et al., 2015; Purkey et al., 2018). Importantly, we also found that cLTP increases and NMDA-cLTD decreases AKAP palmitoylation and spine targeting in cultured neurons (Keith et al., 2012), indicating that AKAP palmitoylation is bi-directionally regulated by neuronal activity to modulate its synaptic localization (**Figure 5**). Palmitoylation-mediated recruitment of additional AKAP79 to dendritic spines following cLTP was subsequently found to require DHHC2 expression (Woolfrey et al., 2015), while depalmitoylation-mediated removal of AKAP79 from dendritic spines following cLTD was found to require CaMKII activity, perhaps helping explain recent findings that CaMKII not only mediates LTP but is also required for LTD (Coultrap et al., 2014; Woolfrey et al., 2018). Interestingly, DHHC2 is specifically localized in REs and also palmitoylates PSD-95 to control its PSD clustering (Greaves et al., 2011; Fukata et al., 2013; Woolfrey et al., 2015). Yet, DHHC2 knock-down closely phenocopied that of the AKAP79CS mutant with respect to altered cLTP regulation of RE exocytosis, AKAP spine localization, and AMPAR potentiation, with these phenotypes being rescued by a constitutively lipidated/depalmitoylation resistant N-myristoylated-AKAP79 mutant (Woolfrey et al., 2015).

AKAP150 Palmitoylation-Deficient CS Mutant Knock-In Mice

Functionally, either acute overexpression of AKAP79C36, 129S in neuronal cultures or chronic knock-in of the palmitoylation-deficient AKAP150 CS mutation in mice (**Table 3**) resulted in enhanced basal AMPAR transmission in hippocampal neurons measured by recording of miniature excitatory postsynaptic currents (mEPSCs; Keith et al., 2012; Purkey et al., 2018), thus indicating that AKAP palmitoylation is important for its function as an AMPAR regulator. The enhanced basal AMPAR transmission seen for the AKAP CS mutant in both culture and at CA1 synapses *ex vivo* was associated with a basal increase in synaptic CP-AMPAR activity (Keith et al., 2012; Purkey et al., 2018), which is reminiscent of CaN-anchoring deficient ΔPIX mutant (Sanderson et al., 2012, 2018). However, unlike ΔPIX mice that exhibited impaired LTD and enhanced 1 × 100 Hz HFS LTP, 2–3 week-old AKAP CS mice exhibited normal LTD and selective impairment in CP-AMPAR-dependent LTP induced with 100 Hz HFS but not CP-AMPAR-independent LTP induced with 3 Hz, 90 s 0 mV pairing (Purkey et al., 2018). Thus, in contrast to ΔPIX mice, in AKAP CS mice the basal presence of CP-AMPARs at CA1 synapses appears to be interfering with additional CP-AMPAR recruitment in response to a weaker, brief LTP induction stimulus but not their removal during LTD or their replacement with GluA2-containing AMPARs in response to a stronger, more prolonged LTP induction stimulus. Accordingly, prior induction of LTD in AKAP CS mice to remove CP-AMPARs was able to restore CP-AMPAR synaptic recruitment in response to subsequent induction of LTP/de-depression with brief 1 × 100 Hz HFS (Purkey et al., 2018). Overall, AKAP79/150 palmitoylation appears to regulate a number of important aspects of neuronal function that impact both basal transmission and activity-induced plasticity, including most notably CP-AMPAR synaptic recruitment.

CONCLUSIONS

Overall, by avoiding complications associated with mutating the AMPARs themselves and instead focusing on manipulating upstream kinase/phosphatase regulatory mechanisms, the knock-in mouse studies described above characterizing the roles of AKAP-anchored PKA, CaN, and S-palmitoylation in LTP/LTD have provided a substantial amount of additional evidence for the importance of GluA1 S845 phosphorylation and CP-AMPARs in regulating hippocampal synaptic plasticity. In addition, other studies mentioned above have implicated similar AKAP-PKA/CaN bidirectional control of GluA1 S845 phosphorylation in regulation of CP-AMPAR synaptic recruitment during homeostatic potentiation in cultured hippocampal and cortical neurons. However, a number of important questions remain to be addressed with respect to the CP-AMPAR regulation of synaptic plasticity. In particular, we do not understand the specific route that GluA1 CP-AMPARs travel along on their way to the synapse in terms of trafficking through intracellular recycling stores and the extrasynaptic plasma membrane. While there is evidence that PKA phosphorylation of GluA1 S845 helps prevent endo-lysosomal degradation of GluA1, promotes recycling to the plasma membrane, and stabilizes CP-AMPARs in the extrasynaptic membrane (Ehlers, 2000; Oh et al., 2006; He et al., 2009; Yang et al., 2010; Fernández-Monreal et al., 2012), we still do not know where or how these GluA1 homomeric CP-AMPARs are assembled. Intriguingly, a recent single-molecule trafficking study reported that GluA1 and GluA2 subunit monomers and dimers rapidly exchange (100–200 ms) in and out of tetrameric AMPAR assemblies at the plasma membrane and laterally diffuse in and out of the synapse more readily than tetramers (Morise et al., 2019). Thus, GluA1 homomers could be rapidly assembled from monomers and dimers in response to phosphorylation during plasticity induction, either directly in the synapse or in other compartments *via* subunit exchange. In this regard, the role of AKAP79/150-anchored PKC signaling in CP-AMPAR regulation during LTP perhaps warrants additional investigation, as a recent study indicates that AKAP-PKC mediated phosphorylation of S831 can promote GluA1 homomer formation in a heterologous expression system (Summers et al., 2019). In addition, we do not know whether these AKAP-mediated regulatory mechanisms also control CP-AMPAR mediated plasticity in the hippocampus during pathophysiological states, such as during ischemia and with amyloid-beta exposure during Alzheimer's disease (Liu and Zukin, 2007; Whitcomb et al., 2015), or in other brain regions where changes in CP-AMPAR synaptic incorporation have been observed, such as in the nucleus accumbens and ventral tegmental area in drug addiction models and in the basolateral amygdala in fear extinction learning (Clem and Huganir, 2010; Wolf and Tseng, 2012). Finally, we do not know what specific downstream signaling pathways are being engaged by CP-AMPAR synaptic Ca^{2+} influx to control LTP vs. LTD

and synaptic metaplasticity in the hippocampus or these other brain regions. Thus, a great deal of interesting and potentially impactful research awaits the field in the future.

AUTHOR CONTRIBUTIONS

AP and MD'A wrote this review article and prepared the figures and tables.

FUNDING

American Heart Association (AHA; 16PRE29880006) and NIH/National Institute of Neurological Disorders and Stroke (NINDS; F31NS096815) predoctoral fellowships to AP and NIH/NINDS grant R01NS040701 to MD'A supported this work. The contents are the authors' sole responsibility and do not necessarily represent official AHA or NIH views.

REFERENCES

Adesnik, H., and Nicoll, R. A. (2007). Conservation of glutamate receptor 2-containing AMPA receptors during long-term potentiation. *J. Neurosci.* 27, 4598–4602. doi: 10.1523/JNEUROSCI.0325-07.2007

Ahmad, M., Polepalli, J. S., Goswami, D., Yang, X., Kaeser-Woo, Y. J., Sudhof, T. C., et al. (2012). Postsynaptic complexin controls AMPA receptor exocytosis during LTP. *Neuron* 73, 260–267. doi: 10.1016/j.neuron.2011.11.020

Ancona Esselmann, S. G., Diaz-Alonso, J., Levy, J. M., Bemben, M. A., and Nicoll, R. A. (2017). Synaptic homeostasis requires the membrane-proximal carboxy tail of GluA2. *Proc. Natl. Acad. Sci. U S A* 114, 13266–13271. doi: 10.1073/pnas.1716022114

Aoto, J., Nam, C. I., Poon, M. M., Ting, P., and Chen, L. (2008). Synaptic signaling by all-trans retinoic acid in homeostatic synaptic plasticity. *Neuron* 60, 308–320. doi: 10.1016/j.neuron.2008.08.012

Araki, Y., Zeng, M., Zhang, M., and Huganir, R. L. (2015). Rapid dispersion of SynGAP from synaptic spines triggers AMPA receptor insertion and spine enlargement during LTP. *Neuron* 85, 173–189. doi: 10.1016/j.neuron.2014.12.023

Banke, T. G., Bowie, D., Lee, H., Huganir, R. L., Schousboe, A., and Traynelis, S. F. (2000). Control of GluR1 AMPA receptor function by cAMP-dependent protein kinase. *J. Neurosci.* 20, 89–102. doi: 10.1523/jneurosci.20-01-00089.2000

Barria, A., Muller, D., Derkach, V., Griffith, L. C., and Soderling, T. R. (1997). Regulatory phosphorylation of AMPA-type glutamate receptors by CaM-KII during long-term potentiation. *Science* 276, 2042–2045. doi: 10.1126/science.276.5321.2042

Beattie, E. C., Carroll, R. C., Yu, X., Morishita, W., Yasuda, H., von Zastrow, M., et al. (2000). Regulation of AMPA receptor endocytosis by a signaling mechanism shared with LTD. *Nat. Neurosci.* 3, 1291–1300. doi: 10.1038/81823

Benke, T., and Traynelis, S. F. (2019). AMPA-type glutamate receptor conductance changes and plasticity: still a lot of noise. *Neurochem. Res.* 44, 539–548. doi: 10.1007/s11064-018-2491-1

Bhattacharyya, S., Biou, V., Xu, W., Schluter, O., and Malenka, R. C. (2009). A critical role for PSD-95/AKAP interactions in endocytosis of synaptic AMPA receptors. *Nat. Neurosci.* 12, 172–181. doi: 10.1038/nn.2249

Biederer, T., Kaeser, P. S., and Blanpied, T. A. (2017). Transcellular nanoalignment of synaptic function. *Neuron* 96, 680–696. doi: 10.1016/j.neuron.2017.10.006

Blanpied, T. A., Scott, D. B., and Ehlers, M. D. (2002). Dynamics and regulation of clathrin coats at specialized endocytic zones of dendrites and spines. *Neuron* 36, 435–449. doi: 10.1016/s0896-6273(02)00979-0

Blaschke, M., Keller, B. U., Rivosecchi, R., Hollmann, M., Heinemann, S., and Konnerth, A. (1993). A single amino acid determines the subunit-specific spider toxin block of α-amino-3-hydroxy-5-methylisoxazole-4-propionate/kainate receptor channels. *Proc. Natl. Acad. Sci. U S A* 90, 6528–6532. doi: 10.1073/pnas.90.14.6528

Boehm, J., Kang, M. G., Johnson, R. C., Esteban, J., Huganir, R. L., and Malinow, R. (2006). Synaptic incorporation of AMPA receptors during LTP is controlled by a PKC phosphorylation site on GluR1. *Neuron* 51, 213–225. doi: 10.1016/j.neuron.2006.06.013

Borgdorff, A. J., and Choquet, D. (2002). Regulation of AMPA receptor lateral movements. *Nature* 417, 649–653. doi: 10.1038/nature00780

Bowie, D., and Mayer, M. L. (1995). Inward rectification of both AMPA and kainate subtype glutamate receptors generated by polyamine-mediated ion channel block. *Neuron* 15, 453–462. doi: 10.1016/0896-6273(95)90049-7

Brown, T. C., Tran, I. C., Backos, D. S., and Esteban, J. A. (2005). NMDA receptor-dependent activation of the small GTPase Rab5 drives the removal of synaptic AMPA receptors during hippocampal LTD. *Neuron* 45, 81–94. doi: 10.1016/j.neuron.2004.12.023

Buonarati, O. R., Hammes, E. A., Watson, J. F., Greger, I. H., and Hell, J. W. (2019). Mechanisms of postsynaptic localization of AMPA-type glutamate receptors and their regulation during long-term potentiation. *Sci. Signal.* 12:eaar6889. doi: 10.1126/scisignal.aar6889

Carr, D. W., Hausken, Z. E., Fraser, I. D., Stofko-Hahn, R. E., and Scott, J. D. (1992a). Association of the type II cAMP-dependent protein kinase with a human thyroid RII-anchoring protein. Cloning and characterization of the RII-binding domain. *J. Biol. Chem.* 267, 13376–13382.

Carr, D. W., Stofko-Hahn, R. E., Fraser, I. D., Cone, R. D., and Scott, J. D. (1992b). Localization of the cAMP-dependent protein kinase to the postsynaptic densities by A-kinase anchoring proteins. Characterization of AKAP 79. *J. Biol. Chem.* 267, 16816–16823.

Carroll, R. C., Beattie, E. C., Xia, H., Luscher, C., Altschuler, Y., Nicoll, R. A., et al. (1999a). Dynamin-dependent endocytosis of ionotropic glutamate receptors. *Proc. Natl. Acad. Sci. U S A* 96, 14112–14117. doi: 10.1073/pnas.96.24.14112

Carroll, R. C., Lissin, D. V., von Zastrow, M., Nicoll, R. A., and Malenka, R. C. (1999b). Rapid redistribution of glutamate receptors contributes to long-term depression in hippocampal cultures. *Nat. Neurosci.* 2, 454–460. doi: 10.1038/8123

Chen, L., Lau, A. G., and Sarti, F. (2013). Synaptic retinoic acid signaling and homeostatic synaptic plasticity. *Neuropharmacology* 78, 3–12. doi: 10.1016/j.neuropharm.2012.12.004

Chen, X., Levy, J. M., Hou, A., Winters, C., Azzam, R., Sousa, A. A., et al. (2015). PSD-95 family MAGUKs are essential for anchoring AMPA and NMDA receptor complexes at the postsynaptic density. *Proc. Natl. Acad. Sci. U S A* 112, E6983–E6992. doi: 10.1073/pnas.1517045112

Chen, H., Tang, A. H., and Blanpied, T. A. (2018). Subsynaptic spatial organization as a regulator of synaptic strength and plasticity. *Curr. Opin. Neurobiol.* 51, 147–153. doi: 10.1016/j.conb.2018.05.004

Chen, X., Vinade, L., Leapman, R. D., Petersen, J. D., Nakagawa, T., Phillips, T. M., et al. (2005). Mass of the postsynaptic density and enumeration of three key molecules. *Proc. Natl. Acad. Sci. U S A* 102, 11551–11556. doi: 10.1073/pnas.0505359102

Cho, K. O., Hunt, C. A., and Kennedy, M. B. (1992). The rat brain postsynaptic density fraction contains a homolog of the *Drosophila* discs-large tumor suppressor protein. *Neuron* 9, 929–942. doi: 10.1016/0896-6273(92)90245-9

Choquet, D. (2018). Linking nanoscale dynamics of ampa receptor organization to plasticity of excitatory synapses and learning. *J. Neurosci.* 38, 9318–9329. doi: 10.1523/jneurosci.2119-18.2018

Chung, H. J., Xia, J., Scannevin, R. H., Zhang, X., and Huganir, R. L. (2000). Phosphorylation of the AMPA receptor subunit GluR2 differentially regulates its interaction with PDZ domain-containing proteins. *J. Neurosci.* 20, 7258–7267. doi: 10.1523/jneurosci.20-19-07258.2000

Clem, R. L., and Huganir, R. L. (2010). Calcium-permeable AMPA receptor dynamics mediate fear memory erasure. *Science* 330, 1108–1112. doi: 10.1126/science.1195298

Coghlan, V. M., Perrino, B. A., Howard, M., Langeberg, L. K., Hicks, J. B., Gallatin, W. M., et al. (1995). Association of protein kinase A and protein

phosphatase 2B with a common anchoring protein. *Science* 267, 108–111. doi: 10.1126/science.7528941

Colledge, M., Dean, R. A., Scott, G. K., Langeberg, L. K., Huganir, R. L., and Scott, J. D. (2000). Targeting of PKA to glutamate receptors through a MAGUK-AKAP complex. *Neuron* 27, 107–119. doi: 10.1016/s0896-6273(00)00013-1

Collingridge, G. L., Peineau, S., Howland, J. G., and Wang, Y. T. (2010). Long-term depression in the CNS. *Nat. Rev. Neurosci.* 11, 459–473. doi: 10.1038/nrn2867

Coultrap, S. J., Freund, R. K., O'Leary, H., Sanderson, J. L., Roche, K. W., Dell'Acqua, M. L., et al. (2014). Autonomous CaMKII mediates both LTP and LTD using a mechanism for differential substrate site selection. *Cell Rep.* 6, 431–437. doi: 10.1016/j.celrep.2014.01.005

Craven, S. E., El-Husseini, A. E., and Bredt, D. S. (1999). Synaptic targeting of the postsynaptic density protein PSD-95 mediated by lipid and protein motifs. *Neuron* 22, 497–509. doi: 10.1016/s0896-6273(00)80705-9

Cull-Candy, S., Kelly, L., and Farrant, M. (2006). Regulation of $Ca2^{+}$-permeable AMPA receptors: synaptic plasticity and beyond. *Curr. Opin. Neurobiol.* 16, 288–297. doi: 10.1016/j.conb.2006.05.012

Daw, M. I., Chittajallu, R., Bortolotto, Z. A., Dev, K. K., Duprat, F., Henley, J. M., et al. (2000). PDZ proteins interacting with C-terminal GluR2/3 are involved in a PKC-dependent regulation of AMPA receptors at hippocampal synapses. *Neuron* 28, 873–886. doi: 10.1016/s0896-6273(00)00160-4

Delint-Ramirez, I., Willoughby, D., Hammond, G. R., Ayling, L. J., and Cooper, D. M. (2011). Palmitoylation targets AKAP79 protein to lipid rafts and promotes its regulation of calcium-sensitive adenylyl cyclase type 8. *J. Biol. Chem.* 286, 32962–32975. doi: 10.1074/jbc.M111.243899

Dell'Acqua, M. L., Dodge, K. L., Tavalin, S. J., and Scott, J. D. (2002). Mapping the protein phosphatase-2B anchoring site on AKAP79. Binding and inhibition of phosphatase activity are mediated by residues 315–360. *J. Biol. Chem.* 277, 48796–48802. doi: 10.1074/jbc.m207833200

Dell'Acqua, M. L., Faux, M. C., Thorburn, J., Thorburn, A., and Scott, J. D. (1998). Membrane-targeting sequences on AKAP79 bind phosphatidylinositol-4,5-bisphosphate. *EMBO J.* 17, 2246–2260. doi: 10.1093/emboj/17.8.2246

Derkach, V. A., Oh, M. C., Guire, E. S., and Soderling, T. R. (2007). Regulatory mechanisms of AMPA receptors in synaptic plasticity. *Nat. Rev. Neurosci.* 8, 101–113. doi: 10.1038/nrn2055

Dev, K. K., Nakajima, Y., Kitano, J., Braithwaite, S. P., Henley, J. M., and Nakanishi, S. (2000). PICK1 interacts with and regulates PKC phosphorylation of mGLUR7. *J. Neurosci.* 20, 7252–7257. doi: 10.1523/jneurosci.20-19-07252.2000

Díaz-Alonso, J., Sun, Y. J., Granger, A. J., Levy, J. M., Blankenship, S. M., and Nicoll, R. A. (2017). Subunit-specific role for the amino-terminal domain of AMPA receptors in synaptic targeting. *Proc. Natl. Acad. Sci. U S A* 114, 7136–7141. doi: 10.1073/pnas.1707472114

Diering, G. H., Gustina, A. S., and Huganir, R. L. (2014). PKA-GluA1 coupling *via* AKAP5 controls AMPA receptor phosphorylation and cell-surface targeting during bidirectional homeostatic plasticity. *Neuron* 84, 790–805. doi: 10.1016/j.neuron.2014.09.024

Diering, G. H., Heo, S., Hussain, N. K., Liu, B., and Huganir, R. L. (2016). Extensive phosphorylation of AMPA receptors in neurons. *Proc. Natl. Acad. Sci. U S A* 113, E4920–E4927. doi: 10.1073/pnas.1610631113

Diering, G. H., and Huganir, R. L. (2018). The AMPA receptor code of synaptic plasticity. *Neuron* 100, 314–329. doi: 10.1016/j.neuron.2018.10.018

Dong, H., O'Brien, R. J., Fung, E. T., Lanahan, A. A., Worley, P. F., and Huganir, R. L. (1997). GRIP: a synaptic PDZ domain-containing protein that interacts with AMPA receptors. *Nature* 386, 279–284. doi: 10.1038/386279a0

Dong, H., Zhang, P., Song, I., Petralia, R. S., Liao, D., and Huganir, R. L. (1999). Characterization of the glutamate receptor-interacting proteins GRIP1 and GRIP2. *J. Neurosci.* 19, 6930–6941. doi: 10.1523/jneurosci.19-16-06930.1999

Ehlers, M. D. (2000). Reinsertion or degradation of AMPA receptors determined by activity-dependent endocytic sorting. *Neuron* 28, 511–525. doi: 10.1016/s0896-6273(00)00129-x

Ehlers, M. D. (2007). Secrets of the secretory pathway in dendrite growth. *Neuron* 55, 686–689. doi: 10.1016/j.neuron.2007.08.009

Ehlers, M. D., Heine, M., Groc, L., Lee, M. C., and Choquet, D. (2007). Diffusional trapping of GluR1 AMPA receptors by input-specific synaptic activity. *Neuron* 54, 447–460. doi: 10.1016/j.neuron.2007.04.010

Esteban, J. A., Shi, S.-H., Wilson, C., Nuriya, M., Huganir, R. L., and Malinow, R. (2003). PKA phosphorylation of AMPA receptor subunits controls synaptic trafficking underlying plasticity. *Nat. Neurosci.* 6, 136–143. doi: 10.1038/nn997

Faux, M. C., Rollins, E. N., Edwards, A. S., Langeberg, L. K., Newton, A. C., and Scott, J. D. (1999). Mechanism of A-kinase-anchoring protein 79 (AKAP79) and protein kinase C interaction. *Biochem. J.* 343, 443–452. doi: 10.1042/0264-6021:3430443

Faux, M. C., and Scott, J. D. (1997). Regulation of the AKAP79-protein kinase C interaction by Ca^{2+}/Calmodulin. *J. Biol. Chem.* 272, 17038–17044. doi: 10.1074/jbc.272.27.17038

Fernández-Monreal, M., Brown, T. C., Royo, M., and Esteban, J. A. (2012). The balance between receptor recycling and trafficking toward lysosomes determines synaptic strength during long-term depression. *J. Neurosci.* 32, 13200–13205. doi: 10.1523/jneurosci.0061-12.2012

Fukata, Y., Dimitrov, A., Boncompain, G., Vielemeyer, O., Perez, F., and Fukata, M. (2013). Local palmitoylation cycles define activity-regulated postsynaptic subdomains. *J. Cell Biol.* 202, 145–161. doi: 10.1083/jcb.201302071

Fukata, Y., and Fukata, M. (2010). Protein palmitoylation in neuronal development and synaptic plasticity. *Nat. Rev. Neurosci.* 11, 161–175. doi: 10.1038/nrn2788

García-Nafría, J., Herguedas, B., Watson, J. F., and Greger, I. H. (2016). The dynamic AMPA receptor extracellular region: a platform for synaptic protein interactions. *J. Physiol. Lond.* 594, 5449–5458. doi: 10.1113/jp271844

Gerlai, R., Henderson, J. T., Roder, J. C., and Jia, Z. (1998). Multiple behavioral anomalies in GluR2 mutant mice exhibiting enhanced LTP. *Behav. Brain Res.* 95, 37–45. doi: 10.1016/s0166-4328(98)00002-3

Gladding, C. M., Collett, V. J., Jia, Z., Bashir, Z. I., Collingridge, G. L., and Molnar, E. (2009). Tyrosine dephosphorylation regulates AMPAR internalisation in mGluR-LTD. *Mol. Cell. Neurosci.* 40, 267–279. doi: 10.1016/j.mcn.2008.10.014

Goel, A., Xu, L. W., Snyder, K. P., Song, L., Goenaga-Vazquez, Y., Megill, A., et al. (2011). Phosphorylation of AMPA receptors is required for sensory deprivation-induced homeostatic synaptic plasticity. *PLoS One* 6:e18264. doi: 10.1371/journal.pone.0018264

Gomez, L. L., Alam, S., Smith, K. E., Horne, E., and Dell'Acqua, M. L. (2002). Regulation of A-kinase anchoring protein 79/150-cAMP-dependent protein kinase postsynaptic targeting by NMDA receptor activation of calcineurin and remodeling of dendritic actin. *J. Neurosci.* 22, 7027–7044. doi: 10.1523/jneurosci.22-16-07027.2002

Gorski, J. A., Gomez, L. L., Scott, J. D., and Dell'Acqua, M. L. (2005). Association of an A-kinase-anchoring protein signaling scaffold with cadherin adhesion molecules in neurons and epithelial cells. *Mol. Biol. Cell* 16, 3574–3590. doi: 10.1091/mbc.e05-02-0134

Granger, A. J., and Nicoll, R. A. (2014a). Expression mechanisms underlying long-term potentiation: a postsynaptic view, 10 years on. *Philos. Trans. R. Soc. Lond. B Biol. Sci.* 369:20130136. doi: 10.1098/rstb.2013.0136

Granger, A. J., and Nicoll, R. A. (2014b). LTD expression is independent of glutamate receptor subtype. *Front. Synaptic Neurosci.* 6:15. doi: 10.3389/fnsyn.2014.00015

Granger, A. J., Shi, Y., Lu, W., Cerpas, M., and Nicoll, R. A. (2013). LTP requires a reserve pool of glutamate receptors independent of subunit type. *Nature* 493, 495–500. doi: 10.1038/nature11775

Gray, E. E., Fink, A. E., Sarinana, J., Vissel, B., and O'Dell, T. J. (2007). Long-term potentiation in the hippocampal CA1 region does not require insertion and activation of GluR2-lacking AMPA receptors. *J. Neurophysiol.* 98, 2488–2492. doi: 10.1152/jn.00473.2007

Gray, J. A., Shi, Y., Usui, H., During, M. J., Sakimura, K., and Nicoll, R. A. (2011). Distinct modes of AMPA receptor suppression at developing synapses by GluN2A and GluN2B: single-cell NMDA receptor subunit deletion *in vivo*. *Neuron* 71, 1085–1101. doi: 10.1016/j.neuron.2011.08.007

Greaves, J., and Chamberlain, L. H. (2011). DHHC palmitoyl transferases: substrate interactions and (patho)physiology. *Trends Biochem. Sci.* 36, 245–253. doi: 10.1016/j.tibs.2011.01.003

Greaves, J., Carmichael, J. A., and Chamberlain, L. H. (2011). The palmitoyl transferase DHHC2 targets a dynamic membrane cycling pathway: regulation by a C-terminal domain. *Mol. Biol. Cell* 22, 1887–1895. doi: 10.1091/mbc.e10-11-0924

Greger, I. H., Khatri, L., Kong, X., and Ziff, E. B. (2003). AMPA receptor tetramerization is mediated by Q/R editing. *Neuron* 40, 763–774. doi: 10.1016/s0896-6273(03)00668-8

Groth, R. D., Lindskog, M., Thiagarajan, T. C., Li, L., and Tsien, R. W. (2011). β Ca^{2+}/CaM-dependent kinase type II triggers upregulation of GluA1 to coordinate adaptation to synaptic inactivity in hippocampal neurons. *Proc. Natl. Acad. Sci. U S A* 108, 828–833. doi: 10.1073/pnas.1018022108

Guire, E. S., Oh, M. C., Soderling, T. R., and Derkach, V. A. (2008). Recruitment of calcium-permeable AMPA receptors during synaptic potentiation is regulated by CaM-kinase I. *J. Neurosci.* 28, 6000–6009. doi: 10.1523/jneurosci.0384-08.2008

Havekes, R., Canton, D. A., Park, A. J., Huang, T., Nie, T., Day, J. P., et al. (2012). Gravin orchestrates protein kinase A and β2-adrenergic receptor signaling critical for synaptic plasticity and memory. *J. Neurosci.* 32, 18137–18149. doi: 10.1523/jneurosci.3612-12.2012

He, K., Song, L., Cummings, L. W., Goldman, J., Huganir, R. L., and Lee, H. K. (2009). Stabilization of Ca^{2+}-permeable AMPA receptors at perisynaptic sites by GluR1–S845 phosphorylation. *Proc. Natl. Acad. Sci. U S A* 106, 20033–20038. doi: 10.1073/pnas.0910338106

Henley, J. M., Barker, E. A., and Glebov, O. O. (2011). Routes, destinations and delays: recent advances in AMPA receptor trafficking. *Trends Neurosci.* 34, 258–268. doi: 10.1016/j.tins.2011.02.004

Herlitze, S., Raditsch, M., Ruppersberg, J. P., Jahn, W., Monyer, H., Schoepfer, R., et al. (1993). Argiotoxin detects molecular differences in AMPA receptor channels. *Neuron* 10, 1131–1140. doi: 10.1016/0896-6273(93)90061-u

Herring, B. E., and Nicoll, R. A. (2016). Kalirin and Trio proteins serve critical roles in excitatory synaptic transmission and LTP. *Proc. Natl. Acad. Sci. U S A* 113, 2264–2269. doi: 10.1073/pnas.1600179113

Heynen, A. J., Quinlan, E. M., Bae, D. C., and Bear, M. F. (2000). Bidirectional, activity-dependent regulation of glutamate receptors in the adult hippocampus *in vivo*. *Neuron* 28, 527–536. doi: 10.1016/s0896-6273(00)00130-6

Hiester, B. G., Bourke, A. M., Sinnen, B. L., Cook, S. G., Gibson, E. S., Smith, K. R., et al. (2017). L-tYPE vOLTAGE-gATED Ca^{2+} channels regulate synaptic-activity-triggered recycling endosome fusion in neuronal dendrites. *Cell Rep.* 21, 2134–2146. doi: 10.1016/j.celrep.2017.10.105

Hoffman, D. A., Sprengel, R., and Sakmann, B. (2002). Molecular dissection of hippocampal theta-burst pairing potentiation. *Proc. Natl. Acad. Sci. U S A* 99, 7740–7745. doi: 10.1073/pnas.092157999

Horne, E. A., and Dell'Acqua, M. L. (2007). Phospholipase C is required for changes in postsynaptic structure and function associated with NMDA receptor-dependent long-term depression. *J. Neurosci.* 27, 3523–3534. doi: 10.1523/jneurosci.4340-06.2007

Hoshi, N., Langeberg, L. K., and Scott, J. D. (2005). Distinct enzyme combinations in AKAP signalling complexes permit functional diversity. *Nat. Cell Biol.* 7, 1066–1073. doi: 10.1038/ncb1315

Hosokawa, T., Mitsushima, D., Kaneko, R., and Hayashi, Y. (2015). Stoichiometry and phosphoisotypes of hippocampal AMPA-type glutamate receptor phosphorylation. *Neuron* 85, 60–67. doi: 10.1016/j.neuron.2014.11.026

Huang, K., Yanai, A., Kang, R., Arstikaitis, P., Singaraja, R. R., Metzler, M., et al. (2004). Huntingtin-interacting protein HIP14 is a palmitoyl transferase involved in palmitoylation and trafficking of multiple neuronal proteins. *Neuron* 44, 977–986. doi: 10.1016/j.neuron.2004.11.027

Huganir, R. L., and Nicoll, R. A. (2013). AMPARs and synaptic plasticity: the last 25 years. *Neuron* 80, 704–717. doi: 10.1016/j.neuron.2013.10.025

Ibata, K., Sun, S., and Turrigiano, C. G. (2008). Rapid synaptic scaling induced by changes in postsynaptic firing. *Neuron* 57, 819–826. doi: 10.1016/j.neuron.2008.02.031

Isaac, J. T., Ashby, M. C., and McBain, C. J. (2007). The role of the GluR2 subunit in AMPA receptor function and synaptic plasticity. *Neuron* 54, 859–871. doi: 10.1016/j.neuron.2007.06.001

Jaafari, N., Henley, J. M., and Hanley, J. G. (2012). PICK1 mediates transient synaptic expression of GluA2-lacking AMPA receptors during glycine-induced AMPA receptor trafficking. *J. Neurosci.* 32, 11618–11630. doi: 10.1523/JNEUROSCI.5068-11.2012

Jenkins, M. A., Wells, G., Bachman, J., Snyder, J. P., Jenkins, A., Huganir, R. L., et al. (2014). Regulation of GluA1 α-amino-3-hydroxy-5-methyl-4-isoxazolepropionic acid receptor function by protein kinase C at serine-818 and threonine-840. *Mol. Pharmacol.* 85, 618–629. doi: 10.1124/mol.113.091488

Jensen, V., Kaiser, K. M., Borchardt, T., Adelmann, G., Rozov, A., Burnashev, N., et al. (2003). A juvenile form of postsynaptic hippocampal long-term potentiation in mice deficient for the AMPA receptor subunit GluR-A. *J. Physiol. Lond.* 553, 843–856. doi: 10.1113/jphysiol.2003.053637

Jia, Z., Agopyan, N., Miu, P., Xiong, Z., Henderson, J., Gerlai, R., et al. (1996). Enhanced LTP in mice deficient in the AMPA receptor GluR2. *Neuron* 17, 945–956. doi: 10.1016/s0896-6273(00)80225-1

Jurado, S., Biou, V., and Malenka, R. C. (2010). A calcineurin/AKAP complex is required for NMDA receptor-dependent long-term depression. *Nat. Neurosci.* 13, 1053–1055. doi: 10.1038/nn.2613

Jurado, S., Goswami, D., Zhang, Y., Molina, A. J., Sudhof, T. C., and Malenka, R. C. (2013). LTP requires a unique postsynaptic SNARE fusion machinery. *Neuron* 77, 542–558. doi: 10.1016/j.neuron.2012.11.029

Kameyama, K., Lee, H. K., Bear, M. F., and Huganir, R. L. (1998). Involvement of a postsynaptic protein kinase A substrate in the expression of homosynaptic long-term depression. *Neuron* 21, 1163–1175. doi: 10.1016/s0896-6273(00)80633-9

Kang, R., Wan, J., Arstikaitis, P., Takahashi, H., Huang, K., Bailey, A. O., et al. (2008). Neural palmitoyl-proteomics reveals dynamic synaptic palmitoylation. *Nature* 456, 904–909. doi: 10.1038/nature07605

Kauer, J. A., Malenka, R. C., and Nicoll, R. A. (1988). A persistent postsynaptic modification mediates long-term potentiation in the hippocampus. *Neuron* 1, 911–917. doi: 10.1016/0896-6273(88)90148-1

Kay, H. Y., Greene, D. L., Kang, S., Kosenko, A., and Hoshi, N. (2015). M-current preservation contributes to anticonvulsant effects of valproic acid. *J. Clin. Invest.* 125, 3904–3914. doi: 10.1172/jci79727

Keck, T., Toyoizumi, T., Chen, L., Doiron, B., Feldman, D. E., Fox, K., et al. (2017). Integrating Hebbian and homeostatic plasticity: the current state of the field and future research directions. *Philos. Trans. R. Soc. Lond. B Biol. Sci.* 372:20160158. doi: 10.1098/rstb.2016.0158

Keith, D. J., Sanderson, J. L., Gibson, E. S., Woolfrey, K. M., Robertson, H. R., Olszewski, K., et al. (2012). Palmitoylation of A-kinase anchoring protein 79/150 regulates dendritic endosomal targeting and synaptic plasticity mechanisms. *J. Neurosci.* 32, 7119–7136. doi: 10.1523/JNEUROSCI.0784-12.2012

Kelly, E. E., Horgan, C. P., McCaffrey, M. W., and Young, P. (2011). The role of endosomal-recycling in long-term potentiation. *Cell. Mol. Life Sci.* 68, 185–194. doi: 10.1007/s00018-010-0516-2

Kennedy, M. J., Davison, I. G., Robinson, C. G., and Ehlers, M. D. (2010). Syntaxin-4 defines a domain for activity-dependent exocytosis in dendritic spines. *Cell* 141, 524–535. doi: 10.1016/j.cell.2010.02.042

Kennedy, M. J., and Ehlers, M. D. (2006). Organelles and trafficking machinery for postsynaptic plasticity. *Annu. Rev. Neurosci.* 29, 325–362. doi: 10.1146/annurev.neuro.29.051605.112808

Kessels, H. W., and Malinow, R. (2009). Synaptic AMPA receptor plasticity and behavior. *Neuron* 61, 340–350. doi: 10.1016/j.neuron.2009.01.015

Kim, C. H., Chung, H. J., Lee, H. K., and Huganir, R. L. (2001). Interaction of the AMPA receptor subunit GluR2/3 with PDZ domains regulates hippocampal long-term depression. *Proc. Natl. Acad. Sci. U S A* 98, 11725–11730. doi: 10.1073/pnas.211132798

Kim, C. H., Takamiya, K., Petralia, R. S., Sattler, R., Yu, S., Zhou, W., et al. (2005). Persistent hippocampal CA1 LTP in mice lacking the C-terminal PDZ ligand of GluR1. *Nat. Neurosci.* 8, 985–987. doi: 10.1038/nn1432

Kim, S., Violette, C. J., and Ziff, E. B. (2015). Reduction of increased calcineurin activity rescues impaired homeostatic synaptic plasticity in presenilin 1 M146V mutant. *Neurobiol. Aging* 36, 3239–3246. doi: 10.1016/j.neurobiolaging.2015.09.007

Kim, S., and Ziff, E. B. (2014). Calcineurin mediates synaptic scaling *via* synaptic trafficking of Ca^{2+}-permeable AMPA receptors. *PLoS Biol.* 12:e1001900. doi: 10.1371/journal.pbio.1001900

Klauck, T. M., Faux, M. C., Labudda, K., Langeberg, L. K., Jaken, S., and Scott, J. D. (1996). Coordination of three signaling enzymes by AKAP79, a mammalian scaffold protein. *Science* 271, 1589–1592. doi: 10.1126/science.271.5255.1589

Koike, M., Iino, M., and Ozawa, S. (1997). Blocking effect of 1-naphthyl acetyl spermine on Ca^{2+}-permeable AMPA receptors in cultured rat hippocampal neurons. *Neurosci. Res.* 29, 27–36. doi: 10.1016/s0168-0102(97)00067-9

Kolleker, A., Zhu, J. J., Schupp, B. J., Qin, Y., Mack, V., Borchardt, T., et al. (2003). Glutamatergic plasticity by synaptic delivery of GluR-B(long)-containing AMPA receptors. *Neuron* 40, 1199–1212. doi: 10.1016/s0896-6273(03)00722-0

Kopec, C. D., Li, B., Wei, W., Boehm, J., and Malinow, R. (2006). Glutamate receptor exocytosis and spine enlargement during chemically induced long-term potentiation. *J. Neurosci.* 26, 2000–2009. doi: 10.1523/jneurosci.3918-05.2006

Kristensen, A. S., Jenkins, M. A., Banke, T. G., Schousboe, A., Makino, Y., Johnson, R. C., et al. (2011). Mechanism of Ca^{2+}/calmodulin-dependent kinase II regulation of AMPA receptor gating. *Nat. Neurosci.* 14, 727–735. doi: 10.1038/nn.2804

Kumar, S. S., Bacci, A., Kharazia, V., and Huguenard, J. R. (2002). A developmental switch of AMPA receptor subunits in neocortical pyramidal neurons. *J. Neurosci.* 22, 3005–3015. doi: 10.1523/jneurosci.22-08-03005.2002

Lee, H. K., Barbarosie, M., Kameyama, K., Bear, M. F., and Huganir, R. L. (2000). Regulation of distinct AMPA receptor phosphorylation sites during bidirectional synaptic plasticity. *Nature* 405, 955–959. doi: 10.1038/35016089

Lee, H. K., Kameyama, K., Huganir, R. L., and Bear, M. F. (1998). NMDA induces long-term synaptic depression and dephosphorylation of the GluR1 subunit of AMPA receptors in hippocampus. *Neuron* 21, 1151–1162. doi: 10.1016/s0896-6273(00)80632-7

Lee, H. K., Takamiya, K., Han, J. S., Man, H., Kim, C. H., Rumbaugh, G., et al. (2003). Phosphorylation of the AMPA receptor GluR1 subunit is required for synaptic plasticity and retention of spatial memory. *Cell* 112, 631–643. doi: 10.1016/s0896-6273(00)80632-7

Lee, H. K., Takamiya, K., He, K., Song, L., and Huganir, R. L. (2010). Specific roles of AMPA receptor subunit GluR1 (GluA1) phosphorylation sites in regulating synaptic plasticity in the CA1 region of hippocampus. *J. Neurophysiol.* 103, 479–489. doi: 10.1152/jn.00835.2009

Lee, K. F., Soares, C., and Béïque, J. C. (2013). Tuning into diversity of homeostatic synaptic plasticity. *Neuropharmacology* 78, 31–37. doi: 10.1016/j.neuropharm.2013.03.016.

Lee, K. Y., and Chung, H. J. (2014). NMDA receptors and L-type voltage-gated Ca^{2+} channels mediate the expression of bidirectional homeostatic intrinsic plasticity in cultured hippocampal neurons. *Neuroscience* 277, 610–623. doi: 10.1016/j.neuroscience.2014.07.038

Lee, S. H., Liu, L., Wang, Y. T., and Sheng, M. (2002). Clathrin adaptor AP2 and NSF interact with overlapping sites of GluR2 and play distinct roles in AMPA receptor trafficking and hippocampal LTD. *Neuron* 36, 661–674. doi: 10.1016/s0896-6273(02)01024-3

Leonard, A. S., Davare, M. A., Horne, M. C., Garner, C. C., and Hell, J. W. (1998). SAP97 is associated with the α-amino-3-hydroxy-5-methylisoxazole-4-propionic acid receptor GluR1 subunit. *J. Biol. Chem.* 273, 19518–19524. doi: 10.1074/jbc.273.31.19518

Li, H., Pink, M. D., Murphy, J. G., Stein, A., Dell'Acqua, M. L., and Hogan, P. G. (2012). Balanced interactions of calcineurin with AKAP79 regulate Ca^{2+}-calcineurin-NFAT signaling. *Nat. Struct. Mol. Biol.* 19, 337–345. doi: 10.1038/nsmb.2238

Lin, D. T., Makino, Y., Sharma, K., Hayashi, T., Neve, R., Takamiya, K., et al. (2009). Regulation of AMPA receptor extrasynaptic insertion by 4.1N, phosphorylation and palmitoylation. *Nat. Neurosci.* 12, 879–887. doi: 10.1038/nn.2351

Lisman, J. (1989). A mechanism for the Hebb and the anti-Hebb processes underlying learning and memory. *Proc. Natl. Acad. Sci. U S A* 86, 9574–9578. doi: 10.1073/pnas.86.23.9574

Lisman, J. (2017). Glutamatergic synapses are structurally and biochemically complex because of multiple plasticity processes: long-term potentiation, long-term depression, short-term potentiation and scaling. *Philos. Trans. R. Soc. Lond. B Biol. Sci.* 372:20160260. doi: 10.1098/rstb.2016.0260

Lisman, J. E., Raghavachari, S., and Tsien, R. W. (2007). The sequence of events that underlie quantal transmission at central glutamatergic synapses. *Nat. Rev. Neurosci.* 8, 597–609. doi: 10.1038/nrn2191

Liu, S. Q., and Cull-Candy, S. G. (2000). Synaptic activity at calcium-permeable AMPA receptors induces a switch in receptor subtype. *Nature* 405, 454–458. doi: 10.1038/35013064

Liu, S. J., and Zukin, R. S. (2007). Ca^{2+}-permeable AMPA receptors in synaptic plasticity and neuronal death. *Trends Neurosci.* 30, 126–134. doi: 10.1016/j.tins.2007.01.006

Lledo, P. M., Zhang, X., Sudhof, T. C., Malenka, R. C., and Nicoll, R. A. (1998). Postsynaptic membrane fusion and long-term potentiation. *Science* 279, 399–403. doi: 10.1126/science.279.5349.399

Lu, Y., Allen, M., Halt, A. R., Weisenhaus, M., Dallapiazza, R. F., Hall, D. D., et al. (2007). Age-dependent requirement of AKAP150-anchored PKA and GluR2-lacking AMPA receptors in LTP. *EMBO J.* 26, 4879–4890. doi: 10.1038/sj.emboj.7601884

Lu, W., Man, H., Ju, W., Trimble, W. S., MacDonald, J. F., and Wang, Y. T. (2001). Activation of synaptic NMDA receptors induces membrane insertion of new AMPA receptors and LTP in cultured hippocampal neurons. *Neuron* 29, 243–254. doi: 10.1016/s0896-6273(01)00194-5

Lu, W., and Roche, K. W. (2012). Posttranslational regulation of AMPA receptor trafficking and function. *Curr. Opin. Neurobiol.* 22, 470–479. doi: 10.1016/j.conb.2011.09.008

Lu, W., Shi, Y., Jackson, A. C., Bjorgan, K., During, M. J., Sprengel, R., et al. (2009). Subunit composition of synaptic AMPA receptors revealed by a single-cell genetic approach. *Neuron* 62, 254–268. doi: 10.1016/j.neuron.2009.02.027

Lu, Y., Zhang, M., Lim, I. A., Hall, D. D., Allen, M., Medvedeva, Y., et al. (2008). AKAP150-anchored PKA activity is important for LTD during its induction phase. *J. Physiol. Lond.* 586, 4155–4164. doi: 10.1113/jphysiol.2008.151662

Lüscher, C., Xia, H., Beattie, E. C., Carroll, R. C., von Zastrow, M., Malenka, R. C., et al. (1999). Role of AMPA receptor cycling in synaptic transmission and plasticity. *Neuron* 24, 649–658. doi: 10.1016/s0896-6273(00)81119-8

Lüthi, A., Chittajallu, R., Duprat, F., Palmer, M. J., Benke, T. A., Kidd, F. L., et al. (1999). Hippocampal LTD expression involves a pool of AMPARs regulated by the NSF-GluR2 interaction. *Neuron* 24, 389–399. doi: 10.1016/s0896-6273(00)80852-1

MacGillavry, H. D., Song, Y., Raghavachari, S., and Blanpied, T. A. (2013). Nanoscale scaffolding domains within the postsynaptic density concentrate synaptic AMPA receptors. *Neuron* 78, 615–622. doi: 10.1016/j.neuron.2013.03.009

Magazanik, L. G., Buldakova, S. L., Samoilova, M. V., Gmiro, V. E., Mellor, I. R., and Usherwood, P. N. (1997). Block of open channels of recombinant AMPA receptors and native AMPA/kainate receptors by adamantane derivatives. *J. Physiol.* 505, 655–663. doi: 10.1111/j.1469-7793.1997.655ba.x

Malenka, R. C., Kauer, J. A., Perkel, D. J., Mauk, M. D., Kelly, P. T., Nicoll, R. A., et al. (1989). An essential role for postsynaptic calmodulin and protein kinase activity in long-term potentiation. *Nature* 340, 554–557. doi: 10.1038/340554a0

Malenka, R. C., and Bear, F. M. (2004). LTP and LTD: an embarrassment of riches. *Neuron* 44, 5–21. doi: 10.1016/j.neuron.2004.09.012

Malinow, R., Schulman, H., and Tsien, R. W. (1989). Inhibition of postsynaptic PKC or CaMKII blocks induction but not expression of LTP. *Science* 245, 862–866. doi: 10.1126/science.2549638

Man, H. Y. (2011). GluA2-lacking, calcium-permeable AMPA receptors—inducers of plasticity? *Curr. Opin. Neurobiol.* 21, 291–298. doi: 10.1016/j.conb.2011.01.001

Man, H. Y., Sekine-Aizawa, Y., and Huganir, R. L. (2007). Regulation of α-amino-3-hydroxy-5-methyl-4-isoxazolepropionic acid receptor trafficking through PKA phosphorylation of the Glu receptor 1 subunit. *Proc. Natl. Acad. Sci. U S A* 104, 3579–3584. doi: 10.1073/pnas.0611698104

Mansouri, M. R., Marklund, L., Gustavsson, P., Davey, E., Carlsson, B., Larsson, C., et al. (2005). Loss of ZDHHC15 expression in a woman with a balanced translocation t(X;15)(q13.3;cen) and severe mental retardation. *Eur. J. Hum. Genet.* 13, 970–977. doi: 10.1038/sj.ejhg.5201445

Massey, P. V., and Bashir, Z. I. (2007). Long-term depression: multiple forms and implications for brain function. *Trends Neurosci.* 30, 176–184. doi: 10.1016/j.tins.2007.02.005

Matsuda, S., Mikawa, S., and Hirai, H. (1999). Phosphorylation of serine-880 in GluR2 by protein kinase C prevents its C terminus from binding with glutamate receptor-interacting protein. *J. Neurochem.* 73, 1765–1768. doi: 10.1046/j.1471-4159.1999.731765.x

McCormack, S. G., Stornetta, R. L., and Zhu, J. J. (2006). Synaptic AMPA receptor exchange maintains bidirectional plasticity. *Neuron* 50, 75–88. doi: 10.1016/j.neuron.2006.02.027

Megill, A., Tran, T., Eldred, K., Lee, N. J., Wong, P. C., Hoe, H. S., et al. (2015). Defective age-dependent metaplasticity in a mouse model of Alzheimer's disease. *J. Neurosci.* 35, 11346–11357. doi: 10.1523/jneurosci.5289-14.2015

Meng, Y., Zhang, Y., and Jia, Z. (2003). Synaptic transmission and plasticity in the absence of AMPA glutamate receptor GluR2 and GluR3. *Neuron* 39, 163–176. doi: 10.1016/s0896-6273(03)00368-4

Meyerson, J. R., Kumar, J., Chittori, S., Rao, P., Pierson, J., Bartesaghi, A., et al. (2014). Structural mechanism of glutamate receptor activation and desensitization. *Nature* 514, 328–334. doi: 10.1038/nature13603

Morise, J. K., Suzuki, G. N., Kitagawa, A., Wakazono, Y., Takamiya, K., Tsunoyama, T. A., et al. (2019). AMPA receptors in the synapse turnover by monomer diffusion. *Nat. Commun.* 10:5245. doi: 10.1038/s41467-019-13229-8

Mukai, J., Dhilla, A., Drew, L. J., Stark, K. L., Cao, L., MacDermott, A. B., et al. (2008). Palmitoylation-dependent neurodevelopmental deficits in a mouse model of 22q11 microdeletion. *Nat. Neurosci.* 11, 1302–1310. doi: 10.1038/nn.2204

Mukai, J., Liu, H., Burt, R. A., Swor, D. E., Lai, W. S., Karayiorgou, M., et al. (2004). Evidence that the gene encoding ZDHHC8 contributes to the risk of schizophrenia. *Nat. Genet.* 36, 725–731. doi: 10.1038/ng1375

Mulkey, R. M., Endo, S., Shenolikar, S., and Malenka, R. C. (1994). Involvement of a calcineurin/inhibitor-1 phosphatase cascade in hippocampal long-term depression. *Nature* 369, 486–488. doi: 10.1038/369486a0

Mulkey, R. M., Herron, C. E., and Malenka, R. C. (1993). An essential role for protein phosphatases in hippocampal long-term depression. *Science* 261, 1051–1055. doi: 10.1126/science.8394601

Mulkey, R. M., and Malenka, R. C. (1992). Mechanisms underlying induction of homosynaptic long-term depression in area CA1 of the hippocampus. *Neuron* 9, 967–975. doi: 10.1016/0896-6273(92)90248-c

Muller, D., Joly, M., and Lynch, G. (1988). Contributions of quisqualate and NMDA receptors to the induction and expression of LTP. *Science* 242, 1694–1697. doi: 10.1126/science.2904701

Murphy, J. G., Crosby, K. C., Dittmer, P. J., Sather, W. A., and Dell'Acqua, M. L. (2019). AKAP79/150 recruits the transcription factor NFAT to regulate signaling to the nucleus by neuronal L-type Ca^{2+} channels. *Mol. Biol. Cell* 30, 1743–1756. doi: 10.1091/mbc.e19-01-0060

Murphy, J. G., Sanderson, J. L., Gorski, J. A., Scott, J. D., Catterall, W. A., Sather, W. A., et al. (2014). AKAP-anchored PKA maintains neuronal L-type calcium channel activity and NFAT transcriptional signaling. *Cell Rep.* 7, 1577–1588. doi: 10.1016/j.celrep.2014.04.027

Nabavi, S., Kessels, H. W., Alfonso, S., Aow, J., Fox, R., and Malinow, R. (2013). Metabotropic NMDA receptor function is required for NMDA receptor-dependent long-term depression. *Proc. Natl. Acad. Sci. U S A* 110, 4027–4032. doi: 10.1073/pnas.1219454110

Nair, D., Hosy, E., Petersen, J. D., Constals, A., Giannone, G., Choquet, D., et al. (2013). Super-resolution imaging reveals that AMPA receptors inside synapses are dynamically organized in nanodomains regulated by PSD95. *J. Neurosci.* 33, 13204–13224. doi: 10.1523/JNEUROSCI.2381-12.2013

Newpher, T. M., and Ehlers, M. D. (2008). Glutamate receptor dynamics in dendritic microdomains. *Neuron* 58, 472–497. doi: 10.1016/j.neuron.2008.04.030

Nicoll, R. A. (2017). A brief history of long-term potentiation. *Neuron* 93, 281–290. doi: 10.1016/j.neuron.2016.12.015

Nicoll, R. A., and Roche, K. W. (2013). Long-term potentiation: peeling the onion. *Neuropharmacology* 74, 18–22. doi: 10.1016/j.neuropharm.2013.02.010

Nikandrova, Y. A., Jiao, Y., Baucum, A. J., Tavalin, S. J., and Colbran, R. J. (2010). Ca^{2+}/calmodulin-dependent protein kinase II binds to and phosphorylates a specific SAP97 splice variant to disrupt association with AKAP79/150 and modulate α-amino-3-hydroxy-5-methyl-4-isoxazolepropionic acid-type glutamate receptor (AMPAR) activity. *J. Biol. Chem.* 285, 923–934. doi: 10.1074/jbc.m109.033985

Nishimune, A., Isaac, J. T., Molnar, E., Noel, J., Nash, S. R., Tagaya, M., et al. (1998). NSF binding to GluR2 regulates synaptic transmission. *Neuron* 21, 87–97. doi: 10.1016/s0896-6273(00)80517-6

Noel, J., Ralph, G. S., Pickard, L., Williams, J., Molnar, E., Uney, J. B., et al. (1999). Surface expression of AMPA receptors in hippocampal neurons is regulated by an NSF-dependent mechanism. *Neuron* 23, 365–376. doi: 10.1016/s0896-6273(00)80786-2

O'Brien, R. J., Kamboj, S., Ehlers, M. D., Rosen, K. R., Fischbach, G. D., and Huganir, R. L. (1998). Activity-dependent modulation of synaptic AMPA receptor accumulation. *Neuron* 21, 1067–1078. doi: 10.1016/s0896-6273(00)80624-8

Oh, M. C., Derkach, V. A., Guire, E. S., and Soderling, T. R. (2006). Extrasynaptic membrane trafficking regulated by GluR1 serine 845 phosphorylation primes AMPA receptors for long-term potentiation. *J. Biol. Chem.* 281, 752–758. doi: 10.1074/jbc.m509677200

Oliveria, S. F., Dell'Acqua, M. L., and Sather, W. A. (2007). AKAP79/150 anchoring of calcineurin controls neuronal L-type Ca^{2+} channel activity and nuclear signaling. *Neuron* 55, 261–275. doi: 10.1016/j.neuron.2007.06.032

Oliveria, S. F., Dittmer, P. J., Youn, D. H., Dell'Acqua, M. L., and Sather, W. A. (2012). Localized calcineurin confers Ca^{2+}-dependent inactivation on neuronal L-type Ca^{2+} channels. *J. Neurosci.* 32, 15328–15337. doi: 10.1523/JNEUROSCI.2302-12.2012

Opazo, P., and Choquet, D. (2011). A three-step model for the synaptic recruitment of AMPA receptors. *Mol. Cell. Neurosci.* 46, 1–8. doi: 10.1016/j.mcn.2010.08.014

Opazo, P., Labrecque, S., Tigaret, C. M., Frouin, A., Wiseman, P. W., De Koninck, P., et al. (2010). CaMKII triggers the diffusional trapping of surface AMPARs through phosphorylation of stargazin. *Neuron* 67, 239–252. doi: 10.1016/j.neuron.2010.06.007

Opazo, P., Sainlos, M., and Choquet, D. (2012). Regulation of AMPA receptor surface diffusion by PSD-95 slots. *Curr. Opin. Neurobiol.* 22, 453–460. doi: 10.1016/j.conb.2011.10.010

Osten, P., Srivastava, S., Inman, G. J., Vilim, F. S., Khatri, L., Lee, L. M., et al. (1998). The AMPA receptor GluR2 C terminus can mediate a reversible, ATP-dependent interaction with NSF and α- and β-SNAPs. *Neuron* 21, 99–110. doi: 10.1016/s0896-6273(00)80518-8

Palmer, M. J., Irving, A. J., Seabrook, G. R., Jane, D. E., and Collingridge, G. L. (1997). The group I mGlu receptor agonist DHPG induces a novel form of LTD in the CA1 region of the hippocampus. *Neuropharmacology* 36, 1517–1532. doi: 10.1016/s0028-3908(97)00181-0

Park, J., Chávez, A. E., Mineur, Y. S., Morimoto-Tomita, M., Lutzu, S., Kim, K. S., et al. (2016). CaMKII phosphorylation of TARPγ-8 is a mediator of LTP and learning and memory. *Neuron* 92, 75–83. doi: 10.1016/j.neuron.2016.09.002

Park, M., Penick, E. C., Edwards, J. G., Kauer, J. A., and Ehlers, M. D. (2004). Recycling endosomes supply AMPA receptors for LTP. *Science* 305, 1972–1975. doi: 10.1126/science.1102026

Park, M., Salgado, J. M., Ostroff, L., Helton, T. D., Robinson, C. G., Harris, K. M., et al. (2006). Plasticity-induced growth of dendritic spines by exocytic trafficking from recycling endosomes. *Neuron* 52, 817–830. doi: 10.1016/j.neuron.2006.09.040

Park, P., Sanderson, T. M., Amici, M., Choi, S. L., Bortolotto, Z. A., Zhuo, M., et al. (2016). Calcium-permeable AMPA receptors mediate the induction of the protein kinase a-dependent component of long-term potentiation in the hippocampus. *J. Neurosci.* 36, 622–631. doi: 10.1523/JNEUROSCI.3625-15.2016

Passafaro, M., Piäch, V., and Sheng, M. (2001). Subunit-specific temporal and spatial patterns of AMPA receptor exocytosis in hippocampal neurons. *Nat. Neurosci.* 4, 917–926. doi: 10.1038/nn0901-917

Patterson, M. A., Szatmari, E. M., and Yasuda, R. (2010). AMPA receptors are exocytosed in stimulated spines and adjacent dendrites in a Ras-ERK-dependent manner during long-term potentiation. *Proc. Natl. Acad. Sci. U S A* 107, 15951–15956. doi: 10.1073/pnas.0913875107

Penn, A. C., Zhang, C. L., Georges, F., Royer, L., Breillat, C., Hosy, E., et al. (2017). Hippocampal LTP and contextual learning require surface diffusion of AMPA receptors. *Nature* 549, 384–388. doi: 10.1038/nature23658

Petrini, E. M., Lu, J., Cognet, L., Lounis, B., Ehlers, M. D., and Choquet, D. (2009). Endocytic trafficking and recycling maintain a pool of mobile surface AMPA receptors required for synaptic potentiation. *Neuron* 63, 92–105. doi: 10.1016/j.neuron.2009.05.025

Plant, K., Pelkey, K. A., Bortolotto, Z. A., Morita, D., Terashima, A., McBain, C. J., et al. (2006). Transient incorporation of native GluR2-lacking AMPA receptors during hippocampal long-term potentiation. *Nat. Neurosci.* 9, 602–604. doi: 10.1038/nn1678

Purkey, A. M., Woolfrey, K. M., Crosby, K. C., Stich, D. G., Chick, W. S., Aoto, J., et al. (2018). AKAP150 palmitoylation regulates synaptic incorporation of Ca^{2+}-permeable AMPA receptors to control LTP. *Cell Rep.* 25, 974.e4–987.e4. doi: 10.1016/j.celrep.2018.09.085

Qian, H., Matt, L., Zhang, M., Nguyen, M., Patriarchi, T., Koval, O. M., et al. (2012). β2-Adrenergic receptor supports prolonged theta tetanus-induced LTP. *J. Neurophysiol.* 107, 2703–2712. doi: 10.1152/jn.00374.2011

Qian, H., Patriarchi, T., Price, J. L., Matt, L., Lee, B., Nieves-Cintron, M., et al. (2017). Phosphorylation of Ser^{1928} mediates the enhanced activity of the L-type Ca^{2+} channel $Ca_v1.2$ by the β_2-adrenergic receptor in neurons. *Sci. Signal.* 10:eaaf9659. doi: 10.1126/scisignal.aaf9659

Rácz, B., Blanpied, T. A., Ehlers, M. D., and Weinberg, R. J. (2004). Lateral organization of endocytic machinery in dendritic spines. *Nat. Neurosci.* 7, 917–918. doi: 10.1038/nn1303

Reisel, D., Bannerman, D. M., Schmitt, W. B., Deacon, R. M., Flint, J., Borchardt, T., et al. (2002). Spatial memory dissociations in mice lacking GluR1. *Nat. Neurosci.* 5, 868–873. doi: 10.1038/nn910

Renner, M. C., Albers, E. H., Gutierrez-Castellanos, N., Reinders, N. R., van Huijstee, A. N., Xiong, H., et al. (2017). Synaptic plasticity through activation of GluA3-containing AMPA-receptors. *Elife* 6:e25462. doi: 10.7554/eLife.25462

Robertson, H. R., Gibson, E. S., Benke, T. A., and Dell'Acqua, M. L. (2009). Regulation of postsynaptic structure and function by an A-kinase anchoring protein-membrane-associated guanylate kinase scaffolding complex. *J. Neurosci.* 29, 7929–7943. doi: 10.1523/JNEUROSCI.6093-08.2009

Rosenmund, C., Carr, D. W., Bergeson, S. E., Nilaver, G., Scott, J. D., and Westbrook, G. L. (1994). Anchoring of protein kinase A is required for modulation of AMPA/kainate receptors on hippocampal neurons. *Nature* 368, 853–856. doi: 10.1038/368853a0

Rozov, A., Sprengel, R., and Seeburg, P. H. (2012). GluA2-lacking AMPA receptors in hippocampal CA1 cell synapses: evidence from gene-targeted mice. *Front. Mol. Neurosci.* 5:22. doi: 10.3389/fnmol.2012.00022

Sanderson, J. L., Gorski, J. A., and Dell'Acqua, M. L. (2016). NMDA receptor-dependent LTD requires transient synaptic incorporation of Ca^{2+}-permeable AMPARs mediated by AKAP150-anchored PKA and calcineurin. *Neuron* 89, 1000–1015. doi: 10.1016/j.neuron.2016.01.043

Sanderson, J. L., Gorski, J. A., Gibson, E. S., Lam, P., Freund, R. K., Chick, W. S., et al. (2012). AKAP150-anchored calcineurin regulates synaptic plasticity by limiting synaptic incorporation of Ca^{2+}-permeable AMPA receptors. *J. Neurosci.* 32, 15036–15052. doi: 10.1523/JNEUROSCI.3326-12.2012

Sanderson, J. L., Scott, J. D., and Dell'Acqua, M. L. (2018). Control of homeostatic synaptic plasticity by AKAP-anchored kinase and phosphatase regulation of Ca^{2+}-permeable AMPA receptors. *J. Neurosci.* 38, 2863–2876. doi: 10.1523/JNEUROSCI.2362-17.2018

Seidenman, K. J., Steinberg, J. P., Huganir, R., and Malinow, R. (2003). Glutamate receptor subunit 2 Serine 880 phosphorylation modulates synaptic transmission and mediates plasticity in CA1 pyramidal cells. *J. Neurosci.* 23, 9220–9228. doi: 10.1523/JNEUROSCI.23-27-09220.2003

Selcher, J. C., Xu, W., Hanson, J. E., Malenka, R. C., and Madison, D. V. (2012). Glutamate receptor subunit GluA1 is necessary for long-term potentiation and synapse unsilencing, but not long-term depression in mouse hippocampus. *Brain Res.* 1435, 8–14. doi: 10.1016/j.brainres.2011.11.029

Sheng, M., and Hoogenraad, C. C. (2007). The postsynaptic architecture of excitatory synapses: a more quantitative view. *Annu. Rev. Biochem.* 76, 823–847. doi: 10.1146/annurev.biochem.76.060805.160029

Sheng, M., and Kim, E. (2011). The postsynaptic organization of synapses. *Cold Spring Harb. Perspect. Biol.* 3:a005678. doi: 10.1101/cshperspect.a005678

Shepherd, J. D., and Huganir, R. L. (2007). The cell biology of synaptic plasticity: AMPA receptor trafficking. *Annu. Rev. Cell Dev. Biol.* 23, 613–643. doi: 10.1146/annurev.cellbio.23.090506.123516

Sinnen, B. L., Bowen, A. B., Forte, J. S., Hiester, B. G., Crosby, K. C., Gibson, E. S., et al. (2017). Optogenetic control of synaptic composition and function. *Neuron* 93, 646.e5–660.e5. doi: 10.1016/j.neuron.2016.12.037

Soares, C., Lee, K. F., Nassrallah, W., and Béïque, J. C. (2013). Differential subcellular targeting of glutamate receptor subtypes during homeostatic synaptic plasticity. *J. Neurosci.* 33, 13547–13559. doi: 10.1523/JNEUROSCI.1873-13.2013

Sobolevsky, A. I., Rosconi, M. P., and Gouaux, E. (2009). X-ray structure, symmetry and mechanism of an AMPA-subtype glutamate receptor. *Nature* 462, 745–756. doi: 10.1038/nature08624

Soderling, T. R. (1993). Calcium/calmodulin-dependent protein kinase II: role in learning and memory. *Mol. Cell. Biochem.* 127–128, 93–101. doi: 10.1007/bf01076760

Song, I., Kamboj, S., Xia, J., Dong, H., Liao, D., and Huganir, R. L. (1998). Interaction of the N-ethylmaleimide-sensitive factor with AMPA receptors. *Neuron* 21, 393–400. doi: 10.1016/s0896-6273(00)80548-6

Spacek, J., and Harris, K. M. (1997). Three-dimensional organization of smooth endoplasmic reticulum in hippocampal CA1 dendrites and dendritic spines of the immature and mature rat. *J. Neurosci.* 17, 190–203. doi: 10.1523/JNEUROSCI.17-01-00190.1997

Srivastava, S., and Ziff, E. B. (1999). ABP: a novel AMPA receptor binding protein. *Ann. N Y Acad. Sci.* 868, 561–564. doi: 10.1111/j.1749-6632.1999.tb11329.x

Stein, I. S., Gray, J. A., and Zito, K. (2015). Non-ionotropic NMDA receptor signaling drives activity-induced dendritic spine shrinkage. *J. Neurosci.* 35, 12303–12308. doi: 10.1523/JNEUROSCI.4289-14.2015

Straub, C., and Tomita, S. (2012). The regulation of glutamate receptor trafficking and function by TARPs and other transmembrane auxiliary subunits. *Curr. Opin. Neurobiol.* 22, 488–495. doi: 10.1016/j.conb.2011.09.005

Stubblefield, E. A., and Benke, T. A. (2010). Distinct AMPA-type glutamatergic synapses in developing rat CA1 hippocampus. *J. Neurophysiol.* 104, 1899–1912. doi: 10.1152/jn.00099.2010

Summers, K. C., Bogard, A. S., and Tavalin, S. J. (2019). Preferential generation of Ca^{2+}-permeable AMPA receptors by AKAP79-anchored protein kinase C proceeds *via* GluA1 subunit phosphorylation at Ser-831. *J. Biol. Chem.* 294, 5521–5535. doi: 10.1074/jbc.ra118.004340

Sun, X., Zhao, Y., and Wolf, M. E. (2005). Dopamine receptor stimulation modulates AMPA receptor synaptic insertion in prefrontal cortex neurons. *J. Neurosci.* 25, 7342–7351. doi: 10.1523/JNEUROSCI.4603-04.2005

Sutton, M. A., Ito, H. T., Cressy, P., Kempf, C., Woo, J. C., and Schuman, E. M. (2006). Miniature neurotransmission stabilizes synaptic function *via* tonic suppression of local dendritic protein synthesis. *Cell* 125, 785–799. doi: 10.1016/j.cell.2006.03.040

Swope, S. L., Moss, S. J., Blackstone, C. D., and Huganir, R. L. (1992). Phosphorylation of ligand-gated ion channels: a possible mode of synaptic plasticity. *FASEB J.* 6, 2514–2523. doi: 10.1096/fasebj.6.8.1375568

Tang, A. H., Chen, H., Li, T. P., Metzbower, S. R., MacGillavry, H. D., and Blanpied, T. A. (2016). A trans-synaptic nanocolumn aligns neurotransmitter release to receptors. *Nature* 536, 210–214. doi: 10.1038/nature19058

Tavalin, S. J. (2008). AKAP79 selectively enhances protein kinase C regulation of GluR1 at a Ca^{2+}-calmodulin-dependent protein kinase II/protein kinase C site. *J. Biol. Chem.* 283, 11445–11452. doi: 10.1074/jbc.m709253200

Tavalin, S. J., Colledge, M., Hell, J. W., Langeberg, L. K., Huganir, R. L., and Scott, J. D. (2002). Regulation of GluR1 by the A-kinase anchoring protein 79 (AKAP79) signaling complex shares properties with long-term depression. *J. Neurosci.* 22, 3044–3051. doi: 10.1523/JNEUROSCI.22-08-03044.2002

Terashima, A., Cotton, L., Dev, K. K., Meyer, G., Zaman, S., Duprat, F., et al. (2004). Regulation of synaptic strength and AMPA receptor subunit composition by PICK1. *J. Neurosci.* 24, 5381–5390. doi: 10.1523/JNEUROSCI.4378-03.2004

Thiagarajan, T. C., Piedras-Renteria, E. S., and Tsien, R. W. (2002). α- and βCaMKII. Inverse regulation by neuronal activity and opposing effects on synaptic strength. *Neuron* 36, 1103–1114. doi: 10.1016/s0896-6273(02)01049-8

Thiagarajan, T. C., Lindskog, M., Malgaroli, A., and Tsien, R. W. (2007). LTP and adaptation to inactivity: overlapping mechanisms and implications for metaplasticity. *Neuropharmacology* 52, 156–175. doi: 10.1016/j.neuropharm.2006.07.030

Thiagarajan, T. C., Lindskog, M., and Tsien, R. W. (2005). Adaptation to synaptic inactivity in hippocampal neurons. *Neuron* 47, 725–737. doi: 10.1016/j.neuron.2005.06.037

Thomas, G. M., Hayashi, T., Chiu, S. L., Chen, C. M., and Huganir, R. L. (2012). Palmitoylation by DHHC5/8 targets GRIP1 to dendritic endosomes to regulate AMPA-R trafficking. *Neuron* 73, 482–496. doi: 10.1016/j.neuron.2011.11.021

Tomita, S., Stein, V., Stocker, T. J., Nicoll, R. A., and Bredt, D. S. (2005). Bidirectional synaptic plasticity regulated by phosphorylation of stargazin-like TARPs. *Neuron* 45, 269–277. doi: 10.1016/j.neuron.2005.01.009

Topinka, J. R., and Bredt, D. S. (1998). N-terminal palmitoylation of PSD-95 regulates association with cell membranes and interaction with K^+ channel $K_v1.4$. *Neuron* 20, 125–134. doi: 10.1016/s0896-6273(00)80440-7

Toth, K., and McBain, C. J. (1998). Afferent-specific innervation of two distinct AMPA receptor subtypes on single hippocampal interneurons. *Nat. Neurosci.* 1, 572–578. doi: 10.1038/2807

Traynelis, S. F., Wollmuth, L. P., McBain, C. J., Menniti, F. S., Vance, K. M., Ogden, K. K., et al. (2010). Glutamate receptor ion channels: structure, regulation, and function. *Pharmacol. Rev.* 62, 405–496. doi: 10.1124/pr.109.002451

Tunquist, B. J., Hoshi, N., Guire, E. S., Zhang, F., Mullendorff, K., Langeberg, L. K., et al. (2008). Loss of AKAP150 perturbs distinct neuronal processes in mice. *Proc. Natl. Acad. Sci. U S A* 105, 12557–12562. doi: 10.1073/pnas.0805922105

Turrigiano, G. (2012). Homeostatic synaptic plasticity: local and global mechanisms for stabilizing neuronal function. *Cold Spring Harb. Perspect. Biol.* 4:a005736. doi: 10.1101/cshperspect.a005736

Turrigiano, G. G., Leslie, K. R., Desai, N. S., Rutherford, L. C., and Nelson, S. B. (1998). Activity-dependent scaling of quantal amplitude in neocortical neurons. *Nature* 391, 892–896. doi: 10.1038/36103

Walkup, W. G., Mastro, T. L., Schenker, L. T., Vielmetter, J., Hu, R., Iancu, A., et al. (2016). A model for regulation by SynGAP-α1 of binding of synaptic proteins to PDZ-domain 'Slots' in the postsynaptic density. *Elife* 5:e16813. doi: 10.7554/eLife.16813

Washburn, M. S., and Dingledine, R. (1996). Block of α-amino-3-hydroxy-5-methyl-4-isoxazolepropionic acid (AMPA) receptors by polyamines and polyamine toxins. *J. Pharmacol. Exp. Ther.* 278, 669–678.

Washburn, M. S., Numberger, M., Zhang, S., and Dingledine, R. (1997). Differential dependence on GluR2 expression of three characteristic features of AMPA receptors. *J. Neurosci.* 17, 9393–9406. doi: 10.1523/JNEUROSCI.17-24-09393.1997

Watson, J. F., Ho, H., and Greger, I. H. (2017). Synaptic transmission and plasticity require AMPA receptor anchoring *via* its N-terminal domain. *Elife* 6:e23024. doi: 10.7554/eLife.23024

Weisenhaus, M., Allen, M. L., Yang, L., Lu, Y., Nichols, C. B., Su, T., et al. (2010). Mutations in AKAP5 disrupt dendritic signaling complexes and lead to electrophysiological and behavioral phenotypes in mice. *PLoS One* 5:e10325. doi: 10.1371/journal.pone.0010325

Whitcomb, D. J., Hogg, E. L., Regan, P., Piers, T., Narayan, P., Whitehead, G., et al. (2015). Intracellular oligomeric amyloid-beta rapidly regulates GluA1 subunit of AMPA receptor in the hippocampus. *Sci. Rep.* 5:10934. doi: 10.1038/srep10934

Wild, A. R., and Dell'Acqua, M. L. (2018). Potential for therapeutic targeting of AKAP signaling complexes in nervous system disorders. *Pharmacol. Ther.* 185, 99–121. doi: 10.1016/j.pharmthera.2017.12.004

Wolf, M. E., and Tseng, K. Y. (2012). Calcium-permeable AMPA receptors in the VTA and nucleus accumbens after cocaine exposure: when, how, and why? *Front. Mol. Neurosci.* 5:72. doi: 10.3389/fnmol.2012.00072

Won, S., Levy, J. M., Nicoll, R. A., and Roche, K. W. (2017). MAGUKs: multifaceted synaptic organizers. *Curr. Opin. Neurobiol.* 43, 94–101. doi: 10.1016/j.conb.2017.01.006

Woolfrey, K. M., and Dell'Acqua, M. L. (2015). Coordination of protein phosphorylation and dephosphorylation in synaptic plasticity. *J. Biol. Chem.* 290, 28604–28612. doi: 10.1074/jbc.r115.657262

Woolfrey, K. M., O'Leary, H., Goodell, D. J., Robertson, H. R., Horne, E. A., Coultrap, S. J., et al. (2018). CaMKII regulates the depalmitoylation and synaptic removal of the scaffold protein AKAP79/150 to mediate structural long-term depression. *J. Biol. Chem.* 293, 1551–1567. doi: 10.1074/jbc.m117.813808

Woolfrey, K. M., Sanderson, J. L., and Dell'Acqua, M. L. (2015). The palmitoyl acyltransferase DHHC2 regulates recycling endosome exocytosis and synaptic potentiation through palmitoylation of AKAP79/150. *J. Neurosci.* 35, 442–456. doi: 10.1523/JNEUROSCI.2243-14.2015

Wu, D., Bacaj, T., Morishita, W., Goswami, D., Arendt, K. L., Xu, W., et al. (2017). Postsynaptic synaptotagmins mediate AMPA receptor exocytosis during LTP. *Nature* 544, 316–321. doi: 10.1038/nature21720

Wyllie, D. J., and Nicoll, R. A. (1994). A role for protein kinases and phosphatases in the Ca^{2+}-induced enhancement of hippocampal AMPA receptor-mediated synaptic responses. *Neuron* 13, 635–643. doi: 10.1016/0896-6273(94)90031-0

Xia, J., Chung, H. J., Wihler, C., Huganir, R. L., and Linden, D. J. (2000). Cerebellar long-term depression requires PKC-regulated interactions between GluR2/3 and PDZ domain-containing proteins. *Neuron* 28, 499–510. doi: 10.1016/s0896-6273(00)00128-8

Xu, W. (2011). PSD-95-like membrane associated guanylate kinases (PSD-MAGUKs) and synaptic plasticity. *Curr. Opin. Neurobiol.* 21, 306–312. doi: 10.1016/j.conb.2011.03.001

Yang, Y., Wang, X. B., Frerking, M., and Zhou, Q. (2008). Delivery of AMPA receptors to perisynaptic sites precedes the full expression of long-term potentiation. *Proc. Natl. Acad. Sci. U S A* 105, 11388–11393. doi: 10.1073/pnas.0802978105

Yang, Y., Wang, X. B., and Zhou, Q. (2010). Perisynaptic GluR2-lacking AMPA receptors control the reversibility of synaptic and spines modifications. *Proc. Natl. Acad. Sci. U S A* 107, 11999–12004. doi: 10.1073/pnas.0913004107

Yudowski, G. A., Puthenveedu, M. A., Leonoudakis, D., Panicker, S., Thorn, K. S., Beattie, E. C., et al. (2007). Real-time imaging of discrete exocytic events mediating surface delivery of AMPA receptors. *J. Neurosci.* 27, 11112–11121. doi: 10.1523/JNEUROSCI.2465-07.2007

Zamanillo, D., Sprengel, R., Hvalby, O., Jensen, V., Burnashev, N., Rozov, A., et al. (1999). Importance of AMPA receptors for hippocampal synaptic plasticity but not for spatial learning. *Science* 284, 1805–1811. doi: 10.1126/science.284.5421.1805

Zeng, M., Díaz-Alonso, J., Ye, F., Chen, X., Xu, J., Ji, Z., et al. (2019). Phase separation-mediated TARP/MAGUK complex condensation and AMPA receptor synaptic transmission. *Neuron* 104, 529.e6–543.e6. doi: 10.1016/j.neuron.2019.08.001

Zeng, M., Shang, Y., Araki, Y., Guo, T., Huganir, R. L., and Zhang, M. (2016). Phase transition in postsynaptic densities underlies formation of synaptic complexes and synaptic plasticity. *Cell* 166, 1163.e12–1175.e12. doi: 10.1016/j.cell.2016.07.008

Zhang, M., Patriarchi, T., Stein, I. S., Qian, H., Matt, L., Nguyen, M., et al. (2013). Adenylyl cyclase anchoring by a kinase anchor protein AKAP5 (AKAP79/150) is important for postsynaptic β-adrenergic signaling. *J. Biol. Chem.* 288, 17918–17931. doi: 10.1074/jbc.m112.449462

Zheng, C. Y., Seabold, G. K., Horak, M., and Petralia, R. S. (2011). MAGUKs, synaptic development, and synaptic plasticity. *Neuroscientist* 17, 493–512. doi: 10.1177/1073858410386384

Zhou, Z., Liu, A., Xia, S., Leung, C., Qi, J., Meng, Y., et al. (2018). The C-terminal tails of endogenous GluA1 and GluA2 differentially contribute to hippocampal synaptic plasticity and learning. *Nat. Neurosci.* 21, 50–62. doi: 10.1038/s41593-017-0030-z

Zhou, Q., Xiao, M., and Nicoll, R. A. (2001). Contribution of cytoskeleton to the internalization of AMPA receptors. *Proc. Natl. Acad. Sci. U S A* 98, 1261–1266. doi: 10.1073/pnas.98.3.1261

Zhu, J. J., Esteban, J. A., Hayashi, Y., and Malinow, R. (2000). Postnatal synaptic potentiation: delivery of GluR4-containing AMPA receptors by spontaneous activity. *Nat. Neurosci.* 3, 1098–1106. doi: 10.1038/80614

Conflict of Interest: The authors declare that the research was conducted in the absence of any commercial or financial relationships that could be construed as a potential conflict of interest.

frontiers in Synaptic Neuroscience

ORIGINAL RESEARCH
published: 21 April 2020
doi: 10.3389/fnsyn.2020.00015

Gelatinase Biosensor Reports Cellular Remodeling During Epileptogenesis

*Nathalie Bouquier, Benoit Girard, Juri Aparicio Arias, Laurent Fagni, Federica Bertaso and Julie Perroy**

IGF, Université de Montpellier, CNRS, INSERM, Montpellier, France

Epileptogenesis is the gradual process responsible for converting a healthy brain into an epileptic brain. This process can be triggered by a wide range of factors, including brain injury or tumors, infections, and status epilepticus. Epileptogenesis results in aberrant synaptic plasticity, neuroinflammation and seizure-induced cell death. As Matrix Metalloproteinases (MMPs) play a crucial role in cellular plasticity by remodeling the extracellular matrix (ECM), gelatinases (MMP-2 and MMP-9) were recently highlighted as key players in epileptogenesis. In this work, we engineered a biosensor to report *in situ* gelatinase activity in a model of epileptogenesis. This biosensor encompasses a gelatinase-sensitive activatable cell penetrating peptide (ACPP) coupled to a TAMRA fluorophore, allowing fluorescence uptake in cells displaying endogenous gelatinase activities. In a preclinical mouse model of temporal lobe epilepsy (TLE), the intrahippocampal kainate injection, ACPPs revealed a localized distribution of gelatinase activities, refining temporal cellular changes during epileptogenesis. The activity was found particularly but not only in the ipsilateral hippocampus, starting from the CA1 area and spreading to dentate gyrus from the early stages throughout chronic epilepsy, notably in neurons and microglial cells. Thus, our work shows that ACPPs are suitable molecular imaging probes for detecting the spatiotemporal pattern of gelatinase activity during epileptogenesis, suggesting their possible use as vectors to target cellular reactive changes with treatment for epileptogenesis.

Keywords: activatable cell-penetrating peptides (ACPPs), gelatinase, matrix metalloproteinases (MMPs), epileptogenesis, kainate (KA), molecular imaging probes

OPEN ACCESS

Edited by:
P. Jesper Sjöström, McGill University, Canada

Reviewed by:
Leszek Kaczmarek, Nencki Institute of Experimental Biology (PAS), Poland
Ute Häussler, University of Freiburg, Germany

***Correspondence:**
Julie Perroy
julie.perroy@igf.cnrs.fr

Received: *19 December 2019*
Accepted: *19 March 2020*
Published: *21 April 2020*

Citation:
Bouquier N, Girard B, Aparicio Arias J, Fagni L, Bertaso F and Perroy J (2020) Gelatinase Biosensor Reports Cellular Remodeling During Epileptogenesis. Front. Synaptic Neurosci. 12:15. doi: 10.3389/fnsyn.2020.00015

INTRODUCTION

The biology of excitatory synapses relies on its tetrapartite organization, which includes pre- and post-synaptic neurons, glial cells and the extracellular matrix (ECM) stabilizing synaptic contacts. Matrix Metalloproteinases (MMPs) are key components of the ECM and constitute a large family of proteases, most of which act in the extracellular space (Lukasiuk et al., 2011). Among them, MMP-2 and MMP-9 constitute the class of gelatinases and are amongst the most abundant MMPs in the brain. They have emerged as regulators of diverse biological processes under normal and pathological conditions. These secreted endopeptidases have a significant role in extracellular proteolytic processes at the excitatory synapses. In particular, MMP-9 contributes to the regulation of structural and functional synaptic plasticity (Nagy et al., 2006; Szepesi et al., 2013). It is locally

secreted at the level of dendritic spines in an activity-dependent manner (Konopacki et al., 2007), where it cleaves synaptic cell adhesion molecules and cell surface receptors (Tian et al., 2007; Szepesi et al., 2014), thus shaping dendritic spine morphology (Michaluk et al., 2009, 2011). Hence, disruption of the ECM allows structural and functional synaptic plasticity under physiological conditions, but can also, after an initial brain damage, induce aberrant molecular and cellular remodeling. These molecular modifications, which are still poorly understood, trigger cellular disturbances and disorganization of the networks that can lead to an epileptic brain over weeks.

Epilepsy is a brain disorder characterized by spontaneous and recurrent seizures due to hypersynchronous and excessive neuronal activities. In particular, temporal lobe epilepsy (TLE), the most widespread form of focal epilepsy, arises from epileptic foci located in the temporal neocortex and hippocampus. So far, therapeutic efforts were focused on treating symptoms, such as seizures. However, 30% of TLE patients are still resistant to currently available anti-epileptic drugs, a percentage that has not changed in decades despite the new medication. Hence, new treatments rather targeting the underlying disease mechanisms of the epilepsy pathogenesis should be explored (Terrone et al., 2016; Łukawski et al., 2018). This strategy goes through a better understanding of the establishment of the disease. Epileptogenesis is the mechanism leading to chronic seizures (Pitkänen and Engel, 2014). This dynamic process takes place after an initial insult and converts healthy brain tissue into an epileptic one, with hyper synchronization and hyperexcitability of the neuronal network. It involves a cascade of biological events such as neuronal cell death, proliferation, neuroinflammation, disruption of the blood-brain barrier, neuronal network reorganization and aberrant synaptic plasticity (Pitkänen and Sutula, 2002; Gorter et al., 2015; Łukawski et al., 2018). All these cellular reactive changes, which contribute to the formation of ictogenic neuronal networks, are hereafter included in the term "remodeling." The ECM is a structural scaffold that plays an important role in this detrimental rearrangement (Pitkänen et al., 2014).

Cumulative evidence indicates that gelatinases, and particularly MMP-9, play a fundamental function in epileptogenesis (Ikonomidou, 2014; Khomiak and Kaczmarek, 2018). MMP-9 is upregulated in several epilepsy animal models (Wilczynski et al., 2008) as well as in epileptic patients (Quirico-Santos et al., 2013; Acar et al., 2015). Intrahippocampal injection of kainate (KA) in rodents is an isomorphic epileptogenesis model, which mimics and recapitulates the main clinical features of human TLE. It induces a prolonged seizure, named status epilepticus, that triggers the epileptogenic process, leading to chronic seizures. Evidence of gelatinase implication in seizures was first described by Zhang et al. (1998) showing their upregulation after KA stimulation of rat brain, especially in the hippocampus. The increase of MMP-9 expression (at the mRNA and protein levels) and elevated enzymatic activity in the dentate gyrus play a role in epileptic focus formation (Szklarczyk et al., 2002; Jourquin et al., 2003). MMP-9 was thus proposed as a biomarker to investigate epileptogenesis (Yin et al., 2011; Bronisz and Kurkowska-Jastrzębska, 2016). Because gelatinases are released in a specific time and space-dependent manner at excitatory synapses, precise information about their kinetics of activation is necessary to propose new therapeutic strategies.

In this study, we examined gelatinase activities throughout the epileptogenesis process using an approach based on activatable cell-penetrating peptides (ACPPs). Gelatinase-based ACPPs have already been handled for imaging tumors (Olson et al., 2009, 2010; Nguyen et al., 2010) and ischemic stroke (Chen et al., 2017). We used them in an *in vivo* model of KA-induced epileptogenesis to delineate the gelatinase spatiotemporal activation profile. Not only this tool is of particular interest to finely localize cellular reactive changes during epileptogenesis, but it could also open opportunity for selective and local delivery of therapeutic agents targeted by gelatinase activity.

MATERIALS AND METHODS

Peptide Synthesis

Two peptides were designed from the original publication by Jiang et al. (2004). MMP-2/-9 cleavable ACPP presents the following amino acid sequence: Suc-e8-(Ahx)-PLGLAG-r9-(Ahx)-k(TAMRA)-NH2. As a negative control, a cleavable-resistant ACPP with scrambled linker was synthesized: Suc-e8-(Ahx)-LALGPG-r9-k(Cy5)-NH2. Ahx is a 6-aminohexanoic acid, a flexible hydrophilic linker to facilitate hairpin conformation. Capital letters indicate L-form amino acids and lowercase letters, D-form amino acids. Peptides were N-terminally capped with a succinyl (Suc) group to provide a ninth negative charge equivalent to glutamate without an amino group, and C-termini were amidated. The C-termini were labeled with TAMRA fluorophore coupled to a D-lysine k (Smart Bioscience, Saint-Egrève, France). Peptides were synthesized on a Symphony Synthesizer (Protein Technologies Inc., Tucson, AZ, USA), at a 0.1 mmol scale on a CTC resin (substitution approx. 1.6 mmol/g) and using TAMRA labeled Lysine. Fmoc protecting group was removed using 20% piperidine in DMF and free amine was coupled using ten fold excess of Fmoc amino acids and HCTU/DIEA activation in NMP/DMF (3 × 15 min). The peptide was deprotected and cleaved from the resin with TFA/H2O/1,3-dimethoxybenzene/TIS 92.5/2.5/2.5/2.5 (vol.), then precipitated out in cold diethyl ether. The resulting white solids were washed two times with diethyl ether, resuspended in H_2O/acetonitrile and freeze-dried to afford crude peptide. Finally, fluorophore-labeled peptides were purified by HPLC (C18 reverse-phase column, eluted with 10–40% acetonitrile in water with 0.1% CF3COOH) and lyophilized overnight. The molecular weight of all peptides was confirmed by mass spectroscopy (LC-ESI-MS), and the concentration of each peptide stock solution was verified by UV-vis absorbance.

Cell Culture

Primary cultures of hippocampal neurons were prepared from E18 Wistar rat embryos (Janvier Labs). Briefly, hippocampi were

dissected, treated with 0, 05% trypsin-EDTA, and mechanically disrupted by 10 cycles of aspiration and ejection through a micropipette tip. Dissociated hippocampal cells were seeded on coverslips in 35 mm dishes precoated with 50 μg/ml poly-D-lysine (Sigma–Adrich), in Neurobasal medium containing 2% B27 supplement, 10% heat-inactivated horse serum, 0.5 mM glutamine, and antibiotics (100 U/ml penicillin and 100 mg/ml streptomycin; Gibco). Neurons were maintained in water-saturated 95% air/5% CO_2 at 37°C. The seeding medium was replaced after 20 h with a serum-free neuronal culture medium. After 10 days of culture, the neurons were enriched by treatment with 5 μM cytosine b-D-arabinofuranoside hydrochloride (Sigma–Adrich) for 72 h. The cultures were used for experiments 15 days after plating.

Activation of Gelatinases in Cultures of Hippocampal Neurons

Activation of gelatinases in cultured neurons was performed by exposure to NMDA or glutamate: cells were washed three times with EBSS containing Ca^{2+}, and then stimulated with 100 μM NMDA or 50 μM glutamate for 10 min at 37°C in either absence or presence of Calcium Diethylene Triamine Penta Acetate (Ca-DTPA, 5 mM) a metal chelator and broad-spectrum MMP inhibitor. For β-Dystroglycan expression analysis, cells were further incubated for 10 or 30 min then lysed in 4X SDS sample buffer and denaturated by heating for 5 min at 95°C. For imaging of ACPPs uptake, following the transient NMDA or glutamate application, cells were incubated for 2 h 30 min with 1 μM of ACPPs and then fixed for 15 min with 4% paraformaldehyde (PFA) + 4% sucrose + Hoechst 33258 for nuclei staining. Coverslips were mounted with Mowiol for observation under an epifluorescent microscope equipped for optical sectioning (Apotome, Zeiss). The number of TAMRA stained cells was assessed with Cell Profiler, an automated image analysis software. The total number of cells was counted with blue stained nuclei (size range 6.5 μm–26 μm) as well as the number of positive red cells (size range 16 μm–40 μm) with an identical threshold of fluorescence intensity on three independent experiments (number of counted cells >2,000 per condition per experiment on a minimum of 10 fields acquired with a 10× objective).

Western Blot

Neuronal culture lysates containing an equal total amount of protein samples were loaded on 12% SDS-polyacrylamide gels and transferred onto nitrocellulose membranes (GE Healthcare) at 40 V overnight at 4°C. After incubation for 1 h in blocking buffer (PBS, 0.1% Tween-20, and 5% dried non-fat milk), membranes were incubated for 2 h at room temperature with an anti-β-dystroglycan primary antibody (NCL-b-DG, 1:500, Novocastra). The membranes were then incubated with horseradish peroxidase-labeled secondary antibody (Jackson Immuno Research Laboratories) diluted 1:5,000 for 1 h at room temperature. After washing, the immunoblot signals were visualized by enhanced chemiluminescence detection (Western Lightning ECL-Plus, PerkinElmer) and acquired on a ChemiDoc Touch Imaging System (Bio-Rad) controlled by Image Lab software version 3.0 (Bio-Rad). After incubation in a stripping solution (PBS, 0.1% Tween-20, 0.5% sodium azide), the same membranes were re-blotted with an anti-GAPDH (Sigma–Adrich, St. Louis, MO, USA, 1:30,000, G9545) for loading control. For quantification of changes in protein expression levels, band intensities were measured with ImageJ software. The optical density values of β-dystroglycan were normalized to those of GAPDH bands in the same sample and expressed as a percentage of control treatment.

Animals

A total of 58 mice were used in this study. All animal procedures were carried out following the European Communities Council Directive, approved by the French Ministry for Agriculture (2010/63/EU, file# 20170116171220 99) and supervised by the IGF institute's local Animal Welfare Unit (CEEA-LR36). Male C57BL/6 were purchased from Janvier Labs. Animals were housed under standardized conditions with a 12 h light/dark cycle, stable temperature (22 ± 2°C), controlled humidity (55 ± 10%), and food and water *ad libitum*.

Intrahippocampal Kainate Injection Model

The stereotaxic intrahippocampal KA injection is a mouse model of mesial TLE (Bouilleret et al., 1999). Briefly, wild-type C57BL6/J adult male mice (8–16 weeks-old) were intraperitoneally anesthetized with PBS-buffered solution containing 400 mg/kg chloral hydrate, plus a local subcutaneous injection of lidocaine (Xylocaine, AstraZeneca; 4 mg/kg in 50 μl of sterile 0.9% NaCl solution) and placed in a stereotaxic frame using the David Kopf mouse adaptor. All stereotaxic injections were performed using a 10 μl micro-syringe with a stainless steel 33G beveled needle controlled by a micro-pump. Mice were injected in the right dorsal hippocampus (AP = −2; ML = −1.5; DV = −2 mm from Bregma[1]) with 50 nl of a 20 mM solution of kainic acid (KA, 1 nmol; Sigma–Adrich) in 0.9% sterile NaCl. After recovery, the animals were kept under observation for 8–10 h post-injection and displayed non-convulsive status epilepticus defined by characteristic behavioral pattern (long-lasting period of immobility, head deviations, and asymmetric forelimbs movements or rotations). All the KA-injected mice showed DG dispersion when analyzed post-mortem. Control animals were injected with 50 nl of 0.9% sterile NaCl (saline solution) under the same conditions. Stereotaxic injections of ACPP peptide (0.2 nmol, 1 μl at 200 μM) at 200 nl/min were performed ipsilateral and contralateral of saline solution or KA injection (AP = −2.5; ML = ±1.5; DV = −2 mm from Bregma) 7 days before sacrifice. For all ACPPs injection experiments, a total of 52 mice were used. Three independent experiments were performed, with 2–3 animals injected per condition for each experiment.

For EEG recording, six mice were implanted right after KA intrahippocampal injection, at the same coordinates with a bipolar tungsten electrode, as well as skull cortical electrodes on the frontoparietal bone and a reference electrode on

[1]https://scalablebrainatlas.incf.org

the occipital bone. EEG activity was recorded as previously described (Girard et al., 2019) every 2 days during the first week, and then once a week. Briefly, micro connectors on freely moving animals were plugged into an EEG amplifier (Pinnacle Technology Inc.). EEG recordings were performed with parallel video monitoring of animal behavior. Hippocampal seizures were automatically detected using pClamp® software. The threshold for detection of paroxystic activities was set at 3-fold the standard deviation of the signal amplitude without seizures and a 10 ms event duration. Peak detection was visually checked a posteriori. Traces of EEG recordings were classified according to severity scores: score 0: normal activity (control state); score 1: low-voltage background activity; score 2: spikes; score 3: short discharges; score 4: long discharges; score 5: recurrent seizures; score 6: secondarily generalized seizures. Example traces in **Figure 3** illustrate the progression of seizures from KA injection up to the chronic phase.

Tissue Preparation and Immunohistochemistry

One day to 8 weeks after KA injection, mice were anesthetized using pentobarbital (Euthasol®, 400 mg/ml, injected 360 mg/kg) and transcardially perfused with 4% (w/v) PFA. Mouse brains were dissected, postfixed in PFA for 36 h and cut into serial 35 μm-thick coronal sections with a vibratome (VT1000S; Leica). Free-floating sections were rinsed three times in PBS and incubated for 20 min in PBS/0.2% Triton X-100 for permeabilization, and blocked in PBS/3% BSA for 1 h. Slices were then incubated in PBS/1% BSA/ 0.1% Triton X-100 overnight at 4°C with different primary antibodies: chicken anti-GFAP (1:300 dilution, ab4674; Abcam), rabbit anti-Iba1 (1:1,000, #019-19741; Wako), mouse anti-NeuN (1:300, MAB377; Millipore) and rabbit anti-laminin (1:300, L9393; Sigma–Adrich). The day after, sections were rinsed three times for 10 min in PBS and incubated for 2 h with fluorophore-conjugated secondary antibodies: AMCA anti-chicken 1:300, Alexa Fluor 680 anti-rabbit 1:1,000, Alexa Fluor 488 anti-mouse 1:1,000 and nuclear DNA dye Hoechst 33258. The sections were rinsed in PBS three times 10 min before mounting in DPX. At least three slices per animal were processed. Images were acquired with an AxioImager Z1 Zeiss microscope equipped for optical sectioning (Apotome) and with appropriate epifluorescence filters. All parameters were held constant for all sections and for each staining to allow comparison between samples.

Statistical Analysis

Data are presented as the means ± SEM of at least three independent experiments. GraphPad Prism v7.02 software was used to perform statistical analyses. We used the non-parametric Kruskal–Wallis test followed by Dunn's multiple comparison test for Western blot analysis and one-way ANOVA test followed by Tukey's multiple comparison test for immunofluorescence quantification. Statistical significance was determined as $^{*}p < 0.05$; $^{**}p < 0.01$ and $^{***}p < 0.001$.

RESULTS

Neuronal Excitation Induces Endogenous Gelatinase Activation

To characterize the uptake of ACPPs in neuronal cells, we first searched for suitable gelatinase activation conditions *in vitro* in primary cultures of hippocampal neurons. β-dystroglycan (β-DG) was identified previously as a native substrate of MMP-9 that is cleaved in response to enhanced neuronal activity (Michaluk et al., 2007). The proteolytic cleavage of the 43 kDa full-length transmembrane β-DG protein leads to the formation of a 30 kDa product, readily detectable by Western blot. Hence, endogenous gelatinase activation can be indirectly measured by β-DG cleavage assay. We adopted two different protocols of gelatinase activation using transient NMDA (100 μM; Tian et al., 2007), or glutamate (50 μM; Dziembowska et al., 2012) treatments for 10 min. Cleavage of β-DG increased 10 min after the end of stimulation and even more significantly 30 min later (**Figure 1A**; **Supplementary Figures S1, S2**). This cleavage was abolished by applying Ca-DTPA, a broad-spectrum MMP inhibitor (**Figure 1B**). Thus, NMDA or glutamate application causes the activation of endogenous gelatinases.

ACPPs Report Endogenous Gelatinase Activation

We investigated if ACPPs could detect NMDA- or glutamate-induced endogenous gelatinase activation in neurons. ACPPs are peptidic biosensors composed of a polycationic cell-penetrating part connected to a neutralizing polyanion *via* a cleavable linker. In this hairpin conformation, the masking of positive charges prevents biosensor internalization (**Figure 2A**). The linker is a specific target of gelatinases. Upon gelatinases activation, proteolysis of the linker allows the dissociation of the two domains and enables the polycationic CPP to enter cells (Jiang et al., 2004; Aguilera et al., 2009). A red TAMRA fluorophore is coupled to the CPP part (**Figure 2A**). Hence, fluorescence uptake by the cell reports gelatinase activity.

After transient stimulation for 10 min with NMDA or glutamate, neurons were incubated with ACPPs. NMDA or glutamate stimulation strongly increased the number of TAMRA fluorescent cells compared to unstimulated neurons (**Figure 2B**). Ca-DTPA prevented NMDA- or glutamate-induced fluorescence uptake suggesting that gelatinase activation was involved in the process. Moreover, NMDA or glutamate stimulation failed to induce the uptake of scrambled-ACPP that cannot be cleaved by gelatinases (**Figure 2B**). We further quantified a 12-fold increase of gelatinase ACPPs uptake by NMDA or glutamate stimulation, compared to unstimulated condition (**Figure 2C**).

The coherence between results obtained by Western Blot (**Figure 1**) and with gelatinase biosensor in living cells (**Figure 2**) upon enhanced neuronal activity validates the use of ACPPs to report endogenous gelatinase activities by *in situ* detection of TAMRA fluorescence.

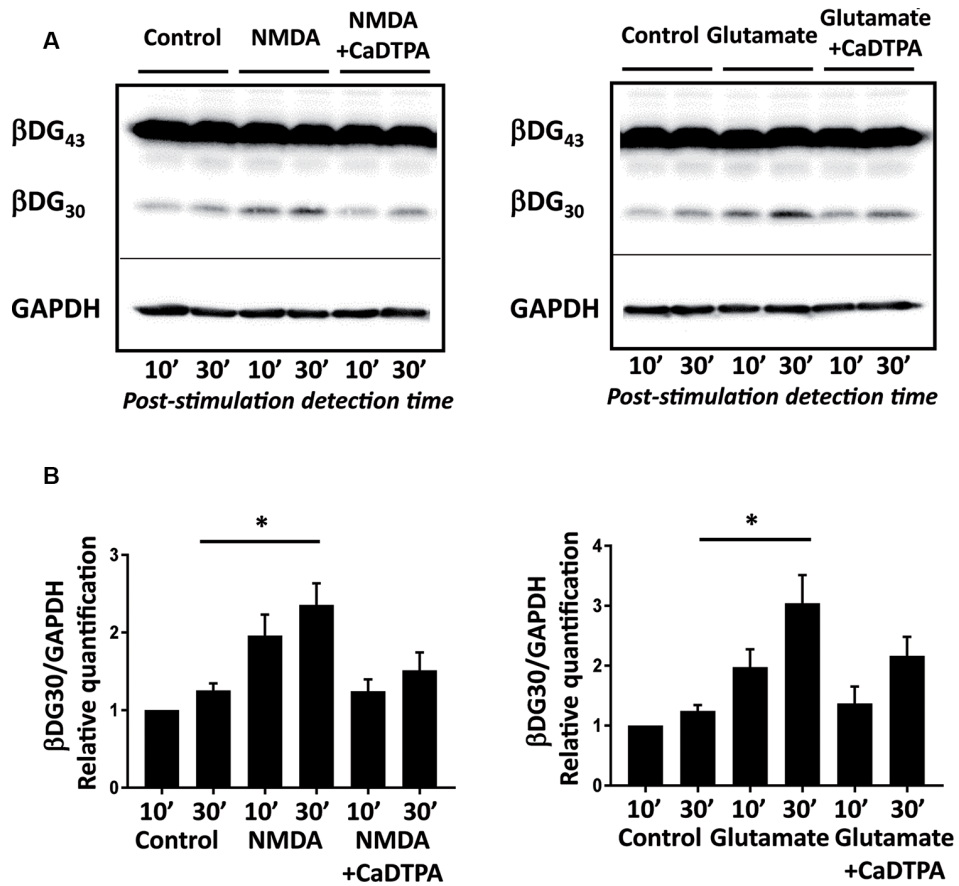

FIGURE 1 | NMDA or glutamate stimulations activate endogenous gelatinases in cultured neurons. **(A)** Rat hippocampal neurons (14 DIV) were stimulated for 10 min with NMDA 100 μM or glutamate 50 μM with or without Ca-DTPA, a metal chelator and a broad range inhibitor of MMPs activity, then incubated for 10 or 30 min before lysis. Endogenous gelatinase activation was detected by cleavage of β-dystroglycan (β-DG), an MMP-9 substrate, by Western Blot. **(B)** Quantification of 30 kD β-DG cleavage product relative to GAPDH as a protein loading control. Graph represents mean values ± SEM (n = 4 independent experiments). Non-parametric Kruskal–Wallis test (p-value = 0.0018 for NMDA experiments and p-value = 0.0003 for glutamate experiments) followed by Dunn's multiple comparison test where $^*p < 0.05$ (control 30 min vs. stimulation 30 min).

ACPPs Report *in vivo* Gelatinase Activity in Epileptogenic Mouse Brain

We next used ACPPs to report gelatinase activity *in vivo*, in a mice model of epileptogenesis. We and others have previously shown that a single intrahippocampal injection of kainic acid (KA) in the right hemisphere of the brain initiates cellular remodeling leading to focal TLE (Bouilleret et al., 1999; Girard et al., 2019). We injected mice unilaterally with KA and ACPPs in both ipsilateral and contralateral sides (**Figure 3A**). Animals were sacrificed at three different time points after KA injection: at 24 h, after 7 days (early phase) or once seizures were spontaneous and chronic (8 weeks, chronic phase, **Figure 3C**). As expected, we observed the characteristic neuronal loss in the CA1 and CA3 areas of the hippocampus and the progressive granular cell dispersion in the dentate gyrus (**Figure 3D**). EEG recordings reported continuous progression of electrical brain activity, from low-voltage background activity 24 h after KA injection, followed by short discharges at 7 days, until recurrent, mature seizures at 8 weeks which are characteristic of an excitation/inhibition imbalance, neuronal hyperexcitability and hyper synchronization (**Figure 3D**).

At the site of KA injection, the spatial distribution of TAMRA fluorescence changed over time, revealing specific patterns of gelatinase activation throughout the epileptogenic process (**Figure 4**). Kinetics in the ipsilateral side is the most informative (**Figures 4D–F,M**). Twenty-four hours after KA injection, red fluorescent positive cells appeared in CA1, in the hilus, and to a less extent in the granular cell and molecular layers (**Figures 3B**, **4D,M**). These data are as per previous studies showing MMP activation by status epilepticus (Szklarczyk et al., 2002; Jourquin et al., 2003), and therefore they validate the ACPPs. Seven days after KA injection, this fluorescent uptake was reinforced, with stronger staining visible in CA1 and in dispersing granular cell layer (**Figures 4E,M**). CA1 is known to be the region where strong rearrangements and cell death occur during epilepsy onset. Indeed, in our experiment, a disturbed laminin staining reported KA-induced cell disorganization and cell death process as soon as 24 h (**Figure 5A**). Laminin is a key component of

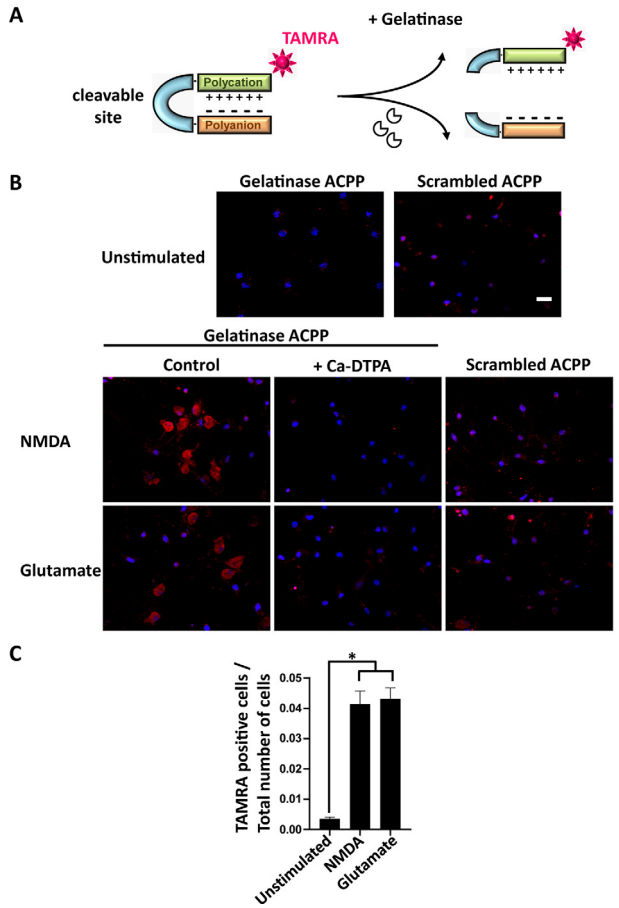

FIGURE 2 | Activatable cell penetrating peptides (ACPPs) can report gelatinase activation by cellular uptake of fluorescence. **(A)** Structure of ACPPs: a cell-penetrating polycationic part (green) is attached to a polyanionic sequence (orange) *via* a cleavable linker (blue). In the presence of active gelatinases (MMP-2/-9), the ACPP is cleaved. The cell-penetrating polycationic part coupled to a TAMRA fluorophore is released and can then enter into surrounding cells. **(B)** Cellular uptake of TAMRA fluorophore induced by NMDA or glutamate transient perfusion. Rat hippocampal neurons (DIV14) were stimulated for 10 min with NMDA (100 μM) or glutamate (50 μM), with or without the broad-spectrum Matrix Metalloproteinase (MMP) inhibitor Ca-DTPA (5 mM), then incubated for 2 h 30 in presence of 1 μM gelatinase ACPPs or an ACCP containing an uncleavable scrambled sequence as a linker (scrambled-ACPP). Hoechst labeled nuclei (blue). Scale bar 20 μm. **(C)** Quantification of the number of TAMRA fluorescent cells in gelatinase-ACPP treated cultures in control, NMDA or glutamate stimulated conditions. The graph represents mean values ± SEM ($n > 30$ fields for each condition, in three independent experiments). One-way ANOVA test (p-value = 0.0264) was performed followed by Tukey's multiple comparison test where $^*p < 0.05$ (control vs. stimulations).

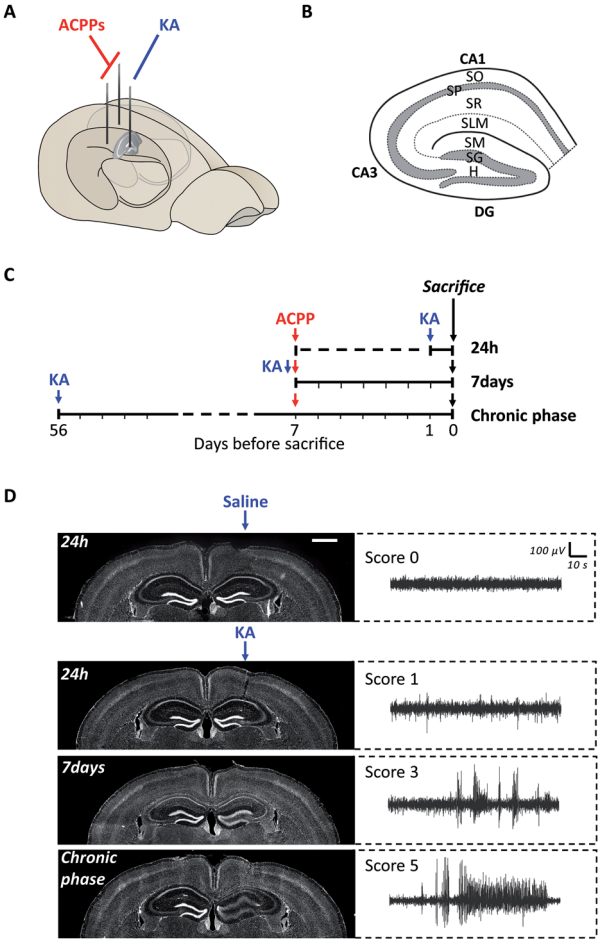

FIGURE 3 | Experimental protocol of ACPPs injection in a mouse model of epileptogenesis. **(A)** Scheme of kainic acid (KA) and ACPPs injections in hippocampal hemispheres. **(B)** Scheme of hippocampal structure and lamination. CA, cornu ammonis; DG, dentate gyrus; H, hilus; SO, stratum oriens; SP, stratum pyramidale; SR, stratum radiatum; SLM, stratum lacunosum-moleculare; SM, stratum moleculare; SG, stratum granulosum. **(C)** Experimental procedure: timeline of injections. **(D)** Hoechst labeled nuclei showing progressive dentate gyrus cell dispersion in KA injected hippocampus, characteristic of epileptogenesis (scale bar: 1 mm). Corresponding EEG recordings representative of the different severity scores are shown on the right. Score 0: normal activity; score 1: low-voltage background activity; score 3: short discharges; score 5: recurrent seizures.

the ECM and a gelatinase substrate (Chen et al., 2003; Gu et al., 2005). Much more vessels were also visible in the KA-injected hemisphere correlating with the progressive disappearance of intact cells in CA1 and dentate gyrus (**Figure 5B**; Sarkar and Schmued, 2010). In the KA-treated hippocampus, the increased ACPP uptake appeared as a negative picture of laminin staining (**Figure 5C**), highlighting gelatinase activity in direct proximity of disorganized cells. In the chronic phase (8 weeks after KA injection, **Figures 4F,M**), red fluorescence stained cells in the diffuse CA1 and the expanded granular cell layer. In the contralateral side, ACPPs localized in CA1 areas 24 h and 7 days after KA injection and in a sparse punctiform staining in the chronic phase. Vessels in stratum lacunosum moleculare were also stained.

Differences between saline (**Figures 4A–C,M**) and KA injections (**Figures 4D–F,M**) were detected. In saline-injected mice, contralateral sites exhibit almost no TAMRA fluorescence. In contrary, ipsilateral injection shows a uniform sparse punctiform staining in the whole hippocampus. This staining, which may reflect a basal gelatinase activation due to inflammation caused by the injection itself, is more important

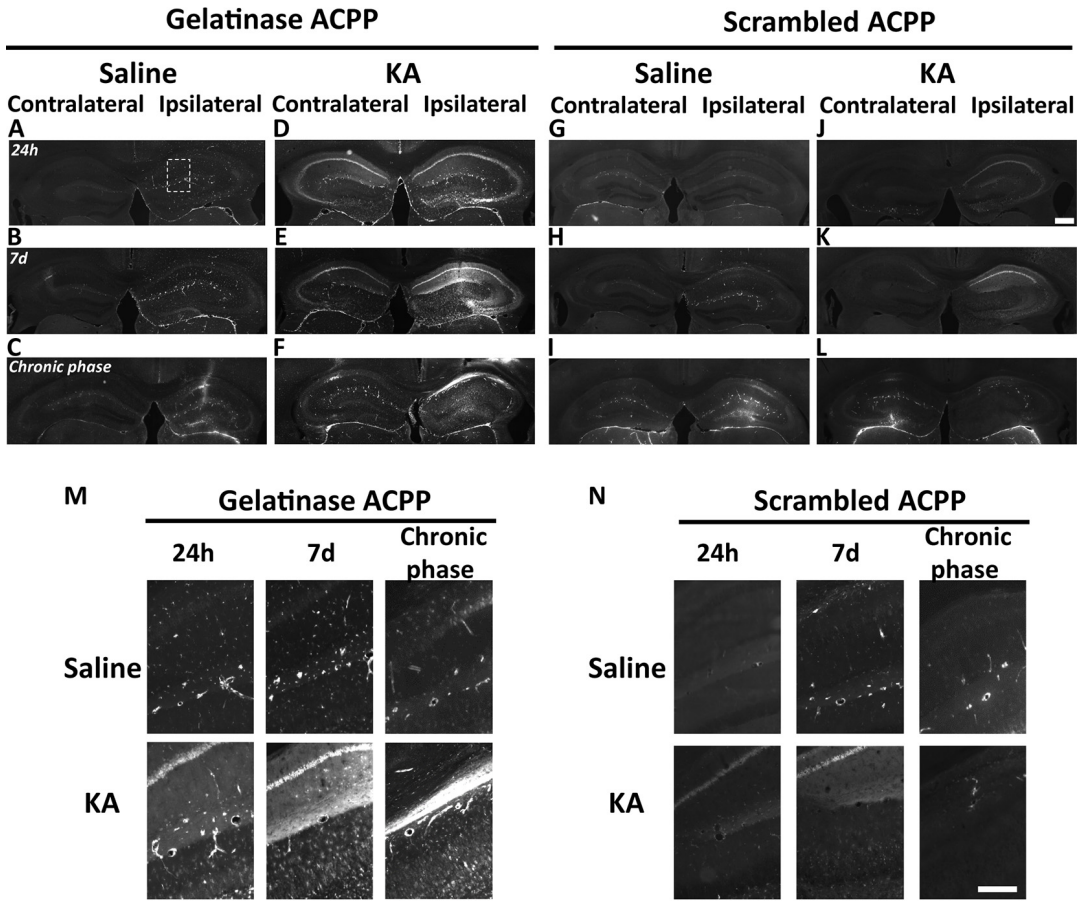

FIGURE 4 | Detection of *in vivo* gelatinase activity by cleavage of ACPPs in the epileptogenic mouse brain. **(A–L)** TAMRA ACPP fluorescence in mice brains injected with KA **(D–F,J–L)** or saline solution **(A–C,G-I)** in the right hippocampus, and gelatinase-ACPP **(A–F)** or scrambled-ACPP **(G–L)** in ipsi- and contralateral sites. Mice were sacrificed 24 h, 7 days or 8 weeks after KA injection (n = 3 independent experiments, two or three animals injected per condition for each experiment). **(M,N)** Enlarged image of the outlined area in panel **(A)** showing TAMRA Gelatinase- **(M)** or Scrambled- **(N)** ACPP fluorescence in the ipsilateral hippocampus. Scale bars: **(J)**, 500 μm, **(N)** 250 μm.

after 1 week of exposure but negligible compared to the KA-injected hippocampus (magnifications of the ipsilateral side are provided in **Figure 4M**). No particular staining was noticed with saline injections during the chronic phase, except in vessels.

Finally, the cleavage-resistant scrambled peptide was used as control (**Figures 4G–L,N**) and indicates TAMRA fluorescence background. In the saline-injected hippocampus (**Figures 4G–I**), no TAMRA fluorescence uptake was detected in the contralateral side and slight staining in microvasculature was noticed in the ipsilateral side (**Figure 4N**). In the KA-injected hippocampus (**Figures 4J–L,N**), a weak red signal probably due to neuronal death was observed in CA1 structure in the ipsilateral side only, but much weaker than the fluorescence of gelatinase ACPP samples. The scrambled peptide, therefore, validated the specificity of fluorescence uptake, essentially induced by gelatinase substrate cleavage.

ACPPs Reveal Cell-Type-Specific Kinetics of Gelatinase Activity During Epileptogenesis

To investigate in which cell type gelatinases are activated, we performed immunostaining with markers for neurons (NeuN), microglia (Iba1) and astrocytes (GFAP; **Figure 6**).

In the KA-injected hippocampus, 24 h after injection gelatinase activity reported by fluorescence uptake correlated with NeuN in CA1 neurons (**Figure 6A**). A sparse homogenous staining of microglia was detected in the same area (**Figure 6D**). After 1 week, the fluorescence uptake in neurons in the stratum pyramidale was further increased (**Figure 6B**), together with neurons from the granular cell layer and hilus (**Figure 6K**). We noticed a concomitant increase of gelatinase activity in microglia and astrocytes from the molecular layer (**Figures 6N,Q**). Finally, in the chronic phase, dispersed neurons from the stratum

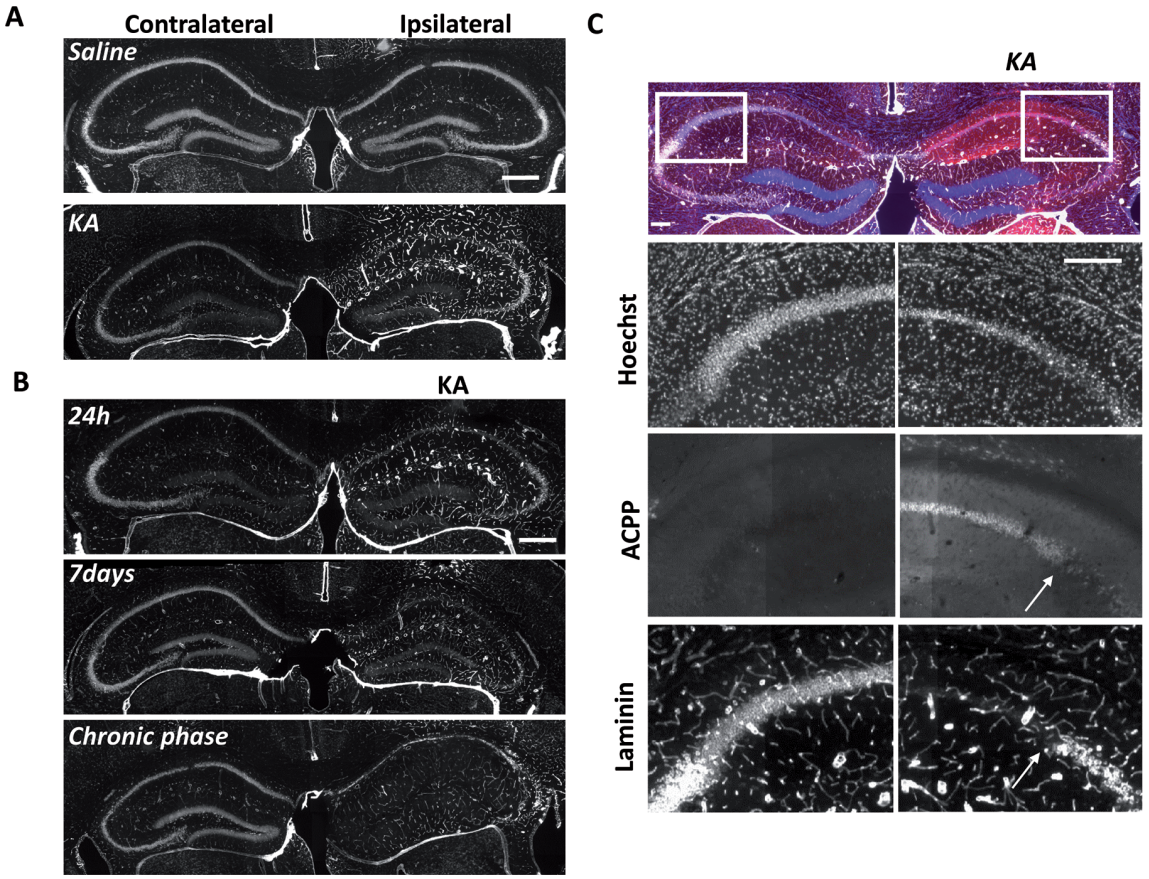

FIGURE 5 | Uptake of ACPP is superimposed to loss of neuronal laminin in KA treated brain. **(A)** Laminin immunoreactivity in saline or KA-injected hippocampus 24 h after injection. **(B)** Progressive changes of laminin expression during the different phases of epileptogenesis. **(C)** Magnification of laminin loss in CA1–CA2 region 7 days after KA injection. The white arrow shows the limit between ACPP uptake and intact laminin (right panels), whereas no TAMRA fluorescence is detectable in the contralateral side and laminin is intact. TAMRA ACPPs (red), Laminin (white), Hoechst (blue). Scale bars: **(A,B)** 500 μm, **(C)** 200 μm.

pyramidale and granular cell layer displayed gelatinase activity (**Figures 6C,L**). At that stage, microglia still displayed gelatinase activity in molecular and granular cell layers, while astrocytes did not (**Figures 6O,R**). We also noticed in the contralateral part a sparse ACPP positive microglia staining in the chronic phase (data not shown), revealing that inflammation also occurs in the contralateral side of the epileptic brain. In saline-injected conditions the punctiform ACPP fluorescence uptake corresponded to Iba1 positive cells, confirming our previous hypothesis that a basal gelatinase activation by microglia was due to the injection *per se* (not shown).

These data reveal a cell-type-specific temporal and spatial pattern of activation throughout the epileptogenic process. In particular, the common marker along the process is the microglia, confirming an essential role for neuroinflammation in epileptogenesis.

DISCUSSION

The present work reports the *in situ* gelatinase activation during epileptogenesis using ACPPs. To this end, we engineered a biosensor which enters cells upon gelatinase activation. Cell fluorescence uptake of ACPPs but not uncleavable scrambled forms validate the specificity of the biosensor to report gelatinase activity. This gelatinase activity appears as the negative picture of an intact ECM stained by laminin, confirming that the biosensor is staining cells undergoing remodeling in the vicinity of ECM disruption. Cellular remodeling reported by the ACPPs confirmed the main features of KA-induced epileptogenesis (Pernot et al., 2011), in particular the fact that CA1 is one of the main regions suffering strong rearrangements during epilepsy onset, therefore validating the utility of ACPPs as a biomarker of cellular reorganizations during epileptogenesis. Taking gelatinase-sensitive ACPPs as biomarker of cellular remodeling, we here refine the spatio-temporal pattern of specific cell-types disorganization during epileptogenesis. We found that structural changes in CA1 during status epilepticus, in particular in neurons from the stratum pyramidale in the ipsilateral side, is followed shortly after by dentate gyrus disorganization from hilus to granular cell and molecular layers. In the epileptic brain, cellular

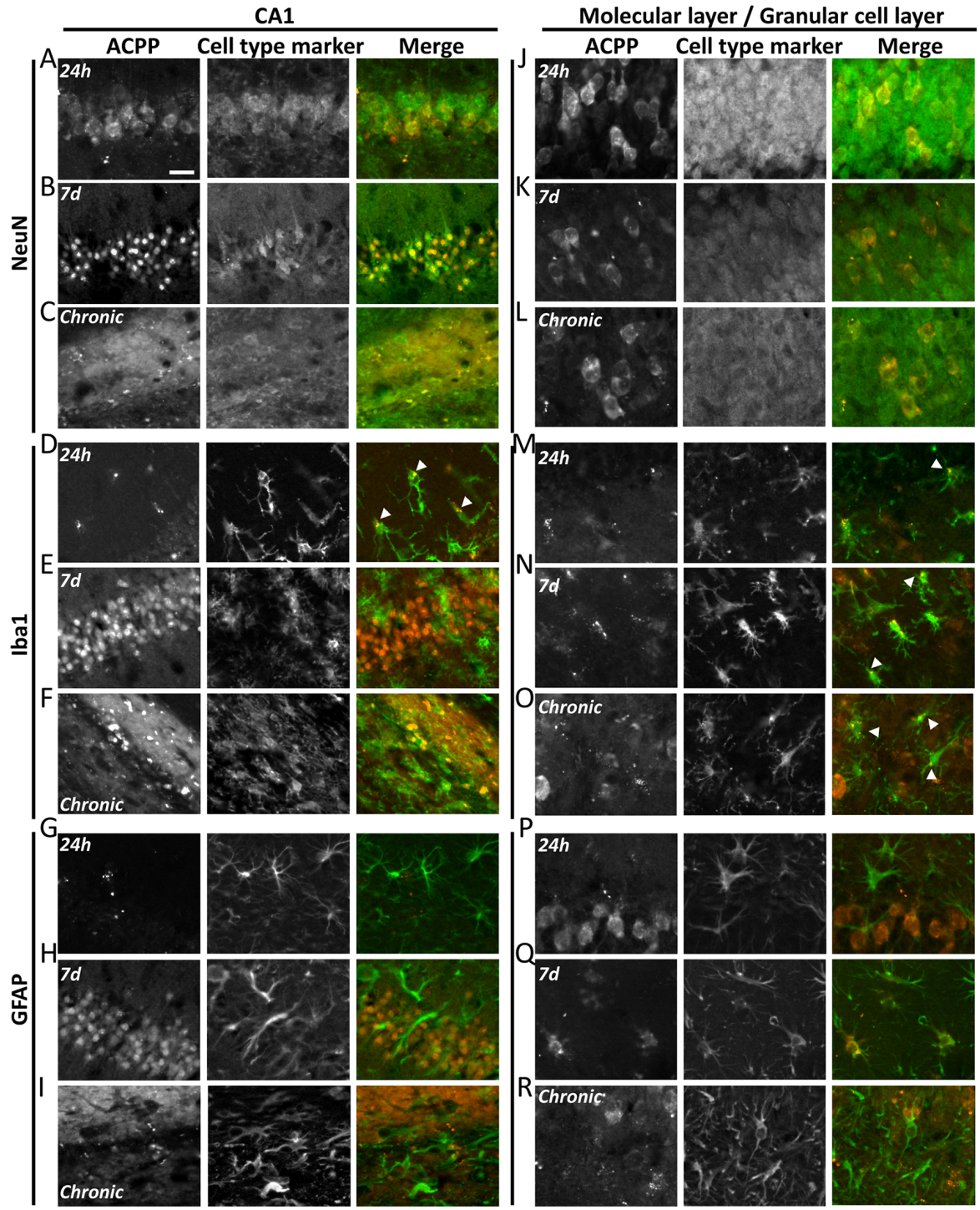

FIGURE 6 | ACPPs reveal cell-type-specific kinetics of gelatinase activity during epileptogenesis. The gelatinase spatiotemporal activation profile was observed with gelatinase-ACPP uptake in CA1 and molecular and granular layers of KA-injected hippocampi at 24 h, 7 days after KA injection or during the chronic phase. Slices were stained with neurons marker NeuN **(A–C,J–L)**, microglial marker Iba1 **(D–F,M–O)** or astrocytic marker GFAP **(G–I,P–R)**. Merge of the cell type marker (green) and TAMRA ACPP (orange) are shown. *n* = 3 independent experiments, two or three animals injected per condition for each experiment, three slices per mouse were used. Scale bar 20 μm.

remodeling still occurs in diffuse CA1 and expanded granular cell layer. Microglia activation appears as an early phenomenon, lasting all along the epileptogenesis process, while astrocytes remodeling is more transient. Interestingly,

these rearrangements are not restricted to the ipsilateral side since in the contralateral hippocampus, ACPPs reports cellular rearrangement in CA1 area 24 h and 7 days after KA injection and a sparse punctiform staining in the chronic phase, due to weaker but prolonged inflammatory processes in the epileptic brain. In KA-injected mice, the absence of fluorescence background with scrambled-ACPPs (no cell death) in the contralateral side together with gelatinase-ACPPs uptake in microglia cells may support a role of neuroinflammation in neuronal cell death protection (Zattoni et al., 2011).

Our study shows that only isolated cells incorporate the ACPP but not surrounding cells, suggesting that the cleaved peptide does not diffuse away from the gelatinase activity but is rather up-taken immediately. We took a profit on this property to identify specific cell-types undergoing remodeling during epileptogenesis. An interesting point is the ACPP colocalization in activated microglial cells in the hippocampal region suggesting a significant role of gelatinases in neuroinflammation as well as the importance of inflammation in epileptogenesis. This observation is consistent with the fact that microglia are among the main sources of gelatinases while they play an important role in epileptogenesis (Kalozoumi et al., 2018). We used gelatinase ACPPs in a preclinically relevant mouse model of TLE, achieved by intrahippocampal application of KA. The initial status epilepticus triggers a massive cellular reorganization over a few days/weeks (early phase), followed by spontaneous chronic seizures around 3 weeks post-SE. This model leads to severe alterations, such as ipsilateral loss of CA1 neurons, dentate gyrus dispersion, and focal hippocampal seizures and inflammation. Those events are spatiotemporally restricted and imply a cell-specific and activity-driven modification of the pericellular environment. In this context, gelatinases are locally secreted at excitatory synapses with proteolytic activity in extracellular space, especially close to dendritic spines of hippocampal neurons following KA stimulation (Konopacki et al., 2007). The localization of ACPPs' is following previous findings showing an upregulation of MMP-9 expression (mRNA and protein levels) and enzymatic activity in the hippocampal dentate gyrus after KA treatment (Zhang et al., 1998; Szklarczyk et al., 2002; Wilczynski et al., 2008). Yet Szklarczyk et al. (2002) showed stronger activity in molecular and granule cell layers whereas, in our experiments, ACPPs uptake happened more in CA1 and hilus after 24 h of exposition, where cell death occurs. However, these differences in gelatinase activation might be due to nuances in animal models, as previous studies were performed mainly 24 h only after KA injection and KA was administered intraperitoneally. The time course after status epilepticus and the severity of the cellular alterations depend on the studied model and can thus affect the profile of molecular changes. Other epileptic models could be refined using ACPPs. Finally, here we focused on the hippocampus, but some sparse staining was present in other brain areas such as cortex and striatum (data not shown) which could be explained by ACPPs uptake far from the KA application site. An alternative hypothesis is that ACPPs stain hippocampal projections, which would allow reporting with high spatio-temporal resolution neuronal networks undergoing remodeling during epileptogenesis. To get the full picture of cellular remodeling during epileptogenesis, gelatinase activity in other brain regions could also be explored.

Tools are required to assess gelatinase activity *in vivo* and *in vitro* to decipher their various functions such as extracellular remodeling. ACPPs display a polycationic cell-penetrating part composed of D-arginine residues attached *via* a cleavable L-amino acid linker (PLGLAG) to a matching polyanionic sequence of D-glutamate residues. ACPPs adopt a hairpin confirmation due to neutralization between the polyanionic amino acids and the cell-penetrating polycations. When the linker is cleaved by active gelatinases, the two parts dissociate and ACPPs deliver their payload inside the cell (here a TAMRA fluorescent molecule) *via* endocytosis. Our results are consistent with prior findings that ACPPs can be cleaved by secreted MMP-2/-9 and the released CPPs are incorporated into cells displaying the gelatinase activity, for example, tumor cells (Jiang et al., 2004; Aguilera et al., 2009; Olson et al., 2009) and ischemic zones (Chen et al., 2017).

Different techniques to detect MMP-2/-9 proteolytic activity have been used, including the commonly employed *in situ* zymography, based on dye-quenched-gelatin, a fluorogenic gelatinase substrate. The main drawback of these probes is their limited spatiotemporal resolution. A FRET-based biosensor was also recently described (Stawarski et al., 2014) but its use requires exogenous surexpression. In contrast, ACPPs appear as a more reliable and ready-to-use technique to detect *in vivo* MMP-2/-9 activity. The main advantages of ACPPs are the possibility to be used *in vivo*, the fact that they are readily imageable (contrary to the indirect classical zymography technique), and can be adapted to other proteases. We chose to detect the total activation of gelatinases instead of the cleavage of one specific substrate to reliably report ECM disruption and associated cellular remodeling; but on the other hand, in our experiments, we cannot discriminate the involvement of MMP-2 vs. MMP-9, although the latter seems to be the predominant enzyme responsible for these processes (Khomiak and Kaczmarek, 2018). The next improvements would include the design of an MMP-9-specific ACPP. Among the wide range of various substrates for MMP-9, the PRSLS sequence described by Fudala et al. (2012) could be a good candidate. Furthermore, ACPPs could be visualized with the recently developed brain optical clearing technique iDISCO for a 3D mapping of gelatinase activity in the epileptogenic brain at different times. This approach would offer a global overview of proteolytic events, including long-range projections that might be affected by the local KA treatment.

Efforts to improve the precise temporal relationship of cellular reactive changes during epileptogenesis could provide biomarkers (Engel and Pitkänen, 2019) and promote therapeutic intervention in the epileptogenic process (Pitkänen and Lukasiuk, 2011; Goldberg and Coulter, 2014). Because

gelatinases are released in a specific time and space-dependent manner, precise information about their kinetics of activation could be used to target anti-epileptogenic drugs in a controlled-delivery manner, fusing a pharmacological compound to ACPPs instead of the fluorescent TAMRA reporter. Gelatinase activity itself could be tuned in cells undergoing remodeling. MMP-9 is indeed the predominant gelatinase involved in epilepsy and has been proposed to be a potential therapeutic target (Yin et al., 2011). Recent studies on human brain surgery tissues showed an upregulation of MMP-9 in epileptogenic hippocampal lesions of patients with TLE (Li et al., 2012; Konopka et al., 2013; Quirico-Santos et al., 2013). The search for novel MMP inhibitors is ongoing, and recently a new molecule, DP-b99, was shown to impair epileptogenesis in animals (Yeghiazaryan et al., 2014), but further investigation is needed to achieve their controlled spatiotemporal delivery. All these works open up new therapeutic opportunities.

To conclude, our approach to detect gelatinase activation enables an *in situ* molecular imaging, providing an overall view of their distribution over a period at the cellular level after status epilepticus and revealed a microglia-neurons joint involvement during epileptogenesis. Thus ACPPs are *in vivo* targeting agents able to investigate the contribution of gelatinases in physio-pathological processes. Their use as molecular imaging probes is an interesting approach for visualizing enzyme activity and may ultimately allow targeting synaptic dysfunction in neurological disorders, such as the pathogenesis of epilepsy.

DATA AVAILABILITY STATEMENT

All datasets generated for this study are included in the article/**Supplementary Material**.

ETHICS STATEMENT

The animal study was reviewed and approved by the French Ministry for Agriculture (2010/63/EU, file # 2017011617122099) in accordance with the European Communities Council Directive, and supervised by the IGF institute's local Animal Welfare Unit (CEEA-LR36).

AUTHOR CONTRIBUTIONS

NB, BG, LF, FB, and JP designed the experiments, analyzed and interpreted the data. NB performed all molecular biology and *in vitro* experiments. BG, FB, and JA performed intrahippocampal kainate and ACPPs injections all along the epileptogenic process. NB performed tissue preparation, immunohistochemistry and image acquisitions with the help of BG. NB and JP wrote the manuscript with input from FB and BG. JP supervised the project.

FUNDING

This work was supported by the European Research Council (ERC) under the European Union's Horizon 2020 research and innovation program (JP, Grant agreement No. 646788), the Agence Nationale de la Recherche (JP, ANR-13-JSV4-0005-01) and the Région Languedoc-Roussillon (Chercheur d'Avenir) to JP.

ACKNOWLEDGMENTS

We thank the animal facility (iExplore platform of RAM, Montpellier, France), Muriel Asari from the IGF communication service for scheme illustrations and Etienne Audinat (IGF, Montpellier, France) for fruitful discussions.

SUPPLEMENTARY MATERIAL

The Supplementary Material for this article can be found online at: https://www.frontiersin.org/articles/10.3389/fnsyn.2020.00015/full#supplementary-material.

FIGURE S1 | Anti-beta-dystroglycan Western Blot of stimulations of endogenous gelatinases in cultured neurons.

FIGURE S2 | Anti-GAPDH Western Blot (loading control) of stimulations of endogenous gelatinases in cultured neurons.

REFERENCES

Acar, G., Tanriover, G., Acar, F., and Demir, R. (2015). Increased expression of matrix metalloproteinase-9 in patients with temporal lobe epilepsy. *Turk. Neurosurg.* 25, 749–756. doi: 10.5137/1019-5149.jtn.10738-14.0

Aguilera, T. A., Olson, E. S., Timmers, M. M., Jiang, T., and Tsien, R. Y. (2009). Systemic *in vivo* distribution of activatable cell penetrating peptides is superior to that of cell penetrating peptides. *Integr. Biol.* 1, 371–381. doi: 10.1039/b904878b

Bouilleret, V., Ridoux, V., Depaulis, A., Marescaux, C., Nehlig, A., Le Gal La Salle, G., et al. (1999). Recurrent seizures and hippocampal sclerosis following intrahippocampal kainate injection in adult mice: electroencephalography, histopathology and synaptic reorganization similar to mesial temporal lobe epilepsy. *Neuroscience* 89, 717–729. doi: 10.1016/s0306-4522(98)00401-1

Bronisz, E., and Kurkowska-Jastrzębska, I. (2016). Matrix metalloproteinase 9 in epilepsy: the role of neuroinflammation in seizure development. *Mediators Inflamm.* 2016:7369020. doi: 10.1155/2016/7369020

Chen, S., Cui, J., Jiang, T., Olson, E. S., Cai, Q. Y., Yang, M., et al. (2017). Gelatinase activity imaged by activatable cell-penetrating peptides in cell-based and *in vivo* models of stroke. *J. Cereb. Blood Flow Metab.* 37, 188–200. doi: 10.1177/0271678x15621573

Chen, Z. L., Indyk, J. A., and Strickland, S. (2003). The hippocampal laminin matrix is dynamic and critical for neuronal survival. *Mol. Biol. Cell.* 14, 2665–2676. doi: 10.1091/mbc.e02-12-0832

Dziembowska, M., Milek, J., Janusz, A., Rejmak, E., Romanowska, E., Gorkiewicz, T., et al. (2012). Activity-dependent local translation of matrix metalloproteinase-9. *J. Neurosci.* 32, 14538–14547. doi: 10.1523/JNEUROSCI.6028-11.2012

Engel, J. Jr., and Pitkänen, A. (2019). Neuropharmacology biomarkers for epileptogenesis and its treatment. *Neuropharmacology* 167:107735. doi: 10.1016/j.neuropharm.2019.107735

Fudala, R., Ranjan, A. P., Mukerjee, A., Vishwanatha, J. K., Gryczynski, Z., Borejdo, J., et al. (2012). Fluorescence detection of MMP-9. I. MMP-9 selectively cleaves Lys-Gly-Pro-Arg-Ser-Leu-Ser-Gly-Lys peptide. *Curr. Pharm. Biotechnol.* 12, 834–838. doi: 10.2174/138920111795470967

Girard, B., Tuduri, P., Paula, M., Sakkaki, S., Barboux, C., Bouschet, T., et al. (2019). Neurobiology of disease the mGlu7 receptor provides protective effects against epileptogenesis and epileptic seizures. *Neurobiol. Dis.* 129, 13–28. doi: 10.1016/j.nbd.2019.04.016

Goldberg, E. M., and Coulter, D. A. (2014). Mechanisms of epileptogenesis: a convergence on neural circuit. *Nat. Rev. Neurosci.* 14, 337–349. doi: 10.1038/nrn3482

Gorter, J. A., van Vliet, E. A., and Aronica, E. (2015). Epilepsy and behavior status epilepticus, blood—brain barrier disruption, inflammation, and epileptogenesis. *Epilepsy Behav.* 49, 13–16. doi: 10.1016/j.yebeh.2015.04.047

Gu, Z., Cui, J., Brown, S., Fridman, R., Mobashery, S., Strongin, A. Y., et al. (2005). A highly specific inhibitor of matrix metalloproteinase-9 rescues laminin from proteolysis and neurons from apoptosis in transient focal cerebral ischemia. *J. Neurosci.* 25, 6401–6408. doi: 10.1523/JNEUROSCI.1563-05.2005

Ikonomidou, C. (2014). Matrix metalloproteinases and epileptogenesis. *Mol. Cell. Pediatr.* 1:6. doi: 10.1186/s40348-014-0006-y

Jiang, T., Olson, E. S., Nguyen, Q. T., Roy, M., Jennings, P. A., and Tsien, R. Y. (2004). Tumor imaging by means of proteolytic activation of cell-penetrating peptides. *Proc. Natl. Acad. Sci. U S A* 101, 17867–17872. doi: 10.1073/pnas.0408191101

Jourquin, J., Tremblay, E., Décanis, N., Charton, G., Hanessian, S., Chollet, A. M., et al. (2003). Neuronal activity-dependent increase of net matrix metalloproteinase activity is associated with MMP-9 neurotoxicity after kainate. *Eur. J. Neurosci.* 18, 1507–1517. doi: 10.1046/j.1460-9568.2003.02876.x

Kalozoumi, G., Kel-Margoulis, O., Vafiadaki, E., Greenberg, D., Bernard, H., Soreq, H., et al. (2018). Glial responses during epileptogenesis in Mus musculus point to potential therapeutic targets. *PLoS One* 13:e0201742. doi: 10.1371/journal.pone.0201742

Khomiak, D., and Kaczmarek, L. (2018). Matrix metalloproteinase 9 and epileptogenesis—the crucial role of the enzyme and strategies to prevent the disease development *Postepy Biochem.* 64, 222–230. doi: 10.18388/pb.2018_134

Konopacki, F. A., Rylski, M., Wilczek, E., Amborska, R., Detka, D., Kaczmarek, L., et al. (2007). Synaptic localization of seizure-induced matrix metalloproteinase-9 mRNA. *Neuroscience* 150, 31–39. doi: 10.1016/j.neuroscience.2007.08.026

Konopka, A., Grajkowska, W., Ziemiańska, K., Roszkowski, M., Daszkiewicz, P., Rysz, A., et al. (2013). Matrix metalloproteinase-9 (MMP-9) in human intractable epilepsy caused by focal cortical dysplasia. *Epilepsy Res.* 104, 45–58. doi: 10.1016/j.eplepsyres.2012.09.018

Li, S., Yu, S., Zhang, C., Shu, H., Liu, S., and An, N. (2012). Increased expression of matrix metalloproteinase 9 in cortical lesions from patients with focal cortical dysplasia type IIb and tuberous sclerosis complex. *Brain Res.* 1453, 46–55. doi: 10.1016/j.brainres.2012.03.009

Lukasiuk, K., Wilczynski, G. M., and Kaczmarek, L. (2011). Extracellular proteases in epilepsy. *Epilepsy Res.* 96, 191–206. doi: 10.1016/j.eplepsyres.2011.08.002

Łukawski, K., Andres-Mach, M., Czuczwar, M., Łuszczki, J. J., Kruszyński, K., and Czuczwar, S. J. (2018). Mechanisms of epileptogenesis and preclinical approach to antiepileptogenic therapies. *Pharmacol. Rep.* 70, 284–293. doi: 10.1016/j.pharep.2017.07.012

Michaluk, P., Kolodziej, L., Mioduszewska, B., Wilczynski, G. M., Dzwonek, J., Jaworski, J., et al. (2007). β-dystroglycan as a target for MMP-9, in response to enhanced neuronal activity. *J. Biol. Chem.* 282, 16036–16041. doi: 10.1074/jbc.M700641200

Michaluk, P., Mikasova, L., Groc, L., Frischknecht, R., Choquet, D., and Kaczmarek, L. (2009). Matrix metalloproteinase-9 controls NMDA receptor surface diffusion through integrin 1 signaling. *J. Neurosci.* 29, 6007–6012. doi: 10.1523/JNEUROSCI.5346-08.2009

Michaluk, P., Wawrzyniak, M., Alot, P., Szczot, M., Wyrembek, P., Mercik, K., et al. (2011). Influence of matrix metalloproteinase MMP-9 on dendritic spine morphology. *J. Cell Sci.* 124, 3369–3380.doi: 10.1242/jcs.090852

Nagy, V., Bozdagi, O., Matynia, A., Balcerzyk, M., Okulski, P., Dzwonek, J., et al. (2006). Matrix metalloproteinase-9 is required for hippocampal late-phase long-term potentiation and memory. *J. Neurosci.* 26, 1923–1934. doi: 10.1523/JNEUROSCI.4359-05.2006

Nguyen, Q. T., Olson, E. S., Aguilera, T. A., Jiang, T., Scadeng, M., Ellies, L. G., et al. (2010). Surgery with molecular fluorescence imaging using activatable cell-penetrating peptides decreases residual cancer and improves survival. *Proc. Natl. Acad. Sci. U S A* 107, 4317–4322. doi: 10.1073/pnas.0910261107

Olson, E. S., Aguilera, T. A., Jiang, T., Ellies, L. G., Nguyen, Q. T., Wong, E., et al. (2009). *In vivo* characterization of activatable cell penetrating peptides for targeting protease activity in cancer. *Integr. Biol.* 1, 382–393. doi: 10.1039/b904890a

Olson, E. S., Jiang, T., Aguilera, T. A., Nguyen, Q. T., Ellies, L. G., Scadeng, M., et al. (2010). Activatable cell penetrating peptides linked to nanoparticles as dual probes for *in vivo* fluorescence and MR imaging of proteases. *Proc. Natl. Acad. Sci. U S A* 107, 4311–4316. doi: 10.1073/pnas.0910283107

Pernot, F., Heinrich, C., Barbier, L., Peinnequin, A., Carpentier, P., Dhote, F., et al. (2011). Inflammatory changes during epileptogenesis and spontaneous seizures in a mouse model of mesiotemporal lobe epilepsy. *Epilepsia* 52, 2315–2325. doi: 10.1111/j.1528-1167.2011.03273.x

Pitkänen, A., and Engel, J. Jr. (2014). Past and present definitions of epileptogenesis and its biomarkers. *Neurotherapeutics* 11, 231–241. doi: 10.1007/s13311-014-0257-2

Pitkänen, P. A., and Lukasiuk, K. (2011). Mechanisms of epileptogenesis and potential treatment. *Lancet Neurol.* 10, 173–186. doi: 10.1016/s1474-4422(10)70310-0

Pitkänen, A., Ndode-Ekane, X. E., Łukasiuk, K., Wilczynski, G. M., Dityatev, A., Walker, M. C., et al. (2014). "Neural ECM and epilepsy," in *Progress in Brain Research, Vol. 214*, (Finland: Elsevier), 229–262.

Pitkänen, A., and Sutula, T. P. (2002). Review is epilepsy a progressive disorder? Prospects for new therapeutic approaches in temporal-lobe epilepsy. *Lancet Neurol.* 1, 173–181. doi: 10.1016/s1474-4422(02)00073-x

Quirico-Santos, T., Nascimento Mello, A., Casimiro Gomes, A., de Carvalho, L. P., de Souza, J. M., and Alves-Leon, S. (2013). Increased metalloprotease activity in the epileptogenic lesion—lobectomy reduces metalloprotease activity and urokinase-type uPAR circulating levels. *Brain Res.* 1538, 172–181. doi: 10.1016/j.brainres.2013.09.044

Sarkar, S., and Schmued, L. (2010). Kainic acid and 3-Nitropropionic acid induced expression of laminin in vascular elements of the rat brain. *Brain Res.* 1352, 239–247. doi: 10.1016/j.brainres.2010.07.011

Stawarski, M., Rutkowska-Wlodarczyk, I., Zeug, A., Bijata, M., Madej, H., Kaczmarek, L., et al. (2014). Biomaterials Genetically encoded FRET-based biosensor for imaging MMP-9 activity. *Biomaterials* 35, 1402–1410. doi: 10.1016/j.biomaterials.2013.11.033

Szepesi, Z., Bijata, M., Ruszczycki, B., Kaczmarek, L., and Wlodarczyk, J. (2013). Matrix metalloproteinases regulate the formation of dendritic spine head protrusions during chemically induced long-term potentiation. *PLoS One* 8:e63314. doi: 10.1371/journal.pone.0063314

Szepesi, Z., Hosy, E., Ruszczycki, B., Bijata, M., Pyskaty, M., Bikbaev, A., et al. (2014). Synaptically released matrix metalloproteinase activity in control of structural plasticity and the cell surface distribution of GluA1-AMPA receptors. *PLoS One* 9:e98274. doi: 10.1371/journal.pone.0098274

Szklarczyk, A., Lapinska, J., Rylski, M., McKay, R. D. G., and Kaczmarek, L. (2002). Matrix metalloproteinase-9 undergoes expression and activation during dendritic remodeling in adult hippocampus. *J. Neurosci.* 22, 920–930. doi: 10.1523/JNEUROSCI.22-03-00920.2002

Terrone, G., Pauletti, A., Pascente, R., and Vezzani, A. (2016). Preventing epileptogenesis: a realistic goal? *Pharmacol. Res.* 110, 96–100. doi: 10.1016/j.phrs.2016.05.009

Tian, L., Stefanidakis, M., Ning, L., Van Lint, P., Nyman-huttunen, H., Libert, C., et al. (2007). Activation of NMDA receptors promotes dendritic spine development through MMP-mediated ICAM-5 cleavage. *J. Cell Biol.* 178, 687–700. doi: 10.1083/jcb.200612097

Wilczynski, G. M., Konopacki, F. A., Wilczek, E., Lasiecka, Z., Gorlewicz, A., Michaluk, P., et al. (2008). Important role of matrix metalloproteinase 9 in epileptogenesis. *J. Cell Biol.* 180, 1021–1035. doi: 10.1083/jcb.200708213

Yeghiazaryan, M., Rutkowska-Wlodarczyk, I., Konopka, A., Wilczyński, G. M., Melikyan, A., Korkotian, E., et al. (2014). DP-b99 modulates matrix metalloproteinase activity and neuronal plasticity. *PLoS One* 9:e99789. doi: 10.1371/journal.pone.0099789

Yin, P., Yang, L., Zhou, H. Y., and Sun, R. P. (2011). Matrix metalloproteinase-9 may be a potential therapeutic target in epilepsy. *Med. Hypotheses* 76, 184–186. doi: 10.1016/j.mehy.2010.09.013

Zattoni, M., Mura, M. L., Deprez, F., Schwendener, R. A., Engelhardt, B., Frei, K., et al. (2011). Brain infiltration of leukocytes contributes to the pathophysiology of temporal lobe epilepsy. *J. Neurosci.* 31, 4037–4050. doi: 10.1523/JNEUROSCI.6210-10.2011

Zhang, J. W., Deb, S., and Gottschall, P. E. (1998). Regional and differential expression of gelatinases in rat brain after systemic kainic acid or bicuculline administration. *Endocrinology* 10, 3358–3368. doi: 10.1046/j.1460-9568.1998.00347.x

Conflict of Interest: The authors declare that the research was conducted in the absence of any commercial or financial relationships that could be construed as a potential conflict of interest.

frontiers in Synaptic Neuroscience

METHODS
published: 30 April 2020
doi: 10.3389/fnsyn.2020.00019

Procedures for Culturing and Genetically Manipulating Murine Hippocampal Postnatal Neurons

Enora Moutin[1], Anne-Laure Hemonnot[1,2], Vincent Seube[1,2], Nathalie Linck[1,2], François Rassendren[1,2], Julie Perroy[1] and Vincent Compan[1,2]**

[1] Institut de Génomique Fonctionnelle (IGF), University of Montpellier, CNRS, INSERM, Montpellier, France, [2] Laboratoire d'Excellence Canaux Ioniques d'Intérêt Thérapeutique (LabEx ICST), Montpellier, France

Neuronal hippocampal cultures are simple and valuable models for studying neuronal function. While embryonic cultures are widely used for different applications, mouse postnatal cultures are still challenging, lack reproducibility and/or exhibit inappropriate neuronal activity. Yet, postnatal cultures have major advantages such as allowing genotyping of pups before culture and reducing the number of experimental animals. Herein we describe a simple and fast protocol for culturing and genetically manipulating hippocampal neurons from P0 to P3 mice. This protocol provides reproducible cultures exhibiting a consistent neuronal development, normal excitatory over inhibitory neuronal ratio and a physiological neuronal activity. We also describe simple and efficient procedures for genetic manipulation of neurons using transfection reagent or lentiviral particles. Overall, this method provides a detailed and validated protocol allowing to explore cellular mechanisms and neuronal activity in postnatal hippocampal neurons in culture.

Keywords: neurons, postnatal, hippocampus, culture, transfection, transduction, lentivirus

OPEN ACCESS

Edited by:
Kimberly M. Huber, University of Texas Southwestern Medical Center, United States

Reviewed by:
Kenji Hanamura, Gunma University, Japan
Shigeo Takamori, Doshisha University, Japan

****Correspondence:***
Julie Perroy
julie.perroy@igf.cnrs.fr
Vincent Compan
vincent.compan@igf.cnrs.fr

Received: *20 December 2019*
Accepted: *03 April 2020*
Published: *30 April 2020*

Citation:
Moutin E, Hemonnot A-L, Seube V, Linck N, Rassendren F, Perroy J and Compan V (2020) Procedures for Culturing and Genetically Manipulating Murine Hippocampal Postnatal Neurons. Front. Synaptic Neurosci. 12:19. doi: 10.3389/fnsyn.2020.00019

INTRODUCTION

The hippocampus and cortex are two brain areas extensively studied due to their implications in several important neuronal processes including cognition, learning, and memory. Over the past 10 years, major technical breakthrough facilitated *in vivo* studies of these two structures. Despite these advances, *in vitro* models remain the easiest to implement, and are relevant for many applications to study neuronal pathophysiology. In particular, primary neuronal culture is a powerful model to more easily manipulate and observe neurons. This simplified environment facilitates gene manipulation, time-lapse microscopy, electrophysiology and biochemistry, among others. Cultures of dissociated neurons were historically developed from embryonic rats (Banker and Cowan, 1977), but were limited to short term culture (<5 days) or required to co-culture dissociated cells with tissue explants. More complex neuronal culture protocols were later developed for mature neurons and long-term studies. A commonly used method is the 'sandwich' method which requires growing neurons on coverslips on top of a layer of glia cells [for a detailed protocol see Kaech and Banker (2006)]. This model provides cultures of almost pure neurons and is of particular interest to study interaction between astrocytes and neurons dissociated from two different mouse lines. Other approaches have been developed which consist of either growing neurons directly on a confluent glial cell layer or using glia-conditioned medium to maintain neurons in culture for a long period. Culturing neurons without the need of a feeder layer of glial cells was made possible through the formulation of a commercial specific media called Neurobasal

(Brewer et al., 1993). It has been designed with optimized concentrations of each component to promote neuron survival and is lacking some excitatory amino acids that can be toxic for neurons. Supplemented with a serum free supplement called B27, Neurobasal is currently by far the most popular culture media for primary neurons.

Several postnatal culture protocols have been published to produce mouse primary neuronal culture from either very early stage after birth (Ahlemeyer and Baumgart-Vogt, 2005; Beaudoin et al., 2012; Kaar et al., 2017) or adult animals (Eide and McMurray, 2005; Peltier et al., 2010). Postnatal culture presents important advantages such as (i) reducing the number of experimental animals in agreement with the rule of the 3R, as only the pups required for the culture are sacrificed, (ii) genotyping of transgenic animals prior to the culture. Despite these benefits, postnatal culture is still underutilized mainly because of inconsistencies in culture quality compared to embryonic hippocampal dissociated cultures. One explanation for this discrepancy likely comes from the composition of culture media, such as Neurobasal-A, which contains high level of NMDA receptor co-agonist such as L-cysteine or glycine, which can lead to neurotoxicity particularly during long-term postnatal or adult culture (Hogins et al., 2011; Maggioni et al., 2015). Indeed, excitotoxicity increases with the age of culture and correlates with the maturation of neuronal connectivity and the parallel increase of NMDA receptor expression (Peterson et al., 1989; Mattson et al., 1991; Brewer et al., 2007). To overcome these problems, Bardy and colleagues developed a new medium called BrainPhys, which recapitulates the *in vivo* neuronal *milieu intérieur* by adjusting the concentrations of inorganic salts, neuroactive amino acids, and energetic substrates. This medium better supports important neuronal functions and improves physiological neuronal activity on iPSCs- or ESCs-derived human neurons (Bardy et al., 2015).

Here, we thought to develop an optimized culture protocol for postnatal hippocampal neurons. First, we settled a gentle and fast protocol for cell dissociation and plating which can be achieved in less than 2 h, thus improving neuronal survival. Next, we combined the advantage of Neurobasal-A and BrainPhys media for cell plating/growing and for culture maintenance, respectively. Our protocol leads to robust and reproducible hippocampal postnatal cultures that can be successfully prepared from P0 to P3 mice. These cultures present comparable ratios of inhibitory versus excitatory neurons like in embryonic cultures, and provide a neuronal network with a physiological neuronal activity. Finally, we described detailed protocols to produce lentiviral particles and genetically manipulate these cultures either by transient transfection or viral transduction. We also provide few examples of experiments that can be performed on such cultures to manipulate and study neurons.

MATERIALS AND EQUIPMENTS

Animals

All animal procedures were conducted in accordance with the European Communities Council Directive and supervised by the IGF institute's local Animal Welfare Unit (A34-172-41). Mouse pups were obtained from timed-pregnant C57Bl/6j mice. Mice were housed in harem breeding composed of one male and three females. Animals were maintained in a 12 h light/dark cycle (lights on from 7:30 am to 7:30 pm), in stable conditions of temperature (22°C) and humidity (60%). Food and water were available *ad libitum*.

Lentiviral Vectors and Others Plasmids

Packaging plasmid pMD2.G and psPAX2 plasmids were a gift from Didier Trono (Addgene plasmids #12259 and #12260). pAAV-hSyn-VARNAM was a gift from Vincent Pieribone (Addgene plasmid #115554). DRH313: FCK-CheRiff-eGFP and DRH337: AAV-hsyn-CheRiff-eGFP were a gift from Adam Cohen (Addgene plasmids #51693 and #51697). For transgene expression, backbones of pWPT-GFAPprom-RCaMP2, pWPT-CaMKIIαprom-GCaMP6, pWPT-CaMKIIαprom-Venus-NR1A, pWPT-CaMKIIαprom-NLuc-YPet and pWPT-CaMKIIαprom-LIMK-NLuc-YPet plasmids were all derived from pWPT-GFP plasmid (Addgene plasmid #12255). These plasmids were produced by Gibson Assembly (New England Biolabs) after amplification by PCR of GFAP or CaMKIIα promoters and GCaMP6 calcium indicators (amplified from pGP-CMV-GCaMP6s, gift from Douglas Kim & GENIE Project, Addgene plasmid #40753). Others DNA sequences were produced by gene synthesis and sub-cloned in one of the plasmids mentioned above.

Imaging of Dissection Steps and Culture Development

For dissection steps, images were taken using a Canon EOS100D camera with an EFS 18–55 mm objective. To follow the development of neurons during the 14 days of culturing (**Figure 3A**), cells were plated on Ibidi dishes (81166) and representative images were taken at each time point using an Axiovert 40 CFL microscope with a 10X/0.25 objective. At DIV 0 (Day *In Vitro*) images were taken 1 h after cell plating.

Immunocytochemistry

Cell cultures were fixed with 4% paraformaldehyde in PBS solution for 10 min and then permeabilized and blocked with a 3% BSA, 0.1% Triton X-100, PBS solution for 1 h at room temperature. Cultures were then incubated with primary antibodies overnight at 4°C. After washes, cells were incubated with secondary antibodies for 1 h at room temperature, washed, mounted on slides and observed under an Axio-Imager Z1 microscope equipped with appropriate epifluorescence and filters (Carl Zeiss). Image quantification was performed using ImageJ software. Synaptic puncta were quantified using Synapse Counter plug-in for ImageJ on images acquired with a Plan-Apochromat 40X/0.95 objective.

Time-Lapse Calcium and Voltage Imaging

GCaMP6 and VARNAM fluorescences were recorded using a Zeiss Observer Z1 Microscope. For GCaMP6 fluorescence,

microscope was equipped with a Zeiss filterset38 (λex 470/40 – λem 525/50) and a HXP 120C XP Carl Zeiss bulb. For VARNAM fluorescence, microscope was equipped with a 607/70 nm Brightline filter and excitation was performed using 550/15 nm LED with an intensity of 18 mW/mm^2. Neurons were maintained in ACSF medium (in mM): 140 NaCl, 2 $CaCl_2$, 3 KCl, 10 Hepes, 10 D-Glucose. pH was adjusted to 7,4 with NaOH and osmolarity was adjusted to 315 mOsmol using NaCl. Stimulation of CheRiff was induced by LED at 440/20 nm with an intensity of 2 mW/mm^2.

Biochemistry and Synaptosome Preparation

Synaptosomes were prepared from DIV 14 cultures using Syn-PER Synaptic Protein Extraction Reagent (Thermo Fisher Scientific) according to manufacturer instructions; proteins were separated by electrophoresis using 4–12% Bis-Tris Plus Bolt Gels (Thermo Fisher Scientific) and transferred on nitrocellulose membrane (iBlot Transfer Stack from Thermo Fisher Scientific). A solution of PBS supplemented with 0,1% Tween and 5% non-fat milk was used to block the membrane and dilute primary and secondary antibodies.

Electrophysiology

Postnatal hippocampal neurons were recorded in the whole-cell patch-clamp configuration. mEPSCs were recorded on DIV 13 to DIV 15 neurons, at room temperature with a holding potential of −60 mV. The patch pipettes had a resistance around 4 MΩ when filled with the following medium (in mM): 140 CsCl, 0.5 $CaCl_2$, 20 EGTA, 10 Hepes, 10 D-Glucose, 2 ATP-Na_2, with an osmolarity of 300 mOsm and pH 7.2. Neurons were perfused with the following external medium (in mM): 140 NaCl, 2 $CaCl_2$, 3 KCl, 10 Hepes, 10 D-Glucose, 1.5 $MgCl_2$, 0.01 glycine, 0.01 bicucullin, 0.0003 tetrodotoxin. Currents were recorded through an Axopatch 200B amplifier and digitized at 3 kHz. Electrophysiological data were analyzed using the Clampfit 10 software from Axon instruments (Molecular Devices).

Step-by-Step Protocol

Primary Culture of Hippocampal Neurons From Newborn Mice (P0 to P3)

Before starting the coating and the dissection steps, disinfect all the equipment and the laminar culture hood with 70% ethanol. If possible, sterilize tools by autoclaving. Manipulate coverslips using sterile forceps. All solutions have to be sterile.

Coating of Petri dishes and coverslips. Timing 1 h spread over 2 days, at least 1 day before culture.

(1) Thaw a poly-L-ornithine aliquot and dilute it five times in water to get a final concentration of 0.03 mg/mL. Fill the dishes with enough poly-L-ornithine to fully cover the bottom of the dish. As a guideline, we routinely use 1 mL for a 35 mm dish and 50 µL for a well of a 96 well plate. When culturing neurons on coverslips, make sure to remove any bubble remaining between the coverslip and the bottom of the dish.

(2) Incubate overnight at 37°C. This step can be realized 3 days in advance (over the week-end), not earlier.

(3) Wash three times with PBS. Do not remove PBS before you are ready for step 4.

(4) Dilute laminin to get a final concentration of 1 µg/mL in Neurobasal-A (dilution 1/1,000) and fill the dishes immediately after removing PBS. Be sure to cover the bottom of the dish and make sure to remove any bubbles if coverslips are used.

(5) Incubate at 37°C for 4–12 h.

Final settings for dissection, cell dissociation, and plating. Timing: 15 min, just before starting the culture.

The following material is sufficient for one culture prepared for up to eight animals. If doing several cultures of different mouse genotypes in parallel or if culture required more than eight animals, number of material and aliquots described in steps 7 and 8 have to be changed accordingly.

(6) On a clean bench, prepare dissection tools: big and small scissors, 1 pair of forceps, 1 small spatula.

(7) In a culture hood, fill two 60 mm plates with 6 mL cold Hibernate (one to collect the brains and one to dissect hippocampi) and one 15 mL Falcon tube with 2 mL cold hibernate to collect hippocampi. Add 500 µL of Hibernate in a papain aliquot and prepare one syringe of 2 mL and a 0.22 µm filter for later.

(8) Set a water bath at 37°C and warm up the papain aliquot supplemented with Hibernate, the CM+ medium and a 4% BSA aliquot.

(9) If possible, place a binocular microscope in a vertical laminar flow hood. If not, dissection steps can be performed on a clean bench. Prepare small curved scissors and forceps close to the microscope.

Removal of the brain. Timing 1–2 min for each pup.

(10) Euthanize a mouse pup by decapitation using big scissors (**Figure 1A-a,b**) (see **Table 1** for dissection tool references).

(11) By holding the head with the thumb on one side and the index on the other side, cut the skin of the head with small scissors from the caudal region to the extreme rostral region (dotted line on **Figure 1A-c**). Pull the skin on both sides; use the two same fingers to hold it down without pressing on the brain.

(12) Do exactly the same cutting along the skull moving forward slowly with the small scissors to avoid damaging the brain (**Figure 1A-d**). Between the two eyes, make two small incisions in direction of each eye and remove the skull using forceps. If the brain stays attached to the skull, gently insert the tip of the forceps in between and move back and forth.

(13) Place the tip of the spatula under the olfactive bulbs (**Figure 1A-e**) and use it to transfer the brain in the 60 mm dish containing cold Hibernate.

(14) Repeat steps 10 to 13 for each pup, pool the brains in Hibernate. Make sure that brains are all submerged in the Hibernate media.

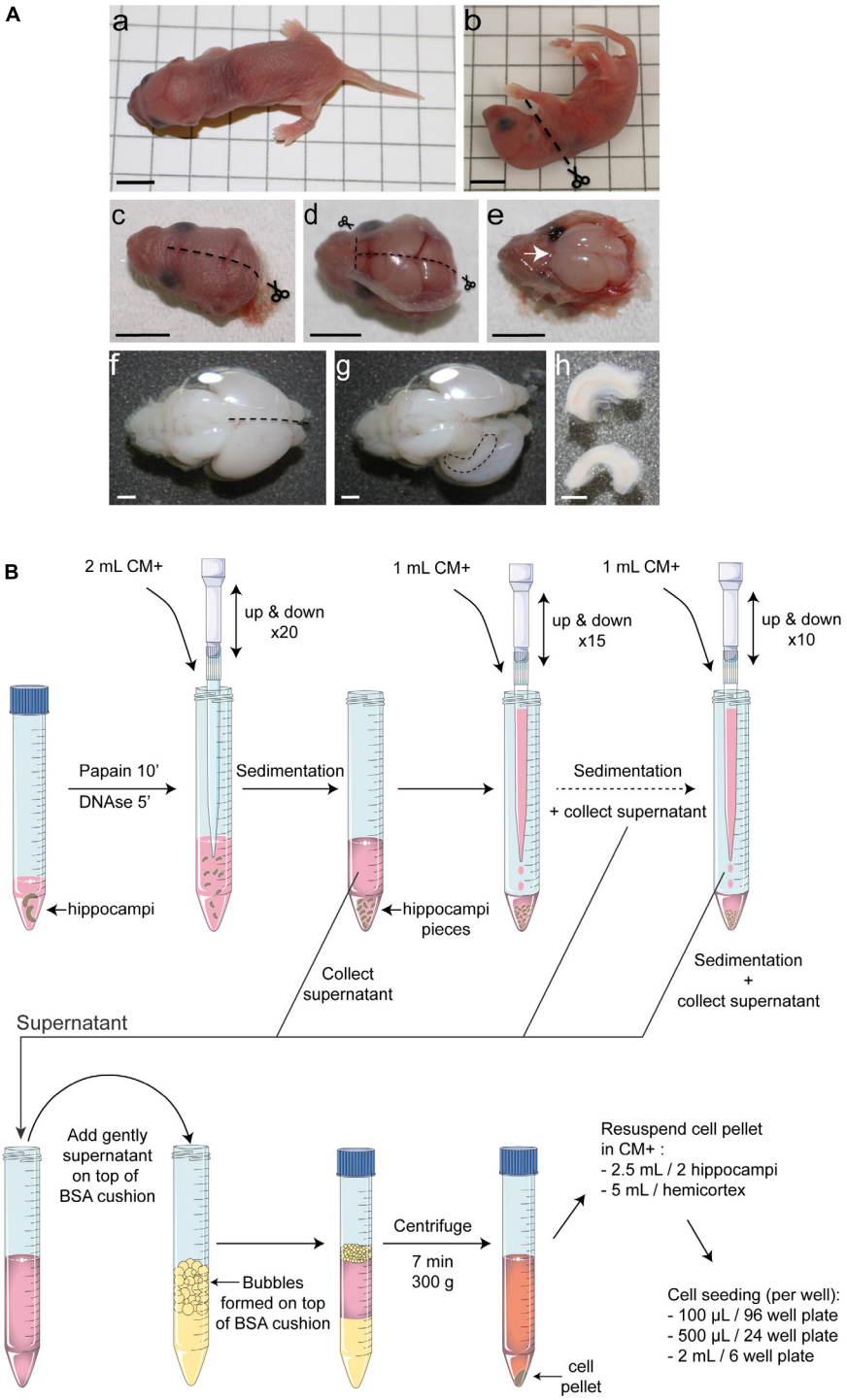

FIGURE 1 | Overview of the protocol for mouse postnatal hippocampal culture. **(A)** Hippocampus dissection. After decapitation **(a–c)**, make a midline incision of the skin on the top of the head, from the back to the extreme rostral region of the brain. **(d)** Do exactly the same cutting along the skull moving forward slowly with the small scissors to avoid damaging the brain. Make two small incisions in direction of each eye and remove the skull. **(e)** Using a small spatula, gently remove the brain and place it into Hibernate medium. **(f)** Using small curved scissors, carefully separate the 2 hemispheres and 'unroll' the cortex from one hemisphere to make the hippocampus visible **(g)**. **(h)** Using small scissors remove the hippocampus. Black scale bar = 5 mm, white scale bar = 1 mm. **(B)** Schematic representation of the enzymatic and mechanical dissociation of cells and plating. Only two hippocampi are represented but this protocol can be applied for up to 16 hippocampi per tube. Hippocampi were collected in Hibernate-A medium, digested using papain at 37°C for 10 min and for five additional minutes in presence of DNase1. After stopping papain activity by adding CM+ media, the tissue was subjected to three rounds of mechanical dissociation using 1,250 µL filtered tips. After adding dissociated tissue on top of a 4% BSA cushion and centrifugation for 7 min at 300 *g*, cells were resuspended in CM+ media and seeded on pre-coated dishes.

TABLE 1 | Reagents, consumables, dissection tools, and antibodies.

	Designation	Supplier, reference	Comments
Reagents	Antibiotics (penicillin and streptomycin)	Gibco, 15140-122	
	B27 supplement	Gibco, 17504044	
	Bovine serum albumin (BSA)	Sigma-Aldrich, A7906-50G	
	BrainPhys	Stemcell Technology, 05790	For culture maintenance
	Cytosine β-D-arabinofuranoside hydrochloride (AraC)	Sigma-Aldrich, C6645	To curb glia proliferation
	DMEM high glucose with Glutamax	Gibco, 61965058	
	DNase I	Roche, 10104159000	
	Fetal bovine serum (FBS)	Gibco, 10270105	Has to be heat inactivated for 30 min at 56°C prior to use
	Glutamax	Gibco, 35050037	
	Glutamine	Gibco, 25030-023	
	Hepes buffer 1M pH7.2 to 7.4	Gibco, 15630-055	
	Hibernate-A	Gibco, A12475-00	For culture dissection
	Laminin	Sigma-Aldrich, L2020	For coating
	Lipofectamine 2000	Invitrogen, 11668019	For transfection
	Neurobasal-A W/O Phenol red	Gibco, 12349015	For culture plating
	Papain	Sigma-Aldrich, P4761	For cellular dissociation
	Polyethylene glycol (PEG)	Sigma-Aldrich, 81253-250G	For lentiviral production
	Poly-L-ornithine hydrobromide	Sigma-Aldrich, P3654	For coating
Consumables	Conical tubes 15 mL	Falcon, CL-TFC55	
	Conical tubes 50 mL	Falcon, CL-TFC20	
	Filter (25 mm diameter, 0.2 μm)	Pall, CL-FS1	For papain filtration
	Filter (37 mm diameter, 0.2 μm)	Pall, CL-FS13	For CM filtration
	Filter (33 mm diameter, 0.45 μm)	Millipore, SLHV033RS	For lentiviral production
	Tips (with filter)	Sorenson, 34000	For physical dissociation
Dissection tools	Dumont #7 Forceps	FST, 11271-29	For dissection – steps 12, 15, 16
	Extra fine Bonn scissors straight	FST, 14084-07	For brain dissection – steps 11, 12
	Spatula	Dominique Dutscher, 037872	For brain removal – step 13
	Vannas spring scissors curved 4 mm cutting edge	FST, 15019-9	For hippocampus dissection – step 14
	Wagner scissors	FST, 14068-11	For pup decapitation – step 10
Primary antibodies	Actin	DSHB, JLA20	Dilution 1:2000 for WB
	CaMKIIα	Millipore, 05-532	Dilution 1:1000 for ICC
	Hoechst 33258	Sigma-Aldrich, B2883	Dilution at 1 μg/mL for ICC
	GFP	Biolabs,TP401	Dilution 1:2000 for ICC and WB
	GluN1	Synaptic systems, 114011	Dilution 1:1000 for WB
	GluR2	Sigma-Aldrich, MAB397	Dilution 1:1000 for WB
	MAP2	Sigma-Aldrich, M4403	Dilution 1:1000 for ICC
	NeuN	Synaptic Systems, 266006	Dilution 1:500 for ICC
	PSD95	ABR, MA1-045	Dilution 1:500 for ICC
	Prox1	Ozyme, BLE925201	Dilution 1:1000 for ICC
	RFP	MBL, PM005	Dilution 1:2000 for ICC and WB
	Synaptophysin	BD Biosciences, 611880	Dilution 1:1000 for ICC
	NeuN-A647	Abcam, Ab19565	Dilution 1:1000 for ICC
	GABA	Sigma, A2052	Dilution 1:2000 for ICC
	Homer1	Synaptic Systems, 160003	Dilution 1:1000 for ICC
Secondary antibodies	Donkey anti-mouse Alexa Fluor 488	Invitrogen, A21206	Dilution 1:1000
	Donkey anti-rabbit Alexa Fluor 350	Invitrogen, A10039	Dilution 1:1000
	Goat anti-chicken Alexa Fluor 594	Molecular Probes, A11012	Dilution 1:1000
	Goat anti-rabbit Alexa Fluor 488	Molecular Probes, A11034	Dilution 1:1000
	Goat anti-rabbit Cy3	Jackson Immunoresearch, 111-165-144	Dilution 1:1000
	Goat anti-mouse Cy3	Jackson Immunoresearch, 115-165-075	Dilution 1:1000

BOX 1 | Preparations to be anticipated prior to postnatal hippocampal culture. In routine experiments, to perform the dissection and plating out neurons in less than 2 h, several preparations and aliquots have to be made in advance:

– To avoid multiple freeze-thaw cycles and to save time, we strongly recommend to aliquot Cytosine β-D-arabinofuranoside hydrochloride AraC (10 mM), B27, glutamax, glutamine, heat inactivated FBS and antibiotics. All these reagents can be stored for months at −20°C.

– Preparation of coverslips for immunocytochemistry. Timing 5 h, at least 2 day before culture.
Clean coverslips can be prepared in advance and can be stored for months. Cell adhesion and polyaminoacids coating will be facilitated by using clean coverslips.
(1) Put coverslips in 1M HCl.
(2) Heat to 50–60°C for 4–8 h with occasional agitation.
(3) Wash the coverslips four times in milliQ water. Be sure to wash out the acid between stuck coverslips.
(4) Rinse coverslips in 100% ethanol.
(5) Store coverslips in 100% ethanol.

– Preparation of Hibernate solution. Timing 5 min.
500 mL Hibernate bottle are supplemented with 5 mL antibiotics and can be stored for weeks at 4°C.

– Preparation of 4% BSA aliquots. Timing 30 min. Can be stored at −20°C for months.
Dissolve 2 g of BSA in 50 mL of Hibernate, to get a final concentration at 4%. Filter using 0.2 μm pore size filter unit and aliquot by 2 mL in 15 mL tubes. Store at −20°C.

– Preparation of DNase I aliquots. Timing 30 min. Can be stored at −20°C for months.
Resuspend DNase powder at 50 mg/mL in 50% glycerol, 2 mM $CaCl_2$, 10 mM Tris pH 7.6, 50 mM NaCl. Always keep the DNase solution on ice during cell culture and put it back at −20°C after use.

– Preparation of poly-L-ornithine aliquots. Timing 30 min. Can be stored at −20°C for months.
Dissolve 100 mg of poly-L-ornithine powder in 700 mL of milliQ water to get an intermediate concentration at 0.15 mg/mL and aliquot by 10 mL in 15 mL Falcon tubes. Store at −20°C.

– Preparation of papain aliquots. Timing 30 min. Can be stored at −20°C for months.
On ice, dispense 2.5 mg of papain in 1.5 mL tubes. Store at −20°C. Papain will be freshly resuspended on the day of culture.

– Preparation of culture media [supplemented (CM+) or not (CM−) with L-glutamine and FBS], see **Table 2***. Timing 30 min. Can be stored at 4°C for up to 2 weeks, to be filtered with 0,22 μm filter unit.*
Depending on the number of pups used, adjust the quantity of media to prepare. Anticipate 3 mL of CM+ and CM− per pup.

Dissection of the hippocampi. Timing 1–2 min for each pup.

(15) Under the microscope, put one brain in a new 60 mm dish containing cold Hibernate. Hold the brain with forceps sunk in the cerebellum. Using small curved scissors, carefully separate the two hemispheres (dotted line on **Figure 1A-f**). Gently 'unroll' the cortex from one hemisphere to make the hippocampus visible. Using small scissors, remove one hippocampus (following the dotted line on **Figure 1A-g**). Repeat this step for the other hemisphere. You can eventually sink the forceps in the first hemisphere to get an easiest access to the other one.
(16) If meninges stay attached to the hippocampi, remove them using two pairs of forceps and transfer hippocampi in the 15 mL Falcon tube containing 2 mL of cold Hibernate (**Figures 1A-h,B**).
(17) Repeat steps 15 and 16 for each brain and pool hippocampi.

Cellular dissociation and plating. Timing 1 h (Figure 1B).

(18) Filter the 500 μL papain aliquot dissolved in Hibernate (step 7) using a 2 mL syringe and a small 0.22 μm filter. Start the dissociation by adding the papain solution to hippocampi. Incubate at 37°C for 10 min.
Troubleshooting: do not use trypsin in place of papain otherwise it will result in an increase of cell death.
(19) Add 50 μL of DNase I. Dissociate tissue mechanically with a 1,250 μL filtered tip (5 up and down) and incubate 5 min at 37°C.
Troubleshooting: the diameter of the tip is critical to get the expected dissociation. We routinely use Sorenson tips [1000 μl (50–1250 μl) XT Barrier – Catalog #34000].
(20) Stop papain activity by adding 2 mL of CM+ and dissociate tissue mechanically with a p1,000 pipette (20 up and down using 1,250 μL filtered tip). Let decant by gravity (1 min), collect supernatant in a new 15 mL Falcon tube and repeat dissociation two times on remaining debris (one with 15 up and down and one with 10) by adding 1 mL of CM+.
(21) Make a lot of bubbles (3 mL on graduations) in the 4% BSA aliquot (see **Box 1**), on top of which add delicately the supernatant.

TABLE 2 | Preparation of culture media.

	Components	Final concentration	Volume for 50 mL aliquot (in mL)
Culture medium + (CM+)	Neurobasal-A	86.5%	43.250
	B27	2%	1
	Glutamax	0.25%	0.125
	L-Glutamine	0.25% – 0.5 mM	0.125
	Antibiotics	1%	0.5
	FBS, heat inactivated	10%	5
Culture medium − (CM−)	BrainPhys	96.75%	48.375
	B27	2%	1
	Glutamax	0.25%	0.125
	Antibiotics	1%	0.5

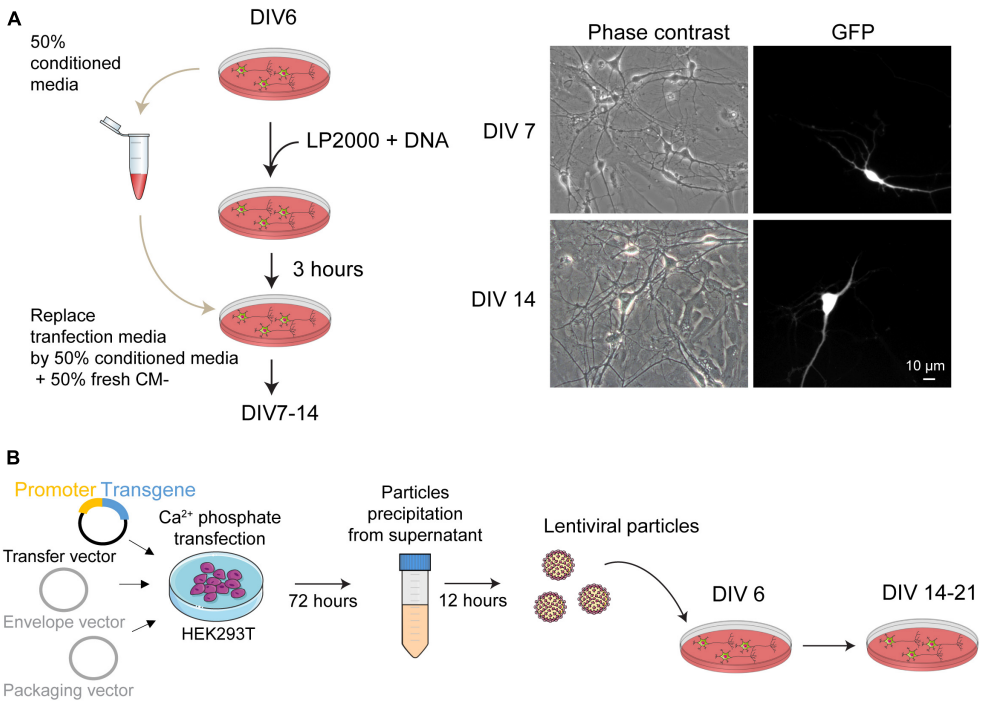

FIGURE 2 | Genetic manipulation of mouse postnatal hippocampal culture. **(A)** (left panel) Schematic representation of the main steps for transgene expression in postnatal hippocampal culture using Lipofectamine2000 as transfection reagent. To reduce cellular toxicity, 3 h after the transfection the medium from the culture dishes is replaced by a solution composed by 50% of conditioned medium collected before the transfection and 50% of fresh CM– media. (right panel) Phase contrast and fluorescence picture of neurons 24 h and 8 days after transfection with a plasmid coding for the GFP protein. **(B)** Overview of the protocol used to produce and purify lentiviral particles from HEK293T cells. These particles are used to transduce the cultures at DIV 6. Expression of the transgene can be detected at DIV 14 and slightly increase until DIV 21.

(22) Centrifuge 7 min at 300 *g* at room temperature.
(23) Resuspend pellet in CM+. For a guideline, we resuspend two hippocampi in 2.5 mL of medium (corresponding to about 500.000 cells/mL).
(24) Remove laminin and directly plate the cells (100 µL for a 96 well plate, 500 µL for a 24 well plate, 1 mL for a 12 well plate and 2 mL for a 6 well plate).
(25) Keep the cultures in an incubator with constant temperature at 37°C and 5% CO_2.

Culture maintenance. Timing 1 h spread over 3 days.

As a general rule, keep in mind that neuronal primary cultures are fragile. Minimize the time that the cells will spend outside the incubator.

(26) To limit glia proliferation, AraC treatment must be performed at DIV 2 during 8 to 18 h. Add AraC diluted in CM− (1 µM final dilution). As a guideline, we routinely dilute 1 µL of AraC 10 mM in 2 mL of CM− and then add 25 µL/well of 96 well plate, 120 µL/well of 24 well plate and 480 µL in a 35 mm dish.
(27) After AraC incubation, replace 80% of media by fresh CM− (80 µL/well of 96 well plate, 400 µL/well of 24 well plate and 1500 µL in a 35 mm dish).
(28) At DIV 6 or 7, proceed to a small replacement of culture medium. As a guideline, we routinely remove 300 µL of the culturing medium and add 400 µL of CM− for a 35 mm dish. If you plan to transfect or transduce the culture, skip this step and directly move to step 29.

Gene Expression

(29) At DIV 6–7, proceed to transfection with plasmid DNA or to transduction with AAV or lentiviruses. All the procedures have to be performed in a culture hood using sterile materials. All work using viruses must be performed after consulting your institution's biosafety committee in order to determine the appropriate biosafety level.

(29a) *Transfection using Lipofectamine2000*
This protocol will lead to a strong and fast expression of the transgene into a low percentage of neurons (less than 5%, **Figure 2A**).
- For the transfection of one 35 mm dish, prepare one tube with 250 µL Neurobasal-A + 2 to 4 µg plasmid DNA and one tube with 250 µL Neurobasal-A + 4 to 8 µL Lipofectamine2000. Wait for 5 min.
- Pool the two tubes together, mix gently by doing few up and down and wait for 20 min.
- Collect half of the medium from the culture dishes to be transfected and save it in a sterile tube. Keep

BOX 2 | Production of lentiviral particles (**Figure 2B**). Timing 4 h spread over 4 days with two waiting days in between. This protocol is adapted from Masuda et al. (2013). Before starting the lentiviral production, prepare the three following solutions that can be stored for months at 4°C:

Solutions for calcium phosphate transfection of HEK293T cells

HBS 2X: to prepare 20 mL, mix 2.8 mL NaCl 2M, 2 mL Hepes 0.5M, 300 μL Na_2HPO_4 0.1M and 14.9 mL milliQ water. Correct pH with NaOH and filter at 0.2 μm in a sterile hood. pH of the HBS solution will strongly influence transfection efficiency. We recommend to prepare four different HBS solution with pH ranging from 6.8 to 7.2. Test transfection efficiency using a plasmid coding for a fluorescent protein such as GFP to determine the optimal pH. If stored properly, HBS solution might be used for years without affecting transfection efficiency.

$CaCl_2$ 1M: dissolve 14.7 g of $CaCl_2$ in 100 mL milliQ water. Filter at 0.2 μm in a culture hood and aliquot per 10 mL.

Solution for lentivirus precipitation

Polyethylene glycol (PEG) solution 4X: to prepare 500 mL, mix 200 g PEG 6,000 with 100 mL milliQ water and agitate. Add 100 mL milliQ water and agitate. Add 40 mL NaCl 5M and agitate. Add 20 mL Hepes 1M pH 7.2–7.4 and agitate. Mix PEG, NaCl, and HEPES in this order or it may dissolve poorly. Adjust pH to 7.4 with NaOH and complete to 500 mL with milliQ water. Autoclave.

(1) *Day 1: cell plating*

Seed HEK293T cells in 10 140 mm Petri dishes at 30–40% density. Adjust final volume to 20 mL using fresh DMEM media (high glucose) supplemented with 1% antibiotics, 1% Glutamax, and 10% FBS. Depending on the quantity of virus to produce, this protocol can be up or downscaled to the appropriate quantity.
Troubleshooting: use only HEK293T cells as this cell line contains the SV40 T-antigen and is competent to replicate vectors carrying the SV40 region of replication.
Incubate the cells for 24 h at 37°C in a humidified incubator with an atmosphere of 5% CO_2.

(2) *Day 2: phosphate calcium transfection*

– Mix 200 μg of the expression vector plasmid, 50 μg of the packaging plasmid pMD2G and 150 μg of the envelope plasmid psPAX2 in a total volume of 8,250 μL of MilliQ water.
– Troubleshooting: only use plasmid DNA obtained from mid- or maxi-prep and resuspended at a concentration of at least 1 μ g/μ L.
– Add 2,880 μL of $CaCl_2$ 1M and make bubbles during 30 s.
– Incubate the mixture for 20 min at room temperature.
– Add 11,520 μL of HBS 2X in a 50 mL Falcon tube.
– Add DNA mix to the HBS 2X tube drop by drop and make bubbles during 30 s.
– Immediately distribute the mixture in culture dishes (2.3 mL per dish).
– Between 6 and 8 h later, replace media by fresh DMEM (high glucose) supplemented with 1% antibiotics, 1% Glutamax, and only 1% FBS to reduce FBS precipitation.
Troubleshooting: before to replace transfection media, check that DNA precipitates are visible around cells using a 40X objective.
– Incubate 72 h at 37°C in a humidified incubator with an atmosphere of 5% CO_2.

(3) *Days 5 and 6: lentivirus concentration by precipitation*

– Filter the cell supernatant (containing lentiviral particles) through a 0.45 μm filter unit and distribute it in six 50 mL Falcon tubes (around 33 mL per tube).
Troubleshooting: filters get easily stuck so change it when pressure is too high; alternatively, centrifuge supernatant at 500 *g* before filtering in order to remove any floating cells and debris.
– Add one third volume of 4X PEG solution (around 11 mL per tube), mix by gently inverting five times.
– Incubate at 4°C overnight.
– Day 6: centrifuge the tubes at 2,600 *g* for 30 min at 4°C and discard the supernatant.
– On ice, resuspend the pellets in a final volume of 300 μL of PBS and make aliquots. Store at −80°C for years.
Troubleshooting: avoid introducing air bubbles when resuspending the virus to keep high transduction efficiency. Freeze-thaw of lentiviruses strongly impairs their efficiency so dispense into aliquots of appropriate volume.

this conditioned medium at 37°C. As a guideline, we routinely remove 1 mL from a 35 mm dish.
- Carefully add the DNA/lipofectamine complexes drop by drop on the cells and put the culture dishes back in the incubator. Wait for 3 h.
- Remove all the medium from the culture dishes and replace by a solution composed by 50% of the conditioned medium collected above and 50% of fresh CM−.
- Expression of your transgene should be detected 24 h later.

(29b) *Transduction with lentiviral particles*

This protocol will lead to a low and slow expression of the transgene into a high percentage of neurons (close to 100% depending on the promoter used for transgene expression, **Figures 2B**, **5**).
- For a 35 mm dish, remove 300 μL of culture media and add a mixture of 400 μL of fresh CM− and 5 μL of lentiviral particles at 10^9 IU/mL (see **Box 2** for lentivirus production and purification). Amount of lentiviruses has to be adapted according to the transgene and the experiment to be performed. As a general guideline, we recommend to test three different concentrations of lentiviral particles to determine the optimal transduction when using a new viral construction.
- There is no need to change media after lentiviral transduction.
- Transgene expression will increase slowly and progressively with days. Depending on transgene and promotor activity, some expression might not be detected before 7 days.

(29c) *Transduction with AAV particles*

This protocol will lead to a high expression of the transgene into a high percentage of neurons (close to 100% depending on the promoter used for transgene expression).

- For a 35 mm dish, remove 300 μL of culture media and add a mixture of 400 μL of fresh CM− and 0.1 μL of lentiviral particles at 10^{11} IU/mL. Amount of AAV has to be adapted according to the transgene and the experiment to be done. As a general guideline, we recommend to test three different concentrations of AAV particles to determine the optimal transduction when using a new viral construction.
- There is no need to change media after AAV transduction.
- Transgene expression will increase rapidly and progressively with days. Depending on transgene and promotor activity, experiments can be performed from the 3^{rd} days after the transduction.

RESULTS

Development and Neuronal Activity of Mouse Postnatal Hippocampal Culture Maintained Either in BrainPhys or in Neurobasal Media

Currently most postnatal neuronal cultures are plated and kept in Neurobasal-A and/or DMEM media. Hippocampal cells were plated with CM+ because its rich composition in supplements might be important to promote cell adhesion and survival. After this initial phase, we thought that using BrainPhys medium (Bardy et al., 2015) instead of Neurobasal-A in the CM− would improve neuronal maintenance as this medium contains less neuroactive components that are likely detrimental for long term postnatal or mature neuronal cultures (Hogins et al., 2011; Maggioni et al., 2015). In embryonic neuronal culture such change in medium composition results in an improvement of action potential generation and synaptic communication and thus in the generation of an *in vitro* model closer to brain physiological conditions (Bardy et al., 2015). Before media change at DIV 3, neurons follow stereotypical developmental steps. First, after plating, neurons are spheres (**Figure 3A-DIV 0**) which start to acquire neurites at DIV 1. Between DIV 1 and DIV 4, these neurites grow and differentiate in axon and dendrites. We first compared basic properties of neurons kept after DIV 3, either in Neurobasal-A- or BrainPhys-containing medium. We did not observe any significant morphological differences between the two conditions of culture. The functional polarization begins approximately 1 week after seeding (DIV 7) with the formation of synapses. Between DIV 7 and DIV 14, a strong ramification of the dendritic tree is observed (**Figure 3A-DIV 14**) as well as the expression of synaptic markers (**Figure 3D**) consistent with the creation of a functional network. These experiments show that mouse postnatal hippocampal cultures kept in BrainPhys- or in Neurobasal-A-containing CM− undergo developmental stages which are similar to those previously described for embryonic culture (Meberg and Miller, 2003; Kaech and Banker, 2006). At DIV 7 and DIV 14, we did not observe any significant difference in neuronal density in cultures kept in Neurobasal-A or in BrainPhys (**Figure 3B**). Importantly, neuronal density was not affected by the age of mouse pups whatever the culture medium composition. Next, we studied the effect of both medium's composition on neuronal excitability. Miniature excitatory post-synaptic currents (mEPSCs) recorded on neurons between DIV 13 and DIV 15 presented a significantly higher amplitude and a fourfold increase in the frequency when maintained in Neurobasal-A compared to BrainPhys (**Figure 3C**). These data support that the composition of culture media used for long term cell culture has important repercussions on neuronal activity. Cultures kept in Neurobasal-A are prone to hyperexcitability, whereas neurons kept in BrainPhys present spontaneous activity with features (amplitude and frequency of mEPSCs) close to what is observed *ex vivo* (Szczot et al., 2010; Thakar et al., 2017; Su et al., 2019). By co-immunostaining pre- and post-synaptic markers (**Figure 3D**), we detected presynaptic and post-synaptic protein clusters and quantify co-localizing puncta, which give an estimation of synaptic connections. We did not observe any significant difference in the number of co-localizing clusters (**Figure 3E**) between cultures maintained in Neurobasal-A and in BrainPhys suggesting that the difference observed in neuronal excitability is not caused by a change in synaptogenesis. We therefore decided to use BrainPhys medium for long term culture.

Neuronal Composition of Mouse Postnatal Hippocampal Culture

We next characterized the cellular composition of postnatal hippocampal culture. First, we analyzed the ratio of excitatory versus inhibitory neurons during culture development. Three main types of neurons are observed in the hippocampus: granular cells and pyramidal cells which are excitatory neurons, and inhibitory interneurons. We performed a triple co-immunostaining using (i) NeuN, a pan neuronal cell marker (Mullen et al., 1992; Iwano et al., 2012; Gusel'nikova and Korzhevskiy, 2015), (ii) CaMKIIα, a marker for hippocampal excitatory neurons (Benson et al., 1992; Sik et al., 1998; Wang et al., 2013; Pelkey et al., 2017), and (iii) Prox1, a granular cell marker (Iwano et al., 2012) (**Figure 4A**). All these markers are not necessarily exclusive and based on data from the literature, we considered that, (i) pyramidal cells are positive for NeuN and CaMKIIα, (ii) granule cells are cells positive for NeuN and Prox1 staining. Most of the granule cells, but not all, might be positive for CaMKIIα (Sola et al., 1999), (iii) inhibitory neurons are cells only positive for NeuN. Stainings were performed at DIV 7 (early stage of culture development) and DIV 14 (mature culture) on cultures from P1 and P3 mouse pups.

Whatever the age of pups, we observed that inhibitory interneurons account for ∼10–15% of the total neuronal cell population at DIV 14 (**Figure 4B**), while the remaining neurons are excitatory (85 to 90%), reflecting neuronal diversity observed *in vivo* in the mouse or rat hippocampus (Pelkey et al., 2017). Presence of inhibitory neurons was confirmed by performing immunostaining using anti-GABA antibody (**Figure 4C**). At DIV 14, GABA-positive and CaMKIIα-negative neurons represent 15,9 ± 5,4% of NeuN-positive neurons. Among excitatory

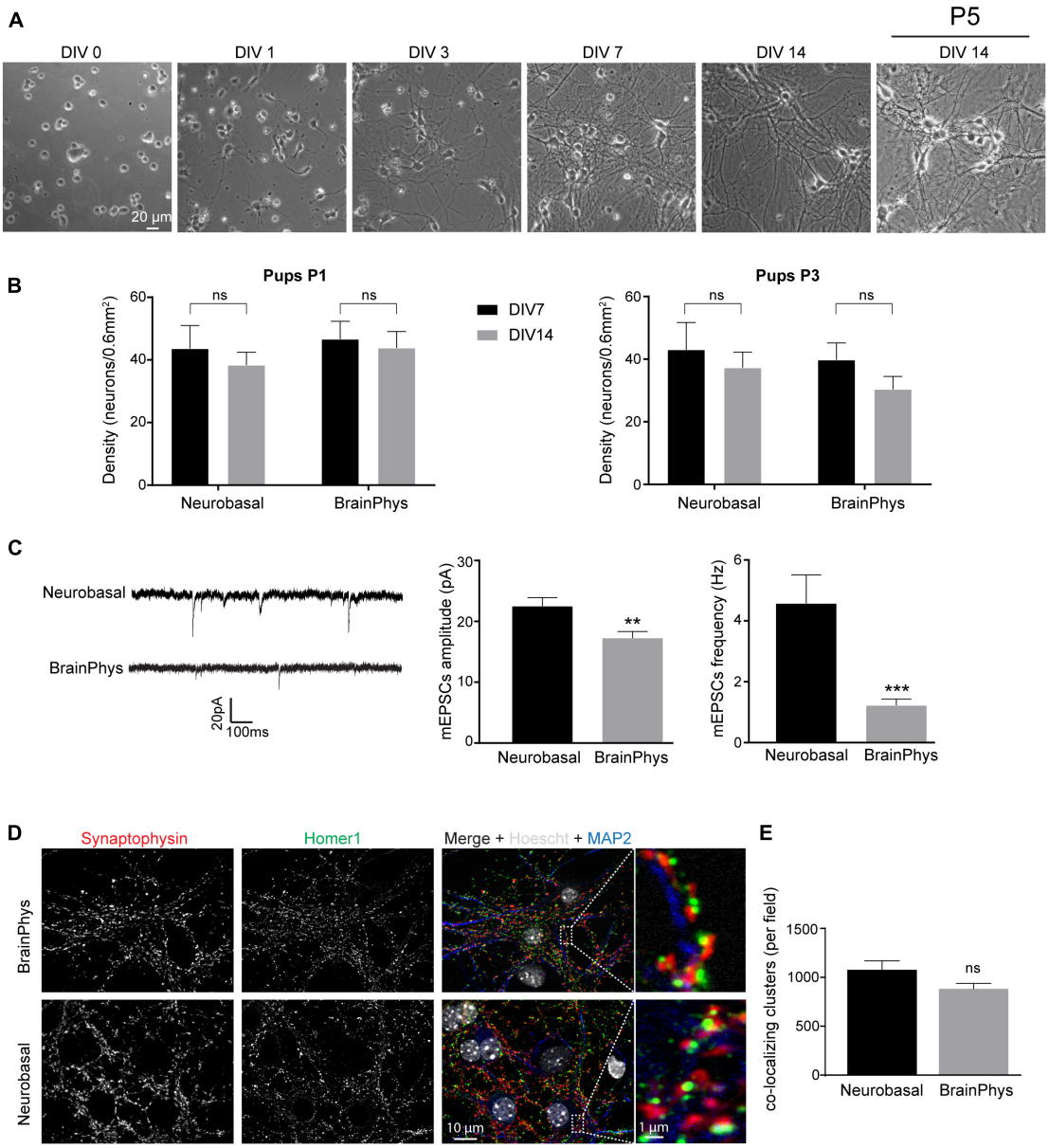

FIGURE 3 | Neuronal morphology and activity in hippocampal culture growth in BrainPhys-containing CM– media. **(A)** Phase contrast images showing the development of a postnatal hippocampal culture. **(B)** Neuronal density of hippocampal culture from P1 (left panel) or P3 (right panel) pups growth in either Neurobasal-A or BrainPhys media. Cultures were fixed at DIV 7 or DIV 14 and neurons stained using NeuN antibody before quantification. Results represent mean + SEM, $N = 3$ independent cultures from P1 pups and P3 pups. At least 357 neurons were analyzed for each condition. Two way ANOVA corrected for multiple comparisons by controlling the False Discovery Rate (FDR). Ns indicates q-value > 0.05. **(C)** mEPSCs frequency and amplitude recorded between DIV 13 and 15 from hippocampal culture maintained in either Neurobasal-A or BrainPhys-containing CM–. Results represent mean + SEM, $N = 27$ and 31 cells were recorded for Neurobasal and BrainPhys condition respectively from four independent cultures done with pups aged between P1 and P2. Mann–Whitney test, **, *** indicate p-value < 0.01, p-value < 0.001, respectively. **(D)** Immunocytochemistry images from DIV 14 cultures stained with antibodies against the presynaptic marker Synaptophysin (Red), the dendritic marker MAP2 (Blue), the post-synaptic marker Homer1 (green) and Hoescht (Gray) in culture maintained in BrainPhys or Neurobasal-A medium. **(E)** Quantification of co-localizing puncta using the ImageJ plug-in called Synapse counter. For **(D,E)**, images were acquired using EC Plan-Neofluar 40X/1.30 and 100X/1.30 objectives respectively. For **(E)**, results represent mean + SEM, $n \geq 12$ fields from $N = 3$ independent cultures from P1 pups. Unpaired t-test, ns indicates p-value > 0.05.

neurons, proportion of granule and pyramidal cells was not affected as well by the age of pups (**Figure 4B**). Pyramidal neurons and granule cells represent around 30 and 60% of the NeuN positive cells, respectively. This is consistent with previous findings showing that postnatal hippocampal culture is mainly composed of granule cells (Wu et al., 2015).

During culture development from DIV 7 to DIV 14, proportion of Prox1$^+$ granule cells, interneurons and pyramidal

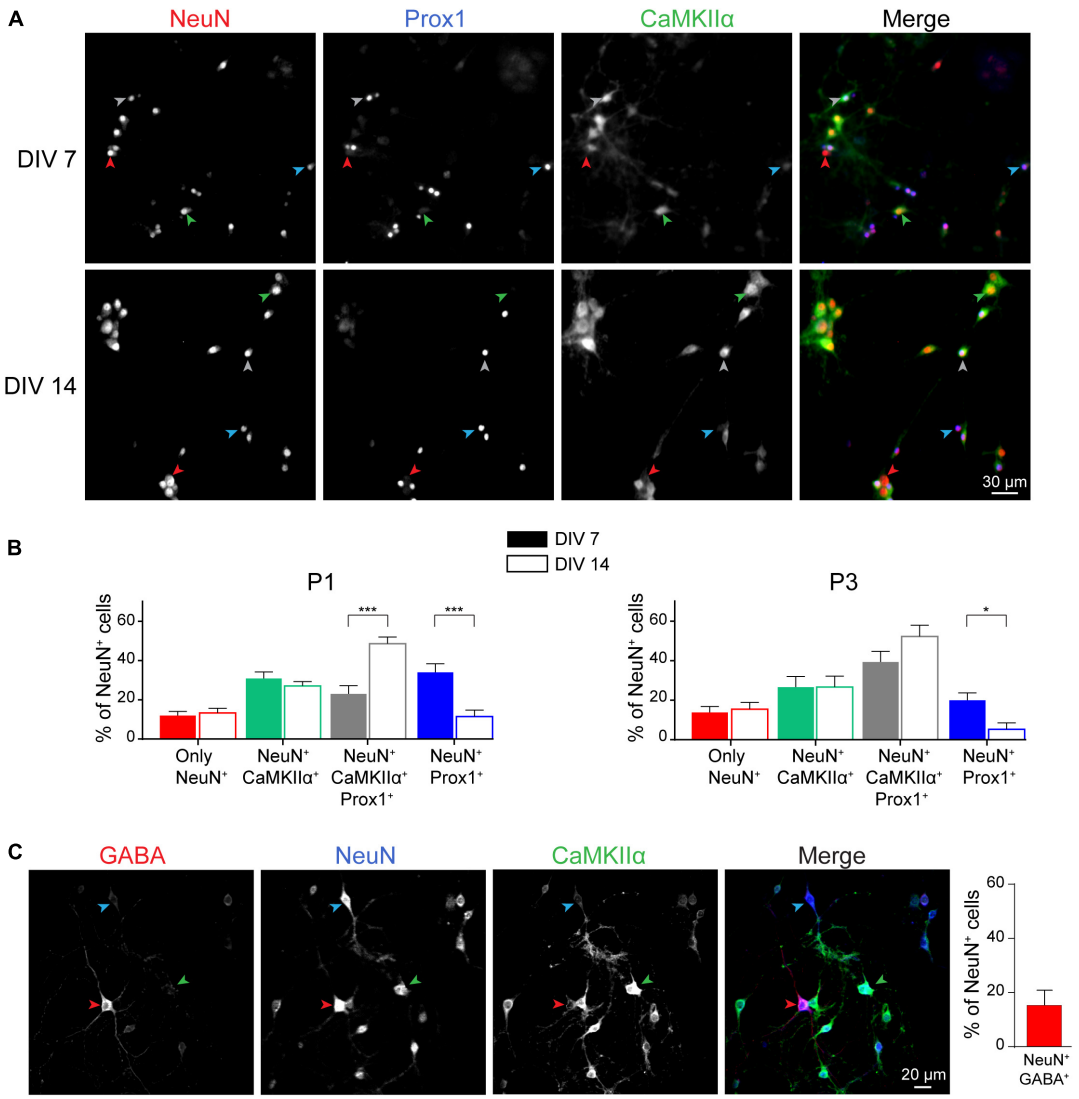

FIGURE 4 | Neuronal cell type characterization of postnatal hippocampal culture. Immunocytochemistry images **(A)** and quantification **(B)** from DIV 7 and 14 cultures stained with antibodies against the neuronal markers NeuN (Red), Prox1 (Blue), and CaMKIIα (green) in culture maintained in BrainPhys medium. Red, Blue, Green and Gray arrow heads indicate cells only $NeuN^+$, $NeuN^+/Prox1^+$, $NeuN^+/CaMKII\alpha^+$ and $NeuN^+/CaMKII\alpha^+/Prox1^+$ respectively. For **(B)**, results represent mean + SEM, $n \geq 8$ fields from $N = 3$ independent cultures from P1 pups and P3 pups. At least 357 neurons were analyzed for each condition. Two way ANOVA corrected for multiple comparisons by controlling the False Discovery Rate (FDR). *, *** indicate q-value < 0.05, q-value < 0.001, respectively.
(C) Immunocytochemistry images from DIV 14 cultures stained with antibodies against the neuronal markers NeuN (Blue), GABA (Red), and CaMKIIα (Green) in culture maintained in BrainPhys medium. Blue, Red, and Green arrow heads indicate cells only $NeuN^+$, $NeuN^+/GABA^+$, and $NeuN^+/CaMKII\alpha^+$ respectively. Results represent mean + SEM, $N = 3$ independent cultures from P1 pups with $n \geq 4$ fields per culture.

cells remain stable. However, we observed a decrease in the percentage of granule cells negative for CaMKIIα and a concomitant increase in the proportion of granule cells positive for this marker (**Figure 4B**). Similar observations were made on culture from P1 and P3 mouse pups.

At DIV 14 the postnatal hippocampal cultures are composed by roughly 50% of glial cells and 50% of neurons (data not shown), whatever the age of pups. Given the importance of glial cells and specially astrocytes in neurons homeostasis (Perea et al., 2009; Robertson, 2018), we believe that this heterogeneity in the culture is beneficial for neuron development, survival and activity as well as for providing an *in vitro* culture model closer to *in vivo* environment.

Tools for Imaging Neuronal Functions

Neuronal culture represents a model of choice to decipher neuronal cell biology at the molecular level, according that these cells are amendable to gene transfer. To that aim we developed a lentiviral approach that allows cell-specific gene expression. As illustrated in **Figure 5**, the present protocol for lentivirus production allows to efficiently genetically manipulate cells of postnatal cultures. We routinely expressed different

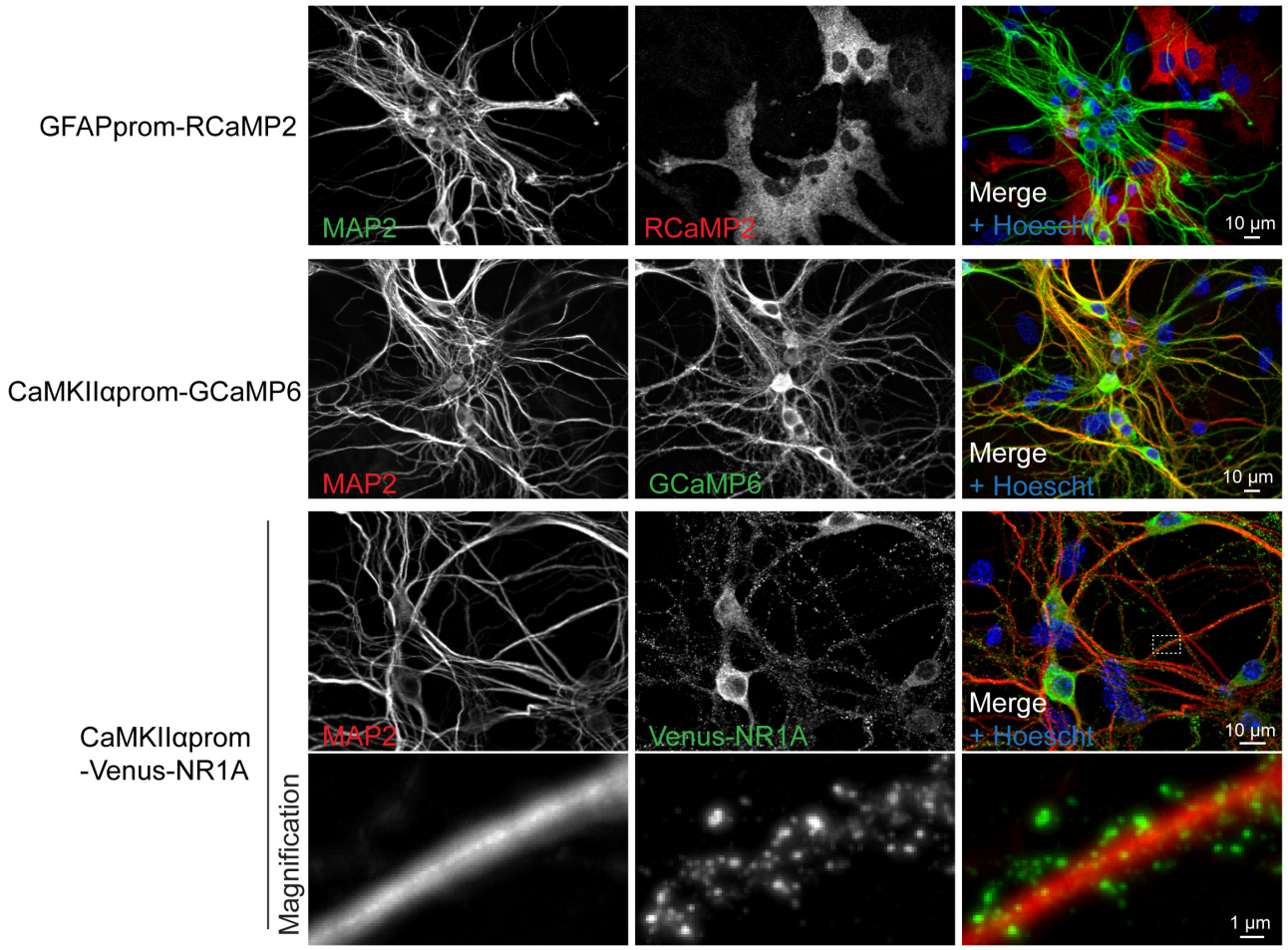

FIGURE 5 | Lentiviral approach allows fine tuning, cell-type specific gene expression. Representative immunocytochemistry images realized on cultures transduced with two genetically encoded calcium indicators (RCaMP2 or GCaMP6) and the NMDA receptor subunit NR1A fused to Venus protein. These constructs were expressed under the control of promoters specific for either neurons (CaMKIIαprom) or astrocytes (GFAPprom). Neurons and nuclei were respectively stained with anti-MAP2 antibody and Hoescht, respectively.

genetically encoded calcium indicators either in astrocytes or in neurons using specific promoters (**Figure 5**). Lentiviral transduction allows low level of transgene expression levels without compromising efficiency in gene delivery. Such features enable a correct targeting of proteins of interest such as NMDA receptor subunit as demonstrated by the punctuate staining of Venus-NR1A subunit observed in dendrites (**Figure 5**).

We usually performed experiments between DIV 14 to DIV 17 when culture is considered mature with a neuronal network composed of stabilized synapses, characterized by spontaneous activity. Results from **Figure 6** highlight examples of experiments that can be achieved using our protocol for culturing and transducing postnatal hippocampal neurons using specific tools dedicated to study neuronal biology. First, to specifically target reporter proteins to spines, we used a palmitoylation motif of the N-terminal tail of LIMK1, as previously described (George et al., 2015). We generated LIMK-NLuc-YPet by fusing this LIMK1's palmitoyl-motif with the N-terminal tail of NLuc-YPet, a fusion protein between the luciferase NLuc and a YFP variant. After transduction and expression in postnatal culture, we compared the subcellular localization of LIMK-NLuc-YPet with that of NLuc-YPet. Synaptosomes were purified at DIV 17 and the different fractions were analyzed by Western Blot. Results from **Figure 6A** show that NLuc-YPet construct is, as expected, indifferently detected in the homogenate, the cytoplasm and the synaptosomal fractions. On the opposite, when fused to the palmitoylation motif, LIMK-NLuc-YPet is preferentially detected in the dendritic spines. Internal controls show that the endogenous proteins actin and AMPA receptors (GluR2) are detected either in the three fractions or specifically in the synaptosomes, respectively. Preferential localization of LIMK-NLuc-YPet at the synapse was also confirmed by immunocytochemistry and co-staining with the post-synaptic marker PSD-95 (**Figure 6B**).

Primary cultures are also convenient for different kinds of functional experiments (**Figures 6C–G**). We first expressed the genetically encoded calcium reporter GCaMP6s under the control of the excitatory neuronal promoter CaMKIIα.

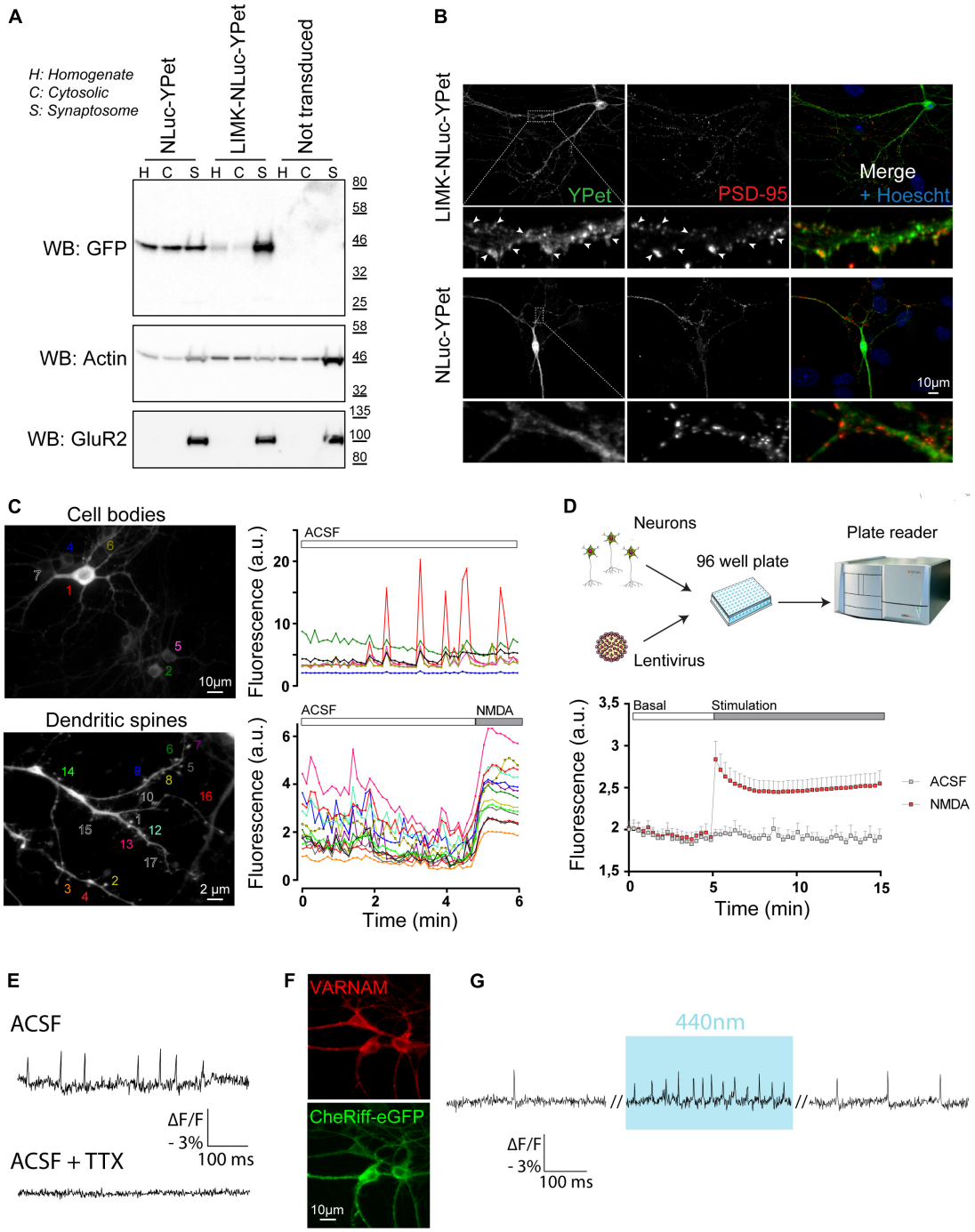

FIGURE 6 | Postnatal hippocampal culture is a simple model to study neuronal function. **(A)** Identification of the subcellular localization of proteins in neurons. After synaptosome purification, expression of endogenous (actin and GluR2) and overexpressed proteins (NLuc-YPet and LIMK-NLuc-YPet) was evaluated by immunoblot in the homogenate (H), the cytosolic fraction (C) and synaptosomes (S). Note that the N-terminal tail of LIMK1 is sufficient to target the cytoplasmic construct NLuc-YPet to dendritic spines. **(B)** Identification of the subcellular localization of proteins in neurons by immunocytochemistry. NLuc-YPet constructs were detected using a GFP antibody recognizing YPet. Dendritic spines were stained using antibodies against PSD-95. **(C)** Calcium recording using videomicroscopy. Spontaneous fluorescence variations of neurons expressing GCaMP6 following lentiviral transduction were recorded for 6 min at 0.15 Hz. Fluorescence intensity was acquired in seven neuronal cell bodies (Top panels) and in 17 different dendritic spines before and after application of 50 µM NMDA (bottom panel). **(D)** Calcium recording using a plate reader. Postnatal culture was seeded in 96 well plate and transduced with lentiviruses coding for GCaMP6 at DIV 7 (top panel). Fluorescence was recorded using an Infinite F500 plate reader for 15 min before and after a control (ACSF) or 50 µM NMDA (NMDA) stimulation. **(E–G)** Monitoring and controlling neuronal activity by light. VARNAM, a red shifted voltage indicator was used to monitor spontaneous **(E)** and light-induced **(G)** neuronal activity at 600 Hz in cells co-expressing the blue shifted channelrhodopsin CheRiff **(F)**. Addition of 0.3 µM TTX completely abolished VARNAM -evoked fluorescence variations.

By imaging fluorescence for 6 min, we detected spontaneous activity in individual neurons, either in cell bodies (**Figure 6C**, top panel) or in dendritic spines (**Figure 6C**, bottom panel). This experiment shows typical recording of neurons with spontaneous calcium waves either asynchronous or synchronous. On dendritic spines, application of 50 μM NMDA induced a robust and prolonged increase in calcium entry (**Figure 6C**, bottom panel). The present protocol for hippocampal postnatal culture is also compatible with 96 well-plate format and GCaMP6 fluorescence can be recorded on cell population using a plate reader (**Figure 6D**).

Second, we provide proof of principle that an all-optical approach can be used on postnatal cultures thereby allowing to optically monitor and control neuronal activity. In neurons after expression of the red shifted voltage indicator VARNAM (Kannan et al., 2018) using AAV-DJ particles, spontaneous action potentials (APs) were resolved by recording fluorescence at a frequency of 600 Hz (**Figure 6E**). Changes in fluorescence were completely abolished after application of TTX. In neurons co-expressing VARNAM and the blue shifted channelrhodopsin CheRiff (**Figure 6F**), light stimulation at 440 nm increased APs frequency (**Figure 6G**) confirming that neuronal activity can be controlled by light in cells expressing CheRiff and recorded through VARNAM fluorescence.

Altogether these data illustrate that our protocols provide an *in vitro* culture model for exploring cellular mechanisms and neuronal activity.

DISCUSSION

Postnatal hippocampal culture represents a convenient model for studying neuronal pathophysiology *in vitro*, especially when using transgenic animals. Most of the current procedures using new born mice are based on protocols originally developed for embryonic culture, resulting to inconsistency in culture quality or limited to P0-P1 pups.

Herein we thought to develop a protocol dedicated to postnatal culture by optimizing the two main steps of the culture, cell dissociation and cell feeding. First, by developing a fast and gentle protocol for cell dissociation we optimized the survival of hippocampal neurons collected from P0 to P3 mice. Contrary to numerous protocols designed for embryonic or postnatal cultures, we found that dissociation of hippocampi with the protease trypsin is detrimental by promoting neuronal death. In our hands, gentle enzymatic tissue digestion using papain is sufficient to dissociate cells preserving neuron survival. Similarly, reducing the mechanical stress by minimizing the trituration procedure results in a cell suspension with a high percentage of viable cells. Neuronal survival was also greatly improved during these different initial steps by keeping hippocampi and dissociated cells in Hibernate medium, a CO_2-independent nutrient medium.

Second, we optimized culture conditions. Neurons are kept in Neurobasal-A medium until DIV 3 since its formulation was designed to favor cell attachment and survival following cell seeding. We found that using BrainPhys medium for long term cell culture results in neurons with reduced spontaneous activity compared to neurons kept in Neurobasal. In BrainPhys kept neurons, mEPSCs parameters are close to what is observed in hippocampal slices where network integrity is conserved (Szczot et al., 2010; Thakar et al., 2017; Su et al., 2019).

This decrease in hyperexcitability observed in BrainPhys is not associated with a change in neuronal survival or in the ratio between excitatory versus inhibitory neurons and is not caused by a delay in synaptogenesis. Indeed, whatever the culture medium used for cell maintenance, our results show that inhibitory neurons represent approximately 15% of the neuronal cells. We speculate that by providing a more physiological environment (Bardy et al., 2015), long term exposure to BrainPhys might regulate expression or post-translational modification of proteins involved in synaptic activity as already described for ARC protein in human neurons and thus facilitate neuronal maturation. This is supported by the observation of a switch of granular neurons from a negative to a positive staining for CaMKIIα during culture development. This switch reflects the development of granule cells toward a mature phenotype given that, (i) before P7, neurogenesis in the dentate gyrus is very active and GCs exhibit immature-like features (Ambrogini et al., 2004; Pedroni et al., 2014), (ii) in rat hippocampus, CaMKIIα mRNA expression increases during developmental stages and reaches a plateau in adult animals (Burgin et al., 1990) and, (iii) in adult mouse hippocampus where neurons are mature, the strongest expression of CaMKIIα is observed in the dentate gyrus (Wang et al., 2013). Thus, the change in CaMKIIα expression observed in our culture might reflect the progressive maturation of granule cells observed after birth.

Given the importance of glial cells in culture maturation and neuronal activity support (for a review see, Perea et al., 2009; Robertson, 2018), we designed a protocol using a low amount of AraC in order to limit rather than stopping glial cell development. In our experimental conditions, glial cells account for approximatively 50% of total cell number. Depending on the study to conduct, one might consider employing higher concentration of AraC to further limit glial cell proportion. However, it must be kept in mind that such treatment might impact neuron survival and/or affect synaptic development and neuronal activity.

We also describe two different approaches to genetically modify neuronal culture. The first method is based on transfection reagent such as Lipofectamine 2000. This approach is very simple to use, is very quick to set up and will result in an overexpression of the transgene. It represents an interesting strategy to express for instance a fluorescent marker in a small percentage of cells and visualize neuronal processing. While Lipofectamine 2000 might be toxic for neurons, we provide here a protocol that limits such toxicity. The second approach is based on the use of lentiviruses. Our protocol adapted from Masuda et al. (2013), is simple (no ultracentrifugation needed) and cost effective. It allows the production and the purification of lentiviral particles suitable for primary neuronal culture transduction. When combined with cell specific promoter, this strategy allows

to target almost 100% of the desired cell type. In addition, because lentivirus lead to the integration of the transgene to the host genome, the use of appropriate promoters results in the expression level of exogenous genes closer to endogenous expression level, compared to other episomal approaches such as AAV transduction and transfection. Low expression level of transgene is illustrated by the correct localization of venus-NR1A subunit observed on **Figure 5**. Indeed, NR1 subunits require to co-assemble with others NMDA subunits to reach the cell surface (McIlhinney et al., 1996, 1998), supporting that in our experiments, expression level of venus-NR1A subunit is compatible with its association with endogenous NMDA subunits. In contrast, overexpression of NR1 tagged subunits using others approaches such as gene gun or transfection reagent result in retention of NR1 subunits and inappropriate localization in neurons (Hall and Soderling, 1997; McIlhinney et al., 1998; Barria and Malinow, 2002). We also routinely use AAV particles for gene manipulation in neurons. Expression of transgene is higher and faster compare to gene delivery using lentiviruses and can be detected 72 h following transduction depending on promoter activity. Purification of AAV particles is far more complex than that of lentiviruses or requires expensive commercial kit. Moreover, higher level transgene expression observed with AAV must be considered carefully including when using genetically encoded calcium indicator [for a review on impact of calcium sensor expression in neurons see McMahon and Jackson (2018)]. We believe that transgene expression using lentiviral particles represents by far the most effective and simple approach for genetic manipulation in culture.

This method for primary neuronal culture was originally designed for hippocampi from P0 to P3 pups. We found it can be extended up to P5 mice for hippocampal neurons without significant increase in neuronal death (**Figure 3A**). This flexibility in the age of pups extends the working time window and dispenses for precise breeding scheduling. This protocol can also be used for cortical neuron cultures from P0-P1 mice (data not shown). In this case, the use of older animals results in a decrease in neuronal survival and less reproducible cultures. Such cortical cultures are of particular interest when performing biochemical experiments where a large number of cells is required, since five 10 cm Petri dishes can be seeded from eight hemispheres (four pups).

Alternatively, this protocol can be adapted to 96 well-plates. Combined with our simple and cost-effective protocol for lentivirus production and neuronal transduction, this protocol of primary neuronal culture is suitable for experiments of automatized drug screening.

DATA AVAILABILITY STATEMENT

The raw data supporting the conclusions of this article will be made available by the authors, without undue reservation, to any qualified researcher.

ETHICS STATEMENT

All animal procedures were conducted in accordance with the European Communities Council Directive and were reviewed and approved by the IGF institute's local Animal Welfare Unit (A34-172-41).

AUTHOR CONTRIBUTIONS

VC and EM contributed conception and design of the study, performed the statistical analysis, and wrote the first draft of the manuscript. VC, EM, A-LH, NL, and VS performed the experiments. NL, A-LH, JP, and FR wrote sections of the manuscript. JP and FR critically revised the data. All authors contributed to manuscript revision, read and approved the submitted version.

FUNDING

This work was supported by the Agence Nationale de la Recherche (VC, ANR-18-CE16-0011-01), the LabEx ICST (FR, 11-LABX-0015), and the European Research Council (ERC) under the European Union's Horizon 2020 Research and Innovation Programme (JP, Grant Agreement No. 646788).

ACKNOWLEDGMENTS

We thank the iExplore animal facility (IGF, Montpellier) and the Arpege plateform (IGF, Montpellier) for the use of plate reader for cell-population BRET. We thank Hélène Hirbec for her assistance with statistical analysis and Yan Chastagnier for his help with synapse counting.

REFERENCES

Ahlemeyer, B., and Baumgart-Vogt, E. (2005). Optimized protocols for the simultaneous preparation of primary neuronal cultures of the neocortex, hippocampus and cerebellum from individual newborn (P0.5) C57Bl/6J mice. *J. Neurosci. Methods* 149, 110–120. doi: 10.1016/j.jneumeth.2005.05.022

Ambrogini, P., Lattanzi, D., Ciuffoli, S., Agostini, D., Bertini, L., Stocchi, V., et al. (2004). Morpho-functional characterization of neuronal cells at different stages of maturation in granule cell layer of adult rat dentate gyrus. *Brain Res.* 1017, 21–31. doi: 10.1016/j.brainres.2004.05.039

Banker, G. A., and Cowan, W. M. (1977). Rat hippocampal neurons in dispersed cell-culture. *Brain Res.* 126, 397–425.

Bardy, C., van den Hurk, , M., Eames, T., Marchand, C., Hernandez, R. V., Kellogg, M., et al. (2015). Neuronal medium that supports basic synaptic functions and activity of human neurons in vitro. *Proc. Natl. Acad. Sci. U.S.A.* 112, E3312–E3312. doi: 10.1073/pnas.1504393112

Barria, A., and Malinow, R. (2002). Subunit-specific NMDA receptor trafficking to synapses. *Neuron* 35, 345–353. doi: 10.1016/s0896-6273(02)00776-6

Beaudoin, G. M., Lee, S. H., Singh, D., Yuan, Y., Ng, Y. G., Reichardt, L. F., et al. (2012). Culturing pyramidal neurons from the early postnatal mouse hippocampus and cortex. *Nat. Protoc.* 7, 1741–1754. doi: 10.1038/nprot.2012.099

Benson, D. L., Isackson, P. J., Gall, C. M., and Jones, E. G. (1992). Contrasting patterns in the localization of glutamic acid decarboxylase and

Ca2+/calmodulin protein kinase gene expression in the rat central nervous system. *Neuroscience* 46, 825–849. doi: 10.1016/0306-4522(92)90188-8

Brewer, G. J., Torricelli, J. R., Evege, E. K., and Price, P. J. (1993). Optimized survival of hippocampal-neurons in B27-Supplemented Neurobasal(Tm), a new serum-free medium combination. *J. Neurosci. Res.* 35, 567–576. doi: 10.1002/jnr.490350513

Brewer, L. D., Thibault, O., Staton, J., Thibault, V., Rogers, J. T., Garcia-Ramos, G., et al. (2007). Increased vulnerability of hippocampal neurons with age in culture: temporal association with increases in NMDA receptor current, NR2A subunit expression and recruitment of L-type calcium channels. *Brain Res.* 1151, 20–31. doi: 10.1016/j.brainres.2007.03.020

Burgin, K. E., Waxham, M. N., Rickling, S., Westgate, S. A., Mobley, W. C., and Kelly, P. T. (1990). In situ hybridization histochemistry of Ca2+/calmodulin-dependent protein kinase in developing rat brain. *J. Neurosci.* 10, 1788–1798.

Eide, L., and McMurray, C. T. (2005). Culture of adult mouse neurons. *Biotechniques* 38, 99–104. doi: 10.2144/05381RR02

George, J., Soares, C., Montersino, A., Beique, J. C., and Thomas, G. M. (2015).). Palmitoylation of LIM Kinase-1 ensures spine-specific actin polymerization and morphological plasticity. *eLife* 4:e06327. doi: 10.7554/eLife.06327

Gusel'nikova, V. V., and Korzhevskiy, D. E. (2015). NeuN As a neuronal nuclear antigen and neuron differentiation marker. *Acta Naturae* 7, 42–47. doi: 10.32607/20758251-2015-7-2-42-47

Hall, R. A., and Soderling, T. R. (1997). Differential surface expression and phosphorylation of the N-methyl-D-aspartate receptor subunits NR1 and NR2 in cultured hippocampal neurons. *J. Biol. Chem.* 272, 4135–4140. doi: 10.1074/jbc.272.7.4135

Hogins, J., Crawford, D. C., Zorumski, C. F., and Mennerick, S. (2011). Excitotoxicity triggered by neurobasal culture medium. *PLoS One* 6:e25633. doi: 10.1371/journal.pone.0025633

Iwano, T., Masuda, A., Kiyonari, H., Enomoto, H., and Matsuzaki, F. (2012). Prox1 postmitotically defines dentate gyrus cells by specifying granule cell identity over CA3 pyramidal cell fate in the hippocampus. *Development* 139, 3051–3062. doi: 10.1242/dev.080002

Kaar, A., Morley, S. J., and Rae, M. G. (2017). An efficient and cost-effective method of generating postnatal (P2-5) mouse primary hippocampal neuronal cultures. *J. Neurosci. Methods* 286, 69–77. doi: 10.1016/j.jneumeth.2017.05.020

Kaech, S., and Banker, G. (2006). Culturing hippocampal neurons. *Nat. Protoc.* 1, 2406–2415. doi: 10.1038/nprot.2006.356

Kannan, M., Vasan, G., Huang, C., Haziza, S., Li, J. Z., Inan, H., et al. (2018). Fast, in vivo voltage imaging using a red fluorescent indicator. *Nat. Methods* 15, 1108–1116. doi: 10.1038/s41592-018-0188-7

Maggioni, D., Monfrini, M., Ravasi, M., Tredici, G., and Scuteri, A. (2015). Neurobasal medium toxicity on mature cortical neurons. *Neuroreport* 26, 320–324. doi: 10.1097/Wnr.0000000000000343

Masuda, T., Tsuda, M., Tozaki-Saitoh, H., and Inoue, K. (2013). Lentiviral transduction of cultured microglia. *Methods Mol. Biol.* 1041, 63–67. doi: 10.1007/978-1-62703-520-0_8

Mattson, M. P., Wang, H., and Michaelis, E. K. (1991). Developmental expression, compartmentalization, and possible role in excitotoxicity of a putative NMDA receptor protein in cultured hippocampal neurons. *Brain Res.* 565, 94–108. doi: 10.1016/0006-8993(91)91740-r

McIlhinney, R. A., Le Bourdelles, B., Molnar, E., Tricaud, N., Streit, P., and Whiting, P. J. (1998). Assembly intracellular targeting and cell surface expression of the human N-methyl-D-aspartate receptor subunits NR1a and NR2A in transfected cells. *Neuropharmacology* 37, 1355–1367. doi: 10.1016/s0028-3908(98)00121-x

McIlhinney, R. A., Molnar, E., Atack, J. R., and Whiting, P. J. (1996). Cell surface expression of the human N-methyl-D-aspartate receptor subunit 1a requires the co-expression of the NR2A subunit in transfected cells. *Neuroscience* 70, 989–997. doi: 10.1016/0306-4522(95)00419-x

McMahon, S. M., and Jackson, M. B. (2018). An inconvenient truth: calcium sensors are calcium buffers. *Trends Neurosci.* 41, 880–884. doi: 10.1016/j.tins.2018.09.005

Meberg, P. J., and Miller, M. W. (2003). Culturing hippocampal and cortical neurons. *Neurons Methods Appl. Cell Biol.* 71, 111–127. doi: 10.1016/S0091-679x(03)01007-0

Mullen, R. J., Buck, C. R., and Smith, A. M. (1992). Neun, a neuronal specific nuclear-protein in vertebrates. *Development* 116, 201–211.

Pedroni, A., Minh do, D., Mallamaci, A., and Cherubini, E. (2014). Electrophysiological characterization of granule cells in the dentate gyrus immediately after birth. *Front. Cell Neurosci.* 8:44. doi: 10.3389/fncel.2014.00044

Pelkey, K. A., Chittajallu, R., Craig, M. T., Tricoire, L., Wester, J. C., and McBain, C. J. (2017). Hippocampal gabaergic inhibitory interneurons. *Physiol. Rev.* 97, 1619–1747. doi: 10.1152/physrev.00007.2017

Peltier, J., Ormerod, B. K., and Schaffer, D. V. (2010). Isolation of adult hippocampal neural progenitors. *Methods Mol. Biol.* 621, 57–63. doi: 10.1007/978-1-60761-063-2_4

Perea, G., Navarrete, M., and Araque, A. (2009). Tripartite synapses: astrocytes process and control synaptic information. *Trends Neurosci.* 32, 421–431. doi: 10.1016/j.tins.2009.05.001

Peterson, C., Neal, J. H., and Cotman, C. W. (1989). Development of N-methyl-D-aspartate excitotoxicity in cultured hippocampal neurons. *Brain Res. Dev. Brain Res.* 48, 187–195. doi: 10.1016/0165-3806(89)90075-8

Robertson, J. M. (2018). The gliocentric brain. *Int. J. Mol. Sci.* 19, 3033. doi: 10.3390/ijms19103033

Sik, A., Hajos, N., Gulacsi, A., Mody, I., and Freund, T. F. (1998). The absence of a major Ca2+ signaling pathway in GABAergic neurons of the hippocampus. *Proc. Natl. Acad. Sci. U.S.A.* 95, 3245–3250. doi: 10.1073/pnas.95.6.3245

Sola, C., Tusell, J. M., and Serratosa, J. (1999). Comparative study of the distribution of calmodulin kinase II and calcineurin in the mouse brain. *J. Neurosci. Res.* 57, 651–662.

Su, Y., Liu, J., Yu, B., Ba, R., and Zhao, C. (2019). Brpf1 haploinsufficiency impairs dendritic arborization and spine formation. Leading to cognitive deficits. *Front. Cell Neurosci.* 13:249. doi: 10.3389/fncel.2019.00249

Szczot, M., Wojtowicz, T., and Mozrzymas, J. W. (2010). GABAergic and glutamatergic currents in hippocampal slices and neuronal cultures show profound differences: a clue to a potent homeostatic modulation. *J. Physiol. Pharmacol.* 61, 501–506.

Thakar, S., Wang, L., Yu, T., Ye, M., Onishi, K., Scott, J., et al. (2017). Evidence for opposing roles of Celsr3 and Vangl2 in glutamatergic synapse formation. *Proc. Natl. Acad. Sci. U.S.A.* 114, E610–E618. doi: 10.1073/pnas.1612062114

Wang, X. J., Zhang, C. Z., Szabo, G., and Sun, Q. Q. (2013). Distribution of CaMKII alpha expression in the brain in vivo, studied by CaMKII alpha-GFP mice. *Brain Res.* 1518, 9–25. doi: 10.1016/j.brainres.2013.04.042

Wu, Y. K., Fujishima, K., and Kengaku, M. (2015). Differentiation of apical and basal dendrites in pyramidal cells and granule cells in dissociated hippocampal cultures. *Plos One* 10:e0118482. doi: 10.1371/journal.pone.0118482

Conflict of Interest: The authors declare that the research was conducted in the absence of any commercial or financial relationships that could be construed as a potential conflict of interest.

frontiers in Synaptic Neuroscience

ORIGINAL RESEARCH
published: 15 June 2020
doi: 10.3389/fnsyn.2020.00021

Adenosine A_1 Receptor-Mediated Synaptic Depression in the Developing Hippocampal Area CA2

Douglas A. Caruana[1,2] *and Serena M. Dudek*[2]*

[1]School of Life and Health Sciences, Aston University, Birmingham, United Kingdom, [2]Neurobiology Laboratory, National Institute of Environmental Health Sciences (NIEHS), National Institutes of Health, Research Triangle Park, NC, United States

Immunolabeling for adenosine A_1 receptors (A_1Rs) is high in hippocampal area CA2 in adult rats, and the potentiating effects of caffeine or other A_1R-selective antagonists on synaptic responses are particularly robust at Schaffer collateral synapses in CA2. Interestingly, the pronounced staining for A_1Rs in CA2 is not apparent until rats are 4 weeks old, suggesting that developmental changes other than receptor distribution underlie the sensitivity of CA2 synapses to A_1R antagonists in young animals. To evaluate the role of A_1R-mediated postsynaptic signals at these synapses, we tested whether A_1R agonists regulate synaptic transmission at Schaffer collateral inputs to CA2 and CA1. We found that the selective A_1R agonist CCPA caused a lasting depression of synaptic responses in both CA2 and CA1 neurons in slices obtained from juvenile rats (P14), but that the effect was observed only in CA2 in slices prepared from adult animals (~P70). Interestingly, blocking phosphodiesterase activity with rolipram inhibited the CCPA-induced depression in CA1, but not in CA2, indicative of robust phosphodiesterase activity in CA1 neurons. Likewise, synaptic responses in CA2 and CA1 differed in their sensitivity to the adenylyl cyclase activator, forskolin, in that it increased synaptic transmission in CA2, but had little effect in CA1. These findings suggest that the A_1R-mediated synaptic depression tracks the postnatal development of immunolabeling for A_1Rs and that the enhanced sensitivity to antagonists in CA2 at young ages is likely due to robust adenylyl cyclase activity and weak phosphodiesterase activity rather than to enrichment of A_1Rs.

Keywords: adenosine, phosphodiesterase, adenylyl cyclase, synapse, long-term depression (LTD), hippocampus

OPEN ACCESS

Edited by:
Alfredo Kirkwood, Johns Hopkins University, United States

Reviewed by:
Julie A. Kauer, Stanford University, United States
Kimberly M. Huber, University of Texas Southwestern Medical Center, United States

***Correspondence:**
Serena M. Dudek
dudek@niehs.nih.gov

Received: *20 February 2020*
Accepted: *04 May 2020*
Published: *15 June 2020*

Citation:
Caruana DA and Dudek SM (2020) Adenosine A_1 Receptor-Mediated Synaptic Depression in the Developing Hippocampal Area CA2. Front. Synaptic Neurosci. 12:21. doi: 10.3389/fnsyn.2020.00021

Abbreviations: Adenosine, 9-β-D-ribofuranosyl-9*H*-purin-6-amine; AP5, 2-amino-5-phosphonovaleric acid; CCPA, 2-chloro-*N*-cyclopentyladenosine; Forskolin, [3*R*-(3α,4aβ,5β,6β,6aα,10α,10aβ,10bα)]-5-(Acetyloxy)-3-ethenyldodecahydro-6,10,10b-trihydroxy-3,4a,7,7,10a-pentamethyl-1*H*-naphtho[2,1-*b*]pyran-1-one; Fostriecin, (6*R*)-5,6-dihydro-6-[(1*E*,3*R*,4*R*,6*R*,7*Z*,9*Z*,11*E*)-3,6,13-trihydroxy-3-methyl-4-(phosphonooxy)-1,7,9,11-tridecatetraenyl]-2*H*-pyran-2-one; KT5720, (9*R*,10*S*,12*S*)-2,3,9,10,11,12-hexahydro-10-hydroxy-9-methyl-1-oxo-9, 12-epoxy-1*H*-diindolo[1,2,3-*fg*:3′,2′,1′-*kl*]pyrrolo[3,4-*i*][1,6]benzodiazocine-10-carboxylic acid; PKI, Protein Kinase A inhibitor fragment (6–22) amide Thr-Tyr-Ala-Asp-Phe-Ile-Ala-Ser-Gly-Arg-Thr-Gly-Arg-Arg-Asn-Ala-Ile-NH_2; Rolipram, 4-[3-(cyclopentyloxy)-4-methoxyphenyl]pyrrolidin-2-one; SB203580, 4-[5-(4-fluorophenyl)-2-[4-(methylsulfonyl)phenyl]-1*H*-imidazol-4-yl]pyridine.

INTRODUCTION

Caffeine acts as a stimulant when consumed by humans, and in some individuals, it may trigger or even exacerbate symptoms of anxiety or psychosis (Lucas et al., 1990; Broderick and Benjamin, 2004). Although the precise cellular mechanisms underlying both the beneficial and detrimental effects of caffeine on cognition remain largely unknown, studies in rodents provide powerful insight into caffeine's mode of action. Strong evidence links adenosine receptors and in particular the A_1 receptor (A_1R) subtype, as major targets of caffeine (Nehlig et al., 1992; Jacobson et al., 1996). Interestingly, mice lacking A_1Rs show increased aggression and anxiety-like behaviors (Giménez-Llort et al., 2002). Indeed, one brain area that has been associated with social aggression and social recognition memory in hippocampal area CA2 (Hitti and Siegelbaum, 2014; Stevenson and Caldwell, 2014; Pagani et al., 2014). This is notable because pyramidal neurons in CA2 show the highest labeling for A_1Rs in the entire hippocampus (Ochiishi et al., 1999). Consistent with the high expression of A_1Rs in CA2 is the observation that caffeine and other A_1R antagonists preferentially enhance excitatory synaptic transmission in area CA2 at concentrations that have little effect on responses in CA1 and CA3 (Simons et al., 2012). This potentiation differs from typical activity-dependent forms of long-term potentiation (LTP) in that it does not require activation of N-methyl-D-aspartate (NMDA) receptors, a rise in postsynaptic calcium, or activity of Ca^{2+}/calmodulin-dependent protein kinase II. It is however, blocked by inhibitors of adenylyl cyclase and postsynaptic protein kinase A (PKA; Simons et al., 2012). Although presynaptic A_1Rs are known to regulate glutamate exocytosis (Dunwiddie and Hoffer, 1980; Prince and Stevens, 1992; Dunwiddie and Masino, 2001), the effects of caffeine on the release probability of neurotransmitter did not differ between areas CA2 and CA1, suggesting that the CA2-specific potentiating effects of A_1R antagonists are due to actions mediated mainly by postsynaptic A_1Rs in CA2 pyramidal neurons (Ochiishi et al., 1999; Simons et al., 2012; but see Muñoz and Solís, 2019).

A difficult finding to reconcile is the observation by Ochiishi et al. (1999) that immunolabeling for the A_1R is uniform in the pyramidal cell layer across the CA fields in young rats, with virtually no difference in labeling between areas CA2 and CA1 at postnatal day 14, the approximate age of animals used previously by Simons et al. (2012). It is only at older ages—P28 and above—that staining for the A_1R is most pronounced in CA2 neurons. Curiously, the robust differences between CA2 and CA1 in their ability to support A_1R-mediated synaptic potentiation do not mirror the developmental expression pattern of the A_1R observed in young rats. Possible explanations to account for this discrepancy may involve key downstream signaling molecules that regulate either the production (*via* adenylyl cyclases) or degradation (*via* phosphodiesterases) of cyclic adenosine monophosphate (cAMP). Because A_1Rs couple to $G_{i/o}$ type G proteins to decrease the activity of adenylyl cyclase and constrain the production of cAMP (Fredholm et al., 2011), we assessed whether activation of A_1Rs would induce synaptic depression in Schaffer collateral inputs to CA2 and CA1. Importantly, we tested whether transmission at these synapses differed in their responses to A_1R agonists in an age-dependent manner. Finally, we tested whether pharmacological manipulation of the postsynaptic signals recruited by activation of A_1Rs would unmask differences in synaptic responses evoked in areas CA1 and CA2 in brain slices prepared from juvenile rats, possibly explaining the differences observed between the two subfields in response to an array of A_1R-selective antagonists, including caffeine.

MATERIALS AND METHODS

Tissue Slices

Methods for obtaining whole-cell voltage-clamp and current-clamp recordings were similar to those described previously (Caruana et al., 2011; Simons et al., 2012; Pagani et al., 2014). Briefly, brain slices were prepared from juvenile (P14–18) male or female Sprague–Dawley rats, as well as from adult males (P60–70; Charles River Laboratories). Animals were anesthetized with sodium pentobarbital (65 mg/kg, i.p.), decapitated and the brains were rapidly removed and transferred into the ice-cold sucrose-substituted artificial cerebrospinal fluid (ACSF) containing (in mM): 240 sucrose, 2.0 KCl, 1 $MgCl_2$, 2 $MgSO_4$, 1 $CaCl_2$, 1.25 NaH_2PO_4, 26 $NaHCO_3$, and 10 D-glucose, and saturated with 95% O_2 and 5% CO_2. Coronal brain slices (340 μm thick) containing the dorsal hippocampus were taken from sections located within −2.30 and −4.30 mm posterior to Bregma (Paxinos and Watson, 1998). Slices were cut using a vibratome (VT1200S, Leica Biosystems) and then placed in a holding chamber containing normal ACSF (warmed to 32°C), and slices recovered for at least 1 h before experimental recordings. Standard ACSF consisted of the following (in mM): 124 NaCl, 2.5 KCl, 2 $MgCl_2$, 2 $CaCl_2$, 1.25 NaH_2PO_4, 26 $NaHCO_3$ and 17 D-glucose. After the recovery period, slices were transferred individually to a recording chamber and visualized using an upright microscope (BX51WI, Olympus Corp.) equipped with differential interference contrast optics, a 40× water-immersion objective and a near-infrared camera (RC300, Dage-MTI). Submerged slices were superfused with oxygenated ACSF at a rate of 2.0 ml/min at room temperature (∼25°C).

Stimulation and Recording

The whole-cell voltage or current-clamp recordings from hippocampal pyramidal neurons were made using patch pipettes filled with a solution containing the following (in mM): 120 K-gluconate, 10 KCl, 3 $MgCl_2$, 0.5 EGTA, 40 HEPES, 2 Na_2-ATP and 0.3 Na-GTP, with pH adjusted to 7.2 by KOH. Electrodes were prepared from borosilicate glass (filamented, 1.5 mm OD; 2.5–3.5 MΩ; King Precision Glass) using a horizontal puller (P-97, Sutter Instrument Co.), and experiments on CA2 neurons were performed only when area CA2 could be distinguished visually from area CA1. Pipettes were placed in contact with somata of visually-identified pyramidal neurons in CA2 and CA1 and gentle suction was applied under voltage

clamp to form a tight seal (1–3 GΩ). Whole-cell configuration was achieved by increased suction, and experiments began after cells stabilized (typically within 10–15 min following break-in). Electrophysiological properties of CA2 neurons such as the amplitude of the sag in response to hyperpolarizing currents, capacitance, or resting membrane potentials, while significantly different from neurons in CA1 or CA3 as a group (Zhao et al., 2007 for the rat; San Antonio et al., 2013; Sun et al., 2017 for mice), were varied enough to make them unreliable indicators of CA2 neuron identity due to the large overlap in values. Therefore, the approximate position of CA2 was estimated based on the appearance of the cells (vs. generally unhealthy-appearing CA3 neurons) and position relative to the upper blade of the dentate gyrus. Differences in pharmacology between presumed CA2 neurons and CA1 neurons provided further evidence that we were recording from different populations of neurons.

Voltage clamp recordings (V_h = −70 mV) were obtained using an Axopatch 200B amplifier (Molecular Devices Inc., San Jose, CA, USA) and displayed on a computer monitor using the software package WinLTP (WinLTP Limited). Recordings were filtered at 5 kHz and digitized at 20 kHz (Digidata 1322A, Molecular Devices Inc., San Jose, CA, USA). No correction was applied to compensate for liquid junction potentials. Only cells with a series *resistance* (R_s) < 25 MΩ and a <20% change in R_s from baseline during an experiment were included for analysis. Synaptic responses in CA2 and CA1 pyramidal neurons were evoked using cluster-style electrodes (CE2C75, FHC Inc.) placed ∼150 μm from recorded neurons in the stratum radiatum at a location intended to stimulate the Schaffer collaterals (see **Figures 1A$_1$,B$_1$**). Synaptic responses were evoked with 0.1 ms constant current pulses delivered using a stimulus isolation unit (BSI-2A, BAK Electronics) and stimulation intensity was adjusted to evoke synaptic currents approximately 75% of maximal amplitude (range; 75–200 μA). Single test pulses or pairs of stimulation pulses (with a 50 ms interpulse interval) were delivered to the Schaffer collaterals every 20 s to evoke excitatory postsynaptic currents (EPSCs). In some experiments, EPSCs were evoked by stimulation intensities ranging from 10 to 200 μA delivered in ascending steps (input-output tests). Protocols for all synaptic recording experiments were configured and controlled using WinLTP. The intrinsic excitability of pyramidal neurons in CA2 and CA1 was determined by measuring changes in membrane potential following the injection of hyperpolarizing and depolarizing current steps in current-clamp mode using the software package pClamp (Molecular Devices Inc., San Jose, CA, USA).

Data Analysis

Evoked synaptic currents were analyzed using the software applications WinLTP and AxoGraph X (AxoGraph Scientific). Peak amplitudes of EPSCs were measured relative to the prestimulus baseline (8–2 ms period before stimulation pulse), and paired-pulse facilitation (PPF) was determined by expressing the amplitude of the second response as a proportion of the amplitude of the first response. During synaptic recordings, input resistance (R_{in}) was calculated by measuring the amplitude of the steady-state current evoked during a −5 mV voltage step (50 ms duration) delivered 100 ms before test stimulation, and R_s was calculated by measuring the peak amplitude of the fast capacitive transient observed at the onset of the voltage step. The coefficient of variation ($1/CV^2$; where C = mean and V = standard deviation) was calculated on the mean amplitude of responses obtained during 10 min epochs of stable recordings of EPSCs using Excel (Microsoft Corporation). The stability of responses was first confirmed by testing the slope of a regression line fit through data points included for $1/CV^2$ analyses, and results for $1/CV^2$ analyses were normalized to the baseline for plotting. The effects of bath- or intracellularly-applied drugs during pharmacological experiments were assessed on the amplitude of averaged EPSCs obtained during 5-min-long epochs recorded at different times during an experiment (latencies specified below). Also, experiments were interleaved so that no single experiment was performed twice in slices prepared from the same animal. All data were expressed as the mean ± SEM and were normalized to baseline recordings for plotting. Changes in response properties were assessed with Prism (GraphPad Software Inc.) using (where appropriate) paired or unpaired samples *t*-tests, one-way ANOVAs, or repeated-measures ANOVAs. *Post hoc* comparisons were made using the Bonferroni or Tukey methods with the alpha level set to $P < 0.05$.

The intrinsic excitability of pyramidal neurons was assessed by counting the number of spikes evoked in response to 500 ms-duration suprathreshold depolarizing current steps (0–100 pA in ascending 20 pA increments) from a constant holding potential (typically rest). Input resistance was calculated by measuring both the peak and the steady-state voltage responses to −100 pA current steps (500 ms in duration), and inward rectification was quantified by expressing the peak input resistance as a proportion of the steady-state resistance (rectification ratio). All data were expressed as the mean ± SEM for plotting, and changes in response properties were assessed using paired samples *t*-tests.

Pharmacology

Unless stated, all compounds used for pharmacological experiments were obtained from Sigma and prepared as concentrated stock solutions (typically 10–50 mM) by dilution in (where appropriate) either distilled water or dimethyl sulfoxide and stored at −20°C until required. Compounds were either bath-applied or loaded intracellularly *via* the patch recording pipette.

RESULTS

Effects of Adenosine and an A$_1$R Agonist on Synaptic Transmission in CA2 and CA1

EPSCs were evoked in CA2 or CA1 by stimulating the Schaffer collaterals. The schematic diagrams are shown in **Figure 1** highlight the placement of stimulating and recording electrodes in coronal slices of the dorsal hippocampus for experiments assessing evoked synaptic responses in area CA2 (**Figure 1A$_1$**) or in area CA1 (**Figure 1B$_1$**). Synaptic responses were stable for

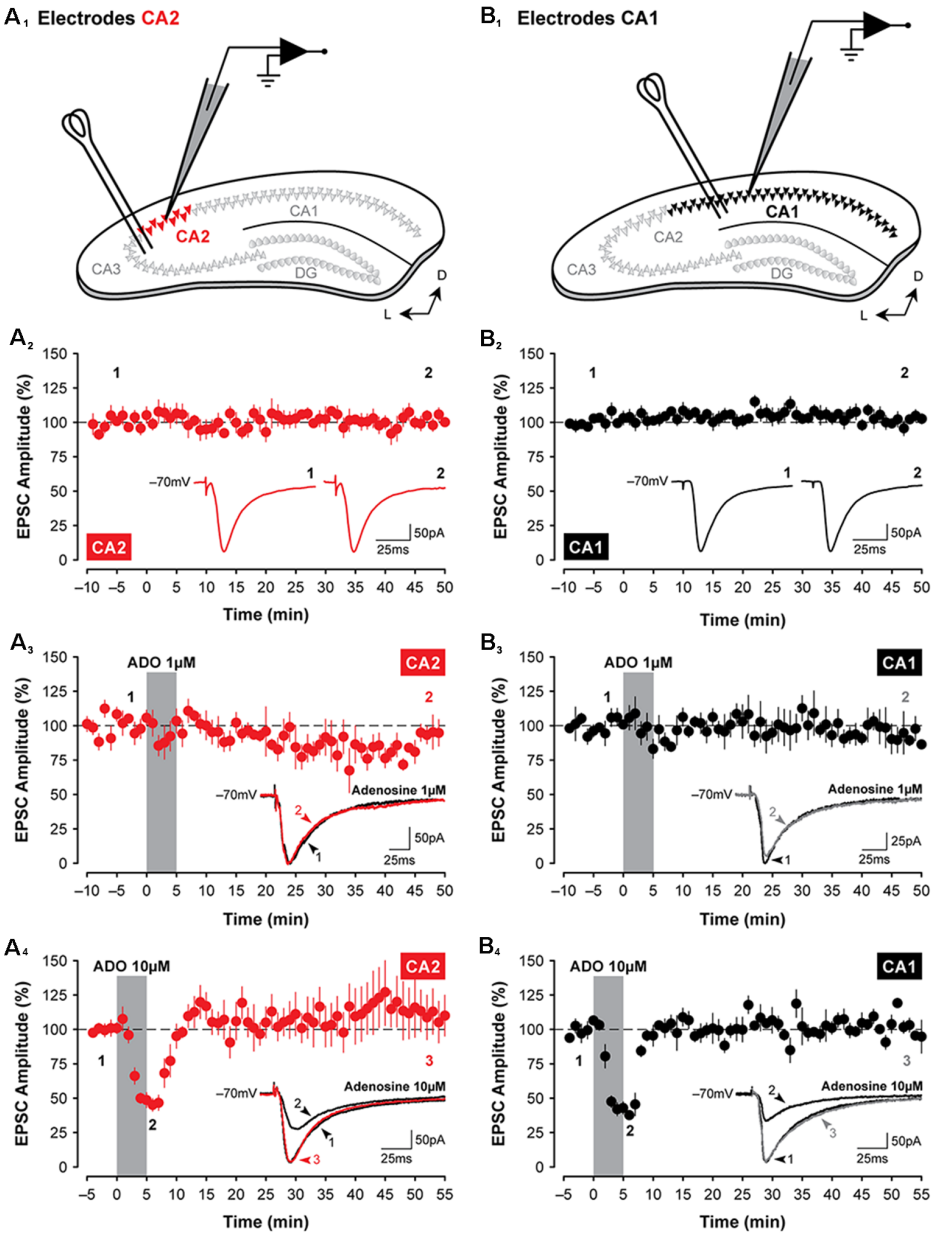

FIGURE 1 | Adenosine has transient suppressive effects on synaptic transmission in hippocampal areas CA2 and CA1. Illustrated are the approximate locations of stimulating electrodes relative to recording electrodes in slices of the dorsal hippocampus (**A$_1$**, CA2, in red; **B$_1$**, CA1, in black; colors are consistent for each figure). Stimulating electrodes were positioned in the stratum radiatum to activate Shaffer Collateral axons. **(A$_2$,B$_2$)** Mean (±SEM) excitatory postsynaptic current (EPSC) amplitudes recorded from CA2 and CA1, respectively, for 60 min without treatment. Data from these graphs are plotted in subsequent figures for statistical comparison. The amplitude of EPSCs has been normalized to the pre-treatment baseline for plotting in this and subsequent figures. Inset traces in **(A$_{2-4}$,B$_{2-4}$)** are averaged EPSCs (average of three consecutive sweeps over a 1-min period in this and subsequent figures) from representative experiments at the times indicated by the numbers. **(A$_{3,4}$,B$_{3,4}$)** Bath-application of adenosine (ADO; obtained from Sigma) for 5 min, indicated by the shaded region, induces only a transient suppression of EPSCs in the hippocampus and only at a concentration of 10 μM **(A$_4$,B$_4$)**. This effect was highly variable and depended on the commercial source of the adenosine (data not shown). Note: recordings were made from slices prepared from juvenile rats (P14 to P18) in this and subsequent figures unless specified otherwise.

60 min (CA2, **Figure 1A$_2$**; CA1, **Figure 1B$_2$**), and the amplitude of EPSCs did not change significantly during the course of interleaved, age-matched and untreated control experiments (CA2, baseline vs. last 5-min, $t_{(5)} = 0.11$, $P = 0.92$, $n = 6$; CA1, baseline vs. last 5-min, $t_{(6)} = 0.37$, $P = 0.72$, $n = 7$). To determine whether activation of adenosine receptors induces a lasting depression of synaptic responses in CA2 neurons, EPSCs were monitored before, during, and after a brief 5-min-long bath-application of adenosine. We found that although 10 μM adenosine significantly suppressed synaptic transmission

during the first 10 min following the onset of drug application (to 51.8 ± 4.8% of baseline, $F_{(1,9)}$ = 10.62, P < 0.01, Bonferroni P < 0.001, n = 5; **Figure 1A$_4$**), responses returned to baseline levels quickly during washout and remained stable for the remainder of the experiment (at 110.21 ± 15.31% of baseline during the last 5-min, Bonferroni P = 0.88). Unlike the potentiating effects of A$_1$R antagonists, which were more pronounced in CA2 (Simons et al., 2012), the effects of adenosine in CA2 did not differ significantly from those in CA1 (compare data shown in **Figures 1A$_{3,4}$,B$_{3,4}$**). Synaptic responses in Schaffer collateral inputs to CA1 were depressed significantly to 43.19 ± 4.71% of baseline ($F_{(1,9)}$ = 89.33, P < 0.0001, Bonferroni P < 0.0001, n = 4, **Figure 1B$_4$**) by 10 μM adenosine and returned quickly to baseline levels during washout (to 102.96 ± 3.01% of baseline, Bonferroni P > 0.999). We note, however, that the adenosine-mediated suppression of EPSCs in both CA2 and CA1 was highly variable and depended on the commercial source of the adenosine, with effects ranging from no suppression of EPSCs (using adenosine obtained from Tocris Bioscience; similar to the non-significant results observed using 1 μM adenosine shown for CA2 in **Figure 1A$_3$**, n = 4; and for CA1 in **Figure 1B$_3$**, n = 4) to brief potentiation (Garaschuk et al., 1992; adenosine from Ascent Scientific; data not shown).

Given the variability of the adenosine-mediated effects described above, we reasoned that the stability of adenosine may be problematic and that use of an A$_1$R agonist may produce more stable and consistent results. Additionally, an agonist would have the advantage of selectivity for the A$_1$R over other adenosine receptor subtypes that are known to be expressed in the hippocampus and would not be subject to degradation by endogenous enzymes. Indeed, a 5-min application of the selective A$_1$R agonist 2-chloro-N6-cyclopentyladenosine (CCPA; Lohse et al., 1988; 100 nM; **Figure 2A$_1$**) induced a robust decrease in the amplitude of synaptic responses recorded in CA2 pyramidal neurons, lasting for at least 50 min. EPSCs were depressed significantly to 32.44 ± 4.27% of baseline within the first 15-min of washout relative to age-matched and untreated control responses ($F_{(1,11)}$ = 7.84, P < 0.05, Bonferroni P < 0.0001, n = 7, **Figure 2B$_1$**), and EPSCs remained significantly depressed at 61.81 ± 9.38% of baseline by the end of the experiment (Bonferroni P < 0.001). The suppression of synaptic responses in CA2 was apparent across a range of stimulation intensities and concentrations of CCPA. The amplitude of synaptic responses in area CA2 increased in proportion to the intensity of electrical stimulation delivered to the Schaffer collaterals, and this was significantly reduced by CCPA when assessed 15 min into the washout period for all but the lowest stimulation intensity tested ($F_{(6,54)}$ = 27.72, P < 0.001, Bonferroni P < 0.001 for 25–200 μA, n = 10, **Figure 2A$_2$**). The effect of CCPA on synaptic responses in CA2 was also tested following bath-application of three different concentrations of CCPA (10 nM, n = 5; 100 nM, n = 7; and 1 μM, n = 1), but a depression of EPSCs lasting longer than 15 min was observed only with the two highest concentrations (see **Figure 2A$_3$**).

Similar to the short-lasting effects of adenosine shown in **Figure 1**, the CCPA-mediated depression of EPSCs observed in CA2 did not differ significantly from the depression induced in area CA1 following the same experimental protocols. Bath-application of 100 nM CCPA significantly depressed the amplitude of EPSCs in CA1 to 24.82 ± 3.12% of baseline within the first 15-min of washout relative to age-matched and untreated control responses ($F_{(1,10)}$ = 22.32, P < 0.001, Bonferroni P < 0.0001, n = 5, **Figure 2B$_4$**), and EPSCs remained significantly depressed at 52.55 ± 8.59% of baseline by the end of the experiment (Bonferroni P < 0.001). And as noted above, the magnitude of the suppression of synaptic responses induced by 100 nM CCPA did not differ between area CA2 and CA1 at the time points assessed ($F_{(1,10)}$ = 0.02, P = 0.893; peak, Bonferroni P = 0.939; last 5-min, Bonferroni P = 0.762; data not shown; see also **Figures 3A$_{2,3}$**). Bath-application of 100 nM CCPA also induced a significant suppression of synaptic responses across a range of stimulation intensities in area CA1 ($F_{(6,48)}$ = 5.26, P < 0.001, Bonferroni P < 0.01 for 25 μA and P < 0.0001 for 50–200 μA, n = 9, **Figure 2B$_2$**), but interestingly, the magnitude of the suppression was greater in area CA2 than in CA1 at the two highest stimulation intensities tested ($F_{(6,102)}$ = 2.51, P < 0.05, Bonferroni P < 0.05 at 150 and 200 μA, respectively; compare **Figures 2A$_2$,B$_2$**). The effect of A$_1$R activation on EPSCs in CA1 was also tested following bath-application of multiple concentrations of CCPA (10 nM, n = 5; 100 nM, n = 5; and 1 μM, n = 1), but similar to area CA2, a depression of synaptic responses lasting longer than 15 min was observed only with the two highest concentrations of CCPA (see **Figure 2B$_3$**). Note that we cannot distinguish between the long-lasting biological effects of A$_1$R activation and incomplete wash-out of the drug with continuing activation of the receptors. These findings suggest that the effects of selective A$_1$R activation, unlike A$_1$R blockade (Simons et al., 2012), are similar in CA1 and CA2 neurons at young postnatal ages (P14 to P18; see **Figures 3A$_{2,3}$**) and closely reflect the developmental expression pattern of A$_1$Rs in the hippocampus (see schematic summary in **Figure 3A$_1$**; Ochiishi et al., 1999).

Developmental Differences in A$_1$R-Mediated Synaptic Depression in the Hippocampus

To determine whether the A$_1$R-mediated depression of EPSCs differs in CA2 and CA1 at an age when A$_1$R expression is known to be highest in area CA2 (Ochiishi et al., 1999; **Figure 3B$_1$**), we tested the effects of 100 nM CCPA on evoked synaptic responses in CA2 and CA1 neurons in slices prepared from adult rats. We found that in slices from adult animals (∼P70), CCPA induced a significantly greater depression of synaptic responses in CA2 than in CA1 ($F_{(1,20)}$ = 6.37, P < 0.05, **Figures 3B$_{2,3}$**). EPSCs were depressed to 53.57 ± 6.66% of baseline levels in area CA2 (n = 6) when assessed at the end of the experiment, whilst responses in CA1 returned to baseline levels (to 83.94 ± 5.12%, n = 6; Bonferroni P < 0.05, **Figures 3B$_{2,3}$**). These data suggest that the A$_1$R-mediated suppression of EPSCs induced by CCPA closely follows the pattern of immunolabeling for A$_1$Rs at both early and late postnatal ages in rats.

Adenosine, acting on A$_1$Rs, has been shown previously to reduce glutamate release (Dunwiddie and Hoffer, 1980;

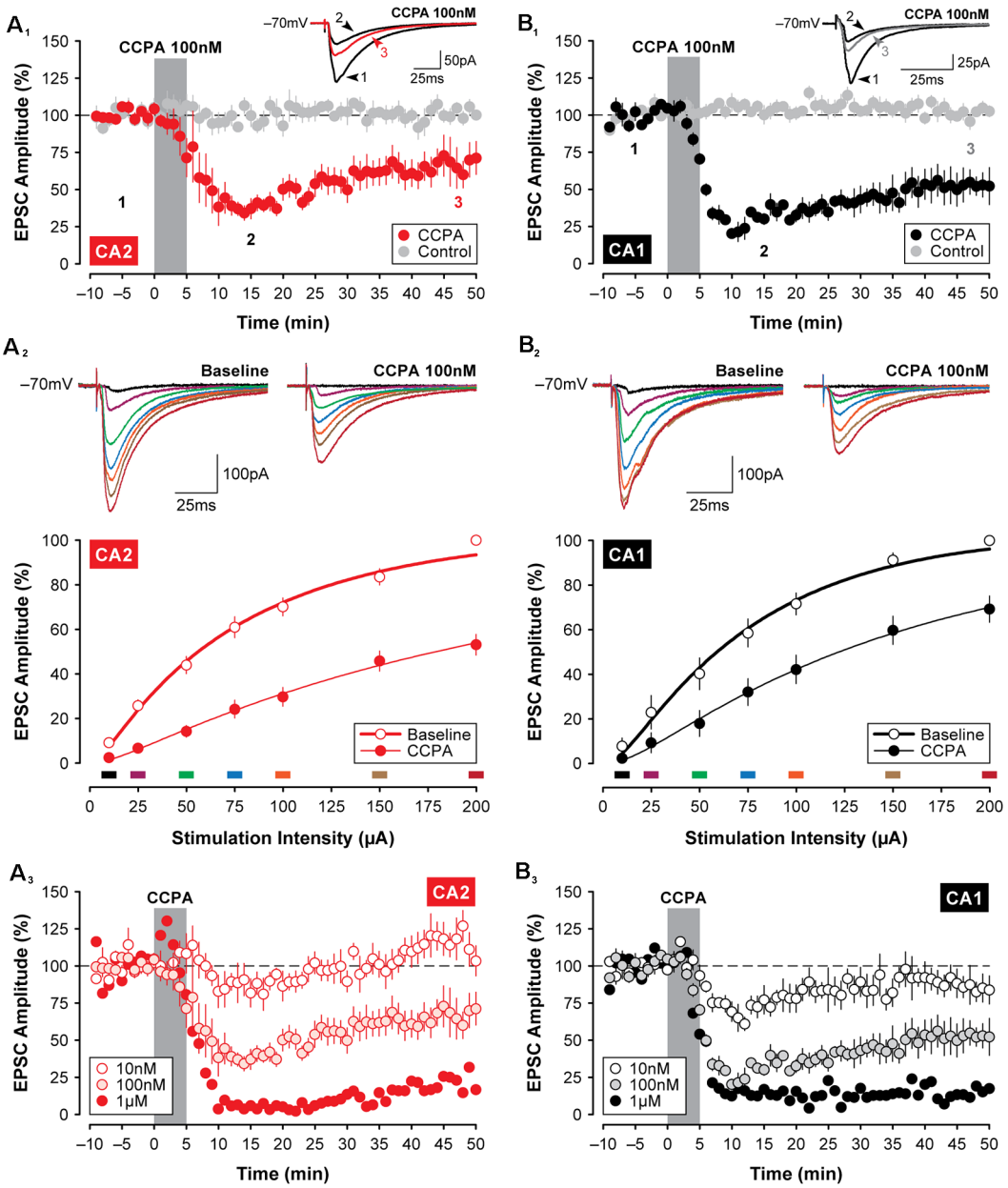

FIGURE 2 | Selective activation of A_1 receptors (A_1Rs) with CCPA induces synaptic depression in both CA2 and CA1. Bath application of the A_1R-selective agonist CCPA (100 nM; gray bar) induced a significant depression in the amplitude of EPSCs in both CA2 **(A_1)** and CA1 **(B_1)**. Inset and averaged traces are from a representative experiment at times indicated by the numbers. Recordings from age-matched and untreated control slices are shown in gray for comparison. **(A_2,B_2)** The depression of EPSCs induced by 100 nM CCPA is evident across a wide range of stimulation intensities when assessed 15-min into the washout period for area CA2 and CA1, respectively. Inset and colored traces (above) are from representative experiments at the stimulation intensities indicated by the corresponding colored bars (below). **(A_3,B_3)** Effects of three doses of CCPA (10 nM, 100 nM, and 1 μM; gray bar) on EPSC amplitudes recorded in CA2 and CA1, respectively. Overall, the effects of CCPA on synaptic function did not differ significantly between areas CA2 and CA1.

Prince and Stevens, 1992). As such, we assessed whether CCPA was acting presynaptically to induce the depression of excitatory synaptic responses observed in both CA2 and CA1 in slices obtained from young animals. One assessment of presynaptic function that is useful in determining whether changes in synaptic transmission can be attributed to changes in the release probability of glutamate is the test of (PPF; Creager et al., 1980; Zucker, 1989; Zucker and Regehr, 2002). Adenosine has been reported to increase PPF, reflecting a decrease in glutamate release from presynaptic terminals (Harris and Cotman, 1985; Dumas and Foster, 1998; Manita et al., 2007). We found that concurrent with the depression in synaptic responses induced by 100 nM CCPA, PPF (using a 50 ms interpulse interval) increased in some cases. The effect was inconsistent across

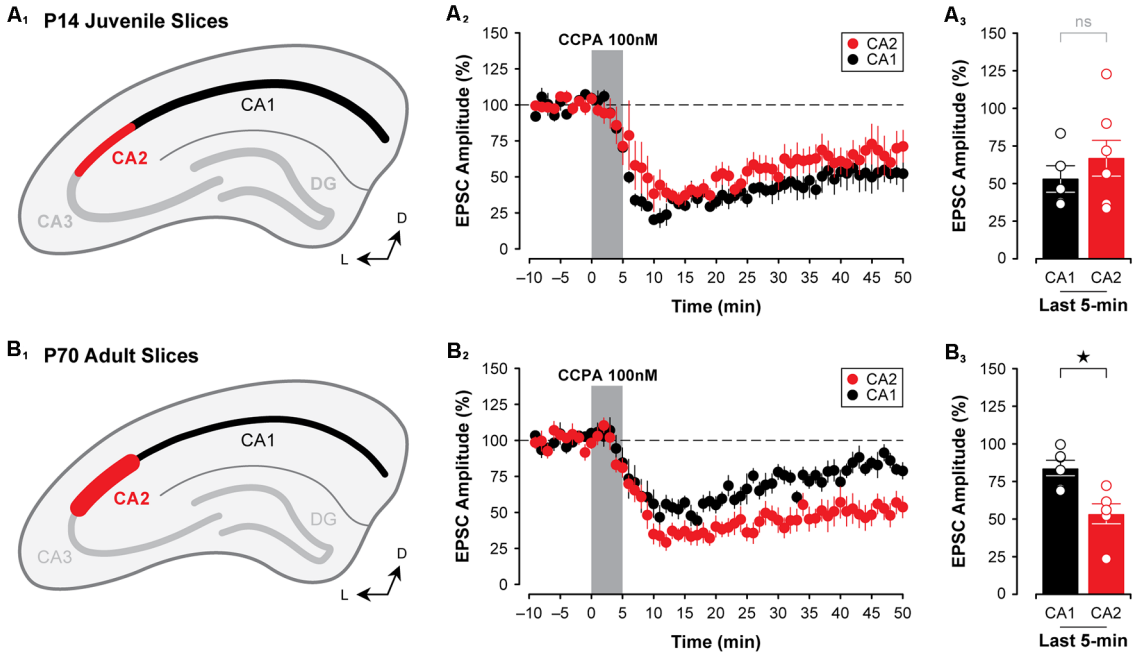

FIGURE 3 | The A$_1$R-mediated depression of EPSPs closely mirrors the developmental expression pattern of A$_1$Rs in CA2 and CA1. Immunolabeling for A$_1$Rs, as reported by Ochiishi et al. (1999), is homogeneous across Ammon's horn in early postnatal development (depicted in **A$_1$**), and A$_1$R expression becomes markedly more pronounced in CA2 and weaker in CA1 during adulthood (depicted in **B$_1$**). Mirroring this is the observation that the CCPA-mediated depression of EPSCs (100 nM) is similar in both CA1 and CA2 in slices obtained from P14 rats **(A$_{2,3}$)**. Further, the A$_1$R-mediated depression induced by CCPA increases with age in CA2, yet decreases with age in CA1 (~P70; **B$_{2,3}$**). *$p < 0.05$, ns, not significant.

slices and did not reach statistical significance in either CA2 (increase to 117.0 ± 8.01% of baseline, $t_{(4)} = 2.14$, $P = 0.099$, $n = 5$, **Figures 4A$_{1,2}$**) or CA1 (increase to 130.1 ± 14.6% of baseline, $t_{(3)} = 2.13$, $P = 0.122$, $n = 4$, **Figures 4B$_{1,2}$**). An additional measure of presynaptic function that may reflect changes induced by the application of CCPA is the coefficient of variation ($1/CV^2$; Caruana et al., 2011; Pagani et al., 2014). Here, $1/CV^2$ was computed for 10-min epochs of stable EPSCs recorded during the baseline period and at the very end of the experiment. Response-to-response variability was increased by CCPA as indicated by a reduction in $1/CV^2$ in both CA2 (to 59.17 ± 6.14% of baseline, $n = 7$, **Figure 4A$_3$**) and CA1 (to 40.48 ± 8.65% of baseline, $n = 5$, **Figure 4B$_3$**), and this suggests that CCPA may have been acting on presynaptic A$_1$Rs to suppress glutamate release and regulate synaptic function. However, the reduction in $1/CV^2$ observed at the end of the experiment did not differ significantly from baseline in either CA2 ($t_{(6)} = 2.23$, $P = 0.066$) or CA1 ($t_{(4)} = 1.95$, $P = 0.123$). Data for $1/CV^2$ analyses obtained during the last 10-min of the experiment were also expressed as a ratio of the baseline and plotted against the CCPA-mediated change in the amplitude of EPSCs for each individual experiment (CA2, **Figure 4A$_4$**, all cells; CA1, **Figure 4B$_4$** all cells), as well as for the pooled data set (CA2, **Figure 4A$_5$**, average; CA1, **Figure 4B$_5$** average). Results shown in **Figures 4A$_5$,B$_5$** indicate that although we observed a significant reduction in the amplitude of EPSCs induced by CCPA in CA2 and CA1, respectively, we found no significant change in the variability of EPSCs to suggest whether CCPA is acting pre- or postsynaptically. Although these data do not rule out the possibility that the suppression of EPSCs in both CA2 and CA1 resulted, in part, from A$_1$R-mediated changes in presynaptic glutamate release, they do argue against a robust involvement of several of the known mechanisms, including regulation of presynaptic calcium, which would have been reflected in the magnitude of PPF observed.

To exclude the possibility that the synaptic depression observed in CA2 and CA1 neurons resulted from A$_1$R-dependent changes in neuronal excitability induced by CCPA, we tested the effects A$_1$R activation on the intrinsic membrane properties of CA2 and CA1 neurons. There was no significant effect of CCPA on the number of action potentials elicited by suprathreshold current injection or on the resting membrane potential of pyramidal neurons in CA2 (spikes, $F_{(9,120)} = 0.03$, $P > 0.99$, $n = 7$, **Figures 5A$_{1,2}$**; RMP, $t_{(6)} = 1.89$, $P = 0.108$, $n = 7$, **Figure 5A$_3$**) or CA1 (spikes, $F_{(9,100)} = 0.36$, $P = 0.95$, $n = 6$, **Figures 5B$_{1,2}$**; RMP, $t_{(5)} = 0.32$, $P = 0.759$, $n = 6$, **Figure 5B$_3$**). Interestingly, although CCPA had no significant effect on the steady-state input resistance of neurons in both CA2 and CA1 (data not shown), there was a significant reduction in the amount of inward rectification induced by CCPA in both CA2 and CA1 pyramidal cells. The rectification ratio decreased from 1.38 ± 0.07 to 1.27 ± 0.07 in area CA2 ($t_{(6)} = 3.70$, $P < 0.05$, $n = 7$, **Figures 5A$_{4,5}$**) and from 1.31 ± 0.03 to 1.19 ± 0.01 in CA1 ($t_{(5)} = 7.82$, $P < 0.001$, $n = 6$, **Figures 5B$_{4,5}$**)

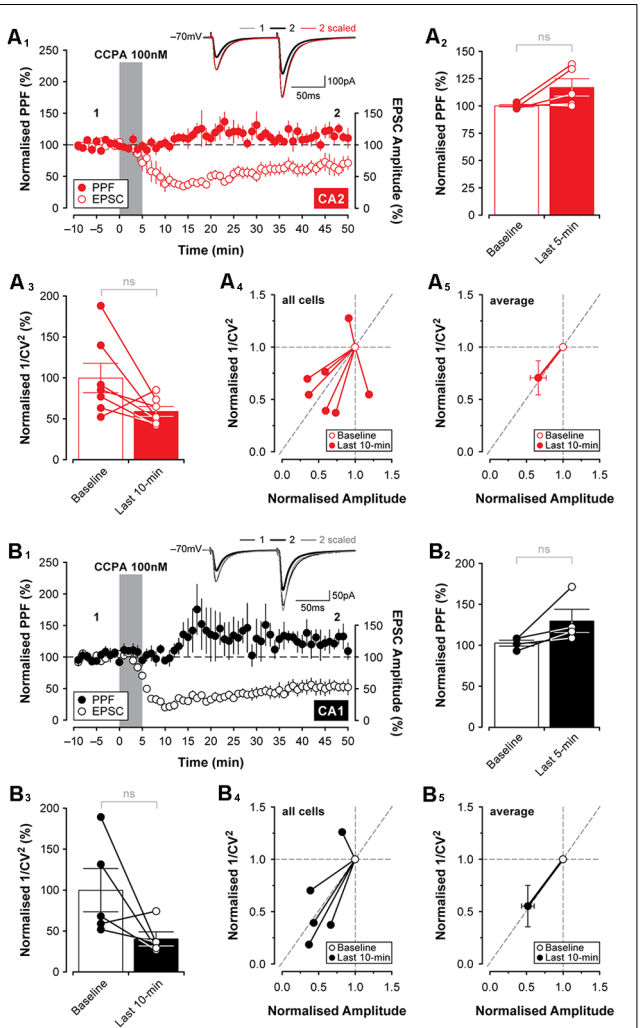

FIGURE 4 | Changes in presynaptic function induced by CCPA do not differ between CA2 and CA1. Paired-pulse facilitation (PPF; 50 ms interpulse interval) did not change significantly following 5-min bath-application of CCPA in area CA2 **($A_{1,2}$)** or area CA1 **($B_{1,2}$)**. The CCPA-mediated depression of EPSCs (open circles) is shown together with PPF (filled circles) for illustration purposes in **(A_1,B_1)**. Inset traces in **(A_1,B_1)** are from representative experiments at the times indicated by the numbers. Note that although CCPA reduced the amplitude of synaptic responses, PPF was unchanged when the responses were scaled to the baseline (inset; scaled) in both CA2 and CA1. **(A_{3-5},B_{3-5})** The coefficient of variation ($1/CV^2$) was computed for 10-min epochs of stable EPSCs recorded during the baseline period and at the end of the experiment. Bath-application of CCPA increased response-to-response variability calculated during the last 10-min of recording as indicated by a slight reduction in $1/CV^2$ for CA2 **(A_3)** and CA1 **(B_3)**, but the reduction was not significantly different from the baseline at either recording site. Normalized $1/CV^2$ for the last 10-min of the experiment is expressed as a ratio of the baseline and plotted against the normalized amplitude of EPSCs for each experiment (CA2, all cells, **A_4**; CA1, all cells, **B_4**) and averaged data (CA2, average, **A_5**; CA1, average, **B_5**). Results are shown in **(A_5,B_5)** indicate that although there is a significant reduction in the amplitude of EPSCs induced by CCPA in CA2 and CA1, respectively, there is no significant change in the variability of evoked responses to suggest whether CCPA was acting on A_1Rs located pre- or postsynaptically. ns, not significant.

following bath-application of 100 nM CCPA. Indeed, there was a marked reduction in the "sag" present in the voltage

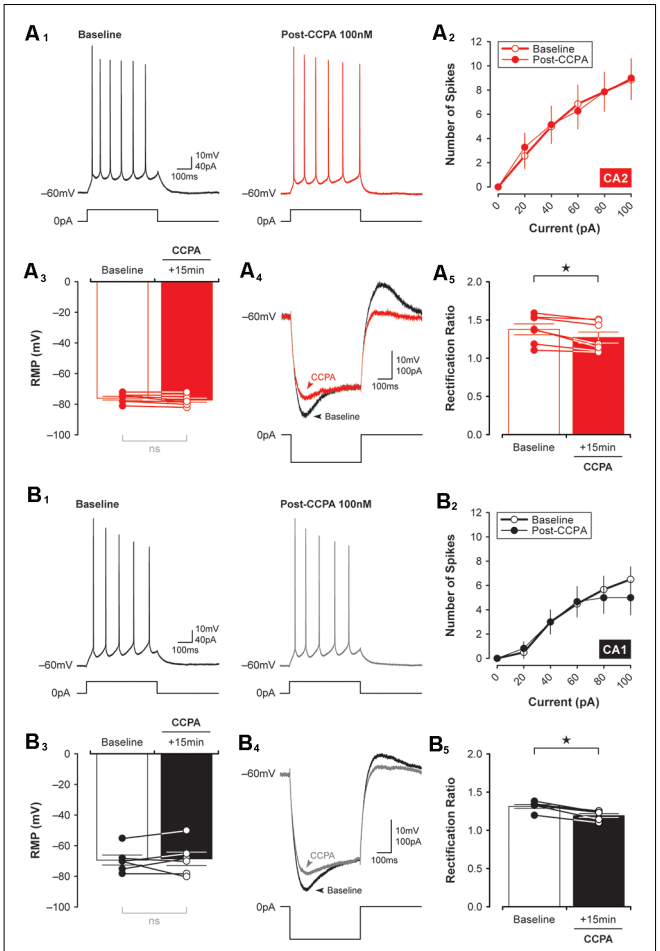

FIGURE 5 | CCPA-mediated changes in inward rectification are similar in both CA2 and CA1. The number of spikes elicited in response to depolarizing current steps was the same in CA2 and CA1 before and 15 min after a brief 5-min-long application of 100 nM CCPA [**A_1,B_1**, representative spikes triggered by a +40 pA current step; **(A_2,B_2)**, input-output data for spikes initiated by suprathreshold injection of multiple current steps up to 100 pA]. There was also no significant change in the resting membrane potential (RMP) of neurons recorded in CA2 **(A_3)** and CA1 **(B_3)** before and after CCPA. Inward rectification was quantified by expressing the peak input resistance as a proportion of the steady-state input resistance (rectification ratio). Rectification ratios decreased significantly following CCPA treatment in both CA2 **($A_{4,5}$)** and CA1 **($B_{4,5}$)**, an effect attributed largely to a CCPA-mediated change in peak input resistance (see representative traces for CA2, **A_4**, and CA1, **B_4**). *$p < 0.05$, ns, not significant.

responses to −100 pA current steps induced by CCPA in both CA2 (**Figure 5A$_4$**) and CA1 (**Figure 5B$_4$**) neurons. These data suggest that activation of A_1Rs has a minimal effect on the overall excitability of principal neurons in the hippocampus and that A_1Rs may regulate the activity of transmembrane currents responsible for inward rectification at hyperpolarized membrane potentials (perhaps *via* the hyperpolarization-activated nonspecific cation current, I_h). Previously, A_1R activation has been shown to activate G-protein-activated K^+ channels (or GIRKS) to inhibit the activity of CA1 neurons (Trussell and Jackson, 1987; Lüscher et al., 1997; Wetherington and Lambert, 2002).

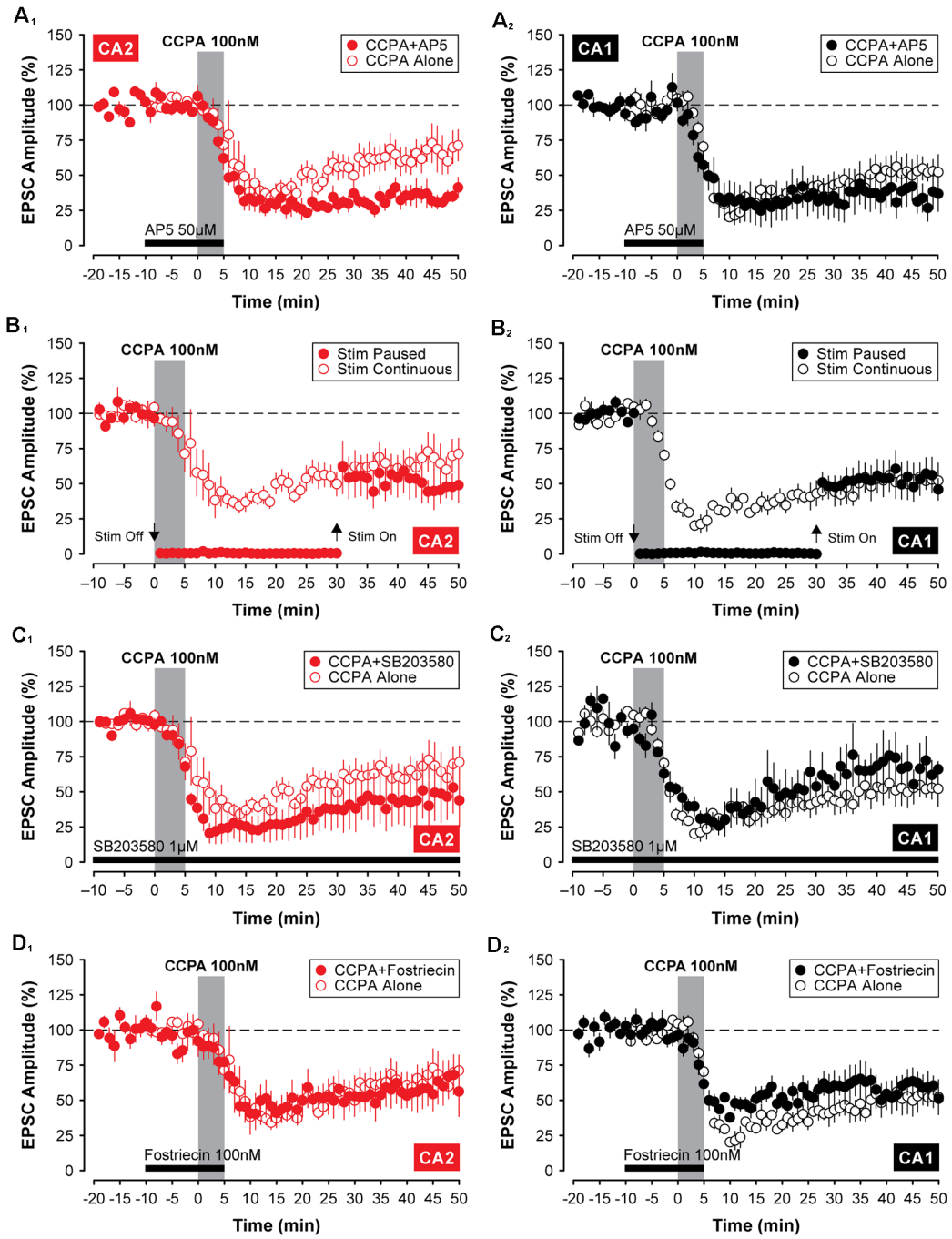

FIGURE 6 | The A_1R-mediated depression of EPSCs in CA2 and CA1 does not require activation of NMDARs, p38 MAP Kinase, or protein phosphatase 2A. Except for a significant *enhancement* of CCPA-induced depression by 50 μM AP5 in area CA2 **(A_1)**, blockade of N-methyl-D-aspartate (NMDA) receptors, p38 MAP kinase or protein phosphatase 2A with 50 μM AP5, 1 μM SB203580 or 100 nM fostriecin (latency indicated by the black bars), respectively, did not affect the depression of EPSCs induced by 5-min bath-application of CCPA in CA2 **(A_1,C_1,D_1)** or CA1 **(A_2,C_2,D_2)**. Also, the constant synaptic drive was not required for the induction of A_1R-mediated synaptic depression in the hippocampus. A temporary pause in the delivery of test stimulation to the Schaffer collaterals for 30 min during and after application of CCPA (Stim Paused) was similarly without effect in either recording site (CA2, **B_1**; CA1, **B_2**).

Mechanisms Underlying the A_1R-Mediated Synaptic Depression in CA2 and CA1

To determine whether the depression of EPSCs induced by CCPA was mechanistically similar to other forms of synaptic depression in the hippocampus, we applied treatments that have been shown to affect synaptic function in other models of synaptic plasticity. Because activity-dependent forms of long-term depression (LTD) can rely on activation of NMDA

receptors (Dudek and Bear, 1992), we tested whether the NMDA receptor antagonist, AP5, would block the CCPA-mediated depression shown in **Figures 2–4**. Co-application of 50 μM AP5 with CCPA was not sufficient to block the A$_1$R-mediated depression of EPSCs in both CA2 and CA1. Indeed, in area CA1, EPSCs were depressed significantly to 33.53 ± 10.15% of baseline when assessed during the last 5-min of the experiment ($F_{(2,14)}$ = 26.78, $P < 0.0001$, n = 5, **Figure 6A$_2$**). Although EPSCs were depressed by the co-application of CCPA and AP5 relative to untreated controls (Tukey $P < 0.0001$), responses did not differ significantly from slices treated with CCPA alone (Tukey P = 0.206). Interestingly, in area CA2, the co-application of AP5 significantly *enhanced* the depression of synaptic transmission induced by CCPA (see **Figure 6A$_1$**). EPSCs were reduced to 34.57 ± 4.32% of baseline in slices treated with both AP5 and CCPA compared to a reduction of only 61.81 ± 9.38% for slices treated with CCPA alone ($F_{(2,15)}$ = 22.66, $P < 0.0001$, n = 5, Tukey $P < 0.05$). It is unclear why blockade of NMDARs facilitates the CCPA-mediated suppression of EPSCs in area CA2, but activation of NMDARs is not a requirement for induction of A$_1$R-mediated synaptic depression in either CA2 or CA1.

We have shown previously that constant synaptic stimulation of the Schaffer collaterals is not required for the induction of A$_1$R-mediated synaptic potentiation in area CA2 (Simons et al., 2012). In the current study, the depression of EPSCs induced by CCPA was also unaffected by a temporary pause in the delivery of test stimulation during the experiment. Responses in CA2 were depressed to 47.11 ± 9.87% of baseline despite test stimulation being suspended for a 30-min period during and after bath-application of CCPA ($F_{(2,15)}$ = 11.83, $P < 0.001$, n = 5; **Figure 6B$_1$**). Although the amplitude of EPSCs was depressed significantly relative to untreated controls (Tukey $P < 0.01$), pausing test stimulation did not affect the magnitude of the CCPA-mediated depression-induced in CA2 once synaptic stimulation was resumed (Tukey P = 0.427; compared to CCPA-treated slices receiving test stimulation every 20 s). Similar results were obtained in recordings made from neurons in area CA1 (EPSCs depressed to 52.21 ± 10.30% of baseline, $F_{(2,14)}$ = 17.51, $P < 0.001$, n = 5; control vs. Stim Paused, Tukey $P < 0.001$; Stim Paused vs. Stim Continuous, Tukey P = 0.999; **Figure 6B$_2$**). These results indicate that repeated test stimulation of the Schaffer collaterals is not a prerequisite for inducing A$_1$R-dependent depression of EPSCs by CCPA.

Previous work has shown that the activity of p38 MAP kinase contributes to A$_1$R-mediated synaptic depotentiation (Liang et al., 2008) and depression (Brust et al., 2006) in CA1 neurons. As such, we tested whether inhibition of p38 MAP kinase would block the induction of CCPA-mediated synaptic depression in Schaffer collateral inputs to CA2 and CA1 neurons in juvenile slices. Inclusion of 1 μM SB203580 in the internal electrode solution was not sufficient to prevent the induction of A$_1$R-dependent synaptic depression in the hippocampus. In area CA2, synaptic responses were significantly depressed to 48.49 ± 18.6% of baseline relative to untreated controls ($F_{(2,14)}$ = 7.21, $P < 0.01$, Tukey $P < 0.05$, n = 4, **Figure 6C$_1$**), and responses did not differ from those evoked in separate experiments in which CCPA was applied without the kinase inhibitor (Tukey P = 0.651). In contrast to previous work, inhibition of p38 MAP kinase also did not block A$_1$R-mediated synaptic depression in hippocampal area CA1. EPSCs were depressed to 64.65 ± 12.09% of baseline by CCPA relative to controls ($F_{(2,12)}$ = 16.78, $P < 0.001$, Tukey $P < 0.05$, n = 3, **Figure 6C$_2$**), and the magnitude of the depression was similar to experiments in which CCPA was applied alone (Tukey P = 0.535). Thus, in slices from juvenile animals, the activity of p38 MAP kinase does not appear to play a significant role in A$_1$R-dependent synaptic depression induced by 100 nM CCPA in either recording site.

There is significant data to support a key role for protein phosphatases in activity-dependent forms of LTD in the hippocampus (Mauna et al., 2011), including protein phosphatase 2A (Stockwell et al., 2015). Here, we investigated whether the inhibiting activity of protein phosphatase 2A with fostriecin would block the A$_1$R-mediated synaptic depression induced by CCPA. Similar to the negative results described above for various other inhibitors, co-application of 100 nM fostriecin with CCPA did not block the A$_1$R-mediated synaptic depression in either CA2 or CA1. The amplitude of EPSCs was reduced significantly to 63.19 ± 14.43% of baseline and to 58.63 ± 7.30% of baseline in CA2 and CA1, respectively, relative to untreated controls (CA2, $F_{(2,16)}$ = 5.03, $P < 0.05$, n = 6, Tukey $P < 0.05$, **Figure 6D$_1$**; CA1, $F_{(2,15)}$ = 19.57, $P < 0.0001$, n = 6, Tukey $P < 0.001$, **Figure 6D$_2$**). Further, the depression of synaptic responses in CA2 and CA1 induced by CCPA in the presence of fostriecin did not differ significantly from the depression induced by CCPA alone (CA2, Tukey P = 0.995; CA2, Tukey P = 0.789). Although we do not provide positive evidence that fostriecin was effective, we note that we used 5 times the concentration found effective for glutamate receptor internalization (Stockwell et al., 2015). Nevertheless, these data suggest that the activity of protein phosphatase 2A is not required for A$_1$R-mediated synaptic depression in the hippocampus and that other A$_1$R-mediated intracellular signals are likely involved.

Divergence in A$_1$R-Mediated Intracellular Signaling in CA2 and CA1 Neurons

Adenosine A$_1$Rs couple to G$_{i/o}$ (Munshi et al., 1991; Dunwiddie and Masino, 2001), and as such, activation of A$_1$Rs by selective agonists should reduce the activity of adenylyl cyclase and constrain the production of cAMP. If the CCPA-mediated synaptic depression in CA2 and CA1 is linked to an A$_1$R-dependent decrease in postsynaptic levels of cAMP then the depression of EPSCs would not necessarily be expected to occur as rapidly as we observe here, even though A$_1$R agonists are known to stimulate internalization of glutamate receptors over long periods (Stockwell et al., 2015). For cAMP levels to drop so precipitously, enzymatic degradation of cAMP would presumably be required. For this reason, we tested whether differences in A$_1$R-mediated synaptic plasticity between areas CA2 and CA1 might reflect regional variations in phosphodiesterase activity in the hippocampus. Indeed, the expression of several isoforms of phosphodiesterase differs across

hippocampal subfields in mice. Specifically, expression of *Pde8b*, *Pde10a*, and *Pde11a* is highest in area CA1, whereas *Pde4d* is expressed exclusively in area CA2 (see **Figure 7A**; Lein et al., 2006). Incidentally, both *Pde8b* and *Pde11a* increase significantly during aging (Kelly et al., 2014). To determine whether inhibition of phosphodiesterase activity mimics effects observed using various A$_1$R antagonists on synaptic transmission in the hippocampus (i.e., induces synaptic potentiation), we bath-applied the phosphodiesterase inhibitor, rolipram, and assessed its effects on evoked synaptic responses in CA2 and CA1. Continuous application of 10 μM rolipram for 50-min induced a slight facilitation of EPSCs in CA2–132.70 ± 13.59% of baseline, but this increase did not differ significantly from control responses (t_{11} = 2.08, P = 0.061, n = 7, **Figure 7B$_1$**). In CA1, however, EPSCs were facilitated to 154.10 ± 14.99% of baseline by rolipram, and this potentiation was significant relative to responses evoked in control experiments (t_{12} = 3.44, $P < 0.01$, n = 7, **Figure 7B$_2$**). Despite this increase, the magnitude of synaptic potentiation induced by rolipram did not differ significantly between CA2 and CA1 ($t_{(12)}$ = 1.06, P = 0.3104, **Figure 7B$_3$**).

Interestingly, rolipram's ability to induce a significant potentiation of EPSCs in area CA1 was coincident with its ability to block the synaptic depression induced by CCPA. For these experiments, slices were first pre-incubated in oxygenated rolipram (10 μM rolipram in normal ASCF) for at least 40 min before being transferred to the recording chamber. This pre-incubation period was then followed by the continuous perfusion of 10 μM rolipram for the entire duration of the experiment. Under these conditions, the A$_1$R-mediated depression of synaptic responses typically induced by 5-min application of CCPA was blocked in Schaffer collateral inputs to CA1 (**Figure 7C$_2$**), but not to CA2 (**Figure 7C$_1$**). In area CA1 of rolipram-treated slices, EPSCs remained stable at 91.80 ± 5.77% of baseline when assessed during the last 5-min of recording, and responses did not differ significantly from untreated controls ($F_{(2,15)}$ = 19.55, $P < 0.0001$, n = 6, Tukey P = 0.432). However, in CA2, rolipram treatment had no effect on the depression induced by CCPA (EPSCs depressed to 60.28 ± 11.79% of baseline, $F_{(2,16)}$ = 6.78, $P < 0.01$, n = 6, Rolipram + CCPA vs. control, Tukey $P < 0.05$). In line with this, the depression of EPSCs was significantly greater in CA2 than in CA1 ($t_{(10)}$ = 2.40, $P < 0.05$,

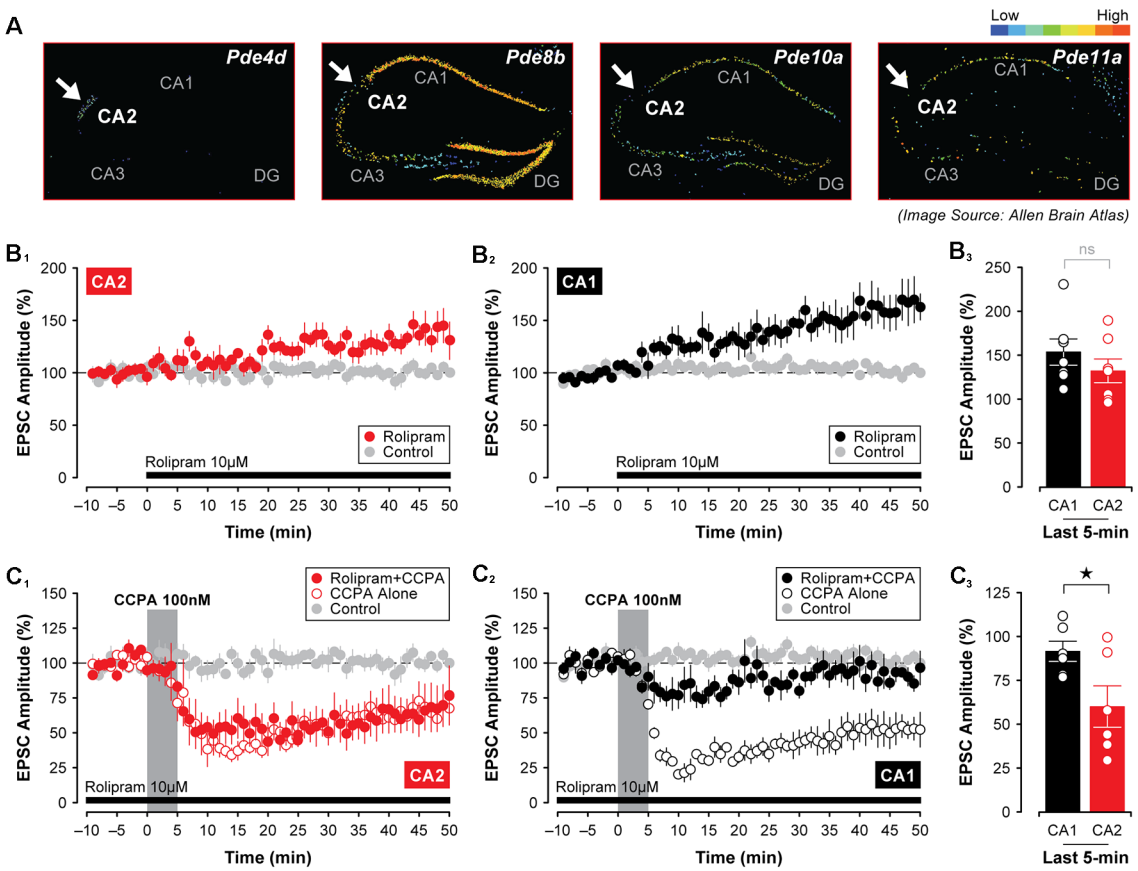

FIGURE 7 | The A$_1$R-mediated depression of synaptic responses in CA1 relies on phosphodiesterase activity. **(A)** The expression of several phosphodiesterases (PDEs) differs in mouse CA1 and CA2 with *Pde4d* showing the highest expression in CA2 (arrow), but with *Pde8b*, *Pde10a*, and *Pde11a* showing the lowest levels in CA2 compared to area CA1 (arrows; Lein et al., 2006). **(B$_{1–3}$)** The PDE inhibitor rolipram (10 μM) induced a slow-onset potentiation of EPSCs that did not differ between CA1 and CA2. However, pre-treating slices with rolipram for 40 min followed by its continuous perfusion throughout the experiment blocked the CCPA-mediated depression of EPSCs in CA1, but not in CA2 **(C$_{1–3}$)**. *$p < 0.05$, ns, not significant.

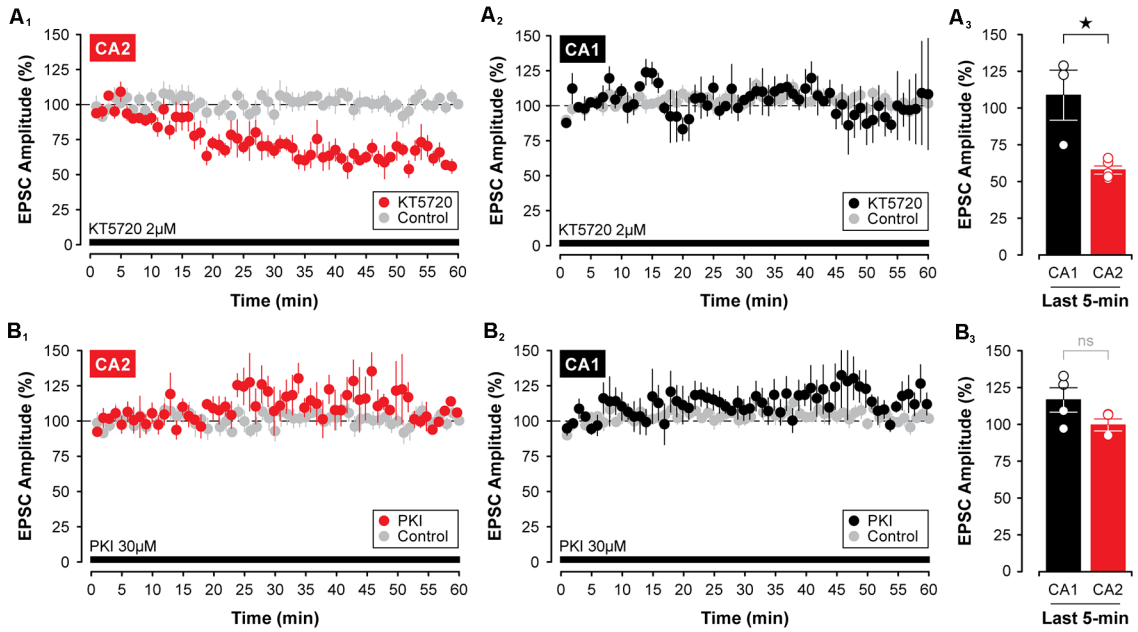

FIGURE 8 | Inhibition of protein kinase A (PKA) with KT5720 induces a slow-onset depression of synaptic transmission in area CA2, but not in area CA1. **(A$_{1-3}$)** Including the PKA inhibitor, KT5720 (2 μM, indicated by the black bar), in the intracellular recording solution caused a significant decrease in the amplitude of EPSC in CA2, but not in CA1. **(B$_{1-3}$)** Interestingly, the internal application of the more selective inhibitor of PKA, PKI (30 μM; black bar), was without effect on EPSCs recorded in CA2 or CA1. PKI was obtained from Santa Cruz Biotechnology. *$p < 0.05$, ns, not significant.

Figure 7C$_3$). This suggests that a mechanism other than robust phosphodiesterase activity may be at work in CA2 neurons to cause synaptic depression in response to A$_1$R agonists.

Although some phosphatases, such as protein phosphatase 2A and protein phosphatase 4, are not required for the decline in synaptic strength induced by CCPA (see **Figures 6D$_{1,2}$**), it is possible that blocking the activity of key protein kinases directly may be sufficient to induce a lasting depression of synaptic transmission in the hippocampus that resembles the depression mediated by activation of A$_1$Rs. This depends critically, though, on whether the depression of EPSCs involves the downregulation of cAMP-dependent protein kinase activity as opposed to regulation of other cAMP-dependent proteins, such as the exchange protein activated by cAMP, or EPAC (Sugawara et al., 2016). Given that PKA is the principal kinase stimulated by the activity of cAMP, we tested two different PKA inhibitors for their efficacy in mimicking the CCPA-mediated depression of EPSCs in CA2 and CA1. Interestingly, 2 μM KT5720, but not 30 μM PKI, in the internal electrode solution, caused a slow-onset depression of synaptic responses in CA2. Indeed, synaptic responses were reduced significantly to 58.01 ± 2.77% of baseline by KT5720 in CA2 relative to untreated controls when assessed during the last 5-min of the experiment ($t_{(9)} = 13.18$, $P < 0.0001$, $n = 5$, **Figure 8A$_1$**). Interestingly, KT5720 had no effect on the amplitude of EPSCs in CA1 (responses remained stable at 108.90 ± 17.06% of baseline, $t_{(8)} = 0.651$, $P = 0.533$, $n = 3$, **Figure 8A$_2$**; CA2 vs. CA1, $t_{(6)} = 3.92$, $P < 0.01$, **Figure 8A$_3$**), and inclusion of PKI in the internal electrode solution had no effect on responses irrespective of recording site (CA2, EPSCs stable at 100.50 ± 4.12%, $t_{(8)} = 0.289$, $P = 0.780$, $n = 4$, **Figures 8B$_{1,3}$**; CA1, EPSCs stable at 117.60 ± 8.24%, $t_{(9)} = 2.21$, $P = 0.054$, **Figures 8B$_{2,3}$**; CA2 vs. CA1, $t_{(6)} = 1.86$, $P = 0.113$, **Figure 8B$_3$**) or concentration (10 μM, data not shown).

Finally, because at least three isoforms of adenylyl cyclase are highly expressed in area CA2 in the mouse (Visel et al., 2006), including *Adcy1*, *Adcy5*, and *Adcy6* (see **Figure 9A**)—an effect observed even in animals as young as P7 (for *Adcy1*, Lein et al., 2006)—we tested whether direct stimulation of adenylyl cyclases could mimic the effects of A$_1$R antagonists and induce synaptic potentiation in area CA2 in slices from juvenile animals. Indeed, bath application of 10 μM forskolin caused a rapid potentiation of EPSCs in CA2 neurons that persisted for the entire duration of the experiment. EPSCs were potentiated to 170.20 ± 10.16% of baseline (**Figure 9B$_1$**, $n = 6$), and this facilitation was significant relative to responses in age-matched and untreated controls ($t_{(10)} = 6.62$, $P < 0.0001$, **Figure 9B$_2$**). As predicted based on our work previously (Simons et al., 2012), there was no effect of forskolin on responses in CA1 neurons (responses remained stable at 118.60 ± 17.89% of baseline, $t_{(11)} = 0.866$, $P = 0.405$, $n = 7$, **Figures 9C$_{1,2}$**). Not surprisingly, the magnitude of the synaptic potentiation induced by forskolin was significantly greater in CA2 than in CA1 ($t_{(11)} = 2.39$, $P < 0.05$, **Figures 9D$_{1,2}$**). Taken together, these data suggest that although A$_1$R expression does not differ substantially across the hippocampus at early postnatal ages, the activity of critical A$_1$R-dependent intracellular signals—including adenylyl cyclase, protein kinase,

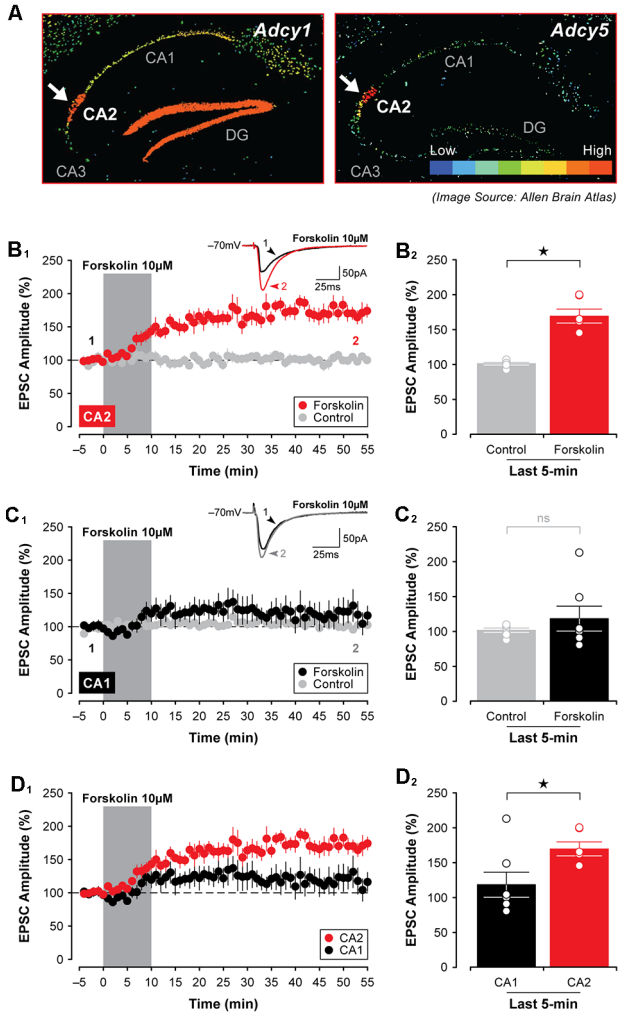

FIGURE 9 | Activation of adenylyl cyclases enhances EPSCs in CA2 in juvenile brain slices. **(A)** Expression of several adenylyl cyclases is greater in CA2, including *Adcy1*, *Adcy5* (shown; arrows), and *Adcy6* (Lein et al., 2006). **(B$_{1,2}$)** Bath-application of the adenylyl cyclase activator, forskolin (10 μM), for 10 min induced a lasting potentiation of EPSCs in area CA2 that was significantly greater than responses in age-matched and untreated control experiments. However, forskolin had no lasting effect on transmission in area CA1 **(C$_{1,2}$)**. **(D$_{1,2}$)** The response to forskolin was significantly greater in CA2 than in CA1 (data re-plotted from **(B$_1$,C$_1$)**. *$p < 0.05$, ns, not significant.

and phosphodiesterase activity—differ considerably between CA1 and CA2, thus resulting in an overall effect that essentially mimics the adult state.

DISCUSSION

In this study, we pursued two lines of inquiry related to adenosine receptor expression in the hippocampus. First, we tested whether the use of a selective A$_1$R agonist to induce synaptic depression in CA2 and CA1 would better reflect changes in the staining pattern of A$_1$Rs in the hippocampus than the application of A$_1$R antagonists, such as caffeine or DPCPX. Second, we tested several of the known intracellular signals linked to activation of A$_1$Rs and whether they might account for the dramatic effects of A$_1$R antagonists observed in CA2 neurons in slices prepared from young animals (Simons et al., 2012). Indeed, both lines of inquiry produced data to support the findings of Ochiishi et al. (1999) in that—at least in Sprague–Dawley rats—A$_1$Rs in the hippocampus are distributed evenly across areas CA2 and CA1 in juvenile animals, and that A$_1$R expression in CA2 neurons increases markedly during typical adolescent development (see **Figure 3**). Our study also highlights critical intracellular signals downstream to activation of A$_1$Rs that contribute to the robust effects of adenosine receptor antagonists observed in area CA2 during early postnatal development, which occur before any enrichment of A$_1$Rs in CA2 pyramidal neurons.

Adenosine receptors localized in presynaptic boutons are known to regulate neurotransmitter release (Prince and Stevens, 1992; Wetherington and Lambert, 2002; Scammell et al., 2003), but they also play critical roles in mediating the activity of key postsynaptic signaling cascades and in controlling intrinsic membrane conductances that affect neuronal excitability (Greene and Haas, 1985; Gerber et al., 1989). Here, we observed several such effects following bath application of the selective A$_1$R agonist CCPA that do not differ between areas CA2 and CA1, including changes in rectification ratios and synaptic function (see **Figures 2**, **5**, respectively) that are similar to those reported previously (Greene and Haas, 1991; Dunwiddie and Masino, 2001). It is unclear, however, whether the lasting effects of CCAP on synaptic and intrinsic excitability shown in the current study are due to A$_1$Rs located pre- or postsynaptically in CA2 and CA1 (but see **Figure 4**). Notably, though, adenosine receptors have been shown to interfere with postsynaptic mechanisms required for the maintenance of activity-dependent forms of LTP in area CA1 (Arai et al., 1990; Rex et al., 2005). The possibility of reversing LTP in CA2 neurons by subsequent activation of A$_1$Rs, however, was not tested in the current study because LTP of synaptic responses rarely occurs in Schaffer collateral inputs to CA2 when performing typical whole-cell slice experiments *in vitro* with 2 mM extracellular calcium in the bathing medium (Zhao et al., 2007; Simons et al., 2009; Chevaleyre and Siegelbaum, 2010). Our data presented here do not rule out a role for A$_1$Rs regulating GABAergic transmission, such as has been described previously (Jeong et al., 2003; Rombo et al., 2014), but we note that Muñoz and Solís (2019) found no effect of picrotoxin on CA1/CA2 differences in caffeine-induced potentiation. This is particularly relevant in light of the findings that CA2 of rats and mice has a higher density of some types of GABAergic interneurons than CA1 (Piskorowski and Chevaleyre, 2013; Botcher et al., 2014).

Regarding the effects of A$_1$R activation on presynaptic terminals, our primary evidence against the idea of a CA1/CA2 difference in presynaptic neurotransmitter release is based on our analysis of PPF. This technique presumes that the identical terminals activated by the first pulse are also activated by the second, and so neurotransmitter release may be underestimated in our experiments to a large degree. We note that although we did not see significant effects of CCPA

(A_1R agonist) on PPF or differences between CA1 and CA2 in slices from juvenile animals, Muñoz and Solís (2019) recently reported that the magnitude of PPF differed between CA1 and CA2 after caffeine (A_1R antagonist) treatment in slices from older animals. The high variance in synaptic responses seen with whole-cell recordings compared with the low variance in responses recorded in field potentials (Muñoz and Solís, 2019) may have also contributed to the differences in findings in the two studies. Additional experiments with more cells may reveal significant findings, but the lack of differences between CA1 and CA2 in: (a) A_1R staining at P14 (Ochiishi et al., 1999), and (b) CCPA-induced depression (**Figure 3**) at P14 is consistent with our findings of modest/variable changes in PPF. Selective disruption of $G_{i/o}$ coupling in the recorded neuron or localized knockout of *Adora1* may eventually resolve the question of the presynaptic effects of adenosine.

Although the developmentally-regulated pattern of immunolabeling for the A_1R in area CA2 first shown by Ochiishi et al. (1999) has not been replicated successfully by us or by others using commercially-available antibodies (Rex et al., 2005), our finding that an A_1R agonist was sufficient to cause an age-dependent change in synaptic function in both CA2 and CA1 directly supports the idea of a developmental shift in the distribution of A_1Rs across the hippocampus (see **Figure 3**). Interestingly, previous immunolabeling work has shown that 5'-nucleotidase—an enzyme required to generate adenosine from ATP—is highly enriched in area CA2 in both the mouse and the gerbil (Lee et al., 1986). Nevertheless, it had yet to be reconciled how a blockade of A_1Rs by caffeine or another A_1R antagonist could induce a robust potentiation of synaptic responses in area CA2 at concentrations that do little in CA1 and CA3 (Simons et al., 2012). Here, we provide evidence showing how several A_1R-mediated intracellular signals differ between areas CA2 and CA1, and this suggests that differences in A_1R-mediated synaptic plasticity observed in slices prepared from juvenile animals may be due to mechanisms other than those linked directly to the expression pattern of A_1Rs in the hippocampus. Specifically, both kinase activity, required for maintaining synaptic responses (see **Figure 8**), and robust response to forskolin in CA2 neurons (see **Figure 9**) indicate that postsynaptic currents in CA2 pyramidal cells are especially sensitive to manipulations of cAMP and changes in substrate phosphorylation, even in tissue obtained from young animals. Alternatively, rolipram-sensitive phosphodiesterase activity, which is required for A_1R-mediated synaptic depression in CA1 but not in CA2 (see **Figure 7**), may be responsible for the blunted potentiating effects of forskolin and various A_1R antagonists in area CA1. Importantly, though, the two are not likely to be mutually exclusive and both may contribute to the relative effectiveness of A_1R antagonists to potentiate EPSCs in slices from young rats. Regional differences in the expression of A_1Rs may be sufficient to explain the differential effects of CCPA on synaptic responses in adult tissue, but they would likely be in addition to any regional differences in intracellular signaling molecules described above. For example, both of the calcium-activated adenylyl cyclases, AC1 and AC8, increase with age in mouse hippocampus (Nicol et al., 2005; Conti et al., 2007). In addition, the antagonist and agonist responses may be controlled by adenosine re-uptake and metabolism pathways, any of which may also be developmentally controlled. Thus the CPPA response, presuming it is neither taken up or metabolized, may reflect partial occlusion by these other factors regulating adenosine tone; caution must be taken when interpreting these data.

The precise mechanism underlying the induction of CCPA-mediated synaptic depression in Schaffer collateral inputs to CA2 and CA1 remains unknown, but it is clear that NMDA receptors or constant synaptic stimulation are not required (see **Figures 6A$_{1,2}$,B$_{1,2}$**). These findings indicate that mechanisms typically involved in the induction of activity-dependent forms of synaptic depression in the hippocampus are not required here [but see Pagani et al. (2014) for mechanisms of Avpr1b-mediated synaptic potentiation in CA2], and this is consistent with the findings of Simons et al. (2012) who demonstrated a role for enhanced activity of PKA in the expression of A_1R-mediated synaptic potentiation in area CA2 induced by caffeine or DPCPX (Simons et al., 2012). Also, previous work examining the effects of the A_1R agonist CPA on glutamate receptor phosphorylation and internalization indicates a key role for protein phosphatase 2A (Stockwell et al., 2015), which has also been implicated in activity-dependent forms of LTD (Mauna et al., 2011). Although we used a different A_1R agonist for a much shorter incubation period than in the previous report, we found no effect of the protein phosphatase 2A inhibitor, fostriecin, on the CCPA-mediated depression of EPSCs in either CA2 or CA1 (see **Figures 6D$_{1,2}$**). We also found that inhibition of p38 MAP kinase, which has been implicated in both adenosine-mediated signaling and NMDA receptor-dependent LTD (Bolshakov et al., 2000; Brust et al., 2006; Liang et al., 2008), was similarly without effect (see **Figures 6C$_{1,2}$**). Thus, although there are several forms of LTD (Sanderson et al., 2016; Pinar et al., 2017), many of which have underlying mechanisms shared with adenosine receptor-mediated reductions in synaptic currents, our data suggest that NMDARs, phosphatase 2A, or p38 MAP kinase are unlikely to be critical for the type CCPA-induced depression reported here. Further studies would be required to determine whether other mechanisms associated with pre- and/or post-synaptic forms of LTD, such as those requiring endocannabinoids or mGluRs, interact with A_1R-mediated depression (Atwood et al., 2014; Kano, 2014; Olmo et al., 2016).

A difficult result to interpret is the observation that internal application of the different protein kinase A inhibitors elicited different effects across the various hippocampal subfields (KT5720 and PKI; see **Figures 8A,B**, respectively). Specifically, KT5720 caused a slow-onset decay in the amplitude of EPSCs recorded in CA2 neurons, yet it had no effect on transmission in CA1 (see **Figures 8A$_{1-3}$**). Interestingly, PKI in the internal electrode solution did not affect synaptic responses evoked in either recording site (see **Figures 8B$_{1-3}$**). Based on the findings of Kameyama et al. (1998) who observed a rundown of responses in CA1 with 10 μM PKI, we had expected a similar result here. However, our initial attempts with 10 μM were without

effect (data not shown), and even a 30 μM concentration of PKI failed to induce changes in synaptic transmission after 1 h of recording (see **Figures 8B$_{1,2}$**). Although possibly the rundown observed with PKI in the previous study was due to the intracellular recording technique (i.e., sharp intracellular recordings using an internal solution containing only salts), we did obtain the expected result with a different PKA inhibitor using a different slice recording protocol (KT5720; whole-cell patch-clamp recordings with ATP and GTP in the internal solution, see **Figure 8A$_1$**). Indeed, the two inhibitors are known to act in slightly different ways to inhibit the activity of PKA, with PKI binding the catalytic subunits of the kinase and KT5720 acting as a competitive antagonist at the ATP binding sites on the catalytic domains (Murray, 2008). KT5720 is thought to be the less selective inhibitor out of the two, raising the possibility that its effects on synaptic responses in CA2 neurons may be due actions on other intracellular kinases, such as MEK or MAPK (Murray, 2008). Alternatively, if the PKA is bound together in complexes, such as AKAPs (Nygren and Scott, 2015), then the PKI binding site may not be accessible to exogenously applied compounds. Nevertheless, we believe that the results here indicate that various targets of PKA, including glutamate receptors, may be differentially regulated in both CA2 and CA1, and this may partly explain the robust potentiating effects of A$_1$R antagonists in area CA2 in slices obtained from young animals despite the lack of any obvious enrichment of A$_1$Rs.

Hippocampal area CA2 has only recently been appreciated for its role in various forms of cognition. Indeed, evidence has been amassed linking CA2 to a wide array of social behaviors. Specifically, lesioning area CA2 or silencing CA2 neurons *via* genetic manipulations to prevent glutamate release results in deficits in social recognition memory (Hitti and Siegelbaum, 2014; Stevenson and Caldwell, 2014), deletion of a CA2-enriched gene, *Avpr1b*, reduces aggressive behavior in mice (Wersinger et al., 2002; Pagani et al., 2014) and optogenetic stimulation of vasopressinergic axons in CA2 enhances social recognition memory (Smith et al., 2016). Although A$_1$Rs are expressed in neurons throughout the brain, if their function is greatest in area CA2 where the receptor is highly concentrated then it is not surprising that an A$_1$R agonist *impairs* social recognition memory and that caffeine *enhances* it (Prediger and Takahashi, 2005). Moreover, A$_1$R knockout mice display no deficits in spatial learning, but they do exhibit pronounced anxiety-like behaviors and aggression (Giménez-Llort et al., 2002, 2005). Finally, chronic administration of caffeine increases aggressive behavior in rats (Fredholm et al., 1999) and enhances both the length and branching pattern of basal dendrites in CA1, including the density of spines on these dendrites (Vila-Luna et al., 2011) which are the main targets of CA2 neurons (Kohara et al., 2013). Thus, links between adenosine receptor function, various social behaviors, and area CA2 may be worthy of further consideration. Our findings indicate that downstream signaling of A$_1$Rs is what distinguishes CA2 from CA2 early in postnatal development. Further, they suggest that the modulation of key neurotransmitter systems in the hippocampus, like adenosine, may differ depending on the stage of development.

DATA AVAILABILITY STATEMENT

The raw data supporting the conclusions of this article will be made available by the authors, without undue reservation, to any qualified researcher.

ETHICS STATEMENT

The animal study was reviewed and approved by the National Institute of Environmental Health Sciences Animal Care and Use Committee.

AUTHOR CONTRIBUTIONS

SD and DC conceived and designed the studies and wrote the manuscript. DC conducted experiments and analyzed data. SD supervised the project.

FUNDING

This research was supported by the Intramural Research Program of the National Institute of Environmental Health Sciences, National Institutes of Health (Z01 ES100221).

REFERENCES

Arai, A., Kessler, M., and Lynch, G. (1990). The effects of adenosine on the development of long-term potentiation. *Neurosci. Lett.* 119, 41–44. doi: 10.1016/0304-3940(90)90750-4

Atwood, B. K., Lovinger, D. M., and Mathur, B. N. (2014). Presynaptic long-term depression mediated by Gi/o-coupled receptors. *Trends Neurosci.* 37, 663–673. doi: 10.1016/j.tins.2014.07.010

Bolshakov, V. Y., Carboni, L., Cobb, M. H., Siegelbaum, S. A., and Belardetti, F. (2000). Dual MAP kinase pathways mediate opposing forms of long-term plasticity at CA3-CA1 synapses. *Nat. Neurosci.* 3, 1107–1112. doi: 10.1038/80624

Botcher, N. A., Falck, J. E., Thomson, A. M., and Mercer, A. (2014). Distribution of interneurons in the CA2 region of the rat hippocampus. *Front. Neuroanat.* 8:104. doi: 10.3389/fnana.2014.00104

Broderick, P., and Benjamin, A. B. (2004). Caffeine and psychiatric symptoms: a review. *J. Okla. State Med. Assoc.* 97, 538–542.

Brust, T. B., Cayabyab, F. S., Zhou, N., and MacVicar, B. A. (2006). p38 mitogen-activated protein kinase contributes to adenosine A1 receptor-mediated synaptic depression in area CA1 of the rat hippocampus. *J. Neurosci.* 26, 12427–12438. doi: 10.1523/JNEUROSCI.4052-06.2006

Caruana, D. A., Warburton, E. C., and Bashir, Z. I. (2011). Induction of activity-dependent LTD requires muscarinic receptor activation in medial prefrontal cortex. *J. Neurosci.* 31, 18464–18478. doi: 10.1523/JNEUROSCI.4719-11.2011

Chevaleyre, V., and Siegelbaum, S. A. (2010). Strong CA2 pyramidal neuron synapses define a powerful disynaptic cortico-hippocampal loop. *Neuron* 66, 560–572. doi: 10.1016/j.neuron.2010.04.013

Conti, A. C., Maas, J. W. Jr., Muglia, L. M., Dave, B. A., Vogt, S. K., Tran, T. T., et al. (2007). Distinct regional and subcellular localization of adenylyl cyclases type

1 and 8 in mouse brain. *Neuroscience* 146, 713–729. doi: 10.1016/j.neuroscience.2007.01.045

Creager, R., Dunwiddie, T., and Lynch, G. (1980). Paired-pulse and frequency facilitation in the CA1 region of the *in vitro* rat hippocampus. *J. Physiol.* 299, 409–424. doi: 10.1113/jphysiol.1980.sp013133

Dudek, S. M., and Bear, M. F. (1992). Homosynaptic long-term depression in area CA1 of hippocampus and effects of N-methyl-D-aspartate receptor blockade. *Proc. Natl. Acad. Sci. U S A* 89, 4363–4367. doi: 10.1073/pnas.89.10.4363

Dumas, T. C., and Foster, T. C. (1998). Late developmental changes in the ability of adenosine A1 receptors to regulate synaptic transmission in the hippocampus. *Dev. Brain Res.* 105, 137–139. doi: 10.1016/s0165-3806(97)00152-1

Dunwiddie, T. V., and Hoffer, B. J. (1980). Adenine nucleotides and synaptic transmission in the *in vitro* rat hippocampus. *Br. J. Pharmacol.* 69, 59–68. doi: 10.1111/j.1476-5381.1980.tb10883.x

Dunwiddie, T. V., and Masino, S. A. (2001). The role and regulation of adenosine in the central nervous system. *Annu. Rev. Neurosci.* 24, 31–55. doi: 10.1146/annurev.neuro.24.1.31

Fredholm, B. B., Bättig, K., Holmén, J., Nehlig, A., and Zvartau, E. E. (1999). Actions of caffeine in the brain with special reference to factors that contribute to its widespread use. *Pharmacol. Rev.* 51, 83–133.

Fredholm, B. B., IJzerman, A. P., Jacobson, K. A., Linden, J., and Müller, C. E. (2011). International union of basic and clinical pharmacology. LXXXI. nomenclature and classification of adenosine receptors–an update. *Pharmacol. Rev.* 63, 1–34. doi: 10.1124/pr.110.003285

Garaschuk, O., Kovalchuk, Y. U., and Krishtal, O. (1992). Adenosine-dependent enhancement by methylxanthines of excitatory synaptic transmission in hippocampus of rats. *Neurosci. Lett.* 135, 10–12. doi: 10.1016/0304-3940(92)90124-p

Gerber, U., Greene, R. W., Haas, H. L., and Stevens, D. R. (1989). Characterization of inhibition mediated by adenosine in the hippocampus of the rat *in vitro*. *J. Physiol.* 417, 567–578. doi: 10.1113/jphysiol.1989.sp017819

Giménez-Llort, L., Fernández-Teruel, A., Escorihuela, R. M., Fredholm, B. B., Tobeña, A., Pekny, M., et al. (2002). Mice lacking the adenosine A1 receptor are anxious and aggressive, but are normal learners with reduced muscle strength and survival rate. *Eur. J. Neurosci.* 16, 547–550. doi: 10.1046/j.1460-9568.2002.02122.x

Giménez-Llort, L., Masino, S. A., Diao, L., Fernández-Teruel, A., Tobeña, A., Halldner, L., et al. (2005). Mice lacking the adenosine A1 receptor have normal spatial learning and plasticity in the CA1 region of the hippocampus, but they habituate more slowly. *Synapse* 57, 8–16. doi: 10.1002/syn.20146

Greene, R. W., and Haas, H. L. (1985). Adenosine actions on CA1 pyramidal neurones in rat hippocampal slices. *J. Physiol.* 366, 119–127. doi: 10.1113/jphysiol.1985.sp015788

Greene, R. W., and Haas, H. L. (1991). The electrophysiology of adenosine in the mammalian central nervous system. *Prog. Neurobiol.* 36, 329–341. doi: 10.1016/0301-0082(91)90005-l

Harris, E. W., and Cotman, C. W. (1985). Effects of synaptic antagonists on perforant path paired-pulse plasticity: differentiation of pre- and postsynaptic antagonism. *Brain Res.* 334, 348–353. doi: 10.1016/0006-8993(85)90230-6

Hitti, F. L., and Siegelbaum, S. A. (2014). The hippocampal CA2 region is essential for social memory. *Nature* 508, 88–92. doi: 10.1038/nature13028

Jacobson, K. A., von Lubitz, D. K. J. E., Daly, J. W., and Fredholm, B. B. (1996). Adenosine receptor ligands: differences with acute versus chronic treatment. *Trends Pharmacol. Sci.* 17, 108–113. doi: 10.1016/0165-6147(96)10002-x

Jeong, H. J., Jang, I. S., Nabekura, J., and Akaike, N. (2003). Adenosine A1 receptor-mediated presynaptic inhibition of GABAergic transmission in immature rat hippocampal neurons. *J. Neurophysiol.* 89, 1214–1222. doi: 10.1152/jn.00516.2002

Kameyama, K., Lee, H. K., Bear, M. F., and Huganir, R. L. (1998). Involvement of a postsynaptic protein kinase A substrate in the expression of homosynaptic long-term depression. *Neuron* 21, 1163–1175. doi: 10.1016/s0896-6273(00)80633-9

Kano, M. (2014). Control of synaptic function by endocanabinoid mediated retrograde signaling. *Proc. Jpn. Acad. Ser. B Phys. Biol. Sci.* 90, 235–250. doi: 10.2183/pjab.90.235

Kelly, M. P., Adamowicz, W., Bove, S., Hartman, A. J., Mariga, A., Pathak, G., et al. (2014). Select 3′,5′-cyclic nucleotide phosphodiesterases exhibit altered expression in the aged rodent brain. *Cell. Signal.* 26, 383–397. doi: 10.1016/j.cellsig.2013.10.007

Kohara, K., Pignatelli, M., Rivest, A. J., Jung, H.-Y., Kitamura, T., Suh, J., et al. (2013). Cell type-specific genetic and optogenetic tools reveal hippocampal CA2 circuits. *Nat. Neurosci.* 17, 269–279. doi: 10.1038/nn.3614

Lee, K. S., Schubert, P., Reddington, M., and Kreutzberg, G. W. (1986). The distribution of adenosine A1 receptors and 5'-nucleotidase in the hippocampal formation of several mammalian species. *J. Comp. Neurol.* 246, 427–434. doi: 10.1002/cne.902460402

Lein, E. S., Hawrylycz, M. J., Ao, N., Ayres, M., Bensinger, A., Bernard, A., et al. (2006). Genome-wide atlas of gene expression in the adult mouse brain. *Nature* 445, 168–176. doi: 10.1038/nature05453

Liang, Y.-C., Huang, C.-C., and Hsu, K.-S. (2008). A role of p38 mitogen-activated protein kinase in adenosine A1 receptor-mediated synaptic depotentiation in area CA1 of the rat hippocampus. *Mol. Brain* 1:13. doi: 10.1186/1756-6606-1-13

Lohse, M. J., Klotz, K. N., Schwabe, U., Cristalli, G., Vittori, S., and Grifantini, M. (1988). 2-Cloro-N6-cyclopentyladenosine: a highly selective agonist at A1 adenosine receptors. *Naunyn Schmiedebergs Arch. Pharmacol.* 337, 687–689. doi: 10.1007/BF00175797

Lucas, P. B., Pickar, D., Kelsoe, J., Rapaport, M., Pato, C., and Hommer, D. (1990). Effects of the acute administration of caffeine in patients with schizophrenia. *Biol. Psychiatry* 28, 35–40. doi: 10.1016/0006-3223(90)90429-6

Lüscher, C., Jan, L. Y., Stoffel, M., Malenka, R. C., and Nicoll, R. A. (1997). G protein-coupled inwardly rectifying K^+ channels (GIRKs) mediate postsynaptic but not presynaptic transmitter actions in hippocampal neurons. *Neuron* 19, 687–695. doi: 10.1016/s0896-6273(00)80381-5

Manita, S., Suzuki, T., Inoue, M., Kudo, Y., and Miyakawa, H. (2007). Paired-pulse ratio of synaptically induced transporter currents at hippocampal CA1 synapses is not related to release probability. *Brain Res.* 1154, 71–79. doi: 10.1016/j.brainres.2007.03.089

Mauna, J. C., Miyamae, T., Pulli, B., and Thiels, E. (2011). Protein phosphatases 1 and 2A are both required for long-term depression and associated dephosphorylation of cAMP response element binding protein in hippocampal area CA1 *in vivo*. *Hippocampus* 21, 1093–1104. doi: 10.1002/hipo.20823

Muñoz, M. D., and Solís, J. M. (2019). Characterisation of the mechanisms underlying the special sensitivity of the CA2 hippocampal area to adenosine receptor antagonists. *Neuropharmacology* 144, 9–18. doi: 10.1016/j.neuropharm.2018.10.017

Munshi, R., Pang, I. H., Sternweis, P. C., and Linden, J. (1991). A1 adenosine receptors of bovine brain couple to guanine nucleotide-binding proteins G_i1, G_i2 and G_o. *J. Biol. Chem.* 266, 22285–22289.

Murray, A. J. (2008). Pharmacological PKA inhibition: all may not be what it seems. *Sci. Signal.* 1:re4. doi: 10.1126/scisignal.122re4

Nehlig, A., Daval, J. L., and Debry, G. (1992). Caffeine and the central nervous system: mechanisms of action, biochemical, metabolic and psychostimulant effects. *Brain Res. Rev.* 17, 139–170. doi: 10.1016/0165-0173(92)90012-b

Nicol, X., Muzerelle, A., Bachy, I., Ravary, A., and Gaspar, P. (2005). Spatiotemporal localization of the calcium-stimulated adenylyl cyclases, AC1 and AC8, during mouse brain development. *J. Comp. Neurol.* 486, 281–294. doi: 10.1002/cne.20528

Nygren, P. J., and Scott, J. D. (2015). Therapeutic strategies for anchored kinases and phosphatases: exploiting short linear motifs and intrinsic disorder. *Front. Pharmacol.* 6:158. doi: 10.3389/fphar.2015.00158

Ochiishi, T., Saitoh, Y., Yukawa, A., Saji, M., Ren, Y., Shirao, T., et al. (1999). High level of adenosine A1 receptor-like immunoreactivity in the CA2/CA3a region of the adult rat hippocampus. *Neuroscience* 93, 955–967. doi: 10.1016/s0306-4522(99)00179-7

Olmo, I. G., Ferreira-Vieira, T. H., and Ribeiro, F. M. (2016). Dissecting the signaling pathways involved in the crosstalk between metabotropic glutamate receptors and cannabinoid type 1 receptors. *Mol. Pharmacol.* 90, 609–619. doi: 10.1124/mol.116.104372

Pagani, J. H., Zhao, M., Cui, Z., Avram, S. K. W., Caruana, D. A., Dudek, S. M., et al. (2014). Role of the vasopressin 1b receptor in rodent aggressive behavior and synaptic plasticity in hippocampal area CA2. *Mol. Psychiatry* 20, 490–499. doi: 10.1038/mp.2014.47

Paxinos, G., and Watson, C. (1998). *The Rat Atlas in Stereotaxic Coordinates*. New York, NY: Academic Press.

Pinar, C., Fontaine, C. J., Triviño-Paredes, J., Lottenberg, C. P., Gil-Mohapel, J., and Christie, B. R. (2017). Revisiting the flip side: Long-term depression of synaptic efficacy in the hippocampus. *Neurosci. Biobehav. Rev.* 80, 394–413. doi: 10.1016/j.neubiorev.2017.06.001

Piskorowski, R. A., and Chevaleyre, V. (2013). Delta-opioid receptors mediate unique plasticity onto parvalbumin-expressing interneurons in area CA2 of the hippocampus. *J. Neurosci.* 33, 14567–14578. doi: 10.1523/JNEUROSCI.0649-13.2013

Prediger, R. D. S., and Takahashi, R. N. (2005). Modulation of short-term social memory in rats by adenosine A_1 and A_{2A} receptors. *Neurosci. Lett.* 376, 160–165. doi: 10.1016/j.neulet.2004.11.049

Prince, D. A., and Stevens, C. F. (1992). Adenosine decreases neurotransmitter release at central synapses. *Proc. Natl. Acad. Sci. U S A* 89, 8586–8590. doi: 10.1073/pnas.89.18.8586

Rex, C. S., Kramár, E. A., Colgin, L. L., Lin, B., Gall, C. M., and Lynch, G. (2005). Long-term potentiation is impaired in middle-aged rats: regional specificity and reversal by adenosine receptor antagonists. *J. Neurosci.* 25, 5956–5966. doi: 10.1523/JNEUROSCI.0880-05.2005

Rombo, D. M., Dias, R. B., Duarte, S. T., Ribeiro, J. A., Lamsa, K. P., and Sebastião, A. M. (2014). Adenosine A_1 receptor suppresses tonic $GABA_A$ receptor currents in hippocampal pyramidal cells and in a defined subpopulation of interneurons. *Cereb. Cortex* 26, 1081–1095. doi: 10.1093/cercor/bhu288

San Antonio, A., Liban, K., Ikrar, T., Tsyganovskiy, E., and Xu, X. (2013). Distinct physiological and developmental properties of hippocampal CA2 subfield revealed by using anti-Purkinje cell protein 4 (PCP4) immunostaining. *J. Comp. Neurol.* 522, 1333–1354. doi: 10.1002/cne.23486

Sanderson, T. M., Hogg, E. L., Collingridge, G. L., and Corrêa, S. A. (2016). Hippocampal metabotropic glutamate receptor long-term depression in health and disease: focus on mitogen-activated protein kinase pathways. *J. Neurochem.* 139, 200–214. doi: 10.1111/jnc.13592

Scammell, T. E., Arrigoni, E., Thompson, M. A., Ronan, P. J., Saper, C. B., and Greene, R. W. (2003). Focal deletion of the adenosine A1 receptor in adult mice using an adeno-associated viral vector. *J. Neurosci.* 23, 5762–5770. doi: 10.1523/JNEUROSCI.23-13-05762.2003

Simons, S. B., Caruana, D. A., Zhao, M., and Dudek, S. M. (2012). Caffeine-induced synaptic potentiation in hippocampal CA2 neurons. *Nat. Neurosci.* 15, 23–25. doi: 10.1038/nn.2962

Simons, S. B., Escobedo, Y., Yasuda, R., and Dudek, S. M. (2009). Regional differences in hippocampal calcium handling provide a cellular mechanism for limiting plasticity. *Proc. Natl. Acad. Sci. U S A* 106, 14080–14084. doi: 10.1073/pnas.0904775106

Smith, A. S., Williams Avram, S. K., Cymerblit-Sabba, A., Song, J., and Young, W. S. III. (2016). Targeted activation of the hippocampal CA2 area strongly enhances social memory. *Mol. Psychiatry* 21, 1137–1144. doi: 10.1038/mp.2015.189

Stevenson, E. L., and Caldwell, H. K. (2014). Lesions to the CA2 region of the hippocampus impair social memory in mice. *Eur. J. Neurosci.* 40, 3294–3301. doi: 10.1111/ejn.12689

Stockwell, J., Chen, Z., Niazi, M., Nosib, S., and Cayabyab, F. S. (2015). Protein phosphatase role in adenosine A1 receptor-induced AMPA receptor trafficking and rat hippocampal neuronal damage in hypoxia/reperfusion injury. *Neuropharmacology* 102, 254–265. doi: 10.1016/j.neuropharm.2015.11.018

Sugawara, K., Shibasaki, T., Takahashi, H., and Seino, S. (2016). Structure and functional roles of Epac2 (Rapgef4). *Gene* 575, 577–583. doi: 10.1016/j.gene.2015.09.029

Sun, Q., Sotayo, A., Cazzulino, A. S., Snyder, A. M., Denny, C. A., and Siegelbaum, S. A. (2017). Proximodistal heterogeneity of hippocampal CA3 pyramidal neuron intrinsic properties, connectivity, and reactivation during memory recall. *Neuron* 95, 656–672. doi: 10.1016/j.neuron.2017.07.012

Trussell, L. O., and Jackson, M. B. (1987). Dependence of an adenosine-activated potassium current on a GTP-binding protein in mammalian central neurons. *J. Neurosci.* 7, 3306–3316. doi: 10.1523/JNEUROSCI.07-10-03306.1987

Vila-Luna, S., Cabrera-Isidoro, S., Vila-Luna, L., Juárez-Díaz, I., Bata-García, J. L., Alvarez-Cervera, F. J., et al. (2011). Chronic caffeine consumption prevents cognitive decline from young to middle age in rats and is associated with increased length, branching, and spine density of basal dendrites in CA1 hippocampal neurons. *Neuroscience* 202, 384–395. doi: 10.1016/j.neuroscience.2011.11.053

Visel, A., Alvarez-Bolado, G., Thaller, C., and Eichele, G. (2006). Comprehensive analysis of the expression patterns of the adenylate cyclase gene family in the developing and adult mouse brain. *J. Comp. Neurol.* 496, 684–697. doi: 10.1002/cne.20953

Wersinger, S. R., Ginns, E. I., O'Carroll, A.-M., Lolait, S. J., and Young, W. S. III. (2002). Vasopressin V1b receptor knockout reduces aggressive behavior in male mice. *Mol. Psychiatry* 7, 975–984. doi: 10.1038/sj.mp.4001195

Wetherington, J. P., and Lambert, N. A. (2002). Differential desensitization of responses mediated by presynaptic and postsynaptic A1 adenosine receptors. *J. Neurosci.* 22, 1248–1255. doi: 10.1523/JNEUROSCI.22-04-01248.2002

Zhao, M., Choi, Y.-S., Obrietan, K., and Dudek, S. M. (2007). Synaptic plasticity (and the lack thereof) in hippocampal CA2 neurons. *J. Neurosci.* 27, 12025–12032. doi: 10.1523/JNEUROSCI.4094-07.2007

Zucker, R. S. (1989). Short-term synaptic plasticity. *Annu. Rev. Neurosci.* 12, 13–31. doi: 10.1146/annurev.ne.12.030189.000305

Zucker, R. S., and Regehr, W. G. (2002). Short-term synaptic plasticity. *Annu. Rev. Physiol.* 64, 355–405. doi: 10.1146/annurev.physiol.64.092501.114547

Conflict of Interest: The authors declare that the research was conducted in the absence of any commercial or financial relationships that could be construed as a potential conflict of interest.

frontiers in Synaptic Neuroscience

ORIGINAL RESEARCH
published: 08 July 2020
doi: 10.3389/fnsyn.2020.00025

Dendritic and Spine Heterogeneity of von Economo Neurons in the Human Cingulate Cortex

Nivaldo D. Correa-Júnior[1†], Josué Renner[2†], Francisco Fuentealba-Villarroel[3], Arlete Hilbig[4] and Alberto A. Rasia-Filho[1,2,3]*

[1] Graduate Program in Biosciences, Universidade Federal de Ciências da Saúde de Porto Alegre (UFCSPA), Porto Alegre, Brazil, [2] Laboratory of Morphology and Physiology, Department of Basic Sciences/Physiology, Universidade Federal de Ciências da Saúde de Porto Alegre, Porto Alegre, Brazil, [3] Graduate Program in Neuroscience, Universidade Federal do Rio Grande do Sul, Porto Alegre, Brazil, [4] Department of Medical Clinics/Neurology, Universidade Federal de Ciências da Saúde de Porto Alegre, Porto Alegre, Brazil

The human cingulate cortex (CC), included in the paralimbic cortex, participates in emotion, visceral responses, attention, cognition, and social behaviors. The CC has spindle-shaped/fusiform cell body neurons in its layer V, the von Economo neurons (VENs). VENs have further developed in primates, and the characterization of human VENs can benefit from the detailed descriptions of the shape of dendrites and spines. Here, we advance this issue and studied VENs in the anterior and midcingulate cortex from four neurologically normal adult subjects. We used the thionin technique and the adapted "single-section" Golgi method for light microscopy. Three-dimensional (3D) reconstructions were carried out for the visualization of Golgi-impregnated VENs' cell body, ascending and descending dendrites, and collateral branches. We also looked for the presence, density, and shape of spines from proximal to distal dendrites. These neurons have a similar aspect for the soma, but features of spiny dendrites evidenced a morphological heterogeneity of CC VENs. Only for the description of this *continuum* of shapes, we labeled the most common feature as VEN 1, which has main dendritic shafts but few branches and sparse spines. VEN 2 shows an intermediate aspect, whereas VEN 3 displays the most profuse dendritic ramification and more spines with varied shapes from proximal to distal branches. Morphometric data exemplify the dendritic features of these cells. The heterogeneity of the dendritic architecture and spines suggests additional functional implications for the synaptic and information processing in VENs in integrated networks of normal and, possibly, neurological/psychiatric conditions involving the human CC.

Keywords: dendritic spines, Golgi method, human brain/cytology, neocortical layer V, modified pyramidal neurons, paralimbic cortex, 3D reconstruction

OPEN ACCESS

Edited by:
Martín Cammarota, Federal University of Rio Grande do Norte, Brazil

Reviewed by:
Zdravko Petanjek, University of Zagreb, Croatia
Francesco Ferraguti, Innsbruck Medical University, Austria

****Correspondence:***
Alberto A. Rasia-Filho
rasiafilho@pq.cnpq.br; rasiafilho@yahoo.com

[†] These authors have contributed equally to this work

Received: *03 March 2020*
Accepted: *26 May 2020*
Published: *08 July 2020*

Citation:
Correa-Júnior ND, Renner J, Fuentealba-Villarroel F, Hilbig A and Rasia-Filho AA (2020) Dendritic and Spine Heterogeneity of von Economo Neurons in the Human Cingulate Cortex. Front. Synaptic Neurosci. 12:25. doi: 10.3389/fnsyn.2020.00025

INTRODUCTION

The cingulate cortex (CC) is part of the "proisocortex" in the paralimbic cortex, which is phylogenetically older than the neocortex along with the evolution of the mammalian brain (Braak, 1979; Kolb and Whishaw, 2015; Pandya et al., 2015). The human CC begins adjacent to the genu of the corpus callosum corresponding to the cortical area 24 of Brodmann and the agranular

anterior limbic area with the subdivision area 33. The CC extends from the precingulate to the area *limitans*, numbered areas 36–38 by von Economo and Koskinas (Triarhou, 2009; see further subdivisions and classification in Vogt, 2015; functional and connectivity-based organization in Cauda et al., 2013; Glasser et al., 2016). The anterior cingulate cortex (ACC), initially considered a component of the superior limbic lobe (Talairach and Tournoux, 1993; Triarhou, 2009), is adjacent to the functionally distinct midcingulate cortex (MCC) (Vogt, 2015). Anterograde and retrograde tracing data showed CC connections with the prefrontal, premotor and motor, orbitofrontal, insular, and anterior temporal cortex as well as with some amygdaloid, hypothalamic, and thalamic nuclei and the periaqueductal gray matter in primates (Nieuwenhuys et al., 1988; Craig, 2002; Watson, 2006; Pandya et al., 2015 and references therein). In our species, the parietal cortex and the ventral striatum are also included (Vogt, 2015). The CC integrates specialized networks for attentional processes/executive functions with sensory, high-order associative and limbic brain areas. In this regard, the human CC elaborates focused attention for problem-solving, goal-directed, and exploratory behaviors; long-term memory and cognitive processing; premotor planning with motivational features; social awareness and emotions as love, trust, empathy, deception, guilt, and fear; feeding and aggression; and sympathetic and parasympathetic responses to modulate heart rate and arterial pressure, respiratory, and gastrointestinal responses (Allman et al., 2001, 2010, 2011a; Watson, 2006; Watson et al., 2006; Xuan et al., 2016; Rangwala et al., 2017 and references therein).

The human CC has a specialized neuronal type with an elongated "spindle-shaped" or rod-shaped cell body in its layer V (Nimchinsky et al., 1995). These cells, named von Economo neurons (VENs; Triarhou, 2009; Seeley et al., 2012), differ morphologically from the adjacent layer V pyramidal neurons (Feldman, 1984; Braak and Braak, 1985) and are larger than small-layer VI fusiform neurons (Nimchinsky et al., 1999). Congruent results with Nissl/thionin staining, Neu-N neuronal nuclear antigen, and immunoreactivity for functional biomarkers (Nimchinsky et al., 1995; Fajardo et al., 2008; Stimpson et al., 2011) identified VENs with vertically oriented fusiform soma and two main perpendicularly oriented primary dendrites emerging from opposite extremes, one directed to the superficial cortical layers and another directed to the white matter (Nimchinsky et al., 1995, 1999; Fajardo et al., 2008; Raghanti et al., 2015; González-Acosta et al., 2018), with few and usually short side braches (Watson, 2006). VENs do not express immunoreactivity for interneuron markers (i.e., parvalbumin, calbindin, or calretinin) but project axons to the subcortical white matter, some entering into the cingulum bundle (Nimchinsky et al., 1995), toward the brainstem or spinal cord regions (Cobos and Seeley, 2015).

The CC VENs have a characteristic phylogenetic and ontogenetic development (Allman et al., 2011a,b; Cauda et al., 2014). The ACC VENs evolved with a clustering pattern in our species and our closest relative living primates, the great apes (Nimchinsky et al., 1999; Allman et al., 2011b; Raghanti et al., 2015). VENs correspond to only 5.6% compared to the number of layer V pyramidal neurons (Nimchinsky et al., 1999) and approximately 3% of all neurons in layer V in the human ACC (Fajardo et al., 2008). Most human VENs mature along with the postnatal brain development (Allman et al., 2010, 2011a; Butti et al., 2013; Raghanti et al., 2015). Indeed, VENs are rare during gestation, and numbers increase during the first 8 months after birth, decrease and reach the adult number at 4–8 years (Allman et al., 2010, 2011a), and remain constant throughout aging in individuals with average cognition, but are comparatively more numerous in individuals ($\geq$ age 80) who show outstanding memory abilities (Gefen et al., 2018).

The pattern of dendritic branching and the presence of pleomorphic spines provide relevant morphological criteria for the classification of neurons (Ramón y Cajal, 1909-1911; Ramón-Moliner, 1962; Braak, 1980; Gabbott et al., 1997; Vásquez et al., 2018). This is an important issue because the dendritic architecture relates to the biophysical properties of the neuron, the membrane available for contacts and integration of excitatory and inhibitory inputs, and the establishment of spatiotemporal domains for the synaptic computations (Spruston, 2008; Spruston et al., 2013; Rollenhagen and Lübke, 2016). Furthermore, dendritic spines are specialized postsynaptic units for most excitatory inputs, increasing the density of synapses in each cell as well as the possibilities for modulation and plasticity of information transmission (Bourne and Harris, 2008; Rochefort and Konnerth, 2012; Spruston et al., 2013; Brusco et al., 2014; Stewart et al., 2014; Woolfrey and Srivastava, 2016). Spines show varied shapes and sizes whose complexity is more evident in the human brain (Ramón y Cajal, 1909-1911; Yuste, 2013; Dall'Oglio et al., 2015). Dendritic spines can have various region-specific and neuron-specific functional implications (Fiala et al., 2002; Hayashi-Takagi et al., 2015; Nakahata and Yasuda, 2018) and show structural changes in neurological and psychiatric disorders (Penzes et al., 2011; Herms and Dorostkar, 2016).

There are few studies describing the dendritic architecture and spine diversity of layer V VENs in the human CC. For example, VENs were reported as fusiform cells with sparse dendritic trees and symmetric apical and basal branches with fewer spines than pyramidal neurons (Watson et al., 2006). Two types of spiny VENs in the human ACC with different dendritic lengths were defined, the small VENs with a total dendritic length of 1,500–2,500 μm and the large ones with 5,000–6,000 μm (Banovac et al., 2019). We obtained further morphological data to depict the heterogeneity of the VENs in the human CC. The VENs in layer V were identified by the thionin technique and further visualized by three-dimensional (3D) reconstruction of Golgi-impregnated neurons. Although having a spindle-shaped cell body with similar longitudinal length, CC VENs show heterogeneity in their dendritic branching pattern, ranging in a morphological *continuum* from sparsely branched to more extensively ramified cells. The 3D images evidenced additional differences in the distribution, density, and shapes of dendritic spines in these VENs. The morphological and likely functional implications are provided below.

MATERIALS AND METHODS

Subjects

The subjects were two men and two women. Age, *postmortem* interval, cause of death, and type of tissue fixation are shown in **Table 1**. All ethical and legal procedures were carried out in accordance with the international regulatory standards based on the Helsinki Declaration of 1964. Written informed consent for brain donation was obtained with a next of kin during an autopsy at the morgue. The privacy rights of subjects were always observed. The Brazilian Ethics Committee from the Federal University of Health Sciences of Porto Alegre (UFCSPA; #62336116.6.0000.5345 and 18718719.7.0000.5345) approved this study.

Donors' clinical and comorbidity information was also obtained by interviewing a next of kin at the morgue. Subjects were reportedly healthy neurologically and psychiatrically, had no previous neurosurgical interventions, and were rated screened for cognitive decline using the "Informant Questionnaire on Cognitive Decline in the Elderly" (IQCODE; Neto et al., 2017). This is a validated interview procedure for which cutoff point scores of $\geq$ 3.27 or 3.48 are considered indicative of dementia in the Brazilian population (Sanchez and Lourenço, 2009; Carrabba et al., 2015). Only cases below these edge values were studied (**Table 1**). Besides, brain tissue from each subject was analyzed histologically and immunohistochemically by a neurologist/neuropathologist (AH) to confirm the absence of common vascular lesions or neurodegenerative disorders (data not shown).

Tissue Processing for the Thionin Staining

All brains were kept immersed in 10% laboratory-grade, unbuffered formaldehyde solution at room temperature (RT) for approximately 5 years before the present procedure. The medial border of the cerebral hemisphere, the corpus callosum, and the characteristic aspect of the CC served as anatomical references (Talairach and Tournoux, 1993). The left hemisphere CC was studied from −36.0 mm to 5.4 mm from anterior to posterior position related to the midpoint of the anterior commissure (plates 5–26 according to Mai et al., 2008).

From each brain, tissue blocks containing the CC were sectioned and postfixed at RT for 30 days using a phosphate buffer solution (PBS, 0.1 M, pH = 7.4) with 4% formaldehyde and 1.5% picric acid. Then, the samples were sectioned in the coronal plane with a vibrating microtome (1000S; Leica, Germany) in an alternating fashion. One series was sectioned at 50 μm for the thionin technique. The other series was sectioned at 200 μm for the Golgi method.

The thionin staining was used to identify the different cells and layers in the CC (**Figures 1**, **2**). Staining began by placing serial sections from each tissue block on gelatin-coated slides and left to dry at RT for 1 day. Afterward, the slides were (1) immersed in a 4% formaldehyde in PBS for 1 week at 4°C protected from light; (2) dried for 1 day at RT and placed in a 70% ethanol solution for another day; (3) immersed in solutions of increasing concentrations of ethanol; (4) cleared in absolute xylene; (5) immersed in decreasing solutions of ethanol and washed in distilled water; (6) immersed in a solution of 0.25% thionin (Merck, Germany) for 3 min; (7) immersed again in solutions of increasing ethanol concentration; (8) dipped in a solution of 95% ethanol with 1% acetic acid and absolute xylene; and (9) mounted with synthetic balsam (Soldan, Brazil) and coverslipped (Dall'Oglio et al., 2013).

The Golgi Method and the 3D Reconstruction Procedure

The "single-section" Golgi method was adapted to provide reliable results for the neuronal cell body and the dendritic and spines features in long-term fixed human brains (Dall'Oglio et al., 2010). The consistency of the present procedure is the same that served for previous characterization of neurons and dendritic spines in subcortical and cortical human brain areas (e.g., the medial and cortical amygdaloid nuclei and the CA3 hippocampal area; Dall'Oglio et al., 2013, 2015; Reberger et al., 2018; Vásquez et al., 2018).

The CC sections were kept for 3 days immersed in the post-fixation solution at RT. Afterward, sections were (1) rinsed in PBS and transferred to a solution of 0.1% osmium tetroxide (Sigma Chemicals Co., United States) in PBS for 20 min; (2) rinsed in PBS and immersed in 3% potassium dichromate (Merck) at 4°C in the dark for 2 days; (3) rinsed again in distilled water, "sandwiched" between coverslips, and placed in a solution of 1.5% silver nitrate (Merck) at RT in the dark for 1 day; (4) washed in distilled water; (5) placed on gelatin-coated histological slides, dried at RT, and dehydrated in an ascending series of ethanol (from 70 to 100% for 3 min each); (6) cleared in ethanol and absolute xylene; and (7) covered with non-acidic synthetic balsam (refractive index = 1.518–1.521, Permount Mounting Medium, EMS, USA or similar product, Soldan, Brazil) and coverslips.

We used the following including criteria to select neurons for analysis: (1) have cell bodies located within the boundaries of the ACC and MCC and in the cortical layer V; (2) have the cell body shape and primary dendrites characteristic of VENs; (3) be isolated from neighboring cells to avoid "tangled" dendrites; (4) have dendrites with defined borders and, as much as possible, tapering after branching or at distal locations; and (5) have dendritic spines distinguishable from the background.

The general morphology of selected neurons was studied at ×260 (using an objective plan apochromatic lens UPlanSApo 0.6 NA, Olympus, Japan) in a light microscope (Olympus BX-61, Japan) equipped with a z-stepping motor and coupled to a CCDDP72 high-performance camera (Olympus, Japan). Each image was acquired after advancing 0.5 μm for each z stack, under high resolution (1360 × 1024 pixels), and submitted to dynamic deconvolution using the Image-Pro Plus 7.0 software (Media Cybernetics, United States) during the acquisition process (Dall'Oglio et al., 2013; Reberger et al., 2018). Files were recorded as.TIFF files. The selected images were converted to 8-bit monochromatic pictures before processing.

We first performed a two-dimensional (2D) reconstruction of Golgi-impregnated neurons by summing microscopic images

TABLE 1 | Characteristics of the human cases.

Cases	Age (years)	Sex	PMI (hours)	IQCODE	Cause of death	Fixation	Technique
1	91	F	≥ 6:00	1.32	Pneumonia	Immersion	Thionin/Golgi
2	62	F	≥ 6:00	3.00	Undetermined	Immersion	Thionin/Golgi
3	79	M	≥ 6:00	3.15	Cardiac Arrest	Immersion	Thionin/Golgi
4	49	M	≥ 6:00	3.00	Undetermined	Immersion	Thionin/Golgi

PMI, post mortem interval; F, female; M, male.

at sequential focal planes that included the cell body and all visible dendrites (**Figure 3**). The features of the soma and the primary dendritic shaft thickness as well as the branching pattern and spatial orientation of main dendritic shafts in the neuropil supported the classification of CC layer V neurons as VENs. Small adjustments of brightness and background contrast were done in final reconstructed images using Adobe Photoshop CS3 software (Adobe Systems, Inc., United States) without altering the original neuronal features.

Based on the 2D general morphology, we performed the 3D reconstruction of VENs using the Neuromantic free software (v1.6.3 programmed in Borland C++ Builder, University of Reading, United Kingdom). Semiautomatic tracing of the cell body and dendrites was done for the original stack of microscopic images acquired along with the three spatial coordinates. Reconstructions were achieved as a sequence of 3D points with an ASCII-based format representing dendritic trees as a series of connected cylinders of varying radii identified by orthogonal lines from edge to edge (Myatt et al., 2012). The luminosity was inverted to allow more details to be observed in the dendritic shafts contrasting with the background. The contrast was adjusted for the visualization of thin branches. Algorithm and image processing are depicted in Myatt et al. (2012). Final images were saved as SWC + format for storing neuron morphologies (Parekh and Ascoli, 2013). Morphometric data were obtained from the L-Measure free software (Scorcioni et al., 2008) using the 3D reconstructed images. Representative examples of VENs in the CC were studied. Values were calculated for the cell body length, main diameter and volume, dendritic diameter of the primary shafts, total number of branches (i.e., the sum obtained starting from primary dendrites, including segments between branching points, and toward the end of tapered main or collateral branches), and total length and total volume of the dendritic tree.

We obtained 33 VENs that randomly fulfilled the including criteria for study. From our sample, 15 neurons were labeled as VEN 1, 10 were VEN 2, and 5 were VEN 3 (see Results). The number of these Golgi-impregnated VENs per studied case and their location in the CC is shown in **Table 2**.

Afterward, for the 3D reconstruction of dendritic spines, bright-field images were acquired at a final magnification of ×1,300 using an ×100 oil immersion objective lens (plan apochromatic UPlanSApo 1.4 NA, Olympus, Japan). Each image was acquired with high resolution (2070 × 1548 pixels) and submitted to dynamic deconvolution using the Image-Pro Plus 7.0 software. Spines were imaged from proximal to distal branches in each neuron studied. Data were obtained by controlling the focus in the "z" axis and acquiring z-stacks at sequential 0.1 μm steps. Corresponding images were stored as.TIFF files and converted to 8-bit monochromatic pictures. Each spiny dendritic segment imaged consisted of approximately 100–200 sequential frames saved as.TIFF files.

Following Reberger et al. (2018), spines were 3D reconstructed using an algorithm performed in the MATLAB software (R2105b, The MathWorks, United States). That is, after processing the gray-scale slices independently or using median 3D filters in smaller sub-volumes, images were processed using the following steps: (a) outlier removal; (b) edge enhancement using a variant of the "unsharp masking method" and image-filtering approach based on domain transforms ("edge-aware"); (c) binarization using an adaptive thresholding approach; (d) false-positive pruning; (e) 2D flood-fill operation with each slice of the binary volume; (f) tricubic interpolation to smooth transitions between adjacent slices; and (g) visualization of the final volume of the sampled images containing the selected dendritic shafts and their spines (Vásquez et al., 2018) using the "Fiji" ImageJ software (Schindelin et al., 2012) with the "Volume Viewer" plug-in[1]. Images had final adjustments of brightness and contrast made in Photoshop CS3 without altering spine counting or classification.

The identification and classification of each type of 3D-reconstructed dendritic spine was based on previous descriptions (Fiala and Harris, 1999; Arellano et al., 2007a,b; Brusco et al., 2010, 2014; González-Ramírez et al., 2014; Dall'Oglio et al., 2015). By rotating the reconstructed images, spines were inspected at different angles to determine their presence and distribution from proximal to distal dendrites and their number, shape, and size (Reberger et al., 2018). For each spine, we observed (1) the presence, length, and diameter of a neck, (2) the number of protrusions from a single stalk, (3) the head diameter, and (4) the head shape. According to these morphological features, spines were classified as (1) thin, (2) stubby, (3) wide, (4) mushroom-like, (5) ramified, (6) having a transitional aspect between these classes, or (7) "atypical" (or "multimorphic") spines with usually more complex and varied shapes (Dall'Oglio et al., 2015 and references therein). Small protrusions extending from the head of a spine were classified as spinules (Brusco et al., 2014; Petralia et al., 2018). Spine density was calculated as the number of spines per dendritic length in proximal and distal segments. We counted 55, 104, and 493 dendritic spines in these segments of representative VENs 1, 2, and 3, respectively.

Not all cells were impregnated by the Golgi method. Therefore, descriptive data are provided for representative VENs

[1]https://imagej.nih.gov/ij/plugins/volumeviewer.html

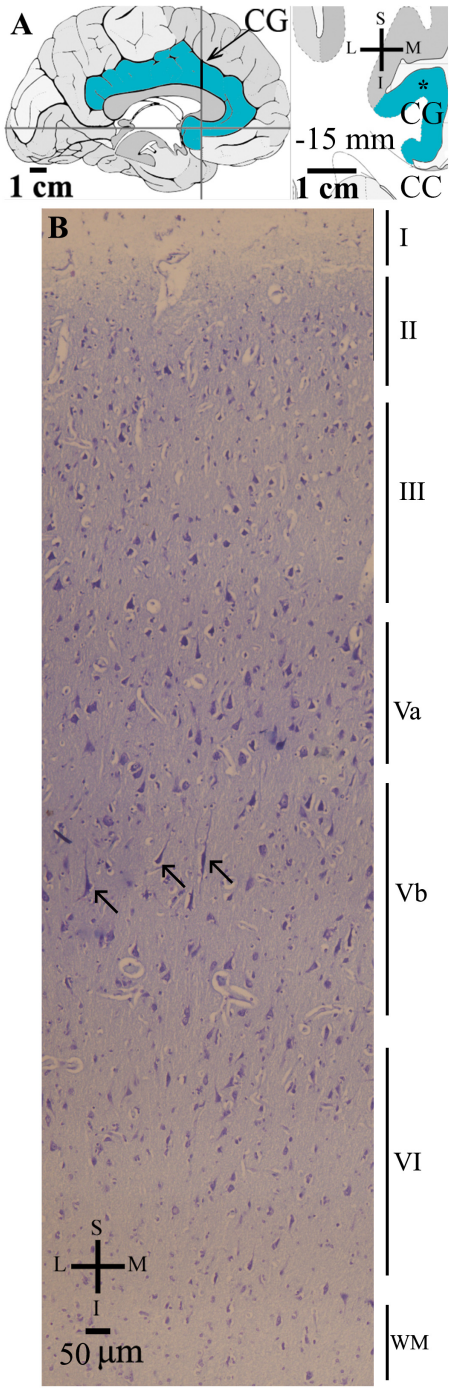

FIGURE 1 | (A) Left: Schematic drawing of the medial view of the human brain showing the location of the cingulate gyrus (CG, highlighted in blue), in this case 15 mm anterior to the midpoint of the anterior commissure. Right: Higher-magnification drawing of the CG. The asterisk represents the approximate location of the brain section used for the study of the cortical cytoarchitecture stained in **(B)**. CC, corpus callosum. Adapted from Mai et al. (2008). **(B)** Photomicrograph of thionin-stained cells in layers I–VI of the human cingulate cortex. Note the characteristic absence of layer IV and a von Economo neuron (indicated by an arrow) with an elongated spindle-shaped cell body and two primary dendrites in layer Vb. WM, white matter. Coordinates: I, inferior; L, lateral; M, medial; S, superior.

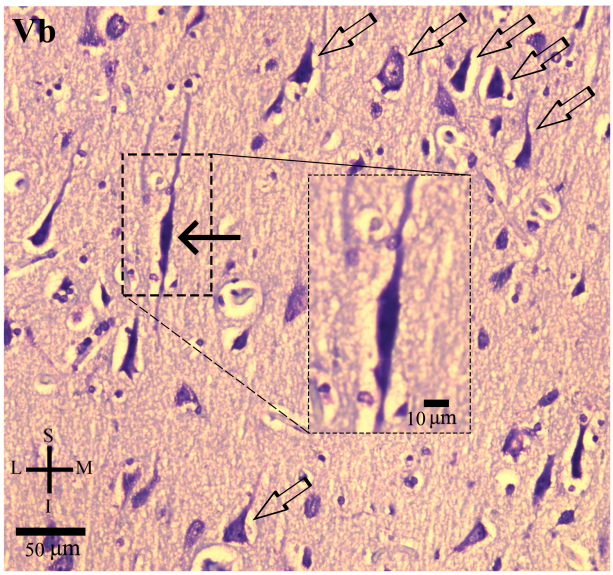

FIGURE 2 | Photomicrograph of thionin-stained cells in the layer Vb of the human cingulate cortex as presented in **Figure 1**. The von Economo neurons (VEN, black solid arrow) are intermingled with pyramidal neurons (open arrows). Higher magnification of VEN (box). Note the characteristic elongated spindle-like cell body and two primary dendrites, one with an ascending direction and another with a descending aspect. Coordinates: I, inferior; L, lateral; M, medial; S, superior.

in layer V of the human CC, but the number of completely impregnated VENs in the ACC and MCC precluded additional extensive statistical analysis. Quantitative data are provided to address how local VENs appear in a *continuum* of morphological features. It has to be mentioned that these morphometric values are not actual ones (as might exist *in vivo*) due to changes in the brain tissue following the *postmortem* period and the various steps of the histological processing (Dall'Oglio et al., 2010, 2013, 2015; Reberger et al., 2018; see also Zeba et al., 2008 for additional discussion). These quantitative data have to be considered with caution and are used as indicators of the relative differences between VENs described here.

All computational procedures were run using Windows Microsoft® (version 10), Intel® Core™ i7-8750H CPU @2.20 GHz, 16.0 GB RAM memory, NVIDIA® GeForce GTX 1051 Ti with 4 GB for image processing.

RESULTS

Thionin-stained sections served to identify the local cortical cytoarchitectonics and, in the CC, the absence of the inner granular layer IV (**Figure 1**). Morphological criteria were used to identify CC VENs in layer V. VENs have a typically large and elongated spindle-shaped cell body with two symmetric, vertically oriented primary dendritic shafts (**Figure 2**). The cell body shape of these cells is similar to those reported by other authors (e.g., Nimchinsky et al., 1995; Allman et al., 2010). All identified VENs in layer V presented the neuronal chromatin

TABLE 2 | Number of Golgi-impregnated VENs in the human cingulate cortex (CC) per studied case.

Case	VEN type 1	VEN type 2	VEN type 3
1	3 [−5.8 mm]		1 [−5.8 mm]
2	4 [−36 mm]		
3	4 [2.7 mm]	3 [2.7 mm]	
4	[−1.3 mm]	7 [−8.3 mm]	4 [4.0 mm]
Total	18	10	5

Approximate location in the CC for the three types of neurons are indicated in the brackets.

aspect and an evident nucleolus. VENs were intermingled with pyramidal neurons and adjacent glial cells (**Figure 2**). The identification of VENs was reinforced by the Golgi results.

Golgi data provided the shape of VEN dendrites and added new information on spines (**Figure 3**). In this regard, all studied VENs are spiny neurons. Dendritic spines showed a variety of shapes and sizes. Their types ranged from small to large stubby and wide, thin and mushroom-like, ramified, transitional aspects and/or more complex shapes with multiple bulbous structures, including double spines (i.e., a spine with a neck ending in a bulb, from which a second neck protruded that will end in another bulb; González-Ramírez et al., 2014; Dall'Oglio et al., 2015). These pleomorphic spines were found either isolated or forming clusters, and with different densities in main and collateral dendritic branches. Spinules were observed in different spine types.

Our results allowed the identification of a *continuum* of dendritic shapes for VENs in the human CC. We selected representative Golgi-impregnated neurons to exemplify the heterogeneity of their dendritic branching pattern (**Figures 4–8** and **Supplementary Videos 1–3**). There is not a strict separation of VENs into different subtypes at this moment. Rather, the general aspect of these neurons was labeled as VENs 1, 2, and 3 only for easy reference when describing the present data.

The *continuum* of VEN shapes ranged from cells with few dendritic branches and sparse simple spines (VEN 1, **Figure 4** and **Supplementary Video 1**), an intermediate aspect regarding the dendritic branching pattern and the slight increase in the number and types of spines (VEN 2, **Figure 5** and **Supplementary Video 2**), and a more profuse dendritic ramification and the highest density of pleomorphic spines beginning close to the soma and extending through distal dendritic segments (VEN 3, **Figures 6**, **7** and **Supplementary Video 3**).

Furthermore, VEN 1 shows both ascending and descending dendrites with a straight course and few ramifications (**Figure 4**), absence or sparse spines in proximal segments (**Figures 4a,d**), and a small increase in spine density toward distal segments (**Figures 4b,c,e,f**). These dendritic spines usually have a simple shape, and most were classified as stubby or wide ones (**Figures 4a–f**), few as atypical ones with spinule (**Figures 4c1,f2**). An example of VEN 1 after 3D reconstruction is shown in **Supplementary Video 1**.

VEN 2 has proximal branching points at both the main ascending and descending primary dendrites (**Figure 5**).

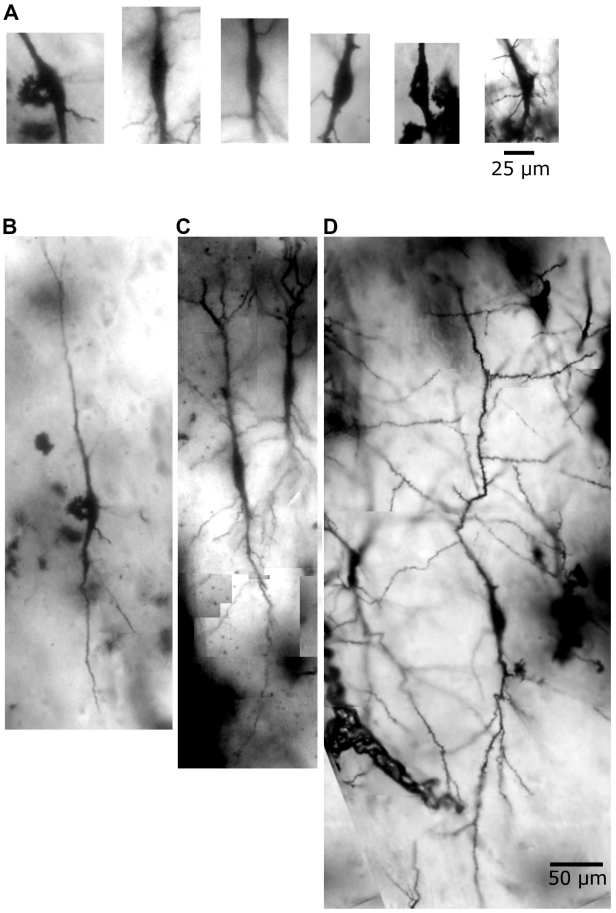

FIGURE 3 | Human *postmortem* Golgi-impregnated von Economo neurons (VENs) in the cingulate cortex as observed in bright-field microscopy. **(A)** Cell body aspect of VENs evidencing a spindle-shaped soma with vertically oriented main primary dendritic shafts. **(B–D)** Golgi-impregnated VENs partially showing the dendritic ramification and spatial orientation. These VENs are shown reconstructed in **Figures 4–8** and **Supplementary Videos 1–3**. Dendritic spines are not quite visible at this magnification. Image adjustment of contrast and brightness made with Photoshop CS3 (Adobe Systems, Inc., United States).

The number of collateral branches is more numerous than VEN 1 but is still limited. The proximal dendritic shafts characteristically show an absence or few spines (**Figures 5a1–3,b1,b2,c1,c2**) usually with stubby and wide (**Figures 5a3,b1,b2**) or atypical shapes (**Figures 5e1,e2**). The presence of intermingled mushroom spines increases in main shaft dendrites from proximal to distal segments (**Figures 5c3,d2,h1,j1**). This also occurs for transitional/atypical spines (**Figures 5c1,c3,e1,h2**). Various large stubby or wide spines were found (**Figures 5g1,h1–3**). Some ramified spines were observed (**Figures 5f2,h2,j1**). Spinules were present in different spine types (**Figures 5c3,d2,e1,l1**). An example of VEN 2 after 3D reconstruction is shown in **Supplementary Video 2**.

VEN 3 displays both high arborization and density of intermingled pleomorphic dendritic spines in main shafts and collateral branches (**Figures 6**, **7** for the descending and

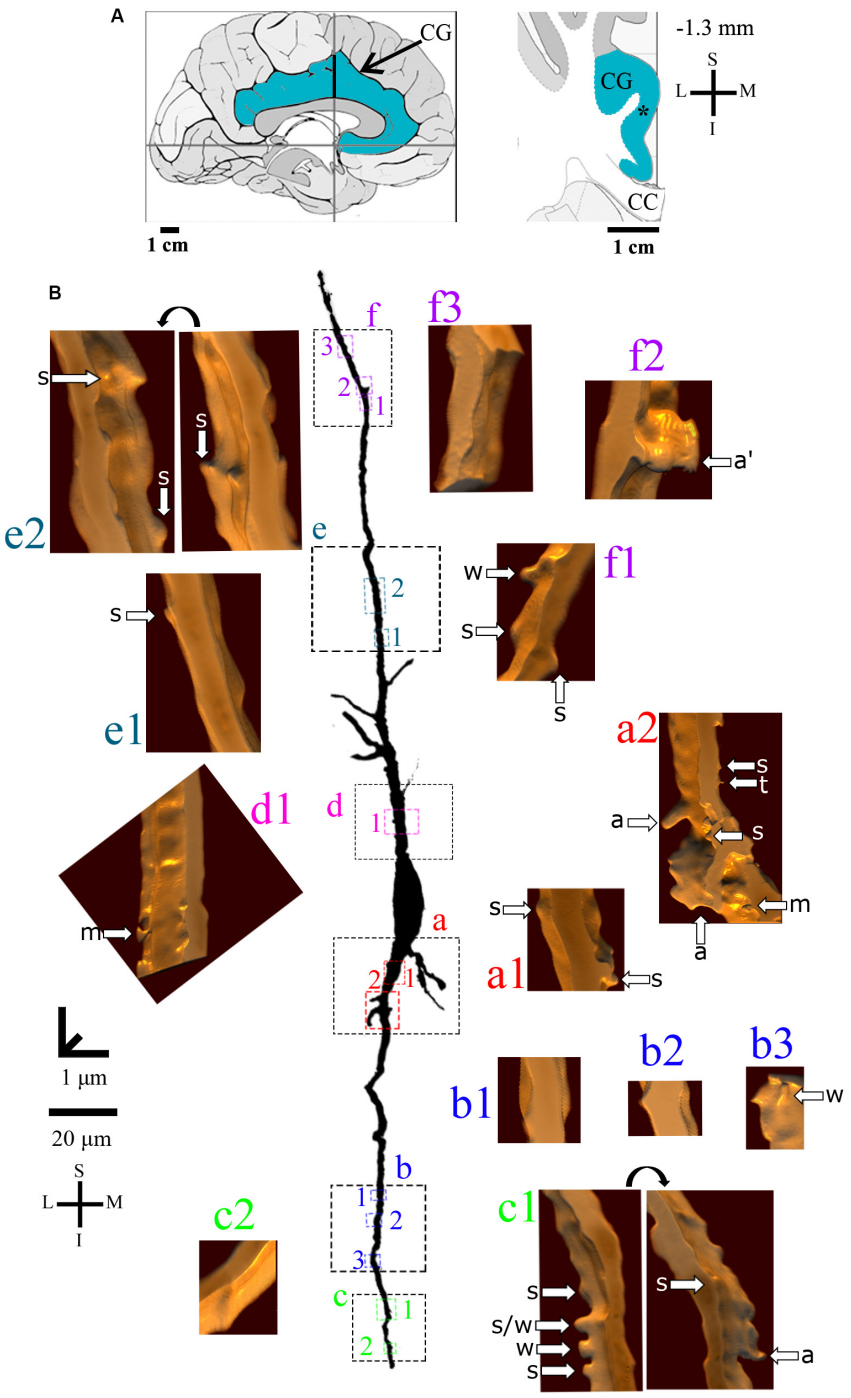

FIGURE 4 | (A) Left: Schematic drawing of the medial view of the human brain showing the location of the cingulate gyrus (CG, highlighted in blue), in this case 1.3 mm anterior to the midpoint of the anterior commissure. Right: Higher-magnification drawing of the CG. The asterisk represents the location of the neuron shown in **(B)**. CC, corpus callosum. Adapted from Mai et al. (2008). Coordinates: I, inferior; L, lateral; M, medial; S, superior. **(B)** Two-dimensional (2D, for the general morphology of this neuron) and three-dimensional (3D, for the dendrites and respective spines) reconstructions of serial bright-field photomicrographs of a representative Golgi-impregnated von Economo neuron (VEN 1) in layer V from the human cingulate cortex. The pial surface is at the top. Note the cell body shape and the main ascending and descending dendritic shafts with a straight course and few ramifications. Proximal to distal dendritic segments (identified by colored letters from "a" to "f") were sampled, and their spines are shown at higher magnification in the adjacent corresponding boxes. Note also the low density of spines and the variety of spine shapes. Spines were classified as stubby (s), wide (w), thin (t), mushroom (m), ramified (r), with a transitional (t/), or atypical aspect (a). Spine types are indicated by arrows after image reconstruction and at different rotating angles. An asterisk with the corresponding spine indicates the presence of a spinule. Image adjustment of contrast made with Photoshop CS3 (Adobe Systems, Inc., United States). Coordinates in **(A,B)**: I, inferior; L, lateral; M, medial; S, superior. Scale = 20 µm for the 2D reconstruction and 1 µm for the 3D reconstructions.

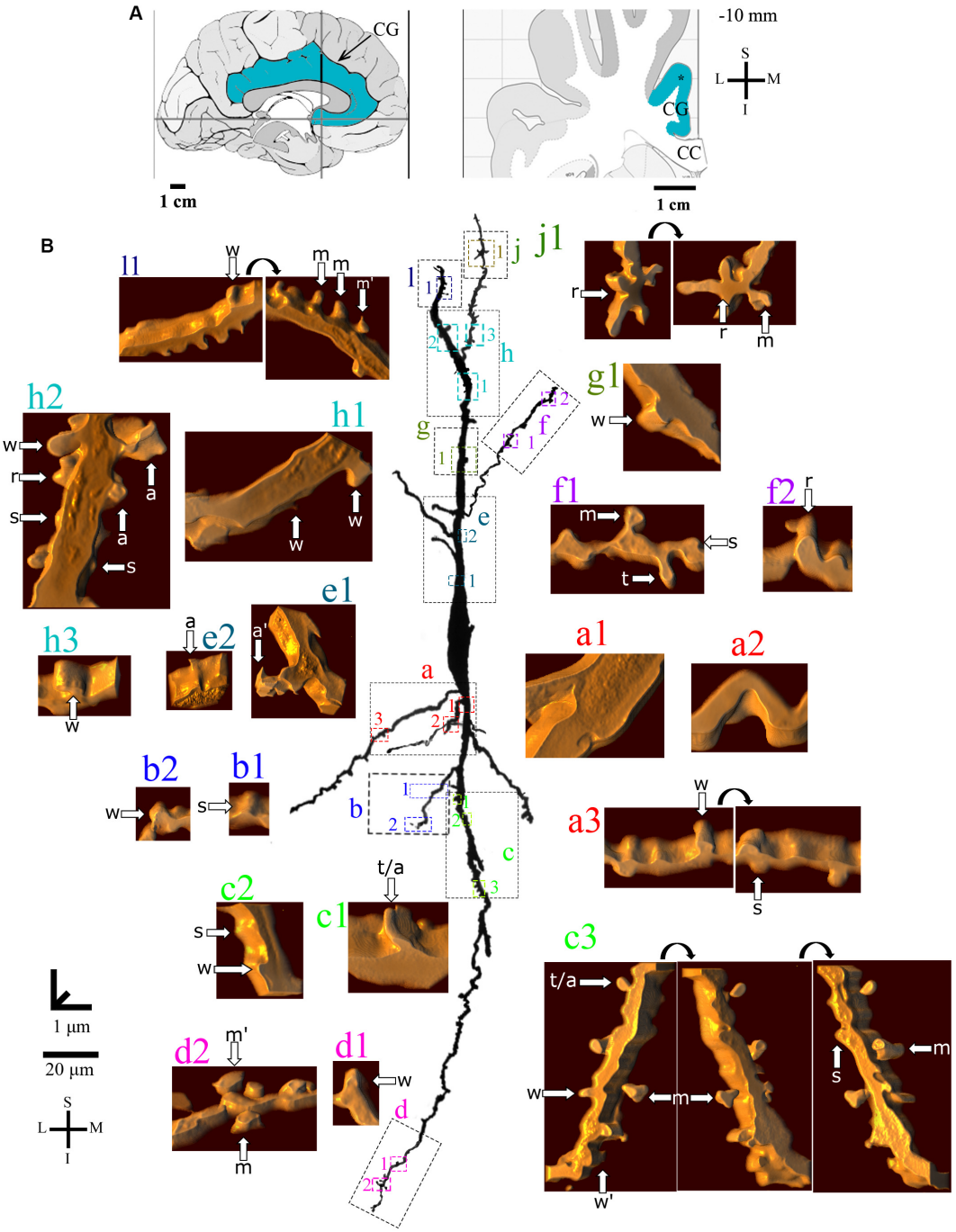

FIGURE 5 | (A) Left: Schematic drawing of the medial view of the human brain showing the location of the cingulate gyrus (CG, highlighted in blue), in this case 10 mm anterior to the midpoint of the anterior commissure. Right: Higher-magnification drawing of the CG. The asterisk represents the location of the neuron shown in **(B)**. CC, corpus callosum. Adapted from Mai et al. (2008). Coordinates: I, inferior; L, lateral; M, medial; S, superior. **(B)** Two-dimensional (2D, for the general morphology of this neuron) and three-dimensional (3D, for the dendrites and respective spines) reconstructions of serial bright-field photomicrographs of a representative Golgi-impregnated von Economo neuron (VEN 2) in layer V from the human cingulate cortex. The pial surface is at the top. Note the cell body shape and the main ascending and descending dendritic shafts, but the presence of more collateral ramifications than VEN 1 shown in **Figure 4**. Proximal to distal dendritic segments (identified by colored letters from "a" to "j") were sampled, and their spines are shown at higher magnification in the adjacent corresponding boxes. Note also the intermediate density of spines and the variety of spine shapes. Spines were classified as stubby (s), wide (w), thin (t), mushroom (m), ramified (r), with a transitional (t/), or atypical aspect (a). Spine types are indicated by arrows after image reconstruction and at different rotating angles. An asterisk with the corresponding spine indicates the presence of a spinule. Image adjustment of contrast made with Photoshop CS3 (Adobe Systems, Inc., United States). Coordinates in **(A,B)**: I, inferior; L, lateral; M, medial; S, superior. Scale = 20 µm for the 2D reconstruction and 1 µm for the 3D reconstructions.

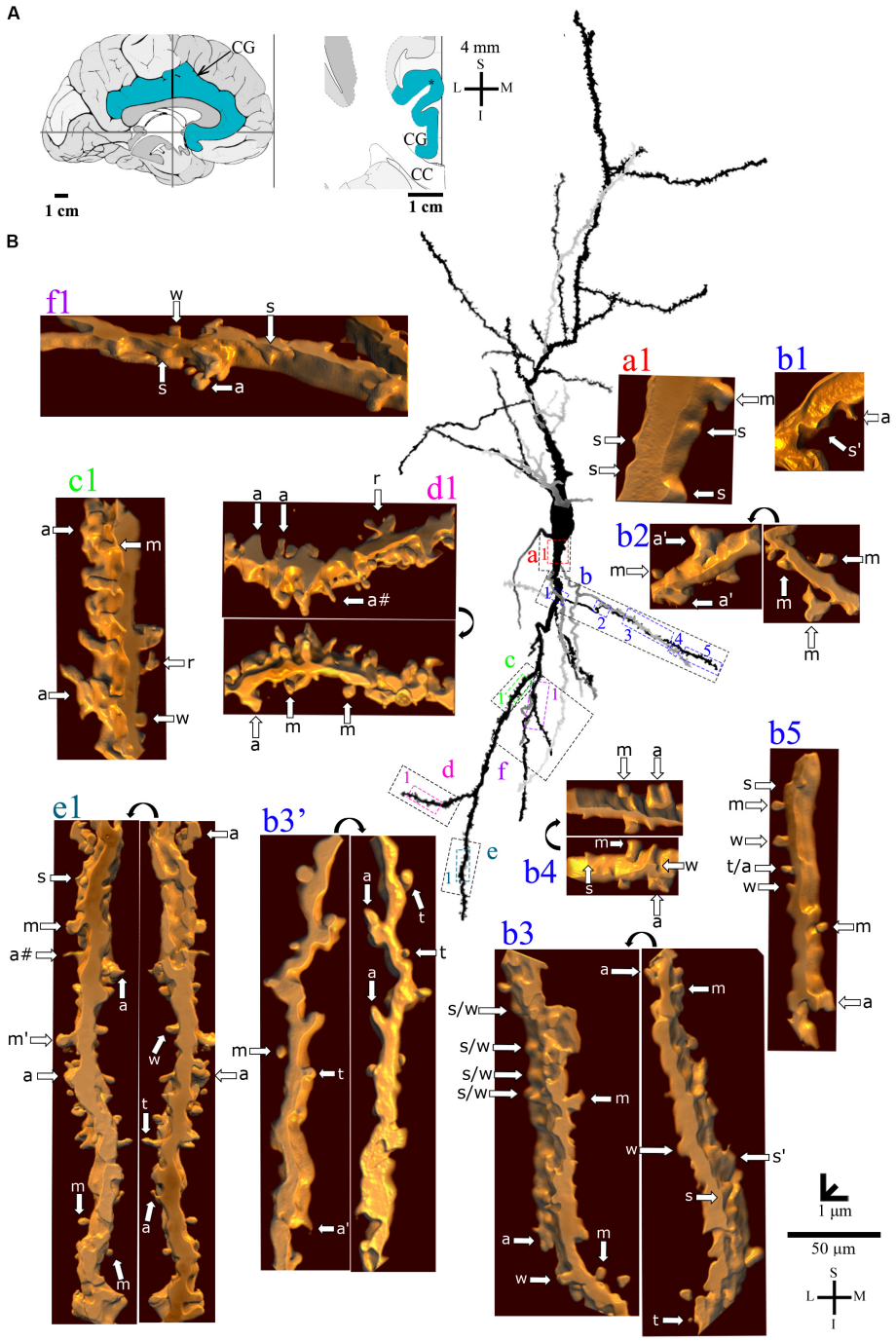

FIGURE 6 | (A) Left: Schematic drawing of the medial view of the human brain showing the location of the cingulate gyrus (CG, highlighted in blue), in this case 4 mm posterior to the midpoint of the anterior commissure. Right: Higher-magnification drawing of the CG. The asterisk represents the location of the neuron shown in **(B)**. CC, corpus callosum. Adapted from Mai et al. (2008). **(B)** Two-dimensional (2D, for the general morphology of this neuron) and three-dimensional (3D, for the dendrites and respective spines) reconstructions of serial bright-field photomicrographs of a representative Golgi-impregnated von Economo neuron (VEN 3) in layer V from the human cingulate cortex. The pial surface is at the top. The descending dendritic branch is shown in more detail for the presence, number, distribution, and shape of pleomorphic dendritic spines. Dendrites in gray contrast with dark ones when they are close branches at different focal planes (e.g., b3' is an upper branch than b3). Proximal to distal dendritic segments (identified by colored letters from "a" to "f") were sampled, and their spines are shown at higher magnification in the adjacent corresponding boxes. Note the high density of spines with different shapes. Spines were classified as stubby (s), wide (w), thin (t), mushroom (m), ramified (r), with a transitional (t/), or atypical aspect (a). Spine types are indicated by arrows after image reconstruction and at different rotating angles. An asterisk with the corresponding spine indicates the presence of a spinule. a* represents a double spine. a# represents an atypical spine with a protrusion resembling a filopodium. Image adjustment of contrast made with Photoshop CS3 (Adobe Systems, Inc., United States). Coordinates in **(A,B)**: I, inferior; L, lateral; M, medial; S, superior. Scale = 50 µm for the 2D reconstruction (compare to **Figures 4**, **5**) and 1 µm for the 3D reconstructions.

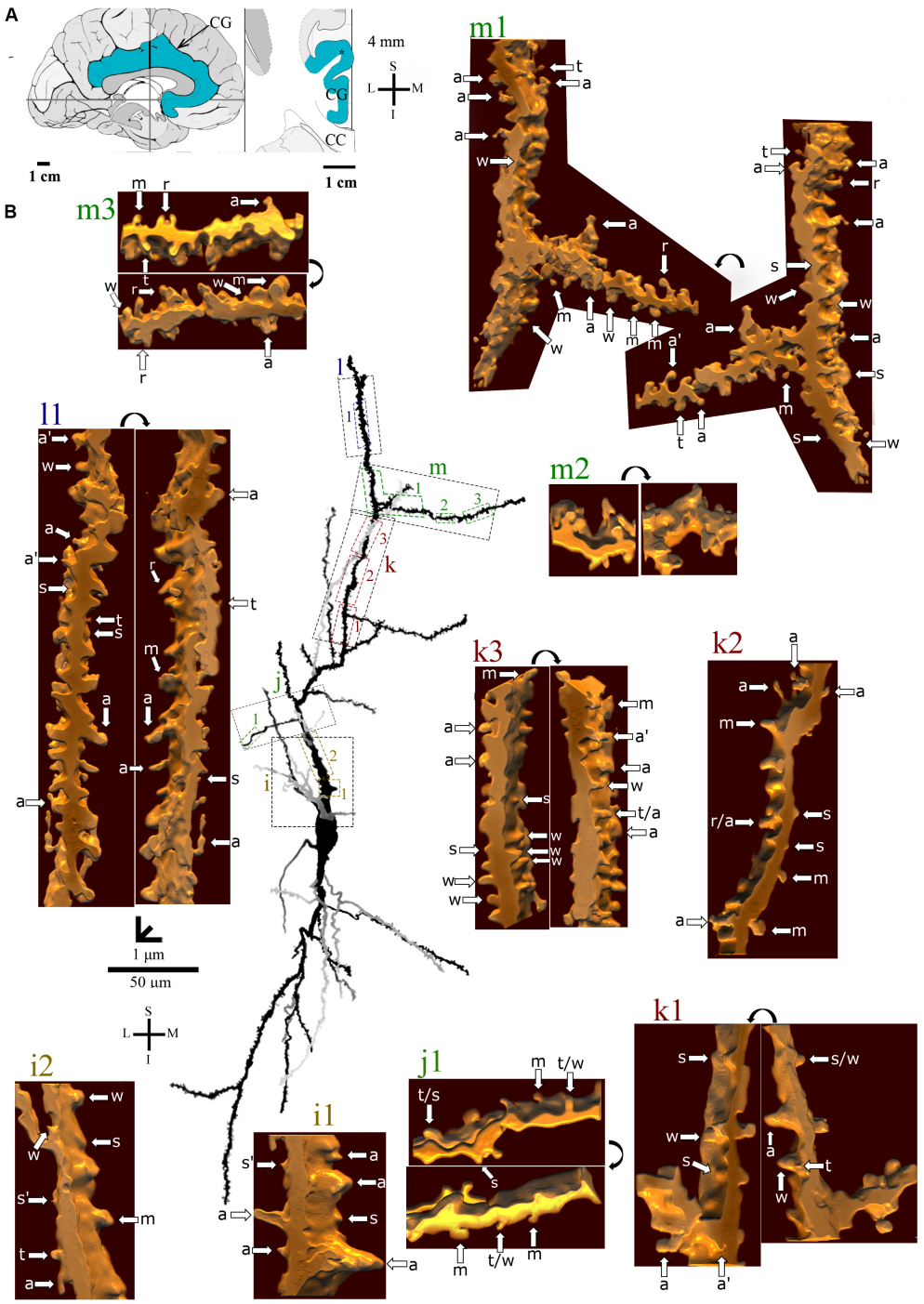

FIGURE 7 | (A) Left: Schematic drawing of the medial view of the human brain showing the location of the cingulate gyrus (CG, highlighted in blue), in this case 4 mm posterior to the midpoint of the anterior commissure. Right: Higher-magnification drawing of the CG. The asterisk represents the location of the neuron shown in **(B)**. CC, corpus callosum. Adapted from Mai et al. (2008). **(B)** Two-dimensional (2D, for the general morphology of this neuron) and three-dimensional (3D, for the dendrites and respective spines) reconstructions of serial bright-field photomicrographs of a representative Golgi-impregnated von Economo neuron (VEN 3) in layer V from the human cingulate cortex. The pial surface is at the top. The ascending dendritic branch is shown in more detail for the presence, number, distribution, and shape of pleomorphic dendritic spines. Dendrites in gray contrast with dark ones when they are close branches at different focal planes. Proximal to distal dendritic segments (identified by colored letters from "i" to "m") were sampled, and their spines are shown at higher magnification in the adjacent corresponding boxes. Note the high density of spines with different shapes. Spines were classified as stubby (s), wide (w), thin (t), mushroom (m), ramified (r), with a transitional (t/), or atypical aspect (a). Spine types are indicated by arrows after image reconstruction and at different rotating angles. An asterisk with the corresponding spine indicates the presence of a spinule. a* represents a double spine. Image adjustment of contrast made with Photoshop CS3 (Adobe Systems, Inc., United States). Coordinates in **(A,B)**: I, inferior; L, lateral; M, medial; S, superior. Scale = 50 µm for the 2D reconstruction (compare to **Figures 4**, **5**) and 1 µm for the 3D reconstructions.

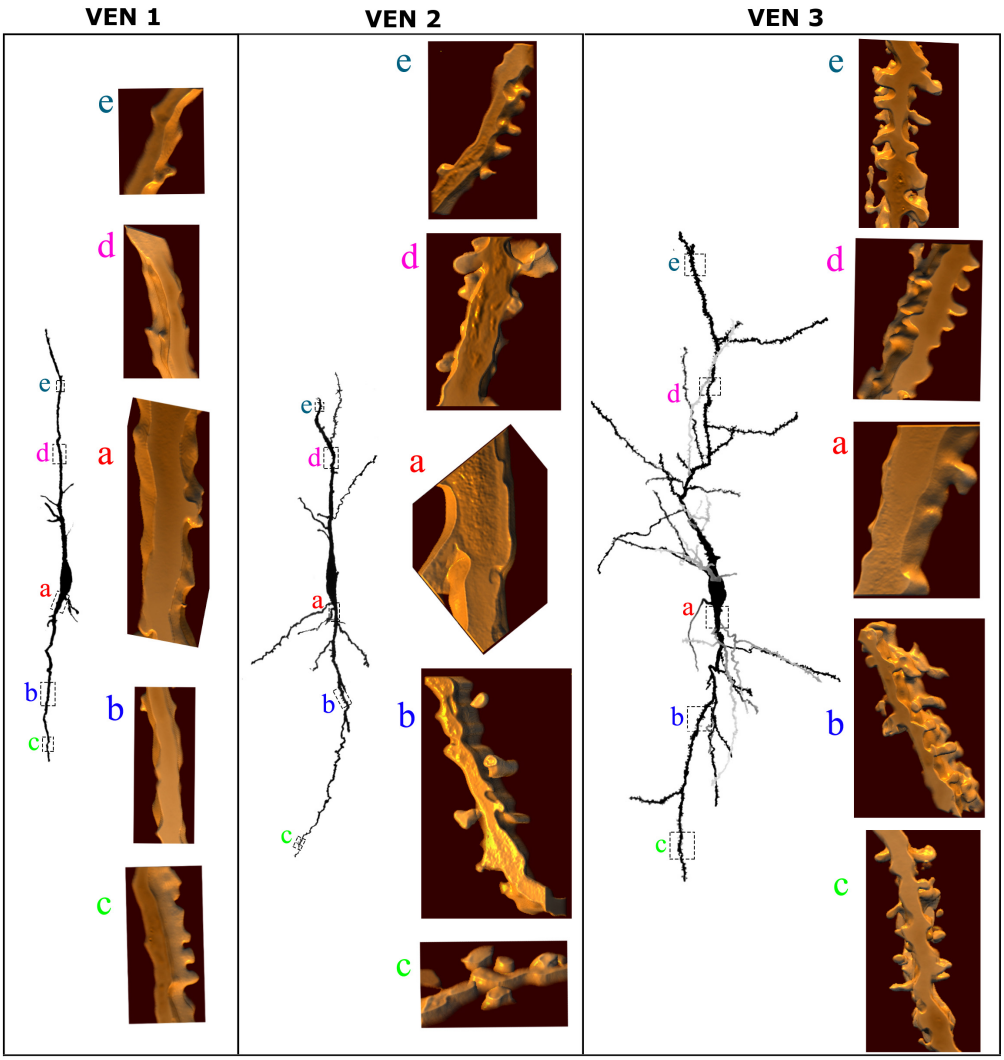

	VEN 1	VEN 2	VEN 3
Cell body			
Axial lenght (μm)	35.7	44.1	43.8
Maximum diameter (μm)	7	8.5	11.4
Area (μm^2)	680.7	1179.4	1134.8
Volume (μm^3)	1067.4	2600.8	2531.0
Dendrites			
Number of branches	21	34	55
Maximum diameter (μm)	2.3	4.9	5.3
Total dendritic lenght (μm)	604.2	948.6	2455.6
Total dendritic area (μm^2)	4023.1	5932.2	14342.2
Total dendritic volume (μm^3)	2505.1	3213.5	7374.6
Spine density			
Proximal	0.6	0.68	1.7
Distal	0.85	1.17	4.2

FIGURE 8 | (Top) Comparison of the morphological features of spindle-shaped von Economo neurons (VENs) from layer V in the human cingulate cortex. There are heterogeneous dendritic features for the morphological *continuum* of VEN 1 (with few dendritic branches and sparse spines), VEN 2 (with intermediate pattern of dendritic ramification and number of dendritic spines), and VEN 3 (with the highest number of dendritic branching points, collateral branches, and pleomorphic spines). Dendritic spines are shown at corresponding segments to illustrate the differences between these cells. Image adjustment of contrast made with Photoshop CS3 (Adobe Systems, Inc., United States). **(Bottom)** Quantitative data were obtained for the representative VENs 1, 2, and 3 shown above. Morphometrical data were obtained for the cell body and in both ascending and descending dendrites (ranging from lower values in VEN 1 and higher in VEN 3). The density of dendritic spines (number of spines per μm) was calculated along proximal to distal branches (segments indicated in section "Results"). Note fewer dendritic values in VEN 1 and 2 and higher ones in VEN 3.

ascending dendrites, respectively). The branching pattern is more profuse and begins close to the cell body in proximal thick branches. Main dendritic shafts maintain the vertical orientation for the ascending and descending branches, whereas the collateral dendrites ramify at different radial angles, including some in a horizontal position (**Figures 6**, **7**). Primary dendrites have various spines, including stubby and wide ones, many atypical aspects, or mushroom shape (**Figures 6a1,b1**, **7i1,i2**), a pattern that also occurs in collateral branches (**Figures 6b2–b5**, **7j1**). The number of pleomorphic dendritic spines increases in intermediate (**Figures 6c1**, **7k2,k3**) and distal segments (**Figures 6d1,e1**, **7m1–3,l1**). There is a myriad of intermingled spines of all sizes and types, i.e., stubby, wide, thin, mushroom, ramified, with transitional shapes, many atypical and complex multimorphic aspects (**Figures 6a–h**, **7i–n**), such as double spines (**Figures 6b3,d1**, **7m1**), and a protrusion resembling a filopodium (**Figure 6e1**). Pleomorphic spines are found spaced from each other (**Figures 6a1,b1,b3**',f1, **7i2,j1,k1**) or, more usually, in clusters along different parts of the same dendritic branch (**Figures 6c1,d1**, **7k3,m1,l1**). Spinules were found in different spine types, such as in stubby (**Figures 6b1,b3**, **7i2**), mushroom (**Figure 6e1**), and atypical spines (**Figures 6b3**', **7k1,k3,l1**). An example of VEN 3 after 3D reconstruction is shown in **Supplementary Video 3**.

The heterogeneity for layer V VENs in the human CC is also exemplified by morphometric data of the cell body and spiny dendrites. All VENs have a spindle-like cell body and close values of somatic longitudinal axis length. The number of branches and total dendritic length as well as the density of proximal and distal spines are more abundant in VEN 3 (**Figure 8**).

DISCUSSION

Golgi-impregnated VENs show a morphological *continuum* of dendritic and spine features in the human CC. The heterogeneity ranges from few dendritic branches in the main ascending and descending dendritic shafts to a higher arborization with many collateral branches. Differences also occurs for the number, shape, and clustering of dendritic spines from proximal to distal segments. Our results add to the characterization of human CC VENs and have likely implications for the synaptic processing in these cells.

Morphological Implications

First, there are some inherent difficulties for the study of the human *postmortem* brain tissue that contrast with quickly fixed tissue samples from other species, including anoxic and autolytic disturbances beyond control. However, we do not have evidence to support that VENs 1 and 2 are artifacts of a worst Golgi impregnation of the more complex VENs 3. Nor was the case for the previously published data showing similar VENs 1 in the human ACC (Watson et al., 2006). Axons are not usually visible using the present Golgi technique. This might be due to an insulating myelin sheath that precludes their silver impregnation. Alternatively, axons might not be arising exclusively from the cell body and it might not be easy to identify their emergence in dendrites. It is also worth mentioning that the Golgi method randomly impregnates a few cells at each time per studied sample. This precluded further comparisons of the number of VENs and the dendritic spine density in each one of these VENs along with the human lifespan, the likely interindividual variability, or the existence of sex differences in our available samples. These are possibilities open to being investigated in future research (see also Mann et al., 2011).

The present Golgi data expanded the Nissl staining characterization of VENs by providing additional features and the heterogeneity of spiny dendrites in this particular population of neuron. Our data are discussed in the context of the current morphological description of the human VENs. The referential work of Nimchinsky et al. (1995) depicted VENs with closely related cell body shapes but with a certain degree of variation in the CC. Accordingly, a neuron "was considered a spindle cell on Nissl-stained material if it had an ovoid nucleus. . . and if it had a basal dendrite that was at least as thick as its apical dendrite. . . spindle neurons were readily distinguishable from pyramidal neurons and exhibited a variety of morphologies. Some were very slender and elongate, with apical and basal dendrites nearly as thick as the soma at its widest point. Others were shorter, more stout, and usually curved. Occasionally, neurons were encountered with a bifid basal dendrite or a third major dendrite emerging from the soma. In addition, lipofuscin deposits were common and were occasionally so large that they distorted the shape of an otherwise very slender neuron. . . Although only neurons with a truly spindle-like morphology were considered for this study, it is probable that these represent one end of a spectrum ranging in morphology from the classical pyramid to the most narrow spindle cell. The significance of this cellular variability is not clear, but it might be related to the cytoarchitectonic variability in this region. . ." (Nimchinsky et al., 1995). We agree with this description. The same possibility for the morphological feature variability of the VEN dendrites and spines was tested here.

VENs would be a subpopulation of pyramidal neurons or "modified pyramidal neurons" (MPN) (Nimchinsky et al., 1995; González-Acosta et al., 2018). Braak (1979) considered layer Vb "slender pyramids or spindles" as MPN in the class of primitively organized Betz-cells in the anterogenual region of the human telencephalon. Banovac et al. (2019) defined "VENs on Golgi staining as a neuron with the following morphological features: an elongated, stick-like cell body gradually continuing into thick apical and basal stem, a brush-like basal stem arborization and an axon origin distant from the cell body." These authors studied cells in the deep part of layer V and, additionally, in the upper part of layer VI in the human left ACC. Accordingly, other local MPN named "bipolar cells" (although with two primary dendrites, i.e., as multipolar neuron) show an oval soma that is "difficult to distinguish from smaller oval VENs based on the cell body and proximal dendritic morphology. . . However, . . . on bipolar modified pyramidal neurons, the prominent basal dendrite is longer, and its thickness decreases gradually without terminal brush-like branching" Banovac et al. (2019). It is still debatable how a "bipolar MPN" with a clear fusiform cell body might differ completely from layer V VENs.

It is worth noting that different nomenclatures would lead to discrepancies in the study of the same nerve cell. For example, Ramón y Cajal (1909-1911) described the morphology of "giant fusiform cells" in the human cingulate gyrus inner "large pyramidal and giant fusiform cell layer" close to "a deep medium-sized pyramidal cell layer." These "fusiform cells have two dendrites, one of which is very long and seems to ascend to layer 1, whereas the other is sometimes rather long and descends before dividing at acute angles into a number of branches." This description of giant fusiform cells close to large pyramidal neurons resembles that of layer V VENs at the same time that differs from small fusiform neurons in the inner layer VI (Nimchinsky et al., 1999). On the other hand, although showing a heterogeneous dendritic branching pattern, CC VENs are cells whose morphological aspect could be separated from other populations of cortical MPNs. No image for the various cortical MPNs corresponds exactly to the VENs in layer V as presented here (compared to **Figure 2** in Braak, 1980; **Figure 6** in Braak and Braak, 1985). These MPNs "deviate substantially from stereotypical pyramidal cells" to include cells with variations in their cellular processes, i.e., the apical dendrite is only a short and very thin process, basal dendrites that do not always have the same diameter and length, and, sometimes, one basal dendrite may be particularly thick and extend in various directions, or cells with various dendrites generated from the lateral surfaces of the soma (Braak, 1980; Braak and Braak, 1985). For example, MPNs from the multiform layer VI of the isocortex emit only two stout dendrites, "one of them is oriented perpendicular to the cortical surface, the other runs in various directions. These cells are therefore referred to as "a pair of compass cells"...with two main dendrites disposed at different angles to each other... The formation of only two main dendrites gives the cell body a triangular or rhombic contour..." (Braak, 1980). The morphological descriptions of MPNs contrast with those for VENs in layer V, their size, and aspects of the cell body shape as well as the orientation and length of the two main primary dendrite shafts.

The criteria for classifying Golgi-impregnated neurons specifically as VENs by Watson et al. (2006) were "an elongated, large soma in layer 5 of the FI or ACC, a prominent basal dendrite, and symmetrical morphology along the horizontal and vertical axes of the cell..." In this regard, there are 29 human neurons labeled as VENs available at the open database "NeuroMorpho.Org"[2] (version 7.8, released 08/19/2019, content: 112244 neurons). Nine of these reconstructed neurons were from the ACC, and 20 others were from the FI. Three of them show a clear "brush-like" basal dendrite, but 26 others do not display that clearly. No VEN specifically in the ACC shows a prominent brush-like basal dendritic branching in this abovementioned sample. We are thus led to consider that "brush-like" basal dendrites of VENs is one of the possible morphological features for VENs, but it might not be the unique morphological feature for the descending branches. Here, although VEN 3 shows the "brush-like basal stem arborization," the examples of VENs 1 and 2 do not have the same specific "brush-like" basal dendrites (**Figure 8**). Otherwise, from the *continuum* of heterogenic shapes of VENs available at NeuroMorpho.org, it would be assumed that 23, 4, and 2 neurons would be VENs 1, 2, and 3, respectively, with similar characteristics as reported here.

[2]http://neuromorpho.org

Functional Implications

The human CC VENs compose a salience detection/attentional frontoparietal network, which may modulate complex function as self-awareness and social interpersonal relationships (Cauda et al., 2013, 2014 and references therein). These VEN functional properties rely on the features of dendritic branches and spines for proper synaptic integration, strength, and plasticity. Yang et al. (2019) combined laser-capture microdissection with RNA sequencing and described the transcriptomic profile of VENs from the human ACC. These authors used pyramidal neurons as reference cells and found 344 genes with VEN-associated expression differences related to morphogenesis, including dendrite branching and axon myelination, and human social–emotional disorders (Yang et al., 2019). The laminar distribution of synapses in the human CC suggests that VENs may be modulated by different neurotransmitters. For example, the cells in layer Vb show moderate to high expression of glutamate AMPA, NMDA, kainate, and mGluR2/3 excitatory receptors; $GABA_A$ and $GABA_B$ inhibitory receptors; adenosine A1 inhibitory receptors; acetylcholine M1 and M3 excitatory receptors, and M2 inhibitory ones; dopamine D1 excitatory receptor; serotonin 2 excitatory receptor; and noradrenalin/adrenalin α1 excitatory and α2 inhibitory receptors (Palomero-Gallagher and Zilles, 2017). Specifically, VENs in the ACC have dopamine D3 and D5 receptors, serotonin-1b and -2b receptors (Watson, 2006), GABA receptor subunit θ, and adrenoceptor α-1A (Dijkstra et al., 2018). Human VENs also characteristically express the activating transcription factor 3 of the CREB protein family likely involved in stress responses and pain sensitivity; interleukin-4 receptor alpha chain linked to inflammatory and allergic reactions; and neuromedin B related to the digestive homeostatic integration, appetite control, gut feelings, and the modulation of appetite with a possible connection of interoception/visceral states with social awareness (Allman et al., 2010; Stimpson et al., 2011; Raghanti et al., 2015). Few human VENs express markers associated with callosal or corticothalamic projections; rather, they prominently express transcription factors of subcerebral projection FEZF2 and CTIP2, which may reach parasympathetic/sympathetic control sites (Cobos and Seeley, 2015). Respectively, the left and the right ACC have been involved with parasympathetic- and sympathetic-associated emotions (Craig, 2005; Cauda et al., 2014; Guo et al., 2016). Our presently described CC VENs could be tested for these neurochemical and functional profiles and compared to other previous data on VENs and MPNs (e.g., Watson et al., 2006; Banovac et al., 2019). Indeed, the "single-section" Golgi method used here was originally developed in rats to be combined with a variety of histochemical procedures (Gabbott and Somogyi, 1984; adapted for humans by Dall'Oglio et al., 2010; but see also Saper, 2005; Zeba et al., 2008).

Human VENs might be considered computationally simple compared to cortical pyramidal neurons, receiving few inputs

within individual mini-columns, and likely providing a rapid cortical radial signal transmission (Watson et al., 2006). The aspect of VENs 3, with more dendrites and spines than VENs 1, adds a high level of complexity to this field. More dendrites and varied spines can greatly enhance the computational power of neurons (Spruston et al., 2013; Brunel et al., 2014; Rollenhagen and Lübke, 2016). The use of theoretical models to simulate the electrophysiological dynamics of the heterogeneous human neurons is an alternative to presume the functions of VENs 1–3 at this moment (Brunel et al., 2014). In this regard, the geometry and the functional properties of more branched dendrites affect the linear and non-linear neuronal processing of information (Oakley et al., 2001; Spruston et al., 2013; Brunel et al., 2014; Rollenhagen and Lübke, 2016). Neocortical dendrites in humans can also have distinctive biophysical properties for signal processing that can enhance both synaptic charge transfer from dendrites to soma and spike propagation along the axon (Eyal et al., 2016). In addition, the spine activity-driven changes related to synaptic demand, stability, and plasticity can show region-specific and neuron-specific characteristics (Chen et al., 2011; Dall'Oglio et al., 2015; Berry and Nedivi, 2017; Nakahata and Yasuda, 2018). Spines of different shapes and sizes differ in the membrane surface available for different receptors and their trafficking, the local electrical and biochemical compartmentalization, the degree of cooperativity between adjacent spines, and/or the capacity to disperse second messengers into the parent dendrite. That is, spines can control signaling mechanisms at individual synapses (Bourne and Harris, 2008; Chen et al., 2011; Brusco et al., 2014). In prefrontal pyramidal neurons, the density of dendritic spines shows a developmental pruning and dynamic remodeling in each phase of the reorganization of cortical circuitries along the first decades of the human lifespan, becoming more stable afterward (Petanjek et al., 2011). All these mentioned features of dendritic spines are open avenues for further studies on the morphological and functional interplay of human VENs.

The impact of the structure and the functions of the different spine shapes (stubby/wide, thin, mushroom, ramified, or transitional/atypical) for the fine-tuned synaptic processing were depicted elsewhere (Arellano et al., 2007a; Rochefort and Konnerth, 2012; Yuste, 2013; Stewart et al., 2014; Dall'Oglio et al., 2015; Tønnesen and Nägerl, 2016; Lu and Zuo, 2017; Nakahata and Yasuda, 2018). Large dendritic spines usually are more stable, have a large postsynaptic density, and make strong connections, whereas small spines can be rather transient (Woolfrey and Srivastava, 2016) and/or indicative of connections with a lower resistance to reach the parent dendrite (Segal, 2010). Different spine types were observed along the VEN dendrites. Spines ranged from few spines in dendrites of VENs 1 to a high number of clustered spines of varied shapes and sizes along the dendritic branches of VENs 3. Clustered dendritic spines can modulate the cooperative interaction between neighboring synapses (Yadav et al., 2012) and the network function, thus influencing storage capacity, learning, and memory (Frank et al., 2018). Tiny protrusions identified as spinules were also reliably observed in different Golgi-impregnated spine types in the human ACC. Spinules are functional elements that modulate cellular trans-endocytosis (Spacek and Harris, 2004), representing additional possibilities for neuronal plasticity (Tao-Cheng et al., 2009), even as active zone-free invaginating structures (see further data in Petralia et al., 2018). Therefore, the morphological features of VENs 1–3 are suggestive of different properties for spatial and temporal synaptic processing regulated at every spiny dendritic segment. This would provide additional emergent properties for neural circuitries integrated for complex human information processing, as occurs in the human prefrontal cortex (Petanjek et al., 2011) and for the CC roles on attention, emotion, visceral responses, consciousness, social judgments, cognition, and adaptive behaviors (Allman et al., 2001, 2011a; Butti et al., 2013; Cauda et al., 2013, 2014; Raghanti et al., 2015; Vogt, 2015). However, it is also important to consider that the dendritic spine-free zone of cortical pyramidal neurons develops late in phylogenesis and ontogenesis (Braak, 1980), which suggest particularities and specializations for the excitatory and inhibitory synaptic processing along the dendritic segments of neurons with more or less spines (Peters et al., 1991; Spruston, 2008; Chen et al., 2011; Spruston et al., 2013; Dall'Oglio et al., 2015).

The development of specialized VENs can also bring about intrinsic vulnerabilities (Allman et al., 2001; Butti et al., 2013; Cauda et al., 2014). Proteomic analysis indicated that cytoskeletal dysfunction can be considered an important component of the neuropathology of the major psychiatric disorders involving the human ACC (Beasley et al., 2006). The ACC neurons – specifically the VENs in some cases – are more vulnerable and damaged in cases of the behavioral variant of the frontotemporal dementia and hindered social–emotional functions (Kim et al., 2012; Gami-Patel et al., 2019; Lin et al., 2019); schizophrenia (Krause et al., 2017); suicide in victims with psychotic disorders (Brüne et al., 2011); deficits in understanding non-literal language, humor, and scenes of social interactions related to partial or complete agenesis of the corpus callosum; the autism spectrum and bipolar disorders (Raghanti et al., 2015 and references therein); Alzheimer's disease (Gefen et al., 2018); altered cardiac vagal tone (Guo et al., 2016); and self-conscious emotional reactivity (Sturm et al., 2013). When further studying VEN shapes and their normal or altered functioning in brain circuitries, it is also important to consider the ". . .great possibility that interaction between psycho-social environments during brain development results in interindividual differences in brain structure observed later in adult human" (Zeba et al., 2008).

CONCLUSION

The human CC shows a *continuum* of morphological features involving the architecture of dendrites and spines of layer V VENs. Our data add to previous morphological studies on the local cytoarchitectonic organization and propose additional functional possibilities for these neurons. The heterogeneity of VENs in the human CC encourages further studies on how these specialized neurons evolved phylogenetically and develop ontogenetically to provide neural

computations that, within various neural networks, enhance the complexity and integrate the information processing in the human brain.

DATA AVAILABILITY STATEMENT

All datasets generated for this study are included in the article/**Supplementary Material**. Data are public at figshare.com using doi: 10.6084/m9.figshare.11368076.

ETHICS STATEMENT

The studies involving human participants were reviewed and approved by The Brazilian Ethics Committee from the Federal University of Health Sciences of Porto Alegre (UFCSPA; #62336116.6.0000.5345 and 18718719.7.0000.5345). The patients' next of kin provided written informed consent for brain donation for use in this study. Written, informed consent was obtained from the individuals' next of kin for the publication of any potentially identifiable data included in this article.

AUTHOR CONTRIBUTIONS

NC-J, JR, FF-V, AH, and AR-F: study concept and design, acquisition of data, and elaboration of the manuscript. NC-J and AR-F: two-dimensional reconstructions. JR and AR-F: three-dimensional reconstructions. NC-J, JR, FF-V, and AR-F: interpretation of data. All authors contributed to the article and approved the submitted version.

FUNDING

This work was supported by the grants from the Brazilian Agencies CAPES and CNPq (Brazilian Ministry of Science Technology and Innovation) "RRID" (Grant Awards Nos. 481992/2010-3 and 306594/2016-1), SCR_002876.

ACKNOWLEDGMENTS

We thankful to M.Sc. Roman Reberger (Germany) and Dr. Claudio R. Jung (UFRGS, Brazil) for their efforts during the original development of the algorithm for 3D reconstruction of dendritic spines. We also thank due to Dr. Lucila L. Gutierrez (UFCSPA, Brazil) for her participation in the first Golgi experiments.

SUPPLEMENTARY MATERIAL

The Supplementary Material for this article can be found online at: https://www.frontiersin.org/articles/10.3389/fnsyn.2020.00025/full#supplementary-material

VIDEO S1 | Three-dimensional reconstruction of layer V Golgi-impregnated VEN 1 from the human cingulate cortex.

VIDEO S2 | Three-dimensional reconstruction of layer V Golgi-impregnated VEN 2 from the human cingulate cortex.

VIDEO S3 | Three-dimensional reconstruction of layer V Golgi-impregnated VEN 3 from the human cingulate cortex.

REFERENCES

Allman, J. M., Hakeem, A., Erwin, J. M., Nimchinsky, E., and Hof, P. (2001). The anterior cingulate cortex. The evolution of an interface between emotion and cognition. *Ann. New York Acad. Sci.* 935, 107–117. doi: 10.1111/j.1749-6632.2001.tb03476.x

Allman, J. M., Tetreault, N. A., Hakeem, A. Y., Manaye, K. F., Semendeferi, K., Erwin, J. M., et al. (2010). The von Economo neurons in frontoinsular and anterior cingulate cortex in great apes and humans. *Brain Struct. Funct.* 214, 495–517. doi: 10.1007/s00429-010-0254-0

Allman, J. M., Tetreault, N. A., Hakeem, A. Y., Manaye, K. F., Semendeferi, K., Erwin, J. M., et al. (2011a). The von economo neurons in the frontoinsular and anterior cingulate cortex. *Ann. N. Y. Acad. Sci.* 1225, 59–71. doi: 10.1111/j.1749-6632.2011.06011.x

Allman, J. M., Tetreault, N. A., Hakeem, A. Y., and Park, S. (2011b). The von Economo neurons in apes and humans. *Am. J. Hum. Biol.* 23, 5–21. doi: 10.1002/ajhb.21136

Arellano, J. I., Benavides-Piccione, R., DeFelipe, J., and Yuste, R. (2007a). Ultrastructure of dendritic spines: correlation between synaptic and spine morphologies. *Front. Neurosci.* 1:131–143. doi: 10.3389/neuro.01.1.1.010.2007

Arellano, J. I., Espinosa, A., Fairén, A., Yuste, R., and DeFelipe, J. (2007b). Non-synaptic dendritic spines in neocortex. *Neuroscience* 145, 464–469. doi: 10.1016/j.neuroscience.2006.12.015

Banovac, I., Sedmak, D., Džaja, D., Jalšovec, D., Jovanov Miloševiæ, N., Rašin, M. R., et al. (2019). Somato-dendritic morphology and axon origin site specify von Economo neurons as a subclass of modified pyramidal neurons in the human anterior cingulate cortex. *J. Anat.* 235, 651–669. doi: 10.1111/joa.13068

Beasley, C. L., Pennington, K., Behan, A., Wait, R., Dunn, M. J., and Cotter, D. (2006). Proteomic analysis of the anterior cingulate cortex in the major psychiatric disorders: evidence for disease-associated changes. *Proteomics* 6, 3414–3425. doi: 10.1002/pmic.200500069

Berry, K. P., and Nedivi, E. (2017). Spine dynamics: are they all the same? *Neuron* 96, 43–55. doi: 10.1016/j.neuron.2017.08.008

Bourne, J. N., and Harris, K. M. (2008). Balancing structure and function at hippocampal dendritic spines. *Ann. Rev. Neurosci.* 31, 47–67. doi: 10.1146/annurev.neuro.31.060407.125646

Braak, H. (1979). Pigment architecture of the human telencephalic cortex. V. Regio anterogenualis. *Cell Tissue Res.* 204, 441–451. doi: 10.1007/bf00233655

Braak, H. (1980). *Architectonics of the Human Telencephalic Cortex*. Berlin: Springer-Verlag.

Braak, H., and Braak, E. (1985). Golgi preparations as a tool in neuropathology with particular reference to investigations of the human telencephalic cortex. *Prog. Neurobiol.* 25, 93–139. doi: 10.1016/0301-0082(85)90001-2

Brüne, M., Schöbel, A., Karau, R., Faustmann, P. M., Dermietzel, R., Juckel, G., et al. (2011). Neuroanatomical correlates of suicide in psychosis: the possible role of von Economo neurons. *PLoS One* 6:e20936. doi: 10.1371/journal.pone.0020936

Brunel, N., Hakim, V., and Richardson, M. J. R. (2014). Single neuron dynamics and computation. *Curr. Opt. Neurobiol.* 25, 149–155.

Brusco, J., Dall'Oglio, A., Rocha, L. B., Rossi, M. A., Moreira, J. E., and Rasia-Filho, A. A. (2010). Descriptive findings on the morphology of dendritic spines in the rat medial amygdala. *Neurosci. Lett.* 483, 152–156. doi: 10.1016/j.neulet.2010.07.083

Brusco, J., Merlo, S., Ikeda, É, T., Petralia, R. S., Kachar, B., Rasia-Filho, A. A., et al. (2014). Inhibitory and multisynaptic spines, and hemispherical synaptic

specialization in the posterodorsal medial amygdala of male and female rats. *J. Comp. Neurol* 522, 2075–2088. doi: 10.1002/cne.23518

Butti, C., Santos, M., Uppal, N., and Hof, P. R. (2013). von Economo neurons: clinical and evolutionary perspectives. *Cortex* 49, 312–326. doi: 10.1016/j.cortex.2011.10.004

Carrabba, L. H. G., Menta, C., Fasolin, E. M., Loureiro, F., and Gomes, I. (2015). Características psicométricas das versões completa e reduzida do IQCODE-BR em idosos de baixa renda e escolaridade. *Rev. Bras. Geriat. Gerontol.* 18, 715–723. doi: 10.1590/1809-9823.2015.14034

Cauda, F., Torta, D. M. E., Sacco, K., D'Agata, F., Geda, E., Duca, S., et al. (2013). Functional anatomy of cortical áreas characterized by Von Economo neurons. *Brain Struct. Funct.* 218, 1–20. doi: 10.1007/s00429-012-0382-9

Cauda, F., Geminiani, G. C., and Vercelli, A. (2014). Evolutionary appearance of von Economo's neurons in the mammalian cerebral cortex. *Front. Hum. Neurosci.* 8:104. doi: 10.3389/fnhum.2014.00104

Chen, X., Leischner, U., Rochefort, N. L., Nelken, I., and Konnerth, A. (2011). Functional mapping of single spines in cortical neurons in vivo. *Nature* 475, 501–505. doi: 10.1038/nature10193

Cobos, I., and Seeley, W. W. (2015). Human von Economo neurons express transcription factors associated with Layer V subcerebral projection neurons. *Cereb. Cortex* 25, 213–220. doi: 10.1093/cercor/bht219

Craig, A. D. (2002). How do you feel? Interoception: the sense of the physiological condition of the body. *Nat. Rev. Neurosci.* 3, 655–666. doi: 10.1038/nrn894

Craig, A. D. (2005). Forebrain emotional asymmetry: a neuroanatomical basis? *Trends Cogn. Sci.* 9, 566–571. doi: 10.1016/j.tics.2005.10.005

Dall'Oglio, A., Dutra, A. C., Moreira, J. E., and Rasia-Filho, A. A. (2015). The human medial amygdala: structure, diversity, and complexity of dendritic spines. *J. Anat.* 227, 440–459. doi: 10.1111/joa.12358

Dall'Oglio, A., Ferme, D., Brusco, J., Moreira, J. E., and Rasia-Filho, A. A. (2010). The "single-section" Golgi method adapted for formalin-fixed human brain and light microscopy. *J. Neurosci. Methods* 189, 51–55. doi: 10.1016/j.jneumeth.2010.03.018

Dall'Oglio, A., Xavier, L. L., Hilbig, A., Ferme, D., Moreira, J. E., Achaval, M., et al. (2013). Cellular components of the human medial amygdaloid nucleus. *J. Comp. Neurol.* 521, 589–611. doi: 10.1002/cne.23192

Dijkstra, A. A., Lin, L. C., Nana, A. L., Gaus, S. E., and Seeley, W. W. (2018). von Economo neurons and fork cells: a neurochemical signature linked to monoaminergic function. *Cereb. Cortex* 28, 131–144. doi: 10.1093/cercor/bhw358

Eyal, G., Verhoog, M. B., Testa-Silva, G., Deitcher, Y., Lodder, J. C., Benavides-Piccione, R., et al. (2016). Unique membrane properties and enhanced signal processing in human neocortical neurons. *eLife* 5:e16553. doi: 10.7554/eLife.16553

Fajardo, C., Escobar, M. I., Buriticá, E., Arteaga, G., Umbarila, J., Casanova, M. F., et al. (2008). von Economo neurons are present in the dorsolateral (dysgranular) prefrontal cortex of humans. *Neurosci. Lett.* 435, 215–218. doi: 10.1016/j.neulet.2008.02.048

Feldman, M. L. (1984). "Morphology of the neocortical pyramidal neuron," in *Cerebral Cortex*, eds E. G. Jones, and A. Peters, (New York, NY: Plenum Press), 107–121.

Fiala, J. C., and Harris, K. M. (1999). "Dendrite structure," in *Dendrites*, eds G. Stuart, N. Spruston, and M. Häusser, (New York, NY: Oxford University Press), 1–34.

Fiala, J. C., Spacek, J., and Harris, K. M. (2002). Dendritic spine pathology: cause or consequence of neurological disorders? *Brain Res. Rev.* 39, 29–54. doi: 10.1016/s0165-0173(02)00158-3

Frank, A. C., Huang, S., Zhou, M., Gdalyahu, A., Kastellakis, G., Silva, T. K., et al. (2018). Hotspots of dendritic spine turnover facilitate clustered spine addition and learning and memory. *Nat. Commun.* 9:422. doi: 10.1038/s41467-017-02751-2

Gabbott, P. L., Jays, P. R., and Bacon, S. J. (1997). Calretinin neurons in human medial prefrontal cortex (areas 24a,b,c, 32', and 25). *J. Comp. Neurol.* 381, 389–410. doi: 10.1002/(sici)1096-9861(19970519)381:4<389::aid-cne1>3.0.co;2-z

Gabbott, P. L., and Somogyi, J. (1984). The 'single' section Golgi-impregnation procedure: methodological description. *J. Neurosci. Methods* 11, 221–230. doi: 10.1016/0165-0270(84)90084-0

Gami-Patel, P., van Dijken, I., van Swieten, J. C., Pijnenburg, Y. A. L., Netherlands Brain Bank, Rozemuller, A. J. M., et al. (2019). Von Economo neurons are part of a larger neuronal population that are selectively vulnerable in C9orf72 frontotemporal dementia. *Neuropathol. Appl. Neurobiol.* 45, 671–680. doi: 10.1111/nan.12558

Gefen, T., Papastefan, S. T., Rezvanian, A., Bigio, E. H., Weintraub, S., Rogalski, E., et al. (2018). Von Economo neurons of the anterior cingulate across the lifespan and in Alzheimer's disease. *Cortex* 99, 69–77. doi: 10.1016/j.cortex.2017.10.015

Glasser, M. F., Coalson, T. S., Robinson, E. C., Hacker, C. D., Harwell, J., Yacoub, E., et al. (2016). A multi-modal parcellation of human cerebral cortex. *Nature* 536, 171–178.

González-Acosta, C. A., Escobar, M. I., Casanova, M. F., Pimienta, H. J., and Buriticá, E. (2018). Von Economo neurons in the human medial frontopolar cortex. *Front. Neuroanat.* 12:64. doi: 10.3389/fnana.2018.00064

González-Ramírez, M. M., Velázquez-Zamora, D. A., Olvera-Cortés, M. E., and González-Burgos, I. (2014). Changes in the plastic properties of hippocampal dendritic spines underlie the attenuation of place learning in healthy aged rats. *Neurobiol. Learn. Mem.* 109, 94–103. doi: 10.1016/j.nlm.2013.11.017

Guo, C. C., Sturm, V. E., Zhou, J., Gennatas, E. D., Trujillo, A. J., Hua, A. Y., et al. (2016). Dominant hemisphere lateralization of cortical parasympathetic control as revealed by frontotemporal dementia. *Proc. Natl. Acad. Sci. U.S.A.* 113, E2430–E2439.

Hayashi-Takagi, A., Yagishita, S., Nakamura, M., Shirai, F., Wu, Y. I., Loshbaugh, A. L., et al. (2015). Labelling and optical erasure of synaptic memory traces in the motor cortex. *Nature* 525, 333–338. doi: 10.1038/nature15257

Herms, J., and Dorostkar, M. M. (2016). Dendritic spine pathology in neurodegenerative diseases. *Ann. Rev. Pathol.* 11, 221–250. doi: 10.1146/annurev-pathol-012615-044216

Kim, E. J., Sidhu, M., Gaus, S. E., Huang, E. J., Hof, P. R., Miller, B. L., et al. (2012). Selective frontoinsular von Economo neuron and fork cell loss in early behavioral variant frontotemporal dementia. *Cereb. Cortex* 22, 251–259. doi: 10.1093/cercor/bhr004

Kolb, B., and Whishaw, I. Q. (2015). *Fundamentals of Human Neuropsychology*. New York, NY: Worth Publishers.

Krause, M., Theiss, C., and Brüne, M. (2017). Ultrastructural alterations of von Economo neurons in the anterior cingulate cortex in schizophrenia. *Anat. Rec.* 300, 2017–2024. doi: 10.1002/ar.23635

Lin, L. C., Nana, A. L., Hepker, M., Hwang, J. L., Gaus, S. E., Spina, S., et al. (2019). Preferential tau aggregation in von economo neurons and fork cells in frontotemporal lobar degeneration with specific MAPT variants. *Acta Neuropathol. Commun.* 7:159.

Lu, J., and Zuo, Y. (2017). Clustered structural and functional plasticity of dendritic spines. *Brain Res. Bull.* 129, 18–22. doi: 10.1016/j.brainresbull.2016.09.008

Mai, J. K., Paxinos, G., and Voss, T. (2008). *Atlas of the Human Brain*. New York, NY: Academic Press.

Mann, S. L., Hazlett, E. A., Byne, W., Hof, P. R., Buchsbaum, M. S., Cohen, B. H., et al. (2011). Anterior and posterior cingulate cortex volume in healthy adults: effects of aging and gender differences. *Brain Res.* 1401, 18–29. doi: 10.1016/j.brainres.2011.05.050

Myatt, D. R., Hadlington, T., Ascoli, G. A., and Nasuto, S. J. (2012). Neuromantic - from semi-manual to semi-automatic reconstruction of neuron morphology. *Front. Neuroinformat.* 6:4. doi: 10.3389/fninf.2012.00004

Nakahata, Y., and Yasuda, R. (2018). Plasticity of spine structure: Local signaling, translation and cytoskeletal reorganization. *Front. Synaptic Neurosci.* 10:29. doi: 10.3389/fnsyn.2018.00029

Neto, E. R., Fonseca, M. K., Guedes, A. C. B., Oliveira, F. H., Hilbig, A., and Fernandez, L. L. (2017). Neuropathological findings in entorhinal cortex of subjects aged 50 years or older and their correlation with dementia in a sample from Southern Brazil. *Dem. Neuropsychol.* 11, 24–31. doi: 10.1590/1980-57642016dn11-010005

Nieuwenhuys, R., Voogd, J., and van Huijzen, C. (1988). *The Human Central Nervous System*. Berlin: Springer-Verlag.

Nimchinsky, E. A., Gilissen, E., Allman, J. M., Perl, D. P., Erwin, J. M., and Hof, P. R. (1999). A neuronal morphologic type unique to humans and great apes. *Proc.Natl. Acad. Sci. U.S.A.* 96, 5268–5273. doi: 10.1073/pnas.96.9.5268

Nimchinsky, E. A., Vogt, B. A., Morrison, J. H., and Hof, P. R. (1995). Spindle neurons of the human anterior cingulate cortex. *J. Comp. Neurol.* 355, 27–37.

Oakley, J. C., Schwindt, P. C., and Crill, W. E. (2001). Dendritic calcium spikes in layer 5 pyramidal neurons amplify and limit transmission of ligand gated dendritic current to soma. *J. Neurophysiol.* 86, 514–527. doi: 10.1152/jn.2001.86.1.514

Palomero-Gallagher, N., and Zilles, K. (2017). Cortical layers: Cyto-, myelo-, receptor- and synaptic architecture in human cortical areas. *Neuroimage* S1053-8119, 30682–30691. doi: 10.1016/j.neuroimage.2017.08.035

Pandya, D. N., Seltzer, B., Petrides, M., and Cipolloni, P. B. (2015). *Cerebral Cortex – Architecture, Connections, and the Dual Origin Concept*. New York, NY: Oxford University Press.

Parekh, R., and Ascoli, G. A. (2013). Neuronal morphology goes digital: a research hub for cellular and system neuroscience. *Neuron* 77, 1017–1038. doi: 10.1016/j.neuron.2013.03.008

Penzes, P., Cahill, M. E., Jones, K. A., VanLeeuwen, J. E., and Woolfrey, K. M. (2011). Dendritic spine pathology in neuropsychiatric disorders. *Nat. Neurosci.* 14, 285–293. doi: 10.1038/nn.2741

Petanjek, Z., Judaš, M., Šimic, G., Rasin, M. R., Uylings, H. B., Rakic, P., et al. (2011). Extraordinary neoteny of synaptic spines in the human prefrontal cortex. *Proc. Natl. Acad. Sci. U.S.A.* 108, 13281–13286. doi: 10.1073/pnas.1105108108

Peters, A., Palay, S. L., and Webster, H. (1991). *The Fine Structure of the Nervous System*. New York, NY: Oxford University Press.

Petralia, R. S., Wang, Y. X., Mattson, M. P., and Yao, P. J. (2018). Invaginating structures in mammalian synapses. *Front. Synaptic Neurosci.* 10:4. doi: 10.3389/fnsyn.2018.00004

Raghanti, M. A., Spurlock, L. B., Uppal, N., Sherwood, C. C., Butti, C., and Hof, P. R. (2015). "von Economo neurons," in *Brain Mapping: An Encyclopedic Reference*, eds K. Zilles and K. Amunts (Amsterdam: Elsevier Inc), 81–91.

Ramón y Cajal (1909-1911). "Histologie Du système nerveux De l'Homme Et Des Vertebrés," in *Paris: Maloine. Translated to English*, eds Swanson, and Swanson, (New York, NY: Oxford University Press).

Ramón-Moliner, E. (1962). An attempt at classifying nerve cells on the basis of their dendritic patterns. *J. Comp.Neurol.* 119, 211–227.

Rangwala, S., Tobin, M., Birk, D., Butts, J. T., Nikas, D., and Hahn, Y. S. (2017). Pica in a child with anterior cingulate gyrus oligodendroglioma: case report. *Ped. Neurosurg.* 52, 279–283. doi: 10.1159/000477816

Reberger, R., DallOglio, A., Jung, C. R., and Rasia-Filho, A. A. (2018). Structure and diversity of human dendritic spines evidenced by a new three-dimensional reconstruction procedure for Golgi staining and light microscopy. *J. Neurosci. Methods* 293, 27–36. doi: 10.1016/j.jneumeth.2017.09.001

Rochefort, N. L., and Konnerth, A. (2012). Dendritic spines: from structure to in vivo function. *EMBO Rep.* 13, 699–708. doi: 10.1038/embor.2012.102

Rollenhagen, A., and Lübke, J. H. R. (2016). "Dendritic Elaboration: morphology and chemistry," in *Neuroscience in the 21st Century*, eds D. W. Pfaff, and N. D. Volkow, (New York, NY: Springer), 225–264. doi: 10.1007/978-1-4939-3474-4_11

Sanchez, M. A. S., and Lourenço, R. A. (2009). Informant questionnaire on cognitive decline in the elderly (IQCODE): adaptação transcultural para uso no Brasil. *Cad. Saúde Púb.* 25, 1455–1465. doi: 10.1590/s0102-311x2009000700003

Saper, C. B. (2005). Editorial: an open letter to our readers on the use of antibodies. *J. Comp. Neurol.* 493, 477–478. doi: 10.1002/cne.20839

Schindelin, J., Arganda-Carreras, I., Frise, E., Kaynig, V., Longair, M., Pietzsch, T., et al. (2012). Fiji: an open-source platform for biological-image analysis. *Nat. Methods* 9, 676–682. doi: 10.1038/nmeth.2019

Scorcioni, R., Polavaram, S., and Ascoli, G. A. (2008). L-Measure: a web-accessible tool for the analysis, comparison and search of digital reconstructions of neuronal morphologies. *Nat. Prot.* 3, 866–876. doi: 10.1038/nprot.2008.51

Seeley, W. W., Merkle, F. T., Gaus, S. E., Craig, A. D., Allman, J. M., and Hof, P. R. (2012). Distinctive neurons of the anterior cingulate and frontoinsular cortex: a historical perspective. *Cereb. Cortex* 22, 245–250. doi: 10.1093/cercor/bhr005

Segal, M. (2010). Dendritic spines, synaptic plasticity and neuronal survival: activity shapes dendritic spines to enhance neuronal viability. *Eur. J. Neurosci.* 31, 2178–2184. doi: 10.1111/j.1460-9568.2010.07270.x

Spacek, J., and Harris, K. M. (2004). Trans-endocytosis via spinules in adult rat hippocampus. *J. Neurosci.* 24, 4233–4241. doi: 10.1523/jneurosci.0287-04.2004

Spruston, N. (2008). Pyramidal neurons: dendritic structure and synaptic integration. *Nat. Rev. Neurosci.* 9, 206–221. doi: 10.1038/nrn2286

Spruston, N., Häusser, M., and Stuart, G. (2013). "Information processing in dendrites and spines," in *Fundamental Neuroscience*, eds L. R. Squire, D. Berg, F. E. Bloom, S. du Lac, A. Ghosh, and N. C. Spitzer, (Waltham: Academic Press), 231–260. doi: 10.1016/b978-0-12-385870-2.00011-1

Stewart, M. G., Popov, V. I., Kraev, I. V., Medvedev, N., and Davies, H. A. (2014). "Structure and complexity of the synapse and dendritic spine," in *The Synapse*, eds V. Pickel, and M. Segal, (New York, NY: Academic Press), 1–20. doi: 10.1016/b978-0-12-418675-0.00001-8

Stimpson, C. D., Tetreault, N. A., Allman, J. M., Jacobs, B., Butti, C., Hof, P. R., et al. (2011). Biochemical specificity of von Economo neurons in hominoids. *Am. J. Hum. Biol.* 23, 22–28. doi: 10.1002/ajhb.21135

Sturm, V. E., Sollberger, M., Seeley, W. W., Rankin, K. P., Ascher, E. A., Rosen, H. J., et al. (2013). Role of right pregenual anterior cingulate cortex in self-conscious emotional reactivity. *Soc. Cogn. Affect. Neurosci.* 8, 468–474. doi: 10.1093/scan/nss023

Talairach, J., and Tournoux, P. (1993). *Referentially Oriented Cerebral MRI Anatomy: An Atlas of Stereotaxic Anatomical Correlations for Gray and White Matter*. New York, NY: Thieme Medical Publishers.

Tao-Cheng, J.-H., Dosemeci, A., Gallant, P. E., Miller, S., Galbraith, J. A., Winters, C. A., et al. (2009). Rapid turnover of spinules at synaptic terminals. *Neuroscience* 160, 42–50. doi: 10.1016/j.neuroscience.2009.02.031

Tønnesen, J., and Nägerl, V. (2016). Dendritic spines as tunable regulators of synaptic signals. *Front. Psych.* 7:101. doi: 10.3389/fpsyt.2016.00101

Triarhou, L. C. (2009). *von Economo and Koskinas' Atlas of Cytoarchitectonics of the Adult Human Cerebral Cortex*. Basel: Karger.

Vásquez, C. E., Reberger, R., Dall'Oglio, A., Calcagnotto, M. E., and Rasia-Filho, A. A. (2018). Neuronal types of the human cortical amygdaloid nucleus. *J. Comp. Neurol.* 526, 2776–2801. doi: 10.1002/cne.24527

Vogt, B. A. (2015). "Mapping cingulate subregions," in *Brain Mapping: An Encyclopedic Reference*, ed. A. W. Toga, (Oxford: Academic Press), 325–339. doi: 10.1016/b978-0-12-397025-1.00230-x

Watson, K. K. (2006). *The von Economo Neurons: From cells to Behavior*. Ph.D Thesis, California Institute of Technology, Pasadena, CA.

Watson, K. K., Jones, T. K., and Allman, J. M. (2006). Dendritic architecture of the von Economo neurons. *Neuroscience* 141, 1107–1112. doi: 10.1016/j.neuroscience.2006.04.084

Woolfrey, K. M., and Srivastava, D. P. (2016). Control of dendritic spine morphological and functional plasticity by small GTPases. *Neural Plast.* 2016:3025948. doi: 10.1155/2016/3025948

Xuan, B., Mackie, M. A., Spagna, A., Wu, T., Tian, Y., Hof, P. R., et al. (2016). The activation of interactive attentional networks. *NeuroImage* 129, 308–319. doi: 10.1016/j.neuroimage.2016.01.017

Yadav, A., Gao, Y. Z., Rodriguez, A., Dickstein, D. L., Wearne, S. L., Luebke, J. I., et al. (2012). Morphologic evidence for spatially clustered spines in apical dendrites of monkey neocortical pyramidal cells. *J. Comp. Neurol.* 520, 2888–2902. doi: 10.1002/cne.23070

Yang, L., Yang, Y., Yuan, J., Sun, Y., Dai, J., and Su, B. (2019). Transcriptomic landscape of von Economo neurons in human anterior cingulate cortex revealed by microdissected-cell RNA sequencing. *Cereb. Cortex* 29, 838–851. doi: 10.1093/cercor/bhy286

Yuste, R. (2013). Electrical compartmentalization in dendritic spines. *Ann. Rev. Neurosci.* 36, 429–449. doi: 10.1146/annurev-neuro-062111-150455

Zeba, M., Jovanov-Miloseviæ, N., and Petanjek, Z. (2008). Quantitative analysis of basal dendritic tree of layer III pyramidal neurons in different areas of adult human frontal cortex. *Coll. Antropol.* 32(Suppl. 1), 161–169.

Conflict of Interest: The authors declare that the research was conducted in the absence of any commercial or financial relationships that could be construed as a potential conflict of interest.

frontiers in Synaptic Neuroscience

MINI REVIEW
published: 10 July 2020
doi: 10.3389/fnsyn.2020.00026

Bidirectional Dysregulation of AMPA Receptor-Mediated Synaptic Transmission and Plasticity in Brain Disorders

Hongyu Zhang[*†‡] *and Clive R. Bramham*[*†]

Department of Biomedicine, University of Bergen, Bergen, Norway

AMPA receptors (AMPARs) are glutamate-gated ion channels that mediate the majority of fast excitatory synaptic transmission throughout the brain. Changes in the properties and postsynaptic abundance of AMPARs are pivotal mechanisms in synaptic plasticity, such as long-term potentiation (LTP) and long-term depression (LTD) of synaptic transmission. A wide range of neurodegenerative, neurodevelopmental and neuropsychiatric disorders, despite their extremely diverse etiology, pathogenesis and symptoms, exhibit brain region-specific and AMPAR subunit-specific aberrations in synaptic transmission or plasticity. These include abnormally enhanced or reduced AMPAR-mediated synaptic transmission or plasticity. Bidirectional reversal of these changes by targeting AMPAR subunits or trafficking ameliorates drug-seeking behavior, chronic pain, epileptic seizures, or cognitive deficits. This indicates that bidirectional dysregulation of AMPAR-mediated synaptic transmission or plasticity may contribute to the expression of many brain disorders and therefore serve as a therapeutic target. Here, we provide a synopsis of bidirectional AMPAR dysregulation in animal models of brain disorders and review the preclinical evidence on the therapeutic targeting of AMPARs.

Keywords: AMPA receptor (AMPAR), synaptic transmission and plasticity, AMPAR trafficking, neurodegenarative diseases, neuropsychiatric disorders, neurodevelopmental disorders

OPEN ACCESS

Edited by:
Carlos B. Duarte,
University of Coimbra, Portugal

Reviewed by:
Graham Hugh Diering,
University of North Carolina at Chapel Hill, United States
Marina E. Wolf,
Oregon Health and Science University, United States

***Correspondence:**
Hongyu Zhang
hongyu.zhang@uib.no
Clive R. Bramham
clive.bramham@uib.no

[†]***ORCID:***
Hongyu Zhang
orcid.org/0000-0001-7152-001X
Clive R. Bramham
orcid.org/0000-0001-5958-7115

[‡]*Lead Contact*

Received: *26 March 2020*
Accepted: *28 May 2020*
Published: *10 July 2020*

Citation:
Zhang H and Bramham CR (2020) Bidirectional Dysregulation of AMPA Receptor-Mediated Synaptic Transmission and Plasticity in Brain Disorders. Front. Synaptic Neurosci. 12:26. doi: 10.3389/fnsyn.2020.00026

INTRODUCTION

Synaptic plasticity is central to memory and other adaptive responses of adult neural circuits. NMDA receptor (NMDAR)-dependent long-term potentiation (LTP) and long-term depression (LTD) are triggered by the activation of NMDARs but expressed by an increase or decrease in the abundance of AMPA receptors (AMPARs) at the postsynaptic membrane, respectively. Postsynaptic LTD induced by the activation of group I metabotropic glutamate receptors (mGluR-LTD) is similarly expressed by a reduction in the number of postsynaptic AMPARs (Luscher and Huber, 2010). AMPARs are tetrameric complexes composed of GluA1, GluA2, GluA3, or GluA4 subunits, with GluA1/2 heteromers dominant at hippocampal CA1 synapses. The number and composition of postsynaptic AMPARs are in a dynamic balance, which is achieved by AMPAR trafficking. AMPAR trafficking involves intracellular transport, endo-/exo-cytosis, recycling, lateral surface diffusion, and degradation (Choquet, 2018). Newly synthesized receptors are transported intracellularly on microtubules from soma to dendrites. Through exocytosis/endocytosis, AMPARs cycle between intracellular and surface pools. Recycling refers to the process by which endocytosed

receptors are returned to the cell surface *via* exocytosis. Surface AMPARs exchange between synaptic and extrasynaptic compartments *via* lateral diffusion and are reversibly trapped at synapses by postsynaptic scaffold proteins, cytoskeletal proteins, adhesion proteins, or extracellular matrix. This continuous exchange of receptors between different pools establishes a dynamic equilibrium (**Figure 1**, top panel). This balance can be shifted in response to neuronal/synaptic activity (Opazo and Choquet, 2011). For example, during LTP, AMPARs are selectively recruited, by lateral diffusion, to the postsynaptic membrane to increase synaptic strength, while exocytosed AMPARs serve as an extrasynaptic reservoir (Makino and Malinow, 2009; Penn et al., 2017). Conversely, during LTD, AMPARs are dispersed, through endocytosis, from the postsynaptic membrane to reduce synaptic transmission. Thus, synaptic strength at single synapses is bidirectionally regulated *via* AMPAR trafficking.

Increasing evidence shows that learning and memory can be modified at the cellular and molecular levels by acute modulation of LTP, LTD, or AMPAR trafficking. For example, fear memory established by associating a foot-shock with optogenetic stimulation of auditory inputs to the amygdala was inactivated by subsequent optogenetic delivery of LTD to the conditioned auditory input and further reactivated by optogenetic delivery of LTP (Nabavi et al., 2014). Moreover, PhotonSABER, an optogenetic tool developed to inhibit AMPAR endocytosis during LTD in a light-dependent manner, was applied in Purkinje cells and inhibited cerebellar motor learning (Kakegawa et al., 2018). Furthermore, immobilization of surface AMPARs by crosslinking approaches markedly impaired hippocampal LTP *in vivo* and also inhibited contextual fear conditioning (Penn et al., 2017). These results support a causal contribution of AMPAR trafficking and synaptic plasticity to learning and memory. Second, they suggest that learning and memory can be manipulated at the molecular level (AMPARs trafficking), as well as at the cellular level by induction of LTP or LTD.

Notably, the dynamic equilibrium of AMPAR trafficking can also be shifted under pathological conditions (**Figure 1**, bottom left and bottom right panels). Increasing evidence suggests that brain region-specific and AMPAR subunit-specific aberrant enhancement or reduction in synaptic transmission or plasticity occurs with many neurodegenerative, neurodevelopmental, and neuropsychiatric disorders. A reversal of these aberrations ameliorates drug-seeking behavior, chronic pain, epileptic seizures, or cognitive deficits. Although the etiology, pathogenesis, and symptoms vary greatly between disorders, the observed restoration of function and mitigation of symptoms suggest that dysregulation of AMPAR-mediated synaptic transmission and plasticity is a convergence point for multiple pathological pathways, rather than a compensatory protective mechanism.

Below, we review the evidence of brain region-specific and AMPAR subunit-specific bidirectional dysregulation of AMAPR-mediated synaptic transmission and plasticity in animal models of several of the most common neurodegenerative, neurodevelopmental and neuropsychiatric disorders. We also review the therapeutic effects exerted by targeting AMPAR subunits or trafficking. We propose that, despite the highly diverse underlying pathologies, dysregulation of AMPARs is a common mechanism in the expression of different diseases, and bidirectional therapeutic targeting of AMPARs may be a promising mitigation strategy for various diseases. Lastly, we discuss the potential therapeutic application of small interfering peptides and aptamers, as well as the need for new optogenetic and optopharmacological tools for elucidating the molecular mechanisms and spatial-temporal dynamics of AMPA regulation in animal models of brain disorders.

Addiction

Addiction is a psychological and physical inability to stop consuming a chemical, despite adverse consequences. Many addictive drugs induce changes in the synaptic composition of AMPARs and alter synaptic plasticity within reward circuitry, such as the ventral tegmental area (VTA), nucleus accumbens (NAc), prefrontal cortex (PFC), dorsal medial striatum (DMS), and amygdala (Ungless et al., 2001; Saal et al., 2003; Wolf, 2016; Cooper et al., 2017). These drugs include cocaine (Conrad et al., 2008), delta(9)-tetrahydrocannabinol (Good and Lupica, 2010), methamphetamine (Scheyer et al., 2016), amphetamine (Saal et al., 2003), benzodiazepines (Tan et al., 2010), nicotine (Marchi et al., 2015), morphine (Madayag et al., 2019), heroin (Van den Oever et al., 2008), and alcohol (Ma et al., 2018). For instance, cocaine exposure or self-administration induced silent synapses, which do not contain AMPARs but only NMDARs, in NAc (Ma et al., 2014; Huang et al., 2015). However, extended withdrawal (e.g., 30–45 days) from cocaine self-administration resulted in the unsilencing of synapses *via* the synaptic insertion of Ca^{2+}-permeable (CP) GluA2-lacking AMPARs. This indicated that CP-AMPARs do not primarily mediate drug-seeking *per se*, but rather contribute to withdrawal-dependent enhancement (incubation) of cocaine-seeking behavior (Conrad et al., 2008; Lee et al., 2013; Ma et al., 2014; Scheyer et al., 2016). Optogenetically induced LTD resulting in CP-AMPAR removal from amygdala-to-NAc synapses attenuated incubation of cocaine craving (Lee et al., 2013). Besides, the application of a mGluR1 positive allosteric modulator, by removing CP-AMPARs from NAc synapses, also reduced the expression of incubated cocaine craving (Loweth et al., 2014). Further evidence suggested that, depending on the input pathway, synaptic insertion of non-CP-AMPARs also underlies cocaine-seeking behavior. In one study, extended cocaine withdrawal evoked the insertion of CP-AMPARs in NAc synapses receiving input from medial PFC, whereas non-CP-AMPARs were inserted at synapses with input from the ventral hippocampus. Optogenetic reversal of plasticity at both inputs abolished cocaine seeking (Pascoli et al., 2014). In another study, extended cocaine withdrawal induced CP-AMPAR insertion in NAc synapses with infralimbic (IL) mPFC input, whereas non-CP-AMPARs were inserted at synapses with prelimbic (PrL) mPFC input. Optogenetic reversal of the plasticity of IL-to-NAc and PrL- to-NAc projections enhanced and reduced, respectively, incubation of cocaine craving (Ma et al., 2014), suggesting a circuit-dependent mechanism. Moreover, optogenetic LTP and LTD induction at projections from mPFC to DMS

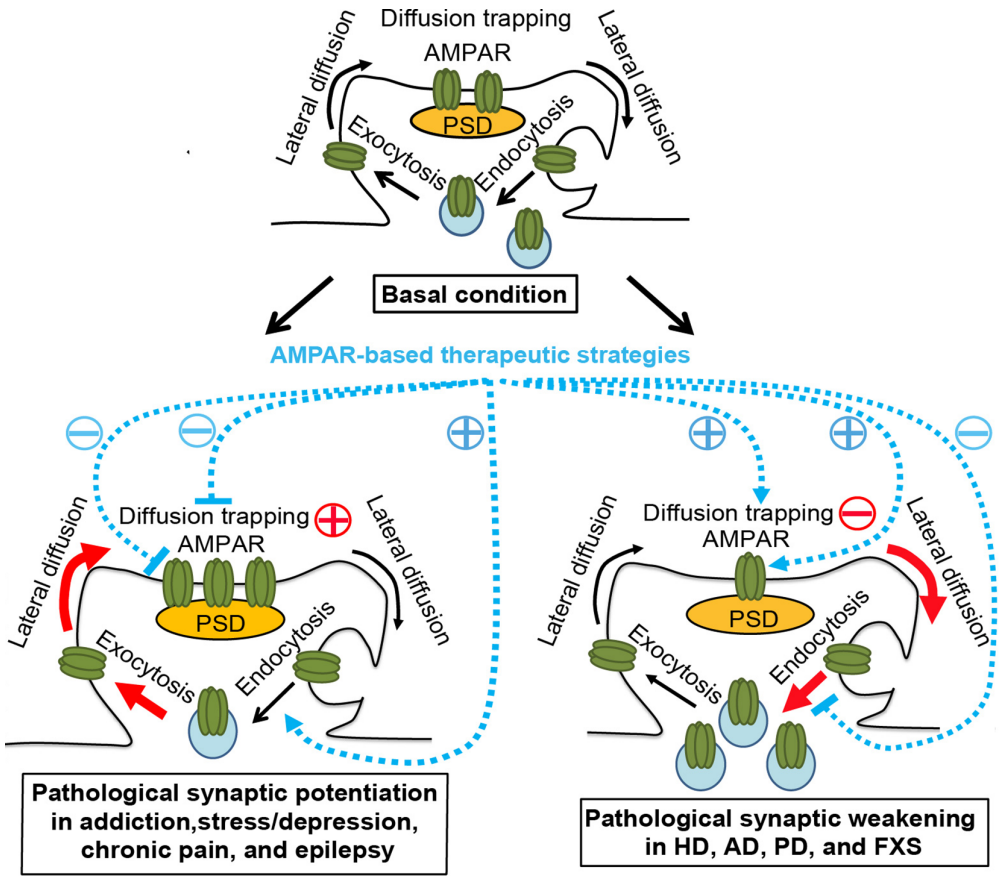

FIGURE 1 | AMPAR trafficking under physiological and pathological conditions and AMPAR-based therapeutic strategies. **Top panel**, basal condition. AMPARs constitutively cycle between intracellular pools and the neuronal surface *via* endocytosis and exocytosis. At the plasma membrane, AMPARs bidirectionally exchange between extrasynaptic and synaptic compartments by lateral diffusion, powered by thermal agitation. This is readily perturbed by protein-protein interactions at postsynaptic sites, where AMPARs are trapped by reversible binding to postsynaptic density (PSD) proteins, cytoskeletal proteins, adhesion proteins, or extracellular matrix. The dynamic equilibrium established between different pools allows the steady state levels of AMPARs at synapses. **Bottom left panel**, pathological conditions, such as addiction, stress/depression, chronic pain, and epilepsy. The equilibrium is shifted towards the accumulation of postsynaptic AMPARs in a region/circuit-specific and subunit-specific manner. This may be due to the enhanced diffusion trapping mechanisms and/or potentiated exocytosis (Red). AMPAR lateral diffusion mediates the recruitment of extrasynaptic AMPARs to the postsynaptic membrane. AMPAR-based therapeutic strategies, which ameliorate drug-seeking behavior, chronic pain, or epileptic seizures in corresponding animal models, include reducing diffusion trapping and/or enhancing endocytosis (such as with optogenetic LTD induction or mGluR1 positive allosteric modulator), or inhibiting AMPAR-mediated currents by AMPAR antagonists. **Bottom right panel**, pathological conditions, such as Huntington's disease (HD), Alzheimer's disease (AD), Parkinson's disease (PD), and fragile X syndrome (FXS). The equilibrium is shifted towards the dispersal of AMPARs from the postsynaptic membrane in hippocampal and cortical neurons, which is linked to cognitive deficits, likely through the impairment of diffusion trapping mechanisms resulting in an increase in AMPAR lateral diffusion, potentiation of endocytosis, and/or suppression of exocytosis (Red). AMPAR-based therapeutic strategies, which improve synaptic plasticity and/or memory in animal models of HD, AD and FXS, include enhancing diffusion trapping mechanisms (such as with tianeptine), blocking endocytosis (such as with mGluR5 antagonists), or enhancing AMPAR function (such as with AMPAR positive allosteric modulators)(Blue). However, the effects of these strategies in human patients remain to be determined. Brain region- and AMPAR subunit-specific treatment is needed.

increased and decreased alcohol-seeking behavior, respectively (Ma et al., 2018). Furthermore, microinjection of NASPM, a synthetic analog of Joro spider toxin that selectively inhibits homomeric GluA1-AMPARs (CP-AMPARs), into the central nucleus of the amygdala, reduced morphine intake of rats (Hou et al., 2020).

Clathrin- and GluA2-dependent AMPAR endocytosis appears to play a crucial role in D-amphetamine-induced behavioral sensitization (Brebner et al., 2005; Choi et al., 2014), morphine-induced place preference (Dias et al., 2012) and cue-induced reinstatement of heroin self-administration (Van den Oever et al., 2008). Blocking regulated AMPAR endocytosis and LTD by GluA2-derived peptide (Tat-GluA2$_{3Y}$) prevented the expression and maintenance of D-amphetamine-induced behavioral sensitization (Brebner et al., 2005; Choi et al., 2014), facilitated the extinction of morphine-induced conditioned place preference (Dias et al., 2012), and reduced heroin seeking (Van den Oever et al., 2008). Collectively, these results suggest a critical role for AMPAR trafficking and AMPAR-mediated plasticity in addictive behavior. Targeting AMPAR subunits or AMPAR trafficking may represent a therapeutic strategy for addiction.

Stress/Depression

Stress in humans is defined as bodily or mental tension caused by physical, mental, or emotional factors.

Stressor exposure promotes the release of hormones from the adrenal gland, such as corticosterone, epinephrine, and norepinephrine (NE). The effect of stress on AMPAR synaptic plasticity is complex and region-specific (McGrath and Briand, 2019). For example, the administration of corticosterone to hippocampal neuronal cultures resulted in time-dependent synaptic accumulation of GluA2-AMPARs, possibly by increasing GluA2-AMPAR surface diffusion (Groc et al., 2008). The regulation of AMPARs was biphasic, with mineralocorticoid receptors (MRs) and glucocorticoid receptors (GRs) mediating early (minutes) and late (hours) responses to corticosterone, respectively. The MR-dependent increase in synaptic AMPAR contents facilitated chemical LTP induction, while the GR-dependent increase occluded chemical LTP (Groc et al., 2008; Krugers et al., 2010). This reflected a saturation process of LTP and also provided a cellular mechanism for the finding that short bath application of corticosterone (100 nM, 5–10 min) to hippocampal slices enhanced the frequency of AMPAR miniature excitatory postsynaptic potentials (mEPSC) in CA1 pyramidal neurons *via* MRs (Karst et al., 2005), while within hours, corticosterone slowly increased the amplitude of AMPAR mEPSC through GRs (Karst and Joëls, 2005) and impaired synaptic potentiation (Kim and Diamond, 2002; Zhang et al., 2013). Notably, the antidepressant tianeptine reversed the corticosterone-induced increase in AMPAR surface diffusion in hippocampal neurons and restored hippocampal LTP in slices from acutely stressed mice (Zhang et al., 2013). This suggests that reversal of AMPAR surface trafficking may contribute to the restoration of hippocampal synaptic plasticity in animal models of stress. Other stressful stimuli, such as NE and emotional stress, induced the phosphorylation and synaptic delivery of GluA1-AMPARs in hippocampal slice cultures, which was thought to lower the threshold for LTP (Hu et al., 2007). It is noteworthy that social defeat stress was shown to reduce the levels of GluA1-AMPAR in the PFC and hippocampus, but elevate its levels in NAc (Yang et al., 2016). Furthermore, stress paradigms that impair hippocampal LTP have been found to facilitate amygdala LTP (Vouimba et al., 2004; Suvrathan et al., 2014). This implies that there may be important region-specific differences in AMPAR regulation and plasticity that need to be taken into account in the development of therapeutics.

Interestingly, increasing evidence suggests that stress facilitates the development of drug addiction. This may be attributed, at least in part, to stress-induced changes in synaptic plasticity (Lo Iacono et al., 2018; McGrath and Briand, 2019). Indeed, drugs of abuse and stress trigger common plasticity mechanisms in midbrain dopamine neurons. Acute stress and *in vivo* administration of drugs of abuse with different molecular mechanisms both enhanced the AMPAR/NMDAR EPSC ratio at excitatory synapses onto midbrain dopaminergic neurons (Saal et al., 2003). Another study found that early stressors such as repeated maternal separation increased TNF levels in the PFC and NAc while reducing GluA2 levels in male but not female rats. Maternally separated male rats display a greater preference for a cocaine-associated context, which was reversed by the TNF inhibitor XPro 1595 through normalizing TNF and GluA2 levels (Ganguly et al., 2019). Notably, chronic stress in humans is associated with higher rates of depression or depressive episodes (Kendler et al., 1999). Thus, the implications of these findings might extend to depression.

Chronic Pain

Chronic pain conditions often have a psychological component in the form of a persistent sensory memory of the pain state, associated with fear, anxiety, and cognitive dysfunction. LTP and LTD in the dorsal horn of the spinal cord and cortical areas, including the anterior cingulate cortex (ACC), are increasingly thought to underlie chronic pain (Bliss et al., 2016). In particular, evidence from genetic and pharmacological studies indicates that the recruitment of GluA1-AMPARs to the postsynaptic membrane contributes to the expression of NMDAR-dependent LTP in the ACC (Toyoda et al., 2007, 2009; Xu et al., 2008; Li et al., 2010), the pathogenesis of chronic inflammation and neuropathic pain (Xu et al., 2008; Li et al., 2010), and chronic visceral pain (Liu et al., 2015; Wang et al., 2015). Analgesic effects were obtained by inhibiting AMPAR-mediated responses or reducing the expression of postsynaptic LTP in the ACC (Li et al., 2010; Chen et al., 2014; Liu et al., 2015; Wang et al., 2015; Zhuo, 2019).

Epilepsy

Epilepsy is a neurological disorder characterized by recurrent and unprovoked seizures, reflecting episodic abnormal synchronized electrical activity in cerebral neuronal networks (Rogawski, 2013). Imbalanced excitatory and inhibitory synaptic transmission is thought to contribute to epilepsy pathogenesis (Bonansco and Fuenzalida, 2016). An elevation of hippocampal AMPAR levels has been reported in both temporal lobe epilepsy (TLE) patients and several animal epilepsy models (Mathern et al., 1998; Lopes et al., 2013). This is supported by a positron emission tomography (PET) tracer study of AMPARs ([11C]K-2), showing that [11C]K-2 uptake is increased in the epileptogenic focus of patients with mesial TLE (Miyazaki et al., 2020). Therapeutic strategies inhibiting AMPA-mediated currents, e.g., AMPAR antagonists, have been developed to treat epilepsy. AMPAR antagonists have been shown to alleviate epileptiform activity in *in vitro* models and confer protection from seizures in many animal seizure models (Rogawski, 2013). In particular, a selective non-competitive AMPAR antagonist, perampanel, has been clinically used to treat patients with partial-onset and tonic-clonic seizures (French et al., 2015a,b; Piña-Garza et al., 2020).

Summary of Addiction, Stress, Chronic Pain, and Epilepsy Models

Taken together, the available data suggest that region- and subunit-specific pathological potentiation of AMPAR-mediated synaptic transmission is a common feature of animal models of addiction, stress, chronic pain, and epilepsy models (**Figure 1**, bottom left panel). In these models, experimental

inhibition of potentiated AMPAR-mediated transmission, eg. using AMPAR antagonists or reversal of enhanced synaptic strength by regulating AMPAR trafficking and redistribution was able to mitigate addictive behavior, chronic pain, and epileptic seizures. In contrast, in the following sections, we review a set of disorders that are characterized by an impaired LTP or enhanced LTD, which has been associated with cognitive deficits.

Huntington's Disease (HD)

Huntington's disease (HD) is an autosomal dominant inherited neurodegenerative disease, clinically characterized by cognitive deficits, psychiatric disturbance, and motor dysfunction. HD is caused by a mutated form of the huntingtin gene and the resulting mutant huntingtin protein (Saudou and Humbert, 2016). Increasing evidence suggests that cognitive and psychiatric disturbances occur in HD gene carriers and HD mouse models well before classical neuropathology or the onset of motor symptom, suggesting that the initial development of the disease results from a cellular dysfunction rather than a loss of neurons (Lemiere et al., 2004; Solomon et al., 2008). Various transgenic and knock-in HD mouse models exhibit impaired hippocampal LTP at the pre- or early-symptomatic stage (Hodgson et al., 1999; Murphy et al., 2000; Zhang et al., 2018). Consistently, behavioral studies reveal the deterioration of hippocampal-associated spatial memory in distinct HD murine models and patients (Chan et al., 2014; Majerová et al., 2012). Recent work has shown that AMPAR surface diffusion is dramatically increased in hippocampal neurons from HD rodent models. This was attributed to deficient brain-derived neurotrophic factor (BDNF)–Tropomyosin related kinase B (TrkB) signaling, which disrupted AMPAR diffusion trapping, i.e., the interaction between transmembrane AMPA receptor regulatory proteins (TARPs) and the PDZ-domain scaffold protein PSD95 (Zhang et al., 2018). The antidepressant tianeptine improved BDNF synthesis and intracellular transport, reversed AMPAR surface diffusion, and restored LTP and hippocampus-dependent memory in different HD mouse models (Zhang et al., 2018). AMPAR positive allosteric modulators (AMPAkines) have also been shown to rescue the deficits in synaptic plasticity and memory in HD mouse models, possibly via upregulating BDNF (Simmons et al., 2009, 2011).

Alzheimer's Disease (AD)

Alzheimer's disease (AD) is a progressive neurodegenerative disease, clinically characterized by early memory deficits and progressive loss of higher cognitive functions. The causes of AD are unclear, but amyloid-β protein (Aβ) and tau are thought to play a central role in the etiology and pathogenesis. Extracellular amyloid plaques (composed of Aβ peptides) and intraneuronal neurofibrillary tangles (composed of tau) are pathological hallmarks of AD (Bloom, 2014). However, increasing evidence suggests that AD begins with synaptic failure before overt neuronal degeneration, which may contribute to the early memory impairments (Selkoe, 2002; Luscher and Huber, 2010; Opazo et al., 2018).

Impaired NMDAR-dependent hippocampal LTP or enhanced LTD are observed in various transgenic AD animal models (Mango et al., 2019). Tau protein appears to be involved in synaptic removal of AMPARs, as clustering of tau fibrils reduced synaptic abundance of AMPARs (Shrivastava et al., 2019). Moreover, Tau protein phosphorylation was involved in a ketamine-induced reduction in surface expression of AMPARs in hippocampal neurons (Li et al., 2019). Besides, mGluR-LTD induced by soluble Aβ oligomers is also thought to contribute to the mental decline in AD (Luscher and Huber, 2010). This appears to result from enhanced GluA2/GluA3-AMPAR endocytosis by Aβ oligomers (Jurado, 2018), which may require the participation of PICK1 (protein interacting with C kinase 1; Alfonso et al., 2014). Of particular note, Aβ-induced synaptic removal of AMPAR *via* endocytosis is necessary and sufficient to induce spine loss (Hsieh et al., 2006), which is in line with the role of GluA2-AMPAR in promoting dendritic spine formation and growth in cultured hippocampal neurons (Saglietti et al., 2007). This suggests that the dysregulation of AMPAR trafficking may have both adverse functional and structural consequences. Moreover, overexpression of the amyloid-precursor protein (APP) or exposure to Aβ oligomers resulted in abnormal enhancement of AMPAR surface diffusion *via* the activation of GluN2B-containing NMDARs (Opazo et al., 2018). Immobilizing AMPARs by crosslinking methods fully rescued spine loss induced by oligomeric Aβ (Opazo et al., 2018). These lines of evidence suggest that targeting of AMPAR trafficking may represent a new therapeutic avenue in AD and HD.

Parkinson's Disease (PD)

Parkinson's disease (PD) is another neurodegenerative disorder associated with loss of dopaminergic neurons of the substantia nigra projection to the striatum, of major importance for motor control. The cause of PD is unknown but is believed to involve both genetic and environmental factors (Kalia and Lang, 2015). PD is not only characterized by motor symptoms but also non-motor symptoms, including cognitive impairment (Bernal-Pacheco et al., 2012; Modugno et al., 2013). The cognitive decline and dementia in PD have been associated with hippocampal dysfunction (Svenningsson et al., 2012; Calabresi et al., 2013; Cosgrove et al., 2015). For example, mutations in PD-associated E3 ubiquitin ligase Parkin have been associated with juvenile-onset PD. Parkin regulates synaptic AMPAR endocytosis *via* its binding and retention of the postsynaptic scaffold protein, homer (Cortese et al., 2016; Zhu et al., 2018). The four common Parkin point mutations (T240M, R275W, R334C, G430D; Zhu et al., 2018) or Parkin knock-down (Cortese et al., 2016) impaired this capacity, reduced surface expression of GluA1- and GluA2-AMPARs, and disrupted glutamatergic synaptic transmission in hippocampal neurons. It should be noted that Parkin is primarily involved in mitochondrial homeostasis (McWilliams and Muqit, 2017). Mitochondria, as energy centers and calcium buffer organelles, may play an important role in the regulation of synaptic plasticity (Todorova and Blokland, 2017). Moreover, PD dementia is considered a

convergence of α-synuclein, tau, and Aβ pathologies (Irwin et al., 2013; Shrivastava et al., 2019). As discussed in the AD section, both tau and Aβ appear to be involved in the removal of synaptic AMPARs (Jurado, 2018; Li et al., 2019; Shrivastava et al., 2019). Thus, PD-related dementia might involve dysregulation of AMPAR trafficking induced by Aβ and tau.

In addition to PD dementia, the motor deficits of PD have also been partially attributed to aberrations in AMPAR plasticity. There is an imbalance in glutamatergic signaling between the direct pathway spiny projection neurons (dSPNs) and indirect pathway SPNs (iSPNs), with LTP (hyper AMPAR signaling) found in iSPNs while LTD (hypo AMPAR signaling) found in dSPNs (Shen et al., 2008; Fieblinger et al., 2014; Shields et al., 2017). In general, activity in the direct-pathway neurons would promote appropriate actions while the indirect-pathway suppresses unnecessary actions or movements. Potentiation or loss of inhibition in the indirect-pathway is thought to contribute to motor dysfunction (Luscher and Huber, 2010; Shields et al., 2017). In support of this idea, the AMPAR antagonist, YM90K, was specifically delivered to the indirect-pathway through the DART (drugs acutely restricted by tethering) technique, that used HaloTag to capture and tether drugs to the cell surface. The treatment profoundly ameliorated motor deficits, such as akinesia in PD animal models (Shields et al., 2017).

Fragile X Syndrome (FXS)

Fragile X syndrome (FXS) is a neurodevelopmental disorder. It is the most common inherited cause of intellectual disability and a prevalent genetic cause of autism spectrum disorder (ASD; Cheng et al., 2017). FXS results from loss-of-function mutations in fragile X mental retardation protein (FMRP), an RNA-binding protein that regulates local translation of a subset of mRNAs at both presynaptic and postsynaptic locations in response to mGluR activation (Luscher and Huber, 2010). One primary consequence of FMRP loss is the enhancement of mGluR-LTD, which depends on GluA1-AMPAR endocytosis (Luscher and Huber, 2010; Cheng et al., 2017). *Fmr*1 knockout mice exhibit enhancement of mGluR-LTD both in the cerebellum and hippocampus (Luscher and Huber, 2010). Various mGluR5 antagonists have entered clinical trials (Berry-Kravis et al., 2018). This strategy aims at normalizing multiple cellular processes including LTD by targeting mGluRs rather than by directly interfering with ionotropic glutamate receptors, which have crucial physiological functions. However, the clinical efficacy of mGluR5 antagonists remains to be determined.

Impaired LTP in *Fmr*1 knockout mice has also been reported in multiple brain regions, such as the hippocampus (Lauterborn et al., 2007; Hu et al., 2008), anterior piriform cortex (Larson et al., 2005), deep-layer visual neocortex (Wilson and Cox, 2007), and ACC (Zhao et al., 2005; Wang et al., 2008). Restoring the synaptic delivery of GluA1-containing AMPARs by enhancing Ras-PI3K-Akt signaling rescued LTP in *Fmr1* KO mice (Hu et al., 2008; Lim et al., 2014). This indicates that targeting of AMPAR trafficking may be a potential therapeutic strategy in FXS.

Summary of AD, HD, PD, and FXS Models

Taken together, the impairment in hippocampal or cortical LTP or the enhancement in LTD has been associated with behavioral and cognitive deficits in animal models of AD, HD, PD, and FXS (**Figure 1**, bottom right panel). Enhancing AMPAR diffusion trapping mechanisms (such as with tianeptine), blocking endocytosis (such as with mGluR5 antagonists), or enhancing AMPAR function (such as with AMPAR positive allosteric modulators) have exhibited therapeutic effects, such as reversal of synaptic plasticity and memory defects in animal models of AD, HD and FXS. However, the effects of these strategies in human patients remain to be determined. Brain region- and AMPAR subunit-specific treatment is needed.

DISCUSSION

While dysregulation of AMPAR synaptic plasticity is emerging as a point of convergence in multiple pathological pathways across several brain disorders, it is unlikely to be the major driver of pathology. Indeed, each brain disorder has a distinct and complex etiology and pathogenesis. Rather, the pathological impact on the excitatory synapse directly influences the expression of the disorders or associated symptoms, and these effects are reversible. Targeting a converging point of multiple pathological pathways, especially in early stages of diseases, such as HD and AD, may be more efficient than targeting any individual pathway. In addition, the pathological potentiation and weakening of synaptic strength both adversely impact the plastic range of the synapse and thus may hamper further plasticity (metaplasticity). Therefore, strategies that can preserve the plastic range of the synapse, eg. regulating AMPAR trafficking, will be beneficial. In particular, modulating AMPAR trafficking leads to AMPAR redistribution without perturbing AMPAR function, which is a great advantage.

Small interfering peptides that target protein-protein interactions are attracting increasing attention as potential therapeutics, partly due to their high binding specificity and affinity, and minimal off-target effects (Fosgerau and Hoffmann, 2015; Havasi et al., 2017). Interfering peptides targeting AMPAR endocytosis were shown effective in preventing the expression of D-amphetamine-induced behavioral sensitization and facilitating the extinction of morphine-induced conditioned place preference in rodent models of drug addiction (Brebner et al., 2005; Dias et al., 2012). We propose that peptides disrupting the diffusion trapping mechanism of AMPARs are an alternative strategy. Though promising, the therapeutic application of cell-penetrating peptides in humans remains challenging (Fosgerau and Hoffmann, 2015; Havasi et al., 2017). As an alternative, aptamers are oligonucleotide molecules that bind to a specific target molecule. For example, attempts have made to design RNA aptamers as AMPAR antagonists (Huang and Niu, 2019). However, there is still a long way to go to translate them into drug options.

A better understanding of the molecular mechanism and dynamics of AMPAR-mediated plasticity may help in the further identification of therapeutic targets. For dissecting

mechanisms, the use of light-sensitive proteins allows fast and reversible manipulation of protein targets with high spatial-temporal precision (Paoletti et al., 2019). The development of optogenetic and optopharmacological tools may help to elucidate the spatial-temporal regulation of AMPAR trafficking in specific cell types and circuits in animal models. For example, genetically-encoded protein photosensors such as LOVTRAP and dimeric Dronpa, have been recently developed (Wang et al., 2016; Zhou et al., 2017). LOVTRAP can be used for reversible light-induced protein dissociation. It requires attaching one of the Zdk/LOV2 pairs to the target protein, and the other to the membrane (Wang and Hahn, 2016). Thus, LOVTRAP technology could serve to manipulate the synaptic anchoring of AMPARs by controlling the interaction between a membrane TARP and a PDZ-containing protein in the PSD. Another example is Dronpa, a reversibly photoswitchable fluorescent protein, which associates and dissociates in response to 400 nm and 500 nm illumination, respectively (Zhou et al., 2017). A generalizable method for optical control of kinases has been recently reported. Photoswitchable kinases, such as psRaf1, psMEK1, psMEK2, and psCDK5, have been successfully generated by attaching two photoswitchable dimeric Dronpa (pdDronpa) domains in the kinase functional domain. The light switch enables the caging and uncaging of the core kinase domain with high temporal and spatial precision (Zhou et al., 2017). This method could be used to elucidate local, synaptic regulation of AMPARs by protein kinases. Furthermore, a study successfully used a freely diffusible photoswitchable quinoxaline-2,3-dione, an antagonist selective for AMPARs, to control action potential firing optically (Barber et al., 2017). Another study developed a technique to inactivate synaptic GluA1 AMPARs *in vivo* using chromophore-assisted light inactivation and erased acquired fear memory in the animals (Takemoto et al., 2017). Thus, optogenetics and optopharmacology emerge as powerful tools for manipulating and interrogating synaptic plasticity with high spatial-temporal precision. Because light does not penetrate tissue easily, applying optogenetic tools in living animals often requires the implantation of invasive optical fibers into the brain. This has limited their applications in humans. Recently, an ultra-sensitive light-responsive molecule, SOUL, has been developed. Once engineered in the neurons inside the brain of mice and monkeys, the neurons can be turned on and off by illumination from outside of the head (Gong et al., 2020). Such non-invasive approaches hold promise for therapeutic optogenetics.

AUTHOR CONTRIBUTIONS

HZ and CB researched data for the article, wrote the article and reviewed and/or edited the manuscript before submission.

FUNDING

Supported by TOPPFORSK grant (249951) from Research Council of Norway to CB; Project Grant (2020/01/FOL) from Bergen Universitetsfond to HZ; Personal Overseas Research Grant (249951/F20) from the Research Council of Norway to HZ; and Project Grant (EuBI_HOZH062) from Euro-BioImaging to HZ.

REFERENCES

Alfonso, S., Kessels, H. W., Banos, C. C., Chan, T. R., Lin, E. T., Kumaravel, G., et al. (2014). Synapto-depressive effects of amyloid β require PICK1. *Eur. J. Neurosci.* 39, 1225–1233. doi: 10.1111/ejn.12499

Barber, D. M., Liu, S. A., Gottschling, K., Sumser, M., Hollmann, M., and Trauner, D. (2017). Optical control of AMPA receptors using a photoswitchable quinoxaline-2,3-dione antagonist. *Chem. Sci.* 8, 611–615. doi: 10.1039/c6sc01621a

Bernal-Pacheco, O., Limotai, N., Go, C. L., and Fernandez, H. H. (2012). Nonmotor manifestations in Parkinson disease. *Neurologist* 18, 1–16. doi: 10.1097/nrl.0b013e31823d7abb

Berry-Kravis, E. M., Lindemann, L., Jonch, A. E., Apostol, G., Bear, M. F., Carpenter, R. L., et al. (2018). Drug development for neurodevelopmental disorders: lessons learned from fragile X syndrome. *Nat. Rev. Drug Discov.* 17, 280–299. doi: 10.1038/nrd.2017.221

Bliss, T. V., Collingridge, G. L., Kaang, B. K., and Zhuo, M. (2016). Synaptic plasticity in the anterior cingulate cortex in acute and chronic pain. *Nat. Rev. Neurosci.* 17, 485–496. doi: 10.1038/nrn.2016.68

Bloom, G. S. (2014). Amyloid-β and tau: the trigger and bullet in Alzheimer disease pathogenesis. *JAMA Neurol.* 71, 505–508. doi: 10.1001/jamaneurol.2013.5847

Bonansco, C., and Fuenzalida, M. (2016). Plasticity of hippocampal excitatory-inhibitory balance: missing the synaptic control in the epileptic brain. *Neural Plast.* 2016:8607038. doi: 10.1155/2016/8607038

Brebner, K., Wong, T. P., Liu, L., Liu, Y., Campsall, P., Gray, S., et al. (2005). Nucleus accumbens long-term depression and the expression of behavioral sensitization. *Science* 310, 1340–1343. doi: 10.1126/science.1116894

Calabresi, P., Castrioto, A., Di Filippo, M., and Picconi, B. (2013). New experimental and clinical links between the hippocampus and the dopaminergic system in Parkinson's disease. *Lancet Neurol.* 12, 811–821. doi: 10.1016/s1474-4422(13)70118-2

Chan, A. W., Xu, Y., Jiang, J., Rahim, T., Zhao, D., Kocerha, J., et al. (2014). A two years longitudinal study of a transgenic Huntington disease monkey. *BMC Neurosci.* 15:36. doi: 10.1186/1471-2202-15-36

Chen, T., Wang, W., Dong, Y. L., Zhang, M. M., Wang, J., Koga, K., et al. (2014). Postsynaptic insertion of AMPA receptor onto cortical pyramidal neurons in the anterior cingulate cortex after peripheral nerve injury. *Mol. Brain* 7:76. doi: 10.1186/s13041-014-0076-8

Cheng, G. R., Li, X. Y., Xiang, Y. D., Liu, D., McClintock, S. M., and Zeng, Y. (2017). The implication of AMPA receptor in synaptic plasticity impairment and intellectual disability in fragile X syndrome. *Physiol. Res.* 66, 715–727. doi: 10.33549/physiolres.933473

Choi, F. Y., Ahn, S., Wang, Y. T., and Phillips, A. G. (2014). Interference with AMPA receptor endocytosis: effects on behavioural and neurochemical correlates of amphetamine sensitization in male rats. *J. Psychiatry Neurosci.* 39, 189–199. doi: 10.1503/jpn.120257

Choquet, D. (2018). Linking nanoscale dynamics of AMPA receptor organization to plasticity of excitatory synapses and learning. *J. Neurosci.* 38, 9318–9329. doi: 10.1523/jneurosci.2119-18.2018

Conrad, K. L., Tseng, K. Y., Uejima, J. L., Reimers, J. M., Heng, L. J., Shaham, Y., et al. (2008). Formation of accumbens GluR2-lacking AMPA receptors mediates incubation of cocaine craving. *Nature* 454, 118–121. doi: 10.1038/nature06995

Cooper, S., Robison, A. J., and Mazei-Robison, M. S. (2017). Reward circuitry in addiction. *Neurotherapeutics* 14, 687–697. doi: 10.1007/s13311-017-0525-z

Cortese, G. P., Zhu, M., Williams, D., Heath, S., and Waites, C. L. (2016). Parkin deficiency reduces hippocampal glutamatergic neurotransmission

by impairing AMPA receptor endocytosis. *J. Neurosci.* 36, 12243–12258. doi: 10.1523/jneurosci.1473-16.2016

Cosgrove, J., Alty, J. E., and Jamieson, S. (2015). Cognitive impairment in Parkinson's disease. *Postgrad. Med. J.* 91, 212–220. doi: 10.1136/postgradmedj-2015-133247

Dias, C., Wang, Y. T., and Phillips, A. G. (2012). Facilitated extinction of morphine conditioned place preference with Tat-GluA2(3Y) interference peptide. *Behav. Brain Res.* 233, 389–397. doi: 10.1016/j.bbr.2012.05.026

Fieblinger, T., Graves, S. M., Sebel, L. E., Alcacer, C., Plotkin, J. L., Gertler, T. S., et al. (2014). Cell type-specific plasticity of striatal projection neurons in parkinsonism and L-DOPA-induced dyskinesia. *Nat. Commun.* 5:5316. doi: 10.1038/ncomms6316

Fosgerau, K., and Hoffmann, T. (2015). Peptide therapeutics: current status and future directions. *Drug Discov. Today* 20, 122–128. doi: 10.1016/j.drudis.2014.10.003

French, J. A., Gil-Nagel, A., Malerba, S., Kramer, L., Kumar, D., and Bagiella, E. (2015a). Time to prerandomization monthly seizure count in perampanel trials: a novel epilepsy endpoint. *Neurology* 84, 2014–2020. doi: 10.1212/wnl.0000000000001585

French, J. A., Krauss, G. L., Wechsler, R. T., Wang, X. F., DiVentura, B., Brandt, C., et al. (2015b). Perampanel for tonic-clonic seizures in idiopathic generalized epilepsy A randomized trial. *Neurology* 85, 950–957. doi: 10.1212/WNL.0000000000001930

Ganguly, P., Honeycutt, J. A., Rowe, J. R., Demaestri, C., and Brenhouse, H. C. (2019). Effects of early life stress on cocaine conditioning and AMPA receptor composition are sex-specific and driven by TNF. *Brain Behav. Immun.* 78, 41–51. doi: 10.1016/j.bbi.2019.01.006

Gong, X., Mendoza-Halliday, D., Ting, J. T., Kaiser, T., Sun, X., Bastos, A. M., et al. (2020). An ultra-sensitive step-function opsin for minimally invasive optogenetic stimulation in mice and macaques. *Neuron* doi: 10.1016/j.neuron.2020.03.032 [Epub ahead of print].

Good, C. H., and Lupica, C. R. (2010). Afferent-specific AMPA receptor subunit composition and regulation of synaptic plasticity in midbrain dopamine neurons by abused drugs. *J. Neurosci.* 30, 7900–7909. doi: 10.1523/jneurosci.1507-10.2010

Groc, L., Choquet, D., and Chaouloff, F. (2008). The stress hormone corticosterone conditions AMPAR surface trafficking and synaptic potentiation. *Nat. Neurosci.* 11, 868–870. doi: 10.1038/nn.2150

Havasi, A., Lu, W., Cohen, H. T., Beck, L., Wang, Z., Igwebuike, C., et al. (2017). Blocking peptides and molecular mimicry as treatment for kidney disease. *Am. J. Physiol. Renal. Physiol.* 312, F1016–F1025. doi: 10.1152/ajprenal.00601.2015

Hodgson, J. G., Agopyan, N., Gutekunst, C. A., Leavitt, B. R., LePiane, F., Singaraja, R., et al. (1999). A YAC mouse model for Huntington's disease with full-length mutant huntingtin, cytoplasmic toxicity and selective striatal neurodegeneration. *Neuron* 23, 181–192. doi: 10.1016/s0896-6273(00)80764-3

Hou, Y. Y., Cai, Y. Q., and Pan, Z. Z. (2020). GluA1 in central amygdala promotes opioid use and reverses inhibitory effect of pain. *Neuroscience* 426, 141–153. doi: 10.1016/j.neuroscience.2019.11.032

Hsieh, H., Boehm, J., Sato, C., Iwatsubo, T., Tomita, T., Sisodia, S., et al. (2006). AMPAR removal underlies Aβ-induced synaptic depression and dendritic spine loss. *Neuron* 52, 831–843. doi: 10.1016/j.neuron.2006.10.035

Hu, H., Qin, Y., Bochorishvili, G., Zhu, Y., van Aelst, L., and Zhu, J. J. (2008). Ras signaling mechanisms underlying impaired GluR1-dependent plasticity associated with fragile X syndrome. *J. Neurosci.* 28, 7847–7862. doi: 10.1523/jneurosci.1496-08.2008

Hu, H., Real, E., Takamiya, K., Kang, M. G., Ledoux, J., Huganir, R. L., et al. (2007). Emotion enhances learning *via* norepinephrine regulation of AMPA-receptor trafficking. *Cell* 131, 160–173. doi: 10.1016/j.cell.2007.09.017

Huang, Z., and Niu, L. (2019). Developing RNA aptamers for potential treatment of neurological diseases. *Future Med. Chem.* 11, 551–565. doi: 10.4155/fmc-2018-0364

Huang, Y. H., Schluter, O. M., and Dong, Y. (2015). Silent synapses speak up: updates of the neural rejuvenation hypothesis of drug addiction. *Neuroscientist* 21, 451–459. doi: 10.1177/1073858415579405

Irwin, D. J., Lee, V. M., and Trojanowski, J. Q. (2013). Parkinson's disease dementia: convergence of α-synuclein, tau and amyloid-β pathologies. *Nat. Rev. Neurosci.* 14, 626–636. doi: 10.1038/nrn3549

Jurado, S. (2018). AMPA receptor trafficking in natural and pathological aging. *Front. Mol. Neurosci.* 10:446. doi: 10.3389/fnmol.2017.00446

Kakegawa, W., Katoh, A., Narumi, S., Miura, E., Motohashi, J., Takahashi, A., et al. (2018). Optogenetic control of synaptic AMPA receptor endocytosis reveals roles of LTD in motor learning. *Neuron* 99, 985.e6–998.e6. doi: 10.1016/j.neuron.2018.07.034

Kalia, L. V., and Lang, A. E. (2015). Parkinson's disease. *Lancet* 386, 896–912. doi: 10.1016/S0140-6736(14)61393-3

Karst, H., Berger, S., Turiault, M., Tronche, F., Schutz, G., and Joels, M. (2005). Mineralocorticoid receptors are indispensable for nongenomic modulation of hippocampal glutamate transmission by corticosterone. *Proc. Natl. Acad. Sci. U S A* 102, 19204–19207. doi: 10.1073/pnas.0507572102

Karst, H., and Joëls, M. (2005). Corticosterone slowly enhances miniature excitatory postsynaptic current amplitude in mice CA1 hippocampal cells. *J. Neurophysiol.* 94, 3479–3486. doi: 10.1152/jn.00143.2005

Kendler, K. S., Karkowski, L. M., and Prescott, C. A. (1999). Causal relationship between stressful life events and the onset of major depression. *Am. J. Psychiatry* 156, 837–841. doi: 10.1176/ajp.156.6.837

Kim, J. J., and Diamond, D. M. (2002). The stressed hippocampus, synaptic plasticity and lost memories. *Nat. Rev. Neurosci.* 3, 453–462. doi: 10.1038/nrn849

Krugers, H. J., Hoogenraad, C. C., and Groc, L. (2010). Stress hormones and AMPA receptor trafficking in synaptic plasticity and memory. *Nat. Rev. Neurosci.* 11, 675–681. doi: 10.1038/nrn2913

Larson, J., Jessen, R. E., Kim, D., Fine, A. K., and du Hoffmann, J. (2005). Age-dependent and selective impairment of long-term potentiation in the anterior piriform cortex of mice lacking the fragile X mental retardation protein. *J. Neurosci.* 25, 9460–9469. doi: 10.1523/jneurosci.2638-05.2005

Lauterborn, J. C., Rex, C. S., Kramar, E., Chen, L. Y., Pandyarajan, V., Lynch, G., et al. (2007). Brain-derived neurotrophic factor rescues synaptic plasticity in a mouse model of fragile X syndrome. *J. Neurosci.* 27, 10685–10694. doi: 10.1523/jneurosci.2624-07.2007

Lee, B. R., Ma, Y. Y., Huang, Y. H., Wang, X., Otaka, M., Ishikawa, M., et al. (2013). Maturation of silent synapses in amygdala-accumbens projection contributes to incubation of cocaine craving. *Nat. Neurosci.* 16, 1644–1651. doi: 10.1038/nn.3533

Lemiere, J., Decruyenaere, M., Evers-Kiebooms, G., Vandenbussche, E., and Dom, R. (2004). Cognitive changes in patients with Huntington's disease (HD) and asymptomatic carriers of the HD mutation--a longitudinal follow-up study. *J. Neurol.* 251, 935–942. doi: 10.1007/s00415-004-0461-9

Li, Y., Ding, R., Ren, X., Wen, G., Dong, Z., Yao, H., et al. (2019). Long-term ketamine administration causes Tau protein phosphorylation and Tau protein-dependent AMPA receptor reduction in the hippocampus of mice. *Toxicol. Lett.* 315, 107–115. doi: 10.1016/j.toxlet.2019.08.023

Li, X. Y., Ko, H. G., Chen, T., Descalzi, G., Koga, K., Wang, H., et al. (2010). Alleviating neuropathic pain hypersensitivity by inhibiting PKMzeta in the anterior cingulate cortex. *Science* 330, 1400–1404. doi: 10.1126/science.1191792

Lim, C. S., Hoang, E. T., Viar, K. E., Stornetta, R. L., Scott, M. M., and Zhu, J. J. (2014). Pharmacological rescue of Ras signaling, GluA1-dependent synaptic plasticity and learning deficits in a fragile X model. *Genes Dev.* 28, 273–289. doi: 10.1101/gad.232470.113

Liu, S. B., Zhang, M. M., Cheng, L. F., Shi, J., Lu, J. S., and Zhuo, M. (2015). Long-term upregulation of cortical glutamatergic AMPA receptors in a mouse model of chronic visceral pain. *Mol. Brain* 8:76. doi: 10.1186/s13041-015-0169-z

Lo Iacono, L., Catale, C., Martini, A., Valzania, A., Viscomi, M. T., Chiurchiu, V., et al. (2018). From traumatic childhood to cocaine abuse: the critical function of the immune system. *Biol. Psychiatry* 84, 905–916. doi: 10.1016/j.biopsych.2018.05.022

Lopes, M. W., Soares, F. M., de Mello, N., Nunes, J. C., Cajado, A. G., de Brito, D., et al. (2013). Time-dependent modulation of AMPA receptor phosphorylation and mRNA expression of NMDA receptors and glial glutamate transporters in the rat hippocampus and cerebral cortex in a pilocarpine model of epilepsy. *Exp. Brain Res.* 226, 153–163. doi: 10.1007/s00221-013-3421-8

Loweth, J. A., Scheyer, A. F., Milovanovic, M., LaCrosse, A. L., Flores-Barrera, E., Werner, C. T., et al. (2014). Synaptic depression *via* mGluR1 positive allosteric

modulation suppresses cue-induced cocaine craving. *Nat. Neurosci.* 17, 73–80. doi: 10.1038/nn.3590

Luscher, C., and Huber, K. M. (2010). Group 1 mGluR-dependent synaptic long-term depression: mechanisms and implications for circuitry and disease. *Neuron* 65, 445–459. doi: 10.1016/j.neuron.2010.01.016

Ma, T., Cheng, Y., Roltsch Hellard, E., Wang, X., Lu, J., Gao, X., et al. (2018). Bidirectional and long-lasting control of alcohol-seeking behavior by corticostriatal LTP and LTD. *Nat. Neurosci.* 21, 373–383. doi: 10.1038/s41593-018-0081-9

Ma, Y. Y., Lee, B. R., Wang, X., Guo, C., Liu, L., Cui, R., et al. (2014). Bidirectional modulation of incubation of cocaine craving by silent synapse-based remodeling of prefrontal cortex to accumbens projections. *Neuron* 83, 1453–1467. doi: 10.1016/j.neuron.2014.08.023

Madayag, A. C., Gomez, D., Anderson, E. M., Ingebretson, A. E., Thomas, M. J., and Hearing, M. C. (2019). Cell-type and region-specific nucleus accumbens AMPAR plasticity associated with morphine reward, reinstatement and spontaneous withdrawal. *Brain Struct. Funct.* 224, 2311–2324. doi: 10.1007/s00429-019-01903-y

Majerová, V., Kalinčík, T., Laczó, J., Vyhnálek, M., Hort, J., Bojar, M., et al. (2012). Disturbance of real space navigation in moderately advanced but not in early Huntington's disease. *J. Neurol. Sci.* 312, 86–91. doi: 10.1016/j.jns.2011.08.016

Makino, H., and Malinow, R. (2009). AMPA receptor incorporation into synapses during LTP: the role of lateral movement and exocytosis. *Neuron* 64, 381–390. doi: 10.1016/j.neuron.2009.08.035

Mango, D., Saidi, A., Cisale, G. Y., Feligioni, M., Corbo, M., and Nistico, R. (2019). Targeting synaptic plasticity in experimental models of Alzheimer's disease. *Front. Pharmacol.* 10:778. doi: 10.3389/fphar.2019.00778

Marchi, M., Grilli, M., and Pittaluga, A. M. (2015). Nicotinic modulation of glutamate receptor function at nerve terminal level: a fine-tuning of synaptic signals. *Front. Pharmacol.* 6:89. doi: 10.3389/fphar.2015.00089

Mathern, G. W., Pretorius, J. K., Leite, J. P., Kornblum, H. I., Mendoza, D., Lozada, A., et al. (1998). Hippocampal AMPA and NMDA mRNA levels and subunit immunoreactivity in human temporal lobe epilepsy patients and a rodent model of chronic mesial limbic epilepsy. *Epilepsy Res.* 32, 154–171. doi: 10.1016/s0920-1211(98)00048-5

McGrath, A. G., and Briand, L. A. (2019). A potential role for microglia in stress- and drug-induced plasticity in the nucleus accumbens: a mechanism for stress-induced vulnerability to substance use disorder. *Neurosci. Biobehav. Rev.* 107, 360–369. doi: 10.1016/j.neubiorev.2019.09.007

McWilliams, T. G., and Muqit, M. M. (2017). PINK1 and Parkin: emerging themes in mitochondrial homeostasis. *Curr. Opin. Cell Biol.* 45, 83–91. doi: 10.1016/j.ceb.2017.03.013

Miyazaki, T., Nakajima, W., Hatano, M., Shibata, Y., Kuroki, Y., Arisawa, T., et al. (2020). Visualization of AMPA receptors in living human brain with positron emission tomography. *Nat. Med.* 26, 281–288. doi: 10.1038/s41591-019-0723-9

Modugno, N., Lena, F., Di Biasio, F., Cerrone, G., Ruggieri, S., and Fornai, F. (2013). A clinical overview of non-motor symptoms in Parkinson's disease. *Arch. Ital. Biol.* 151, 148–168.

Murphy, K. P., Carter, R. J., Lione, L. A., Mangiarini, L., Mahal, A., Bates, G. P., et al. (2000). Abnormal synaptic plasticity and impaired spatial cognition in mice transgenic for exon 1 of the human Huntington's disease mutation. *J. Neurosci.* 20, 5115–5123. doi: 10.1523/jneurosci.20-13-05115.2000

Nabavi, S., Fox, R., Proulx, C. D., Lin, J. Y., Tsien, R. Y., and Malinow, R. (2014). Engineering a memory with LTD and LTP. *Nature* 511, 348–352. doi: 10.1038/nature13294

Opazo, P., and Choquet, D. (2011). A three-step model for the synaptic recruitment of AMPA receptors. *Mol. Cell. Neurosci.* 46, 1–8. doi: 10.1016/j.mcn.2010.08.014

Opazo, P., Viana da Silva, S., Carta, M., Breillat, C., Coultrap, S. J., Grillo-Bosch, D., et al. (2018). CaMKII metaplasticity drives Aβ oligomer-mediated synaptotoxicity. *Cell Rep.* 23, 3137–3145. doi: 10.1016/j.celrep.2018.05.036

Paoletti, P., Ellis-Davies, G. C. R., and Mourot, A. (2019). Optical control of neuronal ion channels and receptors. *Nat. Rev. Neurosci.* 20, 514–532. doi: 10.1038/s41583-019-0197-2

Pascoli, V., Terrier, J., Espallergues, J., Valjent, E., O'Connor, E. C., and Luscher, C. (2014). Contrasting forms of cocaine-evoked plasticity control components of relapse. *Nature* 509, 459–464. doi: 10.1038/nature13257

Penn, A. C., Zhang, C. L., Georges, F., Royer, L., Breillat, C., Hosy, E., et al. (2017). Hippocampal LTP and contextual learning require surface diffusion of AMPA receptors. *Nature* 549, 384–388. doi: 10.1038/nature23658

Piña-Garza, J. E., Rosenfeld, W., Saeki, K., Villanueva, V., Yoshinaga, H., Patten, A., et al. (2020). Efficacy and safety of adjunctive perampanel in adolescent patients with epilepsy: Post hoc analysis of six randomized studies. *Epilepsy Behav.* 104:106876. doi: 10.1016/j.yebeh.2019.106876

Rogawski, M. A. (2013). AMPA receptors as a molecular target in epilepsy therapy. *Acta Neurol. Scand. Suppl.* 197, 9–18. doi: 10.1111/ane.12099

Saal, D., Dong, Y., Bonci, A., and Malenka, R. C. (2003). Drugs of abuse and stress trigger a common synaptic adaptation in dopamine neurons. *Neuron* 37, 577–582. doi: 10.1016/s0896-6273(03)00021-7

Saglietti, L., Dequidt, C., Kamieniarz, K., Rousset, M. C., Valnegri, P., Thoumine, O., et al. (2007). Extracellular interactions between GluR2 and N-cadherin in spine regulation. *Neuron* 54, 461–477. doi: 10.1016/j.neuron.2007.04.012

Saudou, F., and Humbert, S. (2016). The biology of Huntingtin. *Neuron* 89, 910–926. doi: 10.1016/j.neuron.2016.02.003

Scheyer, A. F., Loweth, J. A., Christian, D. T., Uejima, J., Rabei, R., Le, T., et al. (2016). AMPA receptor plasticity in accumbens core contributes to incubation of methamphetamine craving. *Biol. Psychiatry* 80, 661–670. doi: 10.1016/j.biopsych.2016.04.003

Selkoe, D. J. (2002). Alzheimer's disease is a synaptic failure. *Science* 298, 789–791. doi: 10.1126/science.1074069

Shen, W., Flajolet, M., Greengard, P., and Surmeier, D. J. (2008). Dichotomous dopaminergic control of striatal synaptic plasticity. *Science* 321, 848–851. doi: 10.1126/science.1160575

Shields, B. C., Kahuno, E., Kim, C., Apostolides, P. F., Brown, J., Lindo, S., et al. (2017). Deconstructing behavioral neuropharmacology with cellular specificity. *Science* 356:eaaj2161. doi: 10.1126/science.aaj2161

Shrivastava, A. N., Redeker, V., Pieri, L., Bousset, L., Renner, M., Madiona, K., et al. (2019). Clustering of Tau fibrils impairs the synaptic composition of α3-Na^+/K^+-ATPase and AMPA receptors. *EMBO J.* 38:e99871. doi: 10.15252/embj.201899871

Simmons, D. A., Rex, C. S., Palmer, L., Pandyarajan, V., Fedulov, V., Gall, C. M., et al. (2009). Up-regulating BDNF with an ampakine rescues synaptic plasticity and memory in Huntington's Disease knockin mice. *Proc. Natl. Acad. Sci. U S A.* 24, 4906–5011. doi: 10.1073/pnas.0811228106

Simmons, D. A., Mehta, R. A., Lauterborn, J. C., Gall, C. M., and Lynch, G. (2011). Brief ampakine treatements slow the progression of Huntington's disease phenotypes in R6/2 mice. *Nero. Bio. Dis.* 41, 436–444. doi: 10.1016/j.nbd.2010.10.015

Solomon, A. C., Stout, J. C., Weaver, M., Queller, S., Tomusk, A., Whitlock, K. B., et al. (2008). Ten-year rate of longitudinal change in neurocognitive and motor function in prediagnosis Huntington disease. *Mov. Disord.* 23, 1830–1836. doi: 10.1002/mds.22097

Suvrathan, A., Bennur, S., Ghosh, S., Tomar, A., Anilkumar, S., and Chattarji, S. (2014). Stress enhances fear by forming new synapses with greater capacity for long-term potentiation in the amygdala. *Philos. Trans. R. Soc. Lond. B Biol. Sci.* 369:20130151. doi: 10.1098/rstb.2013.0151

Svenningsson, P., Westman, E., Ballard, C., and Aarsland, D. (2012). Cognitive impairment in patients with Parkinson's disease: diagnosis, biomarkers and treatment. *Lancet Neurol.* 11, 697–707. doi: 10.1016/s1474-4422(12)70152-7

Takemoto, K., Iwanari, H., Tada, H., Suyama, K., Sano, A., Nagai, T., et al. (2017). Optical inactivation of synaptic AMPA receptors erases fear memory. *Nat. Biotechnol.* 35, 38–47. doi: 10.1038/nbt.3710

Tan, K. R., Brown, M., Labouebe, G., Yvon, C., Creton, C., Fritschy, J. M., et al. (2010). Neural bases for addictive properties of benzodiazepines. *Nature* 463, 769–774. doi: 10.1038/nature08758

Todorova, V., and Blokland, A. (2017). Mitochondria and synaptic plasticity in the mature and aging nervous system. *Curr. Neuropharmacol.* 15, 166–173. doi: 10.2174/1570159x14666160414111821

Toyoda, H., Wu, L. J., Zhao, M. G., Xu, H., and Zhuo, M. (2007). Time-dependent postsynaptic AMPA GluR1 receptor recruitment in the cingulate synaptic potentiation. *Dev. Neurobiol.* 67, 498–509. doi: 10.1002/dneu.20380

Toyoda, H., Zhao, M. G., Ulzhofer, B., Wu, L. J., Xu, H., Seeburg, P. H., et al. (2009). Roles of the AMPA receptor subunit GluA1 but not GluA2 in synaptic

potentiation and activation of ERK in the anterior cingulate cortex. *Mol. Pain* 5:46. doi: 10.1186/1744-8069-5-46

Ungless, M. A., Whistler, J. L., Malenka, R. C., and Bonci, A. (2001). Single cocaine exposure *in vivo* induces long-term potentiation in dopamine neurons. *Nature* 411, 583–587. doi: 10.1038/35079077

Van den Oever, M. C., Goriounova, N. A., Li, K. W., Van der Schors, R. C., Binnekade, R., Schoffelmeer, A. N., et al. (2008). Prefrontal cortex AMPA receptor plasticity is crucial for cue-induced relapse to heroin-seeking. *Nat. Neurosci.* 11, 1053–1058. doi: 10.1038/nn.2165

Vouimba, R. M., Yaniv, D., Diamond, D., and Richter-Levin, G. (2004). Effects of inescapable stress on LTP in the amygdala versus the dentate gyrus of freely behaving rats. *Eur. J. Neurosci.* 19, 1887–1894. doi: 10.1111/j.1460-9568.2004.03294.x

Wang, H., and Hahn, K. M. (2016). LOVTRAP: a versatile method to control protein function with light. *Curr. Protoc. Cell Biol.* 73, 21.10.21–21.10.14. doi: 10.1002/cpcb.12

Wang, H., Vilela, M., Winkler, A., Tarnawski, M., Schlichting, I., Yumerefendi, H., et al. (2016). LOVTRAP: an optogenetic system for photoinduced protein dissociation. *Nat. Methods* 13, 755–758. doi: 10.1038/nmeth.3926

Wang, H., Wu, L. J., Kim, S. S., Lee, F. J., Gong, B., Toyoda, H., et al. (2008). FMRP acts as a key messenger for dopamine modulation in the forebrain. *Neuron* 59, 634–647. doi: 10.1016/j.neuron.2008.06.027

Wang, J., Zhang, X., Cao, B., Liu, J., and Li, Y. (2015). Facilitation of synaptic transmission in the anterior cingulate cortex in viscerally hypersensitive rats. *Cereb. Cortex* 25, 859–868. doi: 10.1093/cercor/bht273

Wilson, B. M., and Cox, C. L. (2007). Absence of metabotropic glutamate receptor-mediated plasticity in the neocortex of fragile X mice. *Proc. Natl. Acad. Sci. U S A* 104, 2454–2459. doi: 10.1073/pnas.0610875104

Wolf, M. E. (2016). Synaptic mechanisms underlying persistent cocaine craving. *Nat. Rev. Neurosci.* 17, 351–365. doi: 10.1038/nrn.2016.39

Xu, H., Wu, L. J., Wang, H., Zhang, X., Vadakkan, K. I., Kim, S. S., et al. (2008). Presynaptic and postsynaptic amplifications of neuropathic pain in the anterior cingulate cortex. *J. Neurosci.* 28, 7445–7453. doi: 10.1523/JNEUROSCI.1812-08.2008

Yang, B., Zhang, J. C., Han, M., Yao, W., Yang, C., Ren, Q., et al. (2016). Comparison of R-ketamine and rapastinel antidepressant effects in the social defeat stress model of depression. *Psychopharmacology* 233, 3647–3657. doi: 10.1007/s00213-016-4399-2

Zhang, H., Etherington, L. A., Hafner, A. S., Belelli, D., Coussen, F., Delagrange, P., et al. (2013). Regulation of AMPA receptor surface trafficking and synaptic plasticity by a cognitive enhancer and antidepressant molecule. *Mol. Psychiatry* 18, 471–484. doi: 10.1038/mp.2012.80

Zhang, H., Zhang, C., Vincent, J., Zala, D., Benstaali, C., Sainlos, M., et al. (2018). Modulation of AMPA receptor surface diffusion restores hippocampal plasticity and memory in Huntington's disease models. *Nat. Commun.* 9:4272. doi: 10.1038/s41467-018-06675-3

Zhao, M. G., Toyoda, H., Ko, S. W., Ding, H. K., Wu, L. J., and Zhuo, M. (2005). Deficits in trace fear memory and long-term potentiation in a mouse model for fragile X syndrome. *J. Neurosci.* 25, 7385–7392. doi: 10.1523/jneurosci.1520-05.2005

Zhou, X. X., Fan, L. Z., Li, P., Shen, K., and Lin, M. Z. (2017). Optical control of cell signaling by single-chain photoswitchable kinases. *Science* 355, 836–842. doi: 10.1126/science.aah3605

Zhu, M., Cortese, G. P., and Waites, C. L. (2018). Parkinson's disease-linked Parkin mutations impair glutamatergic signaling in hippocampal neurons. *BMC Biol.* 16:100. doi: 10.1186/s12915-018-0567-7

Zhuo, M. (2019). Long-term cortical synaptic changes contribute to chronic pain and emotional disorders. *Neurosci. Lett.* 702, 66–70. doi: 10.1016/j.neulet.2018.11.048

Conflict of Interest: The authors declare that the research was conducted in the absence of any commercial or financial relationships that could be construed as a potential conflict of interest.

frontiers in Synaptic Neuroscience

REVIEW
published: 11 August 2020
doi: 10.3389/fnsyn.2020.00033

Neuroligins and Neurodevelopmental Disorders: X-Linked Genetics

Thien A. Nguyen[1,2], Alexander W. Lehr[1] and Katherine W. Roche[1]**

[1] Receptor Biology Section, National Institute of Neurological Disorders and Stroke, National Institutes of Health, Bethesda, MD, United States, [2] Department of Pharmacology and Physiology, Georgetown University, Washington, DC, United States

Autism spectrum disorder (ASD) is a neurodevelopmental disorder that results in social-communication impairments, as well as restricted and repetitive behaviors. Moreover, ASD is more prevalent in males, with a male to female ratio of 4 to 1. Although the underlying etiology of ASD is generally unknown, recent advances in genome sequencing have facilitated the identification of a host of associated genes. Among these, synaptic proteins such as cell adhesion molecules have been strongly linked with ASD. Interestingly, many large genome sequencing studies exclude sex chromosomes, which leads to a shift in focus toward autosomal genes as targets for ASD research. However, there are many genes on the X chromosome that encode synaptic proteins, including strong candidate genes. Here, we review findings regarding two members of the neuroligin (NLGN) family of postsynaptic adhesion molecules, *NLGN3* and *NLGN4*. Neuroligins have multiple isoforms (NLGN1-4), which are both autosomal and sex-linked. The sex-linked genes, *NLGN3* and *NLGN4*, are both on the X chromosome and were among the first few genes to be linked with ASD and intellectual disability (ID). In addition, there is a less studied human neuroligin on the Y chromosome, NLGN4Y, which forms an X-Y pair with NLGN4X. We will discuss recent findings of these neuroligin isoforms regarding function at the synapse in both rodent models and human-derived differentiated neurons, and highlight the exciting challenges moving forward to a better understanding of ASD/ID.

Keywords: autism, intellectual disabililties, NLGN3, NLGN4X, neuroligin

OPEN ACCESS

Edited by:
Kimberly M. Huber, University of Texas Southwestern Medical Center, United States

Reviewed by:
Dilja Krueger-Burg, University Medical Center Göttingen, Germany
Michele H. Jacob, Tufts University School of Medicine, United States

****Correspondence:***
Thien A. Nguyen
tan30@georgetown.edu
Katherine W. Roche
rochek@ninds.nih.gov

Received: *20 May 2020*
Accepted: *22 July 2020*
Published: *11 August 2020*

Citation:
Nguyen TA, Lehr AW and Roche KW (2020) Neuroligins and Neurodevelopmental Disorders: X-Linked Genetics. Front. Synaptic Neurosci. 12:33. doi: 10.3389/fnsyn.2020.00033

INTRODUCTION

Autism spectrum disorder (ASD) is a highly prevalent neurodevelopmental disorder affecting one in 54 children in the United States. ASD is characterized by deficits in communication and social interaction (Miles, 2011; Fombonne, 2013). Intellectual disability (ID) is characterized by deficits in intellectual functioning and adaptive behavior thus limiting an individual's ability to thrive independently (Raymond, 2006; Lubs et al., 2012; Ellison et al., 2013). Interestingly, both ASD and ID are more prevalent in males (Geschwind, 2011; Miles, 2011; Werling and Geschwind, 2013; Werling et al., 2016), although this strong sex bias in ASD remains unclear. It is notable that a subset of ASD-associated genes are located on the X chromosome indicating that the sex chromosomes may play a role in at least some of the sexual dimorphism in these disorders.

Autism spectrum disorder is divided into two categories: syndromic and nonsyndromic. Syndromic ASD is defined as a condition in patients who already have an existing neurological disorder. For example, a subset of patients with Fragile-X syndrome, tuberous sclerosis, or Rett

syndrome display phenotypes that are attributed to ASD (Singh and Eroglu, 2013; Geschwind and State, 2015). Nonsyndromic ASD accounts for ASD cases that are not linked to any neurological disorders. Before the advancement of next-generation sequencing (NGS), genetic researchers focused on finding rare genetic variants in ASD and ID pedigrees to link genes to these disorders, which led to the association of the neuroligins NLGN3 and NLGN4X to ASD/ID (Jamain et al., 2003; Laumonnier et al., 2004). Other notable genes identified through rare *de novo* mutations and recessive inheritance mutations include *SHANK3*, *CNTNAP2*, *NRXN1*, *PTEN*, *FMR1*, and *TSC1* (Geschwind and State, 2015). Although these cases are rare, functional and genetic studies definitively showed their link with ASD and ID. With NGS becoming cheaper and easier to access, genome wide association studies (GWAS) and whole exome sequencing (WES) studies became the major approaches used to identify common and rare variants for ASD/ID. Large cohort studies continue to identify more genes associated with ASD/ID, including genes that are important in chromatin modification, transcriptional regulation, or are FMRP-associated, embryonically expressed, or affect synaptic function (Sanders et al., 2012; Yu et al., 2013; De Rubeis et al., 2014; Iossifov et al., 2014). Although NGS has dramatically accelerated the identification of new risk genes, it is important to mention that NGS studies often ignore the sex chromosomes due to the limitations for statistical analysis (Wise et al., 2013; No Author List, 2017).

The neuroligin (NLGN) family of postsynaptic cell adhesion molecules have emerged as important factors regulating neuronal development and synaptic transmission. There are five members of the NLGN family in humans and other primates: NLGN1, 2, 3, 4X, and 4Y (Bemben et al., 2015b; Jeong et al., 2017; Südhof, 2017, 2018). However, in rodents, there are only four members: NLGN1, 2, 3, and 4-like (Bolliger et al., 2001, 2008). NLGNs have an isoform-specific localization: NLGN1 is localized to excitatory synapses, NLGN2 at inhibitory synapses, and NLGN3 is at both (Chih et al., 2005; Chubykin et al., 2007; Bemben et al., 2015b). Interestingly human NLGN4X is localized at excitatory synapses, whereas mouse NLGN4-like is at glycinergic synapses (Hoon et al., 2011; Bemben et al., 2015a; Chanda et al., 2016; Marro et al., 2019). NLGN4X and NLGN4Y were historically grouped together and assumed to have the same function due to their almost identical sequence identity. However, recent findings show that a single amino acid difference in NLGN4Y results in a trafficking deficit leading to decreased surface expression and synaptic function (Nguyen et al., 2020).

Neuroligins are highly dynamic, regulated via posttranslational modifications and protein–protein interactions. NLGN1 is phosphorylated by calcium/calmodulin-dependent protein kinase 2 (CaMKII), protein kinase A (PKA), and tyrosine kinases to regulate its function at excitatory synapses (Bemben et al., 2013; Giannone et al., 2013; Letellier et al., 2018; Jeong et al., 2019). Furthermore, a recent paper established that NLGN1-mediated synaptogenic properties are mediated by interacting with Kalirin7, a Rho guanine nucleotide exchange factor (GEF) (Paskus et al., 2019, 2020). Phosphorylation of NLGN2 affects binding with inhibitory scaffolding proteins, thus regulating its function at inhibitory synapses (Poulopoulos et al., 2009; Antonelli et al., 2014; Nguyen et al., 2016). NLGN3 can be cleaved by proteases to reduce its function at synapses (Bemben et al., 2019). Interestingly, the extracellular cleaved fragment of NLGN3 has been identified as a potent mitogen in brain cancer (Venkatesh et al., 2015, 2017). Lastly, NLGN4X can be phosphorylated by protein kinase C (PKC) to enhance excitatory synapses (Bemben et al., 2015a). Together, NLGNs comprise an important class of proteins that are dynamic and have multiple functions at synapses.

Of the NLGN family, *NLGN3*, *NLGN4X*, and *NLGN4Y* are sex-linked with *NLGN3* and *NLGN4X* on the X-chromosome and *NLGN4Y* on the Y-chromosome. Early genetic studies using a family pedigree of ASD/ID probands associated *NLGN3* and *NLGN4X* with ASD/ID (Jamain et al., 2003; Laumonnier et al., 2004) (**Tables 1**, **2**). Interestingly, the majority of cases for NLGN3- and NLGN4X-associated ASD/ID are males. In this review, we provide an overview of the current literature of sex-linked NLGNs functions and their links to ASD/ID.

NLGN3 AND ASD

The first link between ASD and *NLGN3* was revealed from a case study of ASD patients. Jamain et al. (2003) identified a missense mutation in a Swedish family with two affected brothers, one with ASD and the other with Asperger's syndrome. They showed that both probands contain a missense mutation in NLGN3 (NLGN3 R451C), which encodes an arginine instead of a cysteine at amino acid 451 within the extracellular domain (ECD) of NLGN3. The NLGN3 R451C mutant displays a decrease in surface expression compared to WT, and is retained in the ER by binding to the chaperone protein BiP (Chih et al., 2004; Comoletti et al., 2004; De Jaco et al., 2006). Unlike the human specific *NLGN4X*, *NLGN3* is highly conserved across mammals, facilitating the development of knock-in (KI) mouse models to study how NLGN3 mutations affect behavior.

In agreement with molecular studies, the NLGN3 R451C KI mouse displays a significant (∼90%) decrease in protein

TABLE 1 | ASD-associated NLGN3 variants.

Variants	Sex	Inheritance pattern	Primary Phenotype	Additional Comments/References
P104Qfs42X	N/A	N/A	ASD	Kenny et al. (2014)
R195W	N/A	De novo	ASD	Iossifov et al. (2014)
V306M	N/A	Maternal	ASD	Jiang et al. (2013)
V321A	M	Maternal	ASD	Yu et al. (2013)
N390X	N/A	Maternal	ASD	Yuen et al. (2017)
G426S	F	De novo	ASD	Xu et al. (2014)
W433X	M	Maternal	ASD	McRae et al. (2017)
R451C	M	Maternal	ASD	Jamain et al. (2003)
P514S	M × 2	Maternal	ASD	Quartier et al. (2019)
R597W	M × 3	Maternal	ASD	Quartier et al. (2019); Redin et al. (2014)
R617W	M × 2	Maternal	ASD/ID	Redin et al. (2014)
T632A	N/A	Maternal	ASD	Blasi et al. (2006)

TABLE 2 | ASD-associated NLGN4X variants.

Variants	Inheritance Pattern	Sex	Primary Phenotype	Additional Comments/References
G84R	Maternal	M	ASD	Asymptomatic mothers (Xu et al., 2014)
R87W	De novo	M	ASD	Zhang et al. (2009)
P94L	N/A	N/A	N/A	GeneDX submitted on ClinVar with unknown significance
G99S	Maternal	F	ASD	Mother also has learning disability. A brother also has learning disability (Yan et al., 2005)
		M	ASD	Mother also has learning disability. Sibling of above (Yan et al., 2005)
R101Q	Maternal	M	ASD	Nguyen et al. (2020)
V109L	Maternal	M	ID	Nguyen et al. (2020)
Q162K	De novo	F	ASD	Xu et al. (2014)
L211X	N/A	N/A	Anxiety, ADHD, Cerebral palsy	Yuen et al. (2017)
Q274X	Maternal	M	ADHD	Yuen et al. (2017)
A283T	Maternal	M	ASD	Xu et al. (2014)
Q329X	Maternal	M	ASD	Yu et al. (2013)
K378R	Maternal	M	ASD	Pampanos et al. (2009)
		M	ASD	Yan et al. (2005)
396X frameshift 1186t	Maternal	2 × M	Asperger's syndrome/ASD	Jamain et al. (2003)
V403M	Maternal	M	ASD	Have both affected and unaffected siblings (Xu et al., 2014)
429X (nt1253del(AG)	Maternal	13 × M	ASD/ID	Laumonnier et al. (2004)
V454_A457X	De novo	M	ID	Martínez et al. (2016)
V522M	De novo	N/A	TD	Wang et al. (2018)
R704C	Maternal	M	ASD	Unaffected sister (+/–) (Yan et al., 2005)
R766Q	Maternal	M	ASD	Yu et al. (2013)

levels compared to WT. Interestingly, the NLGN3 R451C mutant demonstrated a synaptic transmission gain-of-function phenotype, and these effects are synapse specific. Although the NLGN3 R451C KI mice have reduced protein levels, NLGN3 R451C mice, but not NLGN3 KO mice, display an increase in inhibitory synapses as measured by VGAT and gephyrin immunoreactivity. Furthermore, a concomitant increase in mIPSCs frequency in somatosensory cortex was observed in NLGN3 R451C mice, but not NLGN3 KO mice (Tabuchi et al., 2007). In addition, NLGN3 R451C leads to impaired inhibitory synaptic transmission in PV-neurons in KI animals, unlike the NLGN3 KO; however, both mouse lines show enhanced inhibitory synaptic transmission in cholecystokinin basket cells (Földy et al., 2013). Horn and Nicoll (2018) also provide additional evidence of the synapse-specific function of NLGN3 by showing that knocking down NLGN3 using miRNA specifically affected IPSCs recorded from somatostatin neurons, but not from PV-neurons. In addition, NLGN3 R451C mice, but not NLGN3 KO mice, have a striking phenotype at glutamatergic synapses. In the CA1 region of the hippocampus, NLGN3 R451C mice display an increase in excitatory synaptic transmission (Etherton et al., 2011). Along with this observation, Etherton et al. (2011) saw an increase in dendritic complexity and NMDAR protein levels in NLGN3 R451C mice. In contrast, NLGN3 R451C mice display impaired synaptic transmission at the calyx of Held synapses. Furthermore, Zhang et al. (2017) elegantly demonstrated that the synaptic effect of NLGN3 on the calyx of Held synapses is only observed when NLGN3 is deleted late, but not early, in development. Lastly, NLGN3 R451C KI mice and NLGN3 KO mice share a common synaptic defect at striatal synapses; the deletion or KI of NLGN3 in D1 neurons, but not D2 neurons, results in a decrease in mIPSCs frequency (Rothwell et al., 2014). Taken together, the NLGN3 R451C mutation differentially alter synaptic function depending on neuron and synapse type.

Behavioral analyses of NLGN3 R451C KI mice revealed a deficit in social interaction and an enhancement in spatial learning; however, these findings were not reproduced in a separate independent study, likely due to differences in mouse strains or behavioral protocols (Tabuchi et al., 2007; Chadman et al., 2008; Jaramillo et al., 2014; Lakhani et al., 2019). Another phenotype of ASD is repetitive behavior; and, interestingly, the NLGN3 R451C KI and NLGN3 KO mice share this phenotype despite differences in social interaction and spatial memory paradigms (Rothwell et al., 2014; Burrows et al., 2015). Indeed, NLGN3 R451C KI and NLGN3 KO mice both have an enhanced ability to stay on an accelerated rod (Chadman et al., 2008; Rothwell et al., 2014). Importantly, the repetitive behavior of NLGN3 mutants is due to dysfunction of D1-dopamine receptor-expressing medium spiny neurons, but not D2 neurons. Taken together, the ASD phenotypes of NLGN3 R451C KI and NLGN3 KO mice are circuit- and neuron-specific. Further investigations into which circuits affect the social interaction, spatial memory, and social memory phenotypes in NLGN3 R451C and NLGN3 KO are needed to better understand the mechanisms driving these behavioral deficits in ASD.

Studies in NLGN3 R451C KI and NLGN3 KO mice highlighted a need to better understand the physiological

function of NLGN3. For example, a striking observation in NLGN3 R451C KI mice is a ∼90% reduction in protein levels, while displaying both gain-of-function and loss-of-function phenotypes depending on the type of synapses. Different synaptic phenotypes induced by the single point mutation, NLGN3 R451C, suggest that WT NLGN3 normally functions in a context-dependent manner. Indeed, context-dependent function of NLGNs has been reported in which excitatory synapses are regulated by the relative expression of NLGN1. For example, NLGN1 KO mice display similar spine density as WT animals, but when NLGN1 KO neurons are co-cultured with WT neurons, the NLGN1 KO neurons show a reduction in spine density (Kwon et al., 2012). Applying this model of competition to NLGN3 R451C KI mice to explain the gain-of-function observed in this animal is worthy of investigation. It is also important to carefully study NLGN3 function throughout development. Zhang et al. (2017) demonstrated reduced synaptic transmission at the calyx of Held synapse when NLGN3 is deleted late, but not early, in development. They further showed that when NLGN3 is conditionally knocked out in early development, cerebellin-1 can compensate for the lack of NLGN3.

NLGN4X AND ITS LINK TO ASD

Divergence of NLGN4

Of the ASD-associated genes identified from human genetic screens, NLGNs are of particular interest due to their important function at synapses. Early genetic studies on the X chromosome indicated that a deletion at Xp22.3 was found in ASD/ID probands (Thomas et al., 1999; Zinn et al., 2007). Interestingly, *NLGN4X* is located within this region. Although disease-associated mutations in NLGNs are relatively rare, rigorous genetic studies using probands' pedigrees have established a causal link between NLGN4X and ASD/ID (**Table 2**).

Because *NLGN4X* is a human-specific gene, the discovery of mouse *NLGN4-like* was exciting because it allowed the study of NLGN4 in rodents to probe its role in ASD/ID. Although, there have been enormous advances in the field regarding the synaptic function of NLGN1-3, there are still many gaps in our understanding of the NLGN4 isoforms, which is complicated due to their unusually rapid divergence in humans and rodents. In humans, NLGN4 is sex-linked, and *NLGN4X* and *NLGN4Y* combine to form an X-Y gene pair. However, in mice, NLGN4 exists as a pseudo-autosomal gene often referred to as NLGN4-like. In addition, Maxeiner et al. (2020) observed that mouse NLGN4-like undergoes rapid evolution resulting in changes in protein sequence. Sequence alignment of NLGN4X with NLGN4-like shows seven insertions in NLGN4-like across both the ECD and intracellular domain (ICD). Interestingly, NLGN4 from the rodent infra-orders *castorimorpha*, *hystricomorpha,* and *sciuromorpha* retains similarity to human NLGN4X, whereas the rodent infra-order *myomorpha*, which includes mice, do not. Thus far NLGN4 has not been identified in rats (Bolliger et al., 2008; Maxeiner et al., 2020). Sequence alignment of mouse NLGN4-like, human NLGN4X, and NLGN4Y shows that NLGN4-like only shares ∼60% sequence identity with NLGN4X/4Y, whereas NLGN4X shares ∼97% sequence identity with NLGN4Y (**Figure 1**). A decade of research later, it is now clear that the human and rodent NLGN4 genes do not share the same function as previously assumed.

Human and Mouse NLGN4

Human NLGN4X was first cloned almost two decades ago. In the initial studies, NLGN4X was shown to be expressed and processed in a similar fashion to that of NLGN1. NLGN4X, like NLGN1, is glycosylated, traffics to the cell surface, and can bind to PSD-95 (Bolliger et al., 2001). Furthermore, NLGN4X is found at excitatory synapses. NLGN4X overexpression in mouse hippocampal neurons increases dendritic spine density, but it decreases mEPSCs frequency and amplitude (Chanda et al., 2016; Zhang et al., 2009). However, exogenously expressed human NLGN4X in rat hippocampal slices in combination with NLGN1-3 microRNA to knockdown endogenous NLGN1-3 showed an increase in spine density and a concomitant increase in both AMPAR- and NMDAR-mediated EPSCs (Bemben et al., 2015a). The difference between these two sets of experiments is the presence of endogenous NLGN1-3. It is unclear whether NLGN4X can form heterodimers with NLGN1-3 *in vivo*, although NLGN4X has been shown to form heterodimers with NLGN1 (Poulopoulos et al., 2012). Further investigation into this subject can provide a better understanding of the function of endogenous NLGN4X at synapses.

Using differentiated neurons from human induced pluripotent stem cells (iPS cells), NLGN4X was shown to colocalize with VGLUT and PSD-95, revealing NLGN4X localization at excitatory synapses (Marro et al., 2019). However, in NLGN4X KO differentiated neurons, Marro et al. (2019) did not observe any changes in either EPSCs or IPSCs. It is important to note that although differentiated human neurons from iPS cells can be useful, these differentiated neurons are not fully mature and are lacking NMDARs, a key component of excitatory synapses (Zhang et al., 2013; Quadrato et al., 2017; Marro et al., 2019).

In contrast to NLGN4X, mouse NLGN4-like functions at inhibitory synapses. Localization experiments in mice show that NLGN4-like is at glycinergic inhibitory synapses where it colocalizes with glycine receptors and gephyrin, but not PSD-95 in brainstem, spinal cord, and retina. Moreover, NLGN4-like KO mice were shown to have deficits in glycinergic synaptic transmission (Jamain et al., 2008; Hoon et al., 2011; Zhang et al., 2018). In addition, NLGN4-like also functions at GABAergic synapses (Hammer et al., 2015; Unichenko et al., 2018). In KO NLGN4-like mice, GABAergic synaptic transmission is impaired in hippocampal CA3 region (Hammer et al., 2015). Together, NLGN4-like primarily acts at inhibitory synapses, either glycinergic or GABAergic, whereas human NLGN4X acts at excitatory synapses.

NLGN4-like KO mice were generated over a decade ago and have been characterized extensively. However, the behavioral data have been complicated. For instance, NLGN4-like KO mice were first characterized as having a deficit in social interaction and vocalization (Jamain et al., 2008; El-Kordi et al., 2013; Ju et al., 2014); however, another study using the same NLGN4-like KO mice did not find any deficit in social interaction or

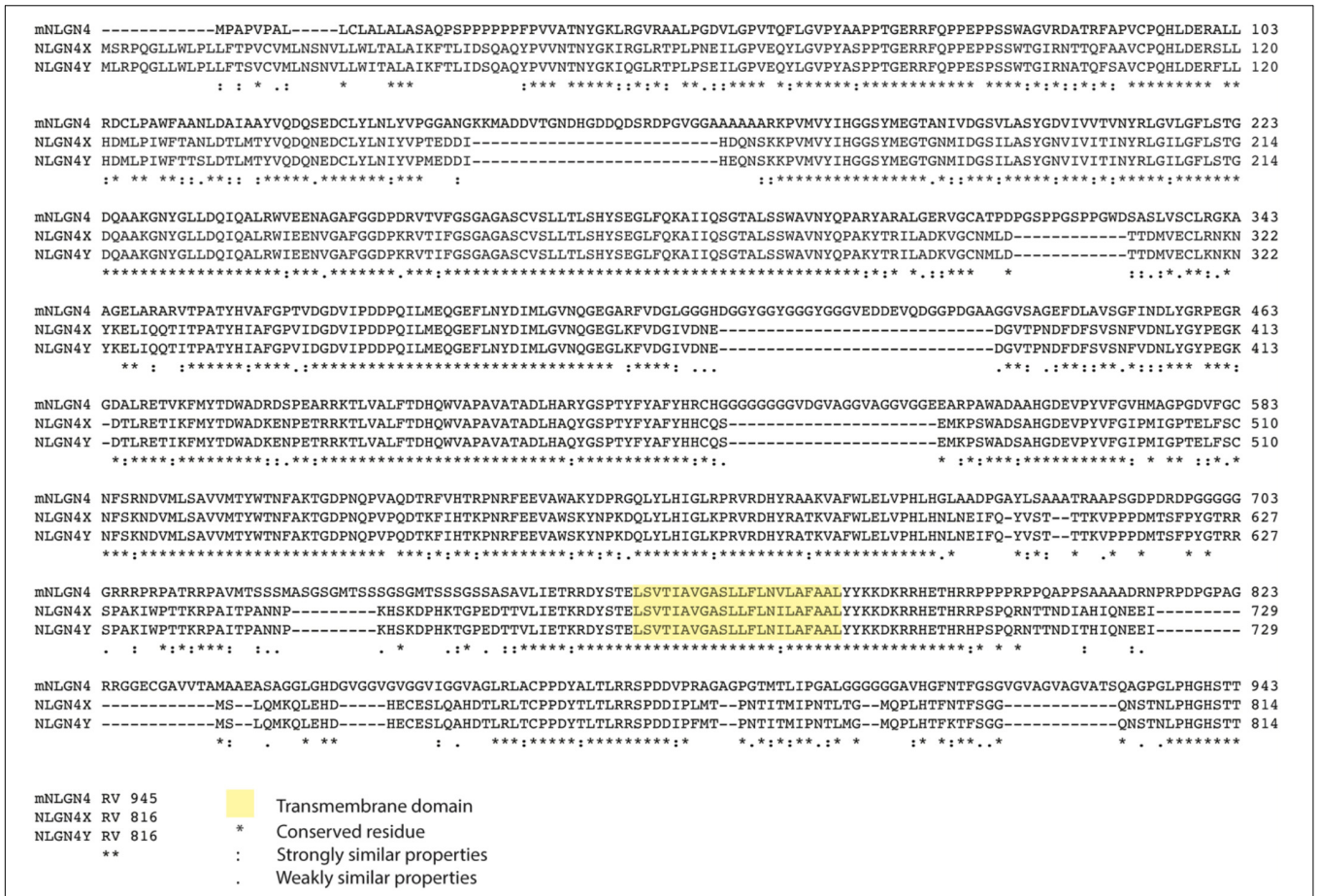

FIGURE 1 | Alignment of NLGN4. Alignment of mouse and human NLGN4s and their conservation.

vocalization (Ey et al., 2012). Although NLGN4-like KO mice provide insights into how this protein may function at synapses, because human NLGN4X and mouse NLGN4-like are divergent, there should be caution in linking mouse NLGN4-like studies with NLGN4X-associated neurodevelopmental disorders.

Lastly, NLGNs are dynamically regulated through posttranslational modifications (Bemben et al., 2015b; Jeong et al., 2017). Similar to NLGN1 and NLGN2, posttranslational modifications have an important role in regulating NLGN4X function (Bemben et al., 2015b; Jeong et al., 2017). NLGN4X is phosphorylated by PKC at T707 (Bemben et al., 2015a). Unlike CaMKII phosphorylation of NLGN1, PKC phosphorylation of NLGN4X does not increase its trafficking to the surface. However, phosphorylated NLGN4X T707 does lead to increases in spine density and aggregation of the excitatory synapse markers VGLUT and PSD-95 (Bemben et al., 2013; Bemben et al., 2015a). In addition, analyses of the NLGN4X phosphomimetic mutation, T707D, reveal significant enhancement of both AMPAR and NMDAR EPSCs compared to WT (Bemben et al., 2015a). How phosphorylated NLGN4X is able to increase excitatory synaptic strength will require additional investigation to reveal the precise mechanisms underlying synaptic potentiation. This topic would benefit from techniques that allow the characterization of spatiotemporal dynamics of PKC phosphorylation of NLGN4X *in vivo*. Furthermore, NLGN4X T707 is conserved in mouse NLGN4-like, but it is unclear whether this residue is phosphorylated in mouse NLGN4-like. Would the phosphorylation of this conserved threonine residue in mouse NLGN4-like enhance synaptic transmission as it does in human NLGN4X? Investigation on the mechanism of phosphorylation and the enhancement of synaptic transmission is a worthy topic to study.

NLGN4X AND ASD/ID

Jamain et al. (2003) first established NLGN4X as causative genes for ASD/ID through screening patients with ASD and Asperger's syndrome, and identified a frameshift mutation (1186insT) in *NLGN4X*, which leads to a premature stop codon at amino acid 396. Interestingly, in addition to the two probands, their mother also carries the mutation, but does not display any autistic symptoms (Jamain et al., 2003). The most convincing case for *NLGN4X* as an ASD/ID risk gene is from a study following a French family with a nonsense mutation in *NLGN4X*. Laumonnier et al. (2004) observed a 2-base-pair deletion in

NLGN4X that resulted in a stop codon at position 429. By documenting the clinical data from this large family, Laumonnier et al. (2004) observed that 13 males with the nonsense mutation were diagnosed with ASD, ID, or pervasive neurodevelopmental disorders, whereas female carriers were unaffected. This finding is remarkable in showing that this mutation in *NLGN4X* follows an X-linked recessive pattern. Many subsequent studies have linked *NLGN4X* with neurodevelopmental disorders, and the recurrent theme is that the majority of affected probands are males (**Table 2**).

Along with frameshift and nonsense mutations, many disease-associated missense mutations have been identified in *NLGN4X*. How might these missense mutations affect NLGN4X function? A missense mutation was identified in two ASD probands resulting in a substitution of an arginine residue to tryptophan (NLGN4X R87W). The NLGN4X R87W variant displays a profound deficit in NLGN4X surface expression, which leads to hypofunction of the protein due to decreased synaptogenesis. Furthermore, expression of NLGN4X R87W results in increased synaptic strength when overexpressed in neurons on a WT background (Zhang et al., 2009). It is puzzling why a variant that failed to induce synaptogenesis on a null background can still enhance synaptic function. Interestingly, a cluster of NLGN4X-associated variants has been identified near the NLGN4X R87W that also display a deficit in surface expression (Nguyen et al., 2020). Because these NLGN4X-associated variants are in the ECD, it is of interest to investigate their ability to bind to neurexin. Using the solved structure of NLGN4X, it was shown that ASD-associated mutations, such as NLGN4X G99S, are located outside of the neurexin binding domain (Fabrichny et al., 2007). These data suggest the observed phenotype from the cluster of NLGN4X-associated mutations is due to a deficit in trafficking.

Another NLGN4X rare variant that has garnered much attention is a substitution in the ICD from arginine to cysteine, NLGN4X R704C (Yan et al., 2005). As discussed above, NLGN4X is phosphorylated by PKC at T707 resulting in an increase in spine numbers and EPSCs (Bemben et al., 2015a). Interestingly, there were significant deficits in phosphorylation of NLGN4X T707 in the NLGN4X R704C variant, and the effects mediated by phosphorylation were abolished (Bemben et al., 2015a). In a separate study, Chanda et al. (2016) expressed NLGN4X R704C in cultured mouse neurons on a WT background and observed an increase in both NMDAR and AMPAR EPSCs compared to WT. Interestingly, neither study observed a change in surface trafficking. The discrepancy in these studies likely results from differences in experimental design, chiefly whether to include or exclude endogenous NLGN1-3. Taken together, NLGN4X R704C displays profound differences, compared to WT, in regulation of excitatory synapses. Using human differentiated neurons from NLGN4X R704C KI hiPSCs, Marro et al. (2019) observed an increase in EPSCs compared to WT. In addition, NLGN4X R704C was shown to increase binding with GluA1, but not PSD-95 (Marro et al., 2019), again revealing that this rare variant has multiple functional effects.

With the advances in stem cell research, it is now possible to study how different NLGN4X variants function in human neurons. Although studies taking this approach provide attractive new tools to study endogenous NLGN4X and its variants, there are pitfalls that needs to be addressed. Use of differentiated neurons from hiPSCs is still in its infancy and synaptic activity from these neurons does not represent the full endogenous nature of a synapse. For instance, it has been shown that differentiated neurons using single transcription expression models lack NMDA receptors (Zhang et al., 2013; Quadrato et al., 2017; Wang et al., 2017; Nehme et al., 2018). These neurons can express NMDARs if, and only if, they are allowed to grow for a long period of time (35+ days). Even so, to date, there is little biochemical evidence that NMDARs are present under these differentiation protocols. For the study of neuroligins, this is particularly problematic as they have been shown to directly interact with NMDARs via their ECDs (Budreck et al., 2013). Thus, although stem cell and differentiation technology are attractive and can be a powerful tool to study human neurons and diseases, a better understanding of the PSD in these neurons is needed before it can be used with great confidence as a model to study synaptic transmission.

NLGN4X AND NLGN4Y

Until recently, the studies on human specific NLGN4s have focused on NLGN4X. However, it is important to explore the function of NLGN4Y as well. NLGN4X and NLGN4Y are remarkably conserved with only 19 amino acid differences between them. Due to this high sequence conservation, the two proteins have been assumed to have the same function (Bemben et al., 2015b; Südhof, 2018); however, this hypothesis had not been experimentally examined until recently. Because NLGN4X/Y are sex-linked genes, an important consideration is the sex-bias in the expression of NLGN4X. Outside of the pseudo autosomal regions (PARs), some genes on the X chromosome can escape X-inactivation thus providing an imbalance of gene dosage between males and females (Carrel and Willard, 2005; Skuse, 2005; Helena Mangs and Morris, 2007; Tukiainen et al., 2017). Interestingly, there are Y-linked genes that are homologs to X-linked genes that escaped X-inactivation in order to balance the gene dosage in males. Furthermore, these X-Y gene pairs have been shown to have an important function in transcription, translation and protein stability (Bellott et al., 2014; Cortez et al., 2014; Hughes and Page, 2015). Together, these studies reveal an important role for genes on the Y chromosome other than sex determining genes. Indeed, comparison of *NLGN4X* and *NLGN4Y* expression in males and females reveals interesting differences. In a large transcriptomic study, *NLGN4Y* was shown to express only in males, as expected; however, *NLGN4X* was shown to express at similar level between males and females (Kang et al., 2011; Trabzuni et al., 2013). To complicate the issue further, a separate study reported that incomplete X-inactivation exists in mammals, and *NLGN4X* partially escapes (Carrel and Willard, 2005; Berletch et al., 2011). Interestingly, in a study using different tissues to study X-inactivation, *NLGN4X* expression is higher in the cortex in female vs. male (Tukiainen et al., 2017). Although gene expression of *NLGN4X* and *NLGN4Y* has been

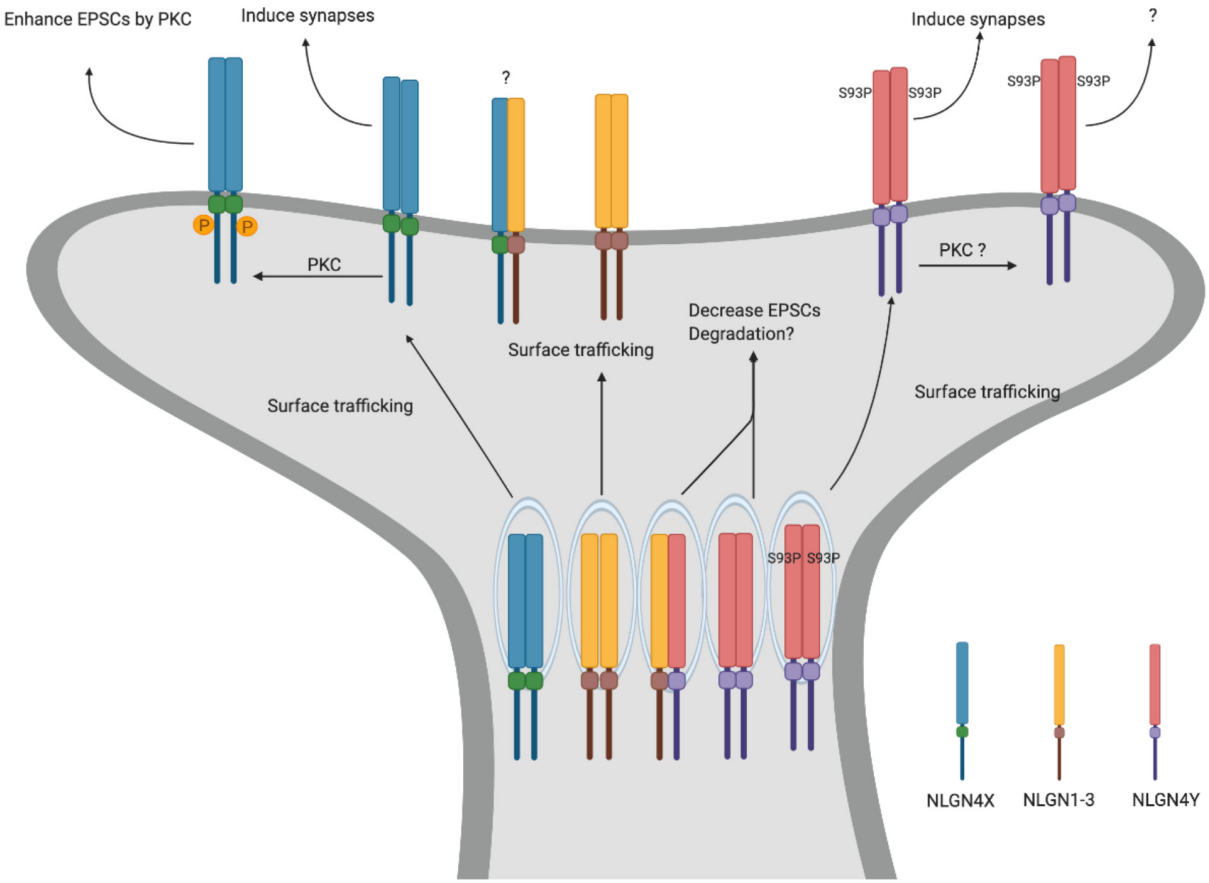

FIGURE 2 | NLGN4X and NLGN4Y function. Schematic for differential trafficking of NLGN4X vs NLGN4Y. NLGN4X can traffic to the surface and induce excitatory synapses. Furthermore, phosphorylation of NLGN4X by PKC drastically enhances excitatory postsynaptic currents (EPSCs). In contrast, NLGN4Y cannot traffic to the surface, thus decreasing EPSCs through binding with other NLGNs.

compared, research comparing NLGN4X and NLGN4Y protein function has lagged behind.

Although it was reasonable to hypothesize that NLGN4X and NLGN4Y served the same function due to their high sequence homology (97%), this hypothesis had never been tested. Interestingly, many ASD/ID variants have been identified in NLGN4X (Jamain et al., 2003; Laumonnier et al., 2004; Yan et al., 2005; Volaki et al., 2013; Xu et al., 2014; Bemben et al., 2015a; Chanda et al., 2016), whereas only one missense mutation has been identified in NLGN4Y (Yan et al., 2008). Furthermore, ASD/ID-associated mutations in NLGN4X selectively affect more males than females, and the reason for this male bias is unknown. This strong male bias observation in NLGN4X-associated diseases, prompted us to focus on NLGN4Y. If NLGN4Y and NLGN4X are functionally redundant, then there should not be a male bias in NLGN4X-associated diseases.

To explore the function of NLGN4Y, in a recent study, we directly compared NLGN4X and NLGN4Y and found that NLGN4Y cannot traffic to the surface to induce synapses (Nguyen et al., 2020). Furthermore, the differential trafficking observed between NLGN4X and NLGN4Y is due to an amino acid difference at position 93, with proline for NLGN4X and serine for NLGN4Y. Indeed, the NLGN4Y S93P mutant was able to efficiently traffic to the surface and induce synapses. Interestingly, there is a cluster of disease-associated NLGN4X variants surrounding the critical amino acid in NLGN4X. Upon analysis, these variants phenocopied the NLGN4Y trafficking deficit and cannot induce synapses (**Figure 2**).

What is the function of NLGN4Y if it cannot get to the surface? Nguyen et al. (2020) demonstrated that NLGN4Y can oligomerize with NLGN1, 2, 3, and 4X and reduce their surface trafficking. In addition, exogenously expressed NLGN4Y on a WT background decreased mEPSCs suggesting NLGN4Y acts to inhibit NLGN1-3 function. However, this study relies on exogenously expressed NLGNs in heterologous cells or rat hippocampal neurons. What the role is for endogenous NLGN4Y in human neurons is an important lingering question.

CONCLUSION

With the advances in NGS technologies, a wide variety of genes have been associated with ASD/ID. However, many of these studies have ignored the sex chromosomes due to the

additional expense and a lack of statistical power. However, historically many genes on the X-chromosome have been linked to ASD/ID by evaluating proband pedigrees. NLGN3 and NLGN4X, both on the X chromosome, were among the first genes associated with ASD/ID. Although NLGN3 and NLGN4X variants only occur in a small population of ASD/ID cases, studies using NLGN3 and NLGN4 mouse models have provided many insights into how disruptions in NLGN3 and NLGN4 function contribute to ASD/ID phenotypes. With advances in stem cell and neuronal differentiation, it is now possible to study NLGN3 and NLGN4X variants using human iPSCs to explore the causality between disruption in sex-linked NLGNs and ASD/ID by examining endogenous human neuroligins. Although neuronal differentiation is an exciting new technology to further our understanding of the human brain, differentiated neurons from human iPSCs are still relatively immature. Further improvement in the technologies to develop reliable mature neurons will be of paramount importance going forward. In addition, the unexpected revelations from the study of NLGN4X and NLGN4Y highlight the need to investigate the often-ignored Y-chromosome. Although many facets of the sex-linked NLGNs have been characterized, many important questions remain unanswered and provide a fertile topic for future investigation into synaptic regulation and to develop therapeutic treatments.

AUTHOR CONTRIBUTIONS

TN and KR wrote the manuscript. AL helped to create table for variants.

FUNDING

This review was supported by the National Institute of Neurological Disorders and Stroke Intramural Research Program (1ZIANS003140-06).

REFERENCES

Antonelli, R., Pizzarelli, R., Pedroni, A., Fritschy, J.-M., Del Sal, G., Cherubini, E., et al. (2014). Pin1-dependent signalling negatively affects GABAergic transmission by modulating neuroligin2/gephyrin interaction. *Nat. Commun.* 5:5066. doi: 10.1038/ncomms6066

Bellott, D. W., Hughes, J. F., Skaletsky, H., Brown, L. G., Pyntikova, T., Cho, T. J., et al. (2014). Mammalian y chromosomes retain widely expressed dosage-sensitive regulators. *Nature* 508, 494–499. doi: 10.1038/nature13206

Bemben, M. A., Nguyen, Q. A., Wang, T., Li, Y., Nicoll, R. A., and Roche, K. W. (2015a). Autism-associated mutation inhibits protein kinase C-mediated neuroligin-4X enhancement of excitatory synapses. *Proc. Natl. Acad. Sci. U.S.A.* 112, 2551–2556. doi: 10.1073/pnas.1500501112

Bemben, M. A., Nguyen, T. A., Li, Y., Wang, T., Nicoll, R. A., and Roche, K. W. (2019). Isoform-specific cleavage of neuroligin-3 reduces synapse strength. *Mol. Psychiatry* 24, 145–160. doi: 10.1038/s41380-018-0242-y

Bemben, M. A., Shipman, S. L., Hirai, T., Herring, B. E., Li, Y., Badger, J. D., et al. (2013). CaMKII phosphorylation of neuroligin-1 regulates excitatory synapses. *Nat. Neurosci.* 17, 56–64. doi: 10.1038/nn.3601

Bemben, M. A., Shipman, S. L., Nicoll, R. A., and Roche, K. W. (2015b). The cellular and molecular landscape of neuroligins. *Trends Neurosci.* 38, 496–505. doi: 10.1016/j.tins.2015.06.004

Berletch, J. B., Yang, F., Xu, J., Carrel, L., and Disteche, C. M. (2011). Genes that escape from X inactivation. *Hum. Genet.* 130, 237–245. doi: 10.1007/s00439-011-1011-z

Blasi, F., Bacchelli, E., Pesaresi, G., Carone, S., Bailey, A. J., and Maestrini, E. (2006). Absence of coding mutations in the X-linked genes neuroligin 3 and neuroligin 4 in individuals with autism from the IMGSAC collection. *Am. J. Med. Genet. Neuropsychiatr. Genet.* 141B, 220–221. doi: 10.1002/ajmg.b.30287

Bolliger, M. F., Frei, K., Winterhalter, K. H., and Gloor, S. M. (2001). Identification of a novel neuroligin in humans which binds to PSD-95 and has a widespread expression. *Biochem. J.* 356(Pt 2), 581–588. doi: 10.1042/0264-6021:3560581

Bolliger, M. F., Pei, J., Maxeiner, S., Boucard, A. A., Grishin, N. V., and Südhof, T. C. (2008). Unusually rapid evolution of Neuroligin-4 in mice. *Proc. Natl. Acad. Sci. U.S.A.* 105, 6421–6426. doi: 10.1073/pnas.0801383105

Budreck, E. C., Kwon, O.-B., Jung, J. H., Baudouin, S., Thommen, A., Kim, H.-S., et al. (2013). Neuroligin-1 controls synaptic abundance of NMDA-type glutamate receptors through extracellular coupling. *Proc. Natl. Acad. Sci. U.S.A.* 110, 725–730. doi: 10.1073/pnas.1214718110

Burrows, E. L., Laskaris, L., Koyama, L., Churilov, L., Bornstein, J. C., Hill-Yardin, E. L., et al. (2015). A neuroligin-3 mutation implicated in autism causes abnormal aggression and increases repetitive behavior in mice. *Mol. Autism* 6:62. doi: 10.1186/s13229-015-0055-7

Carrel, L., and Willard, H. F. (2005). X-inactivation profile reveals extensive variability in X-linked gene expression in females. *Nature* 434, 400–404. doi: 10.1038/nature03479

Chadman, K. K., Gong, S., Scattoni, M. L., Boltuck, S. E., Gandhy, S. U., Heintz, N., et al. (2008). Minimal aberrant behavioral phenotypes of neuroligin-3 R451C knockin mice. *Autism Res.* 1, 147–158. doi: 10.1002/aur.22

Chanda, S., Aoto, J., Lee, S. J., Wernig, M., and Südhof, T. C. (2016). Pathogenic mechanism of an autism-associated neuroligin mutation involves altered AMPA-receptor trafficking. *Mol. Psychiatry* 21, 169–177. doi: 10.1038/mp.2015.20

Chih, B., Afridi, S. K., Clark, L., and Scheiffele, P. (2004). Disorder-associated mutations lead to functional inactivation of neuroligins. *Hum. Mol. Genet.* 13, 1471–1477. doi: 10.1093/hmg/ddh158

Chih, B., Engelman, H., and Scheiffele, P. (2005). Control of excitatory and inhibitory synapse formation by neuroligins. *Science* 307, 1324–1328. doi: 10.1126/science.1107470

Chubykin, A. A., Atasoy, D., Etherton, M. R., Brose, N., Kavalali, E. T., Gibson, J. R., et al. (2007). Activity-dependent validation of excitatory versus inhibitory synapses by neuroligin-1 versus neuroligin-2. *Neuron* 54, 919–931. doi: 10.1016/j.neuron.2007.05.029

Comoletti, D., De Jaco, A., Jennings, L. L., Flynn, R. E., Gaietta, G., Tsigelny, I., et al. (2004). The Arg451Cys-neuroligin-3 mutation associated with autism reveals a defect in protein processing. *J. Neurosci.* 24, 4889–4893. doi: 10.1523/JNEUROSCI.0468-04.2004

Cortez, D., Marin, R., Toledo-Flores, D., Froidevaux, L., Liechti, A., Waters, P. D., et al. (2014). Origins and functional evolution of y chromosomes across mammals. *Nature* 508, 488–493. doi: 10.1038/nature13151

De Jaco, A., Comoletti, D., Kovarik, Z., Gaietta, G., Radiæ, Z., Lockridge, O., et al. (2006). A mutation linked with autism reveals a common mechanism of endoplasmic reticulum retention for the???,??-hydrolase fold protein family. *J. Biol. Chem.* 281, 9667–9676. doi: 10.1074/jbc.M510262200

De Rubeis, S., He, X., Goldberg, A. P., Poultney, C. S., Samocha, K., Cicek, A. E., et al. (2014). Synaptic, transcriptional and chromatin genes disrupted in autism. *Nature* 515, 209–215. doi: 10.1038/nature13772

El-Kordi, A., Winkler, D., Hammerschmidt, K., Kästner, A., Krueger, D., Ronnenberg, A., et al. (2013). Development of an autism severity score for mice using Nlgn4 null mutants as a construct-valid model of heritable monogenic autism. *Behav. Brain Res.* 251, 41–49. doi: 10.1016/j.bbr.2012.11.016

Ellison, J. W., Rosenfeld, J. A., and Shaffer, L. G. (2013). Genetic Basis of Intellectual Disability. *Annu. Rev. Med.* 64, 441–450. doi: 10.1146/annurev-med-042711-140053

Etherton, M., Földy, C., Sharma, M., Tabuchi, K., Liu, X., and Shamloo, M. (2011). Autism-linked neuroligin-3 R451C mutation differentially alters hippocampal and cortical synaptic function. *Proc. Natl. Acad. Sci. U.S.A.* 108, 13764–13769. doi: 10.1073/pnas.1111093108

Ey, E., Yang, M., Katz, A. M., Woldeyohannes, L., Silverman, J. L., Leblond, C. S., et al. (2012). Absence of deficits in social behaviors and ultrasonic vocalizations in later generations of mice lacking neuroligin4. *Genes Brain Behav.* 11, 928–941. doi: 10.1111/j.1601-183X.2012.00849.x

Fabrichny, I. P., Leone, P., Sulzenbacher, G., Comoletti, D., Miller, M. T., Taylor, P., et al. (2007). Structural analysis of the synaptic protein neuroligin and its β-neurexin complex: determinants for folding and cell adhesion. *Neuron* 56, 979–991. doi: 10.1016/j.neuron.2007.11.013

Földy, C., Malenka, R. C., and Südhof, T. C. (2013). Autism-associated neuroligin-3 mutations commonly disrupt tonic endocannabinoid signaling. *Neuron* 78, 498–509. doi: 10.1016/j.neuron.2013.02.036

Fombonne, E. (2013). The epidemiology of autism: a review. *Sci. Ment. Health* 2, 65–82. doi: 10.1017/S0033291799008508

Geschwind, D. H. (2011). Genetics of autism spectrum disorders. *Trends Cogn. Sci.* 15, 409–416. doi: 10.1016/j.tics.2011.07.003

Geschwind, D. H., and State, M. W. (2015). Gene hunting in autism spectrum disorder: on the path to precision medicine. *Lancet Neurol.* 14, 1109–1120. doi: 10.1016/S1474-4422(15)00044-7

Giannone, G., Mondin, M., Grillo-Bosch, D., Tessier, B., Saint-Michel, E., Czöndör, K., et al. (2013). Neurexin-1β binding to neuroligin-1 triggers the preferential recruitment of PSD-95 versus gephyrin through tyrosine phosphorylation of neuroligin-1. *Cell Rep.* 3, 1996–2007. doi: 10.1016/j.celrep.2013.05.013

Hammer, M., Krueger-Burg, D., Tuffy, L. P., Cooper, B. H., Taschenberger, H., Goswami, S. P., et al. (2015). Perturbed hippocampal synaptic inhibition and???-oscillations in a neuroligin-4 knockout mouse model of autism. *Cell Rep.* 13, 516–523. doi: 10.1016/j.celrep.2015.09.011

Helena Mangs, A., and Morris, B. J. (2007). The human pseudoautosomal region (PAR): origin, function and future. *Curr. Genom.* 8, 129–136. doi: 10.2174/138920207780368141

Hoon, M., Soykan, T., Falkenburger, B., Hammer, M., Patrizi, A., Schmidt, K.-F. K.-F., et al. (2011). Neuroligin-4 is localized to glycinergic postsynapses and regulates inhibition in the retina. *Proc. Natl. Acad. Sci. U.S.A.* 108, 3053–3058. doi: 10.1073/pnas.1006946108

Horn, M. E., and Nicoll, R. A. (2018). Somatostatin and parvalbumin inhibitory synapses onto hippocampal pyramidal neurons are regulated by distinct mechanisms. *Proc. Natl. Acad. Sci. U.S.A.* 115, 589–594. doi: 10.1073/pnas.1719523115

Hughes, J. F., and Page, D. C. (2015). The Biology and Evolution of Mammalian Y Chromosomes. *Annu. Rev. Genet.* 49, 507–527. doi: 10.1146/annurev-genet-112414-055311

Iossifov, I., O'Roak, B. J., Sanders, S. J., Ronemus, M., Krumm, N., Levy, D., et al. (2014). The contribution of de novo coding mutations to autism spectrum disorder. *Nature* 515, 216–221. doi: 10.1038/nature13908

Jamain, S., Quach, H., Betancur, C., Råstam, M., Colineaux, C., Gillberg, I. C., et al. (2003). Mutations of the X-linked genes encoding neuroligins NLGN3 and NLGN4 are associated with autism. *Nat. Genet.* 34, 27–29. doi: 10.1038/ng1136

Jamain, S., Radyushkin, K., Hammerschmidt, K., Granon, S., Boretius, S., Varoqueaux, F., et al. (2008). Reduced social interaction and ultrasonic communication in a mouse model of monogenic heritable autism. *Proc. Natl. Acad. Sci. U.S.A.* 105, 1710–1715. doi: 10.1073/pnas.0711555105

Jaramillo, T. C., Liu, S., Pettersen, A., Birnbaum, S. G., and Powell, C. M. (2014). Autism-related neuroligin-3 mutation alters social behavior and spatial learning. *Autism Res.* 7, 264–272. doi: 10.1002/aur.1362

Jeong, J., Pandey, S., Li, Y., Badger, J. D., Lu, W., and Roche, K. W. (2019). PSD-95 binding dynamically regulates NLGN1 trafficking and function. *Proc. Natl. Acad. Sci. U.S.A.* 116, 12035–12044. doi: 10.1073/pnas.1821775116

Jeong, J., Paskus, J. D., and Roche, K. W. (2017). Posttranslational modifications of neuroligins regulate neuronal and glial signaling. *Curr. Opin. Neurobiol.* 45, 130–138. doi: 10.1016/j.conb.2017.05.017

Jiang, Y. H., Yuen, R. K. C., Jin, X., Wang, M., Chen, N., Wu, X., et al. (2013). Detection of clinically relevant genetic variants in autism spectrum disorder by whole-genome sequencing. *Am. J. Hum. Genet.* 93, 249–263. doi: 10.1016/j.ajhg.2013.06.012

Ju, A., Hammerschmidt, K., Tantra, M., Krueger, D., Brose, N., and Ehrenreich, H. (2014). Juvenile manifestation of ultrasound communication deficits in the neuroligin-4 null mutant mouse model of autism. *Behav. Brain Res.* 270, 159–164. doi: 10.1016/j.bbr.2014.05.019

Kang, H. J., Kawasawa, Y. I., Cheng, F., Zhu, Y., Xu, X., Li, M., et al. (2011). Spatio-temporal transcriptome of the human brain. *Nature* 478, 483–489. doi: 10.1038/nature10523

Kenny, E. M., Cormican, P., Furlong, S., Heron, E., Kenny, G., Fahey, C., et al. (2014). Excess of rare novel loss-of-function variants in synaptic genes in schizophrenia and autism spectrum disorders. *Mol. Psychiatry* 19, 872–879. doi: 10.1038/mp.2013.127

Kwon, H.-B., Kozorovitskiy, Y., Oh, W.-J., Peixoto, R. T., Akhtar, N., Saulnier, J. L., et al. (2012). Neuroligin-1-dependent competition regulates cortical synaptogenesis and synapse number. *Nat. Neurosci.* 15, 1667–1674. doi: 10.1038/nn.3256

Lakhani, C. M., Manrai, A. K., Yang, J., Visscher, P. M., Patel, C. J., and Department, B. T. T. (2019). Genetic background effects in neuroligin-3 mutant mice: minimal behavioral abnormalities on C57 background. *Physiol. Behav.* 176, 139–148. doi: 10.1016/j.physbeh.2017.03.040

Laumonnier, F., Bonnet-Brilhault, F., Gomot, M., Blanc, R., David, A., Moizard, M.-P., et al. (2004). X-linked mental retardation and autism are associated with a mutation in the NLGN4 gene, a member of the neuroligin family. *Am. J. Hum. Genet.* 74, 552–557. doi: 10.1086/382137

Letellier, M., Szíber, Z., Chamma, I., Saphy, C., Papasideri, I., Tessier, B., et al. (2018). A unique intracellular tyrosine in neuroligin-1 regulates AMPA receptor recruitment during synapse differentiation and potentiation. *Nat. Commun.* 9:3979. doi: 10.1038/s41467-018-06220-2

Lubs, H. A., Stevenson, R. E., and Schwartz, C. E. (2012). Fragile X and X-linked intellectual disability: four decades of discovery. *Am. J. Hum. Genet.* 90, 579–590. doi: 10.1016/j.ajhg.2012.02.018

Marro, S. G., Chanda, S., Yang, N., Janas, J. A., Valperga, G., Trotter, J., et al. (2019). Neuroligin-4 regulates excitatory synaptic transmission in human neurons. *Neuron* 103, 617.e6–626.e6. doi: 10.1016/j.neuron.2019.05.043

Martínez, F., Caro-Llopis, A., Roselló, M., Oltra, S., Mayo, S., Monfort, S., et al. (2016). High diagnostic yield of syndromic intellectual disability by targeted next-generation sequencing. *J. Med. Genet.* 54, 87–92. doi: 10.1136/jmedgenet-2016-103964

Maxeiner, S., Benseler, F., Krasteva-Christ, G., Brose, N., and Südhof, T. C. (2020). Evolution of the autism-associated neuroligin-4 gene reveals broad erosion of pseudoautosomal regions in rodents. *Mol. Biol. Evol.* 37, 1243–1258. doi: 10.1093/molbev/msaa014

McRae, J. F., Clayton, S., Fitzgerald, T. W., Kaplanis, J., Prigmore, E., Rajan, D., et al. (2017). Prevalence and architecture of de novo mutations in developmental disorders. *Nature* 542, 433–438. doi: 10.1038/nature21062

Miles, J. H. (2011). Autism spectrum disorders-A genetics review. *Genet. Med.* 13, 278–294. doi: 10.1097/GIM.0b013e3181ff67ba

Nehme, R., Zuccaro, E., Ghosh, S. D., Li, C., Sherwood, J. L., Pietilainen, O., et al. (2018). Combining NGN2 programming with developmental patterning generates human excitatory neurons with NMDAR-mediated synaptic transmission. *Cell Rep.* 23, 2509–2523. doi: 10.1016/j.celrep.2018.04.066

Nguyen, Q. A., Horn, M. E., and Nicoll, R. A. (2016). Distinct roles for extracellular and intracellular domains in neuroligin function at inhibitory synapses. *eLife* 5, 1–21. doi: 10.7554/eLife.19236

Nguyen, T. A., Wu, K., Pandey, S., Lehr, A. W., Li, Y., Bemben, M. A., et al. (2020). A cluster of autism-associated variants on X-Linked NLGN4X functionally resemble NLGN4Y. *Neuron* 106, 759.e7–768.e7. doi: 10.1016/j.neuron.2020.03.008

No Author List (2017). Accounting for sex in the genome. *Nat. Med.* 23:1243. doi: 10.1038/nm.4445

Pampanos, A., Volaki, K., Kanavakis, E., Papandreou, O., Youroukos, S., Thomaidis, L., et al. (2009). A substitution involving the NLGN4 gene associated with autistic behavior in the greek population. *Genet. Test. Mol. Biomark.* 13, 611–615. doi: 10.1089/gtmb.2009.0005

Paskus, J. D., Herring, B. E., and Roche, K. W. (2020). Kalirin and trio: RhoGEFs in synaptic transmission, plasticity, and complex brain disorders. *Trends Neurosci.* 43, 505–518. doi: 10.1016/j.tins.2020.05.002

Paskus, J. D., Tian, C., Fingleton, E., Shen, C., Chen, X., Li, Y., et al. (2019). Synaptic kalirin-7 and trio interactomes reveal a gef protein-dependent neuroligin-1 mechanism of action. *Cell Rep.* 29, 2944.e5–2952.e5. doi: 10.1016/j.celrep.2019.10.115

Poulopoulos, A., Aramuni, G., Meyer, G., Soykan, T., Hoon, M., Papadopoulos, T., et al. (2009). Neuroligin 2 drives postsynaptic assembly at perisomatic inhibitory synapses through gephyrin and collybistin. *Neuron* 63, 628–642. doi: 10.1016/j.neuron.2009.08.023

Poulopoulos, A., Soykan, T., Tuffy, L. P., Hammer, M., Varoqueaux, F., and Brose, N. (2012). Homodimerization and isoform-specific heterodimerization of neuroligins. *Biochem. J.* 446, 321–330. doi: 10.1042/BJ20120808

Quadrato, G., Nguyen, T., Macosko, E. Z., Sherwood, J. L., Min Yang, S., Berger, D. R., et al. (2017). Cell diversity and network dynamics in photosensitive human brain organoids. *Nature* 545, 48–53. doi: 10.1038/nature22047

Quartier, A., Courraud, J., Thi Ha, T., McGillivray, G., Isidor, B., Rose, K., et al. (2019). Novel mutations in NLGN3 causing autism spectrum disorder and cognitive impairment. *Hum. Mutat.* 40, 2021–2032. doi: 10.1002/humu.23836

Raymond, F. L. (2006). X linked mental retardation: a clinical guide. *J. Med. Genet.* 43, 193–200. doi: 10.1136/jmg.2005.033043

Redin, C., Gérard, B., Lauer, J., Herenger, Y., Muller, J., Quartier, A., et al. (2014). Efficient strategy for the molecular diagnosis of intellectual disability using targeted high-throughput sequencing. *J. Med. Genet.* 51, 724–736. doi: 10.1136/jmedgenet-2014-102554

Rothwell, P. E., Fuccillo, M. V., Maxeiner, S., Hayton, S. J., Gokce, O., Lim, B. K., et al. (2014). Autism-associated neuroligin-3 mutations commonly impair striatal circuits to boost repetitive behaviors. *Cell* 158, 198–212. doi: 10.1016/j.cell.2014.04.045

Sanders, S. J., Murtha, M. T., Gupta, A. R., Murdoch, J. D., Raubeson, M. J., Willsey, A. J., et al. (2012). De novo mutations revealed by whole-exome sequencing are strongly associated with autism. *Nature* 485, 237–241. doi: 10.1038/nature10945

Singh, S. K., and Eroglu, C. (2013). Neuroligins provide molecular links between syndromic and nonsyndromic autism. *Sci. Signal.* 6:re4. doi: 10.1126/scisignal.2004102

Skuse, D. H. (2005). X-linked genes and mental functioning. *Hum. Mol. Genet.* 14, 27–32. doi: 10.1093/hmg/ddi112

Südhof, T. C. (2017). Synaptic neurexin complexes: a molecular code for the logic of neural circuits. *Cell* 171, 745–769. doi: 10.1016/j.cell.2017.10.024

Südhof, T. C. (2018). Towards an understanding of synapse formation. *Neuron* 100, 276–293. doi: 10.1016/j.neuron.2018.09.040

Tabuchi, K., Blundell, J., Etherton, M. R., Hammer, R. E., Liu, X., Powell, C. M., et al. (2007). A neuroligin-3 mutation implicated in autism increases inhibitory synaptic transmission in mice. *Science* 318, 71–76. doi: 10.1126/science.1146221

Thomas, N. S., Sharp, A. J., Browne, C. E., Skuse, D., Hardie, C., and Dennis, N. R. (1999). Xp deletions associated with autism in three females. *Hum. Genet.* 104, 43–48. doi: 10.1007/s004390050908

Trabzuni, D., Ramasamy, A., Imran, S., Walker, R., Smith, C., Weale, M. E., et al. (2013). Widespread sex differences in gene expression and splicing in the adult human brain. *Nat. Commun.* 4:2771. doi: 10.1038/ncomms3771

Tukiainen, T., Villani, A. C., Yen, A., Rivas, M. A., Marshall, J. L., Satija, R., et al. (2017). Landscape of X chromosome inactivation across human tissues. *Nature* 550, 244–248. doi: 10.1038/nature24265

Unichenko, P., Yang, J. W., Kirischuk, S., Kolbaev, S., Kilb, W., Hammer, M., et al. (2018). Autism related neuroligin-4 knockout impairs intracortical processing but not sensory inputs in mouse barrel cortex. *Cereb. Cortex* 28, 2873–2886. doi: 10.1093/cercor/bhx165

Venkatesh, H. S., Johung, T. B., Caretti, V., Noll, A., Tang, Y., Nagaraja, S., et al. (2015). Neuronal activity promotes glioma growth through neuroligin-3 secretion. *Cell* 161, 803–816. doi: 10.1016/j.cell.2015.04.012

Venkatesh, H. S., Tam, L. T., Woo, P. J., Lennon, J., Nagaraja, S., Gillespie, S. M., et al. (2017). Targeting neuronal activity-regulated neuroligin-3 dependency in high-grade glioma. *Nature* 549, 533–537. doi: 10.1038/nature24014

Volaki, K., Pampanos, A., Kitsiou-Tzeli, S., Vrettou, C., Oikonomakis, V., Sofocleous, C., et al. (2013). Mutation screening in the Greek population and evaluation of NLGN3 and NLGN4X genes causal factors for autism. *Psychiatr. Genet.* 23, 198–203. doi: 10.1097/YPG.0b013e3283643644

Wang, C., Ward, M. E., Chen, R., Liu, K., Tracy, T. E., Chen, X., et al. (2017). Scalable production of iPSC-derived human neurons to identify tau-lowering compounds by high-content screening. *Stem Cell Rep.* 9, 1221–1233. doi: 10.1016/j.stemcr.2017.08.019

Wang, S., Mandell, J. D., Kumar, Y., Sun, N., Morris, M. T., Arbelaez, J., et al. (2018). De novo sequence and copy number variants are strongly associated with tourette disorder and implicate cell polarity in pathogenesis. *Cell Rep.* 24, 3441.e12–3454.e12. doi: 10.1016/j.celrep.2018.08.082

Werling, D. M., and Geschwind, D. H. (2013). Understanding sex bias in autism spectrum disorder. *Curr. Opin. Neurol.* 26, 146–153. doi: 10.1097/WCO.0b013e32835ee548

Werling, D. M., Parikshak, N. N., and Geschwind, D. H. (2016). Gene expression in human brain implicates sexually dimorphic pathways in autism spectrum disorders. *Nat. Commun.* 7:10717. doi: 10.1038/ncomms10717

Wise, A. L., Gyi, L., and Manolio, T. A. (2013). EXclusion: toward integrating the X chromosome in genome-wide association analyses. *Am. J. Hum. Genet.* 92, 643–647. doi: 10.1016/j.ajhg.2013.03.017

Xu, X., Xiong, Z., Zhang, L., Liu, Y., Lu, L., Peng, Y., et al. (2014). Variations analysis of NLGN3 and NLGN4X gene in Chinese autism patients. *Mol. Biol. Rep.* 41, 4133–4140. doi: 10.1007/s11033-014-3284-5

Yan, J., Feng, J., Schroer, R., Li, W., Skinner, C., Schwartz, C. E., et al. (2008). Analysis of the neuroligin 4Y gene in patients with autism. *Psychiatr. Genet.* 18, 204–207. doi: 10.1097/YPG.0b013e3282fb7fe6

Yan, J., Oliveira, G., Coutinho, A., Yang, C., Feng, J., Katz, C., et al. (2005). Analysis of the neuroligin 3 and 4 genes in autism and other neuropsychiatric patients. *Mol. Psychiatry* 10, 329–332. doi: 10.1038/sj.mp.4001629

Yu, T. W., Chahrour, M. H., Coulter, M. E., Jiralerspong, S., Okamura-Ikeda, K., Ataman, B., et al. (2013). Using whole-exome sequencing to identify inherited causes of autism. *Neuron* 77, 259–273. doi: 10.1016/j.neuron.2012.11.002

Yuen, R. K. C., Merico, D., Bookman, M., Howe, J. L., Thiruvahindrapuram, B., Patel, R. V., et al. (2017). Whole genome sequencing resource identifies 18 new candidate genes for autism spectrum disorder. *Nat. Neurosci.* 20, 602–611. doi: 10.1038/nn.4524

Zhang, B., Gokce, O., Hale, W. D., Brose, N., and Südhof, T. C. (2018). Autism-associated neuroligin-4 mutation selectively impairs glycinergic synaptic transmission in mouse brainstem synapses. *J. Exp. Med.* 215, 1543–1553. doi: 10.1084/jem.20172162

Zhang, B., Seigneur, E., Wei, P., Gokce, O., Morgan, J., and Südhof, T. C. (2017). Developmental plasticity shapes synaptic phenotypes of autism-associated neuroligin-3 mutations in the calyx of Held. *Mol. Psychiatry* 22, 1483–1491. doi: 10.1038/mp.2016.157

Zhang, C., Milunsky, J. M., Newton, S., Ko, J., Zhao, G., Maher, T. A., et al. (2009). A neuroligin-4 missense mutation associated with autism impairs neuroligin-4 folding and endoplasmic reticulum export. *J. Neurosci.* 29, 10843–10854. doi: 10.1523/JNEUROSCI.1248-09.2009

Zhang, Y., Pak, C. H., Han, Y., Ahlenius, H., Zhang, Z., Chanda, S., et al. (2013). Rapid single-step induction of functional neurons from human pluripotent stem cells. *Neuron* 78, 785–798. doi: 10.1016/j.neuron.2013.05.029

Zinn, A. R., Roeltgen, D., Stefanatos, G., Ramos, P., Elder, F. F., Kushner, H., et al. (2007). A Turner syndrome neurocognitive phenotype maps to Xp22.3. *Behav. Brain Funct.* 3:24. doi: 10.1186/1744-9081-3-24

Conflict of Interest: The authors declare that the research was conducted in the absence of any commercial or financial relationships that could be construed as a potential conflict of interest.

frontiers in Molecular Neuroscience

ORIGINAL RESEARCH
published: 10 September 2020
doi: 10.3389/fnmol.2020.00161

The Fragile X Mental Retardation Protein Regulates Striatal Medium Spiny Neuron Synapse Density and Dendritic Spine Morphology

Jessica L. Huebschman[1,2], *Kitzia S. Corona*[1], *Yuhong Guo*[1] *and Laura N. Smith*[1,2]*

[1]Department of Neuroscience and Experimental Therapeutics, Texas A&M University Health Science Center, Bryan, TX, United States, [2]Texas A&M Institute for Neuroscience, Texas A&M University, College Station, TX, United States

The fragile X mental retardation protein (FMRP), an RNA-binding protein that mediates the transport, stability, and translation of hundreds of brain RNAs, is critically involved in regulating synaptic function. Loss of FMRP, as in fragile X syndrome (FXS), is a leading monogenic cause of autism and results in altered structural and functional synaptic plasticity, widely described in the hippocampus and cortex. Though FXS is associated with hyperactivity, impaired social interaction, and the development of repetitive or stereotyped behaviors, all of which are influenced by striatal activity, few studies have investigated the function of FMRP here. Utilizing a cortical-striatal co-culture model, we find that striatal medium spiny neurons (MSNs) lacking FMRP fail to make normal increases in PSD95 expression over a short time period and have significant deficits in dendritic spine density and colocalized synaptic puncta at the later measured time point compared to wildtype (WT) MSNs. Acute expression of wtFMRP plasmid in *Fmr1* KO co-cultures results in contrasting outcomes for these measures on MSNs at the more mature time point, reducing spine density across multiple spine types but making no significant changes in colocalized puncta. FMRP's KH2 and RGG RNA-binding domains are required for normal elimination of PSD95, and interruption of these domains slightly favors elimination of immature spine types. Further, KH2 is required for normal levels of colocalized puncta. Our data are largely consistent with a basal role for FMRP and its RNA-binding domains in striatal synapse stabilization on developing MSNs, and in light of previous findings, suggest distinct regional and/or cell type-specific roles for FMRP in regulating synapse structure.

Keywords: striatum, dendritic spine, RNA-binding proteins, FXS, synapse structure, morphology

OPEN ACCESS

Edited by:
P. Jesper Sjöström, McGill University, Canada

Reviewed by:
Aurore Thomazeau, Research Institute of the McGill University Health Center, Canada
Barbara Bardoni, UMR7275 Institut de Pharmacologie Moléculaire et Cellulaire (IPMC), France

***Correspondence:**
Laura N. Smith
laura.smith@tamu.edu

Received: *02 June 2020*
Accepted: *05 August 2020*
Published: *10 September 2020*

Citation:
Huebschman JL, Corona KS, Guo Y and Smith LN (2020) The Fragile X Mental Retardation Protein Regulates Striatal Medium Spiny Neuron Synapse Density and Dendritic Spine Morphology. Front. Mol. Neurosci. 13:161. doi: 10.3389/fnmol.2020.00161

INTRODUCTION

The fragile X mental retardation protein (FMRP) is an RNA-binding protein encoded by the *Fmr1* gene, which regulates the transport, stability, and translation of hundreds of brain RNAs, many of which are critically involved in synaptic function. FMRP contains several RNA-binding motifs, including three K-homology (KH0, KH1, and KH2) domains and a C-terminal

arginine-glycine-glycine (RGG) box, which associate with "kissing complex" and "G-quadruplex" RNA structures, respectively (Schaeffer et al., 2001; Darnell et al., 2005a; Myrick et al., 2015). Loss of FMRP, as observed in fragile X syndrome (FXS), is a leading monogenic cause of autism and intellectual disability, and is characterized by altered structural and functional synaptic plasticity throughout the brain (Irwin et al., 2001; Nimchinsky et al., 2001; Huber et al., 2002; Antar et al., 2006; Grossman et al., 2006; Pfeiffer et al., 2010; Bagni et al., 2012; Smith et al., 2014; Neuhofer et al., 2015). Of note, a single point mutation in FMRP's KH2 domain (I304N) reliably abolishes its interactions with "kissing complex" RNAs and polyribosomes *in vitro* (Darnell et al., 2005a), though no kissing complex motifs have yet been identified in FMRP targets, including those in a high confidence dataset (Darnell et al., 2011; Ascano et al., 2012; Anderson et al., 2016; Maurin et al., 2018). However, the I304N mutation does result in a particularly severe form of FXS (De Boulle et al., 1993; Feng et al., 1997), and truncations and point mutations in the RGG domain have been identified in individuals exhibiting FXS symptoms (Handt et al., 2014; Okray et al., 2015; Suhl and Warren, 2015), implicating both domains in the disease pathology.

Abnormalities in synapse density and dendritic spine morphology have been widely reported in human patients and animal models of FXS, with most studies indicating an increase in synapse and spine density, particularly of immature or transient spine types, throughout the cortex and hippocampus (Antar et al., 2006; Grossman et al., 2006; Pfeiffer and Huber, 2007; He and Portera-Cailliau, 2013). FMRP also regulates mGluR5-dependent hippocampal long-term depression (Huber et al., 2002) and changes in cortical GluR1 surface expression (Wang et al., 2008). In cultured *Fmr1* knockout (KO) hippocampal cells, acute expression of wildtype (WT) FMRP reduces synapse number in a manner dependent on its KH2, but not its RGG, RNA-binding domain (Pfeiffer and Huber, 2007), while FMRP having both the KH2 and RGG domains intact is required for activity-dependent synapse elimination by the myocyte enhancer factor 2 (MEF2) transcription factor (Pfeiffer et al., 2010), differentially implicating these domains in various forms of synaptic plasticity. FMRP also regulates numerous presynaptic activities, including translation-independent ion channel trafficking and stabilization, neurotransmitter release, and axon growth cone dynamics (Antar et al., 2006; Centonze et al., 2008; Deng et al., 2013; Ferron et al., 2020). Interestingly, while FMRP regulates localization of presynaptic voltage-gated calcium channels independently of new protein synthesis, mutations in the RGG RNA binding domain are sufficient to impair the protein-protein interactions necessary for this function (Ferron et al., 2020), highlighting a broader role for these domains in regulating synaptic plasticity.

Few studies have examined FMRP's function outside of the cortex and hippocampus. However, FXS is associated with hyperactivity, impaired social interaction, and the development of repetitive, or stereotyped behaviors, all of which are influenced by striatal activity, suggesting that FMRP may regulate synaptic function in this region, as well (Langen et al., 2011; Bagni et al., 2012; Báez-Mendoza and Schultz, 2013; Yael et al., 2019). Inhibitory transmission is enhanced in the striatum of *Fmr1* KO mice, despite a significant decrease in the number of GABAergic synapses (Centonze et al., 2008), but little is known about FMRP's striatal role in regulating plasticity. In the ventral striatum, lack of FMRP has been associated with deficits in presynaptic function and decreased stubby-type dendritic spine density (nucleus accumbens, shell region; Smith et al., 2014), a sharp contrast with the increases in spine density reported in cortex and hippocampus. While these initial studies suggest it may have a unique striatal function, the full extent of FMRP's regulation of synapses throughout this region remains largely unknown. Here, we sought to establish the role of FMRP in regulating striatal excitatory synapse number and dendritic spine morphology, and determine whether this function is dependent upon the KH2 or RGG RNA-binding motifs.

MATERIALS AND METHODS

Animals

Trio or pairwise breeding was conducted under standard laboratory conditions, in ventilated cages with a 12-h light/dark cycle (on at 06:00) and *ad libitum* access to standard mouse chow and water. Littermate embryos on a C57BL/6N background, either WT (male) and *Fmr1* KO (male and female) or *Fmr1* KO only (male and female), were generated with $Fmr1^{-/y}$ and $Fmr1^{-/+}$ or $Fmr1^{-/y}$ and $Fmr1^{-/-}$ breeders, respectively. All procedures were conducted in compliance with the Texas A&M University Institutional Animal Care and Use Committee (Protocol #: 2017-0234).

Primary Cortical-Striatal Co-culture

Dissociated cortical-striatal co-cultures were prepared on embryonic day 16 (ED16) using previously described protocols (Penrod et al., 2011). Briefly, pregnant mice were euthanized by CO_2 asphyxiation, and embryos were removed and rapidly genotyped by PCR. Cortical tissue (roughly corresponding to the prefrontal cortex) and the combined medial and lateral ganglionic eminences were collected by region and genotype into separate 15 ml conical tubes containing fresh Ca^{2+}/Mg^{2+}-free Hank's Balance Salt Solution with 10 mM HEPES (CMF-HBSS). After tissue had settled to the bottom of the tubes, CMF-HBSS was replaced with 0.25% trypsin digestion solution (10× Trypsin-EDTA, Sigma–Aldrich T4174). Tissue was incubated in digestion solution for 30 min at 37°C, after which cells were centrifuged at 1,000× *g* for 5 min and digestion solution was replaced with neuronal plating media (10 mM HEPES, 10 mM sodium pyruvate, 0.5 mM glutamine, 12.5 μM glutamate, 10% Newborn Calf Serum, 0.6% glucose in Earl's Minimal Essential Media). Following trituration, dissociated cells were counted using trypan blue and a hemocytometer. Cells were plated on coverslips coated with poly-D-lysine (PDL; Fisher ICN10269410) and laminin (Thermo Fisher 23017015) at a total density of 2×10^5 cells/35 mm dish (two parts striatal to three parts cortical). After 1 h, plating media was replaced with neuronal growth media [Neurobasal, Thermo Fisher 21103049; 50× B27, Thermo Fisher 17504-044; 0.5 mM L-glutamine (Q), Sigma G7513]. Cultures were kept at

37°C/5% CO_2 and half of the media per plate was replaced every 3–4 days with new growth media. Cultures were designated for either synaptic puncta or dendritic spine analysis; for each measurement, two to three replicates (separate cultures/litters) were used per group. In relevant studies, calcium phosphate transfection was performed at day *in vitro* (DIV) eight to introduce green fluorescent protein (GFP) alone, or various forms of enhanced (E)GFP-tagged FMRP. The WT (wtFMRP-EGFP), arginine/glycine-rich box (RGG) deletion (lacking amino acids RRGDGRRRGGGGRGQGGRGRGGGFKGN; ΔRGG-FMRP-EGFP), and I304N point mutant (KH2 domain; I304N-FMRP-EGFP) forms of FMRP-EGFP were under control of the endogenous human *Fmr1* promoter, as described (Darnell et al., 2005b; Pfeiffer and Huber, 2007). For spine analysis, cells were transfected with mCherry, either alone or in addition to the above constructs, at the same time point. At designated time points (DIV 10 or 14), cells were fixed in 4% paraformaldehyde (PFA)/4% sucrose (15 min) at room temperature, washed in 1× PBS (three times), and stored at 4°C protected from light until staining.

Immunocytochemistry and Fluorescent Microscopy

For synaptic puncta experiments, fixed cells were blocked in 10% goat serum (30 min) and permeabilized in 0.2% Triton-X (10 min) at room temperature. A second blocking step (10 min) was used, as recommended for the preservation of fine cell structures (Penrod et al., 2011). Cells were incubated overnight (shaking, 4°C) in primary antibody diluted in PBS with 1% goat serum (synapsin Ia and Ib, Millipore Sigma AB1543, 1:500; PSD95 Millipore Sigma MABN 68, 1:200). Afterwards, cells were rinsed with PBS and incubated (1 h) at room temperature in goat anti-rabbit Alexa-Fluor 647, goat anti-mouse Alexa-Fluor 488 (untransfected), or goat anti-mouse Alexa-Fluor 594 (transfected) secondary antibodies (Thermo Fisher, 1:1,000) diluted in PBS with 1% goat serum and 0.2% Triton-X. Following final rinses in PBS, coverslips were mounted on microscope slides with Vectashield antifade mounting medium (Vector Labs H-1000) for imaging.

Fluorescence was detected using an Olympus FV1000 confocal microscope with a 60× (puncta) or 100× (spines) oil immersion lens. Intact medium spiny neurons (MSNs) were identified for analysis by their soma size (10–20 μm) and dendritic arborization, as indicated by expression of PSD95 (puncta, untransfected cells), GFP (puncta, transfected cells), or mCherry (spines). For synaptic puncta experiments, *z*-stacks encompassing the entirety of the cell soma and visible processes were collected using a step size of 0.50 μm. For dendritic spine experiments, a *z*-stack (step size 0.45 μm) of mCherry fluorescence from an isolated region of a single secondary or higher order dendritic branch (≥20 μm) from each cell was collected for analysis. To minimize crossover of GFP fluorescence emission, GFP+ cells were first identified *via* epifluorescence and then, using the 543 nm laser, mCherry positivity was confirmed and a *z*-stack of the dendritic branch was collected. When collecting a multi-channel image that included both GFP and mCherry signals, mCherry was first collected alone for reconstruction before proceeding to multi-channel imaging, minimizing photobleaching and ensuring that images collected for spine analyses were captured with only the 543 nm laser active.

Synaptic Puncta Analysis

Maximum intensity projection images were generated in Fiji (Schindelin et al., 2012) from acquired *z*-stacks using the Extended Depth of Field plugin (Aguet et al., 2008), and used to generate cell reconstructions with the NeuronJ plugin (Meijering et al., 2004). Reconstructions of MSNs were built from either the PSD95 (basal experiments) or GFP (transfection experiments) projection images. Points of fluorescent intensity above a set threshold for PSD95 and synapsin I, as well as points of colocalization, defined as overlap between PSD95 and synapsin I signals, were quantified along dendritic tracings in a radius of approximately 70 μm in all directions from the soma of interest using the SynapCountJ2 plugin (Mata et al., 2016). Dendritic diameter was set to 20 pixels, or approximately 3.12 μm, and only points of fluorescent intensity above threshold within this dendritic area were included in analysis. Thresholds were defined for each cell individually as a set number of standard deviations (*untransfected cells*: 3 or 4; *transfected cells*: 2 or 3; for PSD95 and synapsin I, respectively) above the average fluorescent signal from that cell's maximum intensity projection image, not varying within experiment.

Dendritic Spine Analysis

MSN dendritic branches and spines were reconstructed from *z*-stacks using the semi-automated Filament Tracer tool in Imaris (Bitplane, Oxford Instruments). Morphological characteristics, including spine head and neck diameter, branching, and length were used to classify dendritic spines based on previously described criteria (Harris et al., 1992; Jedynak et al., 2007). Briefly, spines having head diameters ≥0.55 μm, which also exceeded the diameter of the spine neck, were considered mushroom type. Spines with a spine head <0.55 μm but still greater than the spine neck diameter were classified as thin type. When head diameter equaled or was less than spine neck diameter, length determined categorization as either filopodia (>1.0 μm) or stubby type (≤1.0 μm). Spines with single or multiple branch points were categorized as branched or thorny, respectively, regardless of other measurements. Spine density was calculated for each cell as the number of spines (total or by type) over the length of the reconstructed dendritic branch.

Statistical Analysis

All statistical analysis and results are listed in **Supplementary Table S1**. Synaptic puncta and total dendritic spine density were analyzed with one- (plasmid) or two-way (genotype × time point) between-subjects analysis of variance (ANOVA). Densities of spines by type were analyzed using two-way (genotype × spine type or plasmid × spine type) mixed ANOVAs, where spine type was a within-subjects variable. Significant interactions were followed by additional ANOVAs (one-way), paired *t*-tests, and/or Bonferroni *post hoc* analyses, as appropriate, to evaluate simple main effects (SMEs).

When Mauchly's test of sphericity was significant, either Greenhouse–Geisser (G–G; when $\varepsilon < 0.75$) or Huynh–Feldt (H–F; when $\varepsilon > 0.75$) corrections were used. All statistics were performed using GraphPad Prism or SPSS software. Significance was set at $\alpha = 0.05$.

RESULTS

FMRP Mediates Striatal Excitatory Synapse Number

To determine FMRP's role in regulating excitatory synapse number, we compared expression of presynaptic (synapsin I) and postsynaptic (PSD95) markers, quantified as distinct puncta above a set threshold (see "Materials and Methods" section), along dendritic branches of cultured WT and *Fmr1* KO MSNs at DIV 10 and 14 (**Figure 1A**). Synapsin Ia is fairly stably expressed, at least in cultured embryonic hippocampal cells, over the time points represented here (Ferreira et al., 2000), and with little exception, synapsin I is expressed in all neurons (presynaptic), and appearance is tightly linked to synaptic ontogenesis (De Camilli et al., 1983). There is additional evidence in other culture systems that pre- and postsynaptic proteins are stably present at or before DIV 10, largely preceding, but ultimately associated with, the development of spines or synapses (Ahmari et al., 2000; Prange and Murphy, 2001). We observed no significant main effects or interactions of genotype or day on expression of the presynaptic marker, synapsin I (**Figure 1B**). For expression of the postsynaptic marker, PSD95, two-way ANOVA showed a significant interaction between day and genotype ($F_{(1,236)} = 4.13$, $p < 0.05$). Follow-up Bonferroni analysis of this interaction revealed a significant SME of day for WT cells ($p < 0.001$), with density of PSD95 puncta being significantly higher on MSNs at DIV 14 (**Figure 1C**). We next quantified density of colocalized synapsin I and PSD95 puncta staining, as a measure of structural excitatory synapses. Two-way ANOVA of colocalized puncta revealed significant main effects of day ($F_{(1,236)} = 13.13$, $p < 0.001$) and genotype ($F_{(1,236)} = 6.639$, $p < 0.05$; **Figure 1D**). SMEs were observed for day within the WT group ($p < 0.01$), with DIV 14 greater than DIV 10, and for genotype within the DIV 14 time point ($p < 0.05$), where WT had significantly more colocalized puncta than *Fmr1* KO cells.

Striatal *Fmr1* KO MSNs Have Reduced Dendritic Spine Density

To more clearly determine the role of FMRP in regulating excitatory postsynaptic structure, we next compared dendritic spine density and morphology in cultured WT and *Fmr1* KO MSNs transfected with mCherry plasmid at DIV 14 (**Figure 2A**). An unpaired *t*-test showed a significant difference in total spine density between WT and KO cells ($t_{(98)} = 5.382$, $p < 0.0001$; **Figure 2B**), with *Fmr1* KO cells having significantly lower overall density. All spines were classified based on structural features (see "Materials and Methods" section) as thin, filopodia, stubby, mushroom, branched, or thorny type. Two-way mixed ANOVA indicated a significant interaction between genotype and spine classification ($F_{(5,490)} = 5.323$, $p < 0.0001$). Follow-up analysis revealed significant SMEs of genotype for thin ($p < 0.0001$), filopodia ($p < 0.01$), and stubby ($p < 0.0001$) spine types (**Figure 2C**), with the KO group having significantly lower spine density than the WT for each.

FMRP's RNA-Binding Domains Mediate Striatal Synaptic Markers

Acute expression of FMRP drives synapse elimination in hippocampal cells in a manner dependent on its KH2 RNA-binding domain (Pfeiffer and Huber, 2007). Given our basal findings, we next wanted to determine the effect of acute expression of FMRP, as well as the role of its KH2 and RGG RNA-binding domains, in regulating striatal excitatory synapse number. To do so, we compared pre-, post-, and colocalized synaptic puncta density in *Fmr1* KO cells transfected with plasmids expressing wtFMRP-EGFP, GFP alone, I304N-FMRP-EGFP, or ΔRGG-FMRP-EGFP at the DIV 14 time point (**Figure 3A**). For density of synapsin I puncta, one-way ANOVA showed a significant main effect of plasmid ($F_{(3,152)} = 5.67$, $p = 0.001$), with Bonferroni *post hoc* analysis indicating significantly greater density in the ΔRGG group compared to either the wtFMRP ($p < 0.01$) or I304N ($p < 0.01$) groups (**Figure 3B**). Analysis of PSD95 puncta density also revealed a significant main effect of plasmid ($F_{(3,152)} = 11.5$, $p < 0.0001$). Follow-up testing showed that cells receiving the wtFMRP plasmid had significantly lower PSD95 density compared to all other groups (GFP, $p < 0.0001$; I304N, $p < 0.01$; ΔRGG, $p < 0.0001$), and PSD95 density for the I304N group was significantly lower than that of the ΔRGG group ($p < 0.05$; **Figure 3C**). One-way ANOVA of colocalized puncta densities showed a significant main effect of plasmid ($F_{(3,152)} = 5.262$, $p < 0.01$), with Bonferroni follow-up analysis indicating that puncta density in the ΔRGG group was significantly higher than that of the GFP (KO; $p < 0.05$) and I304N ($p < 0.05$) groups (**Figure 3D**).

FMRP's RNA-Binding Domains Mediate MSN Dendritic Spine Morphology

Given our findings that FMRP's RNA-binding domains are involved in regulating synapse, and particularly PSD95, density, we next compared dendritic spine density and morphology between *Fmr1* KO cells transfected with plasmids expressing mCherry (for spine analysis) and either wtFMRP-EGFP, GFP, I304N-FMRP-EGFP, or ΔRGG-FMRP-EGFP (**Figure 4A**). For total spine density, one-way ANOVA revealed a significant main effect of plasmid ($F_{(3,143)} = 4.586$, $p < 0.01$), with Bonferroni *post hoc* analyses indicating significant decreases in spine density in the wtFMRP ($p < 0.05$), I304N ($p < 0.05$), and ΔRGG ($p < 0.01$) groups compared to the GFP (KO) control group (**Figure 4B**, inset). When spines were considered by type, a two-way mixed ANOVA showed a significant interaction between spine classification and plasmid ($F_{(15,715)} = 1.76$, $p < 0.05$). Follow-up Bonferroni analysis indicated that expression of ΔRGG significantly decreased the density of filopodia spines ($p < 0.05$), and the I304N group trended towards a significantly decreased thin spine density ($p = 0.067$), each compared to the GFP (KO) group (**Figure 4B**). The relative frequency distribution of

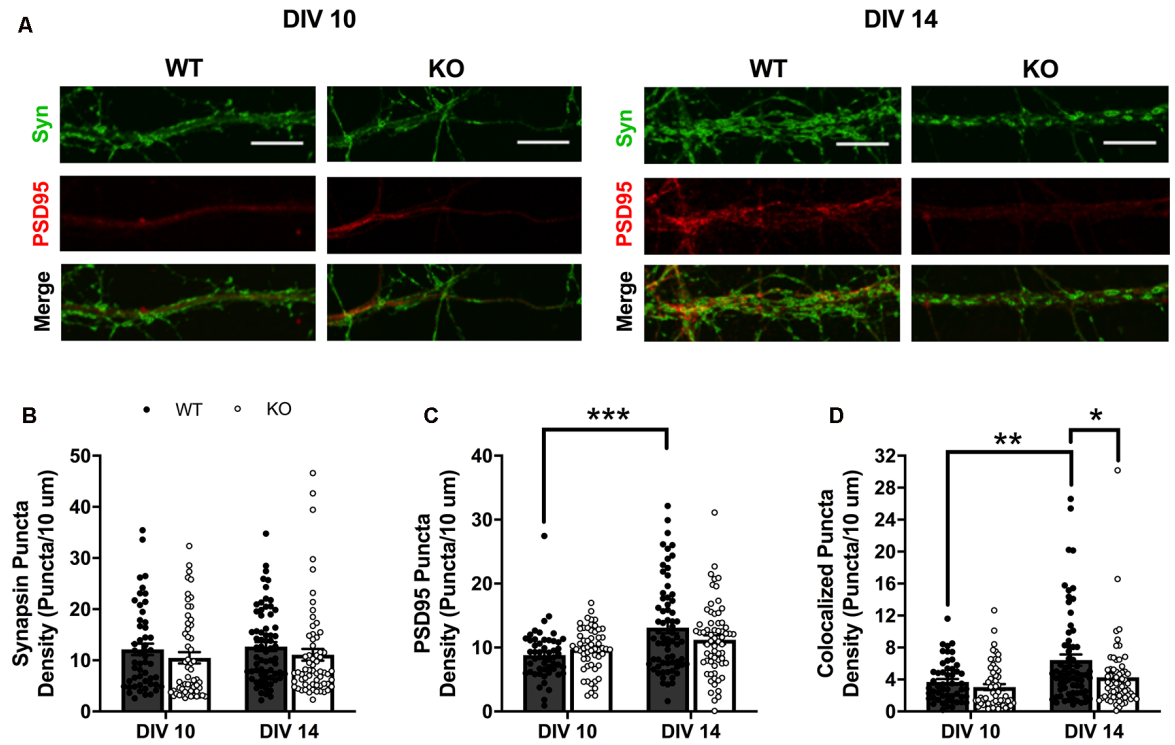

FIGURE 1 | Expression of presynaptic (synapsin I; green) and postsynaptic (PSD95; red) markers in wildtype (WT) and *Fmr1* knockout (KO) medium spiny neurons (MSNs) at day *in vitro* (DIV) 10 and 14 (**A**; scale bars are 10 μm). Synapsin I expression did not vary between genotypes or across the two time-points (**B**; two-way analysis of variance, ANOVA). WT cells have significantly increased density of PSD95 at DIV 14 compared to DIV 10, but KO cells show no change in expression level between the two time points (**C**; two-way ANOVA). Only WT cells increase the density of colocalized pre- and postsynaptic markers from DIV 10 to 14, with KO cells showing a significant deficit at DIV 14 compared to WT counterparts (**D**; two-way ANOVA). Significant Bonferroni comparisons are indicated (*$p < 0.05$, **$p < 0.01$, ***$p < 0.001$); data shown are mean ± SEM.

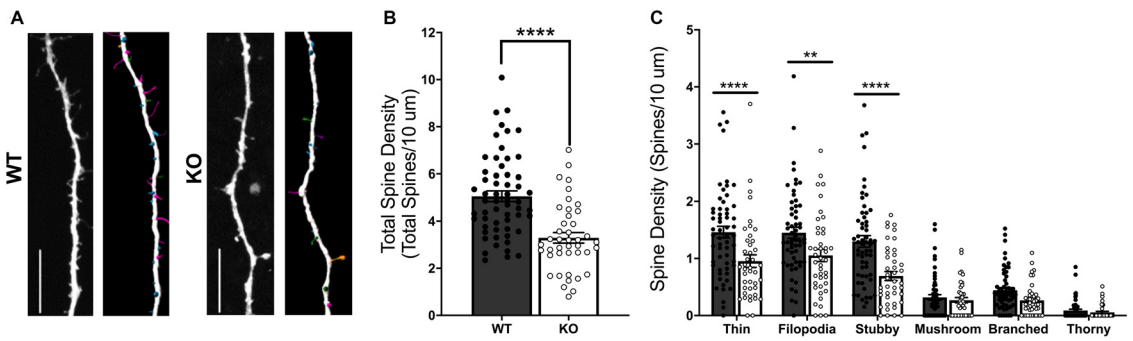

FIGURE 2 | Dendritic spine analysis of WT and *Fmr1* knockout (KO) striatal MSNs at day *in vitro* (DIV) 14 (**A**; scale bars 10 μm). KO cells have a significant deficit in total dendritic spine density (**B**; unpaired *t*-test), as well as deficits in thin, filopodia, and stubby spine type densities (**C**; two-way RM ANOVA). Significant Bonferroni comparisons are indicated (**$p < 0.01$, ****$p < 0.0001$); data shown are mean ± SEM.

spine types for each group is displayed in **Figure 4C**. We also observed differences in spine head diameter between groups, with one-way ANOVA showing a significant main effect of plasmid ($F_{(3,5241)} = 53.08$, $p < 0.0001$). Bonferroni *post hoc* analyses indicated that, compared to the GFP (KO) group, spines in the I304N and ΔRGG groups had significantly greater average head diameter ($p < 0.0001$ and $p < 0.001$, respectively), and there was a trend toward significance for wtFMRP spines to be of greater head diameter than GFP (KO; $p = 0.055$). In addition, the I304N group spines had significantly greater average head diameter than either the wtFMRP ($p < 0.0001$) or the ΔRGG ($p < 0.0001$) groups (**Figure 4D**).

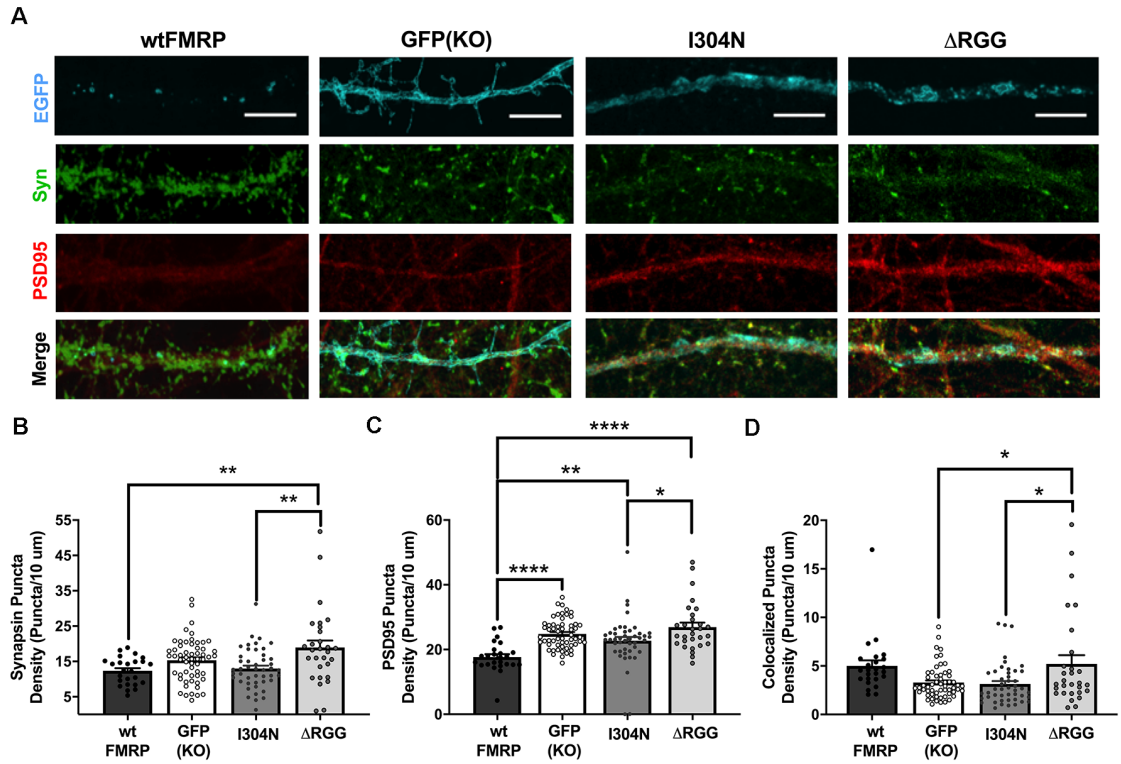

FIGURE 3 | Expression of presynaptic (synapsin I; green) and postsynaptic (PSD95; red) markers at day *in vitro* (DIV) 14 in *Fmr1* knockout (KO) MSNs transfected with either green fluorescent protein (GFP) alone, or various forms of EGFP-tagged FMRP (**A**; scale bars are 10 μm). Cells transfected with ΔRGG-FMRP have a higher density of synapsin than those transfected with wt- or I304N-FMRP (**B**; one-way ANOVA). Cells transfected with wt-FMRP had significantly decreased density of PSD95 puncta, while those transfected with I304N- or ΔRGG-FMRP did not differ from GFP (KO) controls (**C**; one-way ANOVA). Cells transfected with ΔRGG-FMRP had a greater density of colocalized synapsin and PSD95 puncta compared to those transfected with I304N-FMRP and GFP (KO) controls (**D**; one-way ANOVA). Significant Bonferroni comparisons are indicated (*$p < 0.05$, **$p < 0.01$, ****$p < 0.0001$); data shown are mean ± SEM.

DISCUSSION

Much of what is known about the neural function of FMRP, an RNA-binding protein that regulates RNA transport, stability, and translation, has been discovered in cortex and hippocampus (Huber et al., 2002; Antar et al., 2006; Grossman et al., 2006; Zang et al., 2013). Work done in hippocampal cells suggests key roles for FMRP and its KH2 RNA-binding domain in reducing synapse number (Pfeiffer and Huber, 2007). Using a cortical-striatal co-culture system, here we report findings consistent with a basal role for FMRP in promoting striatal dendritic spine and excitatory synapse number. Striatal WT MSNs show a significant increase in synapse count, associated with an increase in postsynaptic marker (PSD95) expression, which emerges between DIV 10 and 14. During the same time frame, *Fmr1* KO MSNs fail to increase PSD95 expression and at DIV 14 show an overall deficit in spine density compared to WT MSNs. On the other hand, similar to hippocampal cells, acute expression of FMRP in KO co-culture reduces striatal MSN spine density at DIV 14, though colocalized puncta do not show the same effect. By also making comparisons with mutant forms of FMRP, we show complex and unexpected roles for FMRP's RNA-binding domains in this process.

Measuring basal differences in *Fmr1* KO and WT MSNs in co-culture, we find a reduction in colocalized synapsin I and PSD95 puncta in KO cells at DIV 14 that is accompanied by deficits in thin, filopodia, and stubby spine densities. While thin and filopodia spine types are considered immature and generally represent newly formed spines that will be either eliminated or stabilized into more mature, sometimes larger spine morphologies (Maletic-Savatic et al., 1999; Holtmaat et al., 2005; Petrak et al., 2005; Zuo et al., 2005), stubby spines are considered more stable and likely to contribute to stronger synaptic connections (Kasai et al., 2003). Comparing *Fmr1* KO to WT MSNs in slices prepared from NAc shell, we previously helped to identify a basal deficit in stubby spines, in particular, in adult KO mice (Smith et al., 2014). Our current *in vitro* findings strengthen our *in vivo* observations and suggest that these striatal deficits in spine morphology in FXS may be present across the lifespan. Observations in early postnatal hippocampal development (first week) similarly suggest that postsynaptic expression of FMRP promotes synapse function and maturation (Zang et al., 2013), and by adulthood, hippocampal, as well as cortical, *Fmr1* KO spine deficits generally manifest as excessive numbers of immature spine types (Antar et al., 2006; Grossman et al., 2006; He and Portera-Cailliau, 2013). Work performed

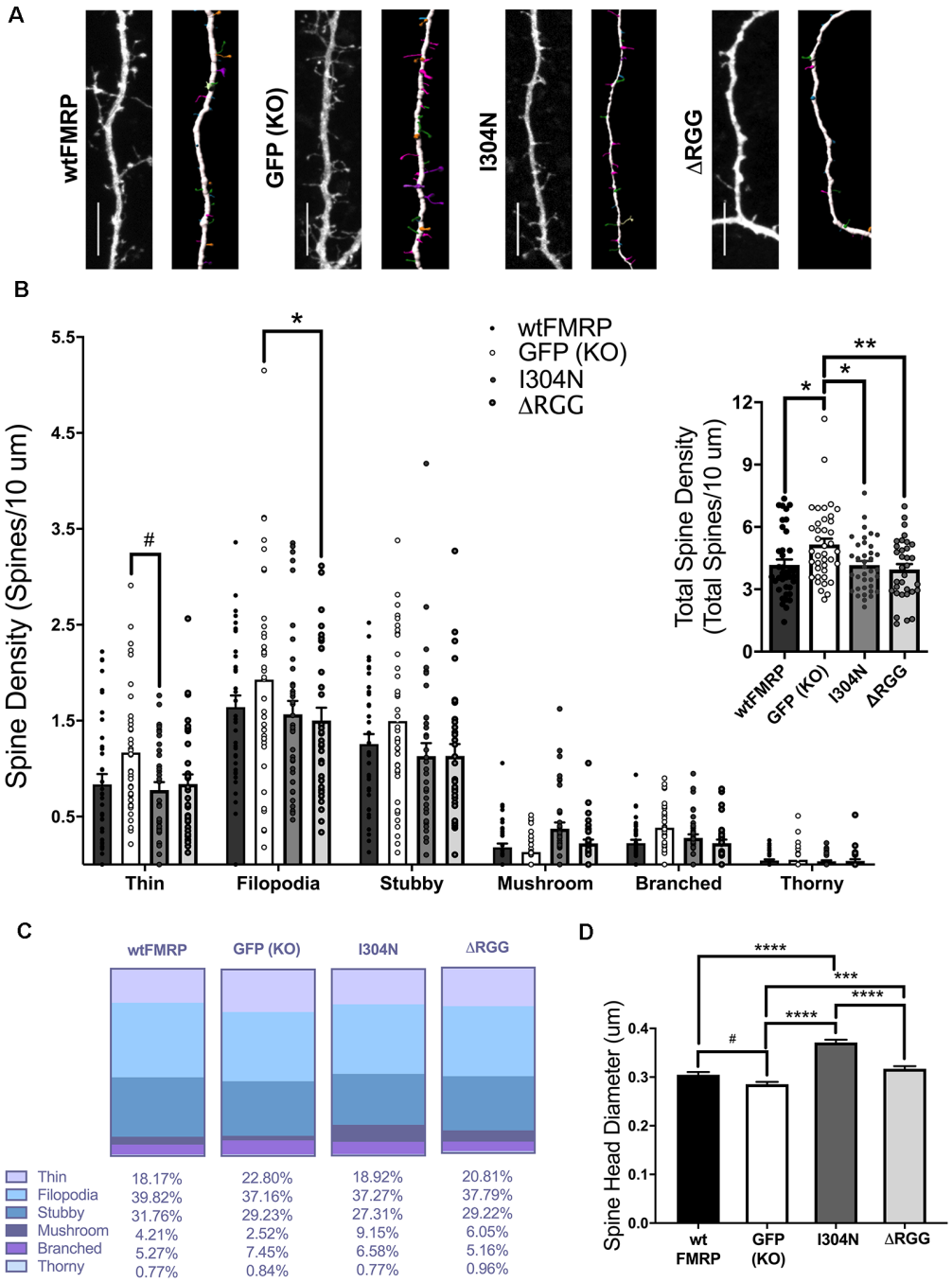

FIGURE 4 | Dendritic spine analysis of striatal MSNs at day *in vitro* (DIV) 14, following transfection with plasmids expressing mCherry and either wtFMRP-EGFP, GFP, I304N-FMRP-EGFP, or ΔRGG-FMRP-EGFP (**A**; scale bars 10 μm). Groups receiving either wtFMRP-or mutant FMRP-expressing plasmids had significantly decreased total spine density compared to the GFP (*Fmr1* KO) control group (**B**; one-way ANOVA). The ΔRGG group had a significantly decreased density of filopodia spines, and the I304N group trended towards significantly decreased thin spines, compared to GFP (KO) control (**B**; two-way RM ANOVA). Relative distribution of spine types for each group is shown in panel **(C)**. Compared to the GFP (KO) group, spines in the I304N and ΔRGG group had greater spine head diameter (**D**; one-way ANOVA). Bonferroni comparisons are indicated ($^{\#}p < 0.1$, $^{*}p < 0.05$, $^{**}p < 0.01$, $^{***}p < 0.001$, $^{****}p < 0.0001$); data shown are mean ± SEM.

in cultured *Fmr1* KO cortical cells identifies involvement of the synaptic adhesion molecule calsyntenin-1 (CLSTN1), an FMRP target mRNA (Darnell et al., 2011), as a potential mechanism for FMRP-mediated spine stabilization (Cheng et al., 2019). Indeed, it may be that a role for FMRP in spine stabilization is at the heart of these different adult morphological observations, manifesting differently depending on regional or cell type environmental conditions, including those that drive FMRP-dependent synapse

elimination (Pfeiffer et al., 2010) to a greater or lesser degree. Notably, we and others have reported increased MSN spine densities, of either elongated (>1 μm; Neuhofer et al., 2015) or thin type (Smith et al., 2014), more similar to hippocampus or cortex, for the NAc core subregion of *Fmr1* KO mice, indicating that absence of FMRP *in vivo* drives different dendritic phenotypes even within striatal subregions.

In contrast to observations under basal conditions, we find that acute expression of wtFMRP-GFP in striatal *Fmr1* KO cells significantly *decreases* both PSD95 puncta number and overall dendritic spine density compared to GFP expression alone (KO). Indeed, FMRP is known to mediate activity-dependent synapse weakening and elimination in the brain (Weiler and Greenough, 1999; Pfeiffer et al., 2010; Zang et al., 2013). For example, acute expression of wtFMRP in *Fmr1* KO hippocampal dissociated and slice cultures reduces total PSD95 and synapsin (unspecified) puncta, an interpretation that was bolstered by measurements of miniature excitatory postsynaptic current frequency (Pfeiffer and Huber, 2007). However, in our study, while we also observe reductions in PSD95 puncta counts and spine density in wtFMRP-treated cells, a similar effect is not present for colocalized puncta—a feature representative of functional synapses (Ippolito and Eroglu, 2010; Verstraelen et al., 2018). In fact, while numbers of colocalized puncta align well with overall spine density in our studies of basal conditions, when we perturb the KO cell environment with acute availability of FMRP, these outcomes no longer align, at least at the examined time point (DIV 14). For example, I304N- and ΔRGG-FMRP expression each result in overall spine densities that are significantly below KO and comparable to wtFMRP; however, despite this fact, ΔRGG-FMRP-treated striatal cells have normal levels of colocalized puncta, expressing significantly more than either the GFP (KO) or I304N-FMRP groups. It may be that greater pre- and postsynaptic availability increases opportunities for successful colocalization in the ΔRGG group; however, future studies should determine whether such putative synaptic alignments are occurring with proper relevance to experience and whether they affect behavioral outcomes *in vivo*.

Notably, while both mutant forms of FMRP decrease overall spine density, they fail to decrease PSD95 puncta. These seemingly contradictory outcomes could occur if existing spines in these groups express greater numbers of postsynaptic (PSD95) proteins, or "nanomodules," a phenomenon recently described (Hruska et al., 2018). While the current study does not address this question, we do observe that I304N- and ΔRGG-FMRP-expressing cells exhibit specific decreases in immature spine types (thin and filopodia, respectively), whereas wtFMRP-expressing cells show a more general decrease in density across multiple types. Spines in the I304N group also, on average, show a significantly greater average spine head diameter than that of any other group. Spine head diameter and volume positively correlate with PSD95 expression, and not all new or transient spines (i.e., thin, filopodia types) will acquire PSD95 puncta (Cane et al., 2014), so it may be that FMRP's KH2 and RGG domains are not required for elimination of immature dendritic spines that lack stable incorporation of PSD95. We emphasize that the RGG domain is dispensable for synapse elimination in hippocampal cells, while the 1304N mutation has been shown to disrupt this and other hippocampal cellular functions (Pfeiffer and Huber, 2007). The fact that our results in striatal cells do not entirely align with synapse elimination after acute presentation of FMRP suggests that we may be observing mixed states of synapse and spine elimination, stabilization, and/or homeostatic recovery. These outcomes are likely complicated by the myriad roles FMRP plays in structural plasticity, dependent in different ways on the protein domains examined here. As one example, FMRP's RGG domain is required to limit forward trafficking of N-type Ca^{2+} channels to the presynaptic active zone (Ferron et al., 2020), a process important to early synaptogenesis (Pravettoni et al., 2000; Rieckhof et al., 2003), which may contribute to the increased synapsin labeling and normal levels of colocalized puncta that we observe in the ΔRGG-FMRP-expressing group. In any case, our findings add to our understanding of FXS, suggesting distinctions in FMRP's role for different brain regions and/or cell types.

We note that striatal cells in experiments described here were co-cultured alongside cortical cells of the same genotype. In transfection experiments, while only MSNs expressing the transfected plasmid (GFP+) were analyzed, these cells likely received excitatory cortical and inhibitory MSN collateral input from other successfully transfected cells, as well as input from *Fmr1* KO untransfected cells. Thus, we cannot rule out the influence of abnormal presynaptic signaling, such as that described previously (Deng et al., 2013; Patel et al., 2013). However, a study specifically investigating cortico-striatal signaling reported enhanced GABAergic, but normal glutamatergic, transmission onto striatal cells in *Fmr1* KO mice (Centonze et al., 2008), suggesting that our findings do not likely result from abnormal excitatory cortical cell input. In any case, there is abundant evidence of FMRP's importance in the postsynapse across various brain regions in many aspects of synapse plasticity, including synaptogenesis (Wang et al., 2018), synaptic scaling and synaptic strength (Soden and Chen, 2010), as well as synapse elimination (Pfeiffer and Huber, 2007). We also note that general KO striatal spine deficits were the impetus for this work. While many spines on MSNs appose cortical projections, axonal collateral terminals from other nearby MSNs, despite being inhibitory, are also commonly found contributing to asymmetric synapses in the striatum (Wilson and Groves, 1980), thus we did not differentiate presynaptic puncta by type. Lastly, because wtFMRP is introduced to *Fmr1* KO cells in our acute transfection studies, it is possible that the previous absence of FMRP underlies the discrepancy between these and our basal condition experiments. Indeed, FMRP is normally present during embryonic development and its absence results in, among other things, aberrant gene expression and impaired differentiation of neural progenitor cells (Sunamura et al., 2018). Additional studies will be needed to parse the influence of FMRP's pre- and postsynaptic functions, as well as potential developmental roles, on striatal MSN dendritic morphology.

FMRP is a critical player in synapse regulation, with much of its function discovered in brain regions that are characterized by relatively high densities of glutamatergic neurons and excitatory transmission. The striatum, largely made up of relatively

quiescent, GABAergic inhibitory MSNs, plays a major role in motor activation, as well as social and repetitive behaviors, all of which are detrimentally affected in FXS. While FMRP-mediated synapse elimination is likely contributing to observed outcomes in striatal MSNs, similar to findings in hippocampal cells, results from both our basal and acute transfection studies indicate a critical role for FMRP in striatal synapse stabilization during this early time period. Given that forms of FXS and intellectual disability have been linked to mutations disrupting specific domains of FMRP, including KH2 and RGG, our work also supports the idea that appropriately nuanced treatment approaches may be most effective. Moving forward, it will be important to investigate FMRP's pre- and postsynaptic functions in striatum and the consequences of both total and domain-specific disruption of FMRP on both cell physiological and behavioral function.

DATA AVAILABILITY STATEMENT

The raw data supporting the conclusions of this article will be made available by the authors, without undue reservation.

ETHICS STATEMENT

The animal study was reviewed and approved by the Texas A&M University Institutional Care and Use Committee.

AUTHOR CONTRIBUTIONS

JH contributed to the design, acquisition, analysis, interpretation, and writing of the manuscript. KC contributed to the acquisition, analysis, and revision of the manuscript. YG contributed to the design, acquisition, and revision of the manuscript. LS contributed to the design, acquisition, analysis, interpretation, and writing of the manuscript.

FUNDING

This research was supported by Texas A&M University internal funding.

ACKNOWLEDGMENTS

Use of the Texas A&M Microscopy and Imaging Center is acknowledged. We thank Catherina Tovar Pensa for synaptic puncta analysis assistance.

SUPPLEMENTARY MATERIAL

The Supplementary Material for this article can be found online at: https://www.frontiersin.org/articles/10.3389/fnmol.2020.00161/full#supplementary-material.

REFERENCES

Aguet, F., Ville, D. V. D., and Unser, M. (2008). Model-based 2.5-d deconvolution for extended depth of field in brightfield microscopy. *IEEE Trans. Image Process.* 17, 1144–1153. doi: 10.1109/TIP.2008.924393

Ahmari, S. E., Buchanan, J., and Smith, S. J. (2000). Assembly of presynaptic active zones from cytoplasmic transport packets. *Nat. Neurosci.* 3, 445–451. doi: 10.1038/74814

Anderson, B. R., Chopra, P., Suhl, J. A., Warren, S. T., and Bassell, G. J. (2016). Identification of consensus binding sites clarifies FMRP binding determinants. *Nucleic Acids Res.* 44, 6649–6659. doi: 10.1093/nar/gkw593

Antar, L. N., Li, C., Zhang, H., Carroll, R. C., and Bassell, G. J. (2006). Local functions for FMRP in axon growth cone motility and activity-dependent regulation of filopodia and spine synapses. *Mol. Cell. Neurosci.* 32, 37–48. doi: 10.1016/j.mcn.2006.02.001

Ascano, M. Jr., Mukherjee, N., Bandaru, P., Miller, J. B., Nusbaum, J. D., Corcoran, D. L., et al. (2012). FMRP targets distinct mRNA sequence elements to regulate protein expression. *Nature* 492, 382–386. doi: 10.1038/nature11737

Báez-Mendoza, R., and Schultz, W. (2013). The role of the striatum in social behavior. *Front. Neurosci.* 7:233. doi: 10.3389/fnins.2013.00233

Bagni, C., Tassone, F., Neri, G., Hagerman, R., Bagni, C., Tassone, F., et al. (2012). Fragile X syndrome: causes, diagnosis, mechanisms and therapeutics. *J. Clin. Invest.* 122, 4314–4322. doi: 10.1172/JCI63141

Cane, M., Maco, B., Knott, G., and Holtmaat, A. (2014). The relationship between PSD-95 clustering and spine stability *in vivo*. *J. Neurosci.* 34, 2075–2086. doi: 10.1523/JNEUROSCI.3353-13.2014

Centonze, D., Rossi, S., Mercaldo, V., Napoli, I., Ciotti, M. T., De Chiara, V., et al. (2008). Abnormal striatal GABA transmission in the mouse model for the fragile X syndrome. *Biol. Psychiatry* 63, 963–973. doi: 10.1016/j.biopsych.2007.09.008

Cheng, K., Chen, Y.-S., Yue, C.-X., Zhang, S.-M., Pei, Y.-P., Cheng, G.-R., et al. (2019). Calsyntenin-1 negatively regulates ICAM5 accumulation in postsynaptic membrane and influences dendritic spine maturation in a mouse model of fragile X syndrome. *Front. Neurosci.* 13:1098. doi: 10.3389/fnins.2019.01098

Darnell, J. C., Fraser, C. E., and Mostovetsky, O. (2005a). Kissing complex RNAs mediate interaction between the fragile-X mental retardation protein KH2 domain and brain polyribosomes. *Genes Dev.* 19, 903–918. doi: 10.1101/gad.1276805

Darnell, J. C., Mostovetsky, O., and Darnell, R. B. (2005b). FMRP RNA targets: identification and validation. *Genes Brain Behav.* 4, 341–349. doi: 10.1111/j.1601-183x.2005.00144.x

Darnell, J. C., Van Driesche, S. J., Zhang, C., Hung, K. Y. S., Mele, A., Fraser, C. E., et al. (2011). FMRP stalls ribosomal translocation on mRNAs linked to synaptic function and autism. *Cell* 146, 247–261. doi: 10.1016/j.cell.2011.06.013.

De Boulle, K., Verkerk, A. J. M. H., Reyniers, E., Vits, L., Hendrickx, J., Van Roy, B., et al. (1993). A point mutation in the FMR-1 gene associated with fragile X mental retardation. *Nat. Genet.* 3, 31–35. doi: 10.1038/ng0193-31

De Camilli, P., Cameron, R., and Greengard, P. (1983). Synapsin I (protein I), a nerve terminal-specific phosphoprotein: I. Its general distribution in synapses of the central and peripheral nervous system demonstrated by immunofluorescence in frozen and plastic sections. *J. Cell Biol.* 96, 1337–1354. doi: 10.1083/jcb.96.5.1337

Deng, P.-Y., Rotman, Z., Blundon, J. A., Cho, Y., Cui, J., Cavalli, V., et al. (2013). FMRP regulates neurotransmitter release and synaptic information transmission by modulating action potential duration *via* BK channels. *Neuron* 77, 696–711. doi: 10.1016/j.neuron.2012.12.018

Feng, Y., Absher, D., Eberhart, D. E., Brown, V., Malter, H. E., and Warren, S. T. (1997). FMRP associates with polyribosomes as an mRNP and the I304N mutation of severe fragile X syndrome abolishes this association. *Mol. Cell* 1, 109–118. doi: 10.1016/s1097-2765(00)80012-x

Ferreira, A., Kao, H.-T., Feng, J., Rapoport, M., and Greengard, P. (2000). Synapsin III: developmental expression, subcellular localization and role in axon formation. *J. Neurosci.* 20, 3736–3744. doi: 10.1523/JNEUROSCI.20-10-03736.2000

Ferron, L., Novazzi, C. G., Pilch, K. S., Moreno, C., Ramgoolam, K., and Dolphin, A. C. (2020). FMRP regulates presynaptic localization of neuronal voltage gated calcium channels. *Neurobiol. Dis.* 138:104779. doi: 10.1016/j.nbd.2020.104779

Grossman, A. W., Elisseou, N. M., McKinney, B. C., and Greenough, W. T. (2006). Hippocampal pyramidal cells in adult Fmr1 knockout mice exhibit an immature-appearing profile of dendritic spines. *Brain Res.* 1084, 158–164. doi: 10.1016/j.brainres.2006.02.044

Handt, M., Epplen, A., Hoffjan, S., Mese, K., Epplen, J. T., and Dekomien, G. (2014). Point mutation frequency in the FMR1 gene as revealed by fragile X syndrome screening. *Mol. Cell. Probes* 28, 279–283. doi: 10.1016/j.mcp.2014.08.003

Harris, K., Jensen, F., and Tsao, B. (1992). Three-dimensional structure of dendritic spines and synapses in rat hippocampus (CA1) at postnatal day 15 and adult ages: implications for the maturation of synaptic physiology and long-term potentiation. *J. Neurosci.* 12, 2685–2705. doi: 10.1523/JNEUROSCI.12-08-j0001.1992

He, C. X., and Portera-Cailliau, C. (2013). The trouble with spines in fragile X syndrome: density, maturity and plasticity. *Neuroscience* 251, 120–128. doi: 10.1016/j.neuroscience.2012.03.049

Holtmaat, A. J. G. D., Trachtenberg, J. T., Wilbrecht, L., Shepherd, G. M., Zhang, X., Knott, G. W., et al. (2005). Transient and persistent dendritic spines in the neocortex *in vivo*. *Neuron* 45, 279–291. doi: 10.1016/j.neuron.2005.01.003

Hruska, M., Henderson, N., Le Marchand, S. J., Jafri, H., and Dalva, M. B. (2018). Synaptic nanomodules underlie the organization and plasticity of spine synapses. *Nat. Neurosci.* 21, 671–682. doi: 10.1038/s41593-018-0138-9

Huber, K. M., Gallagher, S. M., Warren, S. T., and Bear, M. F. (2002). Altered synaptic plasticity in a mouse model of fragile X mental retardation. *Proc. Natl. Acad. Sci. U S A* 99, 7746–7750. doi: 10.1073/pnas.122205699

Ippolito, D. M., and Eroglu, C. (2010). Quantifying synapses: an immunocytochemistry-based assay to quantify synapse number. *J. Vis. Exp.* 45:2270. doi: 10.3791/2270

Irwin, S. A., Patel, B., Idupulapati, M., Harris, J. B., Crisostomo, R. A., Larsen, B. P., et al. (2001). Abnormal dendritic spine characteristics in the temporal and visual cortices of patients with fragile-X syndrome: a quantitative examination. *Am. J. Med. Genet.* 98, 161–167. doi: 10.1002/1096-8628(20010115)98:2<161::aid-ajmg1025>3.0.co;2-b

Jedynak, J. P., Uslaner, J. M., Esteban, J. A., and Robinson, T. E. (2007). Methamphetamine-induced structural plasticity in the dorsal striatum. *Eur. J. Neurosci.* 25, 847–853. doi: 10.1111/j.1460-9568.2007.05316.x

Kasai, H., Matsuzaki, M., Noguchi, J., Yasumatsu, N., and Nakahara, H. (2003). Structure-stability-function relationships of dendritic spines. *Trends Neurosci.* 26, 360–368. doi: 10.1016/s0166-2236(03)00162-0

Langen, M., Durston, S., Kas, M. J. H., van Engeland, H., and Staal, W. G. (2011). The neurobiology of repetitive behavior: . . . and men. *Neurosci. Biobehav. Rev.* 35, 356–365. doi: 10.1016/j.neubiorev.2010.02.005

Maletic-Savatic, M., Malinow, R., and Svoboda, K. (1999). Rapid dendritic morphogenesis in CA1 hippocampal dendrites induced by synaptic activity. *Science* 283, 1923–1927. doi: 10.1126/science.283.5409.1923

Mata, G., Heras, J., Morales, M., Romero, A., and Rubio, J. (2016). *SynapCountJ: A Tool for Analyzing Synaptic Densities in Neurons.* Rome, Italy: SCITEPRESS-Science and Technology Publications, Limited.

Maurin, T., Lebrigand, K., Castagnola, S., Paquet, A., Jarjat, M., Popa, A., et al. (2018). HITS-CLIP in various brain areas reveals new targets and new modalities of RNA binding by fragile X mental retardation protein. *Nucleic Acids Res.* 46, 6344–6355. doi: 10.1093/nar/gky267

Meijering, E., Jacob, M., Sarria, J.-C. F., Steiner, P., Hirling, H., and Unser, M. (2004). Design and validation of a tool for neurite tracing and analysis in fluorescence microscopy images. *Cytometry A* 58, 167–176. doi: 10.1002/cyto.a.20022

Myrick, L. K., Hashimoto, H., Cheng, X., and Warren, S. T. (2015). Human FMRP contains an integral tandem agenet (Tudor) and KH motif in the amino terminal domain. *Hum. Mol. Genet.* 24, 1733–1740. doi: 10.1093/hmg/ddu586

Neuhofer, D., Henstridge, C. M., Dudok, B., Sepers, M., Lassalle, O., Katona, I., et al. (2015). Functional and structural deficits at accumbens synapses in a mouse model of fragile X. *Front. Cell. Neurosci* 9:100. doi: 10.3389/fncel.2015.00100

Nimchinsky, E. A., Oberlander, A. M., and Svoboda, K. (2001). Abnormal development of dendritic spines in FMR1 knock-out mice. *J. Neurosci.* 21, 5139–5146. doi: 10.1523/JNEUROSCI.21-14-05139.2001

Okray, Z., de Esch, C. E., Van Esch, H., Devriendt, K., Claeys, A., Yan, J., et al. (2015). A novel fragile X syndrome mutation reveals a conserved role for the carboxy-terminus in FMRP localization and function. *EMBO Mol. Med.* 7, 423–437. doi: 10.15252/emmm.201404576

Patel, A. B., Hays, S. A., Bureau, I., Huber, K. M., and Gibson, J. R. (2013). A target cell-specific role for presynaptic fmr1 in regulating glutamate release onto neocortical fast-spiking inhibitory neurons. *J. Neurosci.* 33, 2593–2604. doi: 10.1523/JNEUROSCI.2447-12.2013

Penrod, R. D., Kourrich, S., Kearney, E., Thomas, M. J., and Lanier, L. M. (2011). An embryonic culture system for the investigation of striatal medium spiny neuron dendritic spine development and plasticity. *J. Neurosci. Methods* 200, 1–13. doi: 10.1016/j.jneumeth.2011.05.029

Petrak, L. J., Harris, K. M., and Kirov, S. A. (2005). Synaptogenesis on mature hippocampal dendrites occurs *via* filopodia and immature spines during blocked synaptic transmission. *J. Comp. Neurol.* 484, 183–190. doi: 10.1002/cne.20468

Pfeiffer, B. E., and Huber, K. M. (2007). Fragile X mental retardation protein induces synapse loss through acute postsynaptic translational regulation. *J. Neurosci.* 27, 3120–3130. doi: 10.1523/JNEUROSCI.0054-07.2007

Pfeiffer, B. E., Zang, T., Wilkerson, J. R., Taniguchi, M., Maksimova, M. A., Smith, L. N., et al. (2010). Fragile X mental retardation protein is required for synapse elimination by the activity-dependent transcription factor MEF2. *Neuron* 66, 191–197. doi: 10.1016/j.neuron.2010.03.017

Prange, O., and Murphy, T. H. (2001). Modular transport of postsynaptic density-95 clusters and association with stable spine precursors during early development of cortical neurons. *J. Neurosci.* 21, 9325–9333. doi: 10.1523/JNEUROSCI.21-23-09325.2001

Pravettoni, E., Bacci, A., Coco, S., Forbicini, P., Matteoli, M., and Verderio, C. (2000). Different localizations and functions of L-type and N-type calcium channels during development of hippocampal neurons. *Dev. Biol.* 227, 581–594. doi: 10.1006/dbio.2000.9872

Rieckhof, G. E., Yoshihara, M., Guan, Z., and Littleton, J. T. (2003). Presynaptic N-type calcium channels regulate synaptic growth. *J. Biol. Chem.* 278, 41099–41108. doi: 10.1074/jbc.M306417200

Schaeffer, C., Bardoni, B., Mandel, J.-L., Ehresmann, B., Ehresmann, C., and Moine, H. (2001). The fragile X mental retardation protein binds specifically to its mRNA *via* a purine quartet motif. *EMBO J.* 20, 4803–4813. doi: 10.1093/emboj/20.17.4803

Schindelin, J., Arganda-Carreras, I., Frise, E., Kaynig, V., Longair, M., Pietzsch, T., et al. (2012). Fiji: an open-source platform for biological-image analysis. *Nat. Methods* 9, 676–682. doi: 10.1038/nmeth.2019

Smith, L. N., Jedynak, J. P., Fontenot, M. R., Hale, C. F., Dietz, K. C., Taniguchi, M., et al. (2014). Fragile X mental retardation protein regulates synaptic and behavioral plasticity to repeated cocaine administration. *Neuron* 82, 645–658. doi: 10.1016/j.neuron.2014.03.028

Soden, M. E., and Chen, L. (2010). Fragile X protein FMRP is required for homeostatic plasticity and regulation of synaptic strength by retinoic acid. *J. Neurosci.* 30, 16910–16921. doi: 10.1523/JNEUROSCI.3660-10.2010

Suhl, J. A., and Warren, S. T. (2015). Single-nucleotide mutations in fmr1 reveal novel functions and regulatory mechanisms of the fragile X syndrome protein FMRP. *J. Exp. Neurosci.* 9, 35–41. doi: 10.4137/jen.s25524

Sunamura, N., Iwashita, S., Enomoto, K., Kadoshima, T., and Isono, F. (2018). Loss of the fragile X mental retardation protein causes aberrant differentiation in human neural progenitor cells. *Sci. Rep.* 8:11585. doi: 10.1038/s41598-018-30025-4

Verstraelen, P., Van Dyck, M., Verschuuren, M., Kashikar, N. D., Nuydens, R., Timmermans, J.-P., et al. (2018). Image-based profiling of synaptic connectivity in primary neuronal cell culture. *Front. Neurosci.* 12:389. doi: 10.3389/fnins.2018.00389

Wang, H., Wu, L.-J., Kim, S. S., Lee, F. J. S., Gong, B., Toyoda, H., et al. (2008). FMRP acts as a key messenger for dopamine modulation in the forebrain. *Neuron* 59, 634–647. doi: 10.1016/j.neuron.2008.06.027

Wang, X., Zorio, D. A. R., Schecterson, L., Lu, Y., and Wang, Y. (2018). Postsynaptic FMRP regulates synaptogenesis *in vivo* in the developing

cochlear nucleus. *J. Neurosci.* 38, 6445–6460. doi: 10.1523/JNEUROSCI.0665-18.2018

Weiler, I. J., and Greenough, W. T. (1999). Synaptic synthesis of the fragile X protein: possible involvement in synapse maturation and elimination. *Am. J. Med. Genet.* 83, 248–252. doi: 10.1002/(sici)1096-8628(19990402)83:4<248::aid-ajmg3>3.0.co;2-1

Wilson, C. J., and Groves, P. M. (1980). Fine structure and synaptic connections of the common spiny neuron of the rat neostriatum: a study employing intracellular injection of horseradish peroxidase. *J. Comp. Neurol.* 194, 599–615. doi: 10.1002/cne.901940308

Yael, D., Tahary, O., Gurovich, B., Belelovsky, K., and Bar-Gad, I. (2019). Disinhibition of the nucleus accumbens leads to macro-scale hyperactivity consisting of micro-scale behavioral segments encoded by striatal activity. *J. Neurosci.* 39, 5897–5909. doi: 10.1523/JNEUROSCI.3120-18.2019

Zang, T., Maksimova, M. A., Cowan, C. W., Bassel-Duby, R., Olson, E. N., and Huber, K. M. (2013). Postsynaptic FMRP bidirectionally regulates excitatory synapses as a function of developmental age and MEF2 activity. *Mol. Cell. Neurosci.* 56, 39–49. doi: 10.1016/j.mcn.2013.03.002

Zuo, Y., Lin, A., Chang, P., and Gan, W.-B. (2005). Development of long-term dendritic spine stability in diverse regions of cerebral cortex. *Neuron* 46, 181–189. doi: 10.1016/j.neuron.2005.04.001

Conflict of Interest: The authors declare that the research was conducted in the absence of any commercial or financial relationships that could be construed as a potential conflict of interest.

frontiers in Synaptic Neuroscience

HYPOTHESIS AND THEORY
published: 02 October 2020
doi: 10.3389/fnsyn.2020.590403

The Synapse Diversity Dilemma: Molecular Heterogeneity Confounds Studies of Synapse Function

Seth G. N. Grant[1,2]* *and Erik Fransén*[3,4]

[1] Genes to Cognition Programme, Centre for Clinical Brain Sciences, University of Edinburgh, Edinburgh, United Kingdom, [2] Simons Initiative for the Developing Brain, Centre for Discovery Brain Sciences, University of Edinburgh, Edinburgh, United Kingdom, [3] Department of Computational Science and Technology, School of Electrical Engineering and Computer Science, KTH Royal Institute of Technology, Stockholm, Sweden, [4] Science for Life Laboratory, KTH Royal Institute of Technology, Solna, Sweden

Recent studies have shown an unexpectedly high degree of synapse diversity arising from molecular and morphological differences among individual synapses. Diverse synapse types are spatially distributed within individual dendrites, between different neurons, and across and between brain regions, producing the synaptome architecture of the brain. The spatial organization of synapse heterogeneity is important because the physiological activation of heterogeneous excitatory synapses produces a non-uniform spatial output of synaptic potentials, which confounds the interpretation of measurements obtained from population-averaging electrodes, optrodes and biochemical methods that lack single-synapse resolution. Population-averaging measurements cannot distinguish between changes in the composition of populations of synapses and changing synaptic physiology. Here we consider the implications of synapse diversity and its organization into synaptome architecture for studies of synapse physiology, plasticity, development and behavior, and for the interpretation of phenotypes arising from pharmacological and genetic perturbations. We conclude that prevailing models based on population-averaging measurements need reconsideration and that single-synapse resolution physiological recording methods are required to confirm or refute the major synaptic models of behavior.

Keywords: synaptome, LTP, electrophysiology, synapse proteome, synapse heterogeneity, synaptic computation

OPEN ACCESS

Edited by:
Pierre Paoletti, Institut National de la Santé et de la Recherche Médicale (INSERM), France

Reviewed by:
Joris De Wit, VIB & KU Leuven Center for Brain & Disease Research, Belgium
Michele H. Jacob, Tufts University School of Medicine, United States

***Correspondence:**
Seth G. N. Grant
seth.grant@ed.ac.uk

Received: *01 August 2020*
Accepted: *15 September 2020*
Published: *02 October 2020*

Citation:
Grant SGN and Fransén E (2020) The Synapse Diversity Dilemma: Molecular Heterogeneity Confounds Studies of Synapse Function. Front. Synaptic Neurosci. 12:590403. doi: 10.3389/fnsyn.2020.590403

INTRODUCTION

Synapse diversity has been known for many decades from pharmacological, physiological and neurochemical studies that have led to the standard classifications of excitatory and inhibitory synapses and different neurotransmitter systems. In the past two decades, studies of the synapse proteome have revealed a high degree of molecular complexity (Husi et al., 2000; Collins et al., 2006; Coba et al., 2009; Bayes et al., 2011, 2012, 2017; Distler et al., 2014). A typical synapse in the mammalian brain occupies a volume of 1 μm^3 (Bayes et al., 2011) and can potentially house several million individual protein molecules. Approximately 10% of the proteins encoded by the ~23,000 genes in the human genome are found in synapses.

Proteins are not expressed equally in all synapses; instead, different synapses (types and subtypes) express combinations of proteins (Husi et al., 2000; Micheva et al., 2010; Frank et al., 2016, 2017; Zhu et al., 2018; Cizeron et al., 2020). There is a potentially vast synapse diversity that could arise from the combinatorial expression of synapse proteins (Grant, 2007, 2018a,b; Micheva et al., 2010; O'Rourke et al., 2012; Zhu et al., 2018; Cizeron et al., 2020). Molecularly distinct synapses are differentially distributed within the dendritic tree of individual neurons, and different neurons (even within the same class) have different synapse distributions. Every brain region is characterized by a "signature" of synapse composition (Zhu et al., 2018; Cizeron et al., 2020), which together result in a 3D spatial architecture of the brain, known as the synaptome architecture (Zhu et al., 2018; Cizeron et al., 2020). We recently studied the brain-wide distribution of excitatory synapse types across the mouse lifespan and observed temporal trajectories in synapse parameters and regional compositional signatures (Cizeron et al., 2020). Synapse diversity and its organization into the spatiotemporal lifespan synaptome architecture (Cizeron et al., 2020) most likely reflect a concerted set of genetic programs (Frank et al., 2016, 2017; Frank and Grant, 2017; Skene et al., 2017; Zhu et al., 2018; Grant, 2019; Cizeron et al., 2020).

The hippocampal formation of the mammalian brain has attracted much attention as an experimental preparation because its circuitry is amenable to electrophysiological recording of synaptic transmission (Bliss and Collingridge, 1993; Basu and Siegelbaum, 2015; Nicoll, 2017). Slices of hippocampal tissue can be maintained in an organ bath and the strength of synaptic transmission is measured using a stimulating electrode placed into the extracellular space of an afferent fiber bundle (e.g., Schaffer collateral-commissural pathway that projects from the CA3 region to CA1 stratum radiatum) and a recording electrode placed in the dendritic population of apical dendrites of the postsynaptic pyramidal neurons (e.g., CA1 stratum radiatum, CA1sr). Stimulation protocols typically trigger action potentials in many axon fibers that travel to the presynaptic terminal and cause release of neurotransmitter (glutamate) onto dozens to hundreds of postsynaptic dendritic spines (**Figure 1**). The electrode records the sum of the individual postsynaptic responses (field excitatory postsynaptic response, fEPSP), which is used as the measure of synaptic strength. Other methods record from the soma or dendrites of individual neurons (e.g., cell-attached patch electrodes) and sum the synaptic responses (**Figure 1**).

Synapse diversity within hippocampal CA1 pyramidal neurons has been described using molecular and morphological approaches. Dye filling experiments show that a single pyramidal neuron in the rat contains ∼32,000 synapses, of which >90% are excitatory (Megias et al., 2001). Molecular studies of these excitatory synapses using synaptome mapping approaches, which quantify the intensity, size and shape of synapses expressing postsynaptic scaffold proteins PSD95 and SAP102, show that the CA1sr has the highest synaptic diversity of any mouse brain region (Zhu et al., 2018; Cizeron et al., 2020). Postsynaptic proteins are differentially distributed along the length of the apical dendritic arborization of CA1 pyramidal neurons, producing synapses of different sizes and amounts of protein organized into gradients (Broadhead et al., 2016; Zhu et al., 2018; Cizeron et al., 2020). Comparison of the dendritic arborizations of adjacent neurons along the medial-to-lateral axis also shows a gradient of synaptic parameters (Zhu et al., 2018; Cizeron et al., 2020). Gradients of diverse synapses are also observed in the striatum and regions of the neocortex (Zhu et al., 2018). Thus, electrophysiological recordings measure the population average of these heterogeneous synapses. The recordings not only average the responses and lose the specific information from individual synapses, but also fail to inform on the spatial location of the different synapses.

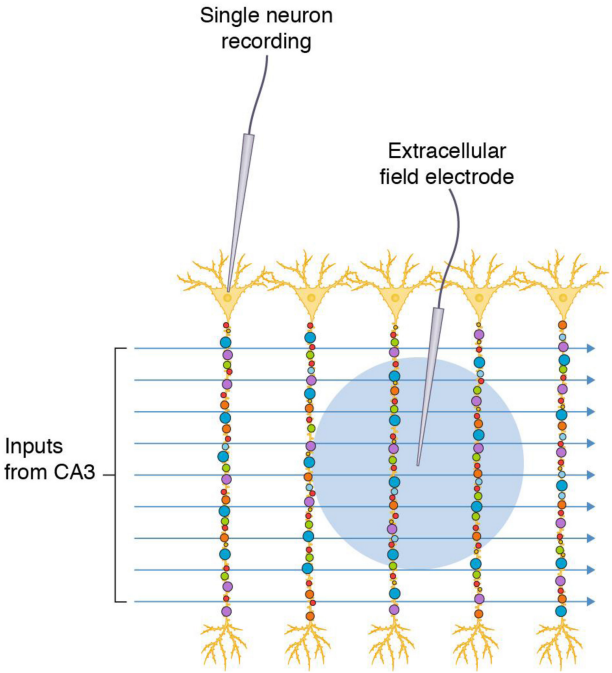

FIGURE 1 | Commonly used electrophysiological methods record responses from synapse populations and do not inform on individual synapses. Populations of diverse synapses in the CA1 stratum radiatum of the hippocampal formation (small colored circles) are distributed on the apical dendrites of pyramidal neurons. Axon inputs from CA3 are stimulated and recording electrodes access populations of synapses in a single neuron by direct recording or populations of neurons by recording in the extracellular space (blue circle indicates the area from which synaptic potentials are detected).

The problem of population-averaged assays in biological systems has long been recognized in the context of cellular diversity (Altschuler and Wu, 2010). The overriding assumption is that the population average represents the mechanism(s) operating within individual cells (or synapses) within the population. Population-averaged measurements are known to confound the interpretation of cellular signaling pathways and the roles of cellular subtypes in physiological processes and to poorly reflect the internal states of the majority of the cells, any subpopulation of cells, or even any single cell (Altschuler and Wu, 2010). These problems equally apply to the

biology of synapse heterogeneity but have received little attention (O'Rourke et al., 2012).

Population-averaged recordings of synapse physiology that are correlated with behavioral measures assume that all synapses have equal relevance to the behavioral output. However, it is possible, perhaps even highly likely, that only some synapses are relevant for a particular behavior (referred to below as "behavior-relevant synapses"). Similarly, studies of cellular heterogeneity have demonstrated the important roles of small subpopulations of cells or single cells with the population (e.g., cancer cells) (Altschuler and Wu, 2010). The spatial organization of synaptic heterogeneity is important because the physiological activation of heterogeneous excitatory synapses produces a non-uniform spatial output of synaptic potentials (Grant, 2018b; Zhu et al., 2018; Cizeron et al., 2020), and this introduces a host of problems for the interpretation of measurements obtained from a population-averaging electrode. With this background, we will consider how synapse diversity and its spatial organization impact on the interpretation of physiological, genetic, pharmacological and behavioral studies.

FUNCTIONAL CONSIDERATIONS OF HETEROGENOUS EXCITATORY SYNAPSES

We will first consider a simple model that contrasts a population of homogeneous with heterogeneous excitatory synapses recorded using a single electrode (**Figure 2**). The populations consist of 16 synapses, each represented as a circle. The "homogeneous population" is composed of one type of synapse (**Figure 2A**), whereas the "heterogeneous population" comprises three types (**Figure 2B**). These synapse types have different molecular compositions and physiological properties: a single action potential generates a 1 mV potential from type 1 (a weak synapse), 2 mV from type 2 (a medium strength synapse) and 3 mV from type 3 (a strong synapse). There is a non-random spatial organization (synaptome architecture) to the heterogeneous population, where the top two layers are type 2 synapses, the third layer is type 3 and the fourth layer is type 1 (**Figure 2B**). When these two populations are stimulated with a single action potential, there are distinct spatial maps of synaptic responses observable at single-synapse resolution. However, the population recording does not detect the spatial differences (or synapse diversity) and the summed response (Σ_{pop}) in both populations is the same (Σ_{pop} = 32 mV). In other words, electrophysiological methods that record population measurements are blinded to the diversity of synapses and their spatial organization.

Next we will consider how population recordings could confuse the interpretation of synaptic plasticity in heterogeneous populations of synapses (**Figure 3**). Here we will contrast two stimulation protocols: one that results in long-term potentiation (LTP) and another that results in long-term depression (LTD). Both the homogeneous and heterogeneous populations show LTP (Σ_{pop} increases from control) and LTD (Σ_{pop} decreases from control). However, unlike the homogeneous population where

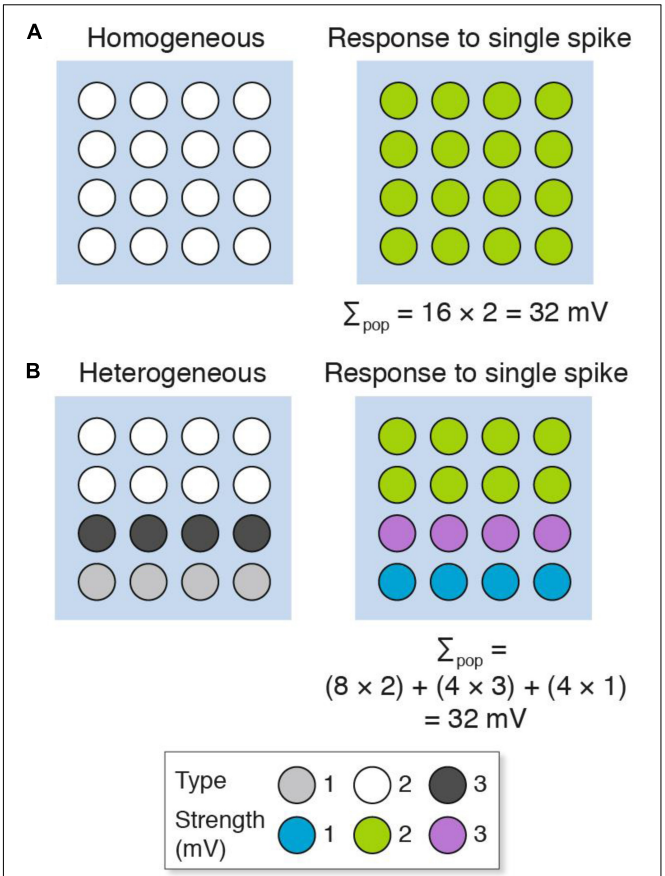

FIGURE 2 | Populations of **(A)** homogeneous and **(B)** heterogeneous synapses can show the same overall response. The key shows three synapse types and their strength. Σ_{pop}, summed response for each population.

all the synapses either strengthen or weaken, the heterogeneous populations show physiological diversity at the single-synapse level: some synapses strengthen and others weaken. If the specific synapses (or subsets) within each population were to have distinct physiological outputs (for example, because of their location within the dendritic tree) then the population recording could not be relied upon to inform us if their output was increased or decreased in either the LTP or LTD experiment.

The failure of population recordings to discriminate spatial effects of heterogeneous synapse populations has important implications for those experiments that attempt to correlate physiological and behavioral properties. For the purposes of this discussion, we will assume that a subset of synapses within the population drive a circuit that controls the behavior (behavior-relevant synapses). An increase in synaptic strength recorded in the whole population of synapses (LTP) would not necessarily correlate with an increase in synaptic strength in the behavior-relevant synapses and so there would not be a correlation between LTP and learning. Thus, if we assume that LTP is the causal mechanism of learning (Bliss and Collingridge, 1993), then synapse diversity could be invoked to explain why dissociations between the direction or strength of change in LTP and learning

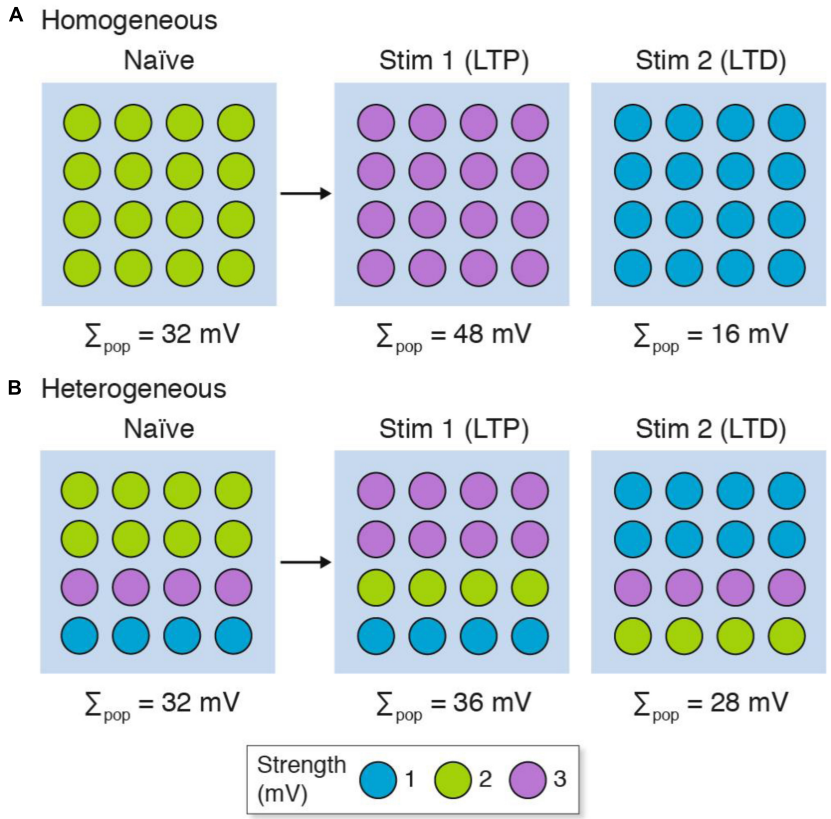

FIGURE 3 | LTP and LTD in populations of **(A)** homogeneous and **(B)** heterogeneous synapses. The strength of the synapse populations in **Figure 2** are shown before (naïve) and after LTP (Stim 1) and LTD (Stim 2) induction. Although both homogeneous and heterogeneous populations show LTP and LTD, only some synapses in the heterogeneous populations reflect the population measure and subpopulations of synapses can show opposite phenotypes (i.e., LTD in individual synapses when the population shows LTP, and vice versa). The key shows three synapse types and their strength. Σ_{pop}, summed response for each population.

do not necessarily refute that model. However, the LTP-learning model is itself based on population-averaging measurements (Bliss and Lømo, 1973; Bliss and Collingridge, 1993; Basu and Siegelbaum, 2015; Nicoll, 2017) and must therefore be questioned in the same light. If we do not start with the *a priori* assumption that LTP is the mechanism of learning, then population-averaging recordings of synapses cannot be used to support the model because it cannot be safely assumed that all synapses are functioning in the same way, as shown in **Figure 3B**. Therefore, experiments that do not resolve the physiological properties of individual synapses and rely on population measurements cannot be used to support or rebut the LTP model of learning.

A substantial body of literature describes changes in LTP and LTD during the postnatal developmental period and has suggested that these changes are important for learning in critical periods (Fox, 1992; Feldman et al., 1999; Kirkwood et al., 1995; Ge et al., 2007). Our recent study of the lifespan synaptome architecture shows a dramatic increase in excitatory synapse diversity during the postnatal developmental period, with every brain region undergoing major compositional changes in heterogeneous synapses (Cizeron et al., 2020). Thus, although the electrophysiological studies have been interpreted as changes in long-term synaptic strength through synaptic plasticity of existing synapses, a radical suggestion, which remains formally possible, is that there could be circumstances where there are no changes in long-term synapse strength mediated by plasticity but changes in the composition of synapse populations. Nevertheless, stimulation of single presynaptic terminals can induce short-term plasticity indicating that at least this form of plasticity occurs at single synapses (Vandael et al., 2020). Untangling the relative contribution of synaptic plasticity and changing populations of synapses to the long-term changes in synaptic strength will require physiological and molecular studies of synapses at single-synapse resolution.

INTERPRETATION OF PHARMACOLOGICAL PERTURBATIONS OF DIVERSE SYNAPSES

It has long been known that drugs bind to proteins, and because synapses contain different proteins then drugs will target different synapses. This logic has been at the heart of the majority of neuropharmacological therapies and interventions that target neurotransmitter systems. Here we will illustrate how synapse diversity can confound the interpretation of

pharmacological experiments. We will use the LTP models in **Figure 3** and incorporate the NMDA receptor (NMDAR) into our homogeneous and heterogeneous synapses. For simplicity, we will assume the standard position in the literature – that patterns of neural activity can activate the NMDAR and postsynaptic signaling pathways lead to strengthening of synapses (Nicoll, 2017). In our model of homogeneous synapses (**Figure 4A**), which all express the NMDAR (NMDAR+1), LTP is induced in all synapses (**Figure 4A1**) and pharmacological blockade of NMDAR prevents LTP induction (**Figure 4A2**). In our model of heterogeneous synapses (**Figure 4B**), we have synapses that express (NMDAR+) and those lacking (NMDAR−) NMDARs (**Figure 4B**). The NMDAR+ synapses are divided into two groups: NMDAR+1 synapses, which are the same as those in the homogenous population model (**Figure 4A**); and NMDAR+2 synapses, which fail to produce LTP when stimulated. Examples of subtypes of NMDA receptors with differential protein interactions and roles in LTP have been described (Ryan et al., 2013; Frank et al., 2016, 2017; Frank and Grant, 2017). As shown in **Figure 4B1**, stimulating this heterogeneous population of synapses produces LTP in the overall population, whereas at the single-synapse level we see LTP in only half the synapses (NMDAR+1), with the other synapses either unchanged (NMDAR+2) or weakened (NMDAR−).

Next we will repeat this experiment in the presence of a drug that blocks the NMDAR (**Figures 4A2,B2**). Both homogeneous and heterogeneous populations show no overall change in synaptic strength; in other words, LTP is blocked. However, on closer inspection of individual synapses, we find that within the heterogeneous population some synapses show LTP (NMDAR+2) whereas others show LTD (NMDAR−). These simulations show that in an experiment in which there is diversity in the expression of the NMDAR and downstream signaling molecules, a misleading interpretation can be drawn of the synaptic changes within the population. As noted above, if these subpopulations are of differing relevance to behavioral outputs then the population measures would give a misleading interpretation of both the electrophysiological and pharmacological data. The scenarios we portray are not unrealistic as studies of spike timing-dependent plasticity show that a given pattern of pre- and post-synaptic activation induces LTP at some synapses and induces LTD at other synapses (Brzosko et al., 2019). Moreover, the neuromodulatory neurotransmitters can convert the LTD to LTP and vice versa (Brzosko et al., 2019).

In addition to considering the action of drugs that target neurotransmitters these principles apply to signaling and metabolic enzymes, which are known to have differential distributions (Roy et al., 2018a,b). If synapses showed different rates of protein synthesis then protein synthesis inhibitors would exert different phenotypes on individual synapses. There are well-documented examples of dissociations between protein synthesis and long-term memory, which remain unexplained (Routtenberg and Rekart, 2005; Gold, 2008), potentially because of synapse diversity.

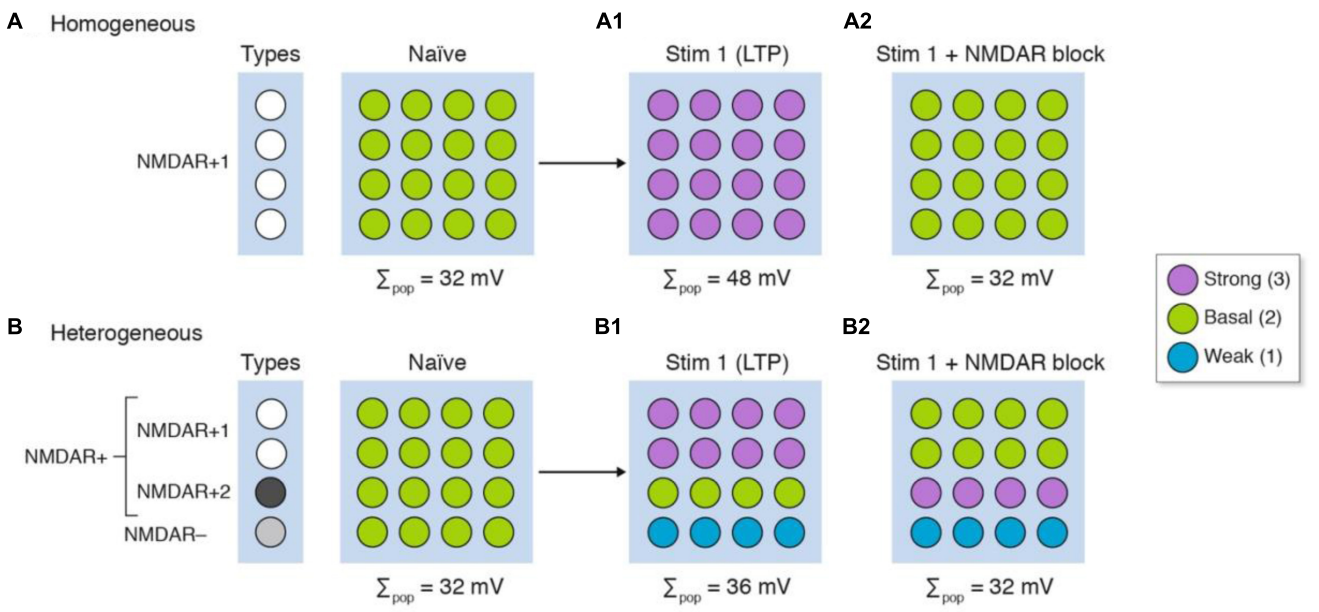

FIGURE 4 | The differing molecular composition of individual synapses confounds the interpretation of signaling mechanisms. Three types of synapse are illustrated in four rows: NMDAR+ synapses, which express the NMDA receptor, are divided into NMDAR+1 synapses that have an enzyme used for NMDAR induction of LTP, and NMDAR+2 synapses which lack the enzyme; and NMDAR− synapses that do not express NMDA receptors but can be weakened by synaptic stimulation. After stimulation (Stim 1), LTP is induced in all the homogeneous synapses **(A1)** but in only half the heterogeneous synapse populations **(B1)** even though LTP is measured in the whole population. The same experiment performed in the presence of an NMDA receptor blocker **(A2,B2)** shows that the population measure of LTP is blocked. However, there are synaptic physiological changes in the heterogeneous population that remain undetected **(B2)**.

INTERPRETING GENETIC PERTURBATIONS IN DIVERSE SYNAPSES

Genetic perturbations (e.g., knockout mice, knockdown approaches) will change the molecular composition of individual synapses and thereby alter their signaling properties in a way that is similar to the pharmacological model presented above (**Figure 4**). In addition to this mechanism, we have previously described "synaptome reprograming" in mice carrying gene mutations (Zhu et al., 2018; Grant, 2019). Broadly speaking, synaptome reprograming changes one heterogeneous population of synapses into a different population (**Figure 5**). We will consider two versions of synaptic reprograming that occur with gene mutations: (i) where the spatial location of the different synapses has changed (**Figure 5**, mutation 1); and (ii) where the numbers of synapse types and their spatial location have changed (**Figure 5**, mutation 2).

After an LTP-inducing stimulation, the response of mutation 1 is the same as wild type, but the mutant synaptome produces different outputs from those synapses located in rows 2 and 4. If these were behavior-relevant synapses, then this would produce behavioral differences to the wild type without an apparent difference in LTP. The response of mutation 2 is a different spatial output to the wild type and mutation 1 and an overall lower LTP. The behavioral output will depend on the relative importance of synapses in different locations. Together, these examples illustrate how genetic mutations could produce a change in LTP and have any number of effects (increase, decrease or no change) on behavior.

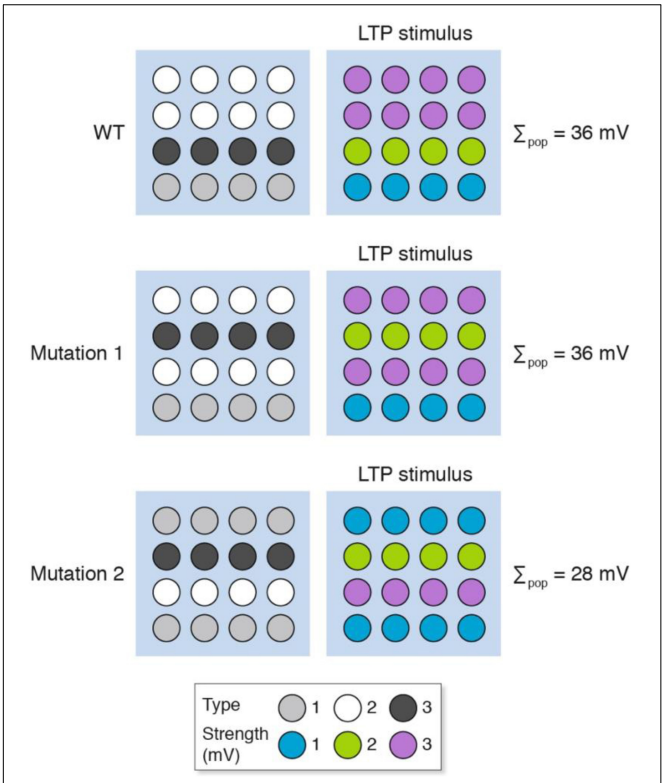

FIGURE 5 | Synaptome reprograming by gene mutations alters the spatial distribution of heterogeneous synapses. The wild-type synaptome map, which is composed of three synapse types, provides an overall population measure (Σ_{pop}) after LTP induction of 36 mV. With mutation 1, the spatial distribution of synapses has changed but the total LTP is the same as for wild type (Σ_{pop} = 36 mV). Mutation 2, however, has altered the representation of synapse types (more type 1 and fewer type 2) and an LTP-inducing stimulus shows less LTP than the wild type.

These simulations have implications for the interpretation of population recording in mutant organisms. In the presence of synaptic diversity it is not possible to conclude the physiological properties of individual synapses or the potential contribution to a behavioral output without knowing the physiological changes in each synapse and the spatial location of the synapse. With synaptome reprograming, the spatial reorganization of synapse types complicates the interpretation of basal physiological differences between wild type and mutant, and of differences that arise after a stimulation protocol that induces LTP.

DISCUSSION

The vast majority of electrophysiological studies of synaptic function employ methods that record from populations of synapses. Moreover, EEG and fMRI signals are assumed to stem largely from populations of synapses. Data from these experiments have been highly influential; for example, they have been used to support the hypothesis that an increase in stable synaptic strength can account for learning and for how behaviors change during development. These models are based on the assumption that the synapses are homogeneous and therefore the population measure can be extrapolated to reflect the physiology of the individual synapses. However, in the presence of synapse diversity, the population measure does not accurately inform on the physiological properties of individual synapses. As we have argued, there can be a dissociation between the population measure and the changes in subsets of synapses. Moreover, in the presence of a genetic, pharmacological or other biochemical perturbation that changes the molecular composition of synapses and/or their spatial location, the interpretation of the data is further confounded.

Synapse diversity interferes in many different ways with the interpretation of electrophysiological experiments that record populations of synapses. Phenotypic dissociations between electrophysiology and behavior using pharmacological and genetic approaches are confounded. Indeed, there have been many examples where LTP and learning have been dissociated with pharmacological and genetic approaches. These dissociations could be explained by synapse diversity and synaptome reprograming. Although synapse diversity and synaptome reprograming could be used to dismiss a dissociation, we need to recognize that the null hypothesis itself (that LTP is the causal mechanism of learning) is also subject to the same confound because the experiments that have shown the correlation between synapse strength and learning are themselves based on population measurements of synapse physiology.

An important area of molecular neuroscience has been the dissection of signaling pathways from neurotransmitter receptors. These experiments have almost universally used synapse population measures (e.g., hippocampus slices bathed in drugs), and the phenotypes of different molecular perturbations are assumed to reflect the "pathways" inside the homogenous synapses. However, the molecular targets of these drugs and the proteins comprising the signaling pathways can differ between synapses, and the physiological outputs could therefore represent changes in the relative contributions of different synapse types rather than the efficacy of the putative pathway. This problem has previously been described in the context of cellular heterogeneity (Altschuler and Wu, 2010). Synapse electrophysiology is not the only area of synaptic biology that is bedeviled by synapse diversity. Many biochemical studies involve extracting proteins from populations of synapses (e.g., western blotting) and neurochemical approaches obtain measurements from large populations of synapses.

It is also important to recognize that homogenous synapses can have differential physiological outputs depending on their spatial location in the dendritic tree (Spruston, 2008). When considering the physiological importance of synapses, it is therefore necessary to consider the spatial location and the molecular, morphological and functional characteristics of each synapse. This underlines the conceptual and practical importance of the synaptome architecture (Grant, 2018b; Zhu et al., 2018; Cizeron et al., 2020). The first synaptome maps that describe the synaptome architecture of the mouse and human brain are now emerging (Zhu et al., 2018; Cizeron et al., 2020; Curran et al., 2020). In the same way that neuronal types are being reclassified and atlased using genomic methods, we expect that there will be new classifications of synapses and synaptome atlases, which will be key reference resources. Linking synaptome and connectome atlases will enable an understanding of the physiological properties of specific circuits and synapse types to be integrated with electrophysiological and behavioral mechanisms.

Until single-synapse resolution physiological responses can be correlated with the known molecular constituents of the recorded synapses, it will not be possible to safely interpret population-based physiological studies. Importantly, the current models of synaptic mechanisms and their relevance to behavior will need to be re-examined before we can have confidence in their validity. This does not mean we are arguing against populations of synapses as important carriers of information, but rather to emphasize the need for identification of synapse type. In this regard, optical approaches to molecular imaging offer an increasingly powerful set of tools capable of resolving the molecular composition of individual synapses and their functional properties. Synaptic proteins could be genetically labeled (using fluorescent proteins (Zhu et al., 2018) or self-labeling tags (Masch et al., 2018)) to identify synapse subtypes together with simultaneous optical recording using genetically encoded functional reporters (e.g., Ca^{2+}, voltage indicators), or dyes that fill dendritic spines, or labels that reveal the dynamic nanoarchitecture of synapses (Masch et al., 2018; Wegner et al., 2018). Electrophysiological stimulation of individual presynaptic terminals of mossy fibers paired with postsynaptic recording in the CA3 region using patch electrodes is a powerful approach that can be coupled with Ca^{2+} chelators that modify the biochemical properties of individual synapses (Vyleta and Jonas, 2014) and has the potential to be combined with molecular labeling methods that distinguish individual synapses. Ideally, the recording systems would not use "whole cell recording" of individual postsynaptic events, but direct recording from individual postsynaptic terminals. Although the characterization of synapse diversity and synaptome architecture raises problems for the existing literature, it also opens completely new models of physiology and behavior based on the functional diversity of molecularly distinct synapses (Grant, 2018b; Zhu et al., 2018).

DATA AVAILABILITY STATEMENT

All datasets generated for this study are included in the article, further inquiries can be directed to the corresponding author/s.

AUTHOR CONTRIBUTIONS

All authors listed have made a substantial, direct and intellectual contribution to the work, and approved it for publication.

FUNDING

This work was supported by the Wellcome Trust (Technology Development Grant No. 202932), the European Research Council (ERC) under the European Union's Horizon 2020 Research and Innovation Programe (695568 SYNNOVATE), and the Simons Foundation Autism Research Initiative (529085).

ACKNOWLEDGMENTS

We thank D. Maizels for artwork, C. Davey for editing, and Tom O'Dell for helpful comments.

REFERENCES

Altschuler, S. J., and Wu, L. F. (2010). Cellular heterogeneity: do differences make a difference? *Cell* 141, 559–563. doi: 10.1016/j.cell.2010.04.033

Basu, J., and Siegelbaum, S. A. (2015). The corticohippocampal circuit, synaptic plasticity, and memory. *Cold Spring Harb. Perspect. Biol.* 7:a021733. doi: 10.1101/cshperspect.a021733

Bayes, A., Collins, M. O., Croning, M. D. R., van de Lagemaat, L. N., Choudhary, J. S., Grant, S. G. N. (2012). Comparative study of human and mouse

postsynaptic proteomes finds high compositional conservation and abundance differences for key synaptic proteins. *PLoS One* 7:e46683. doi: 10.1371/journal.pone.0046683

Bayes, A., Collins, M. O., Reig-Viader, R., Gou, G., Goulding, D., Izquierdo, A., et al. (2017). Zebrafish synapse proteome complexity, evolution and ultrastructure. *Nat. Commun.* 8:14613. doi: 10.1038/ncomms14613

Bayes, A., van de Lagemaat, L. N., Collins, M. O., Croning, M. D. R., Whittle, I. R., Choudhary, J. S., et al. (2011). Characterization of the proteome, diseases and evolution of the human postsynaptic density. *Nat. Neurosci.* 14, 19–21. doi: 10.1038/nn.2719

Bliss, T. V., and Collingridge, G. L. (1993). A synaptic model of memory: long-term potentiation in the hippocampus. *Nature* 361, 31–39. doi: 10.1038/361031a0

Bliss, T. V., and Lømo, T. (1973). Long-lasting potentiation of synaptic transmission in the dentate area of the anaesthetized rabbit following stimulation of the perforant path. *J. Physiol.* 232, 331–356. doi: 10.1113/jphysiol.1973.sp010273

Broadhead, M. J., Horrocks, M. H., Zhu, F., Muresan, L., Benavides-Piccione, R., DeFelipe, J., et al. (2016). PSD95 nanoclusters are postsynaptic building blocks in hippocampus circuits. *Sci. Rep.* 6:24626. doi: 10.1038/srep24626

Brzosko, Z., Mierau, S. B., and Paulsen, O. (2019). Neuromodulation of spike-timing-dependent plasticity: past. *Present Future Neuron* 103, 563–581. doi: 10.1016/j.neuron.2019.05.041

Cizeron, M., Qiu, Z., Koniaris, B., Gokhale, R., Komiyama, N. H., Fransén, E., et al. (2020). A brain-wide atlas of synapses across the mouse lifespan. *Science* 369, 270–275. doi: 10.1126/science.aba3163

Coba, M. P., Pocklington, A. J., Collins, M. O., Kopanitsa, M. V., Uren, R. T., Swamy, S., et al. (2009). Neurotransmitters drive combinatorial multistate postsynaptic density networks. *Sci. Signal.* 2:ra19. doi: 10.1126/scisignal.2000102

Collins, M. O., Husi, H., Yu, L., Brandon, J. M., Anderson, C. N. G., Blackstock, W. P., et al. (2006). Molecular characterization and comparison of the components and multiprotein complexes in the postsynaptic proteome. *J. Neurochem.* 97(Suppl. 1), 16–23. doi: 10.1111/j.1471-4159.2005.03507.x

Curran, O. E., Qiu, Z., Smith, C., and Grant, S. G. (2020). A single-synapse resolution survey of PSD95-positive synapses in twenty human brain regions. *Eur. J. Neurosci.* doi: 10.1111/ejn.14846

Distler, U., Schmeisser, M. J., Pelosi, A., Reim, D., Kuharev, J., Weiczner, R., et al. (2014). In-depth protein profiling of the postsynaptic density from mouse hippocampus using data-independent acquisition proteomics. *Proteomics* 14, 2607–2613. doi: 10.1002/pmic.201300520

Feldman, D., Nicoll, R., and Malenka, R. (1999). Synaptic plasticity at thalamocortical synapses in developing rat somatosensory cortex: LTP, LTD, and silent synapses. *J. Neurobiol.* 41, 92–101. doi: 10.1002/(sici)1097-4695(199910)41:1<92::aid-neu12>3.0.co;2-u

Fox, K. (1992). A critical period for experience-dependent synaptic plasticity in rat barrel cortex. *J. Neurosci.* 12, 1826–1838. doi: 10.1523/jneurosci.12-05-01826.1992

Frank, R. A., and Grant, S. G. (2017). Supramolecular organization of NMDA receptors and the postsynaptic density. *Curr. Opin. Neurobiol.* 45, 139–147. doi: 10.1016/j.conb.2017.05.019

Frank, R. A., Komiyama, N. H., Ryan, T. J., Zhu, F., O'Dell, T. J., Grant, S. G. N. (2016). NMDA receptors are selectively partitioned into complexes and supercomplexes during synapse maturation. *Nat. Commun.* 7:11264. doi: 10.1038/ncomms11264

Frank, R. A. W., Zhu, F., Komiyama, N. H., and Grant, S. G. N. (2017). Hierarchical organization and genetically separable subfamilies of PSD95 postsynaptic supercomplexes. *J. Neurochem.* 142, 504–511. doi: 10.1111/jnc.14056

Ge, S., Yang, C.-H., Hsu, K.-S., Ming, G.-L., and Song, H. (2007). A critical period for enhanced synaptic plasticity in newly generated neurons of the adult brain. *Neuron* 54, 559–566. doi: 10.1016/j.neuron.2007.05.002

Gold, P. E. (2008). Protein synthesis inhibition and memory: formation vs amnesia. *Neurobiol. Learn. Mem.* 89, 201–211. doi: 10.1016/j.nlm.2007.10.006

Grant, S. G. (2007). Toward a molecular catalogue of synapses. *Brain Res. Rev.* 55, 445–449. doi: 10.1016/j.brainresrev.2007.05.003

Grant, S. G. N. (2018a). Synapse molecular complexity and the plasticity behaviour problem. *Brain Neurosci. Adv.* 2:2398212818810685. doi: 10.1177/2398212818810685

Grant, S. G. N. (2018b). The synaptomic theory of behavior and brain disease. *Cold Spring Harb. Symp. Quant. Biol.* 83, 45–56. doi: 10.1101/sqb.2018.83.037887

Grant, S. G. N. (2019). Synapse diversity and synaptome architecture in human genetic disorders. *Hum. Mol. Genet.* 28, R219–R225. doi: 10.1093/hmg/ddz178

Husi, H., Ward, M. A., Choudhary, J. S., Blackstock, W. P., and Grant, S. G. (2000). Proteomic analysis of NMDA receptor-adhesion protein signaling complexes. *Nat. Neurosci.* 3, 661–669. doi: 10.1038/76615

Kirkwood, A., Lee, H.-K., and Bear, M. F. (1995). Co-regulation of long-term potentiation and experience-dependent synaptic plasticity in visual cortex by age and experience. *Nature* 375, 328–331. doi: 10.1038/375328a0

Masch, J.-M., Steffens, H., Fischer, J., Engelhardt, J., Hubrich, J., Keller-Findeisen, J., et al. (2018). Robust nanoscopy of a synaptic protein in living mice by organic-fluorophore labeling. *Proc. Natl. Acad. Sci.* 115, E8047–E8056.

Megias, M., Emri, Z., Freund, T. F., and Gulyas, A. I. (2001). Total number and distribution of inhibitory and excitatory synapses on hippocampal CA1 pyramidal cells. *Neuroscience* 102, 527–540. doi: 10.1016/s0306-4522(00)00496-6

Micheva, K. D., Busse, B., Weiler, N. C., O'Rourke, N., and Smith, S. J. (2010). Single-synapse analysis of a diverse synapse population: proteomic imaging methods and markers. *Neuron* 68, 639–653. doi: 10.1016/j.neuron.2010.09.024

Nicoll, R. A. (2017). A brief history of long-term potentiation. *Neuron* 93, 281–290. doi: 10.1016/j.neuron.2016.12.015

O'Rourke, N. A., Weiler, N. C., Micheva, K. D., and Smith, S. J. (2012). Deep molecular diversity of mammalian synapses: why it matters and how to measure it. *Nat. Rev. Neurosci.* 13, 365–379. doi: 10.1038/nrn3170

Routtenberg, A., and Rekart, J. L. (2005). Post-translational protein modification as the substrate for long-lasting memory. *Trends Neurosci.* 28, 12–19. doi: 10.1016/j.tins.2004.11.006

Roy, M., Sorokina, O., McLean, C., Tapia-González, S., DeFelipe, J., Armstrong, J. D., et al. (2018a). Regional diversity in the postsynaptic proteome of the mouse brain. *Proteomes* 6:31. doi: 10.3390/proteomes6030031

Roy, M., Sorokina, O., Skene, N., Simonnet, C., Mazzo, F., Zwart, R., et al. (2018b). Proteomic analysis of postsynaptic proteins in regions of the human neocortex. *Nat. Neurosci.* 21, 130–138. doi: 10.1038/s41593-017-0025-9

Ryan, T. J., Kopanitsa, M. V., Indersmitten, T., Nithianantharajah, J., Afinowi, N. O., Pettit, C., et al. (2013). Evolution of GluN2A/B cytoplasmic domains diversified vertebrate synaptic plasticity and behavior. *Nat. Neurosci.* 16, 25–32. doi: 10.1038/nn.3277

Skene, N. G., Roy, M., and Grant, S. G. (2017). A genomic lifespan program that reorganises the young adult brain is targeted in schizophrenia. *eLife* 6:e17915.

Spruston, N. (2008). Pyramidal neurons: dendritic structure and synaptic integration. *Nat. Rev. Neurosci.* 9, 206–221. doi: 10.1038/nrn2286

Vandael, D., Borges-Merjane, C., Zhang, X., and Jonas, P. (2020). Short-term plasticity at hippocampal mossy fiber synapses is induced by natural activity patterns and associated with vesicle pool engram formation. *Neuron* 107, 509.e7–521.e7.

Vyleta, N. P., and Jonas, P. (2014). Loose coupling between Ca^{2+} channels and release sensors at a plastic hippocampal synapse. *Science* 343, 665–670. doi: 10.1126/science.1244811

Wegner, W., Mott, A. C., Grant, S. G., Steffens, H., and Willig, K. I. (2018). In vivo STED microscopy visualizes PSD95 sub-structures and morphological changes over several hours in the mouse visual cortex. *Sci. Rep.* 8, 1–11.

Zhu, F., Cizeron, M., Qiu, Z., Benavides-Piccione, R., Kopanitsa, M. V., Skene, N. G., et al. (2018). Architecture of the mouse brain synaptome. *Neuron* 99, 781.e10–799.e10. doi: 10.1016/j.neuron.2018.07.007

Conflict of Interest: The authors declare that the research was conducted in the absence of any commercial or financial relationships that could be construed as a potential conflict of interest.

frontiers in Synaptic Neuroscience

HYPOTHESIS AND THEORY
published: 11 March 2021
doi: 10.3389/fnsyn.2021.616607

The Subcortical-Allocortical-Neocortical *continuum* for the Emergence and Morphological Heterogeneity of Pyramidal Neurons in the Human Brain

Alberto A. Rasia-Filho[1,2], Kétlyn T. Knak Guerra[2], Carlos Escobar Vásquez[2], Aline Dall'Oglio[1], Roman Reberger[3], Cláudio R. Jung[4] and Maria Elisa Calcagnotto[2,5]*

[1] Department of Basic Sciences/Physiology and Graduate Program in Biosciences, Universidade Federal de Ciências da Saúde de Porto Alegre, Porto Alegre, Brazil, [2] Graduate Program in Neuroscience, Universidade Federal do Rio Grande do Sul, Porto Alegre, Brazil, [3] Medical Engineering Program, Friedrich-Alexander-Universität Erlangen-Nürnberg, Erlangen, Germany, [4] Institute of Informatics, Universidade Federal do Rio Grande do Sul, Porto Alegre, Brazil, [5] Neurophysiology and Neurochemistry of Neuronal Excitability and Synaptic Plasticity Laboratory, Department of Biochemistry and Biochemistry Graduate Program, Universidade Federal do Rio Grande do Sul, Porto Alegre, Brazil

OPEN ACCESS

Edited by:
Kimberly M. Huber, University of Texas Southwestern Medical Center, United States

Reviewed by:
Zdravko Petanjek, University of Zagreb, Croatia
Humberto Salgado, Universidad Autónoma de Yucatán, Mexico

***Correspondence:**
Alberto A. Rasia-Filho
aarf@ufcspa.edu.br; rasiafilho@yahoo.com

Received: *12 October 2020*
Accepted: *01 February 2021*
Published: *11 March 2021*

Citation:
Rasia-Filho AA, Guerra KTK, Vásquez CE, Dall'Oglio A, Reberger R, Jung CR and Calcagnotto ME (2021) The Subcortical-Allocortical-Neocortical continuum for the Emergence and Morphological Heterogeneity of Pyramidal Neurons in the Human Brain. Front. Synaptic Neurosci. 13:616607. doi: 10.3389/fnsyn.2021.616607

Human cortical and subcortical areas integrate emotion, memory, and cognition when interpreting various environmental stimuli for the elaboration of complex, evolved social behaviors. Pyramidal neurons occur in developed phylogenetic areas advancing along with the allocortex to represent 70–85% of the neocortical gray matter. Here, we illustrate and discuss morphological features of heterogeneous spiny pyramidal neurons emerging from specific amygdaloid nuclei, in CA3 and CA1 hippocampal regions, and in neocortical layers II/III and V of the anterolateral temporal lobe in humans. Three-dimensional images of Golgi-impregnated neurons were obtained using an algorithm for the visualization of the cell body, dendritic length, branching pattern, and pleomorphic dendritic spines, which are specialized plastic postsynaptic units for most excitatory inputs. We demonstrate the emergence and development of human pyramidal neurons in the cortical and basomedial (but not the medial, MeA) nuclei of the amygdala with cells showing a triangular cell body shape, basal branched dendrites, and a short apical shaft with proximal ramifications as "pyramidal-like" neurons. Basomedial neurons also have a long and distally ramified apical dendrite not oriented to the pial surface. These neurons are at the beginning of the allocortex and the limbic lobe. "Pyramidal-like" to "classic" pyramidal neurons with laminar organization advance from the CA3 to the CA1 hippocampal regions. These cells have basal and apical dendrites with specific receptive synaptic domains and several spines. Neocortical pyramidal neurons in layers II/III and V display heterogeneous dendritic branching patterns adapted to the space available and the afferent inputs of each brain area. Dendritic spines vary in their distribution, density, shapes, and sizes (classified as stubby/wide, thin, mushroom-like, ramified,

transitional forms, "atypical" or complex forms, such as thorny excrescences in the MeA and CA3 hippocampal region). Spines were found isolated or intermingled, with evident particularities (e.g., an extraordinary density in long, deep CA1 pyramidal neurons), and some showing a spinule. We describe spiny pyramidal neurons considerably improving the connectional and processing complexity of the brain circuits. On the other hand, these cells have some vulnerabilities, as found in neurodegenerative Alzheimer's disease and in temporal lobe epilepsy.

Keywords: amygdaloid complex, hippocampus, cerebral cortex, human dendritic spines, 3D reconstruction, Alzheimer's disease, temporal lobe epilepsy

"*. . . the cerebral cortex is similar to a garden filled with trees, the pyramidal cells, which, thanks to intelligent culture, can multiply their branches, sending their roots deeper and producing more and more varied and exquisite flowers and fruits.*" (Ramón y Cajal, 1894a)

INTRODUCTION

Ramón y Cajal (1894b) described cortical pyramidal neurons (or "psychic cells") as "progressively larger and more complex in ascending the animal scale. . . to assume that at least part of its increased functional role is a result of increased morphological complexity. . . In descending the vertebrate ladder, the shape of the psychic cell becomes simpler, with its length and volume decreasing in parallel. . . differences are in microscopic form and the relative volume of particular components used in (brain) construction." In humans, pyramidal neurons are found in forebrain structures (Ramón y Cajal, 1894b, Ramón y Cajal, 1909–1911), but not in the striatum, the cerebellum, the brainstem, or in the spinal cord (Spruston, 2008). These cells develop in the "anatomic limbic system" or "greater limbic lobe" (Miller and Vogt, 1995; Wyss and van Groen, 1995; Gloor, 1997; Heimer et al., 2008) and are found in the heterogeneous allocortex and neocortex layers (i.e., except in cortical layer I, from layers II to VI and their subdivisions; Miller and Vogt, 1995; Andersen et al., 2007; DeFelipe, 2011), accounting for approximately 70–85% of all cells in the cerebral gray matter (Nieuwenhuys, 1994; DeFelipe, 2011; Kolb and Whishaw, 2015).

Pyramidal neurons have been studied using complementary techniques, from the Nissl (or thionine) staining and the Golgi silver impregnation procedure to different approaches for intracellular microinjection of fluorescent dyes, serial sections for ultrastructural connectional and neurochemical profiles, *in vitro* and *in vivo* electrophysiological recordings, computational and *in silico* models (Ramón y Cajal, 1909–1911; Lorente de Nó, 1934; Szentágothai, 1978; Mountcastle, 1979; Braak, 1980; Peters and Jones, 1984; Sims and Williams, 1990; Peters et al., 1991; McCormick et al., 1993; Segev et al., 1995; Somogyi et al., 1998; Valverde et al., 2002; Andersen et al., 2007; Spruston, 2008; Larriva-Sahd, 2010; Ramaswamy and Markram, 2015; Eyal et al., 2018; Soltesz and Losonczy, 2018; Cembrowski and Spruston, 2019; Oruro et al., 2019; Benavides-Piccione et al., 2020). For example, the Golgi method adapted for formalin-fixed human brain and light microscopy provides images of pyramidal dendrites and spine shapes from different cortical and subcortical regions (Dall'Oglio et al., 2010; Reberger et al., 2018; Vásquez et al., 2018; Correa-Júnior et al., 2020). This can eventually add fundamental data to identify the brain cellular components and their connectivity toward physiology and behavior, as well as for modeling and theory approaches on neural structure and integrated functions of human brain areas (see a current discussion in Zeng, 2020).

The "typical" or "classical" morphological attributes of an adult spiny pyramidal neuron include: (1) a triangular/conical soma; (2) basal dendrites with opposing origins from the base of the perikaryon and closely ramified branches extending radially outward; (3) an apical dendrite arising from the apex of the cell body with some collaterals branches but maintaining a straight course until the terminal ramification near the cortical surface; (4) an heterogeneous distribution of spines from proximal to distal dendrites; and (5) an axon that descends toward the white matter (Feldman, 1984; Peters and Jones, 1984; for further information see Nieuwenhuys, 1994). These features typically refer to thick-tufted pyramidal neurons in the neocortical internal pyramidal layer V of various species (e.g., rats, mice, monkeys, and humans; Feldman, 1984; Peters and Jones, 1984; Ledergerber and Larkum, 2010; Ramaswamy and Markram, 2015; Wang et al., 2018). The study of pyramidal neurons is vast, and we still do not have a complete picture of the integrated functions of these abundant cells in the most complex neural processing, such as consciousness, cognition, abstract thinking, creativity, and social emotions (see relevant data in Anderson et al., 2009; DeFelipe, 2011; Marín-Padilla, 2014; Ramaswamy and Markram, 2015; Cembrowski and Spruston, 2019 and references therein). Morphology is a crucial step to proceed on this endeavor (Ramón y Cajal, 1894b; DeFelipe, 2011).

Here, we illustrate and discuss the morphological findings of three-dimensional (3D) reconstruction of heterogeneous pyramidal neurons with pleomorphic dendritic spines in the anatomical and functional subcortical-allocortical-neocortical *continuum* in the human brain (from adult males; samples and methodological procedures are described in Dall'Oglio et al., 2010, 2013, 2015; Reberger et al., 2018; Vásquez et al., 2018). Our aim is not to exhaustively elaborate the data available in the literature. Additional references can be found in the articles cited here. Instead, we would like to highlight and instigate further 3D morphological studies on the emergence and development of human pyramidal neurons, including the features of dendritic

spine number and shapes, as essential steps for understanding the integrative capacities of these neurons in distinct, functionally specialized brain areas (Spruston, 2008; Luebke, 2017; Soltesz and Losonczy, 2018; Cembrowski and Spruston, 2019; Benavides-Piccione et al., 2020). These human data encourage further efforts on elaborating the cell heterogeneity and synaptic processing in dendritic domains and spines of pyramidal cells settled from specific amygdaloid nuclei to neocortical areas in both normal and pathological conditions. In this regard, pyramidal neurons show vulnerabilities and involvement in Alzheimer's disease (AD) and epilepsy, as described below.

THE MORPHOLOGICAL HETEROGENEITY OF PYRAMIDAL NEURONS

"Typical" Pyramidal and "Pyramidal-Like" Neurons

The classification of a neuron as a pyramidal cell type includes morphological features that show considerable diversity in each brain area within and across species (Ramón y Cajal, 1894b; Feldman, 1984; Nieuwenhuys, 1994; Spruston, 2008; Ledergerber and Larkum, 2010; Bianchi et al., 2013; Luebke, 2017; Soltesz and Losonczy, 2018; Cembrowski and Spruston, 2019; Gouwens et al., 2019; Benavides-Piccione et al., 2020). From a morphological standpoint, heterogeneous pyramidal neurons can have a small to large cell body with triangular, spherical, ovoid, rhomboidal, and irregular forms, basal dendrites with varied branching pattern and radial extension, and an apical dendrite with different terminal tuft aspect (Feldman, 1984). Large thick-tufted pyramidal neurons in neocortical layer V have basal and apical dendrites whose length would integrate afferent connections across different layers. However, there are variations in these cells for their basal ramification, apical bifurcation, and tapering as a horizontal tuft in the superficial cortical layers (Morishima and Kawaguchi, 2006; Wang et al., 2018). In the rat frontal cortex, two populations of layer V pyramidal neurons that project to the striatum differ in apical dendrite initial shaft diameter and the distal tuft area, length, and branch points in layer I (Morishima and Kawaguchi, 2006). That is, cells in the superficial layer V show tufted or slender apical dendrites, whereas cells in the deeper layer V have a reduced or absent apical tuft (Morishima and Kawaguchi, 2006). Furthermore, the apical dendrites of deeper layer VI pyramidal neurons may not reach layer I as a terminal tuft; rather, these dendrites taper at midcortical levels in the neocortex of rats and monkeys (Braak, 1980; Feldman, 1984; Ledergerber and Larkum, 2010).

"Typical" pyramidal neurons have a main apical dendritic shaft directed toward the pial surface of the neocortex. "Pyramidal-like" neurons show most features of a pyramidal shape (Gloor, 1997; Luis de la Iglesia and Lopez-Garcia, 1997) although they can have an apical dendrite branching close to the cell body and with different orientation in the neuropil (Vásquez et al., 2018). For example, the pyramidal-like neurons in the human cortical nucleus of the amygdaloid complex (posterior part, PCo) have a triangular cell body, two basal dendrites of a similar thickness, and one main thick dendrite emerging at the apex of the soma. The primary and short "apical" dendrite of these cells may not be directed to the nuclear external surface (Vásquez et al., 2018; shown below). Pyramidal-like neurons in the basolateral amygdaloid nuclei show three to five primary dendrites. One of them is at the somatic apex, it is longer than the others, and has no preferred spatial orientation (Braak and Braak, 1983; Gloor, 1997). These pyramidal-like neurons are not arranged in evident layers and are not oriented in parallel alongside one another (Gloor, 1997). Pyramidal-like neurons also show a pyramidal or piriform soma in the rat allocortex (subiculum), one thicker apical dendrite projecting across the molecular layer into the hippocampal fissure, and thinner basal projections into the alveus white matter (Mattia et al., 1997), or a more complex dendritic architecture in the *stratum oriens* of CA2 to CA1 regions of *Proechimys* (Scorza et al., 2011).

"Modified Pyramids"

Lorente de Nó (1934) used the term "modified pyramids" for the main components of the "Ammon's horn and fascia dentata" in man and monkey. Peters and Jones (1984) refer to modified pyramids when "there are other cells which are modified in form, but nonetheless are easily recognized as having pyramidal features" as those in the neocortical layer II (even with short, divaricated, or absent apical dendrites) or with a rather oval cell body, thin apical dendrite, and basal dendrites radiating out in all directions in neocortical layer IV. Modified pyramids refer to a great variety of cellular shapes (Braak, 1980). In the human isocortical multiform layer VI, modified pyramidal neurons "deviate substantially from stereotypical pyramidal cells" including cells with a short and thin apical dendrite, basal dendrites with different diameters and lengths, one thick basal dendrite extending in various directions or various dendrites generated from the lateral surfaces of the soma (Braak, 1980; Braak and Braak, 1985). In the piriform cortex, modified pyramids include bi-horn, spindle-, triangular-, and crescent-shaped cells (reviewed in Larriva-Sahd, 2010). "Inverted" pyramidal neurons in neocortical layer VI display an "apical" dendrite directed toward the white matter (Feldman, 1984; Steger et al., 2013). Other neurons were also considered variations (or specializations) of pyramidal neurons, such as the Meynert-Cajal cells in layer IVb of the primary visual cortex (Hof and Morrison, 1990), the Meynert neurons in layer Vb of the striate area (Braak, 1980), the large Betz cells in layer Vb of the primary motor cortex (Braak, 1980; Feldman, 1984), and the von Economo neurons (VENs) in the frontoinsular and anterior cingulate cortices, for example (Butti et al., 2013; Banovac et al., 2019; for VENs particularities see also Cauda et al., 2014; Yang et al., 2019; Correa-Júnior et al., 2020). Then, it is conceivable that the term "pyramidal neuron" might refer to a variety of shapes ranging from "classic" pyramidal, "pyramidal-like," and "modified pyramids" with variable size, somatic shape, dendritic branching pattern, length, and orientation in the neuropil.

DENDRITES AND SPINES IN PYRAMIDAL NEURONS

Besides conserved basic principles of mammalian brain development, evolution also produced significant quantitative and qualitative changes in cell number and shape along with circuit organization in cortical areas (Geschwind and Rakic, 2013; see also Herculano-Houzel et al., 2008; Herculano-Houzel, 2019). The connectivity of pyramidal dendrites in cortical multimodal areas, which receive a broad range of inputs at hierarchically higher association levels of integrative processing, show longer, more branched, and have more spines than in areas that process a specific modality of motor or primary sensory activity (Jacobs et al., 2001; Anderson et al., 2009; Kolb and Whishaw, 2015; Hrvoj-Mihic et al., 2017; González-Burgos et al., 2019). Moreover, cortical pyramidal neurons developed basal and apical dendritic domains with different synaptic receptive fields (Larriva-Sahd, 2002; Andersen et al., 2007; Spruston, 2008; Spruston et al., 2013; Larriva-Sahd, 2014). These dendritic segments can (1) compartmentalize signals and/or sum and organize synchronized transmission of information, both of which provide much more computational capabilities for the dynamic processing of information; (2) use passive and/or active membrane properties; (3) show anterograde and retrograde action potentials; and (4) depending on intrinsic membrane properties, impose refractory periods and/or a selective excitability of a specific segment depending on time and distance in the dendritic tree (Oakley et al., 2001; Andersen et al., 2007; Spruston, 2008; Spruston et al., 2013; Almog and Korngreen, 2014; Kastellakis et al., 2016).

The development of particularly specialized neurons involves the structural remodeling of dendritic branches including the occurrence, distribution, density, size, and shape of dendritic spines. Optimal degrees of synaptic connectivity (Litwin-Kumar et al., 2017) could be then associated with dendritic length and branching pattern, spine features, and the neuronal impedance, conductance, and voltage modulatory properties (Papoutsi et al., 2014). More specifically, spines are multifunctional integrative units (Shepherd, 1996) that increase the packing density of synapses by the convolution and interdigitation of cellular membrane, supporting more synapses without increasing the overall volume of the brain (Bourne and Harris, 2009). Dendritic spines provide an enhanced connectivity, modulation of synaptic processing, strength, and plasticity by considerably increasing the computational possibilities between cells (Anderson et al., 2009; Bourne and Harris, 2009; Rochefort and Konnerth, 2012; Yuste, 2013; Dall'Oglio et al., 2015; Tønnesen and Nägerl, 2016). Spines are specialized postsynaptic elements (see also Shepherd, 1996) that receive most (>90%) excitatory glutamatergic inputs (Rochefort and Konnerth, 2012; Yuste, 2013; Chen et al., 2014). Only a low percentage of spines (although particularly important, Müllner et al., 2015) is contacted by inhibitory γ-aminobutyric acid (GABA)-containing axon terminals (Kubota et al., 2007; Brusco et al., 2014).

Pyramidal neurons in neocortical layers III and V develop spines at different rates across the lifespan (Oga et al., 2017). In monkeys, the number of dendritic spines of pyramidal neurons in the primary visual cortex reduces following the onset of visual experience, whereas in areas of sensory association in the inferotemporal cortex and executive function in the granular prefrontal cortex grow more spines than they lose during the same period (Oga et al., 2017). Human pyramidal neurons also show an ontogenetic development that advances with remodeling dendrites and an increase in the spine number and complexity from the gestational period to birth and onward (Braak, 1980; Ramón y Cajal, 1909–1911; DeFelipe, 2011; Marín-Padilla, 2014). The density of dendritic spines in prefrontal pyramidal neurons have a developmental pruning and dynamic remodeling related to the reorganization of cortical circuitries during the first decades of the human lifespan (Petanjek et al., 2011) and a decline in spine measures latter (>50 years; Jacobs et al., 1997). That is, the human cerebral cortex shows neoteny and heterochrony in cortical circuits development and higher functions elaboration (Geschwind and Rakic, 2013). Furthermore, some pyramidal neurons depart from the general description that proximal dendritic segments are devoid of spines. Human pyramidal neurons can show dendritic spines distributed from proximal (e.g., 0–50 μm, Luengo-Sanchez et al., 2018) to long distal segments, as demonstrated below.

Dendritic Spine Heterogeneity

According to morphological features, spines have been classified as stubby, wide, thin, mushroom-like, ramified, with a transitional aspect between these classes (as 'protospines' or 'multispines,' García-López et al., 2010), or "atypical" (also "multimorphic") with a variety of different shapes, which includes double spines, spines with racemose appendages (with a lobed appearance and various bulbous enlargements and heads), and thorny excrescences (densely packed outgrowths showing fairly large spines with various round heads grouped around the stems) (Fiala and Harris, 1999; Arellano et al., 2007a; González-Burgos et al., 2012; González-Ramírez et al., 2014; Stewart et al., 2014; Dall'Oglio et al., 2015; Correa-Júnior et al., 2020). Small protrusions extending from the spine are spinules (Brusco et al., 2014; Vásquez et al., 2018), which are active zone-free invaginating structures that can participate in synaptic plasticity, including long-term potentiation (Petralia et al., 2018).

Spines are in a *continuum* of sizes and shapes and are found isolated or intermingled and forming groups ("clusters") at the same dendritic branch, between different dendrites of the same neuron, or within the same subpopulation of neurons in a brain area (Fiala and Harris, 1999; Arellano et al., 2007a,b; Chen X. et al., 2011; Yuste, 2013; Rasia-Filho et al., 2012a; Rochefort and Konnerth, 2012; Brusco et al., 2014; Stewart et al., 2014; Dall'Oglio et al., 2015; Vásquez et al., 2018; Zancan et al., 2018). Adult human medial amygdaloid nucleus (MeA) neurons also show filopodium, large and thin dendritic spines with a gemmule appearance, and diverse synaptic arrangements as *en passant*, reciprocal, and serial ones (Dall'Oglio et al., 2015). At the ultrastructural level, spines can be monosynaptic or multisynaptic with contacts at the spine head and neck showing both asymmetric and symmetric characteristics (Dall'Oglio et al., 2015).

The relation between structure and function of the different dendritic spines for the fine-tuned synaptic processing is a matter of investigation and needs to be particularized for each sex, age, cell subpopulation, neural circuit, brain area, species, and specific natural or experimental circumstance (Benavides-Piccione et al., 2002; Arellano et al., 2007a; Bourne and Harris, 2008, 2009; Kasai et al., 2010; Rasia-Filho et al., 2012a; Rochefort and Konnerth, 2012; Yuste, 2013; Stewart et al., 2014; Dall'Oglio et al., 2015; Tønnesen and Nägerl, 2016; Lu and Zuo, 2017; Nakahata and Yasuda, 2018; Zancan et al., 2018). For example, some large dendritic spines can be more stable, have large postsynaptic density (PSD), and make strong connections. The size of the spine head scales with the size of the PSD, the presence and proportion of NMDA to AMPA glutamate receptors, and the amplitude of the excitatory postsynaptic current in mushroom-like spines with macular or perforated PSD (van der Zee, 2015 and references therein). In contrast, small spines would be transient forms (Woolfrey and Srivastava, 2016) and/or indicative of connections with a lower resistance to reach the parent dendrite (Segal, 2010). The length and width of the thin spine neck would determine the degree of electrical and biochemical compartmentalization of the spine (Noguchi et al., 2011; Yuste, 2013; reviewed in Tønnesen and Nägerl, 2016). Long necks in thin spines can impose more resistance and be plastic sites for synaptic coupling (Yuste, 2013).

Mushroom-like spines would standardize local postsynaptic potentials throughout the dendritic tree and reduce the location-dependent variability of excitatory responses (Gulledge et al., 2012). Other modeled distal synapses may not impact the cell's output (Moldwin and Segev, 2019). Ramified spines have additional functional possibilities by displaying postsynaptic receptors on different parts of the spine heads (Verzi and Noris, 2009) with likely temporal and spatial specificity and signaling microdomains (Newpher and Ehlers, 2009; Chen and Sabatini, 2012). Synaptic amplification involving clustered dendritic spines would also enhance input cooperativity among coactive inputs at neighboring synapses (Harnett et al., 2012; Yadav et al., 2012), influencing network plasticity, learning, and memory (Frank et al., 2018; Kastellakis and Poirazi, 2019; for the dendritic mechanisms linking memories and overlapping allocations of synaptic resources see also Kastellakis et al., 2016).

These spine features add a high capacity of activity-dependent regulation and synaptic modulation for pyramidal neurons. This is corroborated by the (1) spatial distribution of spine types across proximal to distal branches; (2) extension and composition of the spine PSD; (3) differences in the composition and function of subcellular cytoskeleton, organelles (e.g., actin or smooth endoplasmic reticulum and mitochondria related to calcium levels modulation and initial synaptic establishment, respectively), dendritic mRNAs, and microRNA; and the (4) compartmentalization for both electrical (voltage coupling of spine and dendrite and vice-versa) and biochemical signals (e.g., affecting the diffusion rate of calcium, second messengers, and enzymes between dendritic shaft and spines) (Harris, 1999; Li et al., 2004; Rochefort and Konnerth, 2012; Yuste, 2013; Spruston et al., 2013; Stewart et al., 2014; Tønnesen and Nägerl, 2016; Hirsch et al., 2018). Because neighboring spines with varying shapes and sizes exist in the same dendritic shafts, "the morphological heterogeneity of spines, even in a small portion of the dendrite, is consistent with the idea that synaptic strength is regulated locally, at the level of each single spine" (Frick and Johnston, 2005; Arellano et al., 2007a,b; Chen X. et al., 2011; Lee et al., 2012; Dall'Oglio et al., 2015). Moreover, the presence of different spines in human pyramidal neurons "aligns well with emerging theoretical models of synaptic learning that demonstrate that synapses exhibiting a gradation of states, each bridged by distinct metaplastic transitions, bestow neural networks with enhanced information storage capacity" (Lee et al., 2012; Dall'Oglio et al., 2015 and references therein). These morphological features of human pyramidal neurons can reflect a more complex subcortical to cortical synaptic processing of sensory, emotional, and cognitive information adapted for species-specific social behaviors (Dall'Oglio et al., 2013, 2015). In summary, (1) most dendritic spines form synapses (Arellano et al., 2007b; see also Berry and Nedivi, 2017); (2) the presence and distribution of these spines are indicative of the neuronal connectivity (Cooke and Woolley, 2005; Chen X. et al., 2011; Chen et al., 2014); (3) spine number and shape implies various synaptic modulatory possibilities (Bourne and Harris, 2007; Yuste, 2013; Dall'Oglio et al., 2015; Tønnesen and Nägerl, 2016); (4) spines can have passive and active properties and their function affect the linear and non-linear neuronal processing of information (Oakley et al., 2001; Spruston et al., 2013; Brunel et al., 2014; Rollenhagen and Lübke, 2016); and (5) spines are cellular specializations with varied plasticity according to each brain area and species (Toni et al., 1999; Dall'Oglio et al., 2015; Hayashi-Takagi et al., 2015; Frank et al., 2018; Bucher et al., 2020).

Implications for the Occurrence of Spiny Pyramidal Neurons

The development of cortical spiny pyramidal neurons has an evolutionary and ontogenetic value *per se* in terms of increased connectivity and integrated functions (Braak, 1980; Nieuwenhuys, 1994; Spruston, 2008; DeFelipe, 2011; Marín-Padilla, 2014; Sedmak et al., 2018; Petanjek et al., 2019). This provided a higher number of neuronal computational possibilities and increased the complexity of assembled cells in each specialized area even that they were limited by an anatomically restricted brain volume (Andersen et al., 2007; Geschwind and Rakic, 2013; Spruston et al., 2013; Marín-Padilla, 2014; Ramaswamy and Markram, 2015; Soltesz and Losonczy, 2018; Cembrowski and Spruston, 2019). Multiple spontaneous evolutionary changes would have increased numbers of neurons in the mammalian cerebral cortex and, although with differences toward primates, affected the average neuronal cell size, its dendritic and axonal arborization (Herculano-Houzel et al., 2014; Herculano-Houzel, 2019). In addition, "not only the increase in size" (i.e., number of cells), "of our brain seems to be responsible for our higher or more abstract mental abilities, but also the specialization of our cortical circuits appears to be critical" (DeFelipe, 2011).

With morphological and functional particularities, pyramidal cells are in the integrated subcortical to allocortical emergence of

the limbic lobe, i.e., from allocortical areas with a primitive to three-layers organization advancing to the neocortical external and internal layers and subdivisions (detailed below). The arrangement of neurons into layers would represent a form of development of proper networks wiring length and space (Guy and Staiger, 2017; see also Chklovskii et al., 2002; Narayanan et al., 2017). However, the cortical functions rely on circuits specified by cell type composition and not only on a strict laminar classification (Guy and Staiger, 2017). In the human prefrontal cortex, pyramidal cell bodies have a cytoarchitectonic organization with stacks of 15–19 somata with apical dendrites arranged into vertically oriented bundles, as distinct clusters at the level of the layers III/V boundary, and forming minicolumns (Gabbott, 2003; see also Buxhoeveden and Casanova, 2002; Rockland, 2010). Pyramidal neurons vary in shape according to functional afferent and efferent features of different cortical loci (Anderson et al., 2009; Scholtens et al., 2014; Gilman et al., 2017; Cembrowski and Spruston, 2019), which change along with the human lifespan (Braak, 1980; Petanjek et al., 2008; Marín-Padilla, 2014; Sedmak et al., 2018; Soltesz and Losonczy, 2018). For example, the morphological complexity of layer V pyramidal neurons progressively increases from primary sensory to primary and supplementary sensory and motor cortices until association and multimodal ones (Kolb and Whishaw, 2015; Ramaswamy and Markram, 2015; see also Jacobs et al., 2001). This also relates to the cyto-, myelo-, receptor- and synaptic architecture of the neocortical layers, as well as differs between allocortical and isocortical areas (Palomero-Gallagher and Zilles, 2017).

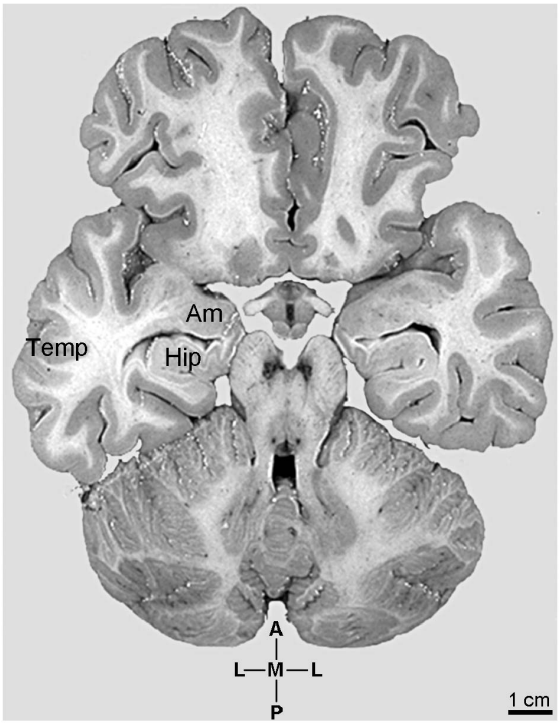

FIGURE 1 | Photographic image of the human brain sectioned transversally at the level of the hypothalamic mammillary bodies to show the anatomical aspect of the continuum involving the emergence and development of pyramidal neurons in specific amygdaloid complex (**Am**) nuclei, hippocampus (**Hip**), and neocortical parietal lobe (**Temp**). Coordinates: A, anterior; L, lateral; M, medial; P, posterior. Adapted from the original image courtesy of the "Digital Anatomist Project." Department of Biological Structure, Copyright, University of Washington, USA 1998 at http://da.si.washington.edu/cgi-bin/DA/imageform.

THE ANATOMICAL AND FUNCTIONAL *continuum* FOR THE EMERGENCE AND DEVELOPMENT OF HUMAN PYRAMIDAL NEURONS

The anatomical *continuum* involving the human pyramidal neurons in the amygdaloid complex nuclei, in CA3 and CA1 hippocampal regions, and neocortex (parietal lobe) is exemplified in **Figure 1**. The morphological complexity of human pyramidal neurons varies from their emergence in the cortical (CoA) and basomedial (BM, but not in the MeA) nuclei of the amygdaloid complex toward the CA3 and CA1 hippocampal regions and the neocortical layers II–VI, with small pyramidal neurons in the upper layers II/III and large pyramidal neurons in the deep layer V. The following images were obtained with the Golgi-impregnation method adapted for the human *postmortem* brain (Dall'Oglio et al., 2010, 2013, 2015; Vásquez et al., 2018). Afterward, we proceeded to the 3D reconstruction of pyramidal neurons aiming further visualization and detailing of the dendritic spines from proximal to distal branches (Reberger et al., 2018; Vásquez et al., 2018; Correa-Júnior et al., 2020). Methodological advantages and technical constraints were outlined in previous reports (e.g., de Ruiter, 1983; Anderson et al., 2009; Dall'Oglio et al., 2010, 2013, Morales et al., 2014; Mohan et al., 2015; Tønnesen and Nägerl, 2016; Reberger et al., 2018).

Human pyramidal-like neurons are present in areas initially considered as subcortical ones (i.e., the amygdaloid complex). These cells can represent the place for the beginning of the limbic lobe (Heimer et al., 2008), phylogenetically and ontogenetically developed to provide further functional features for the amygdaloid and hippocampal areas toward the neocortical lobes and their subdivisions, including the anterior cingulate cortex (Wyss and van Groen, 1995; Gloor, 1997). In this context of "limbic areas" development, the cingulate cortex, part of the "proisocortex" in the paralimbic cortex, is phylogenetically older than the neocortex in the evolution of the mammalian brain (Braak, 1979; Kolb and Whishaw, 2015; Pandya et al., 2015). Nevertheless, by forming part of the neural circuitry for complex social processing, the cingulate cortex is much more than a primitive stage of cortical evolution (Allman et al., 2001; see further data in Vogt, 2015). It is a cytoarchitectonic and functional specialization of the neocortex with participation in emotion, interoceptive and visceral modulation, attention, cognition, and complex perceptions as self-awareness (Allman et al., 2001; Butti et al., 2013; Cauda et al., 2014; Correa-Júnior et al., 2020 and references therein). Likewise, the lateral parietal lobe adjacent to allocortical structures

represents an evolved neocortical structure with primary, associative, and multimodal distributed functions (Nieuwenhuys et al., 1988; Miller and Vogt, 1995; DeFelipe, 2011; Pandya et al., 2015; Kolb and Whishaw, 2015).

Pyramidal-like neurons were found in the "amygdala." However, the "amygdala" is neither an anatomical nor a functional unit (Swanson and Petrovich, 1998; see also Brodal, 1981; Heimer et al., 2008; LeDoux and Schiller, 2009). The amygdaloid complex represents a heterogeneous group of telencephalic nuclei and subnuclei studied according to cytoarchitectonic, neurochemical, connectional, and functional characteristics in different species (Johnston, 1923; Rasia-Filho et al., 2000; de Olmos, 2004; Schumann and Amaral, 2005; Heimer et al., 2008; Schumann et al., 2011; Dall'Oglio et al., 2013; Akhmadeev and Kalimullina, 2015; Janak and Tye, 2015; Olucha-Bordonau et al., 2015; Vásquez et al., 2018). The amygdaloid complex of mammals is composed of pallial (most nuclei and their subdivisions) and subpallial (the MeA and central "extended amygdala," CeA) structures forming parallel circuits (Martínez-García et al., 2007). That is, the amygdaloid complex is composed of both cortical and subcortical origins (de Olmos, 2004; Medina and Abellán, 2012; Akhmadeev and Kalimullina, 2015; Olucha-Bordonau et al., 2015). Interestingly, pyramidal cells are found in brain areas that increased the processing of sensorial information from the environment and from conspecifics. The pyramidal neurons arising in such areas likely associated their cellular shape with more functional possibilities (and vice-versa). For the amygdaloid nuclei, relevant functions might have developed henceforth: (1) for perceiving and elaborating visual and auditory cues; (2) to attribute further emotional valence to these stimuli; (3) to modulate new memories and cognitive abilities; and (4) to expand the behavioral repertoire for complex social interactions between individuals, including judgments of facial expressions and emotional vocalization (Adolphs, 2003; Heimer et al., 2008; Rutishauser et al., 2015; Grisendi et al., 2019) likely contributing to parenting, empathy, happiness, fear, or disgust, for example (see relevant connectional and functional data in Diano et al., 2017). The advancement of both cellular and network processing capacities influenced the gain of species-specific features and adaptive responses. This improvement might lead the human brain networks to reach a higher level of magnitude and complexity from subcortical to cortical areas.

The Amygdaloid Complex and "Cortical-Like Structures" Advancing to the Allocortex and Neocortex

The search for the emergence of pyramidal neurons led to the interface between nuclei of the amygdaloid complex and the hippocampal formation (**Figures 1**, **2A–C**). Pyramidal neurons were also described in the subdivisions of the nucleus basalis of Meynert (based on Nissl staining and composing the cholinergic Ch4 cell group; Mesulam et al., 1983; Saper and Chelimsky, 1984; Liu et al., 2015). Three types of cerebral cortex have been studied: allocortex, periallocortex, and isocortex (Insausti et al., 2017). In rats, the pallial amygdala is considered an initial allocortical structure characterized by superficial layered cortical areas and deep non-layered parts (Olucha-Bordonau et al., 2015). This organization is recognized in the CoA by three cellular layers, i.e., an outer molecular layer (or layer 1), where terminates a direct projection from the olfactory bulbs, and two additional structurally different cellular layers (2 and 3; Olucha-Bordonau et al., 2015). Other nuclei show a cortical appearance and are associated with the olfactory tracts, as the bed nucleus of the accessory olfactory tract and the nucleus of the lateral olfactory tract (Olucha-Bordonau et al., 2015). These nuclei are interposed between the piriform and entorhinal cortices and the cortical amygdala as the rostral cortico-amygdala transition zone between the anterior cortical amygdala and the piriform cortex (Olucha-Bordonau et al., 2015). At the caudal edge of the amygdala, they compose the amygdalo-piriform transition area for the posterolateral cortical amygdala, the caudal piriform cortex, and the lateral entorhinal cortex (or, rather, an "amygdalo-entorhinal transition area"; Olucha-Bordonau et al., 2015).

Transition areas and/or specific nuclei with cellular components suggestive of a primitive cortex are found in the amygdaloid complex of primates (Amaral et al., 1992). In humans, Gloor (1997) included the prepiriform-periamygdaloid segments as part of the evolving mammalian allocortex, homologous with the ventral portion of the lateral pallium of amphibians and reptiles. The prepiriform cortex receives fibers from the lateral olfactory tract, and the periamygdaloid cortex hugs the "amygdala "(Gloor, 1997) medially to the "accessory basal nucleus" (i.e., the BM, Heimer et al., 2008; Janak and Tye, 2015; DiMarino et al., 2016) along the rostral two-thirds of its extent (Schumann and Amaral, 2005). In coronal sections of the human ventromedial area, at the level of the anterior amygdaloid region, it is possible to observe the close position of the prepiriform cortex dorsally, the rostral entorhinal cortex ventromedially, the cortico-amygdaloid transition area, and, at near caudal sections, first appearing, the lateral nucleus, BM, MeA, and CoA (Gloor, 1997). The phylogenetically ancient part of the amygdaloid complex includes both the MeA and CeA (Johnston, 1923). The MeA in the "extended amygdala" has a relatively smaller area than the other grouped nuclei in humans (de Olmos, 2004; Schumann and Amaral, 2005). The MeA occupies a superficial position and forms part of the medial border of the temporal lobe (with the CoA) in the part of the uncus represented by the gyrus semilunaris (Gloor, 1997). Both the MeA and CoA are regarded as "semicortex" in their superficial layers, and true subcortical structures in their deeper portions (Gloor, 1997 and references therein). The MeA subnuclei are involved with the (1) interpretation of environmental cues of conspecific stimuli; (2) processing of multiple sensory information, including direct and indirect olfactory and vomeronasal inputs with social relevance; (3) cellular responses to neural gonadal steroid actions for neuroendocrine secretion; and (4) modulation of reproductive and other social behaviors in rodents (Newman, 1999; Meredith and Westberry, 2004; Choi et al., 2005; Pro-Sistiaga et al., 2007; Rasia-Filho et al., 2012a,b; Petrulis et al., 2017; Petrulis, 2020). Being part of an organized neural network that projects to the bed nucleus of the stria terminalis (see relevant data on arousal behavior in

Rodriguez-Romaguera et al., 2020) and to various hypothalamic and brainstem nuclei, the CeA and MeA subnuclei also participate in social and defensive reactions against innate and learned threats with neuroendocrine, behavioral, and sympathetic/parasympathetic responses to fearful and stressful stimuli (Davis, 1992; LeDoux, 1992; Quirk et al., 1995; Dayas et al., 1999; Rasia-Filho et al., 2000, 2012b; Petrovich et al., 2001; Marcuzzo et al., 2007; Neckel et al., 2012; Petrulis, 2020; Anilkumar et al., 2021). In humans, the extended amygdala responds to the emotional salience of positive and negative affect (Liberzon et al., 2003). The MeA projects to periallocortical, paleocortex, and archicortex, as well as to the insular agranular cortex and ventromedial prefrontal cortex (Everitt, 1995; de Olmos, 2004; Anderson et al., 2009; Petrulis, 2020). These data indicate that the MeA also participates, although with varied magnitude, in parallel circuits with different parts of the evolved neocortex (de Olmos, 2004) for social and emotional processing in our species (reviewed in Petrulis, 2020).

By contrast, the components of the basolateral nuclei are the largest amygdaloid group and, together with the CoA (Stephan et al., 1987), progressed most in size along with the mammalian evolution that led to primates (Gloor, 1997). These nuclei possess more than 50% of all neurons in the human amygdaloid complex (Schumann and Amaral, 2005). The basolateral group nuclei were considered "purely subcortical in location," for none of them reach the surface of the uncus, although showing both cellular components of a "cortical-like" structure (Gloor, 1997) and development related to the allocortical piriform area (Johnston, 1923). The lateral and, afterward, the basal and the BM nuclei are the primary targets of cortical and subcortical afferent projections to the amygdaloid complex in primates (Kelly and Stefanacci, 2009; Janak and Tye, 2015). This developmental feature likely integrates the emergence of an anatomical and functional network from subcortical to allocortical connection endowed with further attributes for complex emotional, cognitive, and social behavior elaborations. For example, the lateral amygdala receives inputs from the hippocampal formation, thalamic and neocortical modality-specific sensory processing areas, integrate them, and display dynamic and plastic responses to signal danger as quickly as possible to initiate defensive behaviors without necessarily requiring additional neocortical processing (Quirk et al., 1995; Rasia-Filho et al., 2000 and references therein).

Neurons in the basolateral group of monkeys selectively change their firing rate by the perception of facial expressions and of specific parts of faces, such as the eyes (Rutishauser et al., 2015). In humans, a subset of amygdala neurons responds to information provided by individual parts of the eye and mouth region, the eyebrow, or wrinkles around the mouth, whereas another subset responds to the entire (whole) aspect of happy or fearful viewed faces (Rutishauser et al., 2011, 2013). This indicates that amygdaloid neurons receive and represent multi-modal sensory inputs for further biological significance and interpretation, relating them with the elaboration of the internal states and social interpretation evoked by faces, encoding the subjective judgment about the emotion perceived, and not only the objective features shown in the face (Wang et al., 2014; Rutishauser et al., 2015; Zheng et al., 2017). The attention associated with the response to stimulus novelty and the amygdalo-hippocampal communication during the encoding of emotional stimuli can be translated into memory and cognition (Rutishauser et al., 2015). The complexity of processing involving the human basolateral amygdala is further exemplified by its implication in late-life depressive symptom severity, associated with the dentate gyrus/hippocampal CA3 field and the lateral entorhinal cortex, during emotional episodic memory (Leal et al., 2017b).

Compared to rats, the large volume of the monkey amygdala (mainly due to the greater basolateral complex neuropil expansion than in the MeA and CeA) relates to a greater number of glial cells relative to neuron number, as well as more dendritic and axonal arborization in primates (Chareyron et al., 2011). Rats also have pyramidal neurons in specific amygdaloid nuclei, but these latter data indicate a higher capacity to process information by the primate amygdaloid cells and circuits. Furthermore, the dendritic arborization of pyramidal neurons in the CA1 hippocampal region is also higher in monkeys than in rats (Altemus et al., 2005). It is likely that the amygdaloid basolateral complex nuclei development parallels the cortical areas with which these nuclei are interconnected in primates (Chareyron et al., 2011), which includes reciprocal connections with the hippocampus (Janak and Tye, 2015), prefrontal cortex, anterior cingulate cortex (Freese and Amaral, 2009; Rutishauser et al., 2015), and primary sensory areas (Chareyron et al., 2011). That is, "the expansion of cortical areas and the greater complexity of cortical information reaching the amygdala are thus associated with a greater development of the amygdala nuclei interconnected with the neocortex" (Chareyron et al., 2011).

Accordingly, it was reasonable to hypothesize that human pyramidal neurons evolved in the amygdaloid basolateral complex and the CoA, but not in the MeA, while progressing onward to further allocortical and neocortical areas. One of the simplest histological approaches to visualize the presence of pyramidal neurons is the use of the Nissl/thionine staining (von Economo, 1927). Stained cells show a roughly triangular cell body shape, a spherical nucleus limiting the perikaryal cytoplasm, an evident nucleolus, and Nissl substance that can be present at the origin of primary dendrites, usually the apical one (Feldman, 1984; see **Figures 2D–L**). Former descriptions for the human MeA mention the presence of few "pyramidal-shaped cells" (Sims and Williams, 1990), "small neurons, some pyramidal, some fusiform or polygonal" (Gloor, 1997), and "pyramidal, multiangular, round, and spindle-shaped cells of different sizes" (de Olmos, 2004). de Olmos (2004) described "a tendency for the neurons of the medial nucleus to form layers, especially superficially, allowing the identification of a cell-poor molecular layer (L1), a superficial dense cell layer (L2), and a deep layer (L3) with somewhat less densely distributed neurons." However, it was not possible to identify pyramidal neurons in the human MeA using the Golgi technique (Dall'Oglio et al., 2013, 2015). Local cells with a triangular cell body (**Figure 2D**) are not characterized by other relevant morphological features commonly associated with pyramidal cells, such as differences in the basal and apical dendritic

thickness, length, and branching pattern (Dall'Oglio et al., 2013). Some of the primary dendrites in these spiny neurons resemble "main" processes extending in the neuropil, with long tapering shafts, and few branching points (**Figure 3**). These human MeA triangular neurons were named "angular" cells (**Figure 3**). They are one among other four Golgi-impregnated multipolar types in this nucleus (Dall'Oglio et al., 2013, 2015). Currently, it is not possible to affirm whether the human MeA neurons are "pure subcortical" or an evolutionary "older" form of (modified) pyramidal neurons that could be included as fusiform, "compass," or multipolar cells according to the classification of Braak (1980). Golgi-impregnated neurons in the rat MeA subnuclei do not resemble pyramidal-like or classic pyramidal cells as well (Marcuzzo et al., 2007; reviewed in Rasia-Filho et al., 2012a,b). Two main types of multipolar neurons were described in the rat posterodorsal MeA: "bitufted" cells with two primary dendrites (i.e., they are not "bipolar" cells with a dendrite and an axon at opposite somatic sites) and stellate ones (with three or more primary dendrites). In addition, no evidence from electrophysiological data support typical pyramidal features for these two types of neurons in the posterodorsal MeA of rats (Dalpian et al., 2019), 50–90% of the total population of rat MeA neurons is GABAergic (Mugnaini and Oertel, 1985), and most of the efferent projections from the MeA are inhibitory GABAergic ones (Swanson and Petrovich, 1998).

On the other hand, de Olmos (2004) described that "...many of the computations required to perform complex tasks are presumably initiated by the activation of neurons in the lateral nucleus" of the amygdaloid complex, which has pyramidal neurons (Sorvari et al., 1996). That is, both the human basolateral amygdaloid complex and the CoA have pyramidal-like and pyramidal neurons (**Figures 2E,F**, **4–6** and **Supplementary Figures 1–3**). Among nine other local neuronal types, Golgi-impregnated pyramidal-like cells in the human posterior CoA usually display a triangular soma, one main thick apical dendrite, and two basal dendrites of a similar thickness at their emerging points (**Figure 4** and **Supplementary Figure 1**). The main apical shaft extends to the CoA surface and ramifies close to the cell body. Basal dendrites have variable branching points and lengths, some of them extending for a considerable distance away from the soma. There is an absence or low density of pleomorphic spines in the proximal dendritic shafts. The number of spines increases along the dendritic length to a moderate density. All types of dendritic spines (i.e., stubby, wide, thin, mushroom-like, ramified, or transitional/atypical ones) are observed, some with large and complex aspects and with a spinule (**Figures 4a–d**; Vásquez et al., 2018).

Thionine and Golgi staining data are congruent on the presence of pyramidal cells in the human BM (Braak and Braak, 1983). Both pyramidal-like (**Figure 5** and **Supplementary Figure 2**) and pyramidal neurons (**Figure 6** and **Supplementary Figure 3**) can be observed in this brain area. Pyramidal-like neurons show characteristic basal dendrites and a short apical dendrite branching close to the cell body (**Figure 5**), whereas pyramidal ones have a longer apical dendrite, various thin collateral branches, and a main ramification distally (**Figure 6**). In both cases, the apical dendrite may not be directed to the pial surface (**Figures 5**, **6**). A high density of pleomorphic spines can be observed in the proximal basal dendrite and along the intermediate to distal apical dendrites in pyramidal-like neurons (**Figures 5a–d**). A moderate to a high density of spines in basal dendrites, proximal collaterals, and distal apical dendrites can occur in pyramidal neurons in the BM (**Figures 6a–d**).

The human periallocortex (i.e., the presubiculum, parasubiculum, and entorhinal cortex) has pyramidal neurons (Insausti et al., 2017). The human CA3 hippocampal region contains pyramidal-like neurons or "short cortical pyramidal neurons" whose shapes are adapted to their position in the relatively small tissue volume. These cells can have primary thick basal dendrites and a short primary apical dendrite oriented to the medial surface of the brain. The main ramification of the apical dendrite is close to the cell body (**Figure 7** and **Supplementary Figure 4**). There is a high density of small spines even in the proximal basal dendrites, and a moderate to high density of pleomorphic spines in intermediate dendritic segments of basal and apical branches, including the presence of thorny excrescences (**Figures 7a–c**; note this same kind of spine in the MeA angular neuron, **Figure 3g**; Dall'Oglio et al., 2015).

The human CA1 hippocampal region shows a variety of pyramidal shapes (**Figures 8**, **9** and **Supplementary Figures 5**, **6**; see Benavides-Piccione et al., 2020 for additional morphological data). For example, some neurons can have basal and apical dendrites with a relative short aspect (**Figures 8a–f** and **Supplementary Figure 5**). Others, located at a deep position, have exceptionally long (at the order of millimeters), straight, and highly spiny apical dendrites with few ramifications (**Figure 9** and **Supplementary Figure 6**). Basal dendrites may not be at opposite somatic poles in this kind of pyramidal neuron (**Figure 9**). In both short and long cells, the apical dendrite is oriented to the surface of the CA1 region. Basal and apical dendrites of local pyramidal neurons can be intermingled within the neuropil (Benavides-Piccione et al., 2020) and have pleomorphic spines (**Figures 8a–f**, **9a–f**). The basal dendrites of the long pyramidal neuron show intermediate to a huge density of pleomorphic spines from proximal to distal segments (**Figure 9a**). The long apical branches also have a huge density of all types of spines, some with spinule (**Figures 9b–f**).

The human neocortex sampled (i.e., the anterolateral temporal lobe) displays a short, small pyramidal neuron in the superficial layers II/III (**Figure 10** and **Supplementary Figure 7**). Basal dendrites branch sparingly and show a low to moderate density of pleomorphic spines (**Figure 10a**). The short apical dendrite has few collaterals, is oriented to the cortical surface, and displays a moderate to high density of spines (**Figure 10b**). Pyramidal neurons in the deep layer V have basal dendrites ramifying horizontally or directed to the adjacent layer VI. The apical dendrite is a long and straight main vertical shaft oriented to the superficial layers with some collateral

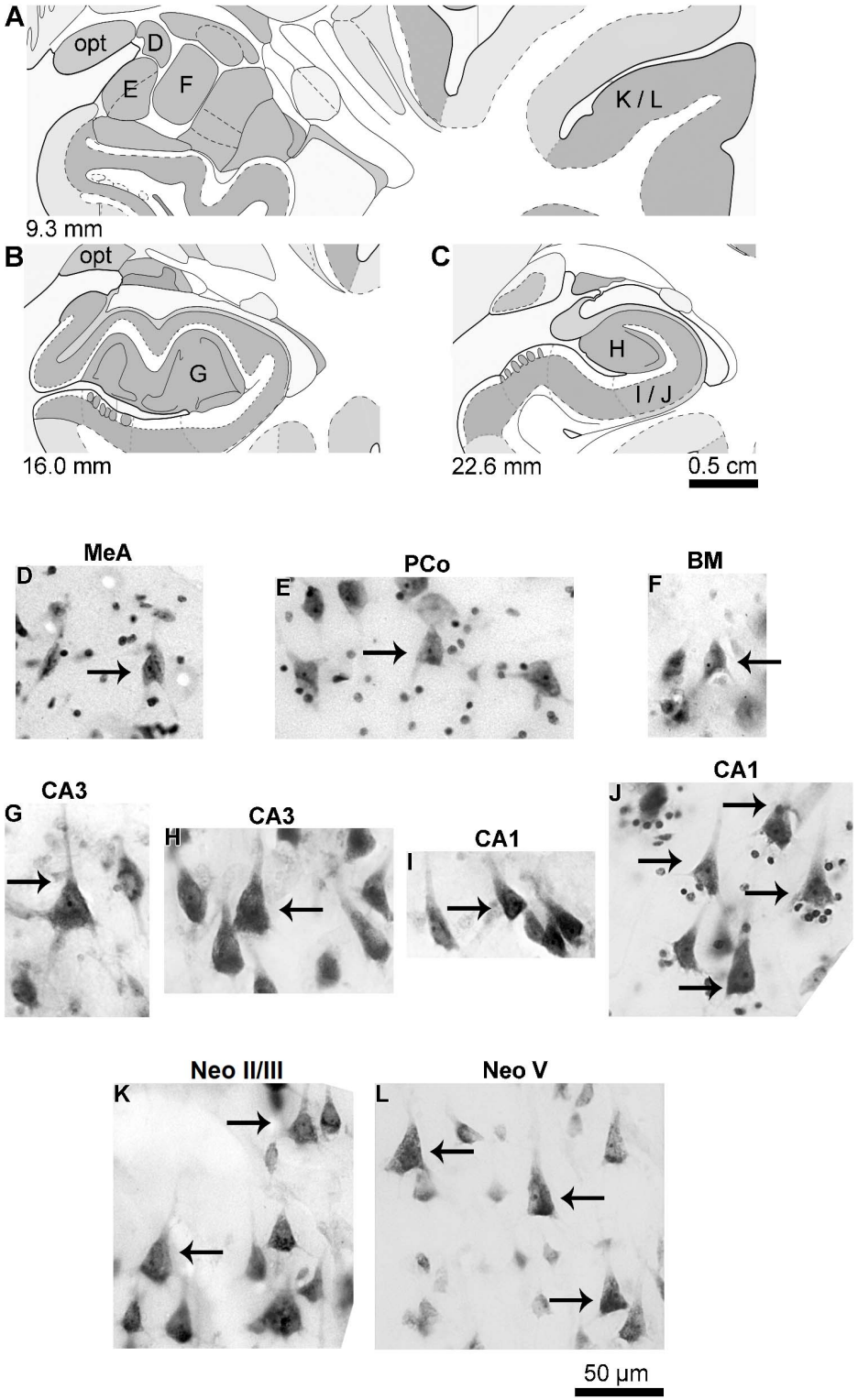

FIGURE 2 | (A–C) Schematic diagrams of coronal sections (from 9.3 to 22.6 mm posterior to the midpoint of the anterior commissure; adapted from Mai et al., 2008) showing the location of the medial (MeA, **D**), cortical (posterior part, PCo, **E**), and basomedial (BM, **F**) amygdaloid nuclei, CA3 **(G,H)** and CA1 **(I,J)** hippocampal regions, and the temporal lobe neocortex layers II/III **(K)** and V **(L)** from where pyramidal neurons were studied in the human (adult male) brain. **(D–L)** Photomicrograph of thionine-stained cells in the studied brain areas. Arrows point to pyramidal neurons, except the angular neuron indicated in the medial amygdaloid nucleus **(D)**. Note the characteristic cell body shape of pyramidal neurons surrounded by other neuron types or small glial cells. Contrast and brightness adjustments were made with Photoshop CS3 software (Adobe Systems, United States). opt, optic tract.

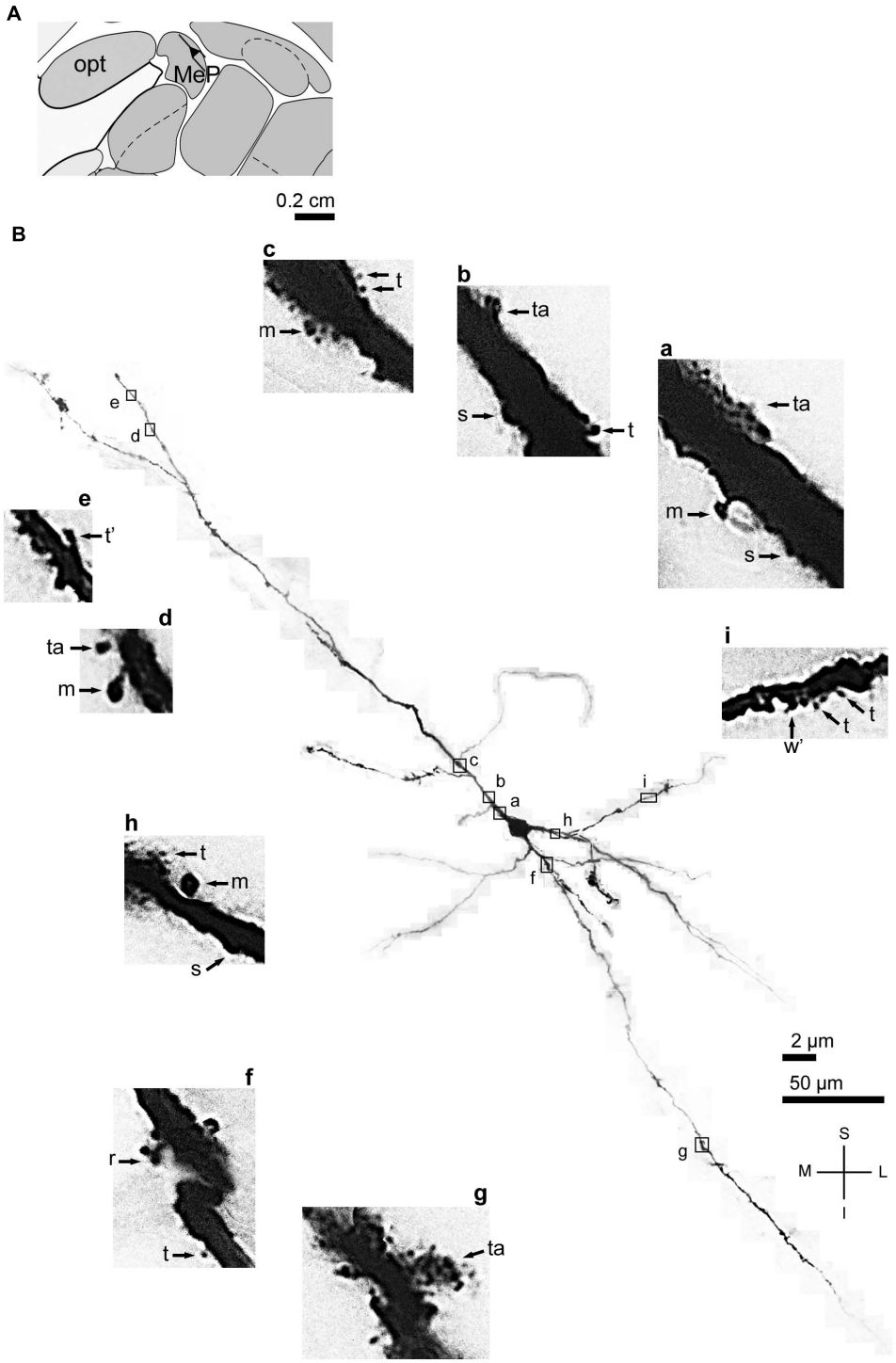

FIGURE 3 | (A) Schematic diagram of a coronal section of the human brain showing the location where a Golgi-impregnated angular spiny neuron was observed (drawn in black) in the medial amygdaloid nucleus (posterior part, MeP; 9.3 mm posterior to the midpoint of the anterior commissure; adapted from Mai et al., 2008) opt, optic tract. **(B)** Digitized and reconstructed light microscopy image of a Golgi-impregnated angular neuron from the human (adult male) MeP. This multipolar cell is not a pyramidal neuron. Note the aspect of three primary dendrites and their length and ramification. The presence, distribution, and varied shapes of dendritic spines are shown in the corresponding inserts **(a-i)** at higher magnification. Dendritic spines were classified as stubby (s), wide (w), thin (t), mushroom (m), ramified (r), and atypical (a) with thorny excrescence aspect (in **g**). t* and w* = spinule in thin and wide spines, respectively. Contrast and brightness adjustments were made with Photoshop CS3 software (Adobe Systems, United States). I, inferior; L, lateral; M, medial; S, superior. Scales = 50 µm for the general view of the neuron and 2 µm for the inserts. Reprinted with permission (license # 4905550516803) from Dall'Oglio et al. (2015); Journal of Anatomy; Copyright 2015 John Wiley & Sons. Inc.

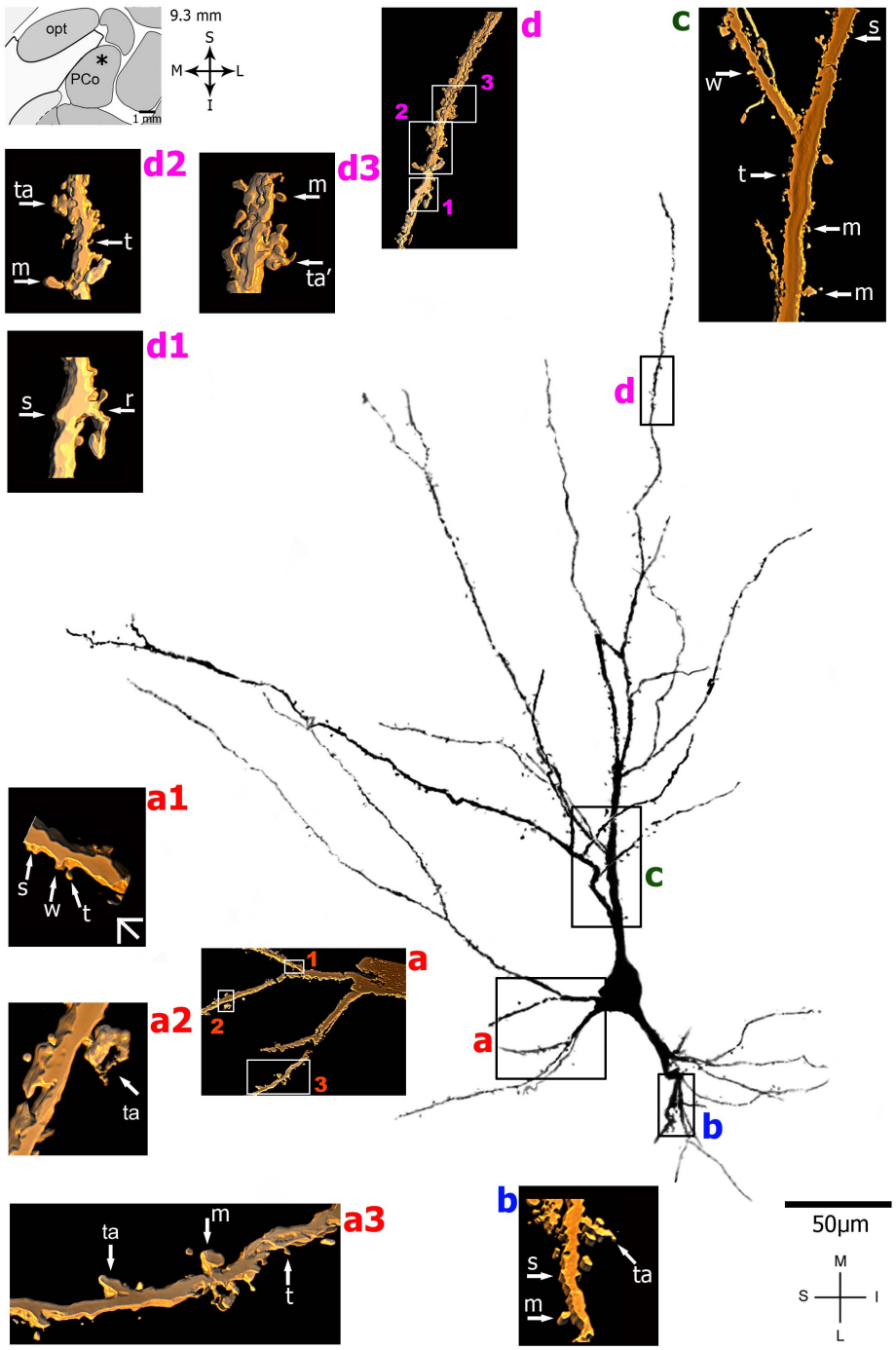

FIGURE 4 | (Left top) Schematic diagram of a coronal section of the human brain showing the location where a Golgi-impregnated pyramidal-like neuron was observed (marked with an asterisk) in the cortical amygdaloid nucleus (posterior part, PCO, 9.3 mm posterior to the midpoint of the anterior commissure; adapted from Mai et al., 2008). opt, optic tract. (**Center and laterals**) Digitized and reconstructed light microscopy image of a Golgi-impregnated pyramidal-like neuron from the human (adult male) PCO. Note the aspect of two primary basal dendrites (marked **a**,**b**) and the primary apical dendrite **(c)**. The presence, distribution, and shape of 3D-reconstructed dendritic spines are shown in the inserts at higher magnification and correspond to the locations of **(a–d)**. Numbers accompanying these letters represent sampled segments of the respective dendrite (in **a1–a3** and **d1–d3**). There is a low density of pleomorphic spines in the proximal basal (**a**) and apical **(c)** dendrites and a moderate density in distal segments (**d1-d3**). Spines were classified as stubby (s), wide (w), thin (t), mushroom-like (m), ramified (r), or transitional/atypical ones (ta). The presence of a spinule is indicated graphically by the apostrophe attached to the corresponding spine (ta' in **d3**). Contrast and brightness adjustments were made with Photoshop CS3 software (Adobe Systems, United States). I, inferior; L, lateral; M, medial; S, superior. Scale = 50 µm for the general view of the neuron and 2 µm for the inserts (the bar shown in **a1** applies to all other images of the 3D reconstructed dendritic branches and spines). This same procedure to demonstrate the 3D reconstructed dendrites and spines will be used for the next figures. Reprinted with permission (License Number 4554940100233) from Vásquez et al. (2018); The Journal of Comparative Neurology, Copyright 2018 Wiley Periodicals, Inc.

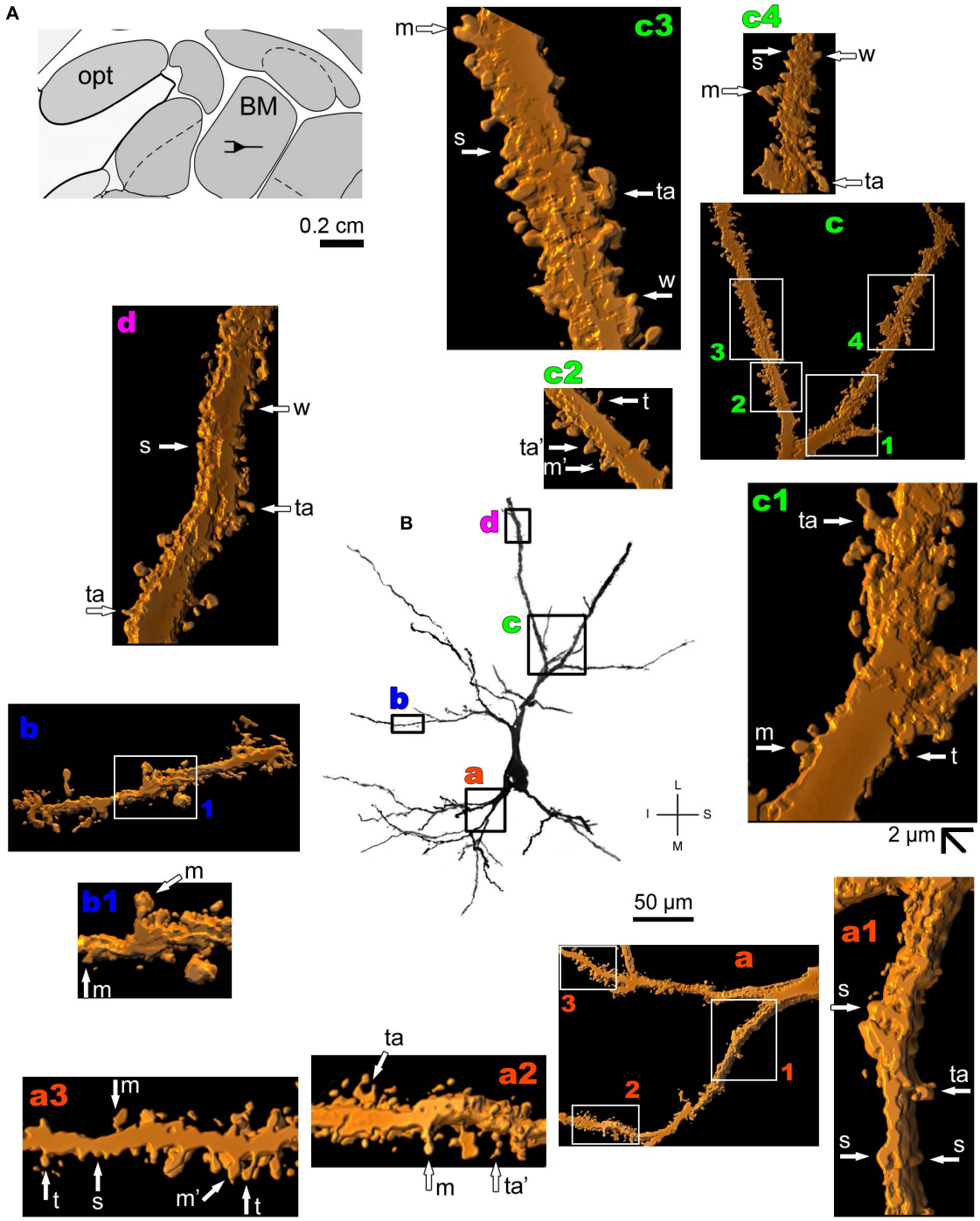

FIGURE 5 | (A) Schematic diagram of a coronal section of the human brain showing the location where a Golgi-impregnated pyramidal-like neuron was observed (drawn in black) in the basomedial amygdaloid nucleus (BM, 9.3 mm posterior to the midpoint of the anterior commissure; adapted from Mai et al., 2008). opt, optic tract. (**B** and laterals) Digitized and reconstructed light microscopy image of a Golgi-impregnated pyramidal-like neuron from the human (adult male) BM. Note the aspect of the primary basal dendrites **(a)** and the primary apical dendrite oriented transversally in the section with its main ramification close to the cell body **(b–d)**. Compare this neuron with the other from the same BM region, but with a different apical dendrite branching aspect shown in **Figure 6**. The presence, distribution, and shape of 3D-reconstructed dendritic spines are shown in the inserts at higher magnification and correspond to the locations of **(a–d)**. Numbers accompanying these letters represent sampled segments of the respective dendrite (in **a1–a3,b1,c1–c4**). There is a high density of spines in the proximal basal dendrite **(a2,a3)** and along the intermediate to distal apical dendrites **(c1–c4,d)**. Spines were classified as stubby (s), wide (w), thin (t), mushroom-like (m) or transitional/atypical ones (ta). In a2, the m spine was identified after rotating the reconstructed image. The presence of a spinule is indicated graphically by the apostrophe attached to the corresponding spine (ta' in **a2** and m' in **a3**). Contrast and brightness adjustments were made with Photoshop CS3 software (Adobe Systems, United States). I, inferior; L, lateral; M, medial; S, superior. Scale = 50 µm for the general view of the neuron and 2 µm for the inserts (the bar shown in **c1** applies to all other images of the 3D reconstructed dendritic branches and spines).

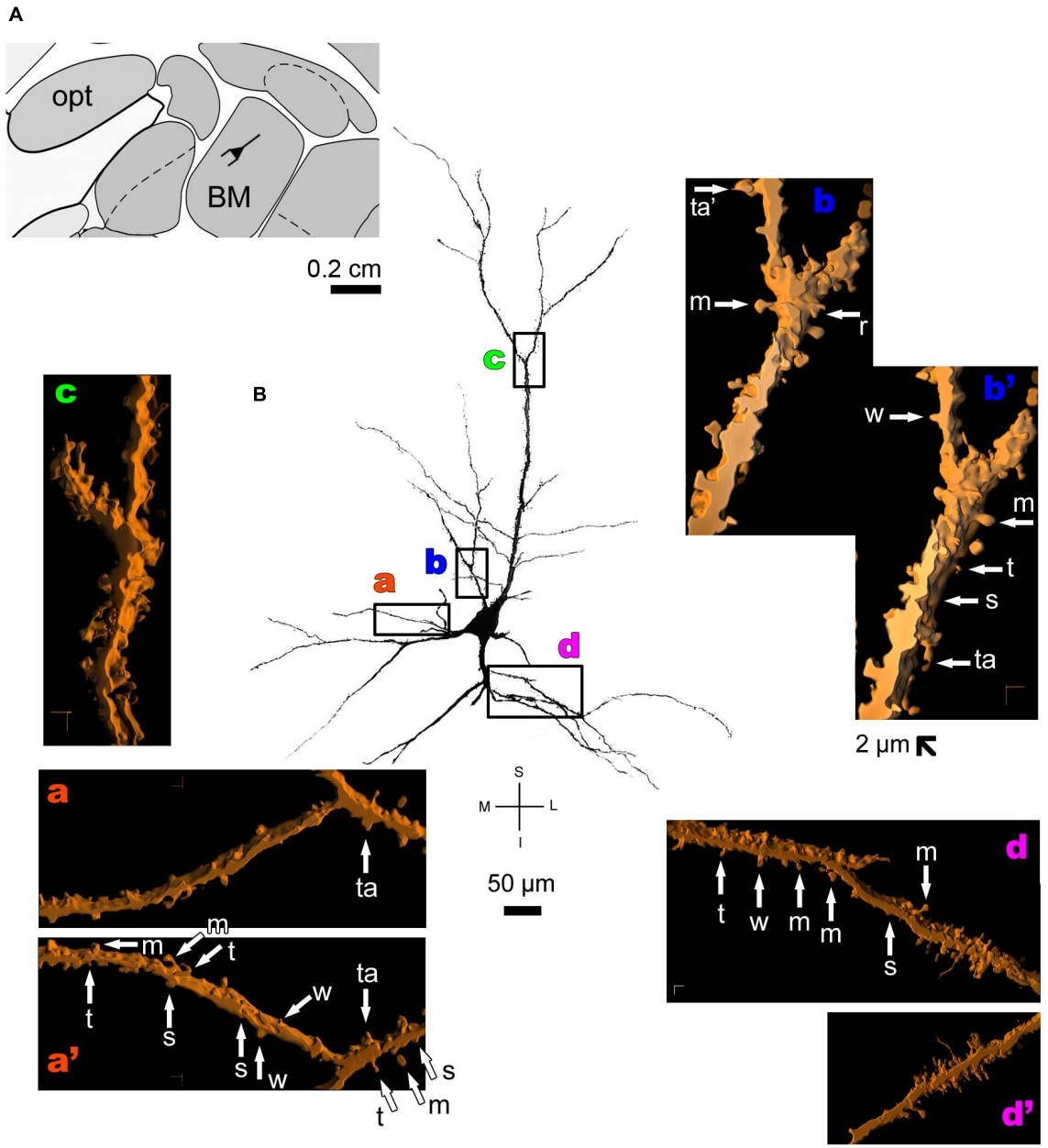

FIGURE 6 | (A) Schematic diagram of a coronal section of the human brain showing the location where a Golgi-impregnated pyramidal neuron was observed (drawn in black) in the basomedial amygdaloid nucleus (BM, 9.3 mm posterior to the midpoint of the anterior commissure; adapted from Mai et al., 2008). opt, optic tract. (**B** and laterals) Digitized and reconstructed light microscopy image of a Golgi-impregnated pyramidal neuron from the human (adult male) BM. Note the aspect of the primary basal dendrites (**a,d**), proximal small branches **(b)**, and the primary apical dendrite oriented obliquely in the section showing its main ramification more distally from the cell body **(c)**. The presence, distribution, and shape of 3D-reconstructed dendritic spines are shown in the inserts at higher magnification and correspond to the locations of **(a–d)**. The apostrophe over these letters represent an image that was rotated in space after 3D reconstruction to detail the pleomorphic dendritic spines **(a',b',d')**. There is a moderate **(a,a')** to high **(d,d')** density of spines in basal dendrites, proximal collaterals **(b,b')**, and distal apical dendrites **(c)**. Spines were classified as stubby (s), wide (w), thin (t), mushroom-like (m), ramified (r) or transitional/atypical ones (ta). The presence of a spinule is indicated graphically by the apostrophe attached to the corresponding spine (ta' in **b**). Contrast and brightness adjustments were made with Photoshop CS3 software (Adobe Systems, United States). I, inferior; L, lateral; M, medial; S, superior. Scale = 50 µm for the general view of the neuron and 2 µm for the inserts (the bar shown in **b'** applies to all other images of the 3D reconstructed dendritic branches and spines).

branches (**Figure 11** and **Supplementary Figure 8**). There is a moderate density of pleomorphic spines in the proximal segments of the basal dendrites (**Figure 11a**). Spines in the apical dendrite show a moderate to high density from proximal to intermediate segments (**Figures 11b,c**) and a moderate density distally (**Figure 11d**).

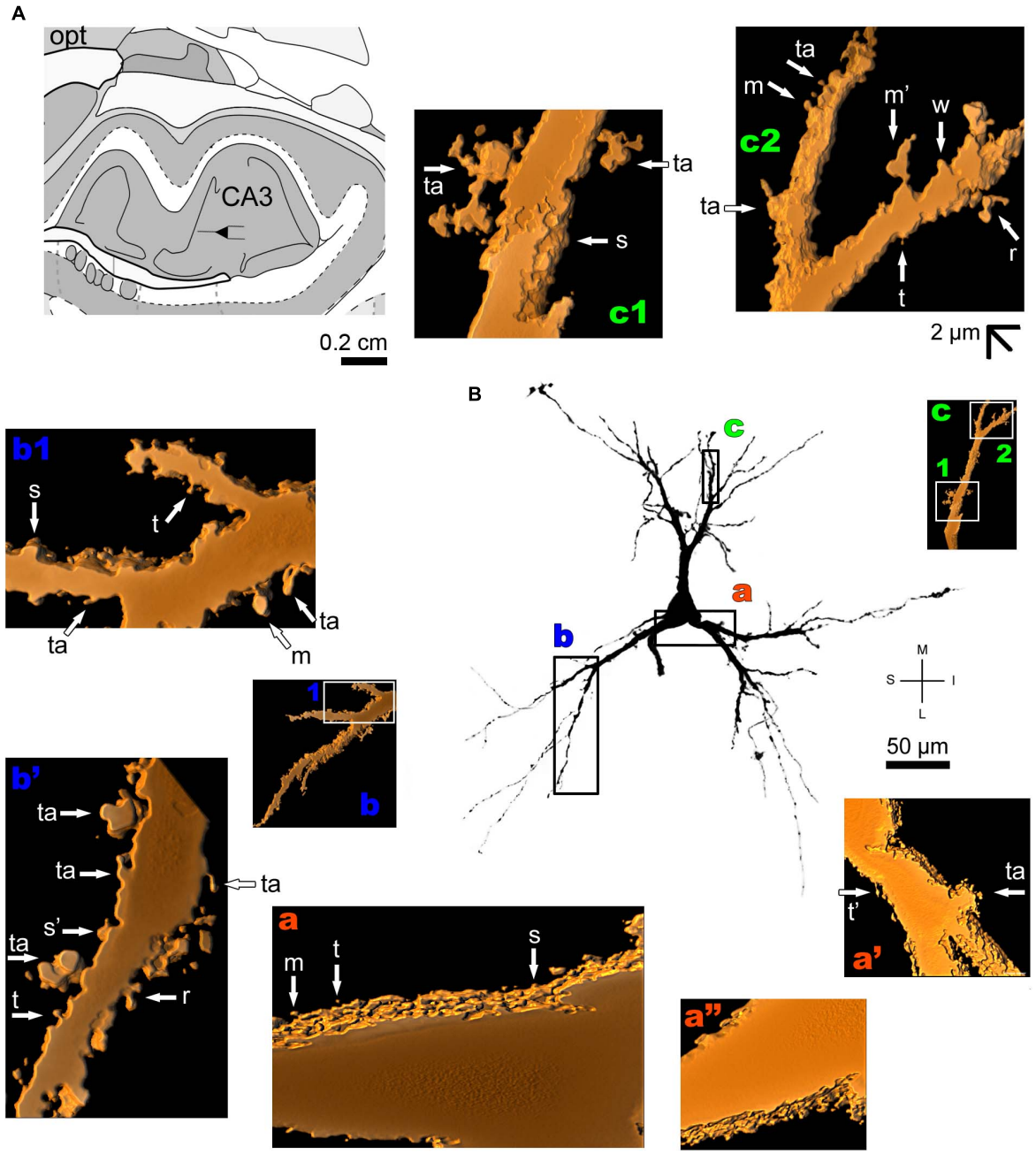

FIGURE 7 | (A) Schematic diagram of a coronal section of the human brain showing the location where a Golgi-impregnated pyramidal neuron was observed (drawn in black) in the CA3 hippocampal region (16 mm posterior to the midpoint of the anterior commissure; adapted from Mai et al., 2008). opt, optic tract. (**B** and laterals) Digitized and reconstructed light microscopy image of a Golgi-impregnated pyramidal neuron from the human (adult male) CA3 hippocampal region. Note the aspect of the primary basal dendrites **(a,b)** and the short primary apical dendrite oriented to the medial surface of the brain with its main ramification close to the cell body **(c)**. The presence, distribution, and shape of 3D-reconstructed dendritic spines are shown in the inserts at higher magnification and correspond to the locations of **(a–c)**. Numbers accompanying these letters represent sampled segments of the respective dendrite (in **b1**,**c1,c2**). The apostrophe over the letters represents an image that was rotated in space after 3D reconstruction to detail the pleomorphic dendritic spines **(a',a",b')**. There is a high density of small spines in the proximal basal dendrite **(a)** and a moderate to high density of pleomorphic spines in intermediate dendritic segments of basal **(b,b1,b')** and apical dendrites **(c1,c2)**. Spines were classified as stubby (s), wide (w), thin (t), mushroom-like (m), ramified (r) or transitional/atypical ones (ta). Note the presence of thorny excrescences in both basal (ta in **a'**,**b'**) and apical (ta in **c1**) dendrites. The presence of a spinule is indicated graphically by the apostrophe attached to the corresponding spine (t' in **a',** s' in **b'**, and m' in **c2**). Contrast and brightness adjustments were made with Photoshop CS3 software (Adobe Systems, United States). I, inferior; L, lateral; M, medial; S, superior. Scale = 50 µm for the general view of the neuron and 2 µm for the inserts (the bar shown in **c2** applies to all other images of the 3D reconstructed dendritic branches and spines).

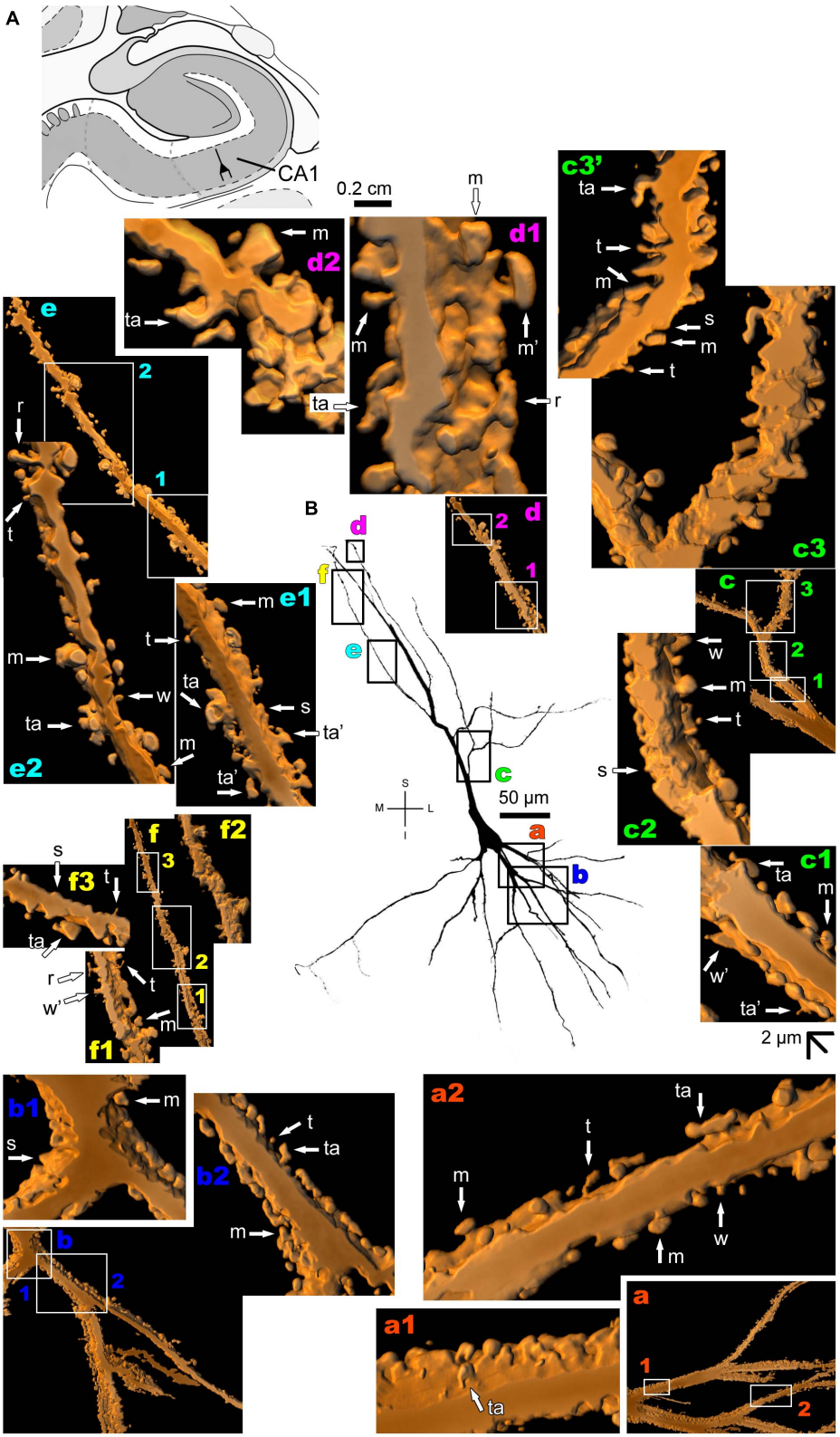

FIGURE 8 | (A) Schematic diagram of a coronal section of the human brain showing the location where a Golgi-impregnated pyramidal neuron was observed (drawn in black) in the CA1 hippocampal region (22.6 posterior to the midpoint of the anterior commissure; adapted from Mai et al., 2008). opt, optic tract. (**B** and laterals) Digitized and reconstructed light microscopy image of a Golgi-impregnated pyramidal neuron from the human (adult male) CA1 hippocampal region. Note the aspect

(Continued)

FIGURE 8 | Continued
and length of the primary basal dendrites **(a,b)** and the main apical dendrite, oriented to the surface of the brain, tapering after collateral ramifications **(c–f)**. Compare this neuron with the next one from the same CA1 region with an apical dendrite that, after bifurcating, have long straight shafts with few collaterals as shown in **Figure 9**. The presence, distribution, and shape of 3D-reconstructed dendritic spines are shown in the inserts at higher magnification and correspond to the locations of **(a–f)**. Numbers accompanying these letters represent sampled segments of the respective dendrite (in **a1**,**a2**,**b1**,**b2**,**c1–c3,d1,d2,e1,e2,f1–f3**). The apostrophe over the letters represents an image that was rotated in space after 3D reconstruction to detail the pleomorphic dendritic spines **(c3')**. There is an intermediate to high density of pleomorphic spines in the proximal segments of the basal **(a,b)** and apical **(c)** dendrites that continues toward distal segments in this latter **(d–f)**. Spines were classified as stubby (s), wide (w), thin (t), mushroom-like (m), ramified (r) or transitional/atypical ones (ta). Note the occurrence of different dendritic spines along the same segments, some relatively isolated (e.g., in **a2**,**e2**) and others in clusters (e.g., **b2**,**c3**,**d1**,**d2**). The presence of a spinule is indicated graphically by the apostrophe attached to the corresponding spine (w' and ta' in **c1,** s' in **b1**, m' in **d1**, ta' in **e1**, and w' in **f1**). Contrast and brightness adjustments were made with Photoshop CS3 software (Adobe Systems, United States). I, inferior; L, lateral; M, medial; S, superior. Scale = 50 μm for the general view of the neuron and 2 μm for the inserts (the bar shown in **(c1)** applies to all other images of the 3D reconstructed dendritic branches and spines).

VULNERABILITY OF HUMAN PYRAMIDAL NEURONS

Although not reductionist, the development of further neural abilities and conscious emotional processing by neural circuits enabled emergent properties with integrated neurophysiological, physicochemical, and mathematical/statistical possibilities. Our evolved nervous tissue organization provided complex motor and social abilities (for speaking, manipulating fire, agricultural techniques, domestication of animals, etc.); language and knowledge transmission between generations (mathematics, medicine, navigation, etc.); abstract thinking, creativity, and artistic expressions (philosophy, painting, creating and playing musical instruments, etc.); technology advancement and various other implications for the human behavior (e.g., see Bunge, 1980; Searle, 1997; Elston, 2003; Persinger and Koren, 2007; DeFelipe, 2011; Geschwind and Rakic, 2013; Marín-Padilla, 2014; Aru et al., 2019; Herculano-Houzel, 2019). The specialized neurons and circuits that provided these higher abilities also show vulnerabilities and are related to complex disorders with variable clinical manifestations in humans (see a parallel discussion and examples in Clowry et al., 2010; Butti et al., 2013; Geschwind and Rakic, 2013; Cauda et al., 2014; Hodge et al., 2019; Correa-Júnior et al., 2020). This implicates the amygdalo-neocortical *continuum* in a broad range of neurological and psychiatric conditions affecting memory, cognition, and mood dysfunction (Carlo et al., 2010; Schumann et al., 2011), as well as in language and social awareness disorders (Yudofsky and Hales, 2004; Geschwind and Rakic, 2013; also see Herculano-Houzel, 2019).

As highlighted by Heimer et al. (2008) for the Vogt's theory of "Pathoklise und Pathoarchitektonik," "certain physiochemical properties of nerve cells that share common morphological characteristics, and often constitute cytoarchitectonically definable areas, confer upon them specific susceptibilities to a variety of pathogenic agents" (Vogt and Vogt, 1922; Gloor, 1997). For example, cortical parts of the greater limbic lobe are "disproportionally targeted by neurofibrillary tangles in Alzheimer's disease, and there is good evidence that this degenerative disease begins in selective non-isocortical parts" within it. "We favor the inclusion of the laterobasal-cortical complex of the amygdala in the limbic lobe. Parts of it are cortex, and the various laterobasal nuclei contain cortical-like neurons aggregated into nuclei segregated by the intrinsic white matter of the amygdala. Moreover, chemoarchitectonic characteristics and connectional patterns. support this viewpoint. The inclusion of the laterobasal amygdaloid complex in the limbic lobe is supported by developmental investigations. . ., which indicate that the laterobasal-cortical amygdala develops in association with the nearby populations of neuronal precursors that ultimately form the cortical mantle. By exclusion, the remaining amygdala, the centromedial complex, belongs to the extended amygdala" (Heimer et al., 2008 and references therein). The current morphological data on the occurrence of pyramidal-like and pyramidal neurons shown here are in line with this former proposition.

Alzheimer's Disease

The amygdaloid nuclei (as well as the allocortical and neocortical areas) that are sites of the emergence and development of pyramidal neurons are also coincident with the neuropathological findings of AD (Morrison et al., 1987; Heun et al., 1997; Merino-Serrais et al., 2011). This is the case for the particularly vulnerable and most severely affected lateral amygdaloid nucleus (de Olmos, 2004), CoA, periamygdaloid cortex (Schmidt et al., 1996), specific pyramidal layers of the parahippocampal region and hippocampus, and functionally organized hierarchical areas of the neocortex (Morrison et al., 1987). Subpopulations of pyramidal neurons with specific anatomical and molecular profiles may show a differential vulnerability in AD (Morrison et al., 1987; Hof and Morrison, 1990; Hof et al., 1990). These neurons display in common high intracellular levels of non-phosphorylated neurofilament protein and a long axonal projection that terminates within the neocortex, hippocampus, or related telencephalic structures (including cells from the locus coeruleus and the nucleus basalis of Meynert; Morrison et al., 1987).

In the context of cellular vulnerability (Morrison et al., 1987; Hof et al., 1990; Braak and Braak, 1991), pyramidal neurons show atrophy of basal and apical dendrites and reduction in the number of dendritic spines with the AD progression (Penzes et al., 2011; Overk and Masliah, 2014). There is a notable atrophy of the amygdaloid nuclei and hippocampus, but also in the nucleus accumbens, putamen, and thalamus (Benzinger et al., 2013), an issue open to debate on secondary atrophy due to reduced connectivity. Neurodegeneration advancing in the limbic lobe harms the dendrites and spines of pyramidal neurons in the subiculum, the CA1 hippocampal region, and the entorhinal cortex in the mesial temporal lobe, further progressing

to involve the nucleus basalis of Meynert and associative areas in the frontal, parietal, and temporal lobes (Hyman et al., 1984; Saper and Chelimsky, 1984; Braak and Braak, 1991; Ishunina and Swaab, 2001; Thompson et al., 2001; Peçanha and Neri, 2007; Serrano-Pozo et al., 2011; Liu et al., 2015). Pyramidal neurons in layers III to VI are severely affected in different parts of the neocortex (Hof and Morrison, 1990; Hof et al., 1990; Arnold et al., 1991; Braak and Braak, 1991). There is also a selective loss of the giant cells of Meynert in the superficial part of layer VI in the human visual cortex (Hof and Morrison, 1990). On the other hand, the corticospinal-projecting Betz cells in motor cortex are not involved in the AD pathology (Morrison et al., 1987).

Brain tissue atrophy along with synaptic dysfunction or loss is linked with symptomatic memory and cognitive decline in AD (Heun et al., 1997; Yudofsky and Hales, 2004; Serrano-Pozo et al., 2011; Dorostkar et al., 2015). However, current experimental, imaging, and biomarkers data provided other important pieces to this scenario of progressive cortical damage. Although not all regions have hypometabolism and atrophy at the same time (Benzinger et al., 2013), it is important to consider that cortical brain circuits can be morphologically and functionally impaired even in the early stages of AD (Huijbers et al., 2015; Palmqvist et al., 2017; Leal et al., 2018). The β-amyloid peptide (Aβ)-related neuroinflammation involves microglial dysfunction and a feedforward harmful cycle in mice (Friker et al., 2020). The accumulation of Aβ begins slowly, years before biomarkers become abnormal (Leal et al., 2018). Nearly every cortical region, with relative initial sparing of entorhinal, precentral, and postcentral cortices, show Aβ deposition 15 years before the expected onset of the symptomatic phase in individuals with autosomal dominant AD (Benzinger et al., 2013). Reduced cortical glucose metabolism and cortical thinning occur 10 and 5 years before the onset of symptoms in the precuneus/posterior cingulate/lateral parietal cortex and in the middle temporal gyrus/lateral prefrontal cortex, respectively (Benzinger et al., 2013). Afterward, atrophy becomes evident in the precuneus, entorhinal, lateral temporal, and lateral parietal cortices, whereas the anterior cingulate cortex increases its thickness (Benzinger et al., 2013).

It is worth noting that Aβ fibrils start to accumulate preferentially in the precuneus, medial orbitofrontal cortex, and posterior cingulate cortex of subjects at preclinical AD stage (Palmqvist et al., 2017). About half of the patients with a mild cognitive impairment show high levels of cortical Aβ deposition, which is more than the percentage of $A\beta^+$ clinically normal older adults (Huijbers et al., 2015). Aβ accumulating APP/PS1 transgenic mice show altered dendritic spines in the hippocampal CA1 *stratum oriens* and *stratum radiatum* with layer-specific decrease in spine neck length and increase of spines with a small head volume (Merino-Serrais et al., 2011). In humans, the initial Aβ accumulation can harm synaptic transmission and is associated with hypoconnectivity between the areas of the "default mode network" and the frontoparietal network (Palmqvist et al., 2017). Autosomal dominant AD mutation carriers also show an inverse correlation between regional and global amyloid deposition and cerebral blood flow as they approached the age of dementia diagnosis (Yan et al., 2018). Amyloid may exacerbate cognitive and vascular dysfunction by a tau-mediated pathway (Albrecht et al., 2020). $A\beta^+$ patients continue toward AD dementia showing high levels of hippocampal activity, increased rates of hippocampal atrophy, and progressive decline in global cognition (Huijbers et al., 2015). That is, the increased hippocampal activity is associated with the levels of Aβ deposition, follows an initial aberrant activity (decreased deactivation) in the default network, and might reflect compensatory neuronal activity striving against memory impairment and/or local excitotoxicity caused by the accumulation of soluble Aβ (Huijbers et al., 2015). The greater hippocampal activation can be detrimental, associated with further Aβ deposition, and cognitive decline (Leal et al., 2017a). Patients with AD can also have subclinical epileptiform activity, indicative of sustained neuronal and network hyperexcitability, while they are at risk for accelerated deleterious effects on cognition (Vossel et al., 2016). Thus, the progression of AD demands the earliest possible detection and treatment of pathological changes before cognitive impairments begin to occur in vulnerable cortical areas (Leal et al., 2018; see additionally Leng et al., 2021).

Temporal Lobe Epilepsy

Temporal lobe epilepsy (TLE) is one of the most common form of focal epilepsy refractory to antiepileptic drugs (Semah et al., 1998; Wiebe, 2000; Kumlien et al., 2002; Téllez-Zenteno and Hernández-Ronquillo, 2012). Seizure-generation and propagation involve the network architecture of limbic structures and neocortical brain regions for the hypersynchrony and hyperexcitability activity, with the midline thalamus serving as a synchronizer (Bertram et al., 1998; Bertram, 2009; Vismer et al., 2015; Wicker and Forcelli, 2016; see additional brain areas in Arakaki et al., 2016; Soper et al., 2016; Wicker et al., 2019). The threshold for kindling to induce limbic seizures in animal models of TLE is significantly lower in structures with pyramidal neurons, such as the amygdaloid complex, hippocampus, entorhinal cortex, piriform cortex (and endopiriform nucleus), olfactory cortex, and interconnected neocortical parts (Gloor, 1997; Vismer et al., 2015; Insausti et al., 2017) when compared to the kindling of other areas, such as the thalamic midline nuclei. Local and remote assemblage of neurons and their microcircuits play an important role in seizure initiation and spreading (Du et al., 1993; Hudson et al., 1993; Natsume et al., 2003; Bertram, 2009; Vismer et al., 2015; Wicker and Forcelli, 2016). For example, the ventrorostral aspect of the piriform cortex encompasses a chemoconvulsant trigger zone particularly named as "*area tempestas*" (reviewed in Vismer et al., 2015).

The amygdaloid complex, the hippocampal formation, and other associated limbic structures are important sites for seizures generation in TLE (Bertram et al., 1998; Mangan et al., 2000; Vismer et al., 2015; Wicker and Forcelli, 2016). In some of them, seizure onset is easier to detect than in others (Bertram et al., 1998; Bertram, 2009). In the hippocampus, which is a laminated cortical structure, the orientation of the pyramidal cell layer generates powerful electrical fields that can be detected by volume conduction at some distance. In addition, the pyramidal neurons in the hippocampus are the

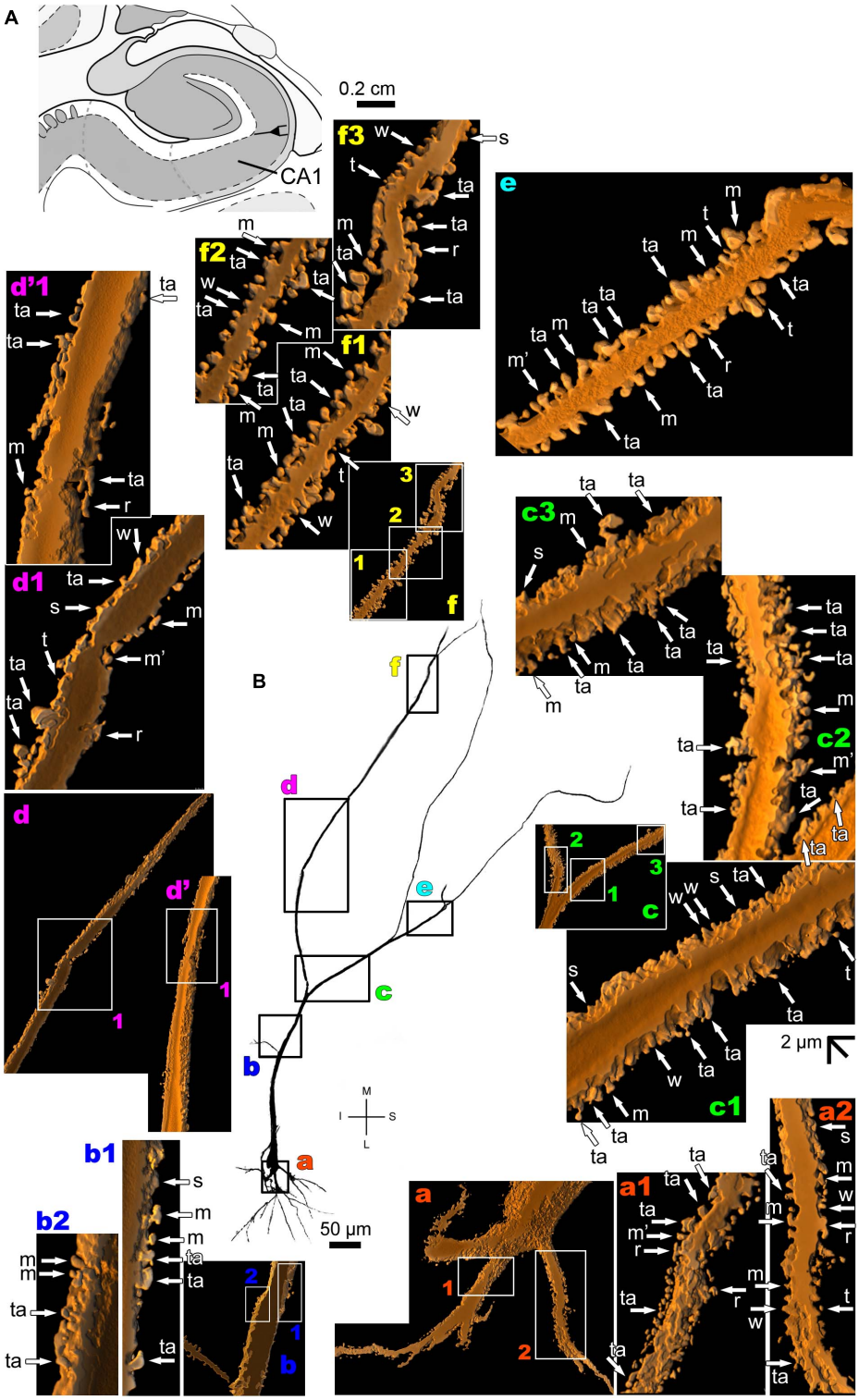

FIGURE 9 | (A) Schematic diagram of a coronal section of the human brain showing the location where a Golgi-impregnated pyramidal neuron was observed (drawn in black) in the CA1 hippocampal region (22.6 posterior to the midpoint of the anterior commissure; adapted from Mai et al., 2008). opt, optic tract. (**B** and laterals) Digitized and reconstructed light microscopy image of a Golgi-impregnated large pyramidal neuron from the human (adult male) CA1 hippocampal region. Note the aspect and length of the primary basal dendrites **(a)** and the main apical dendrite oriented to the surface of the brain, which ramifies sparingly and have long straight shafts **(c–f)**. The presence, distribution, and shape of 3D-reconstructed dendritic spines are shown in the inserts at higher magnification and correspond to the locations of **(a–f)**. Numbers accompanying these letters represent sampled segments of the respective dendrite (in **a1**,**a2**,**b1**,**b2**,**c1–c3**,**d1**,**f1–f3**). The apostrophe

(Continued)

FIGURE 9 | Continued
over the letters represents an image that was rotated in space after 3D reconstruction to detail the pleomorphic dendritic spines **(d',d'1)**. Note the high density of pleomorphic spines in the proximal segments of the basal dendrites **(a1,a2)**, the moderate to high density in spine density in the proximal segments of the apical dendrite **(b1,b2)**, the abundance of types and remarkably high density in intermediate apical segments **(c1–c3)**. Toward the distal parts of the apical dendritic branches, spines show an intermediate (**d1**,**d'1,e**) to an extremely high density of spines close to final shafts **(f1–f3)**. Dendritic spines were classified as stubby (s), wide (w), thin (t), mushroom-like (m), ramified (r) or transitional/atypical ones (ta). Dendritic spines of different shapes occur along the same segments (e.g., **a1**,**c1–c3**,**e**). The presence of a spinule is indicated graphically by the apostrophe attached to the corresponding spine (m' in **a1,d1,e**). Contrast and brightness adjustments were made with Photoshop CS3 software (Adobe Systems, United States). I, inferior; L, lateral; M, medial; S, superior. Scale = 50 μm for the general view of the neuron and 2 μm for the inserts (the bar shown in **(c1)** applies to all other images of the 3D reconstructed dendritic branches and spines).

main mediators of excitatory transmission (Andersen et al., 2007). They receive excitatory inputs and, in turn, make equally powerful excitatory glutamatergic synapses with their target neurons in and outside of the hippocampal formation (Gloor, 1997). The amygdaloid complex is an important site of seizure onset in TLE (Gloor, 1997). Although some amygdaloid nuclei have pyramidal neurons and are another important site of seizure onset in TLE (Gloor, 1997), these amygdaloid cells appear to be not organized in polarized layers as the hippocampus or neocortex, and the electrical field created by these neurons' discharges generate just a small volume conduction outside the structure itself. Nevertheless, specific involvement of amygdala on seizure onset in humans was first observed by Feindel and Penfield (1954) during stimulation of periamygdaloid region in an awake, locally anesthetized patient during a surgery to treat refractory epilepsy. Basolateral amygdala hyperexcitability has also been demonstrated in the chronic kainic acid model in rats (Smith and Dudek, 1997). *In vitro* studies showed that multiple limbic sites (including the basolateral amygdala) have epileptiform discharges associated with prolonged depolarizations and multiple superimposed action potentials (Bertram et al., 1998; Fountain et al., 1998; Bertram, 2009). It remains to be settled whether pyramidal neurons in the human amygdaloid complex have the same electrophysiological properties as other allocortical and neocortical regions and/or behave correspondingly during TLE.

Additional studies with experimental models of TLE and in patients with refractory TLE demonstrated the important participation of the hippocampus on both seizure onset (Yaari and Beck, 2009 and references therein) and maintenance of seizure activity (Alonso-Nanclares et al., 2011) with pronounced changes in intrinsic properties of CA1 pyramidal cells (Jensen and Yaari, 1997; Sanabria et al., 2001; Beck and Yaari, 2008; Chen S. et al., 2011). In hippocampal slices from patients with refractory TLE, the activity of subicular pyramidal cells is associated with epileptiform activity generation (Wozny et al., 2005; Wittner et al., 2009). Most CA2 pyramidal cells can fire spontaneously, depolarize during interictal-like events, and generate independent epileptiform activity (Wittner et al., 2009). Altered expression or modulation of ion channels, can result in abnormal membrane depolarization, such as an up-regulation of T-type Ca^{++} current in dendrites and down-regulation of dendritic I_A that affect the magnitude of the corresponding currents and change the neuronal firing pattern from regular to burst mode (Yaari et al., 2007; Remy et al., 2010). This firing behavior like in the neocortical intrinsically bursting pyramidal cells, under the effect of GABAergic antagonists and threshold stimulation of afferent fibers, can evoke long-latency epileptiform bursts (Tasker et al., 1992). Changes in dendritic ion channels of CA1 pyramidal cells also affect the dynamic of excitatory postsynaptic responses (EPSPs) generated at dendritic sites and the backpropagation of action potentials into the dendritic tree. These dendritic ion channels can be activated by subthreshold EPSPs for spike initiation (Yaari and Beck, 2009 and references therein). The number of axon collaterals of CA1 pyramidal cells also increases in pilocarpine treated rats and in patients with TLE, which indicates that a network reorganization in CA1 contributes to local hyperexcitability via increased backward excitation (Lehmann et al., 2000). The burst discharges of intrinsically bursting CA1 pyramidal neurons can recruit additional neurons via recurrent excitatory connections, contributing to the generation of epileptic discharges (reviewed in Yaari and Beck, 2009). Aberrant synaptic reorganization is evident in the glutamatergic, zinc-containing mossy fibers of granular cell of dentate gyrus and CA3 pyramidal cells as well (Sutula et al., 1988).

Besides the recurrent excitation, selective degeneration of highly vulnerable hippocampal CA1 and CA3 pyramidal neurons is a common structural change related to epilepsy and other neurological disorder as AD and stroke (Medvedeva et al., 2017). Several lines of evidence suggest that glutamate is the neurotransmitter involved in this hippocampal neurodegeneration (reviewed in Lewerenz and Maher, 2015). High levels of glutamate are toxic to select groups of pyramidal cells and, when in subtoxic levels, reduce pyramidal neuron dendrites (Mattson et al., 1989). All zinc-containing neurons are glutamatergic but not all glutamatergic neurons contain zinc (Frederickson et al., 1990). Several glutamatergic releasing pyramidal cells can corelease zinc as those in the CA3 and CA1 regions, prosubicular, piriform cortex, and neocortical layers II-IV and VI (Frederickson et al., 2000; Takeda et al., 2006). With a few exceptions, zinc-containing neurons are located only in the telencephalon forming a vast associational network that reciprocally interconnects limbic, allocortical, and isocortical structures (Frederickson and Moncrieff, 1994, reviewed in Frederickson et al., 2000). Zinc ions are potent modulators of glutamate receptors, especially the NMDA-mediated calcium influx, since the co-release of zinc along with glutamate provides a modulatory mechanism for postsynaptic excitability (Frederickson and Moncrieff, 1994; Calderone et al., 2004; Medvedeva et al., 2017). It is assumed that vesicular zinc at glutamatergic

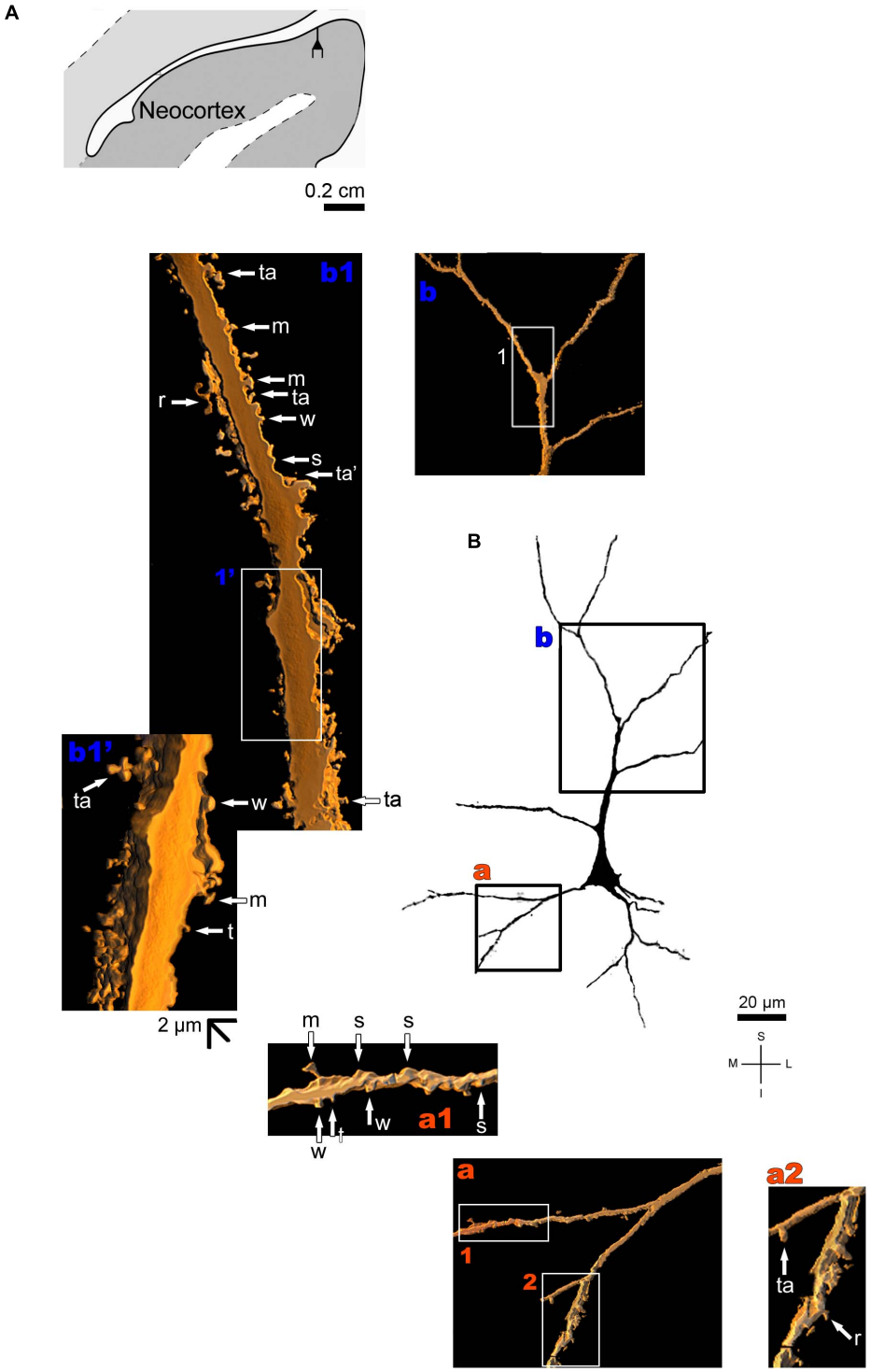

FIGURE 10 | (A) Schematic diagram of a coronal section of the human brain showing the location where a Golgi-impregnated pyramidal neuron was observed (drawn in black) in the layer II/III of the anterolateral temporal lobe (Neocortex, 9.3 mm posterior to the midpoint of the anterior commissure; adapted from Mai et al., 2008). opt, optic tract. (**B** and laterals) Digitized and reconstructed light microscopy image of a Golgi-impregnated small pyramidal neuron from the external layers II/III of the human (adult male) anterolateral temporal neocortex. Compare the length and branching pattern of this neuron in the external pyramidal layer with the one in the internal pyramidal layer V shown in **Figure 11**. Note the aspect and branching pattern of the primary basal dendrites **(a)** and the apical dendrite oriented to the cortical surface **(b)**. The presence, distribution, and shape of 3D-reconstructed dendritic spines are shown in the inserts at higher magnification and correspond to the locations of **(a,b)**. Numbers accompanying these letters represent sampled segments of the respective dendrite (in **a1,a2**,**b1).** The apostrophe over these letters

(Continued)

FIGURE 10 | Continued
represent an image that was rotated in space after 3D reconstruction to detail the pleomorphic dendritic spines **(b1')**. There is a low to moderate density of spines in basal dendrites **(a1,a2)** and a moderate to high density of spines in the apical dendrite **(b1,b1')**. Spines were classified as stubby (s), wide (w), thin (t), mushroom-like (m), ramified (r) or transitional/atypical ones (ta). The presence of a spinule is indicated graphically by the apostrophe attached to the corresponding spine (ta' in **b1**). Contrast and brightness adjustments were made with Photoshop CS3 software (Adobe Systems, United States). I, inferior; L, lateral; M, medial; S, superior. Scale = 20 μm for the general view of the neuron (compare to the other figures) and 2 μm for the inserts (the bar shown in **(b1')** applies to all other images of the 3D reconstructed dendritic branches and spines).

cells (mainly pyramidal-like and pyramidal cells) in the amygdaloid complex, hippocampus, and the perirhinal region is involved in the generation of synaptic plasticity related to neurodevelopment and learning or seizures in TLE (Frederickson and Moncrieff, 1994). Interestingly, the major glutamatergic fibers within the brain stem, thalamus, and cerebellum do not involve pyramidal cells and lack vesicular zinc (Frederickson and Moncrieff, 1994). Although not all pyramidal cells are zinc-containing neurons, the presence of this cell type in an environment with a potent modulation of glutamate receptors, calcium influx, and chances for hyperexcitability would contribute to epileptogenesis in TLE. Moreover, the synchronous firing of thousands of neurons repetitively for many seconds or more during a seizure, with intense release of glutamate and zinc, can induce marked postsynaptic calcium influx and synaptic remodeling. Indeed, patients with refractory TLE and comparable animal models of focal epilepsy have consistently reported a marked decrease in dendritic spine density on hippocampal and neocortical pyramidal cells (Swann et al., 2000). The loss of branches and the occurrence of varicose swellings on the remaining dendrites may alter local electrical signaling and contribute to epileptogenesis and clinical manifestations (Jiang et al., 1998).

Pyramidal cells are crucial but not the only neurons participating in seizure activity. GABAergic interneurons have been implicated in different aspects of seizure formation, contributing to the transition to ictal events through rebound excitation (Chang et al., 2018) and increasing the seizures/ictal activity duration (Khoshkhoo et al., 2017; Cela and Sjöström, 2019). GABAergic inhibition controls excitatory feedback (Naumann and Sprekeler, 2020). That is, the enhanced inhibition of inhibitory interneurons may result in the disinhibition of pyramidal cells with a consequent abnormal increased synchrony in the output of the hippocampus (Wittner et al., 2002). Interestingly, excitatory synapses between pyramidal neurons to subsets of interneuron types in hippocampus and neocortex expressed calcium-permeable AMPA-type glutamate receptors modulating the synaptic dynamics in local circuits (Lalanne et al., 2018). On the other hand, an increased perisomatic inhibition onto CA1 pyramidal cells can contribute to the generation and maintenance of abnormal synchrony in this region during hyperexcitability, interictal spikes, and epileptic seizures in humans with TLE (Wittner et al., 2005; Wittner and Maglóczky, 2017). GABAergic interneurons can also have an excitatory effect, by depolarizing the cells, and building a 'positive feedback circuit' together with glutamatergic pyramidal cells (Khazipov, 2016). In conjunction, these circuits' rearrangements can lead to neuronal synchronization and hyperexcitability in cortical areas (Fujiwara-Tsukamoto et al., 2004).

INTEGRATING PYRAMIDAL MORPHOLOGY ON COMPLEX NETWORKS IN THE HUMAN BRAIN

To detail the nerve cells and their functional organization in multiple circuits is crucial to understand the human brain (Szentágothai, 1978; Ramón y Cajal, 1909–1911; Amaral and Insausti, 1990; Larriva-Sahd, 2002; Elston, 2003; DeFelipe, 2011; Geschwind and Rakic, 2013; Larriva-Sahd, 2014; Glasser et al., 2016; Luebke, 2017; Aru et al., 2019; Zeng, 2020). The neural circuits' architecture dynamically combines the transmission, processing, and integration of information across cellular domains along space and time (Gertler et al., 2008; Spruston et al., 2013). The evolved elaboration and diversity of neural functions and the experience-dependent plasticity amend both discrete and continuous structural heterogeneity of cell types (Ramón y Cajal, 1894b; Holtmaat and Svoboda, 2009; Geschwind and Rakic, 2013; Cembrowski and Spruston, 2019), their dendritic geometry (Luebke, 2017), spine features (Yuste, 2013; Dall'Oglio et al., 2015), and axonal architecture (Beyeler et al., 2018; Rockland, 2020). These morphological aspects can differentiate neurons between species and their functions (DeFelipe, 2011). The pattern of synaptic organization of different pyramidal neurons is elaborated for each cortical area in the human brain, at the same time that is set at the level of each dendritic segment and the modulatory processes made by each spine (Andersen et al., 2007; Bourne and Harris, 2009; Chen and Sabatini, 2012; Spruston et al., 2013; Brusco et al., 2014; Chen et al., 2014; Scholtens et al., 2014; Stewart et al., 2014; Dall'Oglio et al., 2015; Hayashi-Takagi et al., 2015; Palomero-Gallagher and Zilles, 2017; Radler et al., 2020).

The morphological heterogeneity of pyramidal neurons can be observed along the subcortical-allocortex-neocortex *continuum* in the human brain. Pyramidal neurons have spines of all shapes, sizes, and likely functional properties. Indeed, the aspect of the long spiny CA1 hippocampal neuron shown here is impressive (**Figure 9**). The implicit functional complexity related to the huge density and variety of spine shapes along hundreds of dendritic micrometers of this pyramidal neuron would serve to merge the simple architecture of the hippocampus with its diversity of associated functions (Cembrowski and Spruston, 2019). Morphological differences relate to electrophysiological and functional implications for hippocampal pyramidal neurons in the deep and the superficial CA1 sublayers in the rat

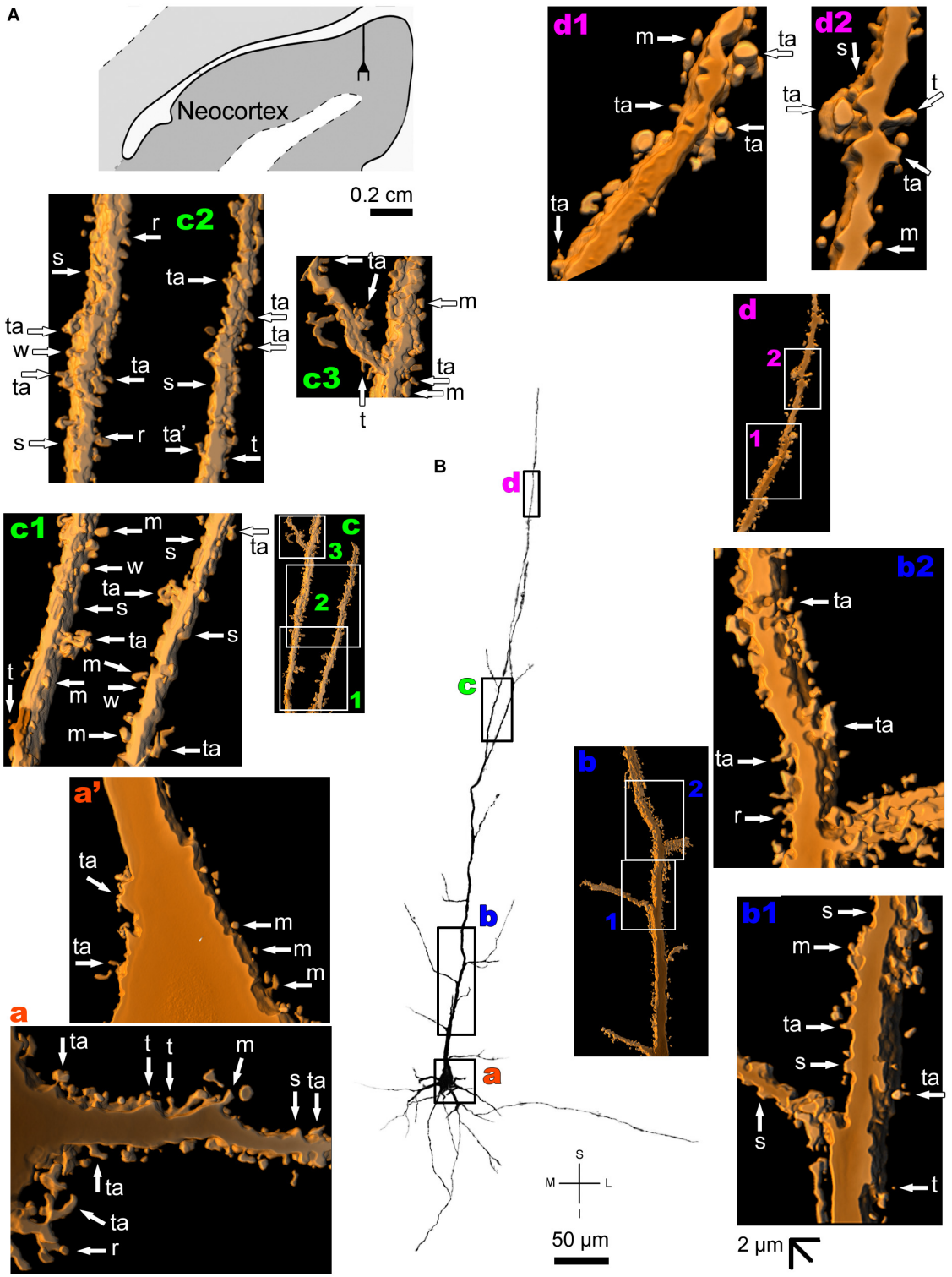

FIGURE 11 | (A) Schematic diagramof a coronal section of the human brain showing the location where a Golgi-impregnated pyramidal neuron was observed (drawn in black) in the layer V of the anterolateral temporal lobe (Neocortex, 9.3 mm posterior to the midpoint of the anterior commissure; adapted from Mai et al., 2008). opt, optic tract. (**B** and laterals) Digitized and reconstructed light microscopy image of a Golgi-impregnated large pyramidal neuron from the internal layer V of the human (adult male) anterolateral temporal neocortex. Note the aspect and length of the primary basal dendrites **(a)** and the main apical dendrite oriented to the surface of the brain with collateral branches and a long straight vertical shaft **(b–d)**. The presence, distribution, and shape of 3D-reconstructed dendritic spines are shown in the inserts at higher magnification and correspond to the locations of **(a–d)**. Numbers accompanying these letters represent sampled segments of the

(Continued)

FIGURE 11 | Continued
respective dendrite (**b1**,**b2**,**c1–c3,d1**,**d2**). The apostrophe over the letters represent an image that was rotated in space after 3D reconstruction to detail the pleomorphic dendritic spines **(a')**. Note the moderate density of pleomorphic spines in the proximal segments of the basal dendrites **(a,a')** and apical dendrite **(b1)**. Moderate to high density of dendritic spines are observed toward intermediate (**b2**) to distal **(c1–c3)** segments of the apical dendrite. Moderate spine density is observed in more distal dendritic shaft **(d1,d2)**. Some spines were observed in the cell body **(a')**. Dendritic spines were classified as stubby (s), wide (w), thin (t), mushroom-like (m), ramified (r) or transitional/atypical ones (ta). As in the other pyramidal neurons, dendritic spines of different shapes and sizes occur along the dendritic segments (e.g., **a**,**b2**,**c1**,**d1**). Contrast and brightness adjustments were made with Photoshop CS3 software (Adobe Systems, United States). I, inferior; L, lateral; M, medial; S, superior. Scale = 50 μm for the general view of the neuron and 2 μm for the inserts (the bar shown in **(b1)** applies to all other images of the 3D reconstructed dendritic branches and spines).

(Mizuseki et al., 2011). We also wonder how many of these human spines would be stable or arise as a plastic response to initiate the cascade of intracellular events for memory formation? Afterward, how many spines would disappear to let the dendritic membrane available for new synapses in a process that has to occur along with decades of the human lifespan. This "within-cell-type heterogeneity may provide the hippocampus the intrinsic flexibility that is needed to meet the diverse and variable demands of the external world" (Cembrowski and Spruston, 2019), as well as our internal states, personal memories and identity, and resilience responses (Rasia-Filho et al., 2018 and references therein).

Consistent with the previous proposition of Heimer et al. (2008), specific nuclei in the amygdaloid complex can be at the beginning of the limbic lobe, merging subcortical and allocortical parts in the basal forebrain. Specific amygdaloid nuclei display pyramidal-like and pyramidal neurons. The geometry of each neuron would be adapted to the nuclear area, the course of afferent pathways, and the local, intrinsic connectional organization. These are likely explanations for specific pyramidal-like neurons display apical dendrites oriented to other spatial directions than the pial surface, when present in transition areas prior to a clear cortical laminar organization. The CA3 and CA1 pyramidal neurons have dendrites with a spatial orientation and functional characteristics related to the hippocampal laminar connectivity. This morphological and functional coupling also occurs for the cytoarchitecture of the neocortical cells in the human brain. The pattern and distribution of inputs amend the dendritic architecture of neurons with distinct basal and apical domains adapted for each tissue volume (Spruston, 2008; Larriva-Sahd, 2014; Cembrowski and Spruston, 2019). It is challenging to consider the degree of normal variability that is possible to occur for these cells and circuits for every one of us. For example, the gray matter volume in the cortical areas related to complex visual-spatial, auditory, motor skills, connectivity of the tracts, and the functional activation overlap of language and music are all significantly larger in musicians than in non-musicians (Gaser and Schlaug, 2003; Bouhali et al., 2020). This is in line with the Ramón y Cajal's (1894a) statement: "it can be admitted as very probable that mental exercise leads to a greater development of the dendritic apparatus and of the system of axonal collaterals in the most utilized cerebral regions. In this way, associations already established among certain groups of cells would be notably reinforced by means of the multiplication of the small terminal branches of the dendritic appendages and axonal collaterals." Moreover, "if a given classical cell type actually embodies a collection of heterogeneous elements, such a cell type could perform a corresponding collection of operations. In the case of cell types that repeat across space, such within-cell-type heterogeneity could facilitate the simultaneous execution of distinct computations through the same apparent circuitry" (Cembrowski and Spruston, 2019).

Going one step further, pyramidal neurons increased their receptive surface and modulatory capabilities by having multiple shaped spines for synaptic processing, compartmentalization, stability, or plasticity with impact on the shaft dendrite and vice-versa (Harris, 1999; Bourne and Harris, 2009; Yuste, 2013). Dendrites operate with linear, sublinear, and supralinear summation of frequency, amplitude, and time window of postsynaptic responses (Tran-Van-Minh et al., 2015). Pre- and postsynaptic plasticity show complementary functions (Mizusaki et al., 2018). The presynaptic element adjusts the speed of learning and controls over postsynaptic firing rates whereas postsynaptic plasticity regulates spike timing and frequency and amplifies the response range (Mizusaki et al., 2018). Another important feature is that spines activated by specific stimuli are found widely distributed on basal and apical dendrites (Chen X. et al., 2011). That is, spines responsive to auditory stimuli are found interspersed on the same dendritic branch, and adjacent spines can respond to different sound frequencies in the mouse cerebral cortex *in vivo* (Chen X. et al., 2011). When synaptic wiring is random, the dimension of a representation formed by many sparsely connected neurons can be higher than that of a smaller number of densely connected elements (Litwin-Kumar et al., 2017). If this model could be applied similarly to dendritic spines, it would be possible that multiple connections in different spines along the pyramidal dendrites would provide a high-dimensional representation and output pattern to different ensembles of inputs (adapting data from Litwin-Kumar et al., 2017). On the other hand, it is possible that both the scattered and the clustered synaptic processing can be relevant for the dendritic integration strategies and to determine which prominent dendritic mechanism will be recruited for postsynaptic summation (Tran-Van-Minh et al., 2015). "The recruitment of synapses that participate in the encoding and expression of memory is neither random nor uniform. . . The clustering of synapses may emerge from synapses receiving similar input, or via many processes that allow for crosstalk between nearby synapses within a dendritic branch,

leading to cooperative plasticity. Clustered synapses can act in concert to maximally exploit the non-linear integration potential of the dendritic branches in which they reside. Their main contribution is to facilitate the induction of dendritic spikes and dendritic plateau potentials, which provide advanced computational and memory-related capabilities to dendrites and single neurons" (Kastellakis and Poirazi, 2019). In conjunction, these findings indicate that the diversity of operations in pyramidal spines provide an exceptional repertoire for the integration of postsynaptic potentials at each spiny dendritic segment and more "functional output codes" for each cell.

Notably, human pyramidal neurons are not merely "scaled-up" versions of neurons found in other species but have improved structural and encoding capabilities properties (Mohan et al., 2015). Single-cell RNA-sequencing datasets revealed particularities in gene expression, morphology, proportions, and laminar distributions of cell types in our cerebral cortex (Hodge et al., 2019). There are also species-specific differences in key molecules that regulate synaptic plasticity (Beed et al., 2020). Human CA1 pyramidal neurons have larger apical and basal dendrites with higher branching complexity than mice (Benavides-Piccione et al., 2020). Human pyramidal neurons in layers II/III of the temporal cortex have threefold larger dendritic length and increased branch complexity with longer segments than in macaque and mouse (Mohan et al., 2015). *In silico*, human pyramidal cells with larger dendritic trees track the activity of synaptic inputs with higher temporal precision, enabling efficient information transfer from inputs to output within cortical neurons (Gorioununova et al., 2019). Coexisting synapses on dendritic shafts and axo-spiny contacts at different distances from the soma in the dendritic arbor influence the neuron's excitatory and inhibitory integrative capacity (Megías et al., 2001; Kubota et al., 2007; Anderson et al., 2009; Spruston et al., 2013; Bucher et al., 2020). There is also a high level of interdependence between dendritic excitability and synaptic plasticity, i.e., activity-dependent regulation of dendritic excitability induces synaptic plasticity, and synaptic plasticity affects dendritic computations (see Ramaswamy and Markram, 2015). Spines add more plasticity to synaptic transmission, serving as time-space encoding and decoding devices, and involving varied number and intermingled shapes and sizes for a moment-to-moment activity and engrams. Human dendritic spines have neck length about 30% longer and 100% more volume than in the somatosensory cortex of mice (DeFelipe, 2011 and references therein). The monkey prefrontal cortex layer III pyramidal neurons have spatially (non-random) clustered dendritic spines (mushroom-like and stubby ones) predominantly concentrated in apical terminal branches (Yadav et al., 2012). The same pattern was not found in basal and apical dendritic segments of layer III pyramidal neurons from frontal, temporal, and cingulate cortex in humans (two males; Morales et al., 2014).

Let us then consider that the morphological heterogeneity of human pyramidal neurons also implies likely differences in functional properties. There is a high degree of synaptic diversity arising from molecular and morphological differences among individual synapses and spatially distributed within individual dendrites, between different neurons, and across and between brain regions, which can produce a non-uniform spatial output of synaptic potentials (Grant and Fransén, 2020). The intra-individual and inter-individual differences associated with the potential structural plasticity of the pyramidal dendritic spines imply much more probabilistic possibilities for the functional organization of the human cortical areas. How would all these pyramidal features in each specific area encode, integrate, and determine the conscious identity of each of us? There is no complete explanation for this question yet. Adding to the variations of the shape and connectivity of pyramidal neurons in different human brain areas (Jacobs et al., 1997, 2001), this scenario is enriched by: (1) the stereological estimation of 12.2 million neurons in the amygdaloid complex (approximately 8.5 million in the basolateral nuclei; Schumann and Amaral, 2005); (2) 2.7 million pyramidal neurons in CA2-3 and 16 million pyramidal neurons in CA1 (West and Gundersen, 1990); (3) 16 billion cortical neurons (Herculano-Houzel et al., 2014); and (4) 5 billion neurons in the temporal lobe of humans (Pakkenberg and Gundersen, 1997; see von Bartheld et al., 2016 for a review). When estimating the number of neurons and of the synaptic profiles within cubes of cortical tissue (50 μm wide by 50 μm thick) in the layer V of the human anterolateral temporal cortex, there are 21 neurons and 958,890 synapses, which gives approximately 30,000 synapses per neuron, 90% being asymmetric and 10% symmetric ones (DeFelipe, 2011). Multi-sites non-linear signals and large excitatory synapses/cell (∼30,000) can enhance the computational capabilities for the comparatively short human temporal layer II/III pyramidal neurons (Eyal et al., 2018). Pyramidal neurons in the prefrontal cortex can have up to 23 times more dendritic spines than those in the primary visual area (Elston, 2003). Moreover, human temporal pyramidal neurons possess unique biophysical membrane properties that significantly enhances both synaptic charge-transfer from dendrites to soma and spike propagation along the axon (Eyal et al., 2016). The axon hillock location relative to the soma or dendrite is finely tuned with the somatodendritic capacitive load in thick-tufted pyramidal neuron in neocortical layer V (Hamada et al., 2016). Finally, by miniaturization of computational gating, it was calculated that the human cerebral cortex executes over 1.2 zetta logical operations per second without combusting the brain by the released heat (Georgiev et al., 2020).

We focused our work on pyramidal neurons, but we should not dismiss other important issues as: (1) the interneurons needed for the cortical functioning (the "neurons with short axon" described by Ramón y Cajal, 1909–1911; Fairén et al., 1984; McCormick et al., 1993; Gabbott et al., 1997; Kubota et al., 2007; Larriva-Sahd, 2014; Jiang et al., 2015; Ramaswamy and Markram, 2015; Gouwens et al., 2019); (2) the whole-genome and transcriptome studies for cell origin and evolution and, more specifically, for the heterogeneous pyramidal neurons across the cortical areas (Hill and Walsh, 2005; Thompson et al., 2008; Geschwind and Rakic, 2013; Arendt et al., 2016; Cembrowski and Spruston, 2019; Writing Committee for the Attention-Deficit/Hyperactivity Disorder, et al., 2020); (3) the spine structure modulation by microRNA epigenetic actions

(Park et al., 2019) or by other neurotransmitters than glutamate (e.g., dopamine; Yagishita et al., 2014; Iino et al., 2020); and (4) the contiguous glia with regional functional and morphological specializations (Hodge et al., 2019), plasticity, heterogeneity (Chai et al., 2017), cooperativity for synaptic communication, remodeling, and integration with axons, dendrites, spines, and the extracellular matrix (Dityatev and Rusakov, 2011; Stewart et al., 2014; Chai et al., 2017; Mederos et al., 2018; Arizono et al., 2020; Chioma et al., 2020).

We have shown images from males. Nevertheless, pyramidal neurons in the rat CA1 hippocampal region are subject to various modulatory factors that can affect spine number and shape depending on sex steroids, such as fluctuations in estrogen and progesterone circulating levels and the expression of aromatase (Woolley et al., 1990; Brusco et al., 2008; Yague et al., 2010; Hansberg-Pastor et al., 2015; Sheppard et al., 2019; Barreto-Cordero et al., 2020). Indeed, morphological differences related to sex were reported for human insular pyramidal neurons (Anderson et al., 2009) and for the hippocampal estrogen receptor-α localization in neurofibrillary tangles along with AD (Wang et al., 2016). The modulatory effects of gonadal hormones on human neuronal and glial structure and circuits are another avenue open to further research (e.g., Cahill, 2006; Gobinath et al., 2017; Fogazzi et al., 2020).

CONCLUDING REMARKS

Here, we discussed the emergence and heterogeneity of pyramidal neurons, as well as the dendritic spine diversity in specific amygdaloid nuclei at the beginning of the limbic lobe, progressing along with allocortical and neocortical areas in the human brain. Additional morphological and functional contributions to this field are welcome and can employ and/or expand the present 3D reconstruction procedure in other human brain areas. The involvement of pyramidal neurons (Pierri et al., 2003; Petanjek et al., 2019) and dendritic spines in normal development or in neurological and psychiatric dysfunctions is an important ongoing research field (Ferrer et al., 1986; Ferrer and Gullotta, 1990; Fiala et al., 2002; Blazquez-Llorca et al., 2011; Merino-Serrais et al., 2011; Penzes et al., 2011; Dorostkar et al., 2015; Ramaswamy and Markram, 2015; Herms and Dorostkar, 2016; Chioma et al., 2020). The use of computational tools to explore structural and functional relations of human pyramidal neurons (Toharia et al., 2016) with a model-based clustering mathematical approach for dendritic spines can add theoretical predictions on the functional features of human pyramidal neurons and their integrated synaptic processing (Luengo-Sanchez et al., 2018). We would like to contribute with additional information on the morphological heterogeneity observed in human pyramidal neurons and spines, relevant to elucidate much of the neural processing across various parts of the human brain and in comparative studies with other species (DeFelipe, 2011; Geschwind and Rakic, 2013; Soltesz and Losonczy, 2018 Cembrowski and Spruston, 2019).

DATA AVAILABILITY STATEMENT

All data are available as shown in the present report. Additional data can be requested directly from the authors.

ETHICS STATEMENT

The studies involving human participants were reviewed and approved by The Brazilian Ethics Committee from the Federal University of Health Sciences of Porto Alegre (UFCSPA; #43059115.4.0000.5345, #48771715.5.0000.5345, #06273619.7.0000.5345, and #18718719.7.0000.5345) and Universidade Federal do Rio Grande do Sul (UFRGS; #18718719.7.3001.5347). The next of kin provided written informed consent for brain donation and for use in this kind of study. There is no potentially identifiable data for any individual included in this article.

AUTHOR CONTRIBUTIONS

AR-F, KG, CV, AD, RR, CJ, and MC: study concept and design. AR-F, CV, and AD: acquisition of data. AR-F, KG, CV, and AD: two-dimensional reconstructions. AR-F, KG, RR, and CJ: three-dimensional reconstructions. AR-F, KG, CV, AD, RR, CJ, and MC: interpretation of data and elaboration of the manuscript. All authors contributed to the article and approved the submitted version.

FUNDING

Grants from the Brazilian Agencies CAPES and CNPq [Brazilian Ministry of Science Technology and Innovation "RRID" (Grant Awards Numbers 481992/2010-3 and 306594/2016-1)], SCR_002876.

ACKNOWLEDGMENTS

Authors are thankful to the relatives for the donation of brain tissue samples for the kind of study. This work was awarded with the "Austregésilo" Prize from the National Academy of Medicine (Brazil) in 2016. AR-F and CJ are CNPq researchers.

SUPPLEMENTARY MATERIAL

The Supplementary Material for this article can be found online at: https://www.frontiersin.org/articles/10.3389/fnsyn.2021.616607/full#supplementary-material

Supplementary Figure 1 | Three-dimensional reconstruction of a Golgi-impregnated pyramidal-like neuron from the human cortical amygdaloid nucleus.

Supplementary Figure 2 | Three-dimensional reconstruction of a Golgi-impregnated pyramidal-like neuron from the human basomedial amygdaloid nucleus.

Supplementary Figure 3 | Three-dimensional reconstruction of a Golgi-impregnated pyramidal neuron from the human basomedial amygdaloid nucleus.

Supplementary Figure 4 | Three-dimensional reconstruction of a Golgi-impregnated pyramidal neuron from the human CA3 hippocampal region.

Supplementary Figure 5 | Three-dimensional reconstruction of a Golgi-impregnated small pyramidal neuron from the human CA1 hippocampal region.

Supplementary Figure 6 | Three-dimensional reconstruction of a Golgi-impregnated large pyramidal neuron from the human CA1 hippocampal region.

Supplementary Figure 7 | Three-dimensional reconstruction of a Golgi-impregnated small pyramidal neuron from the human external layers II/III in the anterolateral temporal neocortex.

Supplementary Figure 8 | Three-dimensional reconstruction of a Golgi-impregnated large pyramidal neuron from the human internal layer V in the anterolateral temporal neocortex.

REFERENCES

Adolphs, R. (2003). Is the human amygdala specialized for processing social information? *Ann. N.Y. Acad. Sci.* 985, 326–340. doi: 10.1111/j.1749-6632.2003.tb07091.x

Akhmadeev, A. V., and Kalimullina, L. B. (2015). Paleoamygdala: the morphogenesis of nuclear-type, paleocortical and intermediate formations in the perial of postnatal development in rats. *Rus. J. Develop. Biol.* 46, 27–32. doi: 10.1134/s1062360415010026

Albrecht, D., Isenberg, A. L., Stradford, J., Monreal, T., Sagare, A., Pachicano, M., et al. (2020). Associations between vascular function and Tau PET are associated with global cognition and amyloid. *J. Neurosci.* 40, 8573–8586. doi: 10.1523/jneurosci.1230-20.2020

Allman, J. M., Hakeem, A., Erwin, J. M., Nimchinsky, E., and Hof, P. (2001). The anterior cingulate cortex. The evolution of an interface between emotion and cognition. *Ann. N.Y. Acad. Sci.* 935, 107–117. doi: 10.1111/j.1749-6632.2001.tb03476.x

Almog, M., and Korngreen, A. (2014). A quantitative description of dendritic conductances and its application to dendritic excitation in layer 5 pyramidal neurons. *J. Neurosci.* 34, 182–196. doi: 10.1523/jneurosci.2896-13.2014

Alonso-Nanclares, L., Kastanauskaite, A., Rodriguez, J.-R., Gonzalez-Soriano, J., and DeFelipe, J. (2011). A stereological study of synapse number in the epileptic human hippocampus. *Front. Neuroanat.* 5:8. doi: 10.3389/fnana.2011.00008

Altemus, K. L., Lavenex, P., Ishizuka, N., and Amaral, D. G. (2005). Morphological characteristics and electrophysiological properties of CA1 pyramidal neurons in macaque monkeys. *Neuroscience* 136, 741–756. doi: 10.1016/j.neuroscience.2005.07.001

Amaral, D. G., and Insausti, R. (1990). "Hippocampal formation," in *The Human Nervous System*, ed. G. Paxinos (New York: Academic Press), 711–755.

Amaral, D. G., Price, J. L., Pitkänen, A., and Carmichael, S. T. (1992). "Anatomical organization of the primate amygdaloid complex," in *The Amygdala: Neurobiological Aspects of Emotion, Memory, and Mental Dysfunction*, ed. J. P. Aggleton (New York: Wiley-Liss), 1–66.

Andersen, P., Morris, R., Amaral, D., Bliss, T., and O'Keefe, J. (2007). *The Hippocampus Book*. New York: Oxford University Press.

Anderson, K., Bones, B., Robinson, B., Hass, C., Lee, H., Ford, K., et al. (2009). The morphology of supragranular pyramidal neurons in the human insular cortex: a quantitative Golgi study. *Cereb. Cortex* 19, 2131–2144. doi: 10.1093/cercor/bhn234

Anilkumar, S., Patel, D., de Boer, S. F., Chattarji, S., and Buwalda, B. (2021). Decreased dendritic spine density in posterodorsal medial amygdala neurons of proactive coping rats. *Behav. Brain Res.* 397:112940. doi: 10.1016/j.bbr.2020.112940

Arakaki, T., Mahon, S., Charpier, S., Leblois, A., and Hansel, D. (2016). The role of striatal feedforward inhibition in the maintenance of absence seizures. *J. Neurosci.* 36, 9618–9632. doi: 10.1523/jneurosci.0208-16.2016

Arellano, J. I., Benavides-Piccione, R., DeFelipe, J., and Yuste, R. (2007a). Ultrastructure of dendritic spines: correlation between synaptic and spine morphologies. *Front. Neurosci.* 1, 131–143. doi: 10.3389/neuro.01.1.1.010.2007

Arellano, J. I, Espinosa, A., Fairén, A., Yuste, R., and DeFelipe, J. (2007b). Non-synaptic dendritic spines in neocortex. *Neuroscience* 145, 464–469. doi: 10.1016/j.neuroscience.2006.12.015

Arendt, D., Musser, J. M., Baker, C. V. H., Bergman, A., Cepko, C., Erwin, D. H., et al. (2016). The origin and evolution of cell types. *Nat. Rev. Genet.* 17, 744–757.

Arizono, M., Krishna Inavalli, V. V. K., Panatier, A., Pfeiffer, T., Angibaud, J., Levet, F., et al. (2020). Structural basis of astrocytic Ca2+ signals at tripartite synapses. *Nat. Commun.* 11:1906. doi: 10.1038/s41467-020-15648-4

Arnold, S. E., Hyman, B. T., Flory, J., Damasio, A. R., and Van Hoesen, G. W. (1991). The topographical and neuroanatomical distribution of neurofibrillary tangles and neuritic plaques in the cerebral cortex of patients with Alzheimer's disease. *Cereb. Cortex* 1, 103–116. doi: 10.1093/cercor/1.1.103

Aru, J., Suzuki, M., Rutiku, R., Larkum, M. E., and Bachmann, T. (2019). Coupling the state and contents of consciousness. *Front. Systems Neurosci.* 13:43. doi: 10.3389/fnsys.2019.00043

Banovac, I., Sedmak, D., Džaja, D., Jalšovec, D., Jovanov Miloševiæ, N., Rašin, M. R., et al. (2019). Somato-dendritic morphology and axon origin site specify von Economo neurons as a subclass of modified pyramidal neurons in the human anterior cingulate cortex. *J. Anat.* 235, 651–669. doi: 10.1111/joa.13068

Barreto-Cordero, L. M., Ríos-Carrillo, J., Roldán-Roldán, G., Rasia-Filho, A. A., Flores, G., Bringas, M. E., et al. (2020). Cyclic changes and actions of progesterone and allopregnanolone on cognition and hippocampal basal (stratum oriens) dendritic spines of female rats. *Behav. Brain Res.* 379:112355. doi: 10.1016/j.bbr.2019.112355

Beck, H., and Yaari, Y. (2008). Plasticity of intrinsic neuronal properties in CNS disorders. *Nat. Rev. Neurosci.* 9, 357–369. doi: 10.1038/nrn2371

Beed, P., Ray, S., Velasquez, L. M., Stumpf, A., Parthier, D., Swaminathan, A., et al. (2020). Species-specific differences in synaptic transmission and plasticity. *Sci. Rep.* 10:16557. doi: 10.1038/s41598-020-73547-6

Benavides-Piccione, R., Ballesteros-Yáñez, I., DeFelipe, J., and Yuste, R. (2002). Cortical area and species differences in dendritic spine morphology. *J. Neurocytol.* 31, 337–346.

Benavides-Piccione, R., Regalado-Reyes, M., Fernaud-Espinosa, I., Kastanauskaite, A., Tapia-González, S., León-Espinosa, G., et al. (2020). Differential structure of hippocampal CA1 pyramidal neurons in the human and mouse. *Cereb. Cortex* 30, 730–752.

Benzinger, T. L. S., Blazey, T., Jack, C. R., Koeppe, R. A., Su, Y., Xiong, C., et al. (2013). Regional variability of imaging biomarkers in ADAD. *Proc. Natl. Acad. Sci. U.S.A.* 110, E4502–E4509.

Berry, K. P., and Nedivi, E. (2017). Spine dynamics: are they all the same? *Neuron* 96, 43–55. doi: 10.1016/j.neuron.2017.08.008

Bertram, E. H. (2009). Temporal lobe epilepsy: where do the seizures really begin? *Epilepsy Behav. Suppl.* 1, 32–37. doi: 10.1016/j.yebeh.2008.09.017

Bertram, E. H., Zhang, D. X., Mangan, P., Fountain, N., and Rempe, D. (1998). Functional anatomy of limbic epilepsy: a proposal for central synchronization of a diffusely hyperexcitable network. *Epilepsy Res.* 32, 194–205. doi: 10.1016/s0920-1211(98)00051-5

Beyeler, A., Chang, C. J., Silvestre, M., Lévêque, C., Namburi, P., Wildes, C. P., et al. (2018). Organization of valence-encoding and projection-defined neurons in the basolateral amygdala. *Cell Rep.* 22, 905–918. doi: 10.1016/j.celrep.2017.12.097

Bianchi, S., Stimpson, C. D., Bauernfeind, A. L., Schapiro, S. J., and Baze, W. B. (2013). Dendritic morphology of pyramidal neurons in the chimpanzee neocortex: regional specializations and comparison to humans. *Cereb. Cortex* 23, 2429–2436. doi: 10.1093/cercor/bhs239

Blazquez-Llorca, L., Garcia-Marin, V., Merino-Serrais, P., Ávila, J., and DeFelipe, J. (2011). Abnormal tau phosphorylation in the thorny excrescences of CA3 hippocampal neurons in patients with Alzheimer's disease. *J. Alzheimer's Dis.* 26, 683–698. doi: 10.3233/jad-2011-110659

Bouhali, F., Mongelli, V., Thiebaut de Schotten, M., and Cohen, L. (2020). Reading music and words: the anatomical connectivity of musicians' visual cortex. *NeuroImage* 212:116666. doi: 10.1016/j.neuroimage.2020.116666

Bourne, J., and Harris, K. M. (2007). Do thin spines learn to be mushroom spines that remember? *Curr. Opin. Neurobiol.* 17, 381–386. doi: 10.1016/j.conb.2007.04.009

Bourne, J. N., and Harris, K. M. (2008). Balancing structure and function at hippocampal dendritic spines. *Ann. Rev. Neurosci.* 31, 47–67. doi: 10.1146/annurev.neuro.31.060407.125646

Bourne, J. N., and Harris, K. M. (2009). "Ultrastructural analysis of spine plasticity," in *Encyclopedia of Neuroscience*, ed. L. R. Squire (New York: Elsevier), 11–17. doi: 10.1016/b978-008045046-9.01771-x

Braak, H. (1979). Pigment architecture of the human telencephalic cortex. V. *Regio anterogenualis*. *Cell Tissue Res.* 204, 441–451. doi: 10.1007/bf00233655

Braak, H. (1980). *Architectonics of the Human Telencephalic Cortex*. Berlin: Springer-Verlag.

Braak, H., and Braak, E. (1983). Neuronal types in the basolateral amygdaloid nuclei of man. *Brain Res. Bull.* 11, 349–365. doi: 10.1016/0361-9230(83)90171-5

Braak, H., and Braak, E. (1985). Golgi preparations as a tool in neuropathology with particular reference to investigations of the human telencephalic cortex. *Prog. Neurobiol.* 25, 93–139. doi: 10.1016/0301-0082(85)90001-2

Braak, H., and Braak, E. (1991). Neuropathological stageing of Alzheimer-related changes. *Acta Neuropathol.* 82, 239–259. doi: 10.1007/bf00308809

Brodal, A. (1981). *Neurological Anatomy*. New York: Oxford University Press.

Brunel, N., Hakim, V., and Richardson, M. J. R. (2014). Single neuron dynamics and computation. *Curr. Op. Neurobiol.* 25, 149–155.

Brusco, J., Merlo, S., Ikeda, ÉT., Petralia, R. S., Kachar, B., Rasia-Filho, A. A., et al. (2014). Inhibitory and multisynaptic spines, and hemispherical synaptic specialization in the posterodorsal medial amygdala of male and female rats. *J. Comp. Neurol.* 522, 2075–2088. doi: 10.1002/cne.23518

Brusco, J., Wittmann, R., de Azevedo, M. S., Lucion, A. B., Franci, C. R., Giovenardi, M., et al. (2008). Plasma hormonal profiles and dendritic spine density and morphology in the hippocampal CA1 stratum radiatum, evidenced by light microscopy, of virgin and postpartum female rats. *Neurosci. Lett.* 438, 346–350. doi: 10.1016/j.neulet.2008.04.063

Bucher, M., Fanutza, T., and Mikhaylova, M. (2020). Cytoskeletal makeup of the synapse: shaft versus spine. *Cytoskeleton* 77, 55–64. doi: 10.1002/cm.21583

Bunge, M. (1980). *The Mind-Body Problem*. Oxford: Pergamon Press.

Butti, C., Santos, M., Uppal, N., and Hof, P. R. (2013). von Economo neurons: clinical and evolutionary perspectives. *Cortex* 49, 312–326. doi: 10.1016/j.cortex.2011.10.004

Buxhoeveden, D. P., and Casanova, M. F. (2002). The minicolumn and evolution of the brain. *Brain Behav. Evol.* 60, 125–151. doi: 10.1159/000065935

Cahill, L. (2006). Why sex matters for neuroscience. *Nat. Rev. Neurosci.* 7, 477–484. doi: 10.1038/nrn1909

Calderone, A., Jover, T., Mashiko, T., Noh, K. M., Tanaka, H., Bennett, M. V., et al. (2004). Late calcium EDTA rescues hippocampal CA1 neurons from global ischemia-induced death. *J. Neurosci.* 24, 9903–9913. doi: 10.1523/jneurosci.1713-04.2004

Carlo, C. N., Stefanacci, L., Semendeferi, K., and Stevens, C. F. (2010). Comparative analyses of the neuron numbers and volumes of the amygdaloid complex in old and new world primates. *J. Comp. Neurol.* 518, 1176–1198.

Cauda, F., Geminiani, G. C., and Vercelli, A. (2014). Evolutionary appearance of von Economo's neurons in the mammalian cerebral cortex. *Front. Hum. Neurosci.* 8:104. doi: 10.3389/fnhum.2014.00104

Cela, E., and Sjöström, P. J. (2019). Novel optogenetic approaches in epilepsy research. *Front. Neurosci.* 13:947. doi: 10.3389/fnins.2019.00947

Cembrowski, M. S., and Spruston, N. (2019). Heterogeneity within classical cell types is the rule: lessons from hippocampal pyramidal neurons. *Nat. Rev. Neurosci.* 20, 193–204. doi: 10.1038/s41583-019-0125-5

Chai, H., Diaz-Castro, B., Shigetomi, E., Monte, E., Octeau, J. C., Yu, X., et al. (2017). Neural circuit-specialized astrocytes: Transcriptomic, proteomic, morphological, and functional evidence. *Neuron* 95, 531–549. doi: 10.1016/j.neuron.2017.06.029

Chang, M., Dian, J. A., Dufour, S., Wang, L., Moradi Chameh, H., Ramani, M., et al. (2018). Brief activation of GABAergic interneurons initiates the transition to ictal events through post-inhibitory rebound excitation. *Neurobiol. Dis.* 109, 102–116. doi: 10.1016/j.nbd.2017.10.007

Chareyron, L. J., Banta Lavenex, P., Amaral, D. G., and Lavenex, P. (2011). Stereological analysis of the rat and monkey amygdala. *J. Comp. Neurol.* 519, 3218–3239. doi: 10.1002/cne.22677

Chen, C.-C., Lu, J., and Zuo, Y. (2014). Spatiotemporal dynamics of dendritic spines in the living brain. *Front. Neuroanat.* 8:28. doi: 10.3389/fnana.2014.00028

Chen, S., and Sabatini, B. L. (2012). Signaling in dendritic spines and spine microdomains. *Curr. Opin. Neurobiol.* 22, 389–396. doi: 10.1016/j.conb.2012.03.003

Chen, S., Su, H., Yue, C., Remy, S., Royeck, M., Sochivko, D., et al. (2011). An increase in persistent sodium current contributes to intrinsic neuronal bursting after status epilepticus. *J. Neurophysiol.* 105, 117–129. doi: 10.1152/jn.00184.2010

Chen, X., Leischner, U., Rochefort, N. L., Nelken, I., and Konnerth, A. (2011). Functional mapping of single spines in cortical neurons in vivo. *Nature* 475, 501–505. doi: 10.1038/nature10193

Chioma, V. C., Kruyer, A., Bobadilla, A.-C., Angelis, A., Ellison, Z., Hodebourg, R., et al. (2020). Heroin seeking and extinction from seeking activate matrix metalloproteinases at synapses on distinct subpopulations of accumbens cells. *Biol. Psych.* doi: 10.1016/j.biopsych.2020.12.004 [Epub ahead of print].

Chklovskii, D. B., Schikorski, T., and Stevens, C. F. (2002). Wiring optimization in cortical circuits. *Neuron* 34, 341–347. doi: 10.1016/s0896-6273(02)00679-7

Choi, G. B., Dong, H. W., Murphy, A. J., Valenzuela, D. M., Yancopoulos, G. D., Swanson, L. W., et al. (2005). Lhx6 delineates a pathway mediating innate reproductive behaviors from the amygdala to the hypothalamus. *Neuron* 46, 647–660. doi: 10.1016/j.neuron.2005.04.011

Clowry, G., Molnár, Z., and Rakic, P. (2010). Renewed focus on the developing human neocortex. *J. Anat.* 217, 276–288. doi: 10.1111/j.1469-7580.2010.01281.x

Cooke, B. M., and Woolley, C. S. (2005). Sexually dimorphic synaptic organization of the medial amygdala. *J. Neurosci.* 25, 10759–10767. doi: 10.1523/jneurosci.2919-05.2005

Correa-Júnior, N. D., Renner, J., Fuentealba-Villarroel, F., Hilbig, A., and Rasia-Filho, A. A. (2020). Dendritic and spine heterogeneity of von Economo neurons in the human cingulate cortex. *Front. Synapt. Neurosci.* 12:25. doi: 10.3389/fnsyn.2020.00025

Dall'Oglio, A., Dutra, A. C., Moreira, J. E., and Rasia-Filho, A. A. (2015). The human medial amygdala: structure, diversity, and complexity of dendritic spines. *J. Anat.* 227, 440–459. doi: 10.1111/joa.12358

Dall'Oglio, A., Ferme, D., Brusco, J., Moreira, J. E., and Rasia-Filho, A. A. (2010). The "single-section" Golgi method adapted for formalin-fixed human brain and light microscopy. *J. Neurosci. Methods* 189, 51–55. doi: 10.1016/j.jneumeth.2010.03.018

Dall'Oglio, A., Xavier, L. L., Hilbig, A., Ferme, D., Moreira, J. E., Achaval, M., et al. (2013). Cellular components of the human medial amygdaloid nucleus. *J. Comp. Neurol.* 521, 589–611. doi: 10.1002/cne.23192

Dalpian, F., Rasia-Filho, A. A., and Calcagnotto, M. E. (2019). Sexual dimorphism, estrous cycle and laterality determine the intrinsic and synaptic properties of medial amygdala neurons in rat. *J. Cell Sci.* 132:jcs227793. doi: 10.1242/jcs.227793

Davis, M. (1992). "The role of the amygdala in conditioned fear," in *The Amygdala*, ed. J. P. Aggleton (New York: Wiley-Liss), 255–306.

Dayas, C. V., Buller, K. M., and Day, T. A. (1999). Neuroendocrine responses to an emotional stressor: evidence for involvement of the medial but not the central amygdala. *Eur. J. Neurosci.* 11, 2312–2322. doi: 10.1046/j.1460-9568.1999.00645.x

de Olmos, J. S. (2004). "Amygdala," in *The Human Nervous System*, 2nd Edn, eds G. Paxinos and J. Mai (San Diego: Elsevier), 739–868.

de Ruiter, J. P. (1983). The influence of post-mortem fixation delay on the reliability of the Golgi silver impregnation. *Brain Res.* 266, 143–147. doi: 10.1016/0006-8993(83)91317-3

DeFelipe, J. (2011). The evolution of the brain, the human nature of cortical circuits, and intellectual creativity. *Front. Neuroanat.* 5:29. doi: 10.3389/fnana.2011.00029

Diano, M., Tamietto, M., Celeghin, A., Weiskrantz, L., Tatu, M–K., Bagnis, A., et al. (2017). Dynamic changes in amygdala psychophysiological connectivity reveal distinct neural networks for facial expressions of basic emotions. *Sci. Rep.* 7:45260. doi: 10.1038/srep45260

DiMarino, V., Etienne, Y., and Niddam, M. (2016). *The Amygdaloid Nuclear Complex*. Cham: Springer.

Dityatev, A., and Rusakov, D. A. (2011). Molecular signals of plasticity at the tetrapartite synapse. *Curr. Opin. Neurobiol.* 21, 1–7. doi: 10.1155/2011/734231

Dorostkar, M. M., Zou, C., Blazquez-Llorca, L., and Herms, J. (2015). Analyzing dendritic spine pathology in Alzheimer's disease: problems and opportunities. *Acta Neuropathol.* 130, 1–19.

Du, F., Whetsell, W. O., Abou-Khalil, B., Blumenkopf, B., Lothman, E. W., and Schwarcz, R. (1993). Preferential neuronal loss in layer III of the entorhinal cortex in patients with temporal lobe epilepsy. *Epilepsy Res.* 16, 223–233. doi: 10.1016/0920-1211(93)90083-j

Elston, G. N. (2003). Cortex, cognition and the cell: new insights into the pyramidal neuron and prefrontal function. *Cereb. Cortex* 13, 1124–1138. doi: 10.1093/cercor/bhg093

Everitt, B. (1995). "Limbic lobe and olfactory pathways," in *Gray's Anatomy*, eds M. M. Berry, L. H. Bannister, and S. M. Standring (London: Churchill Livingstone), 1115–1141.

Eyal, G., Verhoog, M. B., Testa-Silva, G., Deitcher, Y., Benavides-Piccione, R., DeFelipe, J., et al. (2018). Human cortical pyramidal neurons: from spines to spikes via models. *Front. Cell. Neurosci.* 12:181. doi: 10.3389/fncel.2018.00181

Eyal, G., Verhoog, M. B., Testa-Silva, G., Deitcher, Y., Lodder, J. C., Benavides-Piccione, R., et al. (2016). Unique membrane properties and enhanced signal processing in human neocortical neurons. *eLife* 5:e16553. doi: 10.7554/eLife.16553

Fairén, A., DeFelipe, J., and Regidor, J. (1984). "Nonpyramidal neurons," in *Cerebral Cortex*, eds E. G. Jones and A. Peters (New York: Plenum Press), 201–253.

Feindel, W., and Penfield, W. (1954). Location of discharge in temporal automatism. *Arch. Neurol. Psychiat.* 72, 605–630. doi: 10.1001/archneurpsyc.1954.02330050075012

Feldman, M. L. (1984). "Morphology of the neocortical pyramidal neuron," in *Cerebral Cortex*, eds E. G. Jones and A. Peters (New York: Plenum Press), 107–121.

Ferrer, I., Fábregues, I., Rairiz, J., and Galofré, E. (1986). Decreased numbers of dendritic spines on cortical pyramidal neurons in human chronic alcoholism. *Neurosci. Lett.* 69, 115–119. doi: 10.1016/0304-3940(86)90425-8

Ferrer, I., and Gullotta, F. (1990). Down's syndrome and Alzheimer's disease: dendritic spine counts in the hippocampus. *Acta Neuropathol.* 79, 680–685.

Fiala, J. C., and Harris, K. M. (1999). "Dendrite structure," in *Dendrites*, eds G. Stuart, N. Spruston, and M. Häusser (New York: Oxford University Press), 1–34. doi: 10.1093/acprof:oso/9780198745273.003.0001

Fiala, J. C., Spacek, J., and Harris, K. M. (2002). Dendritic spine pathology: cause or consequence of neurological disorders? *Brain Res. Rev.* 39, 29–54. doi: 10.1016/s0165-0173(02)00158-3

Fogazzi, D. V., Neary, J. P., Sonza, A., Reppold, C. T., Kaiser, V., Scassola, C. M., et al. (2020). The prefrontal cortex conscious and unconscious response to social/emotional facial expressions involve sex, hemispheric laterality, and selective activation of the central cardiac modulation. *Behav. Brain Res.* 393:112773. doi: 10.1016/j.bbr.2020.112773

Fountain, N. B., Bear, J., Bertram, E. H., and Lothman, E. W. (1998). Responses of deep entorhinal cortex are epileptiform in an electrogenic model of chronic temporal lobe epilepsy. *J. Neurophysiol.* 80, 230–240. doi: 10.1152/jn.1998.80.1.230

Frank, A. C., Huang, S., Zhou, M., Gdalyahu, A., Kastellakis, G., Silva, T. K., et al. (2018). Hotspots of dendritic spine turnover facilitate clustered spine addition and learning and memory. *Nat. Commun.* 9:422. doi: 10.1038/s41467-017-02751-2

Frederickson, C. J., and Moncrieff, D. W. (1994). Zn-containing neurons. *Biol. Signals* 3, 127–139.

Frederickson, C. J., Suh, S. W., Silva, D., Frederickson, C. J., and Thompson, R. B. (2000). Importance of zinc in the central nervous system: the zinc-containing neuron. *J. Nutr.* 130, 1471S–1483S.

Frederickson, R. E., Frederickson, C. J., and Danscher, G. (1990). In situ binding of bouton zinc reversibly disrupts performance on a spatial memory task. *Behav. Brain Res.* 39, 25–33. doi: 10.1016/0166-4328(90)90021-6

Freese, J. L., and Amaral, D. G. (2009). "Neuroanatomy of the primate amygdala," in *The Human Amygdala*, eds P. J. Whalen and E. A. Phelps (New York: Guilford Press), 3–42.

Frick, A., and Johnston, D. (2005). Plasticity of dendritic excitability. *J. Neurobiol.* 64, 100–115. doi: 10.1002/neu.20148

Friker, L. L., Scheiblich, H., Hochheiser, I. V., Brinkschulte, R., Riedel, D., Latz, E., et al. (2020). β-amyloid clustering around ASC fibrils boosts its toxicity in microglia. *Cell Rep.* 30, 3743.e6–3754.e6. doi: 10.1016/j.celrep.2020.02.025

Fujiwara-Tsukamoto, Y., Isomura, Y., Kaneda, K., and Takada, M. (2004). Synaptic interactions between pyramidal cells and interneuron subtypes during seizure-like activity in the rat hippocampus. *J. Physiol.* 557, 961–979. doi: 10.1113/jphysiol.2003.059915

Gabbott, P. L. (2003). Radial organisation of neurons and dendrites in human cortical areas 25, 32, and 32'. *Brain Res.* 992, 298–304. doi: 10.1016/j.brainres.2003.08.054

Gabbott, P. L., Jays, P. R., and Bacon, S. J. (1997). Calretinin neurons in human medial prefrontal cortex (areas 24a,b,c, 32', and 25). *J. Comp. Neurol.* 381, 389–410. doi: 10.1002/(sici)1096-9861(19970519)381:4<389::aid-cne1>3.0.co;2-z

García-López, P., García-Marín, V., and Freire, M. (2010). Dendritic spines and development: towards a unifying model of spinogenesis - a present day review of Cajal's histological slides and drawings. *Neural Plast.* 2010:769207. doi: 10.1155/2010/769207

Gaser, C., and Schlaug, G. (2003). Brain structures differ between musicians and non-musicians. *J. Neurosci.* 23, 9240–9245. doi: 10.1523/jneurosci.23-27-09240.2003

Georgiev, D. D., Kolev, S. K., Cohen, E., and Glazebrook, J. F. (2020). Computational capacity of pyramidal neurons in the cerebral cortex. *Brain Res.* 1748, 147069. doi: 10.1016/j.brainres.2020.147069

Gertler, T. S., Chan, C. S., and Surmeier, D. J. (2008). Dichotomous anatomical properties of adult striatal medium spiny neurons. *J. Neurosci.* 28, 10814–10824. doi: 10.1523/jneurosci.2660-08.2008

Geschwind, D. H., and Rakic, P. (2013). Cortical evolution: judge the brain by its cover. *Neuron* 80, 633–647. doi: 10.1016/j.neuron.2013.10.045

Gilman, J. P., Medalla, M., and Luebke, J. I. (2017). Area-specific features of pyramidal neurons – a comparative study in mouse and Rhesus monkey. *Cereb. Cortex* 27, 2078–2094.

Glasser, M. F., Coalson, T. S., Robinson, E. C., Hacker, C. D., Harwell, J., Yacoub, E., et al. (2016). A multi-modal parcellation of human cerebral cortex. *Nature* 536, 171–178.

Gloor, P. (1997). *The Temporal Lobe and Limbic System*. New York, NY: Oxford University Press.

Gobinath, A. R., Choleris, E., and Galea, L. A. (2017). Sex, hormones, and genotype interact to influence psychiatric disease, treatment, and behavioral research. *J. Neurosci. Res.* 95, 50–64. doi: 10.1002/jnr.23872

González-Burgos, G., Miyamae, T., Krimer, Y., Gulchina, Y., Pafundo, D. E., Krimer, O., et al. (2019). Distinct properties of layer 3 pyramidal neurons from prefrontal and parietal areas of the monkey neocortex. *J. Neurosci.* 39, 7277–7290. doi: 10.1523/jneurosci.1210-19.2019

González-Burgos, I., Rivera-Cervantes, M. C. R., Velázquez-Zamora, D. A., Feria-Velasco, A., and Garcia-Segura, L. M. (2012). Selective estrogen receptor modulators regulate dendritic spine plasticity in the hippocampus of male rats. *Neural Plast.* 2012:309494. doi: 10.1155/2012/309494

González-Ramírez, M. M., Velázquez-Zamora, D. A., Olvera-Cortés, M. E., and González-Burgos, I. (2014). Changes in the plastic properties of hippocampal dendritic spines underlie the attenuation of place learning in healthy aged rats. *Neurobiol. Learn. Mem.* 109, 94–103. doi: 10.1016/j.nlm.2013.11.017

Goriounova, N. A., Heyer, D. B., Wilbers, R., Verhoog, M. B., Giugliano, M., Verbist, C., et al. (2019). Large and fast human pyramidal neurons associate with intelligence. *eLife* 7:e41714.

Gouwens, N. W., Sorensen, S. A., Berg, J., Lee, C., Jarsky, T., Ting, J., et al. (2019). Classification of electrophysiological and morphological neuron types in the mouse visual cortex. *Nat. Neurosci.* 22, 1182–1195.

Grant, S. G., and Fransén, E. (2020). The synapse diversity dilemma: molecular heterogeneity confounds studies of synapse function. *Front. Synaptic Neurosci.* 12:590403. doi: 10.3389/fnsyn.2020.590403

Grisendi, T., Reynaud, O., Clarke, S., and Da Costa, S. (2019). Processing pathways for emotional vocalizations. *Brain Struct. Funct.* 224, 2487–2504. doi: 10.1007/s00429-019-01912-x

Gulledge, A. T., Carnevale, N. T., and Stuart, G. J. (2012). Electrical advantages of dendritic spines. *PLoS One* 7:e36007. doi: 10.1371/journal.pone.0036007

Guy, J., and Staiger, J. F. (2017). The functioning of a cortex without layers. *Front. Neuroanat.* 11:54. doi: 10.3389/fnana.2017.00054

Hamada, M. S., Goethals, S., de Vries, S. I., Brette, R., and Kole, M. H. (2016). Covariation of axon initial segment location and dendritic tree normalizes the somatic action potential. *Proc. Natl. Acad. Sci. U.S.A.* 113, 14841–14846. doi: 10.1073/pnas.1607548113

Hansberg-Pastor, V., González-Arenas, A., Piña-Medina, A. G., and Camacho-Arroyo, I. (2015). Sex hormones regulate cytoskeletal proteins involved in brain plasticity. *Front. Psych.* 6:165. doi: 10.3389/fpsyt.2015.00165

Harnett, M. T., Makara, J. K., Spruston, N., Kath, W. L., and Magee, J. C. (2012). Synaptic amplification by dendritic spines enhances input cooperativity. *Nature* 491, 599–605. doi: 10.1038/nature11554

Harris, K. M. (1999). Structure, development, and plasticity of dendritic spines. *Curr. Op. Neurobiol.* 9, 343–348. doi: 10.1016/s0959-4388(99)80050-6

Hayashi-Takagi, A., Yagishita, S., Nakamura, M., Shirai, F., Wu, Y. I., Loshbaugh, A. L., et al. (2015). Labelling and optical erasure of synaptic memory traces in the motor cortex. *Nature* 525, 333–338. doi: 10.1038/nature15257

Heimer, L., Van Hoesen, G. W., Trimble, M., and Zahm, D. S. (2008). *Anatomy of Neuropsychiatry – The New Anatomy of the Basal Forebrain and Its Implications for Neuropsychiatric Illness*. San Diego, CA: Academic Press.

Herculano-Houzel, S. (2019). Life history changes accompany increased numbers of cortical neurons: a new framework for understanding human brain evolution. *Prog. Brain Res.* 250, 179–216. doi: 10.1016/bs.pbr.2019.06.001

Herculano-Houzel, S., Collins, C. E., Wong, P., Kaas, J. H., and Lent, R. (2008). The basic nonuniformity of the cerebral cortex. *Proc. Natl. Acad. Sci. U.S.A.* 105, 12593–12598. doi: 10.1073/pnas.0805417105

Herculano-Houzel, S., Manger, P. R., and Kaas, J. H. (2014). Brain scaling in mammalian evolution as a consequence of concerted and mosaic changes in numbers of neurons and average neuronal cell size. *Front. Neuroanat.* 8:77. doi: 10.3389/fnana.2014.00077

Herms, J., and Dorostkar, M. M. (2016). Dendritic spine pathology in neurodegenerative diseases. *Ann. Rev. Pathol.* 11, 221–250. doi: 10.1146/annurev-pathol-012615-044216

Heun, R., Mazanek, M., Atzor, K. R., Tintera, J., Gawehn, J., Burkart, M., et al. (1997). Amygdala-hippocampal atrophy and memory performance in dementia of Alzheimer type. *Dement. Geriatr. Cogn. Disord.* 8, 329–336. doi: 10.1159/000106651

Hill, R. S., and Walsh, C. A. (2005). Molecular insights into human brain evolution. *Nature* 437, 64–67. doi: 10.1038/nature04103

Hirsch, M. M., Brusco, J., Vaccaro, T., Margis, R., Moreira, J. E., Gottfried, C., et al. (2018). Sex differences and estrous cycle changes in synaptic plasticity-related microRNA in the rat medial amygdala. *Neuroscience* 379, 405–414. doi: 10.1016/j.neuroscience.2018.03.035

Hodge, R. D., Bakken, T. E., Miller, J. A., Smith, K. A., Barkan, E. R., Graybuck, L. T., et al. (2019). Conserved cell types with divergent features in human versus mouse cortex. *Nature* 573, 61–68.

Hof, P. R., Cox, K., and Morrison, J. H. (1990). Quantitative analysis of a vulnerable subset of pyramidal neurons in Alzheimer's Disease: I. Superior frontal and inferior temporal cortex. *J. Comp. Neurol.* 301, 44–54. doi: 10.1002/cne.903010105

Hof, P. R., and Morrison, J. H. (1990). Quantitative analysis of a vulnerable subset of pyramidal neurons in Alzheimer's disease: II. Primary and secondary visual cortex. *J. Comp. Neurol.* 301, 55–64. doi: 10.1002/cne.903010106

Holtmaat, A., and Svoboda, K. (2009). Experience-dependent structural synaptic plasticity in the mammalian brain. *Nat. Rev. Neurosci.* 10, 647–658. doi: 10.1038/nrn2699

Hrvoj-Mihic, B., Hanson, K. L., Lew, C. H., Stefanacci, L., Jacobs, B., Bellugi, U., et al. (2017). Basal dendritic morphology of cortical pyramidal neurons in Williams syndrome: prefrontal cortex and beyond. *Front. Neurosci.* 11:419. doi: 10.3389/fnins.2017.00419

Hudson, L. P., Munoz, D. G., Miller, L., McLachlan, R. S., Girvin, J. P., and Blume, W. T. (1993). Amygdaloid sclerosis in temporal lobe epilepsy. *Ann. Neurol.* 33, 622–631. doi: 10.1002/ana.410330611

Huijbers, W., Mormino, E. C., Schultz, A. P., Wigman, S., Ward, A. M., Larvie, M., et al. (2015). Amyloid-β deposition in mild cognitive impairment is associated with increased hippocampal activity, atrophy and clinical progression. *Brain* 138, 1023–1035. doi: 10.1093/brain/awv007

Hyman, B. T., Van Hoesen, G. W., Damasio, A. R., and Barnes, C. L. (1984). Alzheimer's disease: cell-specific pathology isolates the hippocampal formation. *Science* 225, 1168–1170. doi: 10.1126/science.6474172

Iino, Y., Sawada, T., Yamaguchi, K., Tajiri, M., Ishii, S., Kasai, H., et al. (2020). Dopamine D2 receptors in discrimination learning and spine enlargement. *Nature* 579, 555–560. doi: 10.1038/s41586-020-2115-1

Insausti, R., Muñoz-López, M., Insausti, A. M., and Artacho-Pérula, E. (2017). The human periallocortex: layer pattern in presubiculum, parasubiculum and entorhinal cortex. A review. *Front. Neuroanat.* 11:84. doi: 10.3389/fnana.2017.00084

Ishunina, T. A., and Swaab, D. F. (2001). Increased expression of estrogen receptor α and β in the nucleus basalis of Meynert in Alzheimer's disease. *Neurobiol. Aging* 22, 417–426. doi: 10.1016/s0197-4580(00)00255-4

Jacobs, B., Driscoll, L., and Schall, M. (1997). Life-span dendritic and spine changes in areas 10 and 18 of human cortex: a quantitative Golgi study. *J. Comp. Neurol.* 386, 661–680. doi: 10.1002/(sici)1096-9861(19971006)386:4<661::aid-cne11>3.0.co;2-n

Jacobs, B., Schall, M., Prather, M., Kapler, E., and Driscoll, L. (2001). Regional dendritic and spine variation in human cerebral cortex: a quantitative Golgi study. *Cereb. Cortex* 11, 558–571. doi: 10.1093/cercor/11.6.558

Janak, P. H., and Tye, K. M. (2015). From circuits to behavior in the amygdala. *Nature* 517, 284–292. doi: 10.1038/nature14188

Jensen, M. S., and Yaari, Y. (1997). Role of intrinsic burst firing, potassium accumulation, and electrical coupling in the elevated potassium model of hippocampal epilepsy. *J. Neurophysiol.* 77, 1224–1233. doi: 10.1152/jn.1997.77.3.1224

Jiang, M., Lee, C. L., Smith, K. L., and Swann, J. W. (1998). Spine loss and other persistent alterations of hippocampal pyramidal cell dendrites in a model of early-onset epilepsy. *J. Neurosci.* 18, 8356–8368. doi: 10.1523/jneurosci.18-20-08356.1998

Jiang, X., Shen, S., Cadwell, C. R., Berens, P., Sinz, F., Ecker, A. S., et al. (2015). Principles of connectivity among morphologically defined cell types in adult neocortex. *Science* 350:aac9462. doi: 10.1126/science.aac9462

Johnston, J. B. (1923). Further contributions to the study of the evolution of the forebrain. *J. Comp. Neurol.* 35, 337–481. doi: 10.1002/cne.900350502

Kasai, H., Hayama, T., Ishikawa, M., Watanabe, S., Yagishita, S., and Noguchi, J. (2010). Learning rules and persistence of dendritic spines. *Eur. J. Neurosci.* 32, 241–249. doi: 10.1111/j.1460-9568.2010.07344.x

Kastellakis, G., and Poirazi, P. (2019). Synaptic clustering and memory formation. *Front. Mol. Neurosci.* 12:300. doi: 10.3389/fnmol.2019.00300

Kastellakis, G., Silva, A. J., and Poirazi, P. (2016). Linking memories across time via neuronal and dendritic overlaps in model neurons with active dendrites. *Cell Rep.* 17, 1491–1504. doi: 10.1016/j.celrep.2016.10.015

Kelly, R., and Stefanacci, L. (2009). "Amygdala: structure and circuitry in primates," in *Encyclopedia of Neuroscience*, ed. L. R. Squire (Oxford: Academic Press), 341–345. doi: 10.1016/b978-008045046-9.00148-0

Khazipov, R. (2016). GABAergic synchronization in epilepsy. *Cold Spring Harb. Perspect. Med.* 6:a022764. doi: 10.1101/cshperspect.a022764

Khoshkhoo, S., Vogt, D., and Sohal, V. S. (2017). Dynamic, cell-type-specific roles for GABAergic interneurons in a mouse model of optogenetically inducible seizures. *Neuron* 93, 291–298. doi: 10.1016/j.neuron.2016.11.043

Kolb, B., and Whishaw, I. Q. (2015). *Fundamentals of Human Neuropsychology*. New York, NY: Worth Publishers.

Kubota, Y., Hatada, S., Kondo, S., Karube, F., and Kawaguchi, Y. (2007). Neocortical inhibitory terminals innervate dendritic spines targeted by thalamocortical afferents. *J. Neurosci.* 27, 1139–1150. doi: 10.1523/jneurosci.3846-06.2007

Kumlien, E., Doss, R. C., and Gates, J. R. (2002). Treatment outcome in patients with mesial temporal sclerosis. *Seizure* 11, 413–417. doi: 10.1053/seiz.2001.0614

Lalanne, T., Oyrer, J., Farrant, M., and Sjöström, P. J. (2018). Synapse type-dependent expression of calcium-permeable AMPA receptors. *Front. Synaptic Neurosci.* 10:34. doi: 10.3389/fnsyn.2018.00034

Larriva-Sahd, J. (2002). Some contributions of Rafael Lorente de Nó to neuroscience: a reminiscence. *Brain Res. Bull.* 59, 1–11. doi: 10.1016/s0361-9230(02)00838-9

Larriva-Sahd, J. A. (2010). Chandelier and interfascicular neurons in the adult mouse piriform cortex. *Front. Neuroanat.* 4:148. doi: 10.3389/fnana.2010.00148

Larriva-Sahd, J. A. (2014). Some predictions of Rafael Lorente de Nó 80 years later. *Front. Neuroanat.* 8:147. doi: 10.3389/fnana.2014.00147

Leal, S. L., Landau, S. M., Bell, R. K., and Jagust, W. J. (2017a). Hippocampal activation is associated with longitudinal amyloid accumulation and cognitive decline. *eLife* 6:e22978. doi: 10.7554/eLife.22978

Leal, S. L., Lockhart, S. N., Maass, A., Bell, R. K., and Jagust, W. J. (2018). Subthreshold amyloid predicts Tau deposition in aging. *J. Neurosci.* 38, 4482–4489. doi: 10.1523/jneurosci.0485-18.2018

Leal, S. L., Noche, J. A., Murray, E. A., and Yassa, M. A. (2017b). Disruption of amygdala-entorhinal-hippocampal network in late-life depression. *Hippocampus* 27, 464–476. doi: 10.1002/hipo.22705

Ledergerber, D., and Larkum, M. E. (2010). Properties of layer 6 pyramidal neuron apical dendrites. *J. Neurosci.* 30, 13031–13044. doi: 10.1523/jneurosci.2254-10.2010

LeDoux, J. E. (1992). "Emotion and amygdala," in *The Amygdala*, ed. J. P. Aggleton (New York, NY: Wiley-Liss), 339–352.

LeDoux, J. E., and Schiller, D. (2009). "The human amygdala: insights from other animals," in *The Human Amygdala*, eds P. J. Whalen and E. A. Phelps (New York, NY: The Guilford Press), 43–60.

Lee, K. F. H., Soares, C., and Béïque, J. C. (2012). Examining form and function of dendritic spines. *Neural Plast.* 2012:704103. doi: 10.1155/2012/704103

Lehmann, T. N., Gabriel, S., Kovacs, R., Eilers, A., Kivi, A., Schulze, K., et al. (2000). Alterations of neuronal connectivity in area CA1 of hippocampal slices from temporal lobe epilepsy patients and from pilocarpine-treated epileptic rats. *Epilepsia* 41(Suppl. 6), S190–S194.

Leng, K., Li, E., Eser, R., Piergies, A., Sit, R., Tan, M., et al. (2021). Molecular characterization of selectively vulnerable neurons in Alzheimer's disease. *Nat. Neurosci.* 24, 276–287. doi: 10.1038/s41593-020-00764-7

Lewerenz, J., and Maher, P. (2015). Chronic glutamate toxicity in neurodegenerative diseases—What is the evidence? *Front. Neurosci.* 9:469. doi: 10.3389/fnins.2015.00469

Li, Z., Okamoto, K.-I., Hayashi, Y., and Sheng, M. (2004). The importance of dendritic mitochondria in the morphogenesis and plasticity of spines and synapses. *Cell* 119, 873–887. doi: 10.1016/j.cell.2004.11.003

Liberzon, I., Phan, K., and Decker, L. (2003). Extended amygdala and emotional salience: a PET activation study of positive and negative affect. *Neuropsychopharmacology* 28, 726–733. doi: 10.1038/sj.npp.1300113

Litwin-Kumar, A., Harris, K. D., Axel, R., Sompolinsky, H., and Abbott, L. F. (2017). Optimal degrees of synaptic connectivity. *Neuron* 93, 1153–1164. doi: 10.1016/j.neuron.2017.01.030

Liu, A. K., Chang, R. C., Pearce, R. K., and Gentleman, S. M. (2015). Nucleus basalis of Meynert revisited: anatomy, history and differential involvement in Alzheimer's and Parkinson's disease. *Acta Neuropathol.* 129, 527–540. doi: 10.1007/s00401-015-1392-5

Lorente de Nó, R. (1934). Studies of the structure of the cerebral cortex. II. Continuation of the study of the ammonic system. *J. Psychol. Neurol.* 46, 113–177.

Lu, J., and Zuo, Y. (2017). Clustered structural and functional plasticity of dendritic spines. *Brain Res. Bull.* 129, 18–22. doi: 10.1016/j.brainresbull.2016.09.008

Luebke, J. I. (2017). Pyramidal neurons are not generalizable building blocks of cortical networks. *Front. Neuroanat.* 11:11. doi: 10.3389/fnana.2017.00011

Luengo-Sanchez, S., Fernaud-Espinosa, I., Bielza, C., Benavides-Piccione, R., Larrañaga, P., and DeFelipe, J. (2018). 3D morphology-based clustering and simulation of human pyramidal cell dendritic spines. *PLoS Comput. Biol.* 14:e1006221. doi: 10.1371/journal.pcbi.1006221

Luis de la Iglesia, J. A., and Lopez-Garcia, C. (1997). A Golgi study of the short-axon interneurons of the cell layer and inner plexiform layer of the medial cortex of the lizard *Podarcis hispanica*. *J. Comp. Neurol.* 385, 565–598. doi: 10.1002/(sici)1096-9861(19970908)385:4<565::aid-cne5>3.0.co;2-1

Mai, J. K., Paxinos, G., and Voss, T. (2008). *Atlas of the Human Brain*. New York, NY: Academic Press.

Mangan, P. S., Scott, C., Williamson, J. M., and Bertram, E. H. (2000). Aberrant neuronal physiology in the basal nucleus of the amygdala in a model of chronic limbic epilepsy. *Neuroscience* 101, 377–391. doi: 10.1016/s0306-4522(00)00358-4

Marcuzzo, S., Dall'Oglio, A., Ribeiro, M. F., Achaval, M., and Rasia-Filho, A. A. (2007). Dendritic spines in the posterodorsal medial amygdala after restraint stress and ageing in rats. *Neurosci. Lett.* 424, 16–21. doi: 10.1016/j.neulet.2007.07.019

Marín-Padilla, M. (2014). The mammalian neocortex new pyramidal neuron: a new conception. *Front. Neuroanat.* 7:51. doi: 10.3389/fnana.2013.00051

Martínez-García, F., Novejarque, A., and Lanuza, E. (2007). "Evolution of the amygdala in vertebrates," in *Evolution of Nervous Systems. A Comprehensive Reference*, ed. J. H. Kaas (Oxford: Elsevier), 255–334. doi: 10.1016/b0-12-370878-8/00139-7

Mattia, D., Kawasaki, H., and Avoli, M. (1997). Repetitive firing and oscillatory activity of pyramidal-like bursting neurons in the rat subiculum. *Exp. Brain Res.* 114, 507–517. doi: 10.1007/pl00005660

Mattson, M. P., Guthrie, P. B., and Kater, S. B. (1989). Intrinsic factors in the selective vulnerability of hippocampal pyramidal neurons. *Prog. Clin. Biol. Res.* 317, 333–351.

McCormick, D. A., Wang, Z., and Huguenard, J. (1993). Neurotransmitter control of neocortical neuronal activity and excitability. *Cereb. Cortex* 3, 387–398. doi: 10.1093/cercor/3.5.387

Mederos, S., González-Arias, C., and Perea, G. (2018). Astrocyte–neuron networks: a multilane highway of signaling for homeostatic brain function. *Front. Synaptic Neurosci.* 10:45. doi: 10.3389/fnsyn.2018.00045

Medina, L., and Abellán, A. (2012). "Subpallial structures," in *The Mouse Nervous System*, eds C. Watson, G. Paxinos, and L. Puelles (Cambridge, MA: Academic Press), 173–220. doi: 10.1016/b978-0-12-369497-3.10007-x

Medvedeva, Y. V., Ji, S. G., Yin, H. Z., and Weiss, J. H. (2017). Differential vulnerability of CA1 versus CA3 pyramidal neurons after ischemia: possible relationship to sources of Zn2+ accumulation and Its entry into and prolonged effects on mitochondria. *J. Neurosci.* 37, 726–737. doi: 10.1523/jneurosci.3270-16.2017

Megías, M., Emri, Z. S., Freund, T. F., and Gulyás, A. I. (2001). Total number and distribution of inhibitory and excitatory synapses on hippocampal CA1 pyramidal cells. *Neuroscience* 102, 527–540. doi: 10.1016/s0306-4522(00)00496-6

Meredith, M., and Westberry, J. M. (2004). Distinctive responses in the medial amygdala to same-species and different-species pheromones. *J. Neurosci.* 24, 5719–5725. doi: 10.1523/jneurosci.1139-04.2004

Merino-Serrais, P., Knafo, S., Alonso-Nanclares, L., Fernaud-Espinosa, I., and DeFelipe, J. (2011). Layer-specific alterations to CA1 dendritic spines in a mouse model of Alzheimer's disease. *Hippocampus* 21, 1037–1044. doi: 10.1002/hipo.20861

Mesulam, M.-M., Mufson, E. J., Levey, A. I., and Wainer, B. H. (1983). Cholinergic innervation of cortex by the basal forebrain: cytochemistry and cortical connections of the septal area, diagonal band nuclei, nucleus basalis (Substantia innominata), and hypothalamus in the rhesus monkey. *J. Comp. Neurol.* 214, 170–197. doi: 10.1002/cne.902140206

Miller, M. W., and Vogt, B. A. (1995). "The cerebral cortex," in *Neuroscience in Medicine*, ed. P. M. Conn (Philadelphia: J.B. Lippincott), 301–317.

Mizusaki, B. E. P., Li, S. S. Y., Costa, R. P., and Sjöström, P. J. (2018). Pre- and postsynaptically expressed spiking-timing-dependent plasticity contribute differentially to neuronal learning. *bioRxiv* [Preprint]. doi: 10.1101/450825

Mizuseki, K., Diba, K., Pastalkova, E., and Buzsáki, G. (2011). Hippocampal CA1 pyramidal cells form functionally distinct sublayers. *Nat. Neurosci.* 14, 1174–1181. doi: 10.1038/nn.2894

Mohan, H., Verhoog, M. B., Doreswamy, K. K., Eyal, G., Aardse, R., Lodder, B. N., et al. (2015). Dendritic and axonal architecture of individual pyramidal neurons across layers of adult human neocortex. *Cereb. Cortex* 25, 4839–4853. doi: 10.1093/cercor/bhv188

Moldwin, T., and Segev, I. (2019). Perceptron learning and classification in a modeled cortical pyramidal cell. *bioRxiv* [Preprint]. doi: 10.1101/464826

Morales, J., Benavides-Piccione, R., Dar, M., Fernaud, I., Rodríguez, A., Anton-Sanchez, L., et al. (2014). Random positions of dendritic spines in human

cerebral cortex. *J. Neurosci.* 34, 10078–10084. doi: 10.1523/jneurosci.1085-14.2014

Morishima, M., and Kawaguchi, Y. (2006). Recurrent connection patterns of corticostriatal pyramidal cells in frontal cortex. *J. Neurosci.* 26, 4394–4405. doi: 10.1523/jneurosci.0252-06.2006

Morrison, J. H., Lewis, D. A., Campbell, M. J., Huntley, G. W., Benson, D. L. I, and Bouras, C. (1987). A monoclonal antibody to non-phosphorylated neurofilament protein marks the vulnerable cortical neurons in Alzheimer's disease. *Brain Res.* 416, 331–336. doi: 10.1016/0006-8993(87)90914-0

Mountcastle, V. B. (1979). "An organizing principle for cerebral function: the unit module and the distributed system," in *The Neurosciences*, eds F. O. Schmitt and F. G. Worden (Cambridge, MA: The MIT Press), 21–42.

Mugnaini, E., and Oertel, W. H. (1985). "An atlas of the distribution of GABAergic neurons and terminals in the rat CNS as revealed by GAD immunohistochemistry," in *Handbook of Chemical Neuroanatomy*, eds A. Björklund and T. Hokfelt (New York, NY: Elsevier), 436–622.

Müllner, F. E., Wierenga, C. J., and Bonhoeffer, T. (2015). Precision of inhibition: dendritic inhibition by individual GABAergic synapses on hippocampal pyramidal cells is confined in space and time. *Neuron* 87, 576–589. doi: 10.1016/j.neuron.2015.07.003

Nakahata, Y., and Yasuda, R. (2018). Plasticity of spine structure: local signaling, translation and cytoskeletal reorganization. *Front. Synaptic Neurosci.* 10:29. doi: 10.3389/fnsyn.2018.00029

Narayanan, R. T., Udvary, D., and Oberlaender, M. (2017). Cell type-specific structural organization of the six layers in rat barrel cortex. *Front. Neuroanat.* 11:91. doi: 10.3389/fnana.2017.00091

Natsume, J., Bernasconi, N., Andermann, F., and Bernasconi, A. (2003). MRI volumetry of the thalamus in temporal, extratemporal, and idiopathic generalized epilepsy. *Neurology* 60, 1296–1300. doi: 10.1212/01.wnl.0000058764.34968.c2

Naumann, L. B., and Sprekeler, H. (2020). Presynaptic inhibition rapidly stabilises recurrent excitation in the face of plasticity. *PLoS Comput. Biol.* 16:e1008118. doi: 10.1371/journal.pcbi.1008118

Neckel, H., Quagliotto, E., Casali, K. R., Montano, N., Dal Lago, P., and Rasia-Filho, A. A. (2012). Glutamate and GABA in the medial amygdala induce selective central sympathetic/parasympathetic cardiovascular responses. *Can. J. Physiol. Pharmacol.* 90, 525–536. doi: 10.1139/y2012-024

Newman, S. W. (1999). The medial extended amygdala in male reproductive behavior. A node in the mammalian social behavior network. *Ann. N.Y. Acad. Sci.* 877, 242–257. doi: 10.1111/j.1749-6632.1999.tb09271.x

Newpher, T. M., and Ehlers, M. D. (2009). Spine microdomains for postsynaptic signaling and plasticity. *Trends Cell Biol.* 19, 218–227. doi: 10.1016/j.tcb.2009.02.004

Nieuwenhuys, R. (1994). The neocortex. An overview of its evolutionary development, structural organization and synaptology. *Anat. Embryol.* 190, 307–337.

Nieuwenhuys, R., Voogd, J., and van Huijzen, C. H. R. (1988). *The Human Central Nervous System*. Berlin: Springer-Verlag.

Noguchi, J., Nagaoka, A., Watanabe, S., Ellis-Davies, G. C., Kitamura, K., Kano, M., et al. (2011). In vivo two-photon uncaging of glutamate revealing the structure-function relationships of dendritic spines in the neocortex of adult mice. *J. Physiol.* 589, 2447–2457. doi: 10.1113/jphysiol.2011.207100

Oakley, J. C., Schwindt, P. C., and Crill, W. E. (2001). Dendritic calcium spikes in layer 5 pyramidal neurons amplify and limit transmission of ligand gated dendritic current to soma. *J. Neurophysiol.* 86, 514–527. doi: 10.1152/jn.2001.86.1.514

Oga, T., Elston, G. N., and Fujita, I. (2017). Postnatal dendritic growth and spinogenesis of layer-V pyramidal cells differ between visual, inferotemporal, and prefrontal cortex of the macaque monkey. *Front. Neurosci.* 11:118. doi: 10.3389/fnins.2017.00118

Olucha-Bordonau, F. E., Fortes-Marco, L., Otero-García, M., Lanuza, E., and Martínez-García, F. (2015). "Amygdala: structure and function," in *The Rat Nervous System*, ed. G. Paxinos (San Diego, CA: Academic Press), 441–490.

Oruro, E. M., Pardo, G. V. E., Lucion, A. B., Calcagnotto, M. E., and Idiart, M. A. P. (2019). Maturation of pyramidal cells in anterior piriform cortex may be sufficient to explain the end of early olfactory learning in rats. *Learn. Mem.* 27, 20–32. doi: 10.1101/lm.050724.119

Overk, C. R., and Masliah, E. (2014). Pathogenesis of synaptic degeneration in Alzheimer's disease and Lewy body disease. *Biochem. Pharmacol.* 88, 508–516.

Pakkenberg, B., and Gundersen, H. J. (1997). Neocortical neuron number in humans: effect of sex and age. *J. Comp. Neurol.* 384, 312–320. doi: 10.1002/(sici)1096-9861(19970728)384:2<312::aid-cne10>3.0.co;2-k

Palmqvist, S., Schöll, M., Strandberg, O., Mattsson, N., Stomrud, E., Zetterberg, H., et al. (2017). Earliest accumulation of β-amyloid occurs within the default-mode network and concurrently affects brain connectivity. *Nat. Commun.* 8:1214. doi: 10.1038/s41467-017-01150-x

Palomero-Gallagher, N., and Zilles, K. (2017). Cortical layers: Cyto-, myelo-, receptor- and synaptic architecture in human cortical areas. *NeuroImage* 197, 716–741. doi: 10.1016/j.neuroimage.2017.08.035

Pandya, D. N., Seltzer, B., Petrides, M., and Cipolloni, P. B. (2015). *Cerebral Cortex – Architecture, Connections, and the Dual Origin Concept*. New York, NY: Oxford University Press.

Papoutsi, A., Kastellakis, G., Psarrou, M., Anastasakis, S., and Poirazi, P. (2014). Coding and decoding with dendrites. *J. Physiol.* 108, 18–27. doi: 10.1016/j.jphysparis.2013.05.003

Park, I., Kim, H. J., Kim, Y., Hwang, H. S., Kasai, H., Kim, J.-H., et al. (2019). Nanoscale imaging reveals miRNA-mediated control of functional states of dendritic spines. *Proc. Natl. Acad. Sci. U.S.A.* 116, 9616–9621. doi: 10.1073/pnas.1819374116

Peçanha, M. A. P., and Neri, V. C. (2007). Estudo neuropatológico e funcional da doença de Alzheimer. *Rev. Cient. FMC* 2, 8–17.

Penzes, P., Cahill, M. E., Jones, K. A., VanLeeuwen, J.-E., and Woolfrey, K. M. (2011). Dendritic spine pathology in neuropsychiatric disorders. *Nat. Neurosci.* 14, 285–293. doi: 10.1038/nn.2741

Persinger, M. A., and Koren, S. A. (2007). A theory of neurophysics and quantum neuroscience: implications for brain function and the limits of consciousness. *Int. J. Neurosci.* 117, 157–175. doi: 10.1080/00207450500535784

Petanjek, Z., Judas, M., Kostoviæ, I., and Uylings, H. B. M. (2008). Lifespan alterations of basal dendritic trees of pyramidal neurons in the human prefrontal cortex: a layer-specific pattern. *Cereb. Cortex* 18, 915–929. doi: 10.1093/cercor/bhm124

Petanjek, Z., Judaš, M., Šimic, G., Rasin, M. R., Uylings, H. B., Rakic, P., et al. (2011). Extraordinary neoteny of synaptic spines in the human prefrontal cortex. *Proc. Natl. Acad. Sci. U.S.A.* 108, 13281–13286. doi: 10.1073/pnas.1105108108

Petanjek, Z., Sedmak, D., Džaja, D., Hladnik, A., Rašin, M. R., and Jovanov-Milosevic, N. (2019). The protracted maturation of associative layer IIIC pyramidal neurons in the human prefrontal cortex during childhood: a major role in cognitive development and selective alteration in autism. *Front. Psychiatry* 14:122. doi: 10.3389/fpsyt.2019.00122

Peters, A., and Jones, E. G. (1984). "Classification of cortical neurons," in *Cerebral Cortex. Functional Properties of Cortical Cells*, eds A. Peters and E. G. Jones (New York, NY: Plenum Press), 107–121.

Peters, A., Palay, S. L., and Webster, H. (1991). *The Fine Structure of the Nervous System*. New York, NY: Oxford University Press.

Petralia, R. S., Wang, Y. X., Mattson, M. P., and Yao, P. J. (2018). Invaginating structures in mammalian synapses. *Front. Synaptic Neurosci.* 10:4. doi: 10.3389/fnsyn.2018.00004

Petrovich, G. D., Canteras, N. S., and Swanson, L. W. (2001). Combinatorial amygdalar inputs to hippocampal domains and hypothalamic behavior systems. *Brain Res. Rev.* 38, 247–289. doi: 10.1016/s0165-0173(01)00080-7

Petrulis, A. (2020). "Structure and function of the medial amygdala," in *Handbook of Behavioral Neuroscience*, eds J. H. Urban and J. A. Rosenkranz (Amsterdam: Elsevier), 39–61. doi: 10.1016/b978-0-12-815134-1.00002-7

Petrulis, A., Fiber, J. M., and Swann, J. M. (2017). "The medial amygdala, hormones, pheromones, social behavior network, and mating behavior," in *Hormones, Brain and Behavior*, 3rd Edn, eds D. W. Pfaff and M. Joëls (Cambridge, MA: Academic Press), 329–343. doi: 10.1016/b978-0-12-803592-4.00011-0

Pierri, J. N., Volk, C. L. E., Auh, S., Sampson, A., and Lewis, D. A. (2003). Somal size of prefrontal cortical pyramidal neurons in schizophrenia: differential effects across neuronal subpopulations. *Biol. Psychol.* 54, 111–120. doi: 10.1016/s0006-3223(03)00294-4

Pro-Sistiaga, P., Mohedano-Moriano, A., Ubeda-Bañon, I., Arroio-Jimenez, M. D. M., and Marcos, P. (2007). Convergence of olfactory and vomeronasal

projections in the rat basal telencephalon. *J. Comp. Neurol.* 504, 346–362. doi: 10.1002/cne.21455

Quirk, G. J., Repa, C., and LeDoux, J. E. (1995). Fear conditioning enhances short-latency auditory responses of lateral amygdala neurons: parallel recordings in the freely behaving rat. *Neuron* 15, 1029–1039. doi: 10.1016/0896-6273(95)90092-6

Radler, M. R., Suber, A., and Spiliotis, E. T. (2020). Spatial control of membrane traffic in neuronal dendrites. *Mol. Cell. Neurosci.* 105:103492. doi: 10.1016/j.mcn.2020.103492

Ramaswamy, S., and Markram, H. (2015). Anatomy and physiology of the thick-tufted layer 5 pyramidal neuron. *Front. Cell. Neurosci.* 9:233. doi: 10.3389/fncel.2015.00233

Ramón y Cajal, S. (1894a). The cronian lecture: la fine structure des centres nerveux. *Proc. Royal Soc. Lond.* 55, 444–468. doi: 10.1098/rspl.1894.0063

Ramón y Cajal, S. (1894b). *New Ideas on the Structure of the Nervous System in Man and Vertebrates*. Paris: Reinwald & Cie.

Ramón y Cajal, S. (1909–1911). *Histologie Du Système Nerveux De l'Homme Et Des Vertebrés*. Paris: Maloine.

Rasia-Filho, A. A., Andrejew, R., and Belló-Klein, A. (2018). "Integrating concepts of resilience from cellular functioning to human behavior," in *Amygdala: Mechanisms, Structure and Role in Disease,* ed. A. Manu (Hauppauge: Nova Science Publishers), 1–30.

Rasia-Filho, A. A., Dalpian, F., Menezes, I. C., Brusco, J., Moreira, J. E., and Cohen, R. S. (2012a). Dendritic spines of the medial amygdala: plasticity, density, shape, and subcellular modulation by sex steroids. *Histol. Histopathol.* 8, 985–1011.

Rasia-Filho, A. A., Haas, D., de Oliveira, A. P., de Castilhos, J., Frey, R., Stein, D., et al. (2012b). Morphological and functional features of the sex steroid-responsive posterodorsal medial amygdala of adult rats. *Mini Rev. Med. Chem.* 12, 1090–1106. doi: 10.2174/138955712802762211

Rasia-Filho, A. A., Londero, R. G., and Achaval, M. (2000). Functional activities of the amygdala: an overview. *J. Psychiatry Neurosci.* 25, 14–23.

Reberger, R., Dall'Oglio, A., Jung, C. R., and Rasia-Filho, A. A. (2018). Structure and diversity of human dendritic spines evidenced by a new three-dimensional reconstruction procedure for Golgi staining and light microscopy. *J. Neurosci. Methods* 293, 27–36. doi: 10.1016/j.jneumeth.2017.09.001

Remy, S., Beck, H., and Yaari, Y. (2010). Plasticity of voltage-gated ion channels in pyramidal cell dendrites. *Curr. Opin. Neurobiol.* 20, 503–509. doi: 10.1016/j.conb.2010.06.006

Rochefort, N. L., and Konnerth, A. (2012). Dendritic spines: from structure to in vivo function. *EMBO Rep.* 13, 699–708. doi: 10.1038/embor.2012.102

Rockland, K. S. (2010). Five points on columns. *Front. Neuroanat.* 4:22. doi: 10.3389/fnana.2010.00022

Rockland, K. S. (2020). What we can learn from the complex architecture of single axons. *Brain Struct. Funct.* 225, 1327–1347. doi: 10.1007/s00429-019-02023-3

Rodriguez-Romaguera, J., Ung, R. L., Nomura, H., Otis, J. M., Basiri, M. L., Namboodiri, V. M. K., et al. (2020). Prepronociceptin-expressing neurons in the extended amygdala encode and promote rapid arousal responses to motivationally salient stimuli. *Cell Rep.* 33:108362. doi: 10.1016/j.celrep.2020.108362

Rollenhagen, A., and Lübke, J. H. R. (2016). "Dendritic elaboration: morphology and chemistry," in *Neuroscience in the 21st Century*, eds D. Pfaff and N. Volkow (New York: Springer), 225–264. doi: 10.1007/978-1-4939-3474-4_11

Rutishauser, U., Mamelak, A. N., and Adolphs, R. (2015). The primate amygdala in social perception – insights from electrophysiological recordings and stimulation. *Trends Neurosci.* 38, 295–306. doi: 10.1016/j.tins.2015.03.001

Rutishauser, U., Tudusciuc, O., Neumann, D., Mamelak, A. N., Heller, A. C., Ross, I. B., et al. (2011). Single-unit responses selective for whole faces in the human amygdala. *Curr. Biol.* 21, 1654–1660. doi: 10.1016/j.cub.2011.08.035

Rutishauser, U., Tudusciuc, O., Wang, S., Mamelak Adam, N., Ross Ian, B., and Adolphs, R. (2013). Single-neuron correlates of atypical face processing in autism. *Neuron* 80, 887–899. doi: 10.1016/j.neuron.2013.08.029

Sanabria, E. R. G., Su, H., and Yaari, Y. (2001). Initiation of network bursts by Ca2- dependent intrinsic bursting in the rat pilocarpine model of temporal lobe epilepsy. *J. Physiol.* 532, 205–216. doi: 10.1111/j.1469-7793.2001.0205g.x

Saper, C. B., and Chelimsky, T. C. (1984). A cytoarchitectonic and histochemical study of nucleus basalis and associated cell groups in the normal human brain. *Neuroscience* 13, 1023–1037. doi: 10.1016/0306-4522(84)90286-0

Schmidt, M. L., Martin, J. A., Lee, V. M.-Y., and Trojanowski, J. Q. (1996). Convergence of Lewy bodies and neurobrillary tangles in amygdala neurons of Alzheimer's disease and Lewy body disorders. *Acta Neuropathol.* 91, 475–481.

Scholtens, L. H., Schmidt, R., de Reus, M. A., and van den Heuvel, M. P. (2014). Linking macroscale graph analytical organization to microscale neuroarchitectonics in the macaque connectome. *J. Neurosci.* 34, 12192–12205. doi: 10.1523/jneurosci.0752-14.2014

Schumann, C. M., and Amaral, D. G. (2005). Stereologial estimation of the number of neurons in the human amygdaloid complex. *J. Comp. Neurol.* 491, 320–329. doi: 10.1002/cne.20704

Schumann, C. M., Bauman, M. D., and Amaral, D. G. (2011). Abnormal structure or function of the amygdala is a common component of neurodevelopmental disorders. *Neuropsychologia* 49, 745–759. doi: 10.1016/j.neuropsychologia.2010.09.028

Scorza, C. A., Araujo, B. H., Leite, L. A., Torres, L. B., Otalora, L. F. P., Oliveira, M. S., et al. (2011). Morphological and electrophysiological properties of pyramidal-like neurons in the stratum oriens of Cornu ammonis 1 and Cornu ammonis 2 area of Proechimys. *Neuroscience* 177, 252–268. doi: 10.1016/j.neuroscience.2010.12.054

Searle, J. R. (1997). *The Mystery of Consciousness*. New York, NY: NYREV.

Sedmak, D., Hrvoj-Mihiæ, B., Džaja, D., Habek, N., Uylings, H. B. M., and Petanjek, Z. (2018). Biphasic dendritic growth of dorsolateral prefrontal cortex associative neurons and early cognitive development. *Croat. Med. J.* 59, 189–202. doi: 10.3325/cmj.2018.59.189

Segal, M. (2010). Dendritic spines, synaptic plasticity and neuronal survival: activity shapes dendritic spines to enhance neuronal viability. *Eur. J. Neurosci.* 31, 2178–2184. doi: 10.1111/j.1460-9568.2010.07270.x

Segev, I., Rinzel, J., and Shepherd, G. M. (1995). *The Theoretical Foundation of Dendritic Function*. Cambridge: The MIT Press.

Semah, F., Picot, M. C., Adam, C., Broglin, D., Arzimanoglou, A., Bazin, B., et al. (1998). Is the underlying cause of epilepsy a major prognostic factor for recurrence? *Neurology* 51, 1256–1262. doi: 10.1212/wnl.51.5.1256

Serrano-Pozo, A., Frosch, M. P., Masliah, E., and Hyman, B. T. (2011). Neuropathological alterations in Alzheimer disease. *Cold Spring Harb. Perspect. Med.* 1:a006189. doi: 10.1101/cshperspect.a006189

Shepherd, G. M. (1996). The dendritic spine: a multifunctional integrative unit. *J. Neurophysiol.* 75, 2197–2210. doi: 10.1152/jn.1996.75.6.2197

Sheppard, P. A. S., Choleris, E., and Galea, L. A. M. (2019). Structural plasticity of the hippocampus in response to estrogens in female rodents. *Mol. Brain* 12:22. doi: 10.1186/s13041-019-0442-7

Sims, K. S., and Williams, R. S. (1990). The human amygdaloid complex: a cytologic and histochemical atlas using Nissl, myelin, acetylcholinesterase and nicotinamide adenine dinucleotide phosphate diaphorase staining. *Neuroscience* 2, 449–472. doi: 10.1016/0306-4522(90)90440-f

Smith, B. N., and Dudek, F. E. (1997). Enhanced population responses in the basolateral amygdala of kainate-treated, epileptic rats in vitro. *Neurosci. Lett.* 222, 1–4. doi: 10.1016/s0304-3940(97)13326-2

Soltesz, I., and Losonczy, A. (2018). CA1 pyramidal cell diversity enabling parallel information processing in the hippocampus. *Nat. Neurosci.* 21, 484–493. doi: 10.1038/s41593-018-0118-0

Somogyi, P., Tamás, G., Lujan, R., and Buhl, E. H. (1998). Salient features of synaptic organisation in the cerebral cortex. *Brain Res. Rev.* 26, 113–135. doi: 10.1016/s0165-0173(97)00061-1

Soper, C., Wicker, E., Kulick, C. V., N'Gouemo, P., and Forcelli, P. A. (2016). Optogenetic activation of superior colliculus neurons suppresses seizures originating in diverse brain networks. *Neurobiol. Dis.* 87, 102–115. doi: 10.1016/j.nbd.2015.12.012

Sorvari, H., Miettinen, R., Soininen, H., and Pitkänen, A. (1996). Parvalbumin-immunoreactive neurons make inhibitory synapses on pyramidal cells in the human amygdala: a light and electron microscopic study. *Neurosci. Lett.* 217, 93–96. doi: 10.1016/0304-3940(96)13067-6

Spruston, N. (2008). Pyramidal neurons: dendritic structure and synaptic integration. *Nat. Rev. Neurosci.* 9, 206–221. doi: 10.1038/nrn2286

Spruston, N., Häusser, M., and Stuart, G. (2013). "Information processing in dendrites and spines," in *Fundamental Neuroscience*, eds L. R. Squire, D. Berg, F. E. Bloom, S. du Lac, A. Ghosh, and N. C. Spitzer (Waltham: Academic Press), 231–260. doi: 10.1016/b978-0-12-385870-2.00011-1

Steger, R., Ramos, R. L., Cao, R., Yang, Q., Chen, C.-C., Dominici, J., et al. (2013). Physiology and morphology of inverted pyramidal neurons in the rodent neocortex. *Neuroscience* 248, 165–179. doi: 10.1016/j.neuroscience.2013.06.004

Stephan, H., Frahm, H. D., and Baron, G. (1987). Comparison of brain structure volumes in insectivores and primates. VII. Amygdaloid components. *J. Hirnforsch* 28, 571–584.

Stewart, M. G., Popov, V. I., Kraev, I. V., Medvedev, N., and Davies, H. A. (2014). "Structure and complexity of the synapse and dendritic spine," in *The Synapse*, eds V. Pickel and M. Segal (New York, NY: Academic Press), 1–20. doi: 10.1016/b978-0-12-418675-0.00001-8

Sutula, T., He, X., Cavazos, J., and Scott, G. (1988). Synaptic reorganization in the hippocampus induced by abnormal functional activity. *Science* 239, 1147–1150. doi: 10.1126/science.2449733

Swann, J. W., Al-Noori, S., Jiang, M., and Lee, C. L. (2000). Spine loss and other dendritic abnormalities in epilepsy. *Hippocampus* 10, 617–625. doi: 10.1002/1098-1063(2000)10:5<617::aid-hipo13>3.0.co;2-r

Swanson, L., and Petrovich, G. (1998). What is the amygdala? *Trends Neurosci.* 21, 323–331. doi: 10.1016/s0166-2236(98)01265-x

Szentágothai, J. (1978). The neuron network of the cerebral cortex: a functional interpretation. *Proc. R. Soc. Lond. B* 201, 219–248. doi: 10.1098/rspb.1978.0043

Takeda, A., Nakajima, S., Fuke, S., Sakurada, N., Minami, A., and Oku, N. (2006). Zinc release from Schaffer collaterals and its significance. *Brain Res. Bull.* 68, 442–447. doi: 10.1016/j.brainresbull.2005.10.001

Tasker, J. G., Peacock, W. J., and Dudek, F. E. (1992). Local synaptic circuits and epileptiform activity in slices of neocortex from children with intractable epilepsy. *J. Neurophysiol.* 67, 496–507. doi: 10.1152/jn.1992.67.3.496

Téllez-Zenteno, J. F., and Hernández-Ronquillo, L. (2012). A review of the epidemiology of temporal lobe epilepsy. *Epilepsy Res. Treat.* 2012:630853. doi: 10.1155/2012/630853

Thompson, C. L., Pathak, S. D., Jeromin, A., Ng, L. L., MacPherson, C. R., Mortrud, M. T., et al. (2008). Genomic anatomy of the hippocampus. *Neuron* 60, 1010–1021.

Thompson, P. M., Mega, M. S., Woods, R. P., Zoumalan, C. I., and Lindshield, C. J. (2001). Cortical change in Alzheimer's disease detected with a disease-specific population-based brain atlas. *Cereb. Cortex* 11, 1–16.

Toharia, P., Robles, O. D., Fernaud-Espinosa, I., Makarova, J., Galindo, S. E., Rodriguez, A., et al. (2016). PyramidalExplorer: a new interactive tool to explore morpho-functional relations of human pyramidal neurons. *Front. Neuroanat.* 9:159. doi: 10.3389/fnana.2015.00159

Toni, N., Buchs, P. A., Nikonenko, I., Bron, C. R., and Muller, D. (1999). LTP promotes formation of multiple spine synapses between a single axon terminal and a dendrite. *Nature* 402, 421–425. doi: 10.1038/46574

Tønnesen, J., and Nägerl, V. (2016). Dendritic spines as tunable regulators of synaptic signals. *Front. Psych.* 7:101. doi: 10.3389/fpsyt.2016.00101

Tran-Van-Minh, A., Cazé, R. D., Abrahamsson, T., Cathala, L., Gutkin, B. S., and DiGregorio, D. A. (2015). Contribution of sublinear and supralinear dendritic integration to neuronal computations. *Front. Cell Neurosci.* 9:67. doi: 10.3389/fncel.2015.00067

Valverde, F., De Carlos, J. A., and López-Mascaraque, L. (2002). "The cerebral cortex of mammals: diversity within unity," in *Cortical Areas: Unity and Diversity*, eds A. Schüz and R. Miller (London: Taylor & Francis), 195–217. doi: 10.1201/9780203299296.pt3

van der Zee, E. A. (2015). Synapses, spines and kinases in mammalian learning and memory, and the impact of aging. *Neurosci. Biobehav. Rev.* 50, 77–85. doi: 10.1016/j.neubiorev.2014.06.012

Vásquez, C. E., Reberger, R., Dall'Oglio, A., Calcagnotto, M. E., and Rasia-Filho, A. A. (2018). Neuronal types of the human cortical amygdaloid nucleus. *J. Comp. Neurol.* 526, 2776–2801. doi: 10.1002/cne.24527

Verzi, D. W., and Noris, O. Y. (2009). A compartmental model for activity-dependent dendritic spine branching. *Bull. Math. Biol.* 71, 1048–1072. doi: 10.1007/s11538-009-9393-y

Vismer, M. S., Forcelli, P. A., Skopin, M. D., Gale, K., and Koubeissi, M. Z. (2015). The piriform, perirhinal, and entorhinal cortex in seizure generation. *Front. Neural Circuits* 9:27. doi: 10.3389/fncir.2015.00027

Vogt, B. A. (2015). "Mapping cingulate subregions," in *Brain Mapping: An Encyclopedic Reference*, ed. A. W. Toga (Oxford: Academic Press), 325–339. doi: 10.1016/b978-0-12-397025-1.00230-x

Vogt, C., and Vogt, O. (1922). Erkrankungen der grosshirnrinde im lichte der topistik, pathoklise und pathoarchitektonik. *J. Psychol. Neurol.* 28, 9–171.

von Bartheld, C. S., Bahney, J., and Herculano-Houzel, S. (2016). The search for true numbers of neurons and glial cells in the human brain: a review of 150 years of cell counting. *J. Comp. Neurol.* 524, 3865–3895. doi: 10.1002/cne.24040

von Economo, C. (1927). *Cellular Structure of the Human Cerebral Cortex, translated and ed. L.Z. Triarhou*. Basel: Karger.

Vossel, K. A., Ranasinghe, K. G., Beagle, A. J., Mizuiri, D., Honma, S. M., Dowling, A. F., et al. (2016). Incidence and impact of subclinical epileptiform activity in Alzheimer's disease. *Ann. Neurol.* 80, 858–870. doi: 10.1002/ana.24794

Wang, C., Zhang, F., Jiang, S., Siedlak, S. L., Shen, L., Perry, G., et al. (2016). Estrogen receptor-α is localized to neurofibrillary tangles in Alzheimer's disease. *Sci. Rep.* 6:20352. doi: 10.1038/srep20352

Wang, S., Tudusciuc, O., Mamelak, A. N., Ross, I. B., Adolphs, R., and Rutishauser, U. (2014). Neurons in the human amygdala selective for perceived emotion. *Proc. Natl. Acad. Sci. U.S.A.* 111, E3110–E3119.

Wang, Y., Ye, M., Kuang, X., Li, Y., and Hu, S. (2018). A simplified morphological classification scheme for pyramidal cells in six layers of primary somatosensory cortex of juvenile rats. *IBRO Rep.* 5, 74–90. doi: 10.1016/j.ibror.2018.10.001

West, M. J., and Gundersen, H. J. (1990). Unbiased stereological estimation of the number of neurons in the human hippocampus. *J. Comp. Neurol.* 296, 1–22. doi: 10.1002/cne.902960102

Wicker, E., Beck, V. C., Kulick-Soper, C., Kulick-Soper, C. V., Hyder, S. K., Campos-Rodriguez, C., et al. (2019). Descending projections from the substantia nigra pars reticulata differentially control seizures. *Proc. Natl. Acad. Sci. U.S.A.* 116, 27084–27094.

Wicker, E., and Forcelli, P. A. (2016). Chemogenetic silencing of the midline and intralaminar thalamus blocks amygdala-kindled seizures. *Exp. Neurol.* 283(Pt A), 404–412. doi: 10.1016/j.expneurol.2016.07.003

Wiebe, S. (2000). Epidemiology of temporal lobe epilepsy. *Can. J. Neurol. Sci.* 27, S6–S10.

Wittner, L., Eross, L., Czirják, S., Halász, P., Freund, T. F., and Maglóczky, Z. (2005). Surviving CA1 pyramidal cells receive intact perisomatic inhibitory input in the human epileptic hippocampus. *Brain* 128, 138–152. doi: 10.1093/brain/awh339

Wittner, L., Eross, L., Szabó, Z., Tóth, S., Czirják, S., Halász, P., et al. (2002). Synaptic reorganization of calbindin-positive neurons in the human hippocampal CA1 region in temporal lobe epilepsy. *Neuroscience* 115, 961–978. doi: 10.1016/s0306-4522(02)00264-6

Wittner, L., Huberfeld, G., Clémenceau, S., Eross, L., Dezamis, E., Entz, L., et al. (2009). The epileptic human hippocampal cornu ammonis 2 region generates spontaneous interictal-like activity in vitro. *Brain* 132, 3032–3046. doi: 10.1093/brain/awp238

Wittner, L., and Maglóczky, Z. (2017). Synaptic reorganization of the perisomatic inhibitory network in hippocampi of temporal lobe epileptic patients. *Biomed. Res. Int.* 2017:7154295. doi: 10.1155/2017/7154295

Woolfrey, K. M., and Srivastava, D. P. (2016). Control of dendritic spine morphological and functional plasticity by small GTPases. *Neural Plast.* 2016:3025948. doi: 10.1155/2016/3025948

Woolley, C. S., Gould, E., Frankfurt, M., and McEwen, B. S. (1990). Naturally occurring fluctuation in dendritic spine density on adult hippocampal pyramidal neurons. *J. Neurosci.* 10, 4035–4039. doi: 10.1523/jneurosci.10-12-04035.1990

Wozny, C., Knopp, A., Lehmann, T. N., Heinemann, U., and Behr, J. (2005). The subiculum: a potential site of ictogenesis in human temporal lobe epilepsy. *Epilepsia* 46(Suppl. 5), 17–21. doi: 10.1111/j.1528-1167.2005.01066.x

Writing Committee for the Attention-Deficit/Hyperactivity Disorder, Autism Spectrum Disorder, Bipolar Disorder, Major Depressive Disorder, Obsessive-Compulsive Disorder, Schizophrenia Enigma Working Groups, et al. (2020). Virtual histology of cortical thickness and shared neurobiology in 6 psychiatric disorders. *JAMA Psychol.* 2020:e202694. doi: 10.1001/jamapsychiatry.2020.2694

Wyss, J. M., and van Groen, T. (1995). "The limbic system," in *Neuroscience in Medicine*, ed. P. M. Conn (Philadelphia: J.B. Lippincott), 321–337.

Yaari, Y., and Beck, H. (2009). Pyramidal cells: intrinsic plasticity of hippocampal CA1 pyramidal cells and its relevance to epileptic discharge and epileptogenesis.

Encyclopedia Basic Epilepsy Res. 9, 1272–1277. doi: 10.1016/B978-012373961-2.00218-6

Yaari, Y., Yue, C., and Su, H. (2007). Recruitment of apical dendritic T-type Ca2+ channels by backpropagating spikes underlies de novo intrinsic bursting in hippocampal epileptogenesis. *J. Physiol.* 580, 435–450. doi: 10.1113/jphysiol.2007.127670

Yadav, A., Gao, Y. Z., Rodriguez, A., Dickstein, D. L., Wearne, S. L., Luebke, J. I., et al. (2012). Morphologic evidence for spatially clustered spines in apical dendrites of monkey neocortical pyramidal cells. *J. Comp. Neurol.* 520, 2888–2902. doi: 10.1002/cne.23070

Yagishita, S., Hayashi-Takagi, A., Ellis-Davies, G. C. R., Urakubo, H., Ishii, S., and Kasai, H. (2014). A critical time window for dopamine actions on the structural plasticity of dendritic spines. *Science* 345, 1616–1620. doi: 10.1126/science.1255514

Yague, J. G., Azcoitia, I., DeFelipe, J., Garcia-Segura, L. M., and Muñoz, A. (2010). Aromatase expression in the normal and epileptic human hippocampus. *Brain Res.* 1315, 41–52. doi: 10.1016/j.brainres.2009.09.111

Yan, L., Liu, C. Y., Wong, K.-P., Huang, S.-C., Mack, W. J., Jann, K., et al. (2018). Regional association of pCASL-MRI with FDG-PET and PiB-PET in people at risk for autosomal dominant Alzheimer's disease. *Neuroimage Clin.* 17, 751–760. doi: 10.1016/j.nicl.2017.12.003

Yang, L., Yang, Y., Yuan, J., Sun, Y., Dai, J., and Su, B. (2019). Transcriptomic landscape of von Economo neurons in human anterior cingulate cortex revealed by microdissected-cell RNA sequencing. *Cereb. Cortex* 29, 838–851. doi: 10.1093/cercor/bhy286

Yudofsky, S. C., and Hales, R. E. (2004). *Essentials of Neuropsychiatry and Clinical Neurosciences*. Arlington: American Psychiatric Publishing.

Yuste, R. (2013). Electrical compartmentalization in dendritic spines. *Ann. Rev. Neurosci.* 36, 429–449. doi: 10.1146/annurev-neuro-062111-150455

Zancan, M., da Cunha, R. S. R., Schroeder, F., Xavier, L. L., and Rasia-Filho, A. A. (2018). Remodeling of the number and structure of dendritic spines in the medial amygdala: from prepubertal sexual dimorphism to puberty and effect of sexual experience in male rats. *Eur. J Neurosci.* 48, 1851–1865. doi: 10.1111/ejn.14052

Zeng, H. (2020). *"Understanding Brain Cell Type Diversity", Webinar: The Future of Brain Health Research, Allen Institute for Brain Science*. Available online at: https://youtu.be/__wCIrvKiUw (accessed October 10, 2020).

Zheng, J., Anderson, K. L., Leal, S. L., Shestyuk, A., Gulsen, G., Mnatsakanyan, L., et al. (2017). Amygdala-hippocampal dynamics during salient information processing. *Nat. Commun.* 8:14413. doi: 10.1038/ncomms14413

Conflict of Interest: The authors declare that the research was conducted in the absence of any commercial or financial relationships that could be construed as a potential conflict of interest.

frontiers in Synaptic Neuroscience

ORIGINAL RESEARCH
published: 11 August 2021
doi: 10.3389/fnsyn.2021.703621

A Multisubcellular Compartment Model of AMPA Receptor Trafficking for Neuromodulation of Hebbian Synaptic Plasticity

Stefan Mihalas[1], *Alvaro Ardiles*[2,3], *Kaiwen He*[4], *Adrian Palacios*[2] *and Alfredo Kirkwood*[4]*

[1] Allen Institute for Brain Science, Seattle, WA, United States, [2] Centro Interdisciplinario de Neurociencia de Valparaíso, Facultad de Ciencias, Universidad de Valparaíso, Valparaíso, Chile, [3] Centro de Neurología Traslacional, Facultad de Medicina, Universidad de Valparaíso, Valparaíso, Chile, [4] Mind Brain Institute, Johns Hopkins University, Baltimore, MD, United States

Neuromodulation can profoundly impact the gain and polarity of postsynaptic changes in Hebbian synaptic plasticity. An emerging pattern observed in multiple central synapses is a pull–push type of control in which activation of receptors coupled to the G-protein Gs promote long-term potentiation (LTP) at the expense of long-term depression (LTD), whereas receptors coupled to Gq promote LTD at the expense of LTP. Notably, coactivation of both Gs- and Gq-coupled receptors enhances the gain of both LTP and LTD. To account for these observations, we propose a simple kinetic model in which AMPA receptors (AMPARs) are trafficked between multiple subcompartments in and around the postsynaptic spine. In the model AMPARs in the postsynaptic density compartment (PSD) are the primary contributors to synaptic conductance. During LTP induction, AMPARs are trafficked to the PSD primarily from a relatively small perisynaptic (peri-PSD) compartment. Gs-coupled receptors promote LTP by replenishing peri-PSD through increased AMPAR exocytosis from a pool of endocytic AMPAR. During LTD induction AMPARs are trafficked in the reverse direction, from the PSD to the peri-PSD compartment, and Gq-coupled receptors promote LTD by clearing the peri-PSD compartment through increased AMPAR endocytosis. We claim that the model not only captures essential features of the pull–push neuromodulation of synaptic plasticity, but it is also consistent with other actions of neuromodulators observed in slice experiments and is compatible with the current understanding of AMPAR trafficking.

Keywords: G-protein coupled receptor, pull-push, long-term potentiation, long-term depression, cortex

Edited by:
P. Jesper Sjöström, McGill University, Canada

Reviewed by:
Mohiuddin Ahmad, University of Oklahoma Health Sciences Center, United States
Jason D. Shepherd, The University of Utah, United States

***Correspondence:**
Alfredo Kirkwood
kirkwood@jhu.edu

Received: *30 April 2021*
Accepted: *05 July 2021*
Published: *11 August 2021*

Citation:
Mihalas S, Ardiles A, He K, Palacios A and Kirkwood A (2021) A Multisubcellular Compartment Model of AMPA Receptor Trafficking for Neuromodulation of Hebbian Synaptic Plasticity. Front. Synaptic Neurosci. 13:703621. doi: 10.3389/fnsyn.2021.703621

INTRODUCTION

Organisms learn about their environment from experiences that are rewarding, aversive, or salient. At an elementary level, learning is thought to result from changes in the strength of specific synaptic connections, changes which in most cases are determined by local patterns of neural activity in a Hebbian manner, which is long-term potentiation (LTP) when pre-synaptic and post-synaptic activities correlate; and long-term depression (LTD) when they do not correlate (Malenka and Nicoll, 1999; Malenka and Bear, 2004). These local synaptic changes, in turn, are subordinated to global behavioral states somehow via the action of the long-range and diffusely

projecting monoaminergic and cholinergic neuromodulatory systems. Hence, understanding the neuromodulation of Hebbian plasticity is central to understanding the mechanisms of learning.

Neuromodulators can activate multiple G-protein coupled receptors (GPCRs) to affect Hebbian plasticity in multiple ways. Hebbian plasticity is initiated by the intracellular Ca^{2+} signal that ensues the activation of postsynaptic NMDA-receptors and/or metabotropic glutamate receptors (mGluRs) and voltage-gated Ca^{2+}channels. When the magnitude of this Ca^{2+}signal exceeds a certain LTD-threshold, it selectively activates phosphatases that promote the removal of AMPA receptors (AMPAR) out of the synapse, and when it exceeds a larger LTP-threshold the Ca^{2+} signal promotes the activation of kinases and the incorporation of AMPARs into the synapse (Malenka and Nicoll, 1999; Shouval et al., 2002; Malenka and Bear, 2004). A wealth of studies has reported that neuromodulators affect this Ca^{2+} signal directly by acting on NMDARs for example, or indirectly by modulating cellular and/or circuit excitability (Faber et al., 2008; Pawlak et al., 2010; Tritsch and Sabatini, 2012; Edelmann and Lessmann, 2013; Meunier et al., 2017; Bari et al., 2020; Fernandez de Sevilla et al., 2021; Lutzu and Castillo, 2021). On the other hand, multiple mechanisms for the expression of NMDA-dependent Hebbian plasticity have been identified. These include the direct exchange of AMPAR between the synapse and internal compartments via exocytosis in LTP, for example (Lledo et al., 1998; Ahmad et al., 2012; Wu et al., 2017), changes in AMPAR unitary conductance (Park et al., 2021), and lateral diffusion of surface AMPARs and their trapping at postsynaptic density compartment (PSD) site, in case of LTP, and their release from the PSD, in the case of LTD (Oh et al., 2006; Derkach et al., 2007; Makino and Malinow, 2009; Newpher and Ehlers, 2009; Choquet, 2018; Diering and Huganir, 2018). These are complex processes that involve AMPAR phosphorylation at specific sites, interactions with multiple synaptic proteins, and possibly transient insertion of calcium-permeable AMPARs (Nicoll, 2017; Buonarati et al., 2019; Purkey and Dell'Acqua, 2020). The recruitment of these mechanisms in different synapses likely varies depending on experimental conditions like the induction protocols used. Hence, like the role of transient insertion of calcium-permeable AMPARs, the contribution of these mechanisms to LTP/D expression is still under debate. In consequence, although neuromodulation also occurs at this stage (Huang et al., 2012), the exact mechanisms are less understood than in the case of neuromodulation of the induction of plasticity.

Despite the diverse receptor targets of neuromodulators, results from several studies are roughly consistent with a simple rule, which is the pull–push regulation of LTP and LTD by receptors coupled to the G-proteins Gs and Gq. According to this rule, Gs-coupled receptors like the D1- dopaminergic receptor or the β-adrenoreceptor, which stimulate cAMP production, tend to promote LTP, but often at the expense of LTD (Thomas et al., 1996; Katsuki et al., 1997; Mockett et al., 2007; Seol et al., 2007; Lin et al., 2008; Huang et al., 2012; Nguyen and Gelinas, 2018; Brzosko et al., 2019). Conversely, Gq-coupled receptors that stimulate the phospholipase C cascade, like the α1-adrenoreceptor or the M1 cholinergic receptor, tend to promote LTD at the expense of LTP (Choi et al., 2005; Seol et al., 2007; Takamatsu et al., 2008; Huang et al., 2012; Hulme et al., 2012). In a previous study examining this pull–push regulation, we showed that it occurs at the level of the expression of plasticity. We also observed that while Gs-coupled receptors inhibit LTD and Gq-coupled receptors inhibit LTP when stimulated individually, and when acting together, they enhance the gain of both LTP and LTD (Seol et al., 2007; Huang et al., 2012). To account for these intriguing interactions between GPCRs, we propose a simple kinetic model in which AMPAR are trafficked in and out of the synapse through perisynaptic (peri-PSD) compartments of limited size (which models the presence of a limited amount of structural anchoring proteins). In the model, the expression of LTP and LTD is limited by the occupancy of AMPARs at the small perisynaptic compartments. GPCRs, in turn, regulate the LTP/D expression by controlling the filling of these perisynaptic compartments. We surmise that the described model captures several essential features of the data observed in the visual cortex and its application could be extended to neuromodulation in other structures.

RESULTS

The trafficking model for the pull–push neuromodulation of Hebbian plasticity is illustrated in **Figure 1**. Essentially, it involves AMPAR trafficking between four saturable membrane compartments and one non-saturable internal endocytic compartment (endo). AMPARs in the PSD contribute to the synaptic conductance, and they can be trafficked to and from small peri-PSD compartments (PeriIN, PeriOut), which do not contribute to the synaptic responses. The model also features the neuromodulation of a direct exchange between the endocytic compartment and unanchored (UA) freely moving AMPARs, a fraction of which contribute to synaptic responses. This was a necessary minimal assumption to model the conspicuous, yet transient changes in synaptic responses induced by GPCR agonists alone (Huang et al., 2012).

We assume that at rest traffic between all the compartments is slow. LTP induction temporarily and selectively increases the traffic rate of AMPARs from the PeriIN to the PSD compartment, thus increasing synaptic conductance (**Figure 1B** left). Conversely, LTD induction temporarily increases the rate of traffic out of the PSD to empty slots in the PeriOut compartment, thus reducing synaptic conductance (**Figure 1B** right). We also assume that the PeriIN and PeriOut compartments have limited capacity. Consequently, LTP and LTD are constrained by the occupancy of these compartments. LTP would be limited by the number of AMPARs anchored at PeriIN and LTD by the number of empty slots at PeriOut.

The key feature of the model is that GPCRs control the expression of LTP and LTD by determining the occupancy of the PeriIN and PeriOut compartments. Activation of GPCRs increases AMPAR traffic of the endocytic compartment with the two perisynaptic compartments and with the UA pool of AMPARs. Gs-coupled receptors increase exocytosis to the PeriIN, the UA AMPARs, and to a lesser extent the PeriOut compartments (**Figure 1C**). Gq-coupled receptors increase the

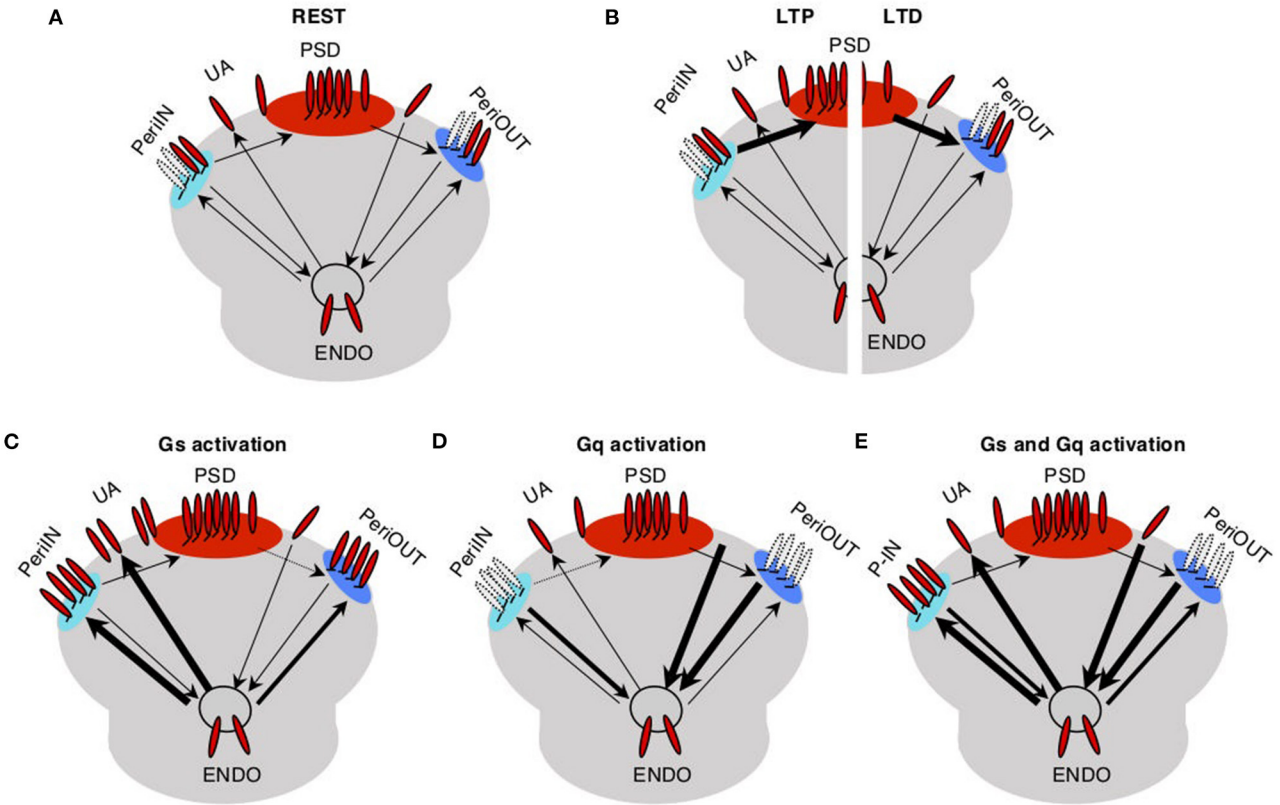

FIGURE 1 | Trafficking model of neuromodulation of Hebbian plasticity. AMPA receptors (red) at the synapse are either anchored at the postsynaptic density compartment (PSD) and in two close compartments (PeriIN, PeriOut), or unanchored. **(A)** Traffic between these synaptic compartments and with an endoplasmatic compartment (Endo) is low at rest (thin arrows). **(B)** Traffic between PSD and P-In, P-Out increases during long-term potentiation (LTP; left) and long-term depression (LTD; right) induction (thick arrows). **(C)** Activation of Gs increases traffic out of the Endo toward the synapse saturating both P-In and P-Out, thus preventing LTD. **(D)** Activation of Gq increases traffic out of the synapse toward the Endo compartment depleting both P-In and P-Out, thus preventing LTP. **(E)** Activation of both Gs and Gq increases the exchange between the synaptic and the Endo compartments, thus enabling/facilitating both, LTP and LTD.

endocytosis from the PeriOut, the UA AMPARs, and to a lesser extent the PeriIN compartments (**Figure 1D**). Thus, activation of Gs-coupled receptors would prevent LTD by saturating the PeriOut compartment (**Figure 1C**), whereas Gq activation would deplete the PeriIN compartment and prevent LTP (**Figure 1D**). The coactivation of Gs- and Gq-coupled receptors would saturate the PeriIN and deplete the PeriOut compartments because of their differential effects on the exchange between the endo and perisynaptic compartments, thus enabling the expression of both LTP and LTD.

The central motivation for the trafficking model outlined above was a study that examined in slices how agonists for β- and α-adrenergic receptors (respectively, coupled to Gs and Gq) affect LTP and LTD induced by pairing conditioning. The study showed that, indeed, activation of β-adrenoreceptors promotes LTP at the expense of LTD, activation of α-adrenoreceptors promotes LTP at the expense of LTD, and, importantly, activation of both together (β- and α-adrenoreceptors) promote both LTP and LTD. We asked, therefore, whether with reasonable assumptions, the trafficking could account for that experimental data on neuromodulation of LTP and LTD. The equations governing the AMPAR trafficking between compartments used in the fitting and the values of the constants and parameters are detailed in the Materials and Methods section. Briefly, the rates of trafficking to and from the PSD compartments during LTP and LTD were assumed to depend on kinases and phosphatases activated by Ca influx during the pairing conditioning, whereas the movement of unanchored AMPARs was assumed limited by lateral diffusion.

To test the model, we first optimized parameters to fit the time course and magnitude of the reported changes in synaptic responses after LTP or LTD induction and after activation of β-and/or α-adrenoreceptors separately. Then we tested the ability of the model to reproduce the interactions between LTP/D and β-and/or α-adrenoreceptors. In the experimental study, the noradrenergic agonists were applied for 10 min, whereas LTP/D were induced with a 2-min pairing of synaptic activation with postsynaptic depolarization delivered by the end of the agonist application (Huang et al., 2012). Parameters optimized included the synaptic size of the compartment, the exchange rates after LTP/D, and the GPCRs activation. The optimization aimed to fit the results reported in Figure 1 of Huang et al. (2012), which capture the essence of the

pull–push nature of the neuromodulation of LTP/D. As shown in **Figure 2**, with adequate parameters and initial values, the changes in synaptic conductance calculated with the model (thick black lines) fit the experimental data (gray circles) in each of the five conditions. Note that in the model LTP and β-adrenoreceptor activation, both potentiate the synaptic response, but through different mechanisms (increasing AMPAR at the PSD or the UA ones) and with opposite effects on the PeriIN compartments. LTP depletes the PeriIN compartment whereas the β-adrenoreceptor saturates it (**Figures 2B,D**). Conversely, LTD and α-adrenoreceptor activation both depress the synaptic response by reducing PSD-anchored and UA AMPARs, respectively, but with opposite effects on the occupancy of the PeriOut compartment (**Figures 2C,E**). On the other hand, coactivation of β- and α-adrenoreceptors modestly affect the synaptic responses, as their effects on the unanchored AMPAR pool cancel out; yet they saturate the PeriIN and deplete the PeriOut compartments (**Figure 2F**).

Subsequently, we checked whether the model accounts for the interactions between LTP/D and the neuromodulators. Indeed, the principal motivation for building the trafficking model was to account that while the activation of β- and α-adrenoreceptors individually prevent LTD and LTP, respectively, together they promote LTP and LTD. In the slice experiments, LTP and LTD were attempted at the end of the 10-min application of the neuromodulators (Huang et al., 2012). In the model, we used that timing sequence, and importantly we used the same values for parameters and constants optimized above in **Figure 2**. As shown in **Figure 3**, there was a clear concordance between the outcomes predicted by the model and the experimental data, both in the magnitude and time course of the changes in synaptic response. Like the activation of β- and α-adrenoreceptors in the slice, in the model Gs activation allows LTP and prevents LTD by saturating the perisynaptic compartments (**Figures 3A,D**), Gq activation allows LTD and prevents LTP by depleting the perisynaptic compartments (**Figures 3B,E**), and the coactivation of Gq and GS allows both LTP and LTD (**Figures 3C,F**).

Finally, we sought experimental support for the idea, central to the model, that neuromodulators can affect perisynaptic AMPARs. To that end, we studied in hippocampal slices the CA3→CA1 synapses, where perisynaptic AMPAR responses can be revealed and quantified by increasing glutamate spillover (Megill et al., 2015) via blocking glutamate uptake with the inhibitor TBOA (see methods). Bath-applied TBOA increases the amplitude and duration of the synaptic responses, reflecting the recruitment of extrasynaptic AMPARs. In the experimental

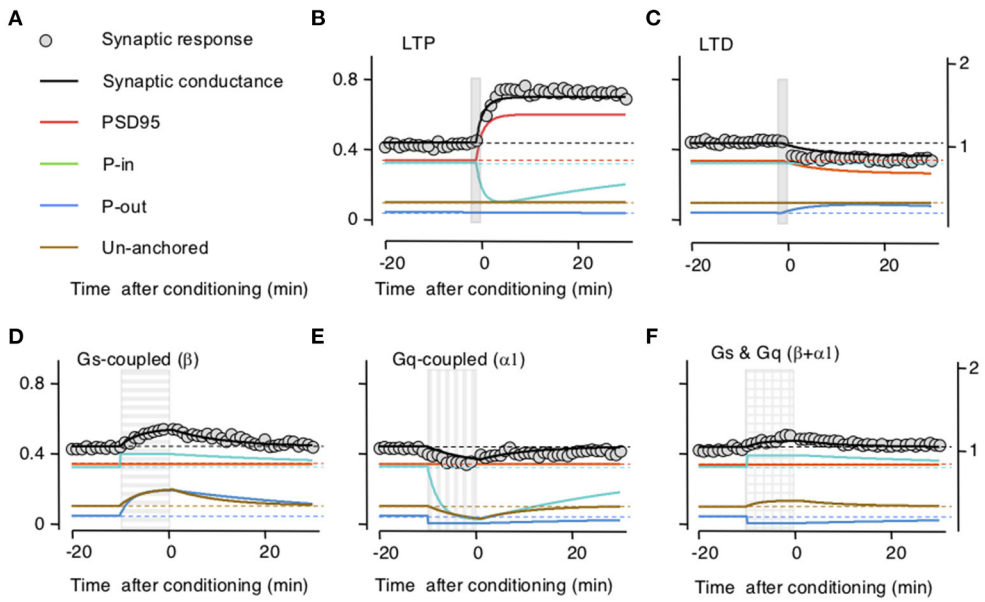

FIGURE 2 | Simulation of how long-term potentiation (LTP)/long-term depression (LTD) induction and the stimulation of Gs and Gq-coupled receptors change the occupancy of the modeled AMPA receptor (AMPAR) compartments. **(A)** Color conventions of the various synaptic compartment described in the remaining panels. Also included are gray circles representing actual synaptic response data from Huang et al. (2012). **(B)** An LTP-induction protocol (vertical gray bar) transiently increases AMPAR traffic onto the postsynaptic density compartment (PSD)95 from the PeriIN compartment, depleting it, but without affecting the PeriOut compartment. This results in a net increase in synaptic conductance with a time course, comparable with changes reported in Huang et al. (2012). Left *Y*-axis: occupancy of synaptic compartments; right *Y*-axis: normalized synaptic response. **(C)** An LTD protocol (vertical gray bar) transiently increases traffic out of the PSP onto the PeriOut compartment, filling it up, and reducing synaptic conductance. **(D)** Stimulation of Gs-coupled receptors (horizontally striped bar) increases AMPAR trafficking from the endosomatic compartment into all but the PSD synaptic compartments causing a transient increase in synaptic conductance. **(E)** Stimulation of Gq-coupled receptors (vertically striped bar) increases AMPAR trafficking to the endosomatic compartment from all but the P synaptic compartments causing a transient decrease in synaptic conductance compartments. **(F)** Stimulation of Gs-and Gq-coupled receptors (checkered bar) increases AMPAR trafficking (in and out) between the endosomal and all but the PDS95 synaptic compartments. This fills up the PeriIN compartment, depletes the PeriOut compartment, and results in a modest transient increase in synaptic conductance.

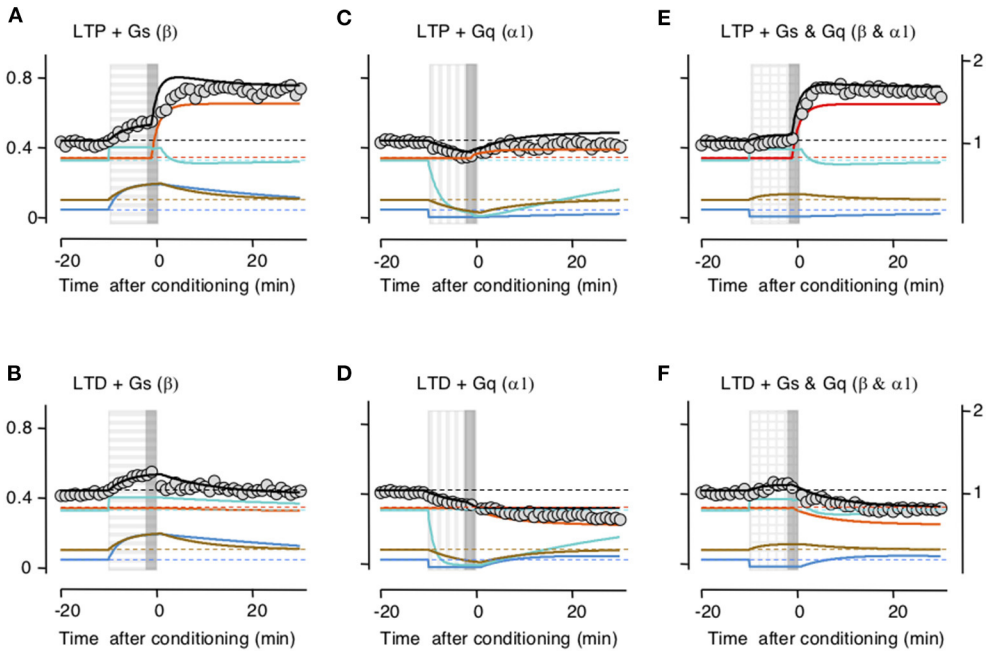

FIGURE 3 | Simulation of how Gs- and Gq-coupled receptors affect the induction of long-term potentiation (LTP) and long-term depression (LTD) by filling and depleting AMPA receptor synaptic compartments. The upper row shows the effects on LTP; the lower row, the effect on LTD. Color conventions of compartments as in **Figure 2**. PerilN: green; PeriOut: blue; Non-anchored: brown; postsynaptic density compartment: red; Synaptic conductance: black; actual data from Huang et al. (2012): gray circles. Left column **(A,B)** shows that Gs-GPCR stimulation (horizontally striped bar) fills up the PerilN and PeriOut compartments, barely affecting the induction (gray vertical bar) of LTP **(A)**, but preventing the induction of LTD **(B)**. The middle column **(C,D)** shows that Gq-GPCR stimulation (vertically striped bar) depletes both the PerilN and the PeriOut compartments, preventing the induction of LTP (C) without affecting the induction of LTD **(D)**. The right column **(E,F)** shows that co-stimulating Gs- and Gq-GPCRs fills up and depletes the PerilN and the PeriOut compartments, respectively, allowing the induction of both LTP **(E)** and LTD **(F)**.

design, we also exploited the previous observation that activation of β- and α-adrenoreceptors have lasting, "priming," effects on LTP and LTD (Huang et al., 2012) that are consistent with lasting changes in the occupancy of the perisynaptic compartments. Thus, we asked how priming with noradrenergic agonists alters the effects of TBOA on synaptic responses recorded extracellularly as field potentials (FP) in CA1. As shown in **Figure 4A**, in the hippocampus, a 10-min pretreatment with the β-adrenergic agonist isoproterenol (Iso: 10 μM) increased the enhancements of the FP induced by bath-applied TBOA (10 μM); conversely, the α-adrenergic agonist methoxamine (Mtx:10 μM) reduced the TBOA-induced FP enhancement. An ANOVA test ($F_{2[2,26]} = 11.22$; $p = 0.0003$) followed by Dunnett's *post-hoc* test confirmed the significance of the differences in the slopes measured 10–15 min after TBOA application. These results are consistent with a scenario in which β-and α-adrenoreceptors, respectively, increase and reduce the pool of extrasynaptic AMPARs. In the visual cortex, on the other hand, TBOA does not affect the synaptic response magnitude, responses collected in the −5 to 0 min interval prior to TBOA application, were comparable with those collected in the 25–30 min interval post TBOA application (paired *t*-test: $p = 0.9616$; **Figure 4B**). This might reflect a smaller capacity of the perisynaptic compartments or a larger distance from the synapse in the visual cortex (see section Discussion).

DISCUSSION

G-protein coupled receptors can facilitate and suppress LTP and LTD in a pull–push manner (Huang et al., 2012). To account for these opposite effects, we developed a simple model where neuromodulators modify the occupancy of two small and saturable perisynaptic compartments that limit the AMPAR traffic in and out of the synapse. This action at the expression level is sufficient to account for the suppression of LTP and LTD by Gs and Gq-coupled receptors, and their paradoxical synergy when simultaneously activated. Note that although GPCRs do affect Ca^{2+} signaling and the kinases and phosphatases involved in LTP/LTD induction (Pawlak et al., 2010; Tritsch and Sabatini, 2012; O'Dell et al., 2015; Meunier et al., 2017; Bari et al., 2020; Fernandez de Sevilla et al., 2021; Lutzu and Castillo, 2021), these actions are not required for the model to work. Indeed, for simplicity, they were not considered in this model. This contrasts with previous models explaining the facilitation of LTP and LTD induction in terms of changes in the kinase and phosphatase signaling pathways (Jedrzejewska-Szmek et al., 2017; Blackwell et al., 2019; Maki-Marttunen et al., 2020). We surmise that the two types of models, those focusing on the facilitation of induction via changes in kinases and phosphatases and this one focusing on the suppression of the expression *via* modulation AMPAR trafficking, are complementary and necessary for

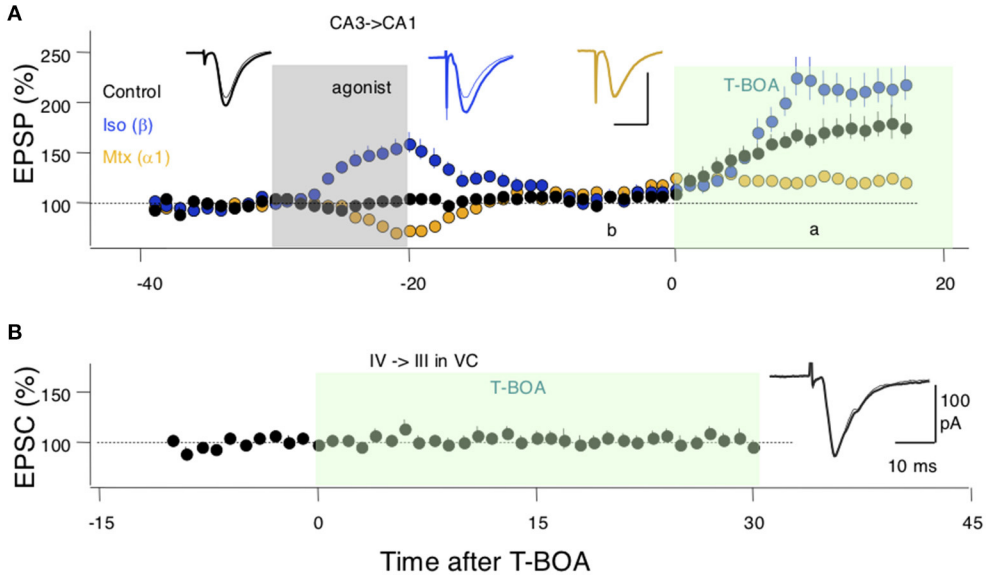

FIGURE 4 | Evidence for an adrenergic modulation of a perisynaptic pool of AMPA receptors (AMPARs). **(A)** In SC-CA1 synapses of the hippocampus bath application of a glutamate uptake blocker (T-BOA: 10 μM. green box) enhances the synaptic responses (black symbols). Pretreating the slices with the agonist for β-adrenergic receptors (coupled to Gs) isoproterenol (Iso: 10 μM for 10 min) potentiates the effects of T-BOA. In contrast, pretreating with an agonist for the a1 adrenergic receptor (coupled to Gq) methoxamine (Mtx: 5 μM for 10 min) reduces the enhancement induced by T-BOA. **(B)** In the visual cortex, T-BOA does not affect synaptic responses suggesting that the pool of perisynaptic AMPARsis too small to be detected. Traces in **(A,B)** are averages of 10 consecutive responses recorded 10 min. before **(B)** and 10 min. after **(A)** the addition of T-BOA. Each symbol in **(A,B)** represents data normalized as % of pre-TBOA baseline and averaged over 1 min.

a comprehensive understanding of the neuromodulation of Hebbian plasticity.

Experimental evidence indicates that GPCRs can regulate LTP and LTD at the expression level independently of the well-documented facilitation of LTP and LTD induction. First, we have shown that the suppression of LTP and LTD by GPCRs is independent of changes in NMDAR activation and cell excitability (Huang et al., 2012). Second, stimulation of GPCRs and LTP/D induction can be dissociated in time. A brief GPCR stimulation epoch can prime the facilitation/suppression of LTP/D elicited even hours later (Tenorio et al., 2010; Huang et al., 2012; Hulme et al., 2012). GPCRs can also act retroactively after plasticity has been induced (Brzosko et al., 2015, 2017, 2019) or attempted (Yagishita et al., 2014; He et al., 2015; Fisher et al., 2017; Shindou et al., 2019). The trafficking model is well-suited to reproduce these temporal features of plasticity neuromodulation. GPCR-induced changes in perisynaptic compartment occupancy and its effect on LTP/D will tend to persist because AMPAR exchange is very slow at rest, following GPCR stimulation at rest. For example, a persistent saturation of these compartments after a brief and strong β-adrenergic stimulation would result in a lasting priming of LTP and lasting suppression of LTD (Huang et al., 2012). Conversely, a lasting depletion of these compartments after α-adrenergic or M1-muscarinic activation would result in the lasting priming of LTD and suppression of LTP (Huang et al., 2012). On the other hand, the retroactive actions of GPCRs, particularly the transformation of silent synaptic eligibility traces onto LTP and LTD, might reflect the combination of residual kinases/phosphatase activity and GPCR-induced changes in the occupancy of the perisynaptic compartments. In sum, the mechanistic dissociation of the induction (NMDAR activation, kinases/phosphatase activities) and the expression of plasticity (AMPAR modification and trafficking) provides a reasonable basis to account for defining temporal features of its neuromodulation.

As mentioned in the introduction, several distinct mechanisms for the expression of postsynaptic Hebbian plasticity have been identified, including lateral diffusion of AMPAR to and from the synapse, direct exchange with internal compartments, and changes in the unitary conductance of AMPAR; yet their relative contribution to LTP/D in different synapses remain unclear. Our model of pull–push neuromodulation, based on data from layer 4→Layer 2/3 cortical synapses, is congruent with lateral diffusion only. How a pull–push neuromodulation could be implemented in the scenario of direct exo- and endocytosis or how GPCRs could affect changes in AMPAR unitary conductance in a pull–push manner remains to be explored, but it is not excluded as a possibility by our model. Our model also features the distinct assumption that AMPAR exchange to and from the PSD is channeled via two perisynaptic compartments whose occupancy, in turn, is controlled by GPCRs and constrains LTP and LTD. We arrived at this two compartments assumption due to the difficulty of fully modeling the simultaneous facilitation of LTP and LTD with a single compartment when Gs and Gq are coactivated. This is because facilitation of LTP by Gs-GPCRs would require saturating the single compartment whereas facilitation of LTD by Gq-GPCRs would require the depletion of that compartment. Simultaneous

activation of Gs-GPCRs and Gq-GPCRs experimentally led to the facilitation of both LTP and LTD, and a parsimonious explanation involves the separation of these compartments. We did not explore other more complicated possibilities, for example, combining a single perisynaptic compartment with more complex schemes of trafficking signaling. The exact nature of these two hypothesized compartments and how GPCRs could control their occupancy remain open questions. A likely candidate mechanism for the occupancy and trafficking control could be the phosphorylation of a distinct constellation of sites in the AMPARs (Diering et al., 2016). In the few cases examined, different GPCRs phosphorylate different subsets of these sites (Hu et al., 2007; Seol et al., 2007; Huang et al., 2014), which in turn would be in tune with the notion of a "phosphorylation code" for AMPAR trafficking (Diering and Huganir, 2018).

Concerning the existence of two perisynaptic compartments, we note that the idea is consistent with the observation of a discrete and defined perisynaptic locus for endocytosis during LTD (Lu et al., 2007). Also consistent with the model are the results of **Figure 4** showing that in the hippocampal slices GPCRs can control bidirectionally perisynaptic AMPARs revealed by blocking glutamate uptake. In visual cortical slices, blocking glutamate uptake did not reveal perisynaptic AMPARs, raising the intriguing possibility that the capacity of these perisynaptic compartments is smaller in cortical synapses than in hippocampal slices or that they are farther away from the synapse.

Finally, the trafficking model for the pull–push neuromodulation makes clear testable predictions. Indeed, a validating aspect of the model was that the values for constants and parameters obtained by fitting the LTP/LTD and Gs/Gq data independently predicted the effects of coactivating Gs and Gq on LTP/D. In Ca1, where the opposite modulation of LTP and LTD by individual GCPRs is well-documented (Katsuki et al., 1997; Mockett et al., 2007; Huang et al., 2012), the model predicts that the coactivation of Gs-GCPR and Gq-GCPR would promote both LTP at LTD. In addition, in CA1 and the visual cortex, the exposure to Gs-GCPR agonists can prime LTP facilitation and LTD suppression for an extended time (Huang et al., 2012). The model predicts that if priming reflects persistent saturation of perisomatic compartments then LTP facilitation and LTD suppression should decay at the same pace. In sum, we surmise that ours is a simple model that accounts for defining features of the pull–push neuromodulation of Hebbian plasticity and makes predictions that can be tested experimentally.

MATERIALS AND METHODS

Slice Experiments

Experiments were performed according to the guidelines for the use of animals approved by the Ethics and Animal Care Committee of Universidad de Valparaíso (BEA064-2015) and the IACUC of Johns Hopkins University (MO14M404). Acute hippocampal or cortical slices were prepared from 1-month-old C57/BL6 mice as previously described (Huang et al., 2012; Ardiles et al., 2014). Briefly, each mouse was sacrificed by decapitation, following an overdose of isoflurane. Hippocampi were rapidly removed and sectioned into 350 μm slices using oxygenated ice-cold dissection buffer [composed of (in mm) 212.7 sucrose, 2.6 KCl, 1.23 NaH_2PO_4, 26 $NaHCO_3$, 10 dextrose, 3 $MgCl_2$, and 1 $CaCl_2$] and recovered at room temperature in artificial CSF [ACSF; composed of (in mm) 124 NaCl, 5 KCl, 1.25 NaH_2PO_4, 26 $NaHCO_3$, 10 dextrose, 1.5 $MgCl_2$, and 2.5 $CaCl_2$]. All recordings were done in a submersion recording chamber perfused with ACSF (29–30°C, 2 ml/min) bubbled with 95% O_2/5% CO_2. For FP recordings, synaptic responses were delivered through a bipolar glass stimulating electrode placed to activate the Schaffer collaterals with a 0.2-ms duration pulse (baseline stimulation at 0.0333 Hz) and recorded from the dendritic field of CA1. EPSCs in layer 2/3 pyramidal cells evoked by layer 4 stimulation were recorded as in Huang et al. (2012). Synaptic responses were digitized and stored online using Igor Pro software (WaveMetrics). To evaluate the neuromodulatory effect of Gs and Gq adrenoceptors, after 15 min of stable baseline, slices were superfused for 10 min with adrenergic agonists isoproterenol (Iso; 10 μm) and methoxamine (Mtx; 5 μm). Then 10 μm dl-threo-β-benzyloxyaspartic acid (TBOA, Tocris Biosciences), a competitive blocker of glutamate transporters, was used to induce spillover of glutamate and to reveal the activity of perisynaptic AMPARs. In these experiments, CA3 was cut away during dissection, and high divalents were added to the ACSF (4 mM $MgCl_2$ and 4 mM $CaCl_2$). Isolated AMPAR-mediated responses were evoked in the presence of 100 μM D,L-APV, and 2.5 μM gabazine. To prevent oxidation, isoproterenol and methoxamine were prepared freshly in ASCF containing sodium ascorbate (40 μM). FP slopes were measured and data are expressed as means ± SEM. All FP and EPSC data had a normal distribution as confirmed by D'Agostino–Pearson normality test. ANOVA and *t*-test were performed in Prism.

Model

Three sets of equations describing the traffic of AMPARs between the PSD, PeriIN, PeriOut, UA, and Endo compartments and the occupancy of PSD, PeriIN, and PeriOut are described below. The set of equations represent three-time intervals, which are modulation, induction, and after induction. The dynamic equations are the same in the three-time intervals but differ in the constants used. The final values for the dynamics in one interval are used as the initial condition for the subsequent interval. The initial condition for the first interval is computed from the analytical solution of the dynamics reaching equilibrium at rest. The suffix A for each compartment denotes sites with anchored AMPAR, the suffix F denotes free sites; thus A plus F represents the total size of each compartment, which is constant in time during our simulations. Values of parameters and constants were chosen to fit the results of Figure 1 in Huang et al. (2012) and are indicated after the equations. Note that in that study, the induction protocols for **Figure 1** were aimed at eliciting maximal plasticity; hence the rates of LTP and LTD, represented by Kin and PP, respectively are not affected by the neuromodulators. The *model was written in Mathematica, and the code is available upon request.

Dynamical Equations

$$
\begin{aligned}
A'_{PeriIN}[t] = &- k_{PeriINEndoM} * A_{PeriIN}[t] + k_{EntdoPeriINM} \\
&* F_{PeriIN}[t] - k_{PeriINPsd} * Kin_{PeriIN}[t] \\
&* A_{PeriIN}[t] * km2Kin/\big(km2Kin + A_{PeriIN}[t]\big) \\
&* F_{Psd}[t] \\
A'_{PeriOut}[t] = &- k_{PeriOutEndoM} * A_{PeriOut}[t] + k_{EntdoPeriOutM} \\
&* F_{PeriOut}[t] + k_{PsdPeriOut} * P_{\rho PeriOut}[t] \\
&* A_{Psd}[t] * km2PP/\big(km2PP + A_{Psd}[t]\big) \\
&* F_{PeriOut}[t] \\
A'_{Psd}[t] = &+ k_{PeriINPsd} * Kin_{PeriIN}[t] * A_{PeriIn}[t] \\
&* km2Kin/\big(km2Kin + A_{PeriIN}[t]\big) * F_{Psd}[t] \\
&- k_{PsdPeriOut} * P_{\rho PeriOut}[t] * A_{Psd}[t] \\
&* km2PP/\big(km2PP + A_{Psd}[t]\big) \quad * F_{PeriOut}[t] \\
A'_{UA}[t] = &- kUA_{EndoM} * A_{UA}[t] + k_{EndoUAM} * A_{Endo}[t] \\
&* F_{UA}[t], \\
Kin'_{PeriIN}[t] = &- k_{Kin} * Kin_{PeriIN}[t] + k_{in}, \\
P\rho'_{PeriOut}[t] = &- k_{P\rho} * P\rho_{PeriOut}[t] + k_{P\rho},
\end{aligned}
$$

The first four equations represent the dynamics of the occupancy of the compartments. The next two equations represent normalized dynamics of the concentrations of kinases and phosphatases. These equations and parameters are identical during the modulation and induction. After induction, the equations are the same, but some of the parameters change. The parameters that change have an index M in the above equations and use the same parameter name without M (see the section Parameter Description) after the induction.

While the dynamical equations are kept general, allowing transitions between multiple compartments, it should be noted that several of these transition constants are zero in the model which reproduces well the observed data.

Initial Conditions

For the modulation period, the initial conditions start from the equilibrium value of the solution for the equations after induction.

For the induction period, the initial conditions are the end of the modulation period with an added step increase for the normalized kinases and phosphatases in the PeriIN and PeriOut compartments (KinPeriINInd, PpPeriOutInd).

For the after-induction period, the initial conditions are the end of the induction period.

Weight

The simulated weight represents the concentration of bound AMPAR in the PSD and the UA compartments. The weight is smoothed with an exponential kernel with time constant tau.

Parameters

It should be noted that given the complexity of the model compared with the number of experimental observations an automatic parameter tuning could not be performed. Therefore, it is important to view these parameters as a possible explanation for the observed data, and not necessarily the only explanation for the observed data. While this is a significant limitation of the current model, we believe the model offers an important conceptual description of the phenomenology, and more precise estimates of the large number of parameters involved would require a vast array of measurements of the biochemical processes involved.

The modulation period lasts 9 min, induction 2, and the total simulation time is 50 min. The unit of time used is minutes.

The total sizes of different compartments are normalized relative to the size of the PSD compartment (TPsd = 1). For the recorded data, there was no clear need to differentiate their respective sizes, and they were all simulated to be equal and quite a bit smaller than the PSD (TAU = TPeriIn = TPeriOut = 0.2).

The rare constants are normalized such that the free AMPAR concentration is 1. While the equations are written in general for the movement of the AMPAR between compartments, the constants characterizing the movement from PeriIn to PSD and PSD to PeriOut are the only non-zero constants (kPeriINPsd = 0.001, kPsdPeriOut = 0.004). Both are very slow, requiring hours to reach equilibrium occupancy (i.e., for the synapse to revert to its background state), and the out rate is higher, resulting in an equilibrium state which is biased toward the PSD anchoring, options being mostly free.

Following LTP or LTD induction, these rates change significantly. They change by a multiplicative factor (KinPeriIN and PpPeriOut), which is time-dependent and abstractly approximates the effects of kinases and phosphatases. These multiplicative factors are computed in the last two dynamic equations. Their values are defined to be normalized to their resting values (the equilibrium solution is defined to be 1 for these variables). Following an LTP induction, KinPeriIn is increased by a factor of KinPeriINInd = 1,000 and reverts to equilibrium with a time constant of kKin = 1/(4 min), while PpPeriOut increases by a factor of PpPeriOutInd = 400 and reverts back to equilibrium with a time constant of kPp = 1/(10 min). The movement to PeriIN and PeriOut compartments is subject to saturation, with saturation half-activations km2Kin = 0.1 and km2Pp = 0.1, which were kept fix at half the size of the Peri compartments.

Lastly, without modulation, the rates from and to the Peri compartments to the Endo(somal) compartment are fixed at 1/(50 min) and from UA to and from Endo at 1/(20 min). Application of beta-agonists leads to an increase of movement from Endo PeriIn by a factor of 100, to PeriOut by a factor of 10, and to UA by a factor of 4.5. Application of alpha agonists leads to an increase in movement to Endo from PeriOut by a factor of 100, from PeriIn by a factor of 10, and from UA by a factor of 2.

DATA AVAILABILITY STATEMENT

The raw data supporting the conclusions of this article will be made available by the authors, without undue reservation.

ETHICS STATEMENT

The animal study was reviewed and approved by Ethics and Animal Care Committee of Universidad de Valparaíso (BEA064-2015).

AUTHOR CONTRIBUTIONS

SM and AK developed the model and wrote the manuscript. SM implemented the model. AA, AP, and AK designed the slice experiments. AA conducted the experiments. All authors contributed to the article and approved the submitted version.

FUNDING

This work was supported by grant R01EY012124 to AK, who was also supported by the NIH grant P01 AG009973. AP was supported by grant MILENIO ICM-ANID P09-022-F and AA by grant FONDECYT 1201342.

ACKNOWLEDGMENTS

The authors thank Dr. Hey-Kyoung Lee for the helpful comments.

REFERENCES

Ahmad, M., Polepalli, J. S., Goswami, D., Yang, X., Kaeser-Woo, Y. J., Sudhof, T. C., et al. (2012). Postsynaptic complexin controls AMPA receptor exocytosis during LTP. *Neuron* 73, 260–267. doi: 10.1016/j.neuron.2011.11.020

Ardiles, A. O., Flores-Munoz, C., Toro-Ayala, G., Cardenas, A. M., Palacios, A. G., Munoz, P., et al. (2014). Pannexin 1 regulates bidirectional hippocampal synaptic plasticity in adult mice. *Front. Cell Neurosci.* 8:326. doi: 10.3389/fncel.2014.00326

Bari, B. A., Chokshi, V., and Schmidt, K. (2020). Locus coeruleus-norepinephrine: basic functions and insights into Parkinson's disease. *Neural Regen. Res.* 15, 1006–1013. doi: 10.4103/1673-5374.270297

Blackwell, K. T., Salinas, A. G., Tewatia, P., English, B., Hellgren Kotaleski, J., and Lovinger, D. M. (2019). Molecular mechanisms underlying striatal synaptic plasticity: relevance to chronic alcohol consumption and seeking. *Eur. J. Neurosci.* 49, 768–783. doi: 10.1111/ejn.13919

Brzosko, Z., Mierau, S. B., and Paulsen, O. (2019). Neuromodulation of spike-timing-dependent plasticity: past, present, and future. *Neuron* 103, 563–581. doi: 10.1016/j.neuron.2019.05.041

Brzosko, Z., Schultz, W., and Paulsen, O. (2015). Retroactive modulation of spike timing-dependent plasticity by dopamine. *eLife* 4:e09685. doi: 10.7554/eLife.09685.017

Brzosko, Z., Zannone, S., Schultz, W., Clopath, C., and Paulsen, O. (2017). Sequential neuromodulation of Hebbian plasticity offers mechanism for effective reward-based navigation. *eLife* 6:e27756. doi: 10.7554/eLife.27756.020

Buonarati, O. R., Hammes, E. A., Watson, J. F., Greger, I. H., and Hell, J. W. (2019). Mechanisms of postsynaptic localization of AMPA-type glutamate receptors and their regulation during long-term potentiation. *Sci. Signal.* 12:eaar6889. doi: 10.1126/scisignal.aar6889

Choi, S., Chang, J., Jiang, B., Seol, G. H., Min, S. S., Han, J. S., et al. (2005). Multiple receptors coupled to PLC gate LTD in visual cortex. *J. Neurosci.* 25, 11433–11443. doi: 10.1523/JNEUROSCI.4084-05.2005

Choquet, D. (2018). Linking nanoscale dynamics of AMPA receptor organization to plasticity of excitatory synapses and learning. *J. Neurosci.* 38, 9318–9329. doi: 10.1523/JNEUROSCI.2119-18.2018

Derkach, V. A., Oh, M. C., Guire, E. S., and Soderling, T. R. (2007). Regulatory mechanisms of AMPA receptors in synaptic plasticity. *Nat. Rev. Neurosci.* 8, 101–113. doi: 10.1038/nrn2055

Diering, G. H., Heo, S., Hussain, N. K., Liu, B., and Huganir, R. L. (2016). Extensive phosphorylation of AMPA receptors in neurons. *Proc. Natl. Acad. Sci. U.S.A.* 113, E4920–4927. doi: 10.1073/pnas.1610631113

Diering, G. H., and Huganir, R. L. (2018). The AMPA receptor code of synaptic plasticity. *Neuron* 100, 314–329. doi: 10.1016/j.neuron.2018.10.018

Edelmann, E., and Lessmann, V. (2013). Dopamine regulates intrinsic excitability thereby gating successful induction of spike timing-dependent plasticity in CA1 of the hippocampus. *Front. Neurosci.* 7:25. doi: 10.3389/fnins.2013.00025

Faber, E. S., Delaney, A. J., Power, J. M., Sedlak, P. L., Crane, J. W., and Sah, P. (2008). Modulation of SK channel trafficking by beta adrenoceptors enhances excitatory synaptic transmission and plasticity in the amygdala. *J. Neurosci.* 28, 10803–10813. doi: 10.1523/JNEUROSCI.1796-08.2008

Fernandez de Sevilla, D., Nunez, A., and Buno, W. (2021). Muscarinic receptors, from synaptic plasticity to its role in network activity. *Neuroscience* 456, 60–70. doi: 10.1016/j.neuroscience.2020.04.005

Fisher, S. D., Robertson, P. B., Black, M. J., Redgrave, P., Sagar, M. A., Abraham, W. C., et al. (2017). Reinforcement determines the timing dependence of corticostriatal synaptic plasticity *in vivo*. *Nat. Commun.* 8:334. doi: 10.1038/s41467-017-00394-x

He, K., Huertas, M., Hong, S. Z., Tie, X., Hell, J. W., Shouval, H., et al. (2015). Distinct eligibility traces for LTP and LTD in cortical synapses. *Neuron* 88, 528–538. doi: 10.1016/j.neuron.2015.09.037

Hu, H., Real, E., Takamiya, K., Kang, M. G., Ledoux, J., Huganir, R. L., et al. (2007). Emotion enhances learning via norepinephrine regulation of AMPA-receptor trafficking. *Cell* 131, 160–173. doi: 10.1016/j.cell.2007.09.017

Huang, S., Rozas, C., Trevino, M., Contreras, J., Yang, S., Song, L., et al. (2014). Associative Hebbian synaptic plasticity in primate visual cortex. *J. Neurosci.* 34, 7575–7579. doi: 10.1523/JNEUROSCI.0983-14.2014

Huang, S., Trevino, M., He, K., Ardiles, A., Pasquale, R., Guo, Y., et al. (2012). Pull-push neuromodulation of LTP and LTD enables bidirectional experience-induced synaptic scaling in visual cortex. *Neuron* 73, 497–510. doi: 10.1016/j.neuron.2011.11.023

Hulme, S. R., Jones, O. D., Ireland, D. R., and Abraham, W. C. (2012). Calcium-dependent but action potential-independent BCM-like metaplasticity in the hippocampus. *J. Neurosci.* 32, 6785–6794. doi: 10.1523/JNEUROSCI.0634-12.2012

Jedrzejewska-Szmek, J., Luczak, V., Abel, T., and Blackwell, K. T. (2017). beta-adrenergic signaling broadly contributes to LTP induction. *PLoS Comput. Biol.* 13:e1005657. doi: 10.1371/journal.pcbi.1005657

Katsuki, H., Izumi, Y., and Zorumski, C. F. (1997). Noradrenergic regulation of synaptic plasticity in the hippocampal CA1 region. *J. Neurophysiol.* 77, 3013–3020. doi: 10.1152/jn.1997.77.6.3013

Lin, Y. W., Yang, H. W., Min, M. Y., and Chiu, T. H. (2008). Inhibition of associative long-term depression by activation of beta-adrenergic receptors in rat hippocampal CA1 synapses. *J. Biomed. Sci.* 15, 123–131. doi: 10.1007/s11373-007-9205-z

Lledo, P. M., Zhang, X., Sudhof, T. C., Malenka, R. C., and Nicoll, R. A. (1998). Postsynaptic membrane fusion and long-term potentiation. *Science* 279, 399–403. doi: 10.1126/science.279.5349.399

Lu, J., Helton, T. D., Blanpied, T. A., Racz, B., Newpher, T. M., Weinberg, R. J., et al. (2007). Postsynaptic positioning of endocytic zones and AMPA receptor cycling by physical coupling of dynamin-3 to Homer. *Neuron* 55, 874–889. doi: 10.1016/j.neuron.2007.06.041

Lutzu, S., and Castillo, P. E. (2021). Modulation of NMDA receptors by G-protein-coupled receptors: role in synaptic transmission, plasticity and beyond. *Neuroscience* 456, 27–42. doi: 10.1016/j.neuroscience.2020.02.019

Maki-Marttunen, T., Iannella, N., Edwards, A. G., Einevoll, G. T., and Blackwell, K. T. (2020). A unified computational model for cortical post-synaptic plasticity. *eLife* 9:e55714. doi: 10.7554/eLife.55714.sa2

Makino, H., and Malinow, R. (2009). AMPA receptor incorporation into synapses during LTP: the role of lateral movement and exocytosis. *Neuron* 64, 381–390. doi: 10.1016/j.neuron.2009.08.035

Malenka, R. C., and Bear, M. F. (2004). LTP and LTD: an embarrassment of riches. *Neuron* 44, 5–21. doi: 10.1016/j.neuron.2004.09.012

Malenka, R. C., and Nicoll, R. A. (1999). Long-term potentiation–a decade of progress? *Science* 285, 1870–1874. doi: 10.1126/science.285.5435.1870

Megill, A., Tran, T., Eldred, K., Lee, N. J., Wong, P. C., Hoe, H. S., et al. (2015). Defective age-dependent metaplasticity in a mouse model of Alzheimer's disease. *J. Neurosci.* 35, 11346–11357. doi: 10.1523/JNEUROSCI.5289-14.2015

Meunier, C. N., Chameau, P., and Fossier, P. M. (2017). Modulation of synaptic plasticity in the cortex needs to understand all the players. *Front. Synaptic Neurosci.* 9:2. doi: 10.3389/fnsyn.2017.00002

Mockett, B. G., Guevremont, D., Williams, J. M., and Abraham, W. C. (2007). Dopamine D1/D5 receptor activation reverses NMDA receptor-dependent long-term depression in rat hippocampus. *J. Neurosci.* 27, 2918–2926. doi: 10.1523/JNEUROSCI.0838-06.2007

Newpher, T. M., and Ehlers, M. D. (2009). Spine microdomains for postsynaptic signaling and plasticity. *Trends Cell Biol.* 19, 218–227. doi: 10.1016/j.tcb.2009.02.004

Nguyen, P. V., and Gelinas, J. N. (2018). Noradrenergic gating of long-lasting synaptic potentiation in the hippocampus: from neurobiology to translational biomedicine. *J. Neurogenet.* 32, 171–182. doi: 10.1080/01677063.2018.1497630

Nicoll, R. A. (2017). A brief history of long-term potentiation. *Neuron* 93, 281–290. doi: 10.1016/j.neuron.2016.12.015

O'Dell, T. J., Connor, S. A., Guglietta, R., and Nguyen, P. V. (2015). beta-Adrenergic receptor signaling and modulation of long-term potentiation in the mammalian hippocampus. *Learn Mem.* 22, 461–471. doi: 10.1101/lm.031088.113

Oh, M. C., Derkach, V. A., Guire, E. S., and Soderling, T. R. (2006). Extrasynaptic membrane trafficking regulated by GluR1 serine 845 phosphorylation primes AMPA receptors for long-term potentiation. *J. Biol. Chem.* 281, 752–758. doi: 10.1074/jbc.M509677200

Park, P., Georgiou, J., Sanderson, T. M., Ko, K. H., Kang, H., Kim, J. I., et al. (2021). PKA drives an increase in AMPA receptor unitary conductance during LTP in the hippocampus. *Nat. Commun.* 12:413. doi: 10.1038/s41467-020-20523-3

Pawlak, V., Wickens, J., Kirkwood, A., and Kerr, J. (2010). Timing is not everything: neuromodulation opens the STDP gate. *Front. Synaptic Neurosci.* 2:146. doi: 10.3389/fnsyn.2010.00146

Purkey, A. M., and Dell'Acqua, M. L. (2020). Phosphorylation-dependent regulation of Ca(2+)-permeable AMPA receptors during hippocampal synaptic plasticity. *Front. Synaptic Neurosci.* 12:8. doi: 10.3389/fnsyn.2020.00008

Seol, G. H., Ziburkus, J., Huang, S., Song, L., Kim, I. T., Takamiya, K., et al. (2007). Neuromodulators control the polarity of spike-timing-dependent synaptic plasticity. *Neuron* 55, 919–929. doi: 10.1016/j.neuron.2007.08.013

Shindou, T., Shindou, M., Watanabe, S., and Wickens, J. (2019). A silent eligibility trace enables dopamine-dependent synaptic plasticity for reinforcement learning in the mouse striatum. *Eur. J. Neurosci.* 49, 726–736. doi: 10.1111/ejn.13921

Shouval, H., Bear, M., and Cooper, L. (2002). A unified model of NMDA receptor-dependent bidirectional synaptic plasticity. *Proc. Natl. Acad. Sci. U.S.A.* 99, 10831–10836. doi: 10.1073/pnas.152343099

Takamatsu, I., Iwase, A., Ozaki, M., Kazama, T., Wada, K., and Sekiguchi, M. (2008). Dexmedetomidine reduces long-term potentiation in mouse hippocampus. *Anesthesiology* 108, 94–102. doi: 10.1097/01.anes.0000296076.04510.e1

Tenorio, G., Connor, S. A., Guevremont, D., Abraham, W. C., Williams, J., O'Dell, T. J., et al. (2010). 'Silent' priming of translation-dependent LTP by ss-adrenergic receptors involves phosphorylation and recruitment of AMPA receptors. *Learn Mem.* 17, 627–638. doi: 10.1101/lm.1974510

Thomas, M. J., Moody, T. D., Makhinson, M., and O'Dell, T. J. (1996). Activity-dependent beta-adrenergic modulation of low frequency stimulation induced LTP in the hippocampal CA1 region. *Neuron* 17, 475–482. doi: 10.1016/S0896-6273(00)80179-8

Tritsch, N. X., and Sabatini, B. L. (2012). Dopaminergic modulation of synaptic transmission in cortex and striatum. *Neuron* 76, 33–50. doi: 10.1016/j.neuron.2012.09.023

Wu, D., Bacaj, T., Morishita, W., Goswami, D., Arendt, K. L., Xu, W., et al. (2017). Postsynaptic synaptotagmins mediate AMPA receptor exocytosis during LTP. *Nature* 544, 316–321. doi: 10.1038/nature21720

Yagishita, S., Hayashi-Takagi, A., Ellis-Davies, G. C., Urakubo, H., Ishii, S., and Kasai, H. (2014). A critical time window for dopamine actions on the structural plasticity of dendritic spines. *Science* 345, 1616–1620. doi: 10.1126/science.1255514

Conflict of Interest: The authors declare that the research was conducted in the absence of any commercial or financial relationships that could be construed as a potential conflict of interest.

Publisher's Note: All claims expressed in this article are solely those of the authors and do not necessarily represent those of their affiliated organizations, or those of the publisher, the editors and the reviewers. Any product that may be evaluated in this article, or claim that may be made by its manufacturer, is not guaranteed or endorsed by the publisher.

Advantages of publishing in Frontiers

OPEN ACCESS
Articles are free to read for greatest visibility and readership

FAST PUBLICATION
Around 90 days from submission to decision

HIGH QUALITY PEER-REVIEW
Rigorous, collaborative, and constructive peer-review

TRANSPARENT PEER-REVIEW
Editors and reviewers acknowledged by name on published articles

Frontiers
Avenue du Tribunal-Fédéral 34
1005 Lausanne | Switzerland

Visit us: www.frontiersin.org
Contact us: frontiersin.org/about/contact

REPRODUCIBILITY OF RESEARCH
Support open data and methods to enhance research reproducibility

DIGITAL PUBLISHING
Articles designed for optimal readership across devices

FOLLOW US
@frontiersin

IMPACT METRICS
Advanced article metrics track visibility across digital media

EXTENSIVE PROMOTION
Marketing and promotion of impactful research

LOOP RESEARCH NETWORK
Our network increases your article's readership